Structural Diversity of Biological Ligands and their Binding Sites in Proteins

Gareth Rhys Stockwell

European Bioinformatics Institute
Hinxton, Cambridge

and

Biomolecular Structure and Modelling Unit
Department of Biochemistry and Molecular Biology
University College London

A thesis submitted to the University of London
in the Faculty of Science for the degree of Doctor of Philosophy

August 2005

ProQuest LLC
789 East Eisenhower Parkway
P.O. Box 1346
Ann Arbor, MI 48106-1346

This document was prepared using the LaTeX typesetting system (Lamport, 1985). Molecular graphics were generated using the PyMOL program (DeLano, 2002). The Dia package (`http://www.gnome.org/projects/dia`) was used to generate many of the diagrams, and statistical analysis and charting was performed using R (Ihaka and Gentleman, 1996), GnuPlot (`http://www.gnuplot.info`) and OpenOffice (`http://www.openoffice.org`).

Abstract

The phenomenon of molecular recognition, which underpins almost all biological processes, is dynamic, complex and subtle. Establishing an interaction between a pair of molecules involves mutual structural rearrangements guided by a highly convoluted energy landscape, the accurate mapping of which continues to elude us. The analysis of interactions between proteins and small molecules has been a focus of intense interest for many years, offering as it does the promise of increased insight into many areas of biology, and the potential for greatly improved drug design methodologies. Computational methods for predicting which types of ligand a given protein may bind, and what conformation two molecules will adopt once paired, are particularly sought after.

The work presented in this thesis aims to quantify the amount of structural variability observed in the ways in which proteins interact with ligands. This diversity is considered from two perspectives: to what extent ligands bind to different proteins in distinct conformations, and the degree to which binding sites specific for the same ligand have different atomic structures.

The first study could be of value to approaches which aim to predict the bound pose of a ligand, since by cataloguing the range of conformations previously observed, it may be possible to better judge the biological likelihood of a newly predicted molecular arrangement. The findings show that several common biological ligands exhibit considerable conformational diversity when bound to proteins. Although binding in predominantly extended conformations, the analysis presented here highlights several cases in which the biological requirements of a given protein force its ligand to adopt a highly compact form. Comparing the conformational diversity observed within several protein families, the hypothesis that homologous proteins tend to bind ligands in a similar arrangement is generally upheld, but several families are identified in which this is demonstrably not the case.

Consideration of diversity in the binding site itself, on the other hand, may be useful in guiding methods which search for binding sites in uncharacterised protein structures: identifying those regions of known sites which are less variable could help to focus the search only on the most important features. Analysis of the diversity of a non-redundant dataset of adenine binding sites shows that a small number of key interactions are conserved, with the majority of the fragment environment being highly variable. Just as ligand conformation varies between protein families, so the degree of binding site diversity is observed to be significantly higher in some families than others.

Taken together, the results of this work suggest that the repertoire of strategies produced by nature for the purposes of molecular recognition are extremely extensive. Moreover, the importance of a given ligand conformation or pattern of interaction appears to vary greatly depending on the function of the particular group of proteins studied. As such, it is proposed that diversity analysis may form a significant part of future large-scale studies of ligand-protein interactions.

Acknowledgements

It is a great pleasure to be able to offer my gratitude to all those whose friendship, advice and support has made this thesis possible.

Firstly I would like to thank my primary supervisor, Janet Thornton, for her unfaltering enthusiasm and encouragement throughout the course of this project. She has been a source of outstanding inspiration, without whom I would never have reached this point. Thanks are also due to my second supervisor Richard Jackson, and my mentor Christine Orengo, both of whom maintained an active interest in this work. The administrative burden of undertaking a Ph.D. was lightened significantly by Gillian Adams, who has been immensely helpful in dealing with forms, contracts, manuscripts and a variety of other issues - always with a smile on her face! This work was funded mainly by the BBSRC, with additional support from EMBL and Inpharmatica.

My time at the EBI has been very enjoyable thanks to members of the Thornton group past and present, many of whom have become good friends as well as colleagues. In particular I wish to thank: Jonathan Barker, for ensuring that our office was always anything but dull; Gail Bartlett, for ensuring that the pranks stayed (at least mostly) on the right side of good taste and decency; Matthew Bashton, for his amusing stories on all topics imaginable; Alex Gutteridge, for being a model of Zen calm to aspire to, both in the office and on the ski slope; Kevin Murray, for teaching me that the light at the end of the tunnel might just be a train; Richard Morris and Rafael Najmanovich, for sharing my view that the Flying Pig is as good a place as any to talk science (and much else besides); James Torrance, for his inimitably dry humour; and Gordon Whamond, for being a friend and housemate for almost three years.

I have benefitted greatly over the last few years from the knowledge and expertise of other members of the group; those to whom I am particularly indebted for numerous enlightening scientific discussions include Tom Funkhouser, Fabian Glaser, Roman Laskowski, Tim Massingham, Richard Morris, Rafael Najmanovich, Irilenia Nobeli, Hannes Ponstingl and Hugh Shanahan. In addition, I thank the other members of the group for contributing to the social atmosphere and always being ready to go to coffee: notably Eric Blanc, Shiri Freilich, Abdullah Kahraman, Marialuisa Pellegrini-Calace, Eugene Schuster, Mike Stevens and (our own) James Watson.

The support of my friends has been invaluable throughout my Ph.D. Although I cannot thank them all here, I would especially like to mention the following people: Daniel Bassett, Rick Muir, Liam O'Flynn, Sam Weatherill and Ed Wood, for some truly momentous nights out; James Howarth and Annabelle Lewis, for regular games of tennis when weather allowed, and trips to the pub when it didn't; Ollie Redfern, for sharing the pain; Andy Pick, for persuading me to abandon common sense and buy the MR2; Ella Hinton, for being such a great and cheery housemate; and Alice Carr, Fred Goldberg, Sam Gray and Barney Jopson, for making my trip to Sri Lanka so memorable. Above all, my thanks go to Debora Lucarelli, for being there for me.

Finally, I wish to thank my parents, Helen and Ian. The importance to me of their love, understanding and support in every circumstance cannot be overstated. Mum and Dad, this is for you.

Contents

List of Figures

List of Tables

List of Algorithms

List of Source Code Listings

Chapter 1

Introduction

The binding of small molecules to proteins lies at the heart of almost all biological processes. Molecular recognition is a vital part of enzyme catalysis, signal transduction and DNA replication to name but three; without it, life could not be sustained. Viewed from a physical perspective, the specific binding of one molecule to another is the result of precise geometric and chemical complementarity between them.

Developing a coherent picture of the principles which underlie intermolecular interactions is therefore of central importance to unravelling the complexities of biological systems. One ultimate aim of computational biology - to be able to accurately model all aspects of a cell - can only be realised if we are able to predict, with atomic-scale precision, the ways in which molecules interact. Since the actions of drugs are determined by the same forces which govern natural protein-ligand interactions, deepening our understanding of molecular recognition may also lead to cheaper, more effective theraputic agents - and perhaps most importantly, fewer undesirable side-effects.

The way in which ligands bind to proteins has been an area of intense interest for many years, with recent innovations in computing technology, allied with increasing availability of biological data, having brought significant advances in our understanding of the subject. The problems of how to predict which ligands a given protein may bind, and the structure of the resulting complex, however, remain unsolved. Despite increasing levels of sophistication in the physical models used to represent protein-ligand interactions, it appears that they are insufficiently accurate to distinguish correct modes of binding from incorrect solutions. Therefore many studies take a more knowledge-based approach, using common patterns of binding observed in protein-ligand complexes to predict putative interactions with new, uncharacterised proteins.

This thesis does not set out to develop a predictive method, but rather to describe and quantify the degree of variation observed in the interactions between a given ligand and the proteins which bind it. The objective of this study is to provide information which can inform future development of predictive methods in this field.

This chapter addresses some questions fundamental to the analysis which follows: What biological roles do ligands play? What is our current understanding of the physical principles underlying molecular recognition? What is the nature of the available structural information on protein-ligand binding? What computational methods have previously been developed? At this stage, the connections between some of these topics are not explicitly spelled out, but will become apparent in later sections of the thesis. The chapter concludes with an outline of the remainder of the thesis.

1.1 Biological ligands

The word ligand derives from the Latin *ligare* (to bind). In chemistry, it usually refers to ions, atoms or functional groups which are covalently bonded to one or more partners. In biochemistry, however, the use of the word is somewhat broader, being applied to any molecule which interacts with a large macromolecule, the type of interaction being either covalent or non-covalent. As a consequence, the term 'ligand' in a biological context comprises an extremely diverse set of molecules, playing a wide range of biological roles.

1.1.1 Biological roles of ligands

1.1.1.1 Provision of energy

Energy is required by biological systems for three main purposes: the performance of mechanical work in muscle contraction and for other cellular movements, the active transport of molecules between cellular compartments, and to power enzymatic reactions involved in biosynthesis. This energy is obtained by chemotrophs through the metabolic breakdown of fuel molecules, and in phototrophs by harvesting free energy from light. In both types of organism, the energy is then stored in the form of chemical bonds. These bonds are made in molecules whose chemical structure is such as to make them convenient stores of energy: that is, which are stable in the absence of a catalyst, but which can be easily persuaded to release their latent energy when it is required.

Adenosine triphosphate (ATP) - see figure 1.2a - is the molecule which universally plays this energy storage role. Its ability to store and release energy derives from the fact that its triphosphate unit contains two phosphoanhydride bonds. These can be hydrolysed to produce ADP and pyrophosphate (P_i), while liberating energy. Although the triphosphate group is thermodynamically unstable - which is to say the free energy of hydrolysis is relatively high (Stryer (1995) cites a value of around 12 kJ mol^{-1} under physiological conditions) - it is *kinetically* stable, meaning that in the absence of a catalyst, ATP is only slowly hydrolysed.

The choice of ATP as the universal energy carrier can be rationalised in part by considering the following contributions to its free energy of hydrolysis:

- **Electrostatic repulsion**. At physiological pH, the triphosphate group is deprotonated, meaning that several negative charges are in close proximity. The electrostatic repulsion between them is relieved when ATP is hydrolysed.
- **Resonance**. The bonding electrons in pyrophosphate are highly delocalised, but less so when the moiety is bonded to ADP. Hydrolysis therefore causes an increase in entropy.
- **Strain**. ATP is often bound along with Mg^{2+}. The divalent coordination of the ion with two of the phosphate groups induces strain in the phosphodiester linkage, thus promoting hydrolysis (see figure 1.1).

There are, however, other biological compounds which possess a phosphodiester linkage to which these arguments would equally apply; why is ATP preferred? One reason that molecules such as phosphoenolpyruvate and creatine are not used as the universal energy carrier is that they actually have a higher phosphoryl potential than ATP, due in part to the ability of the dephosphorylated product to adopt

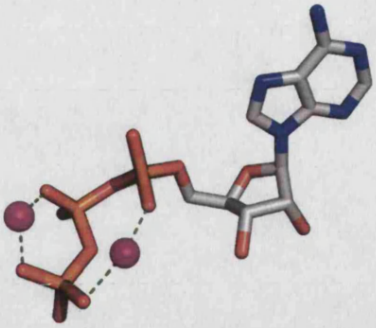

Figure 1.1: Magnesium coordination inducing strain in the ATP phosphate linkage
This ATP molecule is taken from PDB entry 1RDQ, a 1.26Å structure of cAMP-dependent protein kinase. Two magnesium ions are shown as magenta spheres. By coordinating the phosphate oxygens, these ions induce strain into the phosphodiester linkage, thus promoting the hydrolytic cleavage of the terminal phosphate group.

different tautomeric forms. The choice of a molecule with an intermediate phosphoryl potential therefore means that other species can be used as phosphoryl donors during its biosynthesis.

Why, though, is ATP used in preference to other molecules with similar phosphoryl potentials such as GTP or UTP? The reason is less clear, and may be simply due to a fairly arbitrary 'choice' which was made in early evolution.

1.1.1.2 Enabling enzyme catalysis

Ligands which promote enzymatic catalysis are usually termed 'cofactors'. Reviewing the available literature, however, the author was unable to find a single, agreed definition of the term 'cofactor'; the following is adopted as a working definition for the remainder of this thesis:

> *For enzyme-catalysed reactions, an entity other than the enzyme itself which is required for catalysis to occur, and which is not irreversibly changed during the reaction.*

Cofactors are utilised by proteins in order to provide functional groups which cannot be constructed from the repertoire of standard amino acids. Many cofactors are synthesised from vitamins, such as NAD (niacin), FAD (riboflavin / vitamin B_{12}), coenzyme A (pantothenic acid) and thiamine pyrophosphate (thiamine / vitamin B_1). They may be either covalently or non-covalently bound to the enzyme; see §1.2.1 for further discussion of this.

The definition of a cofactor given above deserves comment, since it is not without its problems. Specifically, we need to be careful about what we mean by 'not irreversibly changed during the reaction'. Consider the case of UDP-galactose-4-epimerase, which catalyses the reversible transformation of UDP-glucose to UDP-galactose. These two molecules are identical but for a reversal of the chirality of a single stereocentre. The reaction takes place in two stages: in the first, the 4′ alcohol group is doubly dehydrogenated to form a ketone, with one proton accepted by NAD^+ and one by a base. In the second step, these two protons are returned to the sugar, attaching them in such a way as to reverse the chirality around the C4′ stereocentre. The NAD molecule is thus left unchanged by the overall reaction, acting only as a temporary store of protons and electrons.

Compare this to the reaction catalysed by alcohol dehydrogenase:

$$\text{alcohol} + \text{NAD}^+ \rightleftharpoons \text{acetaldehyde} + \text{NADH} + \text{H}^+$$

After each cycle of this reaction, the cofactor is released from the enzyme in a reduced form, and therefore cannot be said to be unchanged. However, the NAD^+ may be regenerated by other pathways and returned to the enzyme for further enzymatic cycles to take place. Partly by convention, NAD is classified as a cofactor even in cases where the molecule *is* changed during the reaction.

The problem with making exceptions in this way is knowing where to stop. Do we, for example, classify ATP as a cofactor in cases where it is used an an energy source (and is therefore hydrolysed), but does not react directly with a substrate? Here, the ATP, leaving the enzyme as ADP and P_i, then being regenerated via other pathways, is acting similarly to NAD in alcohol dehydrogenase. Again, we fall back to convention, and designate ATP here, and in all reactions in which it is hydrolysed, as a substrate.
Another problematic example is that of coenzyme A. This molecule acts as a ubiquitous scaffold to which other moieties are attached for transportation between compartments, and between pathways. The reactions in which it participates therefore often modify the coenzyme by adding, removing or exchanging its molecular cargo. Nonetheless, it is not usually classified as a substrate.

Here, no distinction is made between the terms 'cofactor' and 'coenzyme'. Some definitions of the former include non-organic entities such as metal ions, reserving 'coenzyme' for organic cofactors. The author prefers not to describe metal ions as cofactors, and all cofactors mentioned here can be assumed to be organic molecules.

1.1.1.3 Signalling and regulation

In many situations, the binding of a ligand plays a communicatory role. This communication may occur between cells, between cellular compartments within a cell, or within a cellular compartment. In the latter case, the communication often forms part of a regulatory circuit.

Binding of Cyclic AMP (cAMP) to the regulatory domain of protein kinase A induces a conformational change which releases the catalytic domain, thus relieving inhibition and allowing it to phosphorylate its target proteins (Krebs, 1989). When GTP binds to G-proteins such as *ras*, its hydrolysis causes a conformational change which releases a catalytic unit which initiates the MAP kinase cascade (Bhattacharya *et al.*, 2004).

In many cases, the product of a given step within a reaction pathway inhibits the activity of an enzyme catalysing an earlier step. This type of feedback inhibition regulates the cellular quantity of the ultimate product of the pathway. An example of this is inhibition of aspartate transcarbamoylase by CTP. Binding of this nucleotide causes an allosteric shift in the hexameric enzyme, which in turn decreases the reaction velocity. Moreover, ATP competes with CTP for occupation of the regulatory sites, and acts as an activator of the enzyme. The overall effect is that the pathway is active when ATP is abundant, and hence energy is available for DNA replication, but when the level of CTP is high, the pathway is suppressed in order to

conserve resources (Hammes, 2002).

1.1.2 Common biological ligands

The major biological ligands may be roughly broken down into the following six classes:

1 Carbohydrates (*e.g.* glucose, fructose, mannose)

2 Peptides (*e.g.* MHC antigens, EGF)

3 Nucleotides and nucleotide derivatives (*e.g.* ATP, NAD, FAD)

4 Lipids (*e.g.* glycerol, phosphatidylcholine)

5 Metal ions (*e.g.* Mg^{2+}, Ca^{2+}, Zn^{2+})

6 Heterocyclic aromatic compounds (*e.g.* heme)

This thesis will be concerned with four ligands from the third class: ATP, GTP, NAD and FAD.

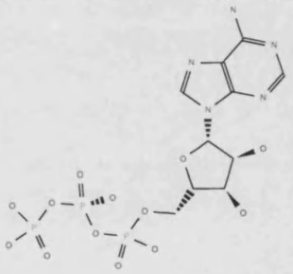

(a) Adenosine triphosphate (ATP)

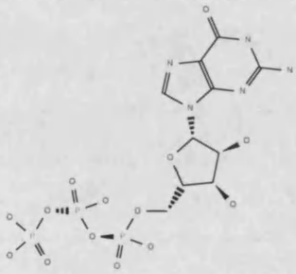

(b) Guanosine triphosphate (GTP)

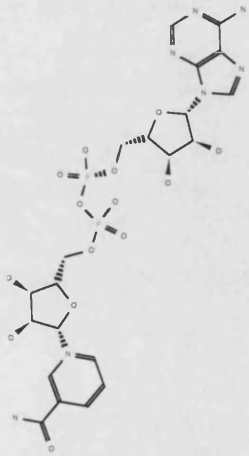

(c) Nicotinamide adenine dinucleotide (NAD)

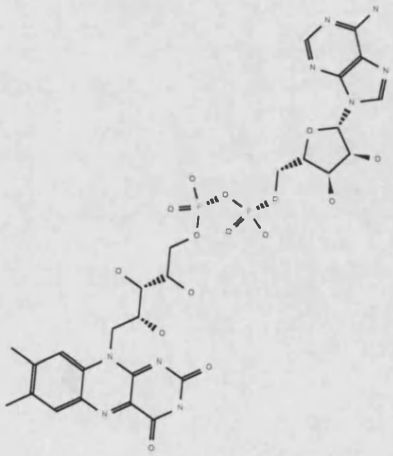

(d) Flavin adenine dinucleotide (FAD)

Figure 1.2: The four ligands chosen for detailed analysis

1.1.2.1 ATP

Adenosine triphosphate (figure 1.2a) consists of the nucleoside adenosine linked to three phosphate groups. The nucleoside is made up of two components: the adenine ring, and a ribose moiety.

The primary role of ATP, as mentioned previously, is as the universal currency of energy. As a result, it is extremely abundant in the cell, with a typical cytosolic concentration of around 3 mM. Resting adult humans turn over approximately half their body weight in ATP each day, and this rate may reach 0.5 kg min^{-1} during strenuous exercise (Stryer, 1995).

Mitchell (1961) proposed a mechanism for ATP generation which he termed the *chemiosmotic hypothesis*. This states that cellular respiration leads to a difference in hydrogen ion concentration (pH) across the mitochondrial membrane, and that the osmotic flux of these protons back out into the cytosol drives the synthesis of ATP. The photosynthesis which takes place in phototrophs leads to a similar proton gradient across the thylakoid membrane of the chloroplast, which can be used to generate ATP in the same way.

Protons are allowed to leave the mitochondrial lumen by passing through a membrane-bound protein called ATP synthase, which catalyses the addition of a phosphate group to ADP. Elucidation of the structure of this enzyme by Walker and colleagues showed that, in addition to its membrane-bound component (known as F_0), ATP synthase includes a large hexameric unit (F_1) which protrudes into the cytosol, and which is linked to F_0 by an extended asymmetric structure known as the γ subunit (Stock *et al.*, 1999). Three of the F_1 subunits contain sites which can bind either ADP or ATP. Proton flux through F_0 causes it to rotate in the membrane, and this in turn causes γ to rotate. Due to its asymmetric structure, rotation of γ compels the subunits of the F_1 component to undergo conformational changes which alter their relative binding affinities for the di- and triphosphate nucleotides. This in turn drives the production of ATP from ADP.

1.1.2.2 GTP

Guanosine triphosphate (figure 1.2b) is identical in structure to ATP, but with the adenine moiety replaced by a guanine group. Unlike adenine, its primary role is not usually to act as a source of energy. GTP often acts as a cellular messenger, for example when binding to G-proteins.

1.1.2.3 NAD

Nicotinamide adenine dinucleotide (NAD) , depicted in figure 1.2c, and the related molecule Nicotinamide adenine dinucleotide phosphate (NADP) are two of the most important cofactors in the cell for redox enzymes such as the lactate and malate dehydrogenases. NADP differs from NAD in that its 2′-hydroxyl group is esterified with a phosphate group.

NAD consists of the nucleosides of nicotinamide and adenine, joined at their C5′ positions by a diphosphate group. The nicotinamide ring is the reactive part of the molecule, due to its capacity to take part in redox reactions. Nicotinamide is structurally similar to nicotine, the addictive substance in tobacco products; the latter is known to compete with nicotinamide for binding sites in the enzymes needed for its absorption, thereby lowering the amounts of nicotinamide available to the cell.

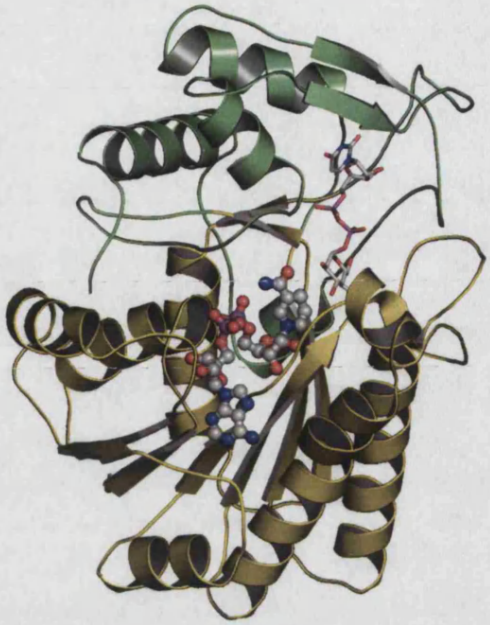

Figure 1.3: Proximity of nicotinamide ring to a substrate
The protein shown here is a UDP-galactose 4-epimerase mutant; PDB entry 1A9Y. The NAD molecule (ball and stick) is shown bound by a canonical Rossmann fold domain (yellow). The substrate (shown with sticks) is bound largely by the catalytic domain (green), which brings it into close proximity with the reactive nicotinamide ring; this is a typical arrangement in NAD(P)-dependent oxidoreductases.

Because their nicotinamide groups are positively charged, the oxidised forms of NAD and NADP are often written NAD^+ and $NADP^+$ respectively. Both cofactors can accept two electrons at a time, in the following reaction

$$NAD^+ + H^+ + 2e^- \rightleftharpoons NADH$$

They may therefore act as oxidising agents in reactions such as the following, in which a secondary alcohol is oxidised to form a ketone

$$NAD^+ + R{-}CHOH{-}R' \rightleftharpoons NADH + R{-}CO{-}R' + H^+$$

The oxidised and reduced forms of nicotinamide are shown in figures 1.4a and 1.4b.

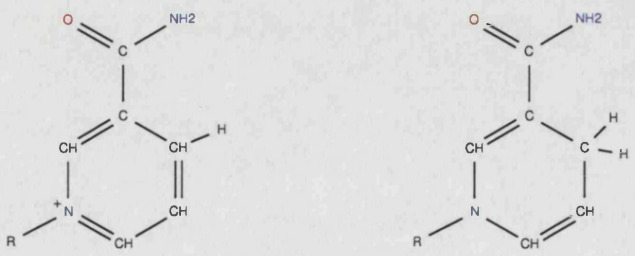

(a) Oxidised form (NAD^+) (b) Reduced form (NADH)

Figure 1.4: The oxidised and reduced forms of nicotinamide

NAD^+ is the major electron acceptor in the oxidation of fuel molecules, which occurs in glycolysis and the

citric acid cycle of cellular respiration. NADP is used almost exclusively for reductive biosynthesis, such as in fatty acid synthesis, and also appears as a reducing agent in the later Calvin cycle of photosynthesis. Like ATP, the reduced forms of NAD and NADP are quite stable in the absence of a catalyst.

1.1.2.4 FAD

Although it is the most common and best-known hydrogen acceptor, nicotinamide is not the only functional group which plays this role - other moieties frequently involved in redox chemistry include the flavin and quinone groups. Approximately 90% of cellular flavin is in the form of Flavin adenine dinucleotide (FAD) (figure 1.2d), in which it is conjugated with an adenine diphosphate moiety. Another relatively common flavin-containing compound is Flavin mononucleotide (FMN) , which is simply a phosphorylated form of flavin. It should be mentioned that neither FAD nor FMN are actually nucleotides, despite their names, since in both cases, the alloxazine ring is bound not to a sugar residue but to an alcohol (ribitol) instead.

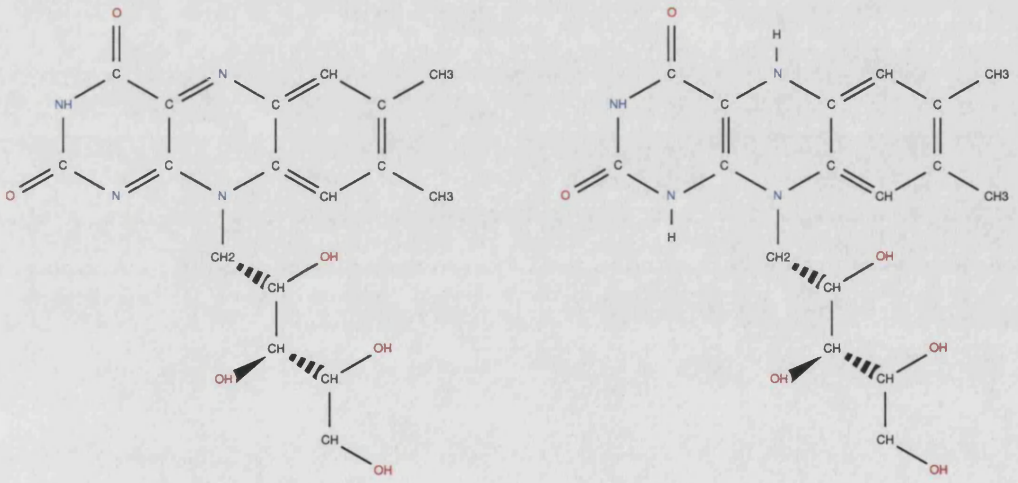

(a) Oxidised form (FAD) (b) Reduced form ($FADH_2$)

Figure 1.5: The oxidised and reduced forms of riboflavin

Like NAD, FAD can also accept 2 electrons. Unlike NAD, it also takes up a proton as well as a hydride ion, as shown in the following reaction

$$\underset{\text{oxidised - yellow}}{\text{FAD}} \overset{+H^+ + e^-}{\rightleftharpoons} \underset{\text{semiquinone - blue}}{\text{FADH}} \overset{+H^+ + e^-}{\rightleftharpoons} \underset{\text{reduced - colourless}}{\text{FADH}_2}$$

The oxidised form of flavin (figure 1.5a) is associated with a vivid yellow colour, which accounts for its name (derived from the Latin *flavus* for yellow). Upon reduction (figure 1.5b), resonance effects in the flavin group are lost, causing the colour to disappear. This loss of resonance means that the redox potential of flavin-containing compounds is affected by factors which stabilise the reduced form. A structural consequence of flavin reduction is that the planarity of the oxidised form tends to be lost (see figure 1.6).

FAD appears as an oxidising agent in a number diverse biological contexts including DNA repair (in the photolyase protein (Weber, 2005)) and control of folding (in oxidoreductin, found in the endoplasmic reticulum). The fact that flavin is a stronger oxidising agent than nicotinamide makes it suitable for its

(a) (b)

Figure 1.6: "Butterfly bending" in the isoalloxine ring
The coordinates of the isoalloxine ring taken from two FAD molecules are shown. (a) The straight form of isoalloxine, from PDB entry 1N62 (carbon monoxide dehydrogenase at 1.09Å). (b) A butterfly form of the isoalloxine group, as observed in PDB entry 1CL0 (thiodoxin reductase at 2.50Å), in which it is in the reduced form. The degree of flavin bending observed in this structure (34° relative to the oxidised form) was found to be the largest in the PDB (Lennon *et al.*, 1999).

role in the electron transport chain, in which FMN mediates electron transfer between carriers that transfer two electrons (*e.g.* NADH) and carriers that can only accept single electrons, such as Fe^{III}.

Common enzymes which utilise FAD as a cofactor include D-amino acid oxidase, glucose oxidase, and xanthine oxidase. FMN is the cofactor for NADH dehydrogenase, an example which illustrates the high oxidative potential of flavin compared to nicotinamide.

1.1.2.5 The ubiquity of the adenosine phosphate scaffold

It is apparent that adenosine phosphate units form a key part of the biochemical repertoire. It has been proposed that their ubiquity may hark back to the ancient origins of life, in which, in addition to their current role as carriers of genetic information, the nucleic acids were also used as catalysts. Prior to the emergence of proteins, RNA enzymes (also known as ribozymes) may have been the dominant type of biocatalyst in primordial life. As stated above, cofactors, and in particular their respective reactive groups, are recruited by enzymes to perform functions which cannot be fulfilled using polypeptides alone. If this recruitment originally occurred before the advent of proteins, it is not surprising that the scaffolds to which many reactive functional groups are attached would be derived from nucleotides.

1.2 Principles of molecular recognition

1.2.1 Covalent versus non-covalent binding of ligands

The interactions between proteins and ligands may be either covalent or non-covalent in nature. This thesis is concerned only with non-covalent interactions, which may be either permanent or transient. If a ligand is permanently bound to a protein, it is sometimes referred to as a 'prosthetic group'; the term 'tightly bound' typically refers to a non-covalently bound prosthetic group.

Heme molecules are the most common prosthetic groups, and may be either covalently bound, as in the c-type cytochromes (Barker and Ferguson, 1999), or non-covalently bound, as in hemoglobin. In the case of cytochrome c, the heme molecule is also a cofactor, since the oxidation state of its iron atom changes as it accepts and releases electrons. Another example of a cofactor which is also a prosthetic group is the

FAD molecule in glutathione reductase, which is irreversibly bound and largely buried. As discussed in the previous section, however, not all cofactors are prosthetic groups - those which leave their enzymes to undergo a 'recycling' step between catalytic cycles are clearly not irreversibly bound.

Regulatory molecules and substrates interact only transiently with their protein partners. The catalytic constant, or turnover number (k_{cat}) for enzymes varies over the range $10^3 - 10^7$ s^{-1}, meaning that for the most efficient enzymes such as catalases, each substrate molecule interacts with the protein for less than 1μs on average (Fersht, 1999). At the other end of the spectrum, the rate of intrinsic GTPase hydrolysis by the G-protein *ras* is approximately 1 hr^{-1}. This rate is significantly increased by the binding of GTPase-activating proteins (GAPs) which therefore promote the inactivation of the G-protein.

The nature of ligand binding has several implications which should be borne in mind when looking at the structure of ligand-protein complexes determined by crystallography. Where a ligand is non-covalently bound to a protein, it is normally secured by several hydrogen-bonding or electrostatic interactions. Since the strength of a covalent bond is roughly ten times that of a hydrogen bond (Jeffrey and Saenger, 1991), covalent attachment of a ligand obviates the need for so many non-covalent interactions.

Another consideration is the temporal relationship of ligand binding to protein folding. In several cases, cofactors have been shown to interact with unfolded polypeptides *in vitro*. By forming specific interactions with parts of the denatured chain, some cofactors can dramatically reduce the entropy of the unfolded state, and therefore speed up the conformational search for the native fold (Higgins *et al.*, 2005). Despite their supposed role in accelerating protein folding, however, not all tightly-bound cofactors are strictly *required* for stabilising the folded protein. In the case of flavoproteins[1], for example, a variety of techniques are available for extracting the flavin-containing cofactor, and then restoring the apoprotein to its native state (Hefti *et al.*, 2003).

The distinction between early and late binding of cofactors is an important one to bear in mind, since the structural rearrangements which can take place during folding imply that the interactions we see in a co-crystallised structure of an early-binding molecule may not necessarily be those which facilitated its initial recognition. Equally, however, extensive side-chain rearrangements are known to occur when ligands bind to fully-folded proteins (Najmanovich *et al.*, 2000). To an extent, therefore, the caveat that experimental observation may not accurately represent the complete biological picture applies to all studies of molecular recognition carried out using X-ray crystallography.

1.2.2 Contributions to the free energy of binding

The non-covalent binding of a protein to a ligand encompasses a range of processes, including the desolvation of parts of the two molecules, conformational rearrangements and the establishment of a variety of different interactions. This section discusses these changes, considering the contribution of each to the binding affinity of the complex.

[1] *i.e.* those which rely on an FAD or FMN cofactor

1.2.2.1 Electrostatic interactions

Types of electrostatic interactions implicated in molecular recognition include salt bridges, hydrogen bonds, dipole-dipole interactions and the interaction with metal ions. Of these, hydrogen bonds are generally recognised to be one of the most important factors. Hydrogen bonds result from an electrostatic attraction between a hydrogen atom bonded to an electronegative atom (such as oxygen or nitrogen), and a lone pair or π-electron system. The electron-withdrawing effect of the hydrogen atom causes the proton of the hydrogen to be de-shielded, thus exposing its positive charge.

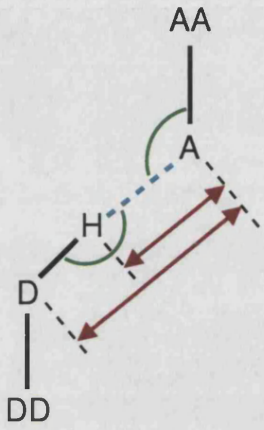

Figure 1.7: Hydrogen bond geometry
The critical distances |HA| and |DA|, and angles $\angle$H A AA and $\angle$D H A are shown. Thresholds applied to these measurements are used to determine whether a given interaction constitutes a valid hydrogen bond.

Establishing a hydrogen bond requires that the geometry of the hydrogen-bonded atoms and their covalent partners obeys fairly strict rules. By analysing hydrogen-bonding interactions in high-resolution protein structures, Baker and Hubbard (1984) stated these as follows (refer to figure 1.7 for the definition of the atoms involved):

- $|\mathrm{HA}| \leq 2.5$ Å
- $|\mathrm{DA}| \leq 3.9$ Å
- $\angle \mathrm{H\,A\,AA} \geq 90\,^{\circ}$
- $\angle \mathrm{D\,H\,A} \sim 180\,^{\circ}$

These criteria mean that hydrogen bonds are strongly directional, and that consequently, establishing a strong hydrogen bonding network between two molecules depends upon their precise orientation relative to one another.

The strength of a hydrogen bond is strongly affected by its environment: the extent to which the two opposing charges are shielded depends on the local dielectric constant. Proximity to polar groups results in an increase in the dielectric constant and therefore a decrease in hydrogen bond strength. This means that hydrogen bonds which are buried within the protein - or in the interface between a protein and its ligand - tend to be stronger than those which occur in solvent-exposed regions.

1.2.2.2 Hydrophobic interactions

When a ligand binds to a protein, some parts of both molecules must be desolvated. This involves rupturing hydrogen bonds between each molecule and the bulk solvent, followed by a reorganisation of water molecules at the interface. The enthalpic cost of breaking protein-solvent and ligand-solvent hydrogen bonds is compensated for by the water molecules which previously formed solvation shells around the two molecules adopting a more structured, clathrate-like arrangement, in which the total number of hydrogen bonds is reduced, but the strength of individual bonds becomes greate , thus yielding an entropic benefit.

This description of desolvation highlights the two main energetic components of the so-called "hydrophobic effect", which describes the unfavourability of exposing a non-polar molecular surface to water. During ligand binding, the hydrophobic effect resulting from unfolding the solvated ligand molecule, and from exclusion of water from the binding pocket, is compensated for by the hydrophobic portions of the two molecules coming into contact with one another. This 'hydrophobic collapse' is thought to be one of the driving forces behind the 'induced fit' which is observed upon ligand binding, and is due to the same physical principles which compel the rapid condensation of the core of many proteins during folding.

Another important type of non-polar interaction is Van der Waals attraction. When atoms are separated by more than a few angstroms, they experience a weak mutual attractive force known as *Van der Waals attraction*[2]. This force originates from the instantaneous dipoles which are set up in each individual atom as a result of the mobility of the electrons which surround their nuclei. When atoms approach one another, the instantaneous dipole in one of them induces a polarity in the other, such that the parts of the two atoms which are juxtaposed have temporary opposite charges. As long as the two atoms remain in proximity, electronic fluctuations in the electron shell of one atom causes corresponding charge redistribution in the other, thus maintaining the attraction. The strength of this attractive force varies with the size of the atoms involved, but is several orders of magnitude less than that of a covalent bond. An example from nature illustrates that Van der Waals interactions can nonetheless be a significant force: remarkably, the unique ability of geckos to cling to smooth surfaces is attributed solely to Van der Waals interactions, rather than to any special chemical properties of the surfaces of their toes (Autumn *et al.*, 2002). Van der Waals attraction between two molecules is related to the degree to which their surfaces have complementary shapes. Shape complementarity is therefore thought to be an important factor in protein-ligand recognition.

1.2.2.3 Conformational restriction

Upon binding, a protein and a ligand each lose three degrees of translational freedom and three degrees of rotational freedom relative to one another. In addition, the rotable bonds in the ligand and in the residues which comprise the binding site are, to some extent, restrained. This entropic cost can in some cases be mitigated against by pre-organisation of the ligand molecule while still in solution.

[2]Van der Waals attraction is also sometimes referred to as the "London force", or as "dispersion forces".

1.3 Structural characterisation of biomolecules

1.3.1 The Protein Data Bank

Since its inception in 1971, the Protein Data Bank (PDB) (Berman *et al.*, 2000) has been the primary worldwide resource for the deposition of biological macromolecular structures[3]. Initially conceived as a warehouse for X-ray crystal structures, the PDB today also holds structures determined by Nuclear Magnetic Resonance (NMR) and cryoelectron microscopy. Prior to July 2002, theoretical models were also permitted to be deposited; this has now been disallowed.

Figure 1.8 illustrates the rate of growth in the size of the PDB. For the first 15 years of its existence, the PDB received less than 100 structures per year, reflecting the time-consuming nature of protein crystallography at that time. Since then, a number of factors have contributed to a significant rise in the rate of PDB deposits. The advent of NMR has meant that the structures of molecules which are not amenable to crystallisation can be determined. Today, NMR structures constitute approximately 15% of the total PDB, as shown in figure 1.9a. Crystallographic methods have seen advances such as Multiple wavelength Anomalous Dispersion (MAD) (Walsh *et al.*, 1999) and Molecular Replacement (MR) (Rossmann, 1990), which allow rapid calculation of initial phases from the raw diffraction data. Cryo-techniques have been developed to reduce radiation damage to crystals caused by the X-ray beam (Garman, 1999), allowing higher-intensity light sources to be deployed. More recently, work on automatically building models into electron density maps has progressed to the extent that, given good data sets, models can be generated entirely without human intervention (Perrakis *et al.*, 1997, Levitt, 2001, Terwilliger, 2000). All of these innovations have had an impact on the speed of the structure determination process.

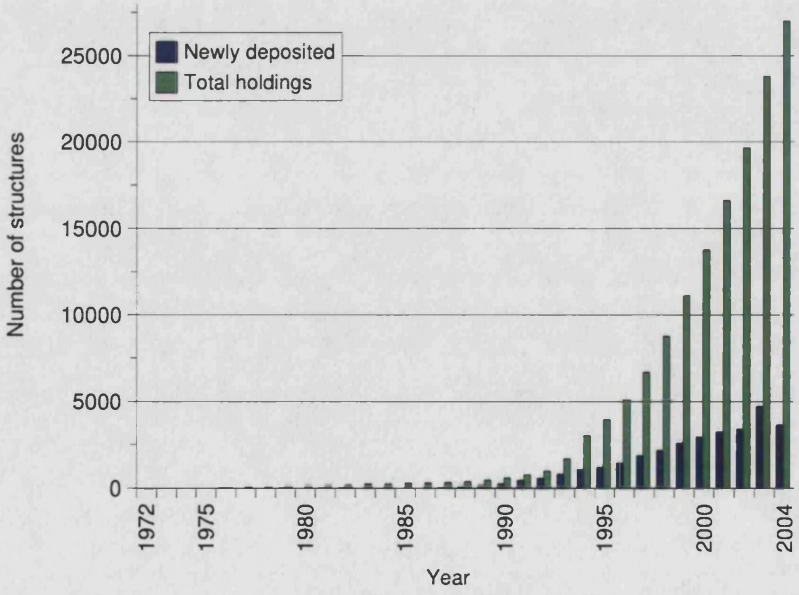

Figure 1.8: Growth in PDB holdings
Data taken from the Research Collaboratory in Structural Bioinformatics (RCSB) website (http://www.rcsb.org).

[3]For a good introduction to the principles of protein structure, the reader is referred to Creighton (1993).

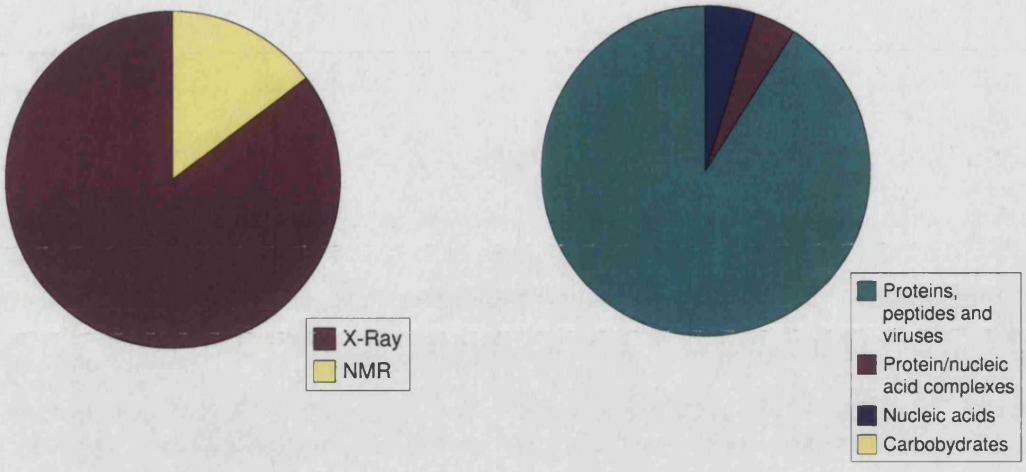

(a) Experimental method (b) Type of complex

Figure 1.9: Types of PDB entry
Distribution of PDB entries, as of October 2004.

Post-processing of PDB data

The PDB remains the primary warehouse for protein structure data. Processed versions of same data, derived from the PDB by application of various algorithms, are available from a number of external sources. The most important of these are described briefly below, as are the post-processing steps carried out by the curators of the PDB itself.

The Protein Quaternary Structure server

The coordinates deposited in the PDB as a result of an X-ray crystallography experiment are those of the *asymmetric unit* (ASU) of the crystal - that is, that fraction of the crystal which contains no internal symmetry, and from which the structure of the entire crystal can be regenerated by the application of crystallographic symmetry operations. While, for some small proteins, these coordinates may correspond to the biologically active form of the molecule, for many larger oligomers, the ASU contains only one or a few of the subunits which make up the complete protein. In other cases, conformational changes undergone by a subset of the proteins in the crystal may result in the ASU containing multiple copies of the macromolecule. Henrick and Thornton (1998) devised an automatic method for determining which of these scenarios is most likely, given the ASU coordinates. The algorithm uses an empirically-determined set of rules based on consideration of the accessible surface area, number of inter-chain salt bridges and disulphide bonds and calculated solvation free energy of folding, for every possible quaternary structure which can be constructed from the original coordinates. Where the program predicts that the ASU represents only a part of a larger assembly, it proceeds to calculate the coordinates of the complete molecule. The resulting predictions and coordinates are available via web- and FTP servers.

The PDB Uniformity project

During its thirty-year lifetime, the PDB has gradually evolved. As the types of data stored in the archive have changed, so the conventions needed to represent this information have been modified. In the early years of

the PDB, this did not present a significant problem since the archive served primarily as a repository from which information was manually retrieved and inspected, and therefore small inconsistencies in the format of the data could be accepted. Lately, however, the PDB is increasingly used as the primary data source for automated, computational batch processing, and thus any lack of uniformity requires, at best, extra effort on the part of the software developers, and at worst, the introduction of heuristics which may be of questionable scientific validity.

In order to solve these problems, the RCSB has recently undertaken a data normalisation project, aimed at identifying inconsistencies in four key types of information - sequence representation, sequence/coordinate mismatches, atom nomenclature and stereochemical labelling (Westbrook *et al.*, 2002). Newly deposited structures are subjected to an automated checking procedure, with potential errors flagged and resolved in partnership with the depositors. Legacy files have been automatically processed, with the 'cleaned' versions of each structure available alongside the original deposition.

The Macromolecular Structure Database

The Macromolecular Structure Database (MSD) (Velankar *et al.*, 2005) is a relational database which stores a range of information about protein and nucleic acid structures, in an integrated and normalised fashion. The primary source of the data stored in the MSD is the PDB, but this data is heavily processed before entry into the relational database. In particular, it is built using a philosophy of 'reference entities'. Each individual ATP molecule in the database is considered to be an instance of an 'idealised' ATP molecule, for example, and is therefore checked to ensure that its complement of atoms, bonds and chiral centres is in agreement with a previously defined reference entry for the ATP compound. The same checks are applied to all chemical entities, thus guaranteeing that the information retrieved when searching the database is internally consistent in terms of its chemical nomenclature.

Another important aspect of data representation in the MSD is that quaternary structure predictions for each entry are stored in the database. As such, the core of the MSD may be thought of as a combination of the normalised PDB data and the information previously dispensed by the PQS. Added to this information is a rich web of links to external databases such as CATH, SCOP, SWISS-PROT and ENZYME, making the MSD a truly integrated resource for information on many aspects of proteins and their structures.

1.3.2 The Cambridge Structural Database

The Cambridge Structural Database (CSD) Allen (2002) is a repository for structures, determined by X-ray crystallography, of small-molecule compounds. The resolution of these structures tends to be considerably higher than those deposited in the PDB, and as such, they have been frequently used in the past as a source of high-quality data on molecular interaction geometries. From the point of view of this study, however, the CSD is not particularly useful, since it does not contain any information on protein-ligand interactions.

1.3.3 Structural genomics

In addition to the technological changes outlined above, the past five years have also seen changes in the approach to structure determination. Until recently, structures tended to be solved by researchers who had a particular interest in the protein concerned, and had therefore expended considerable time and effort to characterise it biochemically. The individual focus was therefore on obtaining insight into the function of particular proteins, by solving their structures. Viewed from a global perspective, however, this has meant that the choice of which proteins to solve has largely been an *ad hoc* one, based on the intrinsic value of each particular structure, rather than on its contribution to our understanding of protein structure, function and evolution on a more general level. Increasingly, researchers from a number of fields have come to the view that obtaining a more uniform sampling of 'protein structure space' would yield many benefits.

Perhaps the most obvious potential benefit of a more systematic approach to structure determination would be an increased understanding of protein evolution. Given that molecular evolution at the sequence level is generally considered to be fairly well understood, the ability to relate changes in protein sequence to modifications of the resulting structure will further illuminate the selective pressures which have caused the evolutionary changes which we can observe today. This endeavour would be greatly assisted by a more rational choice of protein targets.

On a more pragmatic note, having access to the structure of a relatively close neighbour of any protein one may choose, would allow the structure of the new protein to be modelled to reasonable accuracy. In the pharmaceutical industry, there is currently great interest in the feasibility of applying rational drug design to modelled structures; a more uniform coverage of protein space would allow this idea to be explored more thoroughly.

These considerations have led to the initiation of a worldwide program of systematic structure determination, known as Structural Genomics (Burley, 2000). The overall aim of this initiative is to determine the structure of at least one representative protein from each family. In order to achieve this, crystallographers and NMR spectroscopists are altering the way they work, effectively postponing traditional analyses in favour of a high-throughput mode of structure solution.

1.3.4 Structure quality

When assessing the quality of protein structures, one measure which is often used for structures resulting from X-ray crystallography experiments is the resolution. The resolution of a crystallographic structure is determined by the extent of the reflection data which can be collected during the structure determination. The 2-dimensional diffraction pattern which results from the experiment shows concentric rings of scattering peaks, each of which corresponds to a different interplanar distance in the real lattice. The resolution which is quoted is the interplanar spacing for the outermost scattering ring for which data can be reliably collected. It is directly related to the optical definition of resolution - that is, the minimum distance by which two objects may be separated, and may still be visible as two separate objects. The uncertainty in the position of an atom depends both on the resolution of the structure, and the R-factor; on average, the uncertainty in each atomic coordinate in a high-quality structure (R-factor of 0.2 or less) is roughly one fifth to one tenth of the

resolution (Rhodes, 2000). The distribution of reported resolution values for PDB structures determined by X-ray crystallography is shown in figure 1.10.

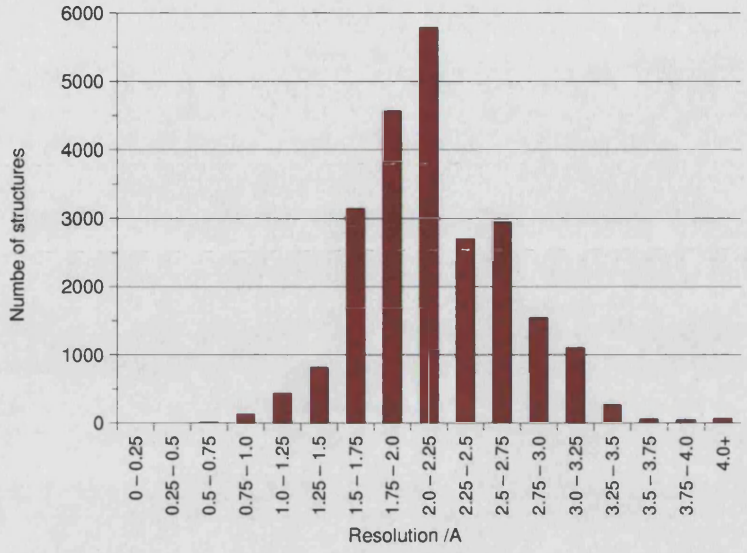

Figure 1.10: Resolution of deposited X-ray structures
This graph shows the distribution of the resolution of PDB entries which were solved by X-ray crystallography, as of October 2004.

Crystals for which data extended beyond about 1.2Å can yield structures in which some of the hydrogen positions can be determined based on the X-ray data alone. Where the resolution is poorer than this, their positions cannot be directly observed; this means that the chemical identity of the terminal side-chain atoms is uncertain for aspartic acid, glutamine and threonine residues, and must be inferred from the protein environment of the side chain. Similarly, the orientation of the imidazole ring of histidine residues cannot be unambiguously determined. These uncertainties can lead to errors in crystal structures, the possibility of which cannot be discounted during studies which depend on precise determination of protein geometry at the atomic level. In recent years, the number of crystal structures being determined to very high-resolution has increased, largely due to the advent of synchotrons which offer very high-intensity light sources.

1.3.5 Non-cognate ligands

Analogues of cognate ligands are routinely used when performing biochemical characterisation of proteins, or when determining their structures. Compounds whose overall structure is similar to a natural ligand, but which are inert, are valuable in obtaining a 'snapshot' of a reaction, halted at a particular step. For example, the ATP analogue ATPγS, in which one oxygen atom on the terminal phosphate group has been replaced by a sulphur atom, hydrolyses much more slowly than the natural ligand. Another example of a substrate analogue which has been used in crystallisation experiments is methotrexate, a folic acid mimic. This binds to dihydrofolate reductase, an enzyme which catalyses the production of an intermediate in the biosynthesis of amino acids and purine nucleotides.

Sometimes, the ligand present in a crystal structure may not even be an analogue of the natural substrate. During crystallisation experiments, many different small molecules are routinely screened to determine

whether any of them encourages the formation of crystals. Some of the ligands thus discovered are only 'structural ligands' - that is, molecules whose binding stabilises the crystal lattice, but which are not thought to be of functional importance to the protein being crystallised.

It is therefore important when analysing protein-ligand interactions obtained from the PDB, to attempt to determine whether the observed complex is likely to be cognate: that is, whether the ligand used in the structure determination experiment is the true biological partner for that protein. Achieving this reliably in an automated manner is challenging, although efforts are currently underway to compile a database of cognate ligands associated with certain proteins (I. Nobeli, personal communication). The work described in this thesis focusses on analysis of interactions between proteins and fairly ubiquitous biological ligands. Therefore in most cases discussed here, we can be fairly confident that the interactions observed are likely to be biologically relevant.

1.3.6 Chemical compound datasets

When working with crystallographic structures of ligands, access to a reference set of chemical compounds can often be of use. Given any chemical compound, we may think of it in terms of several distinct 'levels of abstraction'. The most fundamental of these is a single, *idealised* representation of the molecule. This corresponds to the diagram of the molecule which a chemist may draw. In other words, the idealised representation contains information about the atoms and bonds which make up the molecule - including the atomic number of each atom, the location of any formal charges, and the location and handedness of any chiral stereocentres which may be present. In addition, this representation should contain information about the connectivity of the molecule, including the order of each chemical bond. Additional annotation such as the presence of delocalised or aromatic systems may also be included.

At the other end of the spectrum, we may think of a particular, real *instance* of the molecule, existing in a physical environment. In order to describe such an instance, we should specify additional information such as three-dimensional coordinates of each of its atoms and the distribution of electron density across the volume occupied by the molecule. Of course even this enriched description of the molecule falls short of what would be considered a realistic representation in terms of quantum physics.

The representations of molecular species whose structure has been determined by crystallographic or spectroscopic methods lie at a point intermediate between these two extremes. An X-ray model is a static snapshot of what in reality is a dynamic system; therefore information about molecular motion is to a large extent lost during the structure determination process. Indirectly, the evidence of motion can still be seen in disorded regions, which manifest themselves as blurring of the corresponding electron density. NMR experiments on the other hand yield not one but an ensemble of valid structural solutions. Here, mobile parts of the molecule appear in different conformations among different members of the ensemble.

Given a set of atomic coordinates obtained from X-ray crystallography, building a model into it requires that the chemical identity of the molecule(s) present be identified. This procedure is performed prior to deposition of a structure in the PDB, with the assigned identities being recorded in the PDB residue name fields. For small molecules, however, this assignment is sometimes done inconsistently; therefore it is

desirable to be able to verify the chemical identity of the molecule automatically. Given only the atomic coordinates of a molecule in this frozen state, each labelled with the corresponding chemical element, it is possible to deduce the connectivity of the molecule by reference to a table of standard covalent radii. The resulting topological representation of the molecule is amenable to comparison against a reference dictionary of chemical compounds using graph theoretic methods (see appendix A).

Any number of reference sets of chemical compounds are available, ranging from catalogues of available reagents, through metabolite dictionaries (*e.g.* KEGG COMPOUND, http://www.genome.jp/ligand; ChEBI, http://www.ebi.ac.uk/chebi), to databases of xenobiotic compounds, for example drug molecules (*e.g.* the National Cancer Institute's drug dictionary, http://www.nci.nih.gov). The reference set of chemical compounds used in this work was taken from the MSD, which contains a comprehensive record for each chemical entity found in the PDB. This record contains, along with other data, all the information required for the validation procedure, including *in vacuo* energy-minimised coordinates generated using the CORINA program, which is distributed as part of the CACTVS tool set (Ihlenfeldt *et al.*, 1994).

1.4 Protein structure and evolution

The process of evolution is driven by natural selection acting on variation. Within a population of organisms, those which are best adapted to their environment and circumstances stand a better chance of survival than their peers. Molecular biology has shown us that the source of variations at the level of the organism can be traced to microscopic changes in the molecules which constitute them, which are derived from mutations in the molecules which carry their genetic information. Where mutations occur in the coding regions of genes, they may cause corresponding changes in the proteins encoded by those genes. This change in a protein's primary sequence can, in turn, affect its structure, and hence impact upon the function which it plays within the organism. The cumulative effect of many such changes, occurring over vast timespans, eventually leads to the evolution of proteins with entirely novel structures and functions. This expansion of the protein repertoire is thought to be ultimately responsible for most, if not all of the evolutionary diversity which we see in the living things that surround us.

Proteins which have descended from a common ancestral protein are said to be *homologous*, and may retain similarities in terms of sequence, structure and function. As mutations are accumulated by a protein, these similarities become increasingly hard to detect. It is generally accepted that, in more distant proteins, structure is more conserved than sequence (Chothia, 1984). As a result, while comparison of protein sequences can reveal fairly close evolutionary relationships, taking into account structural information allows the identification of more distant relatives. Specifically, the gross arrangement of secondary structures in a protein - the fold - appears to be particularly well conserved, and therefore proteins with similar folds are often evolutionarily related. Care must be taken in equating structural similarity with evolutionary relatedness, however, since unrelated proteins may converge to a similar fold for functional or physico-chemical reasons.

An examination of pairs of homologous proteins from SCOP showed that some had quite different functions - either two different enzymatic functions, as determined by the enzyme classification (EC) number (IUPAC-

IUB, 1983) - or one enzyme and one non-enzyme (Hegyi and Gerstein, 1999). Russell *et al.* (1998) showed, in a comprehensive analysis of the location of binding sites within structurally superposed SCOP superfamily members, that in approximately 10% of cases, the location was not conserved, suggesting a complete change in function. A comparison of pairs of SCOP domains in conjunction with their EC numbers, (or against FlyBase annotations, in the case of non-enzymes), suggested that precise function is usually only conserved when the sequence identity is above a 40% threshold (Wilson *et al.*, 2000).

Functional congruity between proteins often appears to indicate a common ancestor, but this too can be misleading. A well-known example is the evolution of so-called 'antifreeze proteins' by fish living in very cold waters. These proteins, which prevent the growth of ice crystals in the fishes' bloodstreams, are found in fish indigenous to both the north and south poles. The simplest explanation initially appeared to be that both groups of species inherited the gene for these proteins from a common ancestor prior to their geographical dispersion. In fact, genome analyses have shown that the two populations split long before they developed the antifreeze protein (Chen *et al.*, 1997). This 'reinvention of the wheel' by nature is known as *convergent evolution*, and has been demonstrated several times in diverse systems.

Because of these phenomena, a combination of structural *and* functional likeness is usually taken to be necessary for robust identification of relatedness between proteins whose sequences have diverged beyond detectable levels of similarity. A number of algorithms are now available for the automatic detection of structural similarity between proteins (*e.g.* SSAP (Orengo and Taylor, 1996), DALI (Holm and Sander, 1995), VAST (Madej *et al.*, 1995) and CE (Shindyalov and Bourne, 1998)).

Protein domains and structure classification

Many large proteins can be separated into a number of (semi-)independent units known as domains. There is no single, universally-agreed definition of exactly what constitutes a domain. Biochemists may define a domain as a functional unit of a protein, mediating a certain aspect of a protein's role (*e.g.* "the ligand-binding domain"). Those with a more structural bent tend to talk about domains as being "independent folding units", possessing their own hydrophobic core, and hence often being more amenable to protein crystallography in cases where the structural complexity of a large protein poses experimental difficulties. Those whose focus is more towards the evolutionary aspects of proteins prefer to describe domains as "units of evolution", pointing towards the tendency of new protein functions to be generated not by incremental point mutation, but often by recombination of large 'blocks' of sequence at a time (Patthy, 1991, Baron *et al.*, 1991, Sonnhammer and Kahn, 1994).

In fact, domains often appear to be all of these things at the same time. Any apparent conflict in the definitions given above is due to the intimate inter-relationship of protein sequence, structure and function. Because of the significance of protein domains in evolution, proteins are often compared at the individual domain - rather than whole polypeptide chain - level. Several databases of domains, defined either in terms of their sequence or structure, are available. Here, the focus is on protein structure, and therefore the two pre-eminent structure-based databases of protein domains, CATH (Pearl *et al.*, 2005) and SCOP (Murzin *et al.*, 1995, Andreeva *et al.*, 2004), will be described.

Both CATH and SCOP are hierarchical classifications of protein domains, in which the higher levels separate domains with gross, immediately-recognisable differences in structure (see table 1.1). Moving down through more subtle distinctions, the lower levels contain domains whose structures are practically identical, but which are separated into groups on the basis of sequence identity. Although superficially similar, the two databases have some significant differences, both in terms of the definitions of the various levels in the hierarchy and in the methods used to construct it; commonalities between the two will be covered first, before describing each one separately.

The most basic discriminating feature between protein structures is the type and sequential arrangement of secondary structures which they contain. 98% of protein structures can be separated into four distinct groups: those consisting mainly of α-helices, those made up of β-sheets, those in which helices and sheets alternate (α/β), and those consisting of α and β units which are essentially separate (α+β) (Levitt and Chothia, 1976). The initial levels of CATH and SCOP consist of a separation of domains along roughly these lines. Lower levels cluster domains according to the relative spatial arrangement and/or connection of these secondary structure elements, or in other words, the fold of the domain. Common folds include the Rossmann fold, the immunoglobulin fold and the TIM barrel (see *e.g.* Creighton, 1993).

The number of folds is thought to be significantly fewer than the number of protein families, with recent estimates of the total number of folds in nature ranging between 1,000 and 5,000 (Chothia, 1992, Brenner *et al.*, 1997). As such, each node at the fold level of the hierarchy may contain homologous domains. Alternatively, domains adopting the same fold may be *analagous* - that is, having converged to a similar structure from distinct origins. Below the fold level, domains are clustered into *superfamilies*, within which the criteria described above have been met, suggesting a common evolutionary ancestor. Large superfamilies include the P-loop nucleotide triphosphate hydrolases, the globins and the trypsin-like serine proteases.

Description	CATH level	SCOP level
Overall composition of types of secondary structure.	Class	Class
Gross arrangement of secondary structure elements independent of their connectivity.	Architecture	†
Topological connection of secondary structure elements.	Topology	Fold
Particular similarity in terms of structure and function.	Homology	Superfamily
Identifiable sequence similarity.	Family	Family

Table 1.1: Description of the levels of the CATH and SCOP hierarchies
This table indicates the meaning of each level in two structure-based protein domain classification schema.
(†) SCOP has no level which directly corresponds to CATH's Architecture level; several of the SCOP Class nodes, however, have an architectural component in their description (Orengo *et al.*, 2003).

The CATH database

CATH was first created in 1993. The latest version (2.6.0) classifies 67,054 domains, originating from 45,416 protein chains in 22,478 PDB entries. Its coverage of the PDB entries is therefore approximately 73%. CATH is populated using a semi-automated protocol, invoking manual inspection only in the case of ambiguities. Close homologues are identified using standard pairwise sequence alignment methods (Smith and Waterman,

1981), requiring a match of at least 35% sequence identity over 80% of the length of the longer sequence in order to infer that a pair of domains belong in the same family.

More distant homologues are identified using a profile-based search whereby the new sequence is queried against a library of profiles previously generated for each CATH family using the IMPALA protocol (Schaffer *et al.*, 1999). Any matches found using this approach are then validated using the SSAP program, a dynamic programming method which compares the residue environments of a pair of proteins, and which has been shown to be a robust method for structural comparison (Orengo and Taylor, 1996). Where no homologues are found using the profile search, the input is checked to determine whether it may be a multi-domain protein. This is done using a consensus of three different domain boundary prediction algorithms (Jones *et al.*, 1998); any domains thus found are resubmitted separately to the sequence searches.

For around 15% of new structures, the sequence similarity to existing members of the database is too low to detect. In order to find more distant relatives, the tertiary structures of the domains are compared using a graph-based algorithm (Harrison *et al.*, 2003). Any matches found by this method are then assigned to a superfamily by scanning the protein against a set of superfamily templates generated using the CORA program (Orengo, 1999). If, on the other hand, no match is found (which occurs in about 7% of cases), the domain is compared against all structures in the appropriate class using the more sensitive but slower SSAP program. The domains which are still uncharacterised following this step are manually assigned.

The CATH hierarchy itself differs slightly from the general classification scheme described above. Firstly, CATH does not distinguish between α/β and $\alpha+\beta$ domains. More significantly, the definition of fold is shared across two levels in CATH. The first of these, the 'Architecture' level, describes the overall relative arrangement of secondary structure elements in space, independent of the order of the connecting loops between them. Below this, the 'Topology' level distinguishes between the different ways of connecting up the secondary structure elements.

The SCOP database

SCOP originated in 1994. The latest release (1.67) contains 65,122 domains in 50,285 chains from 24,037 PDB entries (a coverage of 78%). A key difference between CATH and SCOP is that the latter is constructed almost entirely by manual inspection of each new protein structure. A second difference is that the top SCOP level contains a further seven classes ("multi-domain", "membrane and cell surface", "small", "coiled coil", "low resolution", "peptides" and "designed proteins") in addition to those described above.

Proteins are first separated into domains, using a structural definition based on the presence of a independent hydrophobic core and limited contacts to the rest of the structure (Reddy and Bourne, 2003). Class, fold and superfamily are then assigned manually. The clustering of proteins into families is then done principally on the basis of sequence identity (with a 30% cutoff), but in some cases proteins which exhibit structural and functional similarity despite low sequence identity (*e.g.* globins) are placed in the same superfamily.

1.5 Computational studies of ligand binding

A considerable amount of work has been done on developing computational methods to analyse and predict protein-ligand interactions. The particular group of methods focussed upon here are those which, given the atomic coordinates of a functionally uncharacterised protein, attempt to predict which ligand(s) it recognises and, to a greater or lesser degree of accuracy, the coordinates of the bound ligand(s).

As with many areas of computational biology, each can be roughly subdivided into two classes. First, some methods attempt to construct a physically realistic model of the system, explicitly simulating the forces and energies within it. Using this framework, algorithms are then designed whose aim is typically, given two molecules, to search for a low-energy mode of interaction between them. By applying this procedure to each of a library of ligand molecules, the calculated interaction energies are used to score those which are predicted to interact with the protein. The second group of methods may be characterised as being 'knowledge-based'. Starting with the structures of a number of known protein-ligand interactions, these methods attempt to derive patterns which characterise them, and hence which can be used to search for similar interaction sites in uncharacterised proteins. The criterion used to determine which 'hits' are likely to be significant is normally an empirical one, based upon some statistical treatment of the results of the method when applied to a non-redundant calibration set of proteins.

Each approach naturally has both advantages and disadvantages. A physico-chemical modelling approach is attractive, because it offers the possibility of truly understanding the physical laws which govern the process of molecular recognition. If this goal could be achieved, the resulting insight could be applied equally to any molecular system, regardless of whether similar examples had been observed previously. The problem with such approaches is often that, for reasons which are not well understood, the accuracy of the calculated energies is often insufficient to support reliable predictions. In particular, accurate modelling of solvation in macromolecular systems has only recently begun to become a realistic prospect: see *e.g.* Jackson *et al.* (1998).

The primary advantage of knowledge-based approaches is their relative simplicity. Most techniques involve a data mining step, in which patterns are extracted from the data, followed by a pattern recognition step in which techniques such as graph theoretic methods or Geometric Hashing (Lamdan and Wolfson, 1988) are applied in order to search for these patterns in novel structures. One drawback of this approach is that it obviously requires a rich initial data set, in order to provide sufficient information to extract patterns in the first place. Recent increases in the rate of protein structure determination promise a rapid expansion in this data set, which will doubtless fuel the progress of the knowledge-based approaches. Sheer numbers of structures may not be enough for certain studies, however: depending on the degree to which each particular approach is capable of abstracting out general properties from the dataset, some may only work when large numbers of examples of *a particular ligand* are available in the database. Methods which attempt to analyse protein-ligand recognition in terms of interactions between the small functional groups which make up each molecule may be able to circumvent the problem to a degree, but the fact remains that knowledge-based approaches will always be intrinsically less general than those which aim for a fully reductionist treatment of the problem.

1.5.1 Locating the binding site

While in principle, any method capable of searching for favourable interactions between a pair of molecules could simply be applied to the two structures in their entirety, in practice, it is often desirable (and sometimes necessary) to reduce the computational complexity of the problem by first identifying regions of the protein which are likely to contain binding sites.

One common approach is to analyse the geometry of the protein structure in order to find clefts or depressions in its surface. The author of one of the earliest such method, SURFNET (Laskowski, 1995), validated the program by applying it to a set of enzyme structures in which the location of the active site was known. It was reported that, in around 80% of cases, the active site is located in the largest cleft. As such, cleft detection is an effective tool for determining likely binding sites. Although useful, this method is not universally applicable: while some types of compounds are bound in deep clefts, others - for instance carbohydrates (Taroni *et al.*, 2000) - tend to bind to shallow grooves on the protein surface, which cannot be identified using cleft detection. A wide range of algorithms for pocket finding have now been published (Ho and Marshall, 1990, Levitt and Banaszak, 1992, Kleywegt and Jones, 1994, Hendlich *et al.*, 1997, Brady and Stouten, 2000, Binkowski *et al.*, 2003); each has its own technical innovations, but the results produced are broadly similar regardless of the specific method chosen.

An alternative group of methods involve calculating the energy between simple organic probes and the protein, at all points across the surface. Clusters of low-energy points are taken to delineate likely binding pockets. A number of studies involving this type of algorithm have been published (Ringe and Mattos, 1999, Silberstein *et al.*, 2003, Laurie and Jackson, 2005). They report better results that those obtained using geometric approaches; however, the latter are currently the method of choice in high-throughput binding site search applications (Laskowski *et al.*, 2003).

1.5.2 Docking

Docking is a term for computational schemes which attempt to find the 'best' relative positioning of two molecules. Docking has been very thoroughly discussed in a recent review (Halperin *et al.*, 2002); here, those aspects relating to the problem of protein-ligand docking are briefly outlined.

Docking programs attempt to match ligands to proteins based on two criteria: geometric complementarity, and energetic minimisation. These two criteria require quite different representations of the system, and also different search methodologies. Geometry-based docking approaches typically represent the surface of the two molecules using a set of *sparse critical points*, and then use these representations to compute rigid transformations of the two surfaces which maximise shape complementarity, while penalising penetration of one surface into the other. The transformations are often computed using the Geometric Hashing algorithm, which was originally developed for computer vision applications (Lamdan and Wolfson, 1988). This algorithm achieves high performance through an offline pre-processing step which converts the set of points into a translation- and rotation-invariant representation. From this, closely-matching regions between the two surfaces can be quickly identified. Following the translation, scores are calculated on the basis of overlap checks, counts of hydrogen bonds, counts of unsatisfied buried charges, and measures of buried surface area.

Both protein-protein docking and docking of small molecules require an accurate treatment of the energetics of the system, in addition to the geometry. Effective scoring functions for docking must combine treatments of electrostatics, solvation, entropy and van der Waals forces; commonly-used examples include the CHARMM (Brooks *et al.*, 1983) and AMBER (Weiner *et al.*, 1984) force fields. Unlike geometric matching, finding energetically-favourable matches is computationally expensive; the conformational possibilities within even a small spatial region are vast due to the degrees of freedom available to the system[4]. While some components of the energy function - notably the van der Waals term due to the protein - can be calculated in advance and stored on a grid overlaying the system, the need to re-evaluate many potentials at every orientation searched means that even fairly limited docking experiments on small systems can take hours or even days of CPU time. Force field docking methods may either (i) perform an exhaustive scan of solution space in a systematic manner, or (ii) follow a guided progression through some subset of solution space.

While docking can be carried out on bound forms of the two molecules (where co-ordinates of the two components from a co-crystallised complex are the starting point), a more realistic approach is to attempt to dock 'native' or unbound forms of the molecules. This is referred to as 'unbound docking'. The main problem which this poses is how to model the flexibility necessary to take one or both molecules from their 'native' to 'bound' states. Proteins undergo two main types of conformational changes on ligand binding: (i) side chain re-arrangements, which contribute to the entropic component of the binding energy and (ii) backbone movements, which may accompany 'induced fit' (Koshland, 1958). The magnitudes of such changes have been measured by examining cases where proteins are available in both *apo* and *holo* forms. One such study, involving 31 *apo-holo* pairs (Betts and Sternberg, 1999), found that half of the pairs exhibited no more C^{α} and side-chain movement than was observed between different unbound structures of the same protein. However, the greatest movements were seen in the interface residues. In a different study, Najmanovich *et al.* (2000) analysed 353 *apo-holo* pairs of protein-ligand interactions, representing 154 unique protein sequences, and showed that in most cases, only a few residues in the binding pocket underwent significant conformational change on binding.

In *de novo* ligand design methods, the aim is to try to identify favourable interaction sites for fragments of molecules using methods such as GRID (Goodford, 1985), rather than attempting to dock entire ligands. Once a set of probable interactions have been collected, these methods attempt to find molecules with appropriately-positioned functional groups. The most widely used method is the Multiple Copy Simultaneous Search (MCSS) (Miranker and Karplus, 1991), which searches for energetically favourable orientations and positions of functional groups based on the CHARMM energy function. The resulting functionality maps can be used to predict probable ligands by using the HOOK program (Eisen *et al.*, 1994), which generates molecular skeletons by making bonds between the predicted functional groups, screening out unfavourable conformations using a simple van der Waals function.

1.5.3 Knowledge-based ligand prediction

In many cases, a protein's function may be determined by the spatial arrangement of just a few residues or atoms, which mediate ligand binding or catalysis. As such, computational methods which attempt to discover

[4]Three degrees of translational freedom, three axes of rotation, and rotation of bonds in both the protein and the ligand

small structural motifs may, in some cases, be more functionally informative than comparisons at the fold level. Well-studied examples of structural motifs which convey information about a protein's function are the EF-hand which binds calcium (Yap *et al.*, 1999) and the serine protease catalytic triad (Wallace *et al.*, 1996).

Methods which use analogy with previously-observed ligand-protein interactions in order to predict the specificity of a new binding site can be further subdivided into to classes. The first of these may be characterised as 'direct' searches, in that they look for similarities between the new site and a library of known binding sites. If a close match to a given site is found, the new site is inferred to share specificity for the same ligand with the 'hit', with a confidence derived from a prior statistical calibration of the method. In contrast, the second group of methods first deduce interaction propensities between all pairs of atom types or functional groups by determining which combinations are over-represented in a set of known binding sites. These propensities, usually represented in the form of density maps or three-dimensional scatter plots, are then used to infer the atom types which are likely to be found in a binding cavity, given the composition of the surface of the site. Ligands whose structure matches this chemical signature are then sought, with good matches returned as the predicted interaction partners.

1.5.3.1 Similarity-based approaches

Just as for the docking methods, similarity-based binding site search algorithms can be characterised by two properties, namely the way in which the sites are represented, and the method used to search the new site against the library.

Binding sites have been represented using three main approaches. These can be characterised as

- Surface representations: description of the binding site using the molecular surface, or critical points which lie upon it. See *e.g.* Pickering *et al.* (2001), Kinoshita *et al.* (2002).
- Pseudocentre representations: representing the site using a set of points which describe the location of certain functional groups (aromatic rings, hydrogen bond donors/acceptors *etc.*) in space. See *e.g.* Schmitt *et al.* (2002).
- All-atom representations: using the full complement of coordinates of the atoms which line the binding site. See *e.g.* Kobayashi and Go (1997).

Search methods tend to fall into two categories. First among these are graph theoretic methods. As described in appendix A, graph theory provides a powerful and flexible set of tools which may be applied to widely diverse problem domains. Searching for similarities among binding sites, which may be characterised as sets of labelled points lying in a space (and hence simply converted to a graph by adding edges labelled with the Euclidean distance between them) lends itself well to graph-based methods. Various subgraph isomorphism detection algorithms, *e.g.* Bron and Kerbosch (1973), Ullman (1976), can be applied in order to discern the similarities between these graphs. The other technique which is commonly used is geometric hashing.

1.5.3.2 Propensity approaches

These methods can be distinguished on the basis of two criteria: the set of probe types defined, and the type of the data set from which the distributions are obtained.

In the case of X-SITE (Laskowski *et al.*, 1996), 26 atomic probes are defined, based on a previously published list of atom types (Engh and Huber, 1991). Contact preferences are defined relative to 163 three-atom fragments[5], each of which occurs in one or more of the standard amino acid side chains, and which define a coordinate frame. By analysing a set of high-resolution, non-homologous protein structures taken from the PDB, three-dimensional density maps are constructed for each probe/reference-frame pair, which describe the distribution of probe atoms relative to the fragment. Validation on a set of 5 known protein-ligand complexes resulted in correctly predicted atom types for 54-78% of ligand atoms.

The source of the original data for IsoStar (Bruno *et al.*, 1997) is a combination of PDB structures, and coordinates taken from the CSD. It contains distributions constructed in a similar way to those found in X-SITE, except that the probe types in this case are not individual atoms, but rather small functional groups such as hydroxyl moieties or methyl groups. This library is utilised by the SuperStar program to produce contoured propensity maps for putative binding sites. SuperStar was validated on a set of 122 protein-ligand complexes from the PDB. For 80% of the ligand atoms in the test set, the density of the correct probe type at that position was found greater than expected by chance (Verdonk *et al.*, 1999, 2001).

1.5.4 The relationship between ligand specificity and protein function

Identification of the ligand or ligands which bind to a new protein is often cited as an important clue to predicting its function. It is therefore instructive to clarify something of what we mean by the word 'function'.

The inability of this word to encapsulate the many aspects of the role played by one protein in an organism, has been recognised by Skolnick and Fetrow (2000) and Moult and Melamud (2000); meanwhile, the ever-increasing body of knowledge relating to gene and protein function has highlighted a need to explicitly define the vocabulary we use to express this information (Ashburner *et al.*, 2000). A synthesis of the schemes previously presented for the description of protein function leads to the following four complementary classes:

- Physiological function (In which biological processes is the protein involved in the organism?)
- Cellular component (*i.e.* cellular location - is the protein membrane-bound, cytosolic *etc.*)
- Biological process (*e.g.* translation, metabolism)
- Biochemical function (*e.g.* enzyme, transporter)

Of these, protein structure - and in particular, protein-ligand interaction information - allows us access most directly to molecular (or biochemical) function. Moult and Melamud suggested breaking this class further into more fine-grained descriptors:

1 Class (*e.g.* enzyme, DNA-binding protein)

2 Type (*e.g.* protease, transcriptional repressor)

3 Specificity (*e.g.* trypsin-specific protease, *lac* repressor)

A reliable method for the prediction of protein-ligand interactions would give us access to the last of these descriptors. The value of this information would depend in part on the particular ligand predicted: knowing

[5]The X-SITE data set has since been updated to include a wider range of probe types (R.A. Laskowski, personal communication).

that a protein binds ATP does not shed a great deal of light on its function, but learning that it binds glucose 6-phosphate would be more illuminating. It is therefore somewhat paradoxical that the majority of predictive methods are designed and benchmarked on common biological ligands; the hope is that the insight gained from these analyses may allow us to develop methods which also work for less ubiquitous molecules.

1.6 Overview of the Thesis

The work presented in this thesis is an analysis of the structural diversity observed in protein-small molecule interactions. Here, 'variation' means the number of different ways in which proteins have evolved to recognise a given type of ligand. The focus of this thesis is not on the dynamic aspects of structural changes which are known to occur in both molecular partners during the process of molecular recognition. Rather, the intent is to analyse the static structural snapshots of protein-ligand complexes found in the PDB, and to address two questions:

- To what extent does a given ligand adopt different conformations when it is bound by different proteins?
- Among different proteins which bind the same ligand, to what extent do the chemical characteristics of their binding sites differ?

Chapter 2 outlines the design and development of a software library which was used to carry out the analyses described later in the thesis. This library is intended to serve as a generic toolkit for the construction of application programs for structural bioinformatics. Its architecture is discussed in some detail, highlighting those features of its design conferring modularity and reusability.

Chapter 3 describes the methods used in the subsequent analyses. Each technique is presented starting with a discussion of its theoretical basis, before proceeding to an explanation of its application to the particular problem domain of this thesis.

Chapter 4 discusses the generation of a number of datasets of protein-ligand interactions from the PDB. Methods for automatic validation of ligand identity, and clustering of binding sites based on evolutionary relationships between their constituent protein domains are described. Results obtained by applying these methods to the whole PDB are then discussed, allowing certain conclusions about the distribution of ligands with respect to protein families, and *vice versa*, to be drawn.

Chapter 5 consists of an investigation of conformational variability among the structures of bound ligands. Previous observations that ligands tend to bind in extended conformations are quantitatively assessed. By comparing the conformational variability exhibited by ligands bound to unrelated proteins with those bound to proteins from the same superfamily, the hypothesis that ligand conformation is conserved during evolution is tested.

Chapter 6 contains an analysis of the structural and chemical variability in binding sites which recognise a given molecular fragment. Borrowing concepts from sequence analysis, a new method for quantifying

binding site diversity is proposed. This is then applied to binding sites for a number of common ligand fragments, with the aim of determining whether the degree of variation in binding sites is similar among different protein families, and for sites recognising different fragments. Potential applications of this method in knowledge-based binding site prediction are discussed.

Chapter 7 discusses the implications of the findings from the previous chapters, presents the conclusions which can be drawn from them, and suggests future work which could be undertaken.

Chapter 2

The GAMUT library

This chapter describes the design of GAMUT, an object-oriented software library which provides a rich toolset for the development of applications in structural bioinformatics. By providing computationally efficient implementations of a range of commonly-used data structures and algorithms, the library facilitates rapid deployment of solutions to problems in bioinformatics, with a particular focus on those concerned with three-dimensional protein structure data.

In order to explain the motivation for writing the library, a review of recent trends in bioinformatics software development and a survey of projects related to GAMUT are presented. The perceived strengths and weaknesses of these projects are discussed. In the light of the lessons learned from these considerations, the principal design decisions involved in the development of the new software are explored. Implementation details of the library are not considered in depth in this chapter; the interested reader is referred to appendix C.

The project homepage, located at `http://www.ebi.ac.uk/~gareth/gamut`, contains more details on the library.

2.1 A brief history of computational biology

The development and growth of computational biology[1] has been paralleled by - and indeed enabled by advances in both computer hardware and software design techniques (see figure 2.1). The emergence of the field may be traced back to the late 1950s, when crystallographers first began to make use of electronic computers. The rise of scientific computation was enabled intially by the advent of high-level programming languages such as FORTRAN (IBM, 1954). These languages liberated programmers from the need to communicate with computers in assembly language, enabling them instead to write programs which were deliberately similar in style to the mathematical formulae with which they were already acquainted.

Over time, advances in software engineering techniques have been adopted by the computational biology community, with the last decade or so seeing several notable changes. These may be separated into *methodological* and *technological* changes; while clearly inter-related, the two are discussed separately below.

[1] Here, *computational biology* is used as a catch-all term for bioinformatics and crystallographic computation, whose development has been to some extent inter-twined.

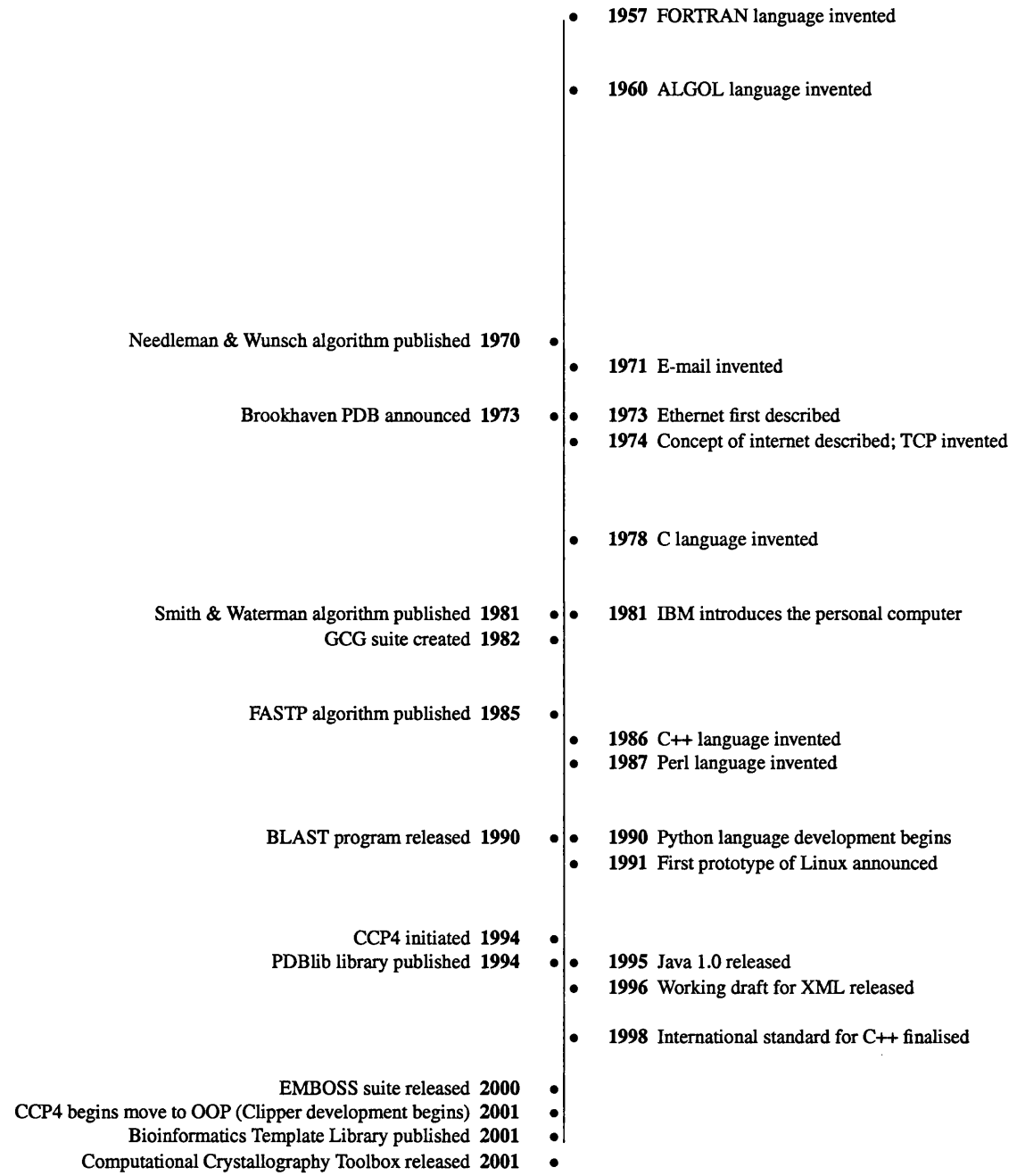

Figure 2.1: Timeline showing key advances in computational biology
The left-hand side of the timeline shows selected developments in computational biology; dates on the right refer to innovations in software technology.

2.1.1 Methodological changes

Early software development in computational biology was very much focussed on a specific, individual problems: *e.g.* writing a program to perform the calculation of a Patterson map from reflection amplitudes. As such, the only constraint on the program design was that it should perform its one job adequately. However, as the use of computers in crystallography became more ubiquitous, the need to develop complete *tool chains* which would work in synchrony with one another became apparent. This need was normally met by the definition of file formats, through which each program in the chain could 'talk' to the next.

The obvious problem with such an approach is that code is redundantly repeated from one tool to the next; if programs X and Y perform two different transformations on electron density maps then, while the code for the transformation itself will differ between the programs, the two are likely to share a lot of 'housekeeping' code for constructing an in-memory representation of the density map, converting between reciprocal- and real-space coordinates, and so forth.

The means for eliminating such redundancy lies in the development of *libraries* of re-usable code. Software libraries may be described as collections of subprograms, which are used to help develop software. Libraries are distinguished from executables in that they are not standalone programs; rather, they consist of 'helper code' which provides services to another independent program or programs. As such, commonly-used routines may be collected into a library, and then employed by any number of application programs. The key requirements in library design, therefore, are that - in addition to performing a particular set of tasks - the library must provide a well-defined interface through which applications may utilise its features. More formally, a software library should satisfy the following requirements:

- **Functionality**: the library must provide a wide enough spectrum of capabilities to make it useful, such that the client[2] is motivated to utilise the library rather than writing custom code.
- **Reusability**: the functionality provided by the library should be flexible enough to be applicable to a range of related problems; without this constraint, a library becomes simply a bespoke software component designed for a single application.
- **Ease of use**: the library should be as user-friendly as possible, meaning that it should provide a clearly documented interface, whose style conforms with existing conventions in the programming language in which it is written.
- **Robustness**: the library should be tolerant to both heavy usage conditions, and to errors in input data.

A good example of a widely-used body of code for computational biology is the CCP4 library (Collaborative Computational Project Number 4, 1994) for crystallographic map manipulation and model building.

2.1.2 Technological changes

Historically, scientific programs have been composed of comparatively simple data structures such as arrays and matrices, with the most commonly required operations being floating-point arithmetic computations. Program structure is also often found to be fairly simple, consisting largely of counting loops and selections.

[2]Throughout this thesis, the term *client* will be used to refer to either the application or the programmer who utilises a library

The prime concern in much scientific programming is efficiency; as such, the languages which initially found favour in the area were those which could offer speed comparable to assembly language programming. However, they were not necessarily the most sophisticated in terms of their control and data structures.

From early, unstructured languages, through structured programming and lately into object-oriented languages, language developments have allowed scientific programmers to model biological data with increasing accuracy and clarity. The programming paradigm currently enjoying the highest profile in computational biology is that of Object-Oriented Programming (OOP) (Meyer, 1997). While, in traditional programming models, data and process are separate parts of a program, the object-oriented approach merges the two together. There are many definitions of an *object*; technically, an object is a software entity which bundles data variables together with the methods which act on this data. More poetically, Meyer characterises the concept of an object using the motto "Ask not first what the system does: As what it does it to!". Conceptually, software objects are able to closely model real-world objects, since they possess the ability to represent both the *state* and *behaviour* of an entity. The object-oriented programming paradigm was adopted for the design of GAMUT.

2.2 Other projects related to GAMUT

At the outset of the work presented in this thesis, it was clear that software posessing a number of capabilities would be required. These capabilities included:

- **Coordinate handling**: the ability to import, represent and manipulate three-dimensional macromolecular coordinate data, including calculations of rigid-body superpositions; methods for classifying atoms into groups according to specified schemas
- **Chemical structure manipulation**: the ability to represent chemical structures, including facilities for detecting common substructures shared by a pair of compounds, identifying rotable bonds, computing graph invariants, and the generation of 2D chemical structure diagrams
- **3D density mapping**: a framework for handling 3D scalar fields, including features such as calculating convolutions, comparing groups of maps and computing isosurface contours
- **Representation of protein structure classifications**: the ability to assign domain identities to individual residues in proteins based on existing structure classification schemes such as CATH and SCOP
- **Miscellaneous utilities**: clustering, database access, linear algebra, computational geometry

It was necessary, therefore, to determine whether libraries providing these features were already available. Several programming libraries for computational biology have recently been described, including a number of object-oriented libraries. These libraries are summarised in table 2.1.

The suitability of the available libraries for the project was assessed in each case according to two main criteria:

- **Ease of use**: Does the library provide an intuitive, well-documented interface? How easily can it be integrated with other systems?
- **Functionality**: Does the library provide the required features?

Predictably, most of the available libraries provided a subset of the required functionality, in addition to other features which were not required. For example, the Clipper library contains very powerful density-map handling facilities, including coordinate transforms, file import/export for several common data formats and comparison of multiple maps. However, at the the outset of the project, Clipper did not have any ability to represent models of macromolecular structure. This pattern was common to all of the libraries surveyed; ultimately, it was felt that developing a new library which provided a full set of the features required would be preferable to attempting to marry several disparate systems.

An additional major motivation for the design and implementation of GAMUT was the percieved educational benefit to the author of undertaking the project. In particular, it was felt that writing a system like GAMUT from scratch would allow the author to gain an understanding of both software design methodologies and algortihmics, which could not be gleaned by simply 'patching together' existing components.

Name	Reference	Description	Language	Active[a]
PDBlib	(Chang *et al.*, 1994)	A class library for modelling structural features of biomolecules at the level which can be parsed from PDB files.	C++	No
MMTK	(Hinsen, 2000)	The Molecular Modelling Toolkit. Provides features including rigid-body fitting, force field minimizations, molecular dynamics, surface calculations.	Python	Yes
BALL	(Kohlbacher and Lenhof, 2000)	Biochemical ALgorithms Library. Extensive collection of data structures and algorithms for development of molecular modelling and simulation applications.	C++	Yes
Clipper	(Cowtan, 2000)	A set of libraries for crystallographic computing. Aimed at aiding the transition of CCP4 developers to object-oriented programming. Provides classes for representation of electron density maps, and frameworks for developing crystallographic phase estimation and model refinement methods.	C++	Yes
BTL	(Pitt *et al.*, 2001)	The Bioinformatics Template Library. Library of components for biocomputing, designed with a strong emphasis on generic programming. Consists largely of generic algorithms in the mould of the Standard Template Library, along with a few specialised data structures.	C++	No
MMDB	(Krissinel, 2002)	The CCP4 coordinate library project. A library intended to help CCP4 developers in working with coordinate files. Provides various high-level tools for working with coordinate files such as orthogonal-fractional coordinate transforms, generation of symmetry mates, and editing molecular structures.	C++	Yes
CACTVS	(Ihlenfeldt *et al.*, 1994)	A research project aiming to change the ways of doing computational chemistry. The functionality of the toolkit is exposed via a scripting layer, but source code for the underlying library is not freely available.	C/Tk	Yes
OpenBabel	(The OpenBabel Team, 2001)	A cross-platform program and library designed to interconvert between many file formats used in molecular modeling and computational chemistry.	C++	Yes
CDK	(Dortu *et al.*, 2000)	Java utitility classes for ChemoInformatics and Computational chemistry.	Java	Yes

Table 2.1: Software development projects related to GAMUT

[a]Whether the project was undergoing active development at the time of writing, to the best of the author's knowledge

2.3 Design of GAMUT

This section describes the overall design of GAMUT, with only limited reference to details of the implementation, which are treated separately in appendix C. The focus of the discussion here is upon the requirements which the library was designed to satisfy.

2.3.1 Design principles

2.3.1.1 Modularity

As described above, GAMUT was conceived as a general-purpose framework for developing structural bioinformatics applications, and as such, provides a wide range of functionality in several distinct areas. It is clear, however, that for any one application, only a subset of this functionality may be required. A key requirement in GAMUT, therefore, is the ability for a client to utilise only the components which are required; this was realised through the following:

- **Object-orientation**: by implementing each data structure and algorithm as an object, each of which is designed with the principle of abstraction in mind, independent software components, each fulfilling a distinct and well-defined role, are made available to the client.
- **Library organisation**: related GAMUT classes, such as the chemistry classes, or density map classes, are collected together in independent modules. This allows the client to utilise only those groups of components which will be required for application development in the area(s) in which he/she is interested.

2.3.1.2 Ease of use

In order to make GAMUT as user-friendly as possible, the following principles were adopted (see also appendix B.1):

- **Consistent, intuitive interface**: functions and variable names are chosen in order to make their use as intuitive as possible. Moreover, naming conventions are used throughout the library, such that functions with the same name in different classes should have the same or comparable effects. The interface is thoroughly documented, as described in §2.4.
- **Idiomatic interface**: the GAMUT interface makes use of numerous design patterns which are in common use in other software components, and are therefore likely to be familiar to potential clients. For example, collections of objects are stored inside *container classes*, and access to them is typically granted through iterators, which prevent array bounds over-runs, and also allow the design of generic algorithms which may operate on a variety of different containers.
- **Simple installation procedure**: to enable portability of the library, standard methods of distribution and installation of the library have been employed: the GNU build tools (Vaughan, 2000), familiar to most UNIX users, are used to configure, compile and install the library.

2.3.2 Robustness

A library will only be utilised if it can be relied upon; therefore a great deal of effort has been spent in making GAMUT as error-free as possible. The key points of this enterprise are:

- **Error tolerance**: where errors may occur during execution of library functions, for example due to erroneous input data, they are checked for, and reported using a system of runtime exceptions.
- **Protecting the programmer**: programming errors are made less likely by removing from the client the burden of memory management: all dynamic memory allocation and deallocation is done within the library itself (see appendix B.2).
- **Self-testing**: a suite of test programs is provided with the library, which should be run once the library itself has been installed. This test suite checks the behaviour of the library in a range of different situations, including several which deliberately invoke errors in order to check GAMUT's exception-handling mechanism. In addition to reassuring the client that his/her installation of the library is working correctly, the testsuite is invaluable during library development, both in checking that recent changes have not inadvertantly introduced bugs into the library, and in evaluating the portability of the system to a number of different platforms.

2.3.3 Choice of language

Once the decision had been taken to design GAMUT in an object-oriented manner, the choice of languages could be substantially narrowed. The three major object-oriented languages currently available are Java (Inc., 1995), C++ (Stroustrup, 1995) and Python (Python Software Foundation, 1990). Each language naturally has its own advantages and disadvantages.

Of the three, Python was the least well-suited to the task: being an interpreted language, its execution speed is typically much slower than that of either of C++ or Java. As such, Python is not suitable for implementation of the numerically-intensive parts of the library, for which efficiency was identified as a priority.

Java was designed from the outset as a cross-platform object-oriented language, and therefore benefits from a clean design, excellent portability and robustness. In addition, there are a large number of high-quality third party Java libraries available. However, certain attractive language features, notably operator overloading and generics (see below) are currently missing from Java. An even more serious impediment to using the language is that the virtual machine architecture needed to provide the ability to run the same program on any platform incurs a significant performance penalty.

C++ was originally conceived as a "C with classes", and as such, owes both good and bad features to C. On the good side, C++ programs can be made to run extremely quickly since the language retains the pointer-manipulation capability of C. This can lead to coding errors, however, and porting C++ code between platforms is recognised to often be troublesome. The mosaic heritage of C++ is often criticised as having led to a language which, although powerful, has become somewhat baroque in its design[3].

[3] An unattributed comment found on the world-wide web describes the language as being *"An octopus made by nailing extra legs onto a dog"*!

C++ provides an extremely high degree of expressivity, due to its support for multiple programming paradigms: in addition to its object-orientation capabilities, C++ allows powerful generic programming techniques to be leveraged, thanks to its template framework. A *template class* is one in which the type of one or more data members is replaced by a 'dummy' or placeholder type. In order to use a template class, it is 'instantiated' by specifying the type(s), which are substituted for the placeholders.

The simplest application of templates is the design of generic objects: for example, one may wish to design a type-safe array object. The array may be implemented as a template class with a single parameter, namely the type of object to be stored in the array. Using this single template, a client is able to instantiate any number of array types, each of which stores a different type of data.

Although the idea of templates is fairly simple, and the number of syntactic rules governing their use within the language is small, templates enable a range of particularly powerful programming techniques to be leveraged using C++. The most exotic of these fall into a group known as 'metaprogramming'. By employing template specialisation and recursion, the compiler can be made to act as an iterpreter, such that parts of C++ programs are effectively executed at compile-time, rather than at run-time, as is normally the case. Alternatively, template metaprogramming can be used to simplify the interface of a complex class using policies and/or typelists. Both of these aspects of metaprogramming were employed in the implementation of GAMUT, and will be discussed further later in this chapter, and in appendices B.4 and B.5.

Since the recent finalisation of an ISO standard for C++ (ISO/IEC Information Technology Task Force, 1998), compiler designers have had a concrete specification to work to, greatly reducing portability problems. One final advantage of C++ is the availability of powerful tools for interfacing with the Python language (Abrahams, 2003), allowing an easy-to-use scripting layer to be wrapped around a C++ library. These features taken together motivated the decision to implement GAMUT in C++.

2.3.4 Architecture of the library

The evolution of a piece of software can often be viewed as a Popperian process. It begins with an initial design, in which the software engineer does his or her best to capture the essence of the problem. This initial conception allows a prototype of the system to be constructed, which fulfils the main requirements identified during the design stage. Inevitably, however, flaws in the design are discovered during the implementation and testing of the software; many design flaws are easily corrected, but every so often, a radical change in the overall design of the system is required. This process of iterative re-design, often involves, in OOP terminology, several *refactoring* steps: elements common to two or more existing classes are abstracted away into a common base class, thereby improving modularity and promoting code re-use. Eventually, the system reaches maturity when all of the features specified in the original design are present, and the system is able to perform the task(s) for which it was designed.

GAMUT has undergone such an evolution of design; a sketch of its final architecture is presented in figure 2.2. It may be seen as consisting of several layers; each of which performs a more specific function than the one before. Within each layer, components which are conceptually related are grouped together into semi-independent modules.

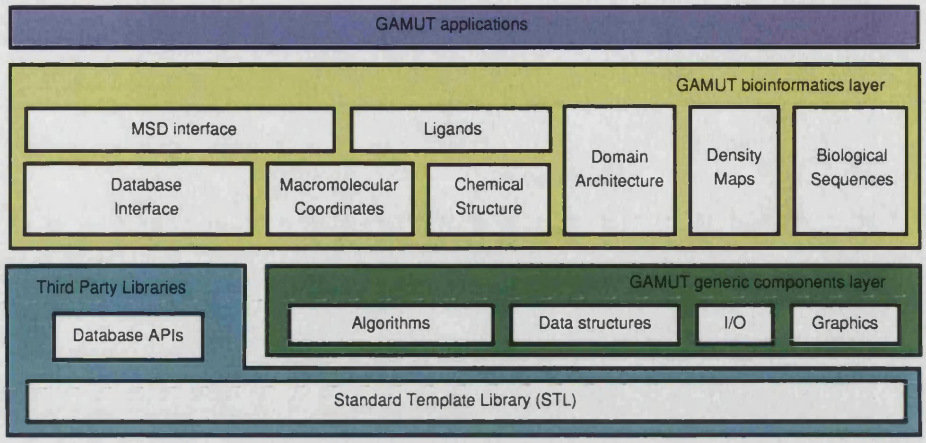

Figure 2.2: Architecture of the GAMUT library
GAMUT consists of several layers, which, reading from the bottom of the picture upwards, are in order of increasingly specialised function.

The lowest layer consists of the C++ Standard Template Library (STL) (Inc., 1994). This is a collection of fundamental data structures such as sets, maps and arrays, an implementation of which is provided with most C++ compilers, and can therefore be assumed to be present on all target platforms for GAMUT. While not strictly part of the GAMUT library, the STL data structures are used as the atomic building blocks from which many of the classes in the higher levels of the library are composed.

2.3.4.1 Generic components

Moving in the direction of increasing specialisation of function, the next layer contains generic data structures, algorithms and utilities. This layer does not contain anything specifically related to biological data; as such, it provides components which are potentially also of use in application areas outside computational biology.

The existence of the generic components layer is largely due to the refactoring process described above, with many classes having begun life as part of the bioinformatics layer, before it was realised that common factors could be abstracted away. A good example of this phenomenon is the tree data. In the first implementation of the macromolecular structure module, the atom, residue and chain classes were designed such that the parent-child relationships between them was explicitly coded into each class. A residue object, for example, contained a pointer to its parent chain, and an array of pointers to its constituent atoms. This meant that code for common tree operations such as adding a child node, or iterating through all children of a given node, were repeated through the atom, residue and polymer classes. In addition, 'housekeeping' code was also repeated: when a residue object is destroyed, it must make sure that the atom objects to which it holds pointers are also destroyed. The chain object holds the same responsibility towards its child residues.

By abstracting the tree concept into its own class, this redundancy was removed: a single node class, which manages the lifetime of, and provides functions for access to its child nodes, now can serve as a base class for the atom, residue and chain classes. This type of abstraction is an example of the *Composite* design pattern (Gamma *et al.*, 1995). Once code for a generic tree is in place, it becomes possible to quickly develop other tree-based data structures - such as those which represent protein domain classification hierarchies like

CATH or SCOP - without re-inventing the wheel.

The key components present in the generic layer are briefly outlined here with a focus upon the aims which were in mind during the design of each one. It should be noted that components similar to several of those provided in GAMUT's generic component layer are now freely available in a third-party C++ library called Boost (The Boost Committee, 1998). These include a generic graph library, linear algebra components, and support for functional programming. Although utilisation of this existing code could have replaced some which was written for GAMUT, the architecture of Boost is such that it is difficult to separate just a few components from the library as a whole[4]. Employing Boost components in GAMUT would have required either distribution of the entire Boost source tree along with GAMUT, or requiring that the user already had Boost installed before downloading GAMUT. Neither of these alternatives was viable.

2.3.4.1.1 Arrays

Classes for representing arrays of objects whose size is fixed at compile-time were required in GAMUT, due to their current absence from the C++ standard. While the language has good support for *dynamic* arrays, through the `std::vector` class, these are not ideal when dealing with arrays whose length is known not to be changeable, for example, when implementing a 3-dimensional vector object. Conversely, the fixed-size array types present in C++ are due to the language's C heritage, and do not provide any of the convenient OOP features of the STL containers. As such, the requirements for the fixed-size array class were that it should be a wrapper for static C arrays, providing an interface as close as possible to that exposed by `std::vector` while maintaining the computational efficiency of the native array types.

In addition to a class for fixed-sized one-dimensional arrays, a three-dimensional array class was required for GAMUT. It should be noted that the author draws a distinction between three-dimensional *arrays*, and three-dimensional *fields*. While both are three-dimensional grids of values, only *fields* are associated with coordinates in three-dimensional space. A field therefore should be thought of as an array which has been *embedded* in a space. The array class should provide the following capabilities:

- **Intuitive indexing**: the client should be able to access data within the array by either providing a three-dimensional address within the grid, or by specifying an index value. The array class should provide means for translating between these two forms of look-up.
- **Views**: by specifying a pair of bounding addresses, the client should be able to identify a block within the array, upon which further operations may be performed. For example, the client must be able to identify a view of the array, and then iterate through all values in that view.
- **Arithmetic operations**: where the type of data stored in the grid supports arithmetic operators, the client should be able to apply these operators to pairs of arrays with compatible dimensions, thereby effecting a cell-by-cell addition, subtraction or multiplication of values. In addition, it should be possible to apply these operations to pairs of arrays with different sizes, as long as the smaller array can be placed somewhere within the larger. This type of operation could be used to update a large scalar field by incrementing a small region using a function stored as an precomputed array of values.

[4]Since the development of GAMUT, a more recent release of Boost which provides a mechanism for installing library components independently has become available.

2.3.4.1.2 Graphs

Graphs, which are discussed in appendix A, are one of the most fundamental data structures in computer science, and are particularly important within GAMUT. Their primary application is in the representation of the atomic connectivity of chemical compounds.

In designing the graph framework for GAMUT, the principal requirements were:

- **A flexible, generic data structure**: the data structure should be able to represent graphs in the same variety of ways that mathematicians use when thinking about them. That is to say, the library should allow one to construct graphs which are directed or undirected, whose connectivity information is stored using adjacency list, edge list or edge matrix, whose edges and vertices may be labelled or unlabelled, *etc.*
- **An intuitive interface**: typical patterns of accessing graph information include iteration through all vertices in a graph, iteration over out-edges of a given vertex, depth-first and breadth-first searches. Mechanisms for performing these should be provided by the library.
- **A consistent interface**: as far as possible, the graph interface should be invariant over the different types of graph described above. That is to say, whether the client is referring to an edge list graph or an adjacency matrix graph, he/she should be able to perform any given operation in the same manner.
- **An extensible algorithm framework**: efficient implementations of commonly-used graph algorithms such as shortest-path methods, cycle perception and isomorphism detection, should be provided. They should be implemented in such a way that, should a client wish to add a new isomorphism algorithm for example, the means for doing so are clear.
- **Graphical representations**: it is often difficult to interpret the results of graph operations without reference to a diagrammatic depiction of the graph. Many graph layout algorithms are available; it was decided that several should be implemented in GAMUT.

2.3.4.1.3 Trees

As described above, a generic tree component was required. The design requirements for the tree classes were as follows:

- **An expressive interface**: clients should be access the data held in the tree by iterating through children of a given node, traversing the tree using depth-first and breadth-first searches, and so on.
- **Automatic lifetime management of nodes**: as described above, parent nodes should take responsibility for the management of the lifetime of their child nodes, in order to avoid memory leaks. A corollary of this is that, when a node n is copied, the copying operation must be *deep*: that is to say, all nodes in the subtree below n must be recursively copied to form a new, independent subtree.
- **Ability to represent different types of trees**: just as the graph framework was designed in order to provide a similar interface, to data structures which internally, may be represented in quite different ways, different types of trees (*e.g.* binary - balanced or unbalanced, N-ary) should expose similar interfaces to the client. Another distinction which may be drawn is between *polymorphic* trees, where the nodes may be of different types (such as the tree of a macromolecular structure, where some nodes

represent residues, others atoms *etc.*), and *monomorphic* trees, such as trees generated by hierarchical clustering algorithms, where each node represents the same type of object, namely a branch in the clustering hierarchy.

2.3.4.1.4 Persistence

A key requirement when developing application programs is the ability to save the state of objects within the program to disk, such that the objects can later be reconstructed from the disk file. This ability to interconvert between volatile, in-memory representations of data, and non-volatile representations such as disk files is known as *persistence*; the actual operation of writing objects to disk is sometimes referred to as *serialisation.* The main issues at hand when designing GAMUT's persistence mechanism were:

- **Platform independence**: files written by a GAMUT application running on one machine should be readable by a GAMUT application running on a different type of platform. The format of the file must not, therefore, be dependent on the features of any particular machine. This is relatively easy to achieve if data is written to text-based files using a common standard such as American Standard Code for Information Interchange (ASCII) . By utilising a text-based file format such as Extensible Markup Language (XML) , complex data can be stored in files which, in addition to being readable on any platform, may also be understood by any application which can parse XML.

  The parsing of a text-based file, however, incurs an overhead on the data recovery process. The alternative is to store data in a binary file format, which can be read in much more rapidly, since the on-disk representation of the data is essentially identical to that held in memory. The disadvantage of using a binary format are that the data is less accessible: whereas an XML file can be inspected using any text editor, and may be parsed by any application which understands XML conventions, a binary file typically can only be interpreted by the program which created it. In addition, storing data in binary files requires consideration of issues such as *endianness*, whereby different types of computer store the bytes of their data in different orders. Transferring files between machines with different endianness requires swapping the byte order within the data.

  At present, the persistence mechanism in GAMUT is binary, for reasons of speed; however, an XML persistence mechanism could be added fairly simply; this would improve the ability of GAMUT applications to communicate with other programs.

- **Versioning**: the information content of a class may change as the software is developed; as such, the information written to disk when an object of that class is serialised, may also change. In order to prevent errors when reading files, it is important to record the version number of the software which created the file, at the start of the data written to disk. On reading the file, this number must be checked against the version of the software performing the read. A mismatch in version number may necessitate an error being generated; on the other hand, newer versions of the software should be backwards-compatible with older file versions.

- **Identity verification**: an additional check which may be added to a persistence mechanism is to verify that the file being read does in fact contain data of the correct type. This means that, in addition to

storing the version number at the head of a data block, each object should write an identifier which specifies that it is of type *X*; if a *Y* object later attempts to read the file, an error will be generated to report the mistake.

- **Indexing**: at an early stage of GAMUT development, it was realised that a means for storing large quantities of data in a form from which specific data items could be rapidly recovered would be advantageous. This data typically takes the form of a large number of objects, each of which can be identified by a small number of 'keys' (*e.g.* numeric indices, or text labels). Third-party database engines could perform this function; however, for such simple data relationships, full relational database capabilities are often not required. Instead, an Indexed Sequential Access Management (ISAM) system was conceived for GAMUT. ISAM storage works by serialising the data objects into one large file, while maintaining a separate file which maps from the keys, to a number which records the location of the appopriate data object in the main data file. In order to access a particular data object, the client needs simply to look up the file offset in the index, and then read from the appropriate position in the archive (see appendix C.1.7.1 for more details).

2.3.4.1.5 Linear algebra

Facilities for basic linear algebra operations, primarily (but not limited to) manipulation of three-dimensional coordinates and transforms, were required for many parts of the library. Many libraries for linear algebra, written in, or compatible with C++, already existed (*e.g.* LAPACK (Anderson *et al.*, 1999) and LEDA (Algorithmic Solutions Software, 2001)). However, these libraries provide capabilities far beyond those required; GAMUT's linear algebra module was designed as lightweight components providing the following features:

- **Vectors and matrices**: classes for the fundamental objects used in linear algebra were designed, including basic operations such as matrix algebra, scalar and cross products *etc.*
- **Matrix decomposition**: singular value decomposition and diagonalisation algorithms

2.3.4.1.6 Computational geometry

Certain geometric operations are common in structural bioinformatics applications; the following were identified as necessary for implementation in GAMUT:

- **Geometric range queries**: structures and algorithms for rapidly determining the set of objects, located in space, which fall inside a given geometric region, such as kd-trees and brick maps. For example, determining the set of residues in contact with a ligand molecule begins with identifying those residues which are in proximity to the ligand; this can be done using a geometric query map.
- **Triangulation**: means for computing and representing triangular meshes, including algorithms for calculating isocontours through scalar fields.

2.3.4.1.7 Graphics

A basic 2D graphics toolkit was designed for GAMUT, in order to allow applications to generate diagrams by providing objects corresponding to geometric primitives such as squares, lines and circles. The graphics

framework was designed such that the in-memory representation of these geometric objects should be separate from the output device. In this way, applications can internally lay out the components of a diagram, then output it in one of a variety of formats (GIF, PostScript (Adobe Systems Incorporated, 1990) *etc.*), simply by selecting the appropriate graphics driver. The graphics framework provides the basis for the graph and tree layout algorithms implemented in the library.

The bioinformatics layer of the library is separated into five main sections, namely the macromolecular structure, chemical structure, domain architecture, density map and sequence modules.

2.3.4.2 Macromolecular structure components

The macromolecular structure module is the largest in the bioinformatics layer. It contains classes for modelling the physical entities which make up a biomolecular structure, as well as classes which represent interactions between atoms within a structure.

The set of fundamental classes needed to model macromolecular structure were fairly clear from the beginning: namely, `Atom`, `Monomer`[5], `Polymer`, `Model` and `Molecule`. Instances of these classes are arranged into a tree whose structure reflects the hierarchical relationship of the corresponding biochemical entities, as shown in figure 2.3; the `Model` class is included in the hierarchy in order to allow us to represent molecules for which there is more than one solution to the structure determination experiment, as is the case for NMR structures. The root of the tree is 'owned' by the `Molecule` object: this means that the lifetime of the objects which constitute a molecule is limited to the lifetime of the molecule itself.

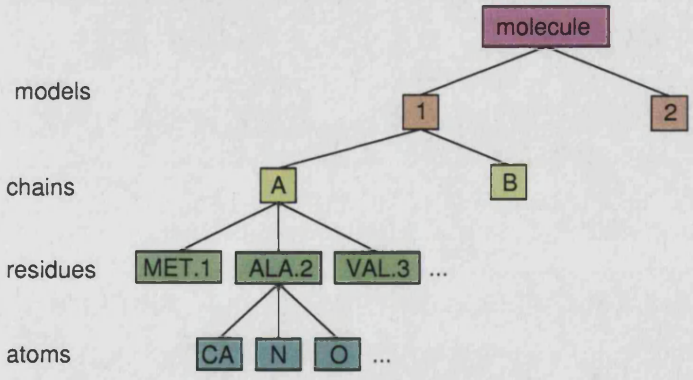

Figure 2.3: Hierarchy of objects which makes up the representation of macromolecular structure

In addition to simply representing the structure itself, the classes in the macromolecular structure module were required to allow the following types of operation:

- **Reading and writing molecular coordinate files**: in order to be able to utilise experimental data, GAMUT needed to have a mechanism for reading macromolecular structures from common file formats. The most widely used is the PDB format; as such, a PDB parser was required.
- **Selection of molecular entities, by identity**: the library should allow clients to perform selections on the molecular tree such as

[5]Throughout this chapter, the term 'monomer' is used interchangably with 'residue', and 'polymer' with 'chain'

  - *select all residues named ALA in chain A*
  - *select all C^{α} atoms except those in glycine residues*

- **Selection of molecular entities, by geometry**: selections should also be possible using geometric criteria, *e.g.*
  - *select all atoms within 4Å of a fixed point, P*
  - *select all residues with at least one atom within 4Å of a fixed point, P*
  - *select all atoms which are within 4Å of a predefined set of atoms, S*
- **Classification of atom or residue types**: the client should be able to specify a scheme for classification of atoms or residues into a number of types. After applying such a classification, it should be possible to easily access all atoms/residues of a particular type, *e.g.* all aliphatic residues.
- **Computation and application of coordinate transforms**: the library should provide the facility for applying coordinate transformations (*i.e.* translations and rigid rotations) to a molecule, or to a subset of its atoms, residues or chains. In addition, it should be able to calculate transformations which perform a least-squares superposition of one set of points (*i.e.* atomic coordinates) onto another.
- **Editing the molecular tree**: clients should be able to edit the molecular tree by adding or removing atoms, residues, chains or models. For example, it should be possible to take a molecule, identify a region of interest (say, a ligand binding site), and then strip away all other parts of the molecule.

2.3.4.3 Chemical structure components

The second module in the bioinformatics layer is concerned with the representation and comparison of chemical structures, primarily their topological connectivity. In order to do this, the chemistry module was designed around a *labelled, undirected graph* data structure in which this information could be easily stored. The primary use of chemical graphs in the library is to serve as *reference structures* against which other graphs may be compared in order to determine the identity of the compound which they represent. In order to perform such a comparison, the ability to derive a chemical graph from the atomic coordinates of a monomer, taken from a crystallographic structure, is required. This allows a dictionary of chemical graphs to be used as a resource for validating the identity of compounds found within, or bound to, protein structures. This process is illustrated schematically in figure 2.4, and is discussed further in chapter 4.

Each vertex in the graph represents an atom, and the following properties were deemed sufficient to describe the characteristics of the atom:

- Atomic number
- Chirality
- Valence
- Number of hydrogens bonded to it
- Formal charge
- Number of 'missing' neighbours
- A string label

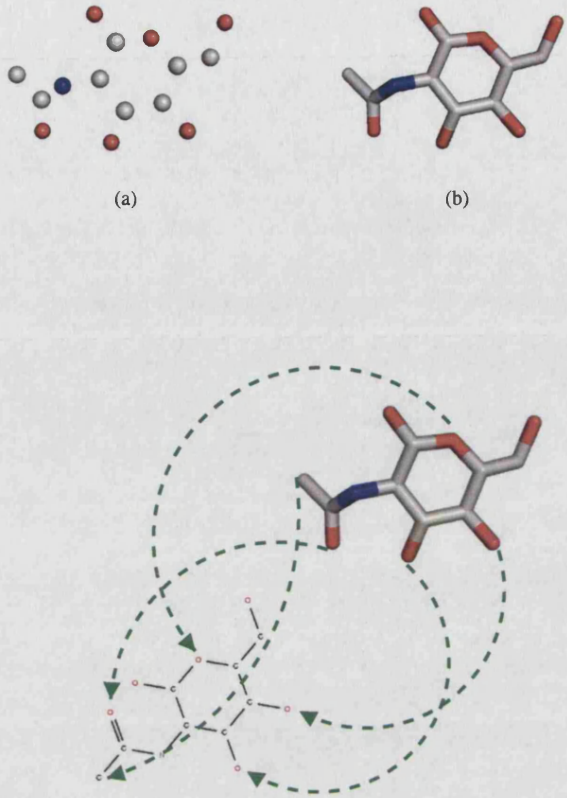

(a) (b)

(c)

Figure 2.4: The process of mapping coordinates of a ligand molecule against a reference compound
The ligand molecule is represented in a crystallographic data file only by its coordinates (a). By referring to a table of standard atomic radii, connectivity information can be added to the molecule (b). This representation of the molecule can then be compared against a reference graph by using a subgraph isomorphism algorithm, thus generating a set of atom-vertex mappings (c).

While the meanings of most of these properties are self-explanatory, the record of missing neighbours should be explained. This field was added in order to better represent molecular fragments. Here, it is desirable to be able to 'mark' the atoms which have incompletely satisfied valence, and which therefore constitute 'attachment points' to which other groups may be bonded. This is illustrated for the case of an adenine moiety in figure 2.5.

In addition to the properties listed above, it was decided that each atom should be optionally associated with a coordinate in 3-dimensional space. This allows the graph object to store energy-minimised coordinates, upon which superpositions can be performed.

Edges in the graph represent chemical bonds; their properties are the type of the bond (single, double, or triple), and an aromaticity flag. Aromatic systems are modelled in GAMUT as alternating single and double bonds, each of which is marked as aromatic.

A system for storing dictionaries of graphs, which may represent idealised conformations of reference compounds, or chemical fragments, was designed using the generic ISAM table component described above.

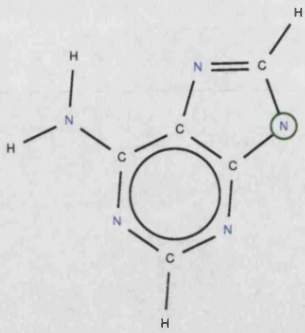

Figure 2.5: Chemical structure diagram showing an adenine fragment
The 'attachment point' at N3 is shown with a green circle.

These dictionaries are named ChemBase archives.

Since the chemical graph class is derived from the generic graph template, any algorithm which is implemented to act on generic graphs, is also applicable to chemical graphs. Therefore, the isomorphism detection and cycle perception algortihms mentioned in §2.3.4.1.2 can be applied to chemical compounds. In addition, a number of algorithms *specifically applicable* to chemical structures were also designed as part of the chemistry component. These were required to do the following:

- **Structure diagram generation**: generation of a 2-dimensional image of a chemical structure, given only the graph object. Note that this layout should not require any 3-dimensional coordinates to begin with; in other words, it should be a true graph layout algorithm rather than an 'unrolling' algorithm such as that utilised in the LIGPLOT program (Wallace *et al.*, 1995).
- **Rotable bond detection**: the ability to identify rotable bonds, allowing compounds to be automatically partitioned into rigid molecular fragments.
- **Torsion angle calculation**: given a rotable bond in a reference graph, facilities for calculating the torsion angle around it.
- **Reading and writing small-molecule structure files**: the ability to parse and write MDL MOL2 files (Dalby *et al.*, 1992).

2.3.4.3.1 Rotable bond detection

For the purposes of the work described in this thesis, rotable bonds are defined as single, acyclic bonds. A ring perception algorithm (see appendix A) had already been implemented, so implementation of the rotable bond detection class was straightforward.

In this thesis, a rotable bond is defined as a bond which

- is single
- is not in a ring
- if broken, yields two fragments consisting of at least two atoms each

The last of these conditions means that only those single, acyclic bonds about which we can *observe* the result of rotation, are considered rotable. For example, neither of the two covalent bonds of a water molecule

are considered rotable, but the carbon-oxygen bond of methanol is.

In order to illustrate the definition of a rotable bond, consider the example shown in figure 2.6. An important point to make regarding the use of rotable bonds in this thesis relates to the effect of hiding hydrogen atoms. Due to the third condition above, certain rotable bonds - specifically, bonds whose rotation does not produce any new conformation of heavy atoms - become non-rotable when hydrogen atoms are neglected. Examples of this type of bond are those to a terminal CH_3, NH_2 or OH group. Since hydrogen atoms are not normally resolved in macromolecular crystal structures, the effect of manipulating these rotors cannot be see in the atomic coordinates.

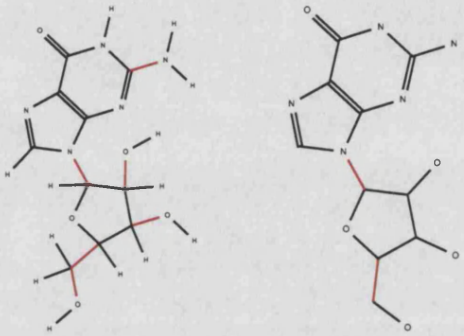

Figure 2.6: Example of the definition of a rotable bond
Rotable bonds are coloured in red. When hydrogens are hidden, several bonds which would previously have been considered rotable, are no longer.

2.3.4.4 *Ligand binding site components*

The chemical structure and macromolecular coordinate components described above provide the basic tools necessary for working with ligands and their binding sites. In order to be able to carry out large-scale surveys of ligand binding across data resources such as the PDB, components for storing information about ligand binding sites were required. In particular, the following three pieces of information about any given ligand should be accessible:

- **Identity**: the location of the ligand molecule in the database; in other words, the identifier of the database entry in which it was found, and the chain and residue codes which uniquely identify the monomer of interest.
- **Reference compound**: the identity of the reference compound to which the coordinate-derived graph was matched.
- **Atom mappings**: mappings from each atom in the ligand as it was found in the PDB, to the corresponding atom of the reference compound.

In addition, we need to store this information in such a way as to enable queries such as the following to be answered:

- *"Find all ligands bound to PDB entry 1xyz"*
- *"Find all ligand molecules called ABC in PDB"*

- *"Find all ligand molecules which matched reference compound graph XYZ"*

As such, three classes were designed: one to store the unique identity of a ligand molecule as it appears in the PDB, one to map PDB atoms onto reference graph vertices, and one to organise this data in an accessible fashion. The latter was designed as an ISAM archive in a similar way to the dictionary of reference graphs.

Further to dealing with the identity of ligand molecules and their correspondance with reference compounds, the ability to conveniently manipulate the atomic coordinates of ligands and their environments was required. In particular, a class which performs the following functions was designed:

- Given the structure of a complete molecule, isolate just the ligand of interest and the residues which constitute its environment, given the ligand identity as described above.
- Compute a transformation which superposes the ligand onto the coordinates of its idealised reference compound.
- Compute a subgraph isomorphism between a part of the ligand molecule and a specified chemical fragment, allowing the calculation of a transformation which superposes just that part of the ligand onto the reference fragment.

2.3.4.5 Density map components

The third part of the bioinformatics layer is concerned with the manipulation of 3-dimensional scalar fields, or density maps. This module is very simple, since a density map is essentially a scalar field. The only added functionality over the generic scalar field classes is the ability to read and write CCP4 format (Collaborative Computational Project Number 4, 1994) density map files, which allow GAMUT density maps to be visualised using standard molecular graphics programs.

2.4 Documentation

A key requirement in library design is that the interface should be well documented. Ideally, the documentation should be *stratified*, providing several views of the system with varying levels of detail, in order to cater for users with different levels of expertise. In other words, a programmer with a basic working knowledge of both the language and the problem domain should be able to quickly build simple applications, by making use of example code and tutorials. On the other hand, developers with in-depth understanding of the language should be able to access detailed information on the structure of the library, while those with expertise in the methods utilised in the library may wish to know algorithmic details.

An accessible documentation system is provided, primarily in the form of web pages (see figure 2.7. These have largely been generated using the Doxygen documentation system (van Heesch, 1997), which processes a list of annotated source code files to generate a set of hyperlinked HTML pages, UNIX manual pages or LaTeX documents.

The on-line documentation contains the following sections:

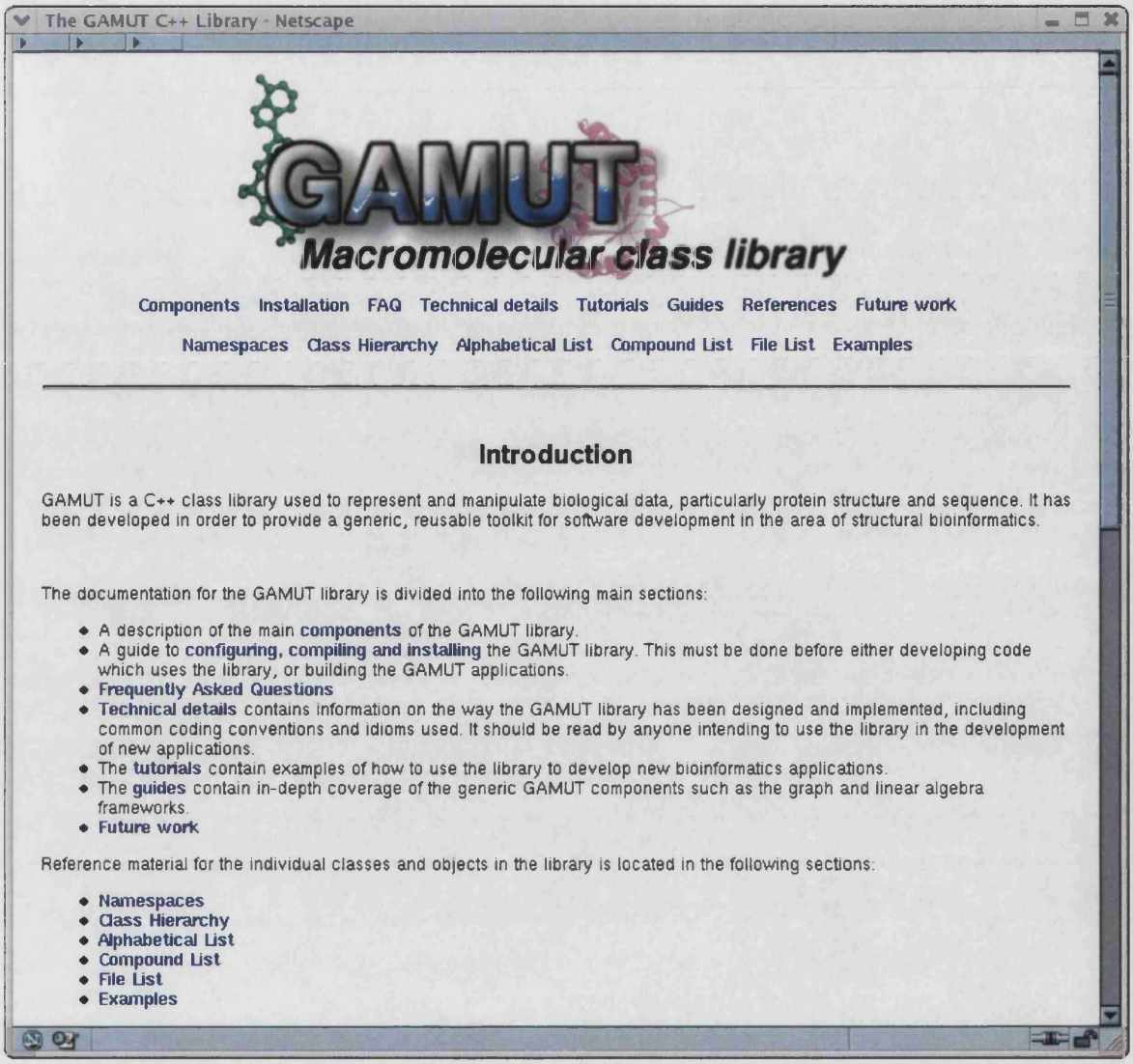

Figure 2.7: A screenshot of the on-line GAMUT documentation

2.4.1 Installation guide

As mentioned previously, the GAMUT configuration and installation system is based upon commonly-used UNIX tools. This means that the installation instructions for the package can afford to be fairly brief; nonetheless, the documentation contains guidance on how best to configure the package for a given system, and how to control which parts of the library are enabled. In addition, instructions are given on how to link GAMUT to third-party libraries, such as the Oracle^{TM} client libraries, which are used in order to allow GAMUT applications to query the MSD.

2.4.2 Tutorials

The bioinformatics-related components of GAMUT are each introduced in a tutorial: for example, in a tutorial for the macromolecular structure module, examples are presented which show how to read a structure from a PDB file, perform queries and transformations upon it, and how to export the data in various file formats. Similar tutorials are provided for using the chemistry, density map, ligand, domains and sequences

components.

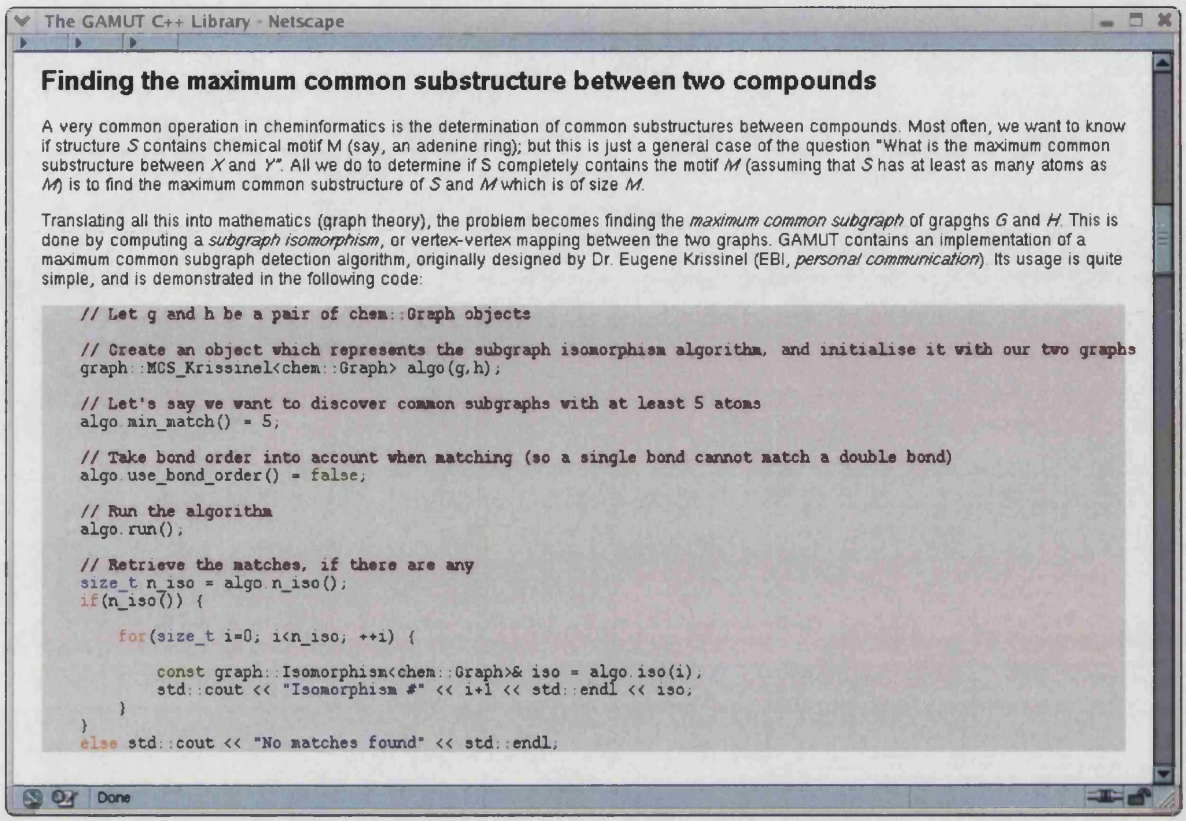

Figure 2.8: Screenshot of part of an on-line GAMUT tutorial

In addition to the tutorials, technical guides are available, which describe in more detail the structure of the generic library components such as the graph, tree, vector and matrix data structures.

2.4.3 API reference

The bulk of the GAMUT documentation consists of a complete reference guide for tha GAMUT Application Programming Interface (API) . For every class in the library, there is a page containing the following:

- A brief description of the role of the class
- A collaboration diagram illustrating the relationship between this and other classes. This is hyperlinked, so that the user can browse around the class hierarchy of the library. A portion of the global class hierarchy diagram is shown in figure 2.9.
- A list of all member functions, including full function signatures and explanation of the usage of the function (see figure 2.10).
- For certain classes, links to example code which demonstrates their use are included

2.5 Summary

The development of a new object-oriented software library for structural bioinformatics has been motivated by outlining the requirements not only of the research project described in this thesis, but of structural

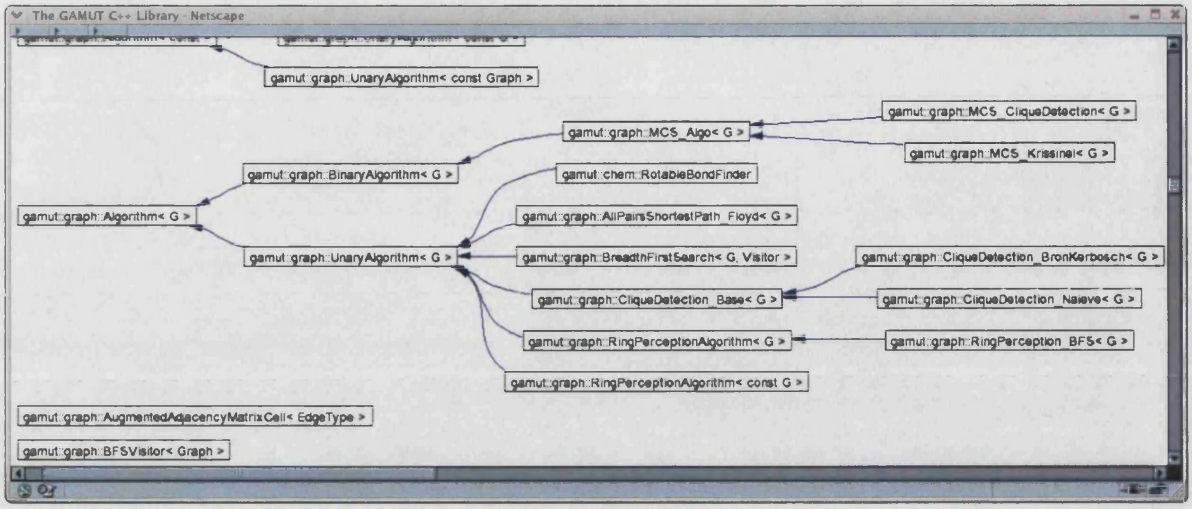

Figure 2.9: The graphical class hierarchy diagram

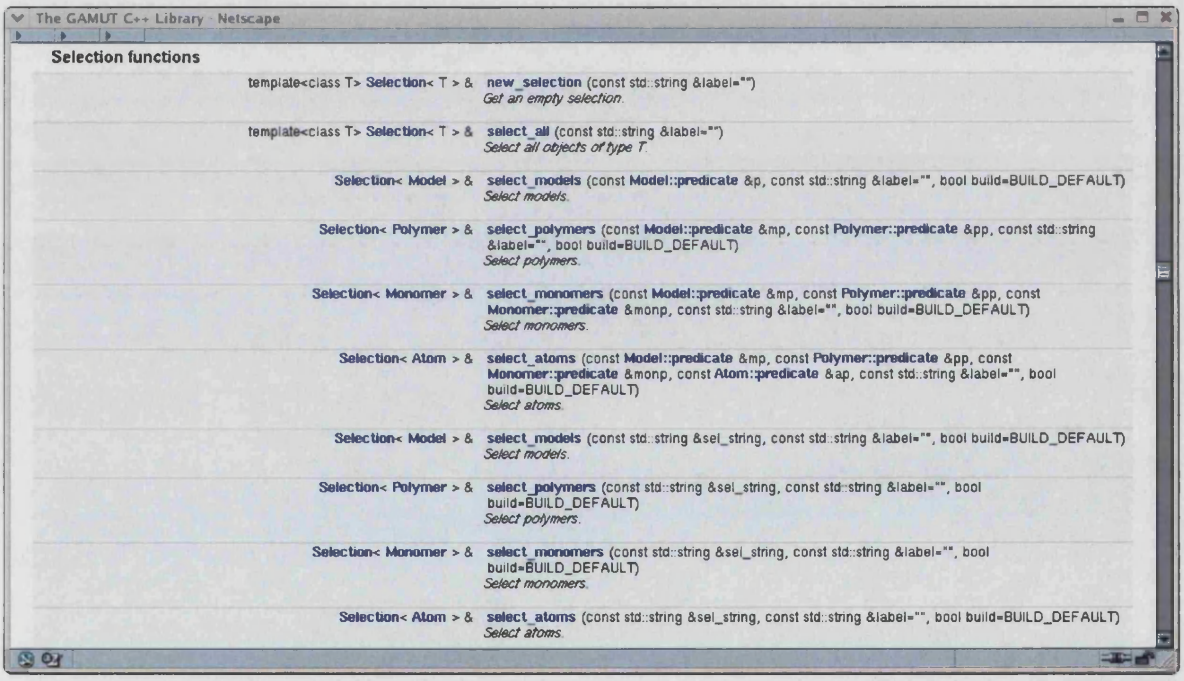

Figure 2.10: Summary of member functions in on-line documentation

bioinformatics applications in general. The design and implementation of the library has been covered in some depth. In the following chapter, the theoretical background of a number of algorithms and methods implemented in GAMUT is discussed. Specific application programs built using GAMUT are discussed in later chapters, where they have been used to perform various analyses.

Chapter 3

Methods

This chapter contains details of the main methods used in the analysis presented subsequently. This discussion will be from a fairly abstract perspective, which is to say that the focus will be upon explaining the theoretical background to each group of methods, and where applicable, examining the advantages and disadvantages of different approaches to a problem. The following chapter will build upon this one by discussing how the methods outlined here were used to construct a pipeline for the generation and analysis of datasets of ligand binding sites. As such, all details of the implementation of the methods are deferred to the following chapter.

3.1 Graph matching

Many problems in bioinformatics can be formulated in terms of graph theory[1], with a common requirement being to compare pairs of graphs in order to determine the degree of similarity between them. Graph matching techniques have been applied to a fairly diverse range of problems in computational biology and chemistry, including automatic chemical reaction mechanism generation (Ratkiewicz and Truong, 2003), chemical database searching (Raymond and Willet, 2002), protein-protein docking (Gardiner *et al.*, 2000), and protein structure comparison (Krissinel and Henrick, 2004b). These, along with numerous other applications, serve to illustrate the power of this particular abstraction.

Graph matching techniques aim to discover subgraph isomorphisms between pairs of graphs. Three types of isomorphism which will be referred to here, are illustrated in 3.1. Isomorphism detection algorithms can typically be broken down into two stages:

1 Determine all pairs of vertices from the two input graphs which may be matched

2 Starting with one such pair of compatible vertices, build up the isomorphism by adding new pairs, checking at each stage that the relationship of the first vertex to the first subgraph is equivalent to the relationship of the second vertex to the second graph

The following sections elaborate on these two steps, and provide several illustrative examples.

[1]Readers unfamiliar with graph theory are referred to appendix A, in which some fundamental concepts are outlined.

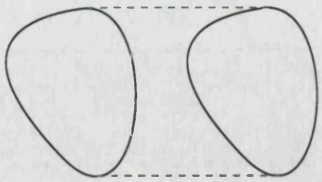

(a) A full graph isomorphism

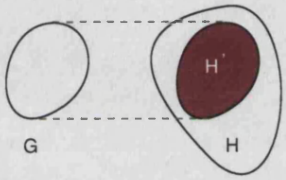

(b) An exact subgraph isomorphism

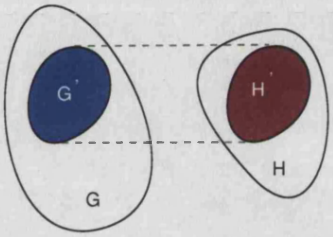

(c) A common subgraph isomorphism

Figure 3.1: Types of graph isomorphism

3.1.1 Vertex and edge compatibility

Before considering the details of graph matching methods, it is necessary to introduce the concept of vertex and edge *compatibility functions*. Graph matching algorithms need to test whether particular pairs of vertices or edges from the two input graphs may potentially be matched in the resulting isomorphism. This is done according to predefined criteria for vertex/edge compatibility. For example, when matching graphs representing chemical structures, the criteria for vertex matching may be that the vertex labels representing atomic number are identical. Alternatively, atoms may be labelled with additional information such as chirality; in this case, the vertex compatibility function can be modified in order to take into account this information during matching.

The boolean functions μ and ν will be used henceforth to represent the vertex and edge compatibility functions respectively. It should be noted here that the function ν by convention matches the *absence* of an edge with any other absent edge. The importance of this will become apparent in the discussion of the construction of association graphs which follows.

Using these functions, our working definition of a common subgraph isomorphism can be stated as follows: For graphs $G = (V,E)$ and $H = (W,F)$ [2], a subgraph ismorphism of size k is defined as $I \subset V \times W$, where X and Y are enumerations of a subset of vertices in V and W respectively, satisfying

$$\mu(v_{x_i}, w_{y_i}) \wedge \nu(e_{x_i x_j}, f_{y_i y_j}) \;\; \forall\, i,j = 1,\ldots,k. \tag{3.1}$$

The problem of finding common subgraphs can be reformulated as that of finding the enumerations $X = \{x_i\}_{i=1}^{k}$ and $Y = \{y_i\}_{i=1}^{k}$ which satisfy 3.1.

[2] As described in appendix A, $G = (V,E)$ indicates that a graph G is defined as a pair of finite sets: the vertices, V, and the edges, E. E is a binary relation on V.

3.1.2 Available methods

The problem of determining the Maximum Common Subgraph (MCS) between two or more graphs is known to be NP-complete (Garey and Johnson, 1979). That is, no algorithm is known which can guarantee to find the MCS between any pair of graphs in polynomial time. The two pre-eminent solutions to the problem are the clique-detection approach, and the backtracking search.

3.1.2.1 Clique detection

Common Subgraph Isomorphism (CSI) discovery by clique detection (Bron and Kerbosch, 1973) is carried out by first constructing an *association graph* A between the input graphs G and H. For every pair of vertices $(v,w) : v \in V, w \in W$, for which $\mu(v,w)$ is true, a vertex a is added to the association graph. Once this process is complete, every pair of vertices $(a,a') \in A$ is checked for edge compatibility. Specifically, if there exist a pair of edges $e = (v,v') \in E$ and $f = (w,w') \in F$ such that $\nu(e,f)$ is true, then an edge $b = (a,a')$ is added to A. It can easily be seen that a clique in A corresponds bijectively[3] to an isomorphism between G and H, and therefore that determination of the largest clique in the association graph leads to the definition of the MCS between the input graphs.

As a simple example, consider the two graphs in figure 3.2. The association graph formed by comparing these graphs is shown in figure 3.3a, and the cliques within it are shown in figure 3.3b. The equivalence between the two largest cliques in the association graph, and the largest isomorphisms between the input graphs, is clear.

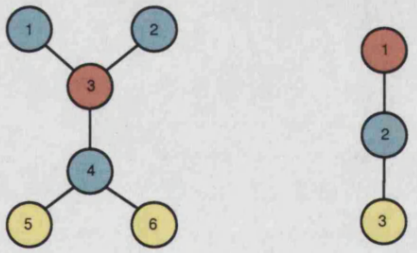

(a) G (b) H

Figure 3.2: Example graphs
The colours represent the vertex properties; numbers are simply indices which are used to refer to each vertex.

3.1.2.2 Backtracking search

The Bron-Kerbosch algorithm is the most efficient available for CSI detection, with a worst-case complexity of $O((mn)^m)$, where n and m are the numbers of vertices in the input graphs ($m \leq n$). When an Exact Subgraph Isomorphism (ESI) is sought, a more efficient algorithm is the backtracking search method (Ullman, 1976).

[3]Formally, a mapping which is both *injective*, *i.e.* one-to-one, and *surjective*. A surjective (or 'onto') mapping is one in which all members of the target set are mapped to.

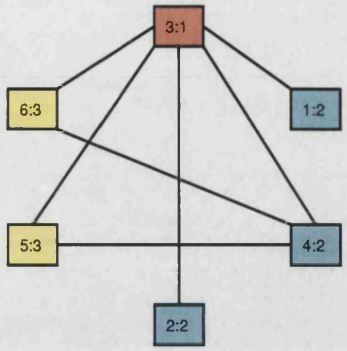

(a) Association graph formed from the example graphs in figure 3.2. Pairs of indices refer to the corresponding vertices of G and H respectively.

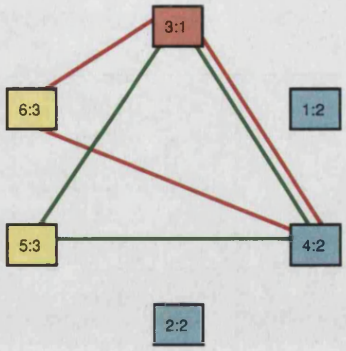

(b) The two 3-vertex cliques in the association graph

Figure 3.3: Graph matching by clique detection
Each clique in the association graph corresponds to an isomorphism between the original two graphs. The two 3-vertex isomorphisms are therefore $\{(3,1),(4,2),(6,3)\}$ and $\{(3,1),(4,2),(5,3)\}$

3.1.2.2.1 Ullman's method

The backtracking search method begins by identifying a single vertex-vertex mapping,

$$v_1 \mapsto w_1 : \mu(v_1, w_1)$$

The algorithm then proceeds by extending the mapping by adding another pair of vertices such that the resulting match still describes a valid isomorphism according to equation 3.1. Given an existing isomorphism consisting of i matched vertex pairs

$$I = \{(v_1, w_1) \cdots (v_i, w_i)\}$$

the match can be extended by mapping $v_{i+1} \mapsto w_{x_{i+1}}$ if the following conditions are satisfied:

$$\mu(v_{i+1}, w_{i+1}) \tag{3.2}$$

$$\forall k \leq i \; e = (v_k, v_{i+1}) \in E \iff f = (w_k, w_{i+1}) \in F \wedge \mathrm{v}(e, f) \tag{3.3}$$

Condition 3.2 merely requires that the new vertex pair satisfy the vertex compatibility function; condition 3.3 stipulates that, for every edge incident on the newly mapped vertex from graph G, there must be a corresponding edge incident on the mapped vertex from H, satisfying the edge compatibility constraint.

Once the mapping I contains m pairs of vertices, the exact subgraph isomorphism has been determined and the algorithm stops. If, on the other hand, the vertex v_i cannot be mapped onto any vertex w_i, the algorithm backtracks by matching the last mapped vertex v_{i-1} onto a vertex from H which has not yet been tried. The progression of Ullman's algorithm applied to the example graphs of figure 3.2 is shown in figure 3.4.

The algorithm described thus far is capable of detecting the exact subgraph isomorphism, but a further optimisation, known as the 'forward checking' procedure, is described in Ullman (1976). The idea is that, for

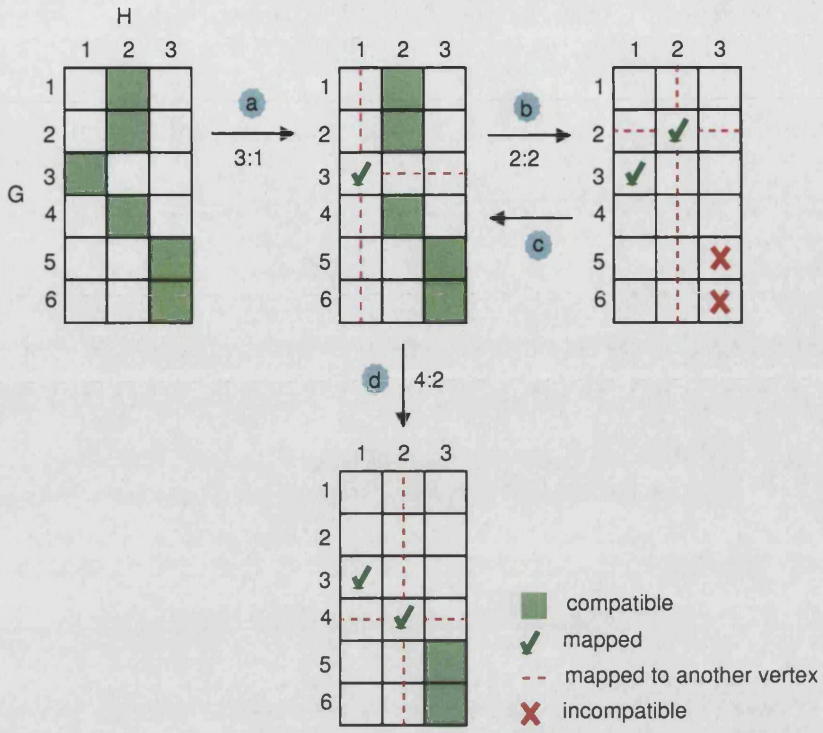

Figure 3.4: Progression of Ullman's algorithm

Diagrammatic representation of the progression of Ullman's algorithm on the example graphs shown in figure 3.2. The algorithm is initiated by identifying all pairs of compatible vertices, shown as green cells in the matrix. (a) vertex G3 is mapped to H1. (b) vertex G2 is mapped to H2. All other mappings to H2 are thus rendered incompatible, as shown by the dotted red lines. Mappings 5:3 and 6:3 are determined incompatible by the forward checking procedure, since H3 is a neighbour of H2, but neither G5 nor G6 are adjacent to H2. (c) no further mappings can be made, so the algorithm backtracks. (d) G4 is mapped to G2. The two ESIs can now be found by mapping either G5 or G6 to H2.

each mapping $v_i \mapsto w_i$, a check is made to see whether there exists at least one mapping for each remaining vertex $v_j : j = i+1, \ldots, m$ which satisfies equation 3.1. If the forward checking fails, the algorithm backtracks immediately, thus eliminating the exploration of unproductive branches of the search tree. This is exemplified by step (c) of figure 3.4.

Ullman's method is described formally in algorithm 3.1. In this version of the algorithm, the conditions of subgraph isomorphism are tested in the 'forward checking' procedure, and are stored in an $m \times n$ binary matrix (**P**), which records whether the i^{th} and j^{th} vertices of G and H respectively are still compatible at each stage of the search.

It can be shown that the worst-case complexity of Ullman's algorithm is $O(m^n n^2)$. However, this only occurs in practice when graphs with high degrees of connectivity and redundancy of labels are used as the input. Chemical graphs have low connectivity, and only moderate label redundancy; as such, the Ullman algorithm tends to exhibit good performance for the purposes for which it has been used in this thesis.

3.1.2.2.2 Krissinel's improved backtracking search

The Ullman algorithm described here searches for *exact subgraph isomorphisms*, with search branches potentially leading to common subgraph ismorphisms being discarded by the forward checking routine. Recently, improvements to the Ullman method have been described which allow searching for common

Main function of the algorithm, called with input graphs G and H
Function ULLMAN($G=(V,E), H=(W,F)$) :
  $m \leftarrow |V|, n \leftarrow |W|$
  assert $m \leq n$

  Initialise the vertex matching candidate matrix $\mathbf{P}$
  $\mathbf{P}=(p_{ij}) : p_{ij} = \begin{cases} 1 & \text{if } \mu(v_i,w_j) \\ 0 & \text{otherwise} \end{cases} \quad \forall\, i=1,\ldots,m; j=1,\ldots,n$

  Initialise set of matched vertex indices to empty
  $I \leftarrow \emptyset$

  Start the recursive part
  BACKTRACK($\mathbf{P}, I$)

Recursive part of the algorithm
$\mathbf{P}$ *is the current vertex mapping candidate matrix; I contains the current match*
Function BACKTRACK($\mathbf{P}, m, I$) :

  $i \leftarrow |I|$
  if $i \geq m$ **then**
    An exact subgraph has been detected - return it
    return (I)

  for each $j=1,\ldots,n$:
    if $\mathbf{P}_{ij}=1$ **then**

      Add the newly matched pair of vertices to the isomorphism
      $I \leftarrow I \cup (v_i,w_j)$

      Update the candidate matrix
      $\mathbf{P}' \leftarrow P, \quad p'_{kj}=0 \;\forall\; k>i$
      if FORWARDCHECK($\mathbf{P}', i, m, n, I$) = true **then**
        BACKTRACK($\mathbf{P}', I$)

      Remove the pair of vertices which failed to match
      $I \leftarrow I - \{(v_i,w_j)\}$

  No match was found - return an empty isomorphism

  return ($\emptyset$)

Function which checks whether a match can potentially be extended
Function FORWARDCHECK($\mathbf{P}, i, m, n, I$) :
  for each $k=i+1,\ldots,n, l=1,\ldots,m$:
    if $p_{kl}=1$ **then**
      for each $(v,w) \in I$:
        if $\nu(e=(v_k,v), f=(w_l,w))$ = false **then**
          $p_{kl} \leftarrow 0$

  Check whether each remaining vertex $v_j : j=i+1,\ldots,n$ *has at least one mapping to H*
  for each $k=i+1,\ldots,n$:
    for each $l=1,\ldots,m$:
      if $p_{kl}=1$ **then**
        Found a mapping for v_k*; go to next vertex*
        next k
    v_k *has no potential mappings - forward checking failed*

    return false

Algorithm 3.1: Ullman's backtracking search algorithm for exact subgraph isomorphism detection

subgraph ismorphisms, and which also improve the performance of the algorithm (Krissinel and Henrick, 2004a).

The ability to detect common subgraph isomorphisms, as opposed to exact subgraph isomorphisms, is easily achieved simply by altering the number of potential mappings which we require to be identified at the forward checking stage. Whereas the original Ullman method requires *all* unmapped vertices from G to have at least one potential mapping to a vertex in H, the Krissinel method simply requires that the maximum achievable match at any point is at least equal to a minimum match parameter, n_0 (and is greater than the largest isomorphism yet found). Varying n_0 allows the user to specify the minimum size of match which is considered to be meaningful in any particular problem. Branches which cannot lead to a match of at least n_0 vertices are not explored.

The Krissinel algorithm achieves performance improvements over the Ullman method via several modifications. The first is to represent the potential vertex mappings, contained in the matrix $\mathbf{P}$ in the original algorithm, using a representation which is more efficient given the frequently sparse nature of P. The Krissinel Vertex Mapping Matrix (VMM) consists of a matrix $\mathbf{M}$ and a vector L. $\mathbf{M}_{ij}$ gives the index of the vertex in H which is mappable onto v_i from G, $j = 1,\ldots,L_i$; L stores the length of each row of $\mathbf{M}$ (*i.e.* the number of vertices mappable onto each vertex of G). This representation reduces the time required to obtain the list of vertices mappable onto v_i when extending the match.

In the example shown previously, each vertex in graph G maps to only one potential candidate in H, so the initial states of $\mathbf{M}$ and L are

$$\mathbf{M} = \begin{pmatrix} 2 & \cdots \\ 2 & \cdots \\ 1 & \cdots \\ 2 & \cdots \\ 3 & \cdots \\ 3 & \cdots \end{pmatrix}, \quad L = (1\,1\,1\,1\,1\,1)$$

In addition, Krissinel *et al.* show that the selection of the next vertex from G to be added to the match, has an impact on performance. Specifically, picking the vertex which has the *fewest* number of potential mappings reduces the runtime of the algorithm to the extent that, on the type of graphs used in their study, it outperforms both the clique detection approach for CSI detection and the original backtracking search for finding ESIs.

	Match metric	Condition	Minimum n_T	Maximum n_T	Minimum match size
1	Tanimoto coefficient	$\tau \geq \tau_{min}$	$\sqrt{\tau_{min}}.n_Q$	$\frac{n_Q}{\sqrt{\tau_{min}}}$	$\sqrt{\frac{\tau_{min}}{1+\tau_{min}}.(n_Q^2+n_T^2)}$
2	Percentage match	$\rho \geq \rho_{min}$	$\rho_{min}.n_Q$	$\frac{n_Q}{\rho_{min}}$	$\rho_{min}.\max(n_Q,n_T)$
3	Mismatch of smaller graph	$\mu_{smaller} \leq \mu_{max}$	1	∞	$\max(1,\min(n_Q,n_T)-\mu_{max})$
4	Mismatch of query graph	$\mu_{query} \leq \mu_{max}$	$\max(1,n_Q-\mu_{max})$	∞	$n_Q-\mu_{max}$
5	Mismatch of larger graph	$\mu_{larger} \leq \mu_{max}$	$\max(1,n_Q-\mu_{max})$	$n_Q+\mu_{max}$	$\max(1,\max(n_Q,n_T)-\mu_{max})$
6	Mismatch of target graph	$\mu_{target} \leq \mu_{max}$	$\max(1,n_Q-\mu_{max})$	$n_Q+\mu_{max}$	$n_T-\mu_{max}$

Table 3.1: Range of target graph sizes which can potentially provide a sufficiently good match
In each expression, n_Q is the size of the query graph, and n_T the size of the target graph. The sizes of the smallest and largest target graphs which can potentially provide a match which satisfies the condition are shown. In practice, the maximum value of n_T for metrics 3 and 4 is the size of the largest target graph in the database. The last column shows the size of the smallest match between the target and a given query graph, which would satisfy the condition.

3.1.3 Match size metrics

When using graph matching methods to identify those members of a database of graphs which exhibit some degree of similarity to a query graph, it is necessary to define a similarity metric. That is, a function which, given the maximum common subgraph isomorphism between a pair of graphs, calculates a scalar value indicating their degree of mutual (dis)similarity.

The following simple functions (where l stands for the number of vertices matched; m and n are the sizes of the two graphs), are commonly used for this purpose:

1 **Tanimoto (or Jaccard) coefficient**. This is a score between 0 and 1, where 1 indicates identity, and 0 indicates no similarity.

$$\tau = \frac{l^2}{m^2 + n^2 - l^2}$$

2 **Percentage identity**. This is also bounded by $[0,1]$.

$$\rho = \frac{l}{\max(m,n)}$$

3 **Mismatch**. The number of vertices from either the smaller or larger of the two graphs, which are not included in the match, may be used as a dissimilarity measure. This obviously has the disadvantage that the size of only one graph is taken into account in the metric.

$$\mu_{smaller} = \min(m,n) - l \mu_{larger} = \max(m,n) - l$$

Alternatively, we may require that the number of mismatched with respect to either the query or target graphs, regardless of which is the smaller, is below a specified threshold.

Any of these metrics may be used as the basis for a condition for accepting or rejecting a match, for example, only matches for which $\tau \geq 0.75$ may be of interest. Given a particular query graph G_Q, it is then possible to compute the range of target graph sizes which could potentially provide a sufficiently good match. These ranges are shown, for each of the match metrics outlined above, in table 3.1. Any target graph whose size falls outside this range can then be immediately excluded from the search, thereby improving its efficiency.

3.2 Clustering

Cluster analysis is concerned with inspecting a set of data to determine whether it contains any underlying structure, in the form of groupings into distinct subsets. Formally, we wish to partition an initial data set of n objects, X, into m clusters C, such that each member of X belongs to exactly one cluster, and so that the union of all clusters is equal to the original set:

$$X = \{x_1, x_2, \ldots, x_n\}$$

$$C = \{c_1, c_2, \ldots, c_m\} \text{ where } c_i \subset X \text{ and } c_i \cap c_j = \emptyset \forall i, j = \{1, \ldots, m\}$$

$$c_1 \cup c_2 \cup \cdots \cup c_m = X$$

The choice of the value m is often not straightforward, and is discussed further below. The use of any clustering method tends to involve several compromises.

3.2.1 Dissimilarity matrices, measures and metrics

The input to most clustering algorithms is a distance matrix $\mathbf{D}$, where the element d_{ij} expressed a measure of the dissimilarity between objects x_i and x_j in the original set. The procedure used to calculate $\mathbf{D}$ from X varies depending on the type of objects being clustered. If the elements of X are vectors of real numbers, for example, the familiar Euclidean distance is often used to populate the dissimilarity matrix:

$$d_{ij} = \sqrt{\sum_{k=1}^{p} (x_{ik} - x_{jk})^2} \quad \text{where } \mathbf{x}_i, \mathbf{x}_j \in \mathbb{R}^p$$

In most cases, the distance measure is required to be a *metric*. A metric d on X is a mapping, $d(x,y) \mapsto \mathbb{R}$, which must satisfy the following conditions for all $x, y, z \in X$:

- **Non-negativity**: $d(x,y) \geq 0$
- **Symmetry**: $d(x,y) = d(y,x)$
- **Triangle inequality**: $d(x,y) \leq d(x,z) + d(y,z)$
- **Reflexivity**: $d(x,x) = 0$

3.2.2 Hierarchical clustering techniques

In hierarchical clustering approaches, a series of consecutive partitions is applied to the data set. These partitions are typically represented in the form of a dendrogram or tree diagram[4]. In order to obtain distinct groupings, a threshold must be specified, the value of which corresponds to physically 'cutting' the dendrogram at that height (see figure 3.5).

Hierarchical clustering methods may be divided into two classes of iterative procedures: agglomerative and divisive.

3.2.2.1 Agglomerative algorithms

As the name suggests, agglomerative algorithms start with n distinct groups, each containing one data point. Each iteration involves fusing a pair of groups, with the end of the process being reached when all data points are in a single group. At each stage of this process, the algorithm must therefore determine which pair of groups are 'closest' to one another; the definition of this inter-group distance is the main

[4]Technically, a rooted, terminally-labelled, weighted tree.

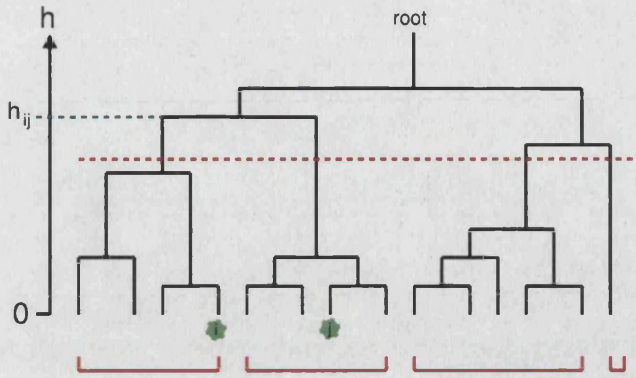

Figure 3.5: An example clustering dendrogram
The value of h corresponding to a chosen pair of data points (i, j) is represented by the height at which the branches of i and j first join. The red dotted line shows an arbitrarily chosen tree cutting threshold; the clusters which would result from this cut are indicated with red braces.

distinguishing characteristic of different agglomerative methods. Common methods are summarised in table 3.2 and illustrated in figure 3.6. When a pair of groups is chosen for fusion, the distance describing their separation is stored, and it is this distance which is represented in the dendrogram as the height of the node which corresponds to the fusion event.

Method	**Definition of the distance between two clusters c_i and c_j**
Single linkage	The minimum distance among pairs consisting of one data point from c_i and one from c_j
Complete linkage	The maximum distance among pairs consisting of one data point from c_i and one from c_j
Group-average	The average of all distances among pairs consisting of one data point from c_i and one from c_j
Centroid	Distance between the centroids of c_i and c_j
Ward's	The increase in the sum of squared distances which would be brought about by the fusion of c_i and c_j

Table 3.2: Agglomerative clustering methods

3.2.2.2 Divisive algorithms

Beginning with a group containing all of the data points, each step of a divisive clustering algorithm involves dividing an existing group into two. As such, two decisions must be made: which cluster to divide, and how best to perform that division. Such algorithms are much more rarely used than agglomerative methods, chiefly because finding the optimal division of a set is computationally demanding. They are not considered further here.

3.2.3 Problems with hierarchical clustering

No clustering method is perfect; indeed some have conspicuous flaws. The simplest hierarchical clustering method, single linkage clustering, is well known to suffer from the problem of *chaining*; that is, the tendency to cluster together, at a relatively low level, groups which are linked by a series of isolated intermediates.

This makes it unsuitable in many cases. Often, methods such as complete linkage are preferred, as they result in compact, globular clusters which agree more closely with our intuitive notion of how the data should be grouped.

Despite the practical problems resulting from its application, single linkage clustering is held by some to be the method with the greatest mathematical appeal. Let us denote the height of the node at which data points i and j join the same cluster with h_{ij}. This value is not the same as the dissimilarity d_{ij} between these two points. The heights are clearly symmetric, and obey the relation

$$h_{ij} \leq \max(h_{ik}\ ,\ h_{jk})$$

which is known as the *ultrametric inequality*. Even if the distance measure is a metric, the metric inequality shown in §3.2.1 is clearly a weaker condition than the ultrametric inequality. The clustering operation therefore can be viewed as a transformation which imposes a constraint that was not satisfied by the original data. It has been shown that, if we require certain properties of a clustering method, including that it should be continuous, single linkage clustering is the only method which satisfies the conditions (Jardine and Sibson, 1971). On the basis of empirical studies which compare the clusters returned by various clustering methods to previously known structure in the data, however, other authors have recommended almost every known method. The conclusion to be drawn is that no one method is ultimately superior; the choice of which to use should be made in the light of each particular problem.

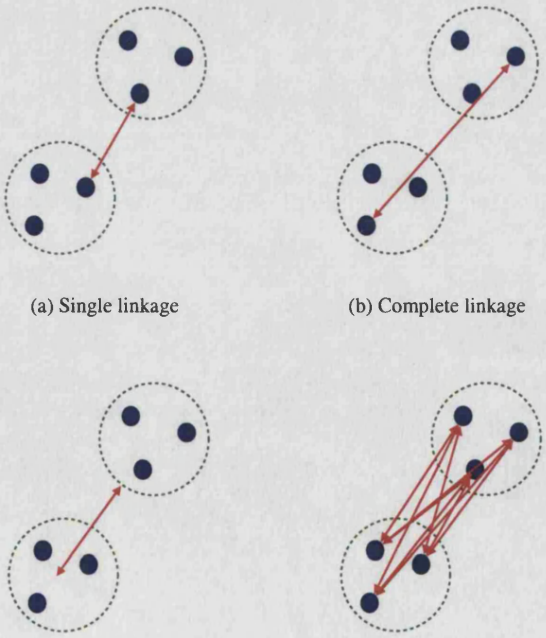

(a) Single linkage (b) Complete linkage

(c) Centroid (d) Group average

Figure 3.6: Agglomerative clustering methods
For each method, the method of calculating inter-cluster distance is illustrated with an arrow. For (d), the distance value is the average of all the arrow lengths.

3.2.4 Validation

A key problem when using clustering is that it is often unclear whether the results obtained by using any one method truly represents any underlying structure in the data. After all, even randomly generated input data will result in a clustering hierarchy - so how does one know if structure has been discovered in, or imposed upon a data set? One way is to try to assess the degree of distortion caused by the clustering method, by comparing the dendrogram heights to the original dissimilarity matrix. This can be done by computing the cophenetic correlation coefficient, which is the product-moment correlation coefficient between the lower half of the distance matrix and the corresponding terms in the cophenetic matrix, **H**, which contains the heights at which each pair of data points first occur in the same cluster:

$$r^2 = \frac{ss_{dh}^2}{ss_{dd}ss_{hh}} = \frac{[\sum_{ij}(d_{ij}-\bar{d})(h_{ij}-\bar{h})]^2}{\sum_{ij}(d_{ij}-\bar{d})^2\sum_{ij}(h_{ij}-\bar{h})^2}$$

This leaves us with the problem of deciding upon a threshold for r above which the dendrogram is deemed to represent the data set with sufficient accuracy. Various values from 0.8 upwards have been suggested (Romesburg, 1984).

More empirical methods for validating clustering results draw on the idea that a clustering solution should be stable. In order to test this, error terms are added to the dissimilarity matrix, or subsets of the original data are excluded (Lanyon, 1985). Comparing the dendrogram thus obtained can provide an indication of the quality of the solution. An example of this type of approach is the bootstrap (Felsenstein, 1985), a non-parametric resampling approach.

3.2.5 Stopping criteria

Assuming that it is valid, the dendrogram in itself provides a valuable insight into the structure of the data set. Sometimes, however, obtaining the tree is only an intermediate step towards dividing the objects into discrete clusters. In order to produce clusters, a threshold height must be specified, as mentioned previously; equivalently, this value may be used as a *stopping criterion* during the agglomeration procedure. As mentioned previously, the choice of this value is not trivial.

Qualitatively, inspection of the dendrogram for large changes in height can indicate a sensible value for the 'best' partition. Several attempts have been made to formalise this decision. One such study suggests that the cut should be made at $\bar{h} + k\sigma_h$, where k is a constant in the range (2.75,3.50) (Mojena, 1977); other approaches are reviewed in (Milligan and Cooper, 1985).

In summary, clustering methods should be applied with care, and their results interpreted while bearing in mind the caveats discussed above.

3.3 Analysis of multidimensional data sets

Much of bioinformatics involves analysing large sets of data, in order to discern relationships between individual objects and patterns shared within subgroups of the data set. Of particular relevance to this work are methods for reducing the dimensionality of a data set.

3.3.1 Principal components analysis

Principal Components Analysis (PCA) (Pearson, 1901) is a method for transforming a set of correlated variables $X_1, X_2, \ldots, X_n$, to m uncorrelated variables $Y_1, Y_2, \ldots, Y_m$, where $m \leq n$ and the variables Y are in decreasing order of their variances.

The result of PCA is a set of linear functions of the original variables, of the form

$$Y_i = e_{1i}X_1 + e_{2i}X_2 + \cdots + e_{ni}X_n$$

with

$$e_{1i}^2 + e_{2i}^2 + \cdots + e_{ni}^2 = 1 \forall i = 1, \ldots n$$

The variances of each of the principal components are denoted $\lambda_1, \lambda_2, \ldots, \lambda_n$, where $\lambda_1 \geq \cdots \geq \lambda_n$.

PCA is carried out by first solving the characteristic equation

$$|\mathbf{S} - \lambda\mathbf{I}| = 0 \tag{3.4}$$

where $\mathbf{S}$ is the sample variance-covariance matrix

$$\mathbf{S} = \begin{pmatrix} \sigma_{X_1}^2 & cov_{X_1X_2} & \cdots & cov_{X_1X_n} \\ cov_{X_1X_2} & \sigma_{X_2}^2 & \cdots & cov_{X_2X_n} \\ \vdots & \vdots & & \vdots \\ cov_{X_1X_n} & cov_{X2_Xn} & \cdots & \sigma_{X_n}^2 \end{pmatrix} \tag{3.5}$$

$$\sigma_X^2 = \frac{1}{n}\sum_{k=1}^{n}(x_k - \bar{x})^2$$

$$cov_{X_iX_j} = \frac{1}{n}\sum_{k=1}^{n}(x_{i_k} - \bar{x_i})(x_{j_k} - \bar{x_j})$$

Note that, in most cases, the input data is standardised before application of PCA, *i.e.* each variable is transformed by subtracting its mean and dividing by its standard deviation. This is in order to prevent the variables with the largest variances from dominating the analysis. If this is the case, $\mathbf{S}$ is replaced with the correlation matrix,

$$\mathbf{S}_{ij} = \frac{1}{n}\sum_{k=1}^{n} x_{ik}x_{jk} \tag{3.6}$$

Since $\mathbf{S}$ must be real and symmetric, the eigenvectors $e_1, \ldots, e_n$ and eigenvalues $\lambda_1, \ldots, \lambda_n$ can be obtained

using diagonalisation. Once the eigenvectors have been obtained, we choose a number m of the original principal components which will be retained (see §3.3.3). Let us define a matrix $\mathbf{E}$ whose columns are the eigenvectors resulting from the solution of equation 3.4

$$\mathbf{E} = \begin{pmatrix} \mathbf{e}_1^T & \mathbf{e}_2^T & \cdots & \mathbf{e}_n^T \end{pmatrix}$$

Now let $\mathbf{F}$ be an $n \times m$ matrix containing the first m rows of $\mathbf{E}$. Given a set of p points in the original n-dimensional space,

$$\mathbf{P} = \begin{pmatrix} \mathbf{x}_1 \\ \mathbf{x}_2 \\ \vdots \\ \mathbf{x}_p \end{pmatrix}$$

the projection is computed as

$$\mathbf{P}' = \mathbf{PF}$$

3.3.2 Multidimensional scaling

Multidimensional Scaling (MDS) (Kruskal and Wish, 1977) is a technique used to determine a map a set of points S onto a new set S' in such a way that the distances between pairs of points in S' is similar to distances between corresponding pairs in S. The classic example used to illustrate dimensionality reduction is that of *map reconstruction*. Imagine that we are presented with a map of the UK and asked to measure all the intercity distances among a set of major cities. This task is trivial, but what about doing the reverse operation? Drawing an accurate map of the locations of the cities given only the matrix of distances between them is much more difficult. It is this type of problem that methods for dimensionality reduction aim to solve.

Formally, given a distance matrix $\mathbf{D} \in^n \mathbb{R}^n$, we wish to determine a matrix $\mathbf{X} \in^m \mathbb{R}^n$, such that

$$||\mathbf{x}_i - \mathbf{x}_j|| \cong d_{ij}$$

In other words, the original distance matrix is represented by a matrix in a lower-dimensional space. In the map reconstruction problem, we reduce the original $n \times n$-dimensional matrix to a 2-dimensional representation. Assuming that the distances in $\mathbf{D}$ are approximately Euclidean, the first step is to apply the Young-Householder factorization theorem (Young and Householder, 1938). This involves applying singular value decomposition (SVD) to the matrix $\mathbf{A}$, where

$$a_{ij} = -\frac{1}{2}(d_{ij}^2 - c_i - c_j + d)$$

$$c_i = \frac{1}{n}\sum_{j=1}^{n} d_{ij}^2$$

$$d = \frac{1}{n^2} \sum_{i,j=1}^{n} d_{ij}^2$$

The SVD method decomposes **A** as follows:

$$\mathbf{A} = \mathbf{U}.\mathbf{W}.\mathbf{V}^T$$

U and **V** are each $n \times n$ column-orthogonal matrices, and **W** is a diagonal matrix. The columns of **U** give the eigenvectors of the decomposition, and the diagonal values of **W** are the corresponding eigenvalues. If the eigenvalues of the decomposition are arranged in order of magnitude so that $\lambda_1 \geq \lambda_2 \geq \lambda_3 \cdots$ and the corresponding eigenvectors, scaled to the length of a unit vector, are denoted $\mathbf{e}_i$, then the matrix **X** is given by

$$\mathbf{X} = \begin{pmatrix} \sqrt{\lambda_1}\mathbf{e}_1^T \\ \sqrt{\lambda_2}\mathbf{e}_2^T \\ \vdots \end{pmatrix}$$

By selecting the first m eigenvectors, where $m < n$, the dimensionality of the original space is reduced.

3.3.3 Choice of the number of dimensions to retain

A key question which must be addressed when performing dimensionality reduction is how to determine the number of dimensions to retain. More specifically, how many dimensions are required to adequately represent any patterns in the original data set? The choice of how many components to retain is usually based on the proportion of the total variance of the original data set which is explained by the combination of these components. The total variance of the original data set is given by the trace of the correlation covariance matrix **S**; therefore, the variance explained by the first m principal components is given by

$$(\lambda_1 + \cdots + \lambda_m)/Tr(\mathbf{S})$$

As for the case of determining clustering thresholds, there are many semi-heuristic rules for determining the proportion of total variance which we wish to capture in the set of m principal components. These include

- Retain all components required to explain at least 80% of the total variance.
- The *scree test*. Typically, the first few eigenvalues of a PCA are of similar magnitude, then there is a sudden drop. The scree test involves plotting the series of eigenvalues and looking for the point of the decrease.
- Broken stick test. Retain all components whose proportion of the total variance is greater than would be expected if the components had been chosen at random.

For some of the analyses presented in this thesis, the aim of PCA/MDS is to project the original data into exactly two dimensions, so they can be plotted in a diagram. When this is the case, a measure of the amount of variance captured by the 2D plot is always provided.

3.4 Geometric range querying

Many applications require the ability to perform *geometric range queries*. These are, in general, problems of the following form: given a set P of N points in a k-dimensional space S, build a data structure such that the set of points which lie inside an arbitrary region $R \in S$ may be quickly determined (see figure 3.7).

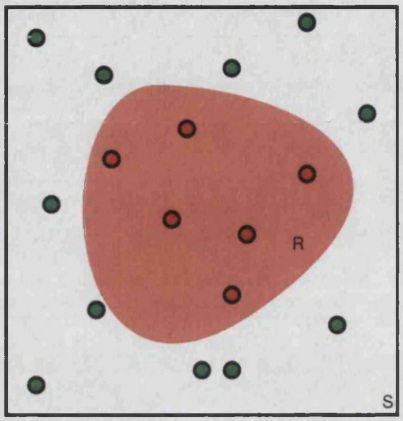

Figure 3.7: Geometric range querying
The set of points which fall inside a region R of the space S, are shown in red.

Two approaches for geometric range querying were assessed: 'brick maps' and kd-trees. The principle behind both methods is to precompute a division of S into a set of smaller partitions T such that one can rapidly compute which members of T are intersected by R. Only points which lie in this subset of T need then be inspected to determine whether they fall inside the region R.

3.4.1 The bricking algorithm

The subdivision procedure used in the bricking algorithm is simple: as the name suggests, the pre-processing step consists of partitioning S into a set of cuboids (bricks). Each brick contains a list of pointers to the objects which fall inside it. In order to quickly process the range query, it is fairly trivial to calculate the set of bricks T which intersect R.

3.4.2 kd-trees

The kd-tree method is somewhat more sophisticated than the bricking algorithm. The subdivision of S is represented as a binary tree, the root node of which consists of the whole initial space. Each node in the rest of the tree is defined by placing a plane through one of the k dimensions, which partitions the set of points in the parent node such that each of its two children receives an equal number of points. The partitioning continues until each leaf node in the tree contains just a single point; this occurs after $log_2(N)$ divisions.

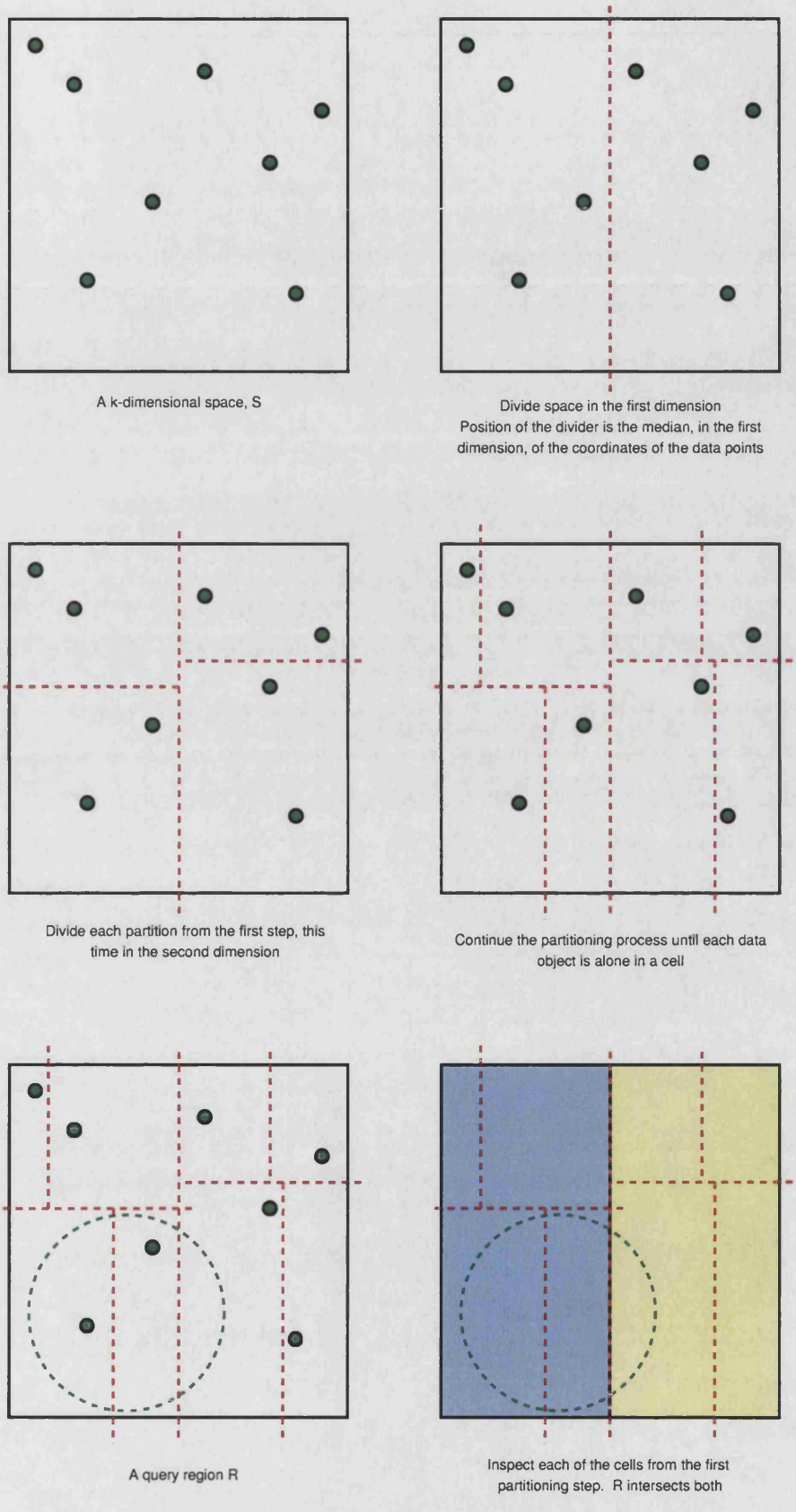

Figure 3.8: kd-tree range querying
Continued overleaf.

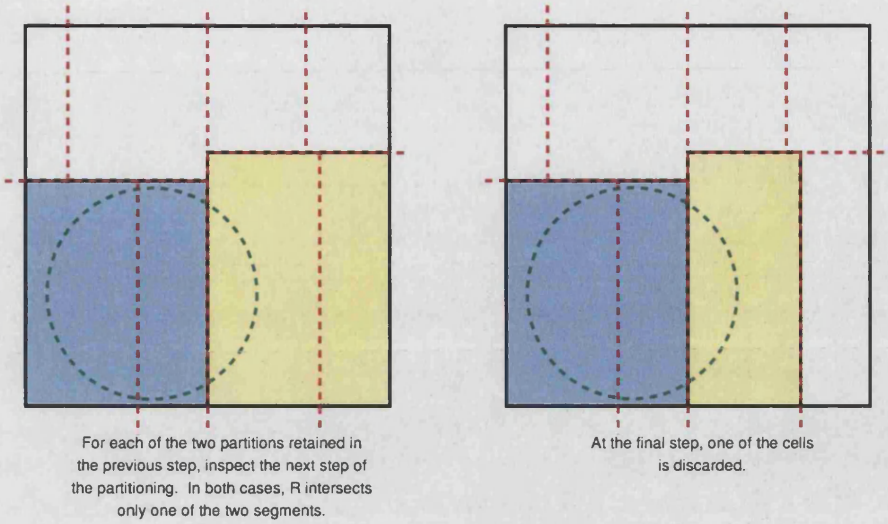

Figure 3.8: kd-tree range querying (continued)

A query on the kd-tree is processed by starting at the root node, and asking whether R intersects the region represented by that node. If so, the same question is asked of the two child nodes, and so forth down the tree. The search down any one branch of the tree is terminated as soon as a node is found whose region does not intersect R. In this way, the search quickly homes in on the regions of S which are intersected by R; the limited set of points in these partitions may then be inspected in turn. The kd-tree method is illustrated in figure 3.8.

It may be seen from the descriptions of the two geometric query methods above, that any region may be used as a query, as long as we may ask of it the following questions:

- Does the region contain a point P?
- Does the region intersect the k-dimensional hypercuboid C? (This is necessary in order to process the query on a kd-tree)
- What is the geometric centre of the region, and what is the distance of its furthest extremity from the centre? (This is the requirement for computing which cells of a brick map we need to inspect)

3.5 Sequence alignment

As discussed in §1.4, identification of overall sequence similarity is a powerful method for inferring structural and functional relationships between proteins based on their primary structure alone. In addition, where several sequences are available for comparison, identification of regions which are particularly well-conserved across all of them can be valuable indicators of functional sites within the proteins.

Achievement of either of these goals involves sequence alignment; that is, identification of equivalent positions between the input sequences. In order to do so, an evolutionary model must first be provided which describes the likelihood of the mutational changes described in §1.4. The aim of any sequence alignment

algorithm is to use this model to deduce the most likely series of evolutionary events which led from one input sequence to another. This proposed evolutionary history then allows the construction of a pairwise alignment between the input sequences.

3.5.1 Pairwise alignment algorithms

The earliest sequence comparison methods computed an alignment between a pair of input sequences, and this is still a common operation today. More recently, methods have been developed which compute a consensus alignment between a group of sequences (Higgins and Sharp, 1989), (Lipman *et al.*, 1989), (Notredame *et al.*, 2000), (Edgar, 2004). However, multiple alignment approaches were not used in this work, and will therefore not be discussed further.

3.5.1.1 Dynamic programming

Dynamic programming (Bellman, 1984) is a general method for solving optimisation problems which can be broken down into independently-solvable sub-problems. In particular, it is applicable when the problem involves making a series of decisions one after another, and where the aim is to find the optimal series of such decisions.

In order to formulate alignment of two sequences $X = (x_1,\ldots,x_m)$ and $Y = (y_1,\ldots,y_n)$ as such a problem, imagine an empty sequence alignment as a matrix with two rows and N columns, where $\max(m,n) \leq N \leq m+n$ holds[5] . Let all cells in this matrix be empty, and place a marker on each of the two input sequences, initially pointing to the first character of each. Now we position ourselves at the first column, and ask how to fill it. Our choices are as follows:

- Populate it with the first character of each of the two sequences.
- Place the first character of the first sequence in the upper cell, but leave the lower cell blank.
- Place the first character of the second sequence in the lower cell, but leave the upper cell blank.

Depending upon which of these options we choose, we must then move one or both of the markers along the input sequences, in order to indicate that a character has been 'used up'. After n iterations of this procedure, the two input markers will have moved forward to positions p and q of the input sequences, and we must choose how to fill the n^{th} column of the alignment matrix:

- Populate it with the p^{th} and q^{th} characters of the input sequences.
- Place the p^{th} character of the first sequence in the upper cell, but leave the lower cell blank.
- Place the q^{th} character of the second sequence in the lower cell, but leave the upper cell blank.

It is clear that the values of p and q, and therefore the nature of the decision to be made at each stage, depends upon the history of decisions which led up to the n^{th} iteration.

[5] To see the reason for the upper bound, consider the worst-case alignment in which the overlapping region of the two sequences contains the maximum possible number of gaps:

$$\begin{pmatrix} x_1 & - & x_2 & - & \cdots & x_m & - & - & \cdots & - \\ - & y_1 & - & y_2 & \cdots & - & y_m & y_{m+1} & \cdots & y_n \end{pmatrix}$$

Assuming without loss of generality that $m \leq n$, the length of the overlapping region is $2m$ and that of the un-aligned region of Y is $n-m$.

To solve the problem, we need to define a scoring scheme which measures the quality of an alignment, based ideally on the biological likelihood of the evolutionary history which it implies. The essential components of this score are a substitution matrix $\mathbf{M} = (\mu_{ij})$ which provides a score for each amino acid type mutating to every other type, and a function which penalises the introduction of gaps into the alignment [6]. The power of dynamic programming derives from noting that the value of the scoring function is local to each column of the alignment, meaning that parts of the alignment can be independently optimised and then concatenated to give the solution. More specifically, we can define the score of a given alignment in terms of the score for the optimal alignment up to the penultimate position, plus the score for the final position alone.

If the score for the optimal alignment up to positions p and q in the two input sequences is denoted A_p^q, and the gap penalty by γ, then we can write

$$A_p^q = \max \begin{cases} A_{p-1}^{q-1} + \mu_{x_p y_q} \\ A_{p-1}^{n} + \gamma \\ A_{p}^{q-1} + \gamma \end{cases} \tag{3.7}$$

By setting $p = m, q = n$, equation 3.7 provides a recursive solution to finding the optimal global alignment, but this is not the most efficient approach, since doing so would likely involve finding the same optimal subalignments multiple times.

Dynamic programming circumvents this problem by systematically computing each subalignment exactly once. Consider the problem of aligning the subsequences $X_p = (x_1, \ldots, x_p)$ and $Y_q = (y_1, \ldots, y_q)$. There are clearly many possible such alignments, but they all have in common the fact that they end with a column containing x_p and y_q. This seems like a trivial observation, but by creating a $m \times n$ matrix populated with the score of the optimal alignment for each value $p = 1, \ldots, m$, $q = 1, \ldots, n$, we produce an organised representation of all the sub-problems which comprise the recursive equation 3.7.

3.5.1.1.1 The Needleman-Wunsch algorithm

The dynamic programming matrix $\mathbf{S}$, consists of m rows, corresponding to the positions of sequence X, and n columns, corresponding to Y. Applying the method of (Needleman and Wunsch, 1970), it is populated as follows:

1 The first row and column are populated with the scores for aligning the appropriate characters.

$$s_{i1} = \mu_{x_i y_1} \forall\, i = 1, \ldots, m$$

$$s_{1j} = \mu_{x_1 y_j} \forall\, j = 1, \ldots, n$$

2 The remaining cells are populated by first calculating three scores corresponding to aligning the appropriate characters, or to inserting a gap into either of the two sequences:

- a_{ij} corresponds to inserting a gap into sequence X. It is calculated by adding the gap penalty γ to

[6] Here the regular gap model, in which extension of existing gaps is not preferred over opening new ones, is assumed. The method may be simply modified to prefer the reverse, by the use of a gap extension penalty.

the score from the cell immediately above.

$$a_{ij} = s_{i-1\ j} + \gamma$$

- b_{ij} corresponds to inserting a gap into sequence Y. It is calculated by adding the gap penalty γ to the score from the cell immediately to the left.

$$b_{ij} = s_{ij-1} + \gamma$$

- c_{ij} corresponds to aligning x_i with x_j. It is calculated by adding μ_{ij} to the score from the cell diagonally to the left and above.

$$c_{ij} = s_{i-1\ j-1} + \mu_{ij}$$

The largest of these three values is then stored in the $(i,j)^{\text{th}}$ cell

$$s_{ij} = \max(a_{ij}, b_{ij}, c_{ij})$$

This procedure for populating **S** can be illustrated by consideration of the following (slightly contrived) simple example. Let $X = (A,B,C,D,C)$ and $Y = (B,D,B,A)$, where we are using an imaginary four-letter alphabet. Now let us suppose that we have the following substitution matrix.

	A	B	C	D
A	10	-5	5	-5
B		10	-5	-7
C			10	-5
D				10

The matrix **S** thus obtained is shown in figure 3.9.

	B	D	B	A
A	-5	-5	-5	10
B	10	-6 -1 -12	-16 -12 5	-1 -6 -10
C	-5	-12 -16 5	-6 -6 -6	10 -17 10
D	-7	-6 -18 5	-17 -6 -2	-1 -13 -11
C	-5	-6 -16 -12	-13 -17 0	-1 -11 3

Figure 3.9: Population of the dynamic programming matrix
The first sequence, X, is arranged down the left-hand side of the matrix; Y is along the top. Within each cell, the upper score (a_{ij}) is the score for inserting a gap into X, the left-hand score (b_{ij}) is for inserting a gap into Y and the bottom-right score (c_{ij}) is for aligning the two sequence characters. The highest score(s) in each cell (s_{ij}) are highlighted.

In order to obtain the alignment itself, one must 'trace back' through the dynamic programming matrix to find the particular series of 'best decisions' which make up the alignment (see figure 3.10).

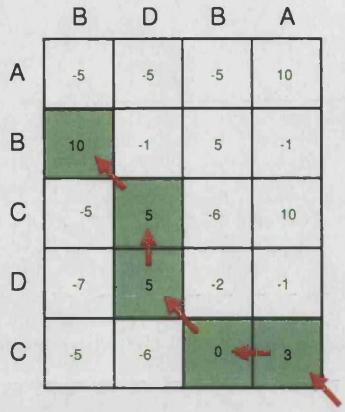

Figure 3.10: Traceback of the dynamic programming matrix
The optimal alignment is found by moving back through the matrix, at each step choosing the highest-scoring subalignment which preceded the current state. This is found by considering the highest-scoring of the left, upper and diagonal neighbouring cells.

The alignment resulting from the traceback of our example matrix is

```
A B C D - C
  |   |   +
B - D B A
```

3.5.1.2 Hidden Markov Models

A more recent family of methods for sequence alignment are based on the concept of the Hidden Markov Model (HMM) . An HMM is a *state machine*, whose output is a series of symbols. The inner workings of an HMM are hidden, but can be inferred using several well-studied algorithms. If an HMM is constructed whose output consists of the two sequences to be aligned, then the inference of the hidden states within it corresponds to finding the most likely series of mutations which would change the first sequence into the second. HMMs were not used in this work, so they are not discussed further.

3.6 Coordinate superposition

Given two sets of coordinates, with a list of correspondances between them, it is common to require a transformation which superposes one coordinate set onto the other. Formally, the requirement for such a transformation is that is should minimise the average squared distance between pairs of corresponding atoms. This quantity, normally referred to as the Root Mean Squared Deviation (RMSD) , is defined for two sets of coordinates P and Q as follows:

$$rmsd(P,Q) = \sqrt{\frac{1}{n}\sum_{i=1}^{n} \|\mathbf{p}_i - \mathbf{q}_i\|^2} \tag{3.8}$$

The superposition problem can be split into two parts: a rotation around the geometric centre of the coordinate set which brings it into the correct orientation, and a translation which superposes the centres of the sets. Let us define the two sets of coordinates X and Y, and require that they are ordered such that the coordinate pair

$(\mathbf{x}_i, \mathbf{y}_i)$ represents a corresponding pair of points. First translate the point sets such that their centroids are at the origin:

$$\mathbf{u}_i = \mathbf{x}_i - \bar{\mathbf{x}}, \mathbf{v}_i = \mathbf{y}_i - \bar{\mathbf{y}}$$

Now, let $\mathbf{R}$ be a rigid rotation matrix. Mathematically speaking, $\mathbf{R}$ must be a member of the *special orthogonal group* SO_3; that is, the subset of the group of orthogonal transformations in 3-space (O_3) whose determinant is 1, and hence which do not reverse orientation. We wish to find the rotation which, when applied to X, minimises the RMSD between the result of the rotation, and the set Y. In other words, we wish to minimise the expression

$$d = \sum_{i=1}^{n} \|\mathbf{R}\mathbf{u}_i - \mathbf{v}_i\|^2 \mid \mathbf{R} \in SO_3 \tag{3.9}$$

3.6.1 Available methods

Early methods for determining optimal superposition of point sets relied upon numerical searches, but several efficient direct methods are now known - see *e.g.* Kearsley (1989). The method used in the current work is due to J. Barker (personal communication), and may be summarised as follows.

Given the point sets U and V as defined above, let $\mathbf{X} = UV^T \in \mathbb{R}^3$. By diagonalising the matrix $\mathbf{X}^T\mathbf{X}$ using the Jacobi algorithm, its eigenvalues $\lambda_1, \lambda_2, \lambda_3$ and eigenvectors $\mathbf{e}_1, \mathbf{e}_2, \mathbf{e}_3$ are obtained. It can be shown that selecting the rotation matrix according to

$$\mathbf{R} = \mathbf{E}(\mathbf{XED})^T$$

where

$$\mathbf{E} = \begin{pmatrix} e_1 & e_2 & e_3 \end{pmatrix}$$

and

$$\mathbf{D} = \begin{pmatrix} \sigma\lambda_1^{-\frac{1}{2}} & 0 & 0 \\ 0 & \lambda_2^{-\frac{1}{2}} & 0 \\ 0 & 0 & \lambda_3^{-\frac{1}{2}} \end{pmatrix}$$

with

$$\sigma = \begin{cases} 1 & \text{if } |\mathbf{X}| \geq 0 \\ -1 & \text{otherwise} \end{cases}$$

minimises the value of d from equation 3.9.

3.6.2 The planarity problem

If the matrix $\mathbf{X}^T\mathbf{X}$ has a rank lower than 3 - that is to say, if it has fewer than 3 linearly independent rows or columns, then one or more of the eigenvalues obtained by its diagonalisation will be zero. It can be seen from the expression for $\mathbf{R}$ above that this would cause the superposition to fail. This situation can arise when all of the points in one of the input sets lie exactly on a plane. While more sophisticated methods exist which

are able to handle these cases gracefully, it was found to be sufficient for the current work merely to test for planarity prior to computing the superposition, and either to report an error if it was detected, or to perturb the points slightly away from the plane.

3.7 Analysis of ligand conformation

The conformation of small molecules - in this case, biological ligands - was studied using several different techniques. The first two, radius of gyration and planarity, provide a general overview of molecular shape, while the calculation of the torsion angles around individual rotable bonds allow the local conformation of individual parts of the molecule to be studied in more detail.

3.7.1 Radius of gyration

The radius of gyration r_g of a solid body is defined by the equation

$$I = mR_g^2$$

where I is the moment of inertia of the body and m is its mass. For a collection of atoms with individual masses $m_1, \ldots, m_n$ and coordinates $\mathbf{x}_1, \ldots, \mathbf{x}_n$, we can therefore write the radius of gyration as

$$r_g = \sqrt{\frac{\sum_{i=1}^{n} m_i \|\mathbf{x}_i - \bar{\mathbf{x}}\|^2}{\sum_{i=1}^{n} m_i}} \tag{3.10}$$

Note that this formula is simply a mass-weighted version of the RMSD given in equation 3.8. It is commonly calculated for proteins using experimental techniques such as Small-angle X-ray Scattering (SAXS) in order to obtain a rough measure of the sphericity of the molecule. For ligands, r_g provides a first approximation of the degree to which the molecule is in an extended or a bent conformation. For an ideal polymer, it can be shown that the mean radius of gyration is linearly related to the mean end-to-end separation (Atkins and de Paula, 2001).

Although the end-to-end distance of a polymer is perhaps a more intuitive way of representing its degree of 'bentness', the radius of gyration is a more general form. Specifically, the definition of end-to-end distance is unambiguous only for simple polymers; where the molecule is branched or cyclic, this quantity no longer has a clear meaning. We could perhaps define the 'ends' of a modestly-branched molecule using an all-pairs shortest path graph algorithm such as Floyd (1962), but the justification for such a measurement would necessarily break down for many of the molecules we would be interested in. The radius of gyration, on the other hand, is calculable for any topology of molecule, and is therefore taken as the preferred method for representing conformational compactness at the gross level.

3.7.2 Torsion angles

The approaches so far in this section have been concerned with representing molecular shape in fairly crude terms; for describing local conformation in detail, torsion angles are a simple but effective tool.

3.7.2.1 Definition

Given four atoms A, B, C and D, where each atom is bonded to the previous one (see figure 3.11), the torsion or dihedral angle represents the relative orientations of the $A-B$ and $C-D$ bonds.

Formally, we define the torsion angle with respect to the four atoms A, B, C and D, τ_{ABCD} as follows

$$\mathbf{e} = \overrightarrow{BC} \times \overrightarrow{BA}$$
$$\mathbf{f} = \overrightarrow{CD} \times \overrightarrow{CB}$$
$$t = \frac{\mathbf{e} \cdot \mathbf{f}}{|\mathbf{e}||\mathbf{f}|}$$
$$\tau_{ABCD} = \begin{cases} \cos^{-1}(t) & \text{if } \mathbf{e} \cdot \overrightarrow{CD} \geq 0 \\ 2\pi - \cos^{-1}(t) & \text{otherwise} \end{cases}$$

Mnemonically, if one imagines looking along the $B-C$ bond, with B closest and oriented such that $B-A$ points vertically upwards, the torsion angle is the clockwise deflection of $C-D$ from 12 o'clock.

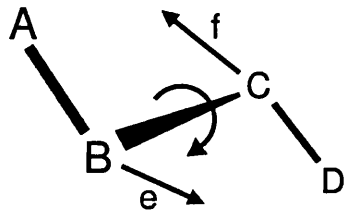

Figure 3.11: Definition of a torsion angle
The torsion angle τ_{ABCD} represents the clockwise deflection of $p(\overrightarrow{CD})$ from $p(\overrightarrow{BA})$, where the transformation p represents projection into a plane normal to $\overrightarrow{CB}$. The vectors $\mathbf{e}$ and $\mathbf{f}$ are constructions used in the calculation of τ_{ABCD}, as described in the text.

Torsion angles are routinely used to describe the conformation of proteins. The shape of the backbone can be completely defined by specifying two torsion angles for each peptide unit. The conventional definitions of these angles are

$$\phi : \text{defined by atoms } C^{i-1} - N^i - C^i_\alpha - C^i$$
$$\psi : \text{defined by atoms } N^i - C^i_\alpha - C^i - N^{i+1}$$

where the superscripts indicate to which peptide unit each atom belongs. The combination of the ϕ and ψ angles for one or more residues is commonly displayed on a two-dimensional Ramachandran plot (Ramachandran and Sasisekharan, 1968). Low-energy orientations of these bonds correspond to the common secondary structure conformations of protein backbones, primarily right-handed α-helices and β-sheets. Comparison of the torsion angles calculated from the coordinate model built into an electron density map with those most statistically favoured for each residue type (Morris *et al.*, 1992) can be used to validate the model building and refinement procedures (Laskowski *et al.*, 1993).

3.7.2.2 Nomenclature

3.7.2.2.1 Angular range nomenclature

The system of Klyne and Prelog (1960) was used for naming angle ranges, with definitions for torsion angles taken from the IUPAC Commission (1974). This system breaks torsion angles firstly into two halves, and then into three equal segments per semicircle, as shown in figure 3.12. Angles in the range $[-90°, 90°)$ are referred to as *syn*, and the rest are called *anti*. The term *periplanar* is applied to angles within $[-30°, 30°]$ and $[150°, -150°]$, while *clinal* refers to angles which fall outside those ranges. Combinations of these terms are used to generate unique names for each of the six segments in the Klyne-Prelog system. The names *cis*, *trans*, *+gauche* and *-gauche* are also sometimes used to refer to angles 0°, 180°, +30° and −30° respectively.

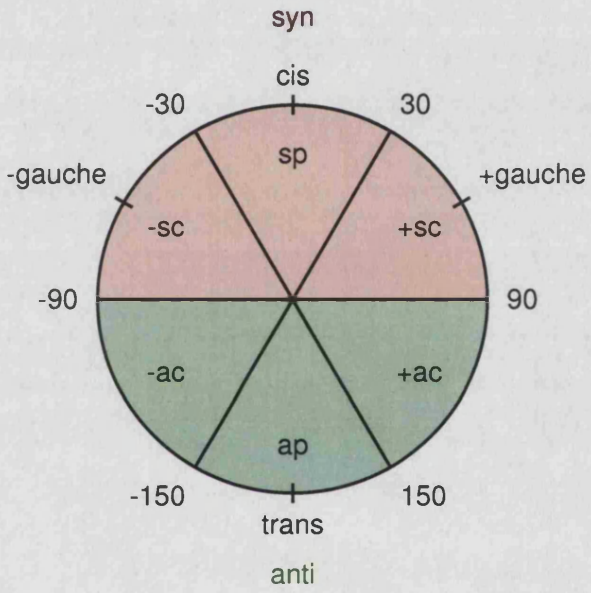

Figure 3.12: The Klyne-Prelog system for angle range nomenclature
Combination of the terms *syn*, *anti*, *clinal* and *periplanar*, defined in the text, lead to the names of the six segments: *synperiplanar* (*sc*), *+synclinal* (*+sc*), *+anticlinal* (*+ac*), *antiperiplanar* (*ap*), *-anticlinal* (*-ac*) and *-synclinal* (*-sc*).

3.7.2.2.2 Bond definitions

When referring to torsion angles of nucleotide derivatives, IUPAC-IUB naming conventions (IUPAC-IUB, 1983) are generally adopted. Figure 3.13 shows two nucleotide triphosphate molecules, ATP and GTP. The angles defined with respect to the standard atom names are listed in table 3.3. The application of these angle definitions to the nucleotide derivatives NAD and FAD is covered in chapter 5.

The torsion angle around the N-glycosidic bond is denoted χ. The atoms which define it depend upon whether the nucleotide is a purine or a pyrimidine, as shown in table 3.3. These are chosen such that the definitions of *syn* and *anti* conformations (§3.7.2.2.1) are consistent with accepted chemical conventions.

One angle for which the definition diverges from IUPAC conventions is ξ. Here, we use this symbol to refer to a P-O bond in the pyrophosphate moiety, with a subscript applied to denote the number of phosphate groups

between the bond and the ribose group. The IUPAC standard is defined with reference to a polynucleotide chain, and therefore uses for ξ as the P-O bond angle within the phosphodiester linkage.

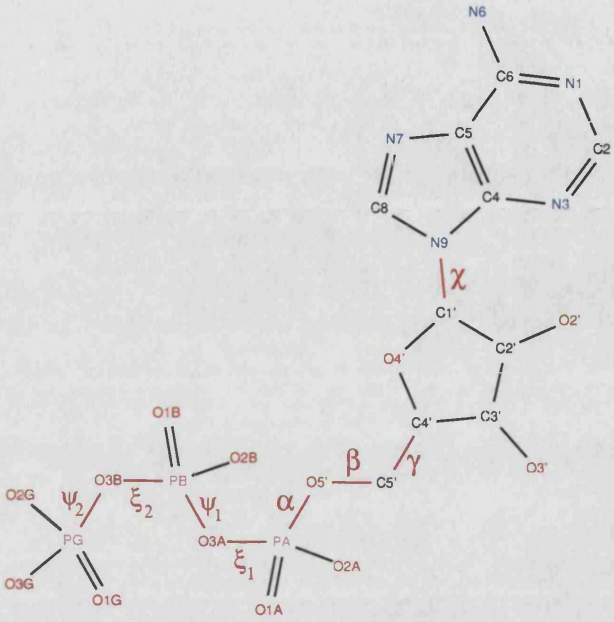

(a) ATP

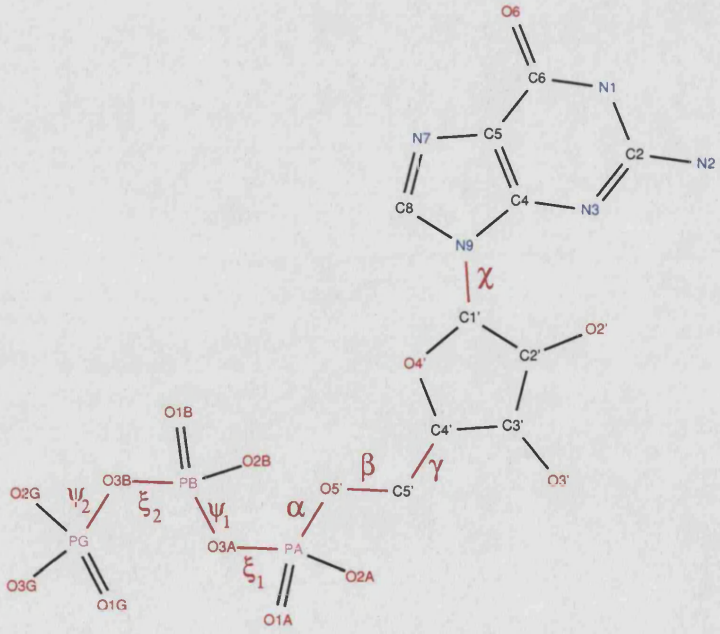

(b) GTP

Figure 3.13: Torsion angles defined for nucleotide triphosphates

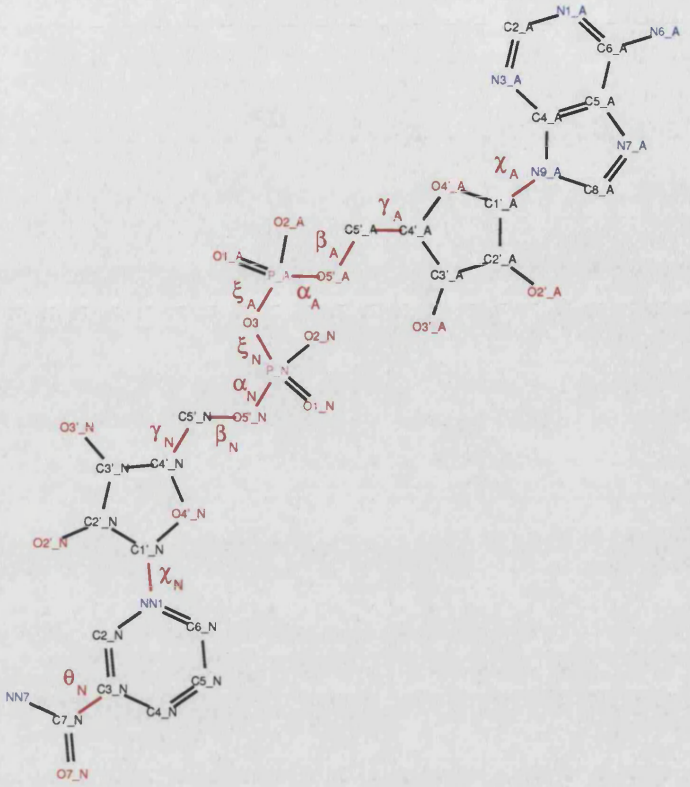

(a) NAD

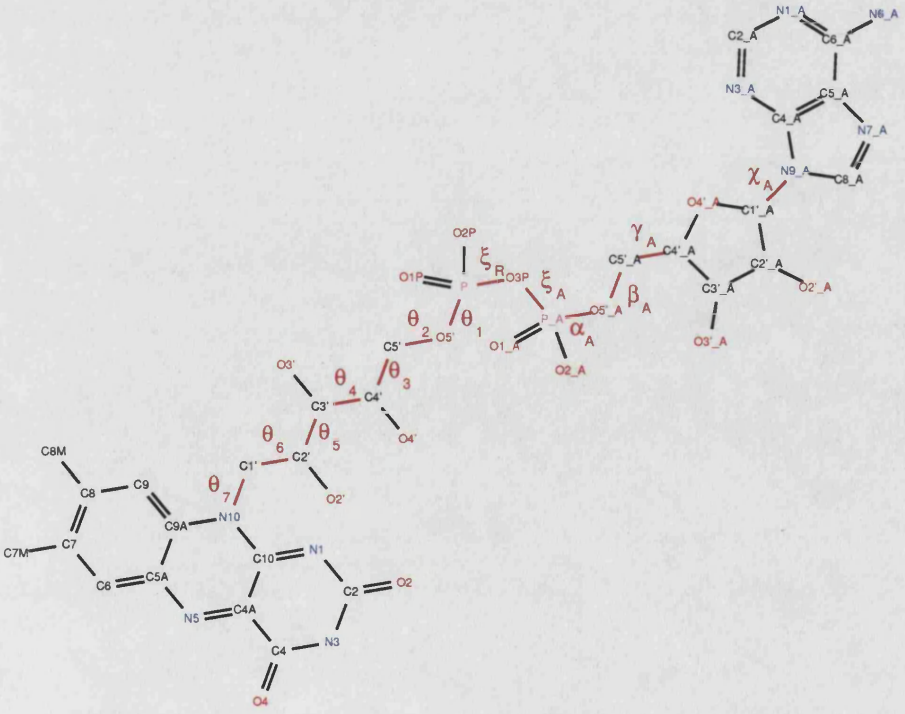

(b) FAD

Figure 3.14: Torsion angles defined for the nucleotide derivatives NAD and FAD

Angle	A	B	C	D
α	O3	PA	O5′	C5′
β	PA	O5′	C5′	C4′
γ	O5′	C5′	C4′	C3′
ξ_1	PB	O3A	PA	O5′
ψ_1	O3B	PB	O3A	PA
ξ_2	PG	O3B	PB	O3A
ψ_2	O3G	PG	O3B	PB
χ_{pur}	O4′	C1′	N9	C4
χ_{pyr}	O4′	C1′	N1	C2

Table 3.3: Definition of torsion angles for nucleotide derivatives
χ_{pur} and χ_{pyr} refer to the definition of the torsion around the N-glycosydic bond for purines and pyrimidines respectively.

3.8 Calculation of solvent-accessible surface area

3.8.1 Molecular surface definitions

The term 'molecular surface' is often used as a catch-all term for several different types of molecular surface. The most commonly used are listed below, and shown graphically in figure 3.15.

- **Van der Waals surface.** Simply the union of those parts of the surfaces of the Van der Waals spheres of each individual atom, which do not fall inside the sphere of any other atom.
- **Connolly surface.** The part of the Van der Waals surface which may be contacted by a solvent sphere. plus the re-entrant surface. This is also known as the contact surface.
- **Lee and Richards surface.** This is commonly known as the 'solvent-accessible surface'. This is defined as the loci traced by the centre of a solvent molecule which is rolled across the surface of the molecule.

3.8.2 kd-tree algorithm for neighbour detection

The method used here to calculate the solvent accessible surface of a molecule, derived from Shrake and Rupley (1973), can be briefly summarised as follows:

1 Generate an evenly-distributed set of points across the expanded-atom surface of the molecule. The expanded-atom surface is constructed by augmenting the Van der Waals radii of the atoms in the molecule with the radius of a solvent molecule.

2 For each surface point, determine whether there is any atom whose Van der Waals sphere occludes a sphere of solvent radius centred at that point. This is done efficiently by using a kd-tree (§3.4).

3 If no such atom exists, the point is classified as solvent-accessible.

The list of solvent-accessible points remaining at the end of the calculation defines the solvent-accessible surface. The density of the initial set of points can then be used to calculate the approximate area of the surface.

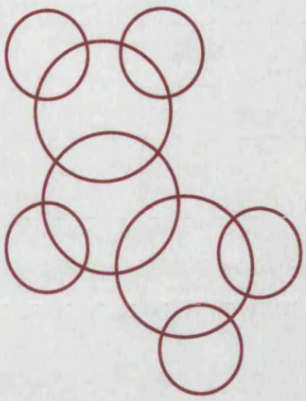

(a) Circles representing the Van der Waals radii of a set of atoms

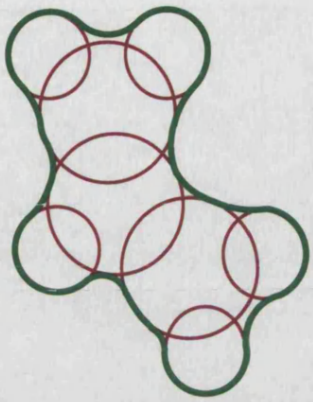

(b) Connolly surface

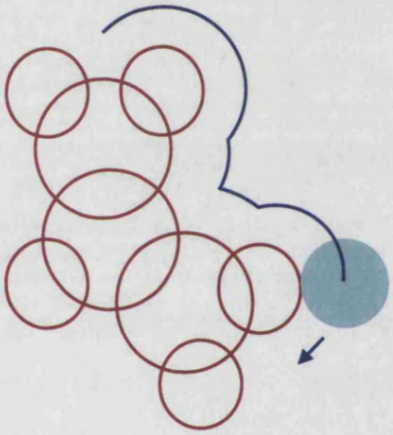

(c) Conceptual method used to construct the Lee & Richards surface

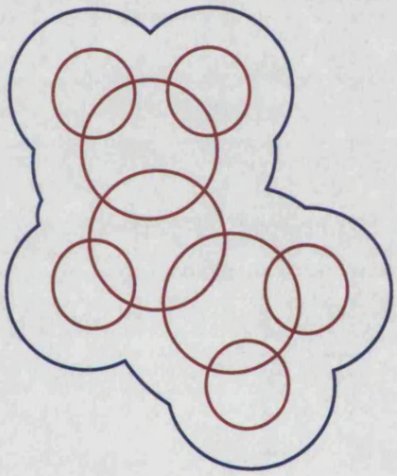

(d) The complete Lee & Richards surface

Figure 3.15: Molecular surface representations

3.8.3 Generation of uniformly distributed surface points

A number of methods for generating the initial set of evenly distributed surface points were considered. Since each of these approaches has its drawbacks, the choice of which to use was to some extent a pragmatic one.

In order to distribute points evenly on the molecular surface, we may first distribute points evenly on the surface of each atom, and then prune away those points which which fall inside the sphere of any other atom.

3.8.3.1 Uniform distribution of points on the unit sphere

A naive approach to randomly distributing points on the unit sphere would be to select the spherical polar coordinates θ and ϕ from the uniform distributions $\theta \in [0, 2\pi)$ and $\phi \in [0, \pi]$. However, we note that the area element

$$d\Omega = \sin\phi \, d\theta \, d\phi \tag{3.11}$$

is a function of ϕ, and that therefore points picked in this way will be more dense towards the poles, and less so at the equator of the sphere.

One solution to this problem is to follow the initial placement step with an iterative refinement which attempts to even out the point density across the surface of the sphere. This can be done by modelling each point as a charged particle; if all points have the same charge, they repel one another, and if their movement is constrained to the spherical surface, this repulsion will lead to a uniform distribution of points. In order to avoid oscillatory motion, a viscosity term is usually added. The problem with such an approach is its computational complexity: each step of the refinement process requires the solution of a differential equation, and depending upon the number of points involved, several hundred iterations may be required to achieve a stable conformation.

Alternatively, direct methods can be used. Inspection of the area element given in equation 3.11 leads to a simple way of eliminating the bias described above. First, we rewrite $d\Omega$ as follows:

$$\begin{aligned} d\Omega &= \sin\phi \, d\theta \, d\phi \\ &= d\theta \, d(\cos\phi) \end{aligned}$$

Evenly distributing points on the surface of the sphere is equivalent to ensuring that any small area upon it is expected to contain the same number of points. In other words, we need to choose distributions for θ and ϕ for which the differentials $d\theta$ and $d(\cos\phi)$ are constant at all values. It is clear that, choosing random variables U and V on $(0,1)$, the following expressions for θ and ϕ satisfy this condition:

$$\begin{aligned} \theta &= 2\pi u \\ \phi &= \cos^{-1}(2v-1) \end{aligned}$$

3.8.3.2 Surface triangulation

An alternative approach is to triangulate the molecular surface, taking either the set of triangular vertices, or the centroids of each triangle as the set of surface points. Such a triangulation can be easily constructed by first representing the occluded volume of the molecule using a regular three-dimensional grid: all points which lie outside the molecule are set to zero, and those inside to unity. Application of an isosurface generation method such as the Marching Cubes algorithm (Lorensen and Cline, 1997) then produces triangles which lie approximately on the molecular surface.

A problem with this approach is that the triangles produced are not guaranteed to be equal in size; deriving a uniformly distributed set of points therefore requires an additional refinement step similar to that described above, in order to make the vertices more evenly distributed. While triangulation is a powerful method for approximating volumetric data of arbitrary shapes therefore, it is not ideally suited to the current problem.

3.8.3.3 Spherical t-designs

A set of N points on the sphere is called a *spherical t-design* if the integral of any polynomial of degree at most t is equal to the average value of that polynomial over the set of N points. Sets of such designs for different values of N and t have been precomputed (Hardin and Sloane, 1996) and are available on the world-wide web from http://www.research.att.com/~njas/sphdesigns. Examples of 3-dimensional spherical designs are shown in figure 3.8.3.3.

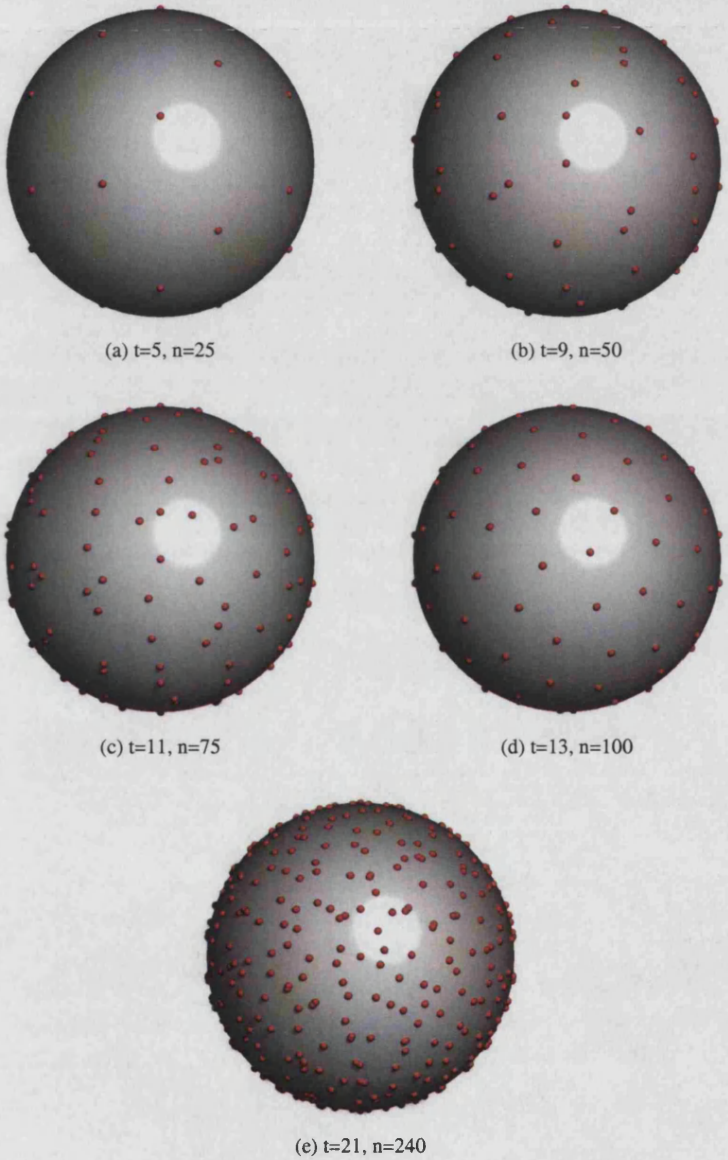

Figure 3.16: Spherical t-designs in three dimensions
For each design, the values of the parameter t and n - the number of points in the design - are given. (Figure courtesy of J. Barker)

The problem of calculating solvent accessible surface area can be formulated as an integral. Let f be a function defined on the expanded-atom-radius surface S of the molecule, whose value is zero at regions of the surface inaccessible to solvent, and unity at solvent-exposed points. Now the total solvent-accessible surface area is given by

$$\int_S f \, dA$$

3.8.3.3.1 Determination of surface point accessibility

In order to determine whether a given point is accessible to solvent, we need to determine whether any atom A is within a distance $d = 2r_{solvent} + r_A$ from the point as shown in figure 3.17. Here, this is done using a kd-tree based search.

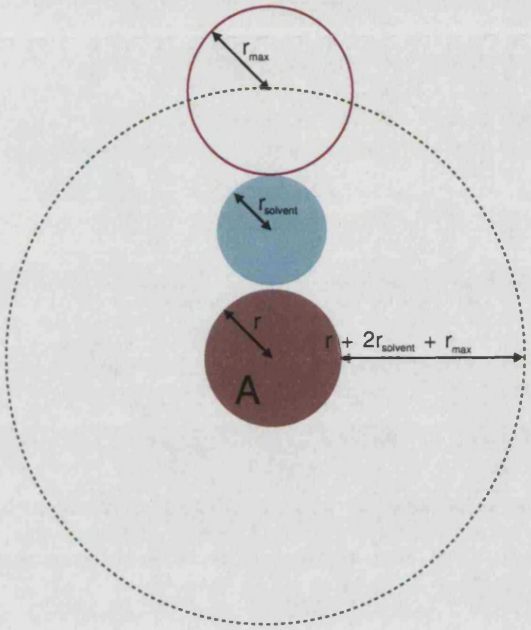

Figure 3.17: Searching for potentially solvent-excluding neighbours
The green circle indicates the volume which must be searched in order to find atoms which may potentially exclude solvent from the surface of atom A.

3.8.4 Caveats

3.8.4.1 Structural water molecules

Before determining the solvent-accessible surface of a molecule whose coordinates have been determined by X-ray crystallography, it is customary first to remove all water molecules from the structure. The implicit assumption here is that these molecules, although immobilised in the crystal (and hence visible in the diffraction pattern), would revert to being part of the bulk solvent were the compound to be returned to its *in vivo* state. This is not always the case, however; some proteins contain *structural water* molecules which do not interchange with bulk solvent. Marking the parts of the protein contacted by these waters as solvent accessible could therefore be said to be erroneous. Automatic discrimination between physiologically-immobilised waters and water of crystallisation is, however, not possible in practice.

3.8.4.2 Internal cavities

The method described above does not distinguish between the external surface of a protein, and that of any internal cavities which it may have. Some proteins, for example the lipocalins (Flower, 1996), many of

which bind small hydrophobic molecules such as retinol, possess large internal cavities. However, since the occurrence of internal cavities of significant size in proteins is thought to be fairly rare, this possibility disregarded here.

3.8.5 Degree of burial

Using the method described above for calculating the solvent-accessible surface of a molecule, we may determine the extent to which a ligand is buried inside a protein. After computing the accessible surface area of the ligand in the absence of the protein coordinates (and also of any water molecules), ASA_{free} and then with the protein atoms replaced, ASA_{bound}, we define the following measure of the degree of burial:

$$frac_{buried} = \frac{ASA_{free} - ASA_{bound}}{ASA_{free}} \tag{3.12}$$

This measure is defined on an atom-by-atom basis. See figure 3.18 for an example.

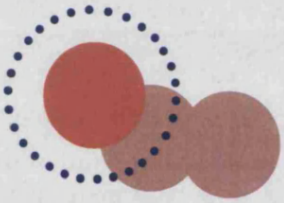

(a) Large spheres represent the atoms of a ligand molecule. Small blue spheres are uniformly-distributed points on the surface of the expanded-atom sphere of the red atom.

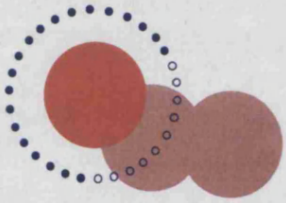

(b) Surface points which are inaccessible to solvent due to the other atoms of the ligand are removed. The remaining solid blue spheres represent the solvent-accessible surface of the ligand atom in the unbound form.

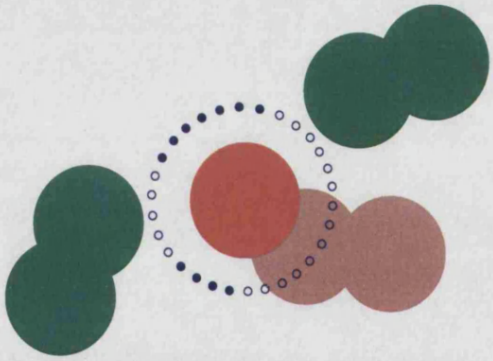

(c) Surface points which are inaccessible to solvent due to protein (green) are removed. The remaining solid blue spheres represent the solvent-accessible surface of the ligand atom in the bound form.

Figure 3.18: Calculation of per-atom solvent accessible surface
Applying equation 3.12, we see that the red atom loses $9/20 = 45\%$ of its solvent-accessible surface upon binding to the protein.

Chapter 4

Generation of datasets

This chapter describes the protocols which were developed in order to generate robust, high-quality data sets for the subsequent analyses presented in this thesis.

The aims are, for each ligand compound of interest:

1 Identify all instances of that compound co-crystallised with protein, which are present in a coordinate repository such as the PDB.
2 Extract the coordinates of each ligand along with its binding site, transforming them such that all ligand molecules lie in a common coordinate frame.
3 Cluster the binding sites based on the evolutionary relatedness of the proteins which comprise them. Each resulting cluster should contain those sites which are from non-identical members of the same homologous superfamily.

The main sections of this chapter, therefore, are as follows. Firstly, the problems involved in the automated creation of good-quality, non-redundant data sets of ligand binding sites are discussed. Secondly, the protocols used to address these problems are described. Thirdly, the architecture of the computational pipeline which implements these protocols is outlined. By applying this procedure to all ligands in the PDB, an overview of the distribution of ligand types with respect to both protein superfamilies and enzyme function is obtained. Finally, datasets for four ligands of particular biological importance,

- ATP
- GTP
- NAD
- FAD

are discussed in more detail. These datasets form the basis of the analyses which follow.

4.1 Protocol for validation of ligand identity

4.1.1 The need for ligand validation

In order to perform a systematic study of ligand binding sites, using co-crystal structures as the data source, an automatic method of identifying ligand molecules is required. In particular, this method should have the following capabilities:

1 Given a crystal structure, identify all ligand molecules.
2 For each ligand, determine its identity; in other words, identify it as being an instance of a particular chemical compound (see §1.3.6).
3 Compute a mapping between each atom in the ligand molecule, as seen in the crystal structure, and the corresponding atom in the reference compound.

A naive approach to achieving this would be simply to parse the PDB file for the structure, then perform the three steps listed above by

1 Finding ligand molecules by looking for HETATM records.
2 For each ligand, reading the residue name, and assigning chemical identity by looking up this name in the RCSB hetgroup dictionary.
3 Mapping each ligand atom to an atom in the reference compound, based on the PDB atom name.

The problem with this simple method is that steps 2 and 3 would frequently fail due to well-known inconsistencies in the data which can be retrieved from the PDB files. Problems may also arise from the fact that this data is the result of an experimental procedure, and therefore contains unavoidable error. Specifically, the following difficulties may be encountered:

- **Inconsistency in naming of compounds.** While PDB files deposited from October 1998 onwards are subject to data uniformity checking (Westbrook *et al.*, 2002), older 'legacy' files may contain compounds whose residue name does not agree with the standard nomenclature.
- **Inconsistency in atom names.** Similarly, atom names are not applied in a uniform manner across entries, so we cannot assume that an atom named 'A' in one instance of compound XYZ refers to the same chemical entity as another atom with the same descriptor.
- **Stereochemical errors.** A chiral stereocentre can be defined by specifying four atoms and their 'handedness'. Where distinct stereoisomers of a compound are found in complex with proteins, those stereoisomers should each have a unique hetgroup identity. Cases can often be found in the PDB, however, in which either the atom labelling or the name of a residue is incorrect, resulting in its chirality, as determined from its coordinates, being inconsistent with that specified for the reference compound.
- **Missing atoms due to insufficient resolution.** Parts of the structure which are mobile, or which exhibit crystal mosaicity, may not produce sufficiently well-defined electron density for reliable model building in that region. This is manifested as missing atoms in the coordinate file. If we later wish to use those atoms as the basis for a coordinate frame, in order to compare different sites binding this molecule, we must first ensure that all atoms in the molecule have well-defined positions.

All of these problems may be circumvented by systematically checking the coordinates of every ligand molecule against a set of reference chemical structures, as described below. It should be noted that, during the time in which this work was carried out, the MSD, which is a 'cleaned up' version of the PDB in which many of the issues discussed above have been alleviated, was released. The reason why it was not used in this study is partly due to issues of time: by the time the database became publicly available, the validation scheme described here had already been implemented. In addition, however, the aims of the MSD's data validation protocols, with respect to ligands, are somewhat different to those of this work, and the author has found examples where the ligand identity assigned by the MSD does not agree either with that provided by this pipeline, nor with that which would be applied on visual inspection. Some of these cases are discussed further below.

4.1.2 The algorithm

The protocol used to identify all ligands in the PDB is outlined as pseudocode in algorithm 4.1. The algorithm attempts to assign a chemical identity to every monomer which is not an amino acid, part of a nucleotide chain, or a solvent molecule. These conditions are tested using a simple screen based on the residue name present in the PDB file; those monomers which remain are identified using a graph-matching procedure.

The procedure is applied to all X-ray crystal structures within the PDB. It should be noted at this point that, where the resolution of the compound is particularly poor, or the crystallographic temperature factors of the ligand atoms are high, the results of this procedure may be suspect. At this stage, however, all ligands are treated equally; a decision can be made later on whether to process only those ligands identified from good quality structures, as determined by, for example, a minimum resolution threshold.

The coordinates of each ligand molecule L are converted into a graph by deducing the connectivity between atoms. This is done by calculating the distances between all pairs of atoms in the monomer. A pair of atoms a_1 and a_2 are considered to be covalently bonded if the separation of their centres d, as calculated from the coordinates in the PDB file, satisfies

$$d \leq r_1 + r_2 + t$$

where r_1 and r_2 are the standard covalent radii of the two atoms, according to a reference table, and t is a tolerance value, which has been set here to 0.2Å. Each atom in the molecule is represented by a vertex whose label corresponds to the atomic number of the atom. Edges are added between vertices whose atoms satisfy the distance cutoff. These edges are unlabelled, since reliable deduction of bond valences and aromaticity from atomic coordinates alone is not a trivial problem: see *e.g.* Labute (2005). The result of this procedure is a graph, G_L, consisting of N_L vertices.

In order to determine the chemical identity of the ligand, G_L must be compared against the database of reference structures $\mathcal{D}$. This search can be made faster by first identifying the subset $\mathcal{S} \subset \mathcal{D}$ which can potentially provide a sufficiently good match against G_L, as described in §3.1.3. Using the expressions shown in table 3.1, it is possible to calculate the range of reference graph sizes (in terms of numbers of vertices) N_{min} and N_{max}, which could potentially provide an acceptable match; the set $\mathcal{S}$ is then given by

```
Function ValidatePDBLigands(PDB P, ChemBase C, MatchCriteria M, MatchSize S) :
  Ligands ← ∅
  for each Entry E ∈ P :
    for each Monomer m ∈ E :
      if not m.is_amino_acid() and not m.is_solvent() then
        Ligands ← Ligands + IdentifyMonomer(m,C,M,S)

Compare connectivity of a given monomer against reference graphs
Function IdentifyMonomer(Monomer m, ChemBase C, MatchCriteria M, MatchSize S) :
  Matches ← ∅

  Convert the coordinates of monomer m into a graph using tables of standard covalent radii
  G1 ← ComputeGraph(m)
  N ← G1.n_vertices()

  Compute the range of target graph sizes which can potentially provide a match against a query of size
  N, satisfying size criterion S
  (Lower,Upper) ← ComputeTargetRange(N,S)

  Compare the monomer graph against all reference graphs within the target range
  M specifies the criteria for identifying pairs of atoms and bonds which can be matched
  for TargetSize ← Lower to Upper :
    for each Graph G2 ∈ C: G2.n_vertices() = TargetSize :
      Matches ← Matches ∪ MatchGraphs(G1,G2,M,S)

  if Matches = ∅ then
    return NoMatch
  else
    return GetBestMatch(Matches)

Function CompareMatches(X,Y) :
  if X.NStereocentreMismatches = Y.NStereocentreMismatches then
    return X.G1.name = X.G2.name
  else
    return X.NStereoCentreMismatches < Y.NStereoCentreMismatches

Function GetBestMatch(Matches) :
  X ← ∅
  for each Match ∈ Matches :
    X ← X + (Match, CheckStereocentres(Match))
  Sort the list X, using the comparison function CompareMatches
  return X[0]

Check correspondance of stereocentre chiralities between monomer and reference graphs
Function CheckStereocentres(M) :
  MisMatches ← 0
  for each Stereocentre S2 ∈ M.G2 :
    Map atoms from reference stereocentre onto the monomer graph
    Stereocentre S1 ← MapChiralCentre(S2,M.G2,M.G1,M)
    Chirality2 ← ComputeChirality(S1)
    Chirality2 ← S2.chirality()
    if Chirality1 ≠ Chirality2 then
      MisMatches ← MisMatches + 1
  return MisMatches
```

Algorithm 4.1: Validation of ligand identity

$$\mathcal{S} = \mathcal{D} : N_{min} \leq N \leq N_{max}$$

By only searching for matches between G_L and the members of $\mathcal{S}$, unproductive comparisons are avoided.

In the present study, mismatches of up to 2 vertices with respect to the reference graph were tolerated. As discussed in §3.1.2.2.2, the fewer the number of mismatches allowed, the faster the matching algorithm runs. Once the matching procedure is complete, stricter conditions on the extent of the match can be applied by using, for example, the subset of the results in which the two graphs matched exactly.

Each reference graph $G_R \in \mathcal{S}$ is compared against G_L using the Krissinel maximum common subgraph ismorphism algorithm (see §3.1, Krissinel and Henrick (2004a)). For the purposes of this stage of the comparison, atoms may be matched if their atomic numbers are identical. Information about charge and chirality is discarded from the reference graph. All bonds are considered compatible; in other words, bond order and aromaticity information, which is present in reference graphs, is ignored for the reasons given above. Since, in most crystal structures, hydrogen atoms are not resolved, hydrogens are ignored during the graph matching procedure. If the size N_S of the maximum common subgraph of G_L and G_R is large enough to satisfy the minimum similarity condition (in this case, $N_S \geq N_R - 2$), the isomorphism is stored.

In most cases, the ligand graph matches just one reference graph, and the chemical identity of the molecule is therefore unambiguously determined. Care must be taken, however, to avoid erroneous matches, which may occur when the atoms of a ligand are poorly resolved in the crystal structure, and the resulting graph is incomplete. An example of this is found in PDB entry 1BI9, a structure of rat retinal dehydrogenase at 2.7Å. Only half of the NAD cofactor is visible in the structure due to crystal disorder, with the result that the resulting derived graph is identical to that of adenosine diphosphate (ADP) (see figure 4.1).

Figure 4.1: The NAD molecule from PDB entry 1BI9
Coordinates for the adenylate part of the molecule (left of picture) are resolved, with the entire nicotinamide nucleotide portion missing. The cleft in which the rest of the cofactor binds is marked.

There is no obvious solution to this problem; the partial resolution applied here is to trust the result of the graph matching only where the name of the reference graph matches the residue name taken from the PDB. In this case, the graph matching procedure becomes a verification of PDB residue names, rather than an *a priori* assignment of chemical identities. This approach is a conservative one in that, while it is unlikely to result in mis-assignment of ligand identity (unless for example the crystallographer mis-labels the partially resolved coordinates of an NAD molecule as ADP!), it may mean that ligands are disregarded as being unidentifiable. Consider the case of a molecule of type 'A', which has been erroneously labelled 'B'. Even if all of the atoms

of the molecule are resolved - and therefore we can in principle determine its identity - because of the name mismatch, the protocol described here would discard it.

In some cases, a single ligand graph matches more than one reference graph with the same degree of similarity. Most often, this occurs when more than one enantiomer of the reference compound is defined. The two compounds L-xylopyranose and L-arabinose (see figure 4.2) are an example of this.

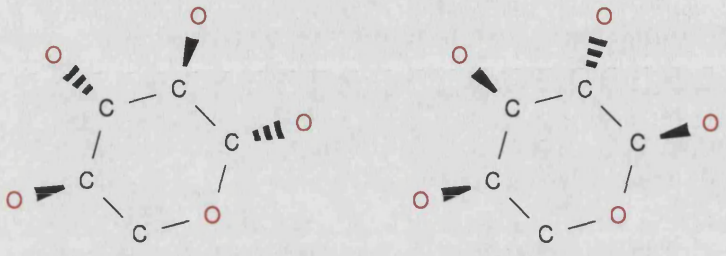

(a) L-xylopyranose (LXC) (b) L-arabinose (ARA)

Figure 4.2: Example of two isomeric compounds
The RCSB hetgroup IDs are given in parentheses.

In order to determine which match to accept, the handedness of any chiral centres present in the compounds can be compared. Each atom of each reference graph is annotated with its chirality. For any atom which is a chiral centre, the indices of its four substituents are also stored, in order of priority [1].

Once an isomorphism exists between the reference graph G_R and the ligand graph G_L, it is trivial to map the five vertices which constitute each chiral stereocentre, to the corresponding five atoms in the ligand molecule. Since, by definition, coordinates are available for those five atoms, the handedness of the chiral stereocentre found in the crystal structure can be deduced.

Calculation of the handedness of a chiral centre is performed as follows

$$\text{chirality} = \begin{cases} \text{R} & \text{if } (\overrightarrow{XB} \times \overrightarrow{XC}) \cdot \overrightarrow{XA} < 0 \\ \text{S} & \text{otherwise} \end{cases}$$

where X is the chiral central atom, and $A-D$ are the four substituents, in order of Cahn-Ingold priority[2]. The difference between the two chiralities can be understood intuitively by arranging the molecule so that one is looking down the $A-X$ bond. Now, if the path which moves through atoms B,C,D is in a clockwise directions, the stereocentre has *rectus* chirality; otherwise, it is *sinister*. The R and S chiralities are shown diagrammatically in figure 4.3.

The number of stereocentres whose chirality is different in the reference graph, to the ligand molecule, is counted. The list of matches is then sorted according to the number of chiral centre mismatches. Where more than one match has the same number of chiral centre mismatches, a match in which the labels of the

[1] At present, these orders are taken from the MSD database which is the source of the chemical reference information. In principal, however, they could be calculated directly from any chemical graph by applying the Cahn-Ingold-Prelog priority rules (Cahn *et al.*, 1966)

[2] Note that only three substituents are required in order to determine the handedness, but the chiral centre must have at least four in order to exist in stereochemically distinct conformations.

two graphs is identical is preferred.

In order to distinguish between molecules which failed to match the reference compound of the same name due to missing or mis-named atoms (or due to the fact that the compound itself was wrongly identified by the crystallographer) and those which failed to match due to incorrect stereochemistry, the following procedure was adopted. If a molecule named P failed to match reference compound P, but instead matched Q, the compounds P and Q were inspected to determine whether they were isomers of one another. This can be done trivially by comparing their graphs, while neglecting chirality information. Where the two compounds are found to be isomers, this fact is recorded, in order to allow the choice at a later date of whether or not to require that compounds strictly match in terms of their stereochemistry.

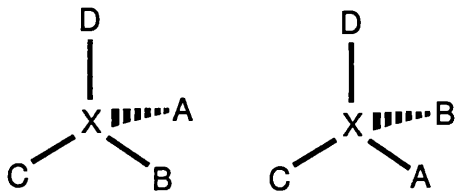

(a) R/+ (b) S/-

Figure 4.3: Convention for referring to the handedness of chiral stereocentres
The atoms A,B,C and D are ordered according to standard priority rules (Cahn *et al.*, 1966). The *rectus* form of the molecule occurs when the vectors $\overrightarrow{XA},\overrightarrow{XB},\overrightarrow{XC}$ form a right-handed set. This is also sometimes referred to as having a positive 'volume sign'. If these vectors form a left-handed set, the chirality is denoted *sinister*, or equivalently, the volume sign is negative.

4.1.3 Weaknesses

The procedure described here has several weaknesses, such as the problem of dealing with missing atoms discussed above. More generally, however, the method suffers from the same problems as any which relies on a reference compound set for chemical identification. As pointed out in Labute (2005), reference sets typically contain molecules in a neutral state, whereas the entity observed in a crystal structure is often a reaction intermediate and therefore may have different atomic charges and/or valences compared to the neutral structure. Nonetheless, the method described here has proven adequate as an automatic means for identifying most ligands correctly.

4.2 Protocol for comparing and clustering ligand binding sites

4.2.1 Aims

The aim of the clustering protocol is to group ligand binding sites according to the relatedness of the proteins which bind them. More specifically, the grouping is made according to the protein *domains* which contact the ligand, since in large, multidomain proteins, it is often the case that only a subset of the protein domains are involved in recognising the ligand. As discussed in §1.4, one way in which proteins can evolve is through 'domain swapping'; as such, relationships may exist between parts of a pair of proteins, which would be missed if the two proteins were compared as a whole.

We wish to obtain several levels of clustering. In order of increasingly coarse-grained groupings, these are:

1 Group together all identical binding sites.
2 Group together all binding sites whose domains could be identified as being related on the basis of sequence similarity alone (that is, whose sequences are more than 35% identical).
3 Group together all binding sites whose domains, although having low sequence identity, have been identified as being evolutionarily related on the basis of conserved structure and/or function.

From here on, these three levels of clustering will be referred to as the first-, second- and third-level clusterings respectively.

4.2.2 Multi-domain binding sites

A common problem which is encountered when performing this type of grouping of functional sites in proteins, be they catalytic sites or ligand binding sites, is how to handle cases where a site is situated at the interface of two or more domains.

To illustrate the problem, consider the two binding sites represented in figure 4.4. Although the majority of each site is contributed by domains which belong to the same homologous superfamily (the 'blue' domain), each ligand also contacts another domain, and this domain comes from a different superfamily in each case. Do we wish to cluster such sites together based on the relatedness of their shared domain, or do we judge the replacement of the red domain with the green one to be a sufficiently large evolutionary step to warrant placing the site in a new cluster?

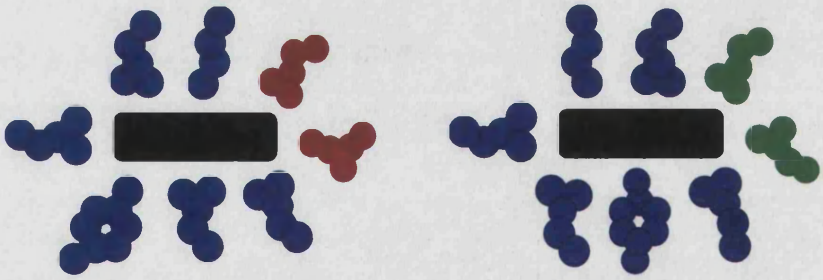

Figure 4.4: Multidomain binding sites
Two binding sites for a given compound are shown; in each, the ligand is represented schematically as a black rectangle. The colour of the residues which contact the ligand indicate the homologous superfamily to which they belong. Note that the domain may mutate so that it presents different chemical groups to the ligand, or so that the position of residues relative to it change. The binding site clustering protocol ignores these local changes and is only concerned with the identity of the domain as a whole.

This type of situation commonly occurs where the ligand in question is an enzymatic cofactor. Here, we often find that a certain conserved cofactor-binding domain is paired with a different catalytic domain in different proteins. An example of this is the Rossmann fold NAD-binding domain found in many oxidoreductases. This domain is found together with a variety of different catalytic domains (Bashton and Chothia, 2002). By interchanging the catalytic units, evolution has been able to generate proteins with new enzymatic activities without needing to re-evolve the capability to recognise and bind the cofactor.

Given that we seek an automatic binding site clustering method, there appears to be no clear-cut solution to the multidomain problem; here, a simple heuristic which gives mostly reasonable clusters is adopted.

4.2.3 The algorithm

Let us define a dissimilarity function, d, which returns a value bounded by $[0,1]$ for each pair of binding sites considered, where higher values indicate that the domain compositions of the two sites are more dissimilar. This function can then be used to populate a distance matrix, to which the clustering methods discussed in §3.2 can be applied.

The steps of the clustering protocol used here are as follows

1 For each site to be clustered, identify the set of residues which contact the ligand. This is done using a simple distance threshold - any residue which has at least one atom within 4Å of any atom of the ligand is considered to be part of the binding site. Note that we do not require that the residue must make an attractive contact with the ligand. This is partly a pragmatic choice, since to do so would be more computationally demanding. It is also motivated by the idea that even residues which do not directly contact the ligand may play an important structural role within the binding site. Ultimately, however, these details are unlikely to significantly affect the clustering result.

2 Annotate all amino acid residues in the binding site according to the domain to which they belong. Here, CATH version 2.6.0 was used, but this annotation could in principle be done according to any other hierarchical domain classification scheme, such as SCOP. Residues which are not annotated as belonging to any domain are marked as unclassified.

3 Decide upon a level, L at which the clustering will be performed. This level must be one of the levels in the domain classification hierarchy. For example, if we want all binding sites composed of domains with similar sequences (to 35% identity) to be grouped together, we should choose the S35 level. If, on the other hand, we want all binding sites composed of domains in the same homologous superfamily to be grouped together (a more coarse-grained clustering), we would choose the H level.

4 For each domain in the binding site, obtain its ancestor within the domain hierarchy, at the level chosen above. In this way, produce a list of all L-level nodes which contribute to the binding site, each one associated with the fraction of the binding site residues which it contributes. Consider the following example.

   Let us imagine a binding site, X, composed of three domains a,b,c, which contribute 2, 3 and 4 residues to the site respectively. In addition, the site contains one residue which is not classified as belonging to a domain (see figure 4.5). We wish to cluster sites at the homologous superfamily level, so the CATH codes for each domain are retrieved, to the fourth level. These are a : 1.2.3.4, b : 1.2.3.4 and c : 5.6.7.8.

   Since domains a and b belong to the same homologous superfamily, their fractional contributions of 0.2 and 0.3 are summed to obtain the total contribution of the 1.2.3.4 family to this site. We can therefore write the composition of X, in terms of homologous superfamilies, as follows

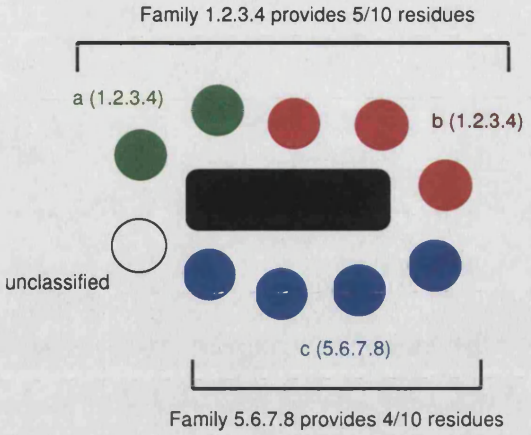

Figure 4.5: Example of binding site domain composition
Binding site residues are represented as circles, with the colour of each one indicating the CATH superfamily of each domain.

$$X = 0.1, \{(1.2.3.4, 0.5), (5.6.7.8, 0.4)\}$$

where the 0.1 represents the fraction of binding site residues which were unclassified. In general, the binding site composition is represented by

$$X = u, \{(x_1, p_1), \ldots, (x_m, p_m)\} : \sum_{i=1}^{m} (p_i) + u = 1 \tag{4.1}$$

where the x_is stand for the L-level ancestors of domains in the binding site, the p_i for their fractional contributions, and where u is the fraction of residues in the binding site which were not classified as being part of any domain.

5 For each pair of binding sites, compute the dissimilarity between their domain compositions, as represented by expression 4.1. The dissimilarity value is calculated as follows. Start with a value of 1. For each L-level node which occurs in both sites, subtract from the current dissimilarity value, the smaller of the two fractional contribution values associated with this node. The result is therefore a number bounded by $[0, 1]$.

Algorithmically,

$$d(X,Y) = 1 - \Sigma_{i=1}^{m} \Sigma_{j=1}^{n} \sigma_{ij}$$

$$\sigma_{ij} = \begin{cases} \min(p_i, q_j) & \text{if } x_i = y_j \\ 0 & \text{otherwise} \end{cases}$$

For example, if we imagine that we have two sites $X = 0.1, \{(1.2.3.4, 0.5), (5.6.7.8, 0.4)\}$ and $Y = 0.2, \{(1.1.1.1, 0.2), (5.6.7.8, 0.6)\}$, the only node shared is 5.6.7.8. The smaller contribution of this node (0.4, to site X) is subtracted from 1, resulting in a dissimilarity value of 0.6.

In order to generate a ligand dataset, firstly any site for which less than 80% of its residues are classified in CATH, is discarded. Then, the groupings (1-3) listed previously are obtained by applying the clustering protocol three times. Firstly, the sites are clustered based on their S95-level annotation. By applying a cutoff

threshold, distinct clusters are obtained. A representative is then chosen from each cluster.

The choice of representative is made on two criteria: firstly, structures which are thought to represent the true biological unit are preferred. This is to prevent the dataset being contaminated by binding sites which, although in reality occurring at a subunit interface, only have half of their coordinates present in the ASU due to crystallographic symmetry. All structures in PQS are annotated according to whether the algorithm predicts that the inter-subunit contacts in the proposed assembly is likely to be biologically relevant, as opposed to simply being crystal packing artefacts. Sites are then ordered according to the resolution of the structure.

Stage	CATH level	Clustering algorithm	Dissimilarity cutoff
A	S95	single linkage	0.4
B	S35	complete linkage	0.4
C	H	complete linkage	0.4

Table 4.1: Clustering steps used to generate ligand datasets
The first stage is done using single-linkage clustering for reasons of efficiency. For certain ligands (*e.g.* HEM), there are many examples in the structure database, meaning that application of complete linkage clustering would be very slow. The choice of clustering algorithm has little influence on the results of this stage. The choice of the dissimilarity threshold of 0.4 was heuristic, being based on visual inspection of the clusters obtained, and assessment of their biological significance.

The representatives from this first stage of clustering are then clustered on their S35-level annotation, and the representatives from this stage are grouped based on H-level annotation. These three stages are summarised in table 4.2.3.

It should be stressed that this protocol clusters binding sites only on the basis of the complement of domains which actually contact the ligand; it does not attempt to cluster proteins as a whole. As such, it is quite possible that binding sites which come from related proteins are placed into separate clusters by this procedure, if the evolution of the protein family has changed the composition of the binding site. Therefore, when reference is made to ligands in the same cluster, this should be read as "ligands contacted by the same combination of related domains".

A caveat to this automated procedure is that ligands may also be placed in separate clusters if they bind in a different sites within the same protein, or if two ligands bind in the *same* site, but in a sufficiently different orientation that the set of domains contacting it are changed.

4.3 Architecture of the processing pipeline

The aim of the pipeline, as stated previously, is to generate, for any specified ligand type, a list of all instances of that compound co-crystallised with proteins, and then to provide a hierarchical grouping of that list based upon the evolutionary relationships between the binding sites. For instance, the pipeline can generate a dataset consisting of all ATP ligands found during the validation process.

While this chapter focusses on whole ligands, at this point, it should be pointed out that the dataset generation pipeline can also be used to collect sets of ligands which share a common fragment. For example, one may

be interested in adenine recognition in general, with the identity of the adenine-containing ligand being unimportant. In this case, a list of all instances of every adenine-containing molecule (*e.g.* AMP, ADP, ATP, NAD, FAD, *etc.*) can be generated. This set of molecules is then clustered using the same domain-based procedure just described, but only those residues which contact the adenine moiety of each molecule are taken into account. Fragment-centric analyses of ligand recognition feature heavily in chapter 6, and will be discussed further at that point.

An overview of the architecture of the pipeline used to generate ligand datasets is shown in figure 4.6. The main stages of the process are as follows:

1 **Populate an archive of reference compounds.** The source of the reference compounds can either be a local instance of the MSDchem database, or otherwise, the user can supply any arbitrary set of compounds in the form of MOL2-format files. In this study, the set of compounds used for ligand validation were obtained from MSDchem. A list of molecular fragments of particular interest were built by hand and used to populate a separate ChemBase archive; this set was used for the the analysis presented in chapter 6.

2 **Build a domain tree.** The hierarchical relationships between nodes in either the CATH or SCOP domain classification schema are stored as a GAMUT binary file. This is for two reasons: firstly, efficiency, since it means that the CATH or SCOP flat-files need only be parsed once, and secondly, to abstract away the differences between the two classifications. Once either CATH or SCOP has been converted into a GAMUT domain tree object, the applications which use it are able to be agnostic as to its original origin.

3 **Perform ligand validation.** Using the archive of reference compounds generated above, and a source of coordinate data, all ligand molecules found in the input structures have their identity determined and recorded by the `build_match_table` program, using the protocol described in §4.1. The source of coordinate data used in this study is the PQS archive; due to the modular nature of the pipeline, any other source of structural data (*e.g.* PDB, MSD) could be in principal be substituted here.

4 **Determine ligand-domain contacts.** For each ligand molecule in the list generated above, the `build_contact_table` program determines the set of protein residues which contact it, by inspection of the coordinates. The domain to which each residue belongs (if it is classified) is found by reference to the domain tree, and the list of domains contacting the ligand is then stored.

5 **Generate ligand dataset.** The dataset produced by the `generate_ligand_dataset` program is in the form of a number of formatted text files which unambiguously identify the ligand molecules matching the description provided, and which indicate to which cluster each ligand belongs at each of the three clustering stages (§4.2). In addition, a file is generated which lists several types of data for each ligand, including the resolution of the structure, its EC number if present, and a summary of the domain composition of the binding site.

Stages 1-4 above need only be carried out once for any given set of structures, and, when the coordinate database is updated, need only be performed on new structures. Since the computationally expensive calculations have then already been carried out, generation of the dataset for a given query is a relatively fast operation. The following sections expand on the details of several of the steps listed above.

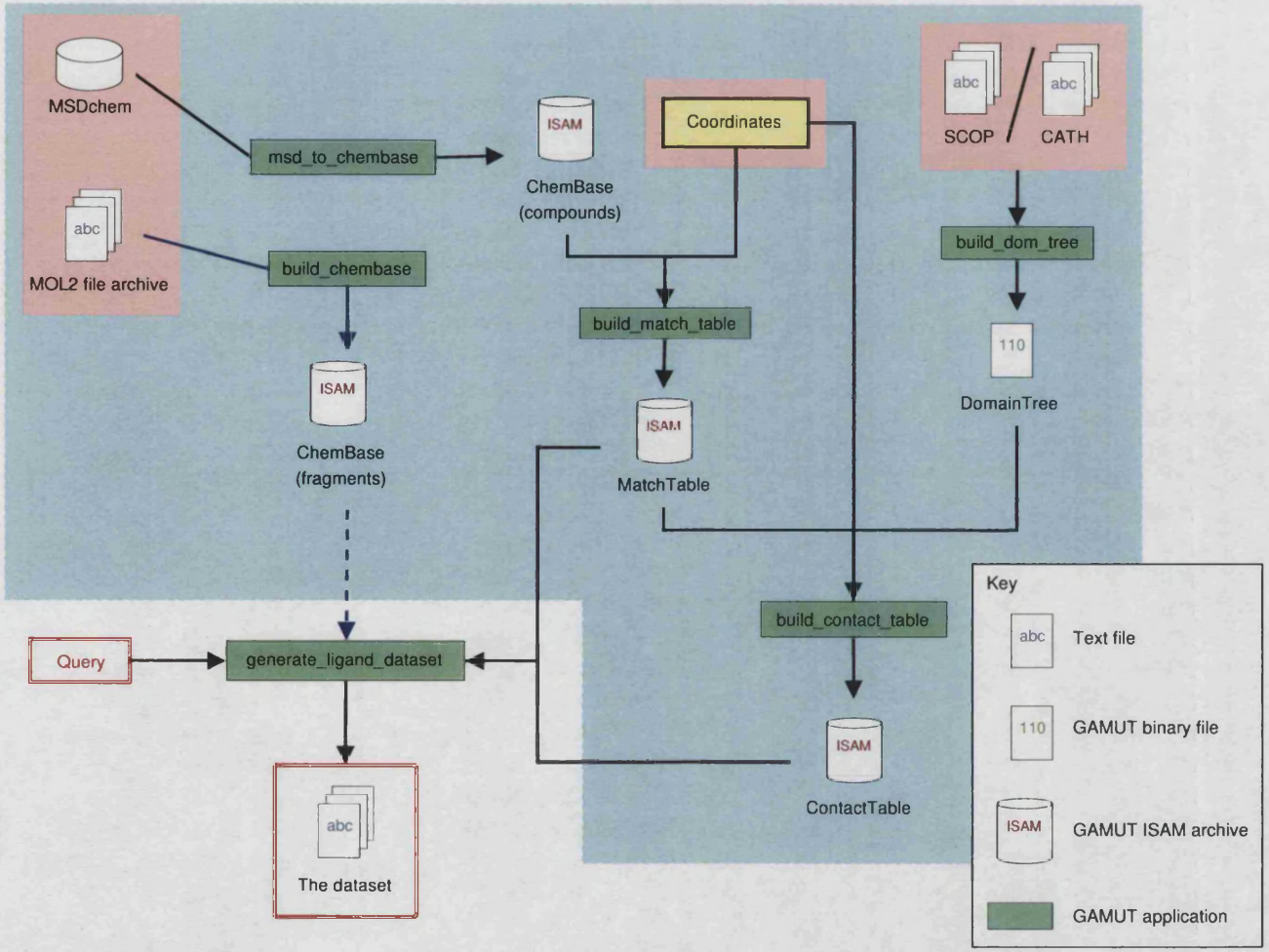

Figure 4.6: Dataset generation pipeline

This diagram shows the main components in the computational pipeline for generation of datasets of ligand binding sites, clustered according to relationships between the proteins. By precalculating and storing certain information, datasets can be rapidly generated on provision of a 'query', which in this context is a definition of a ligand type, or fragment thereof. Pink shaded areas indicate the primary data resources with which the process begins. The blue shaded area encloses the calculations which need only be done once for a given set of structures. The form in which data is stored at each step (*e.g.* relational database, text file, binary file) is indicated pictorially. Blue lines indicate parts of the pipeline used for fragment-centric analyses (chapter 6). The dotted line indicates that the fragment archive is optional at the dataset generation step.

4.3.1 Obtaining the chemical compound data set

Distributed with the GAMUT library are three command-line tools for populating and manipulating ChemBase archives. The first of these, `build_chembase`, simply parses a list of MDL MOL2 files, and creates a new ChemBase archive containing one chemical graph per input file. Since most databases of chemical structures are available in MOL2 format, this application can be used to populate ChemBase archives with data from a variety of sources.

The second ChemBase-related program, `msd_to_chembase`, populates an instance of ChemBase by querying the MSD. The command-line options of this application afford the user a certain degree of control over the subset of MSD compounds which are loaded into the archive. Since the MSD chemical compound table is intended to contain an entry for *every* chemical entity present in the PDB, it contains reference compounds which may not be of interest for a ligand-centric study, such as standard amino acids and nucleotides. Furthermore, the MSD distinguishes between different forms of certain compounds according to their *linking* status: for example, where an amino acid is found to be bound to a protein as a substrate, it is added to the chemical compound dictionary in a separate entry from that which refers to the same amino acid as found in polypeptide chains. This information is encoded in the RCSB_HETTYPE field of the CHEM_COMP MSD table. Using the appropriate combination of `msd_to_chembase` options, the user can specify that certain types of compounds are to be ignored, for example to exclude the 'linking' versions of nucleotide monomers.

The distribution of MSD compounds, according to their RCSB_HETTYPE annotation, is shown in figure 4.7. For all work presented in this thesis, a ChemBase archive consisting of 4857 compounds (those with NON-POLYMER or a saccharide type) was used.

The third program relating to chemical compounds is named `chembase_utils`. As the name suggests, this is something of a "swiss army knife" program, allowing the user to perform a variety of operations including

- extract structures from a ChemBase archive, writing them out as MOL2 or PDB files
- concatenate several ChemBase archives to form a single database
- produce PostScript images of structures stored in an archive
- identify rotable bonds
- identify potential hydrogen-bonding atoms

RCSB_HETTYPE	Number of compounds
D-PEPTIDE LINKING	27
L-PEPTIDE LINKING	439
D-SACCHARIDE ⋆	126
L-SACCHARIDE ⋆	15
SACCHARIDE ⋆	263
DNA LINKING	139
RNA LINKING	94
NON-POLYMER ⋆	4594
Null	258
	5955

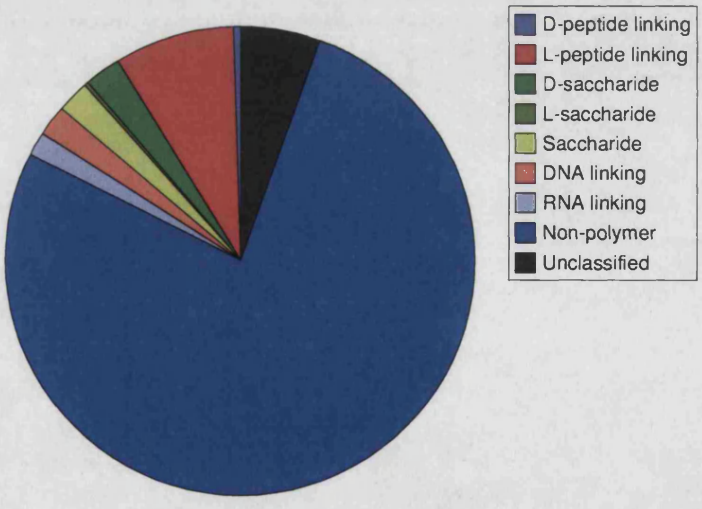

Figure 4.7: Number of compounds in MSD reference dictionary, broken down by RCSB_HETTYPE
Asterisks indicate those classes of compound which were included in the ChemBase archive used for PDB ligand validation

4.3.2 Representation of mappings from molecular structures to reference compounds

A UML diagram summarising the design of the classes for representing the identity of a ligand, and for mapping its atoms to a reference graph (see §2.3.4.3), is shown in figure 4.8. The `Identity` class stores a set of descriptors which uniquely identify a given ligand molecule in the database: namely, the PDB identifier of the entry in which the ligand was found and the chain code, residue name and number used to refer to it in the PDB entry. Each object also stores a flag indicating whether the molecule is covalently or non-covalently bound to a protein.

The `Match` class inherits from `Identity`, therefore each `Match` object also contains the information which identifies a given ligand. In addition, it stores the name of the reference compound to which the ligand was matched during the validation procedure, and a list of indices which represent the mappings from ligand atoms to reference graph vertices.

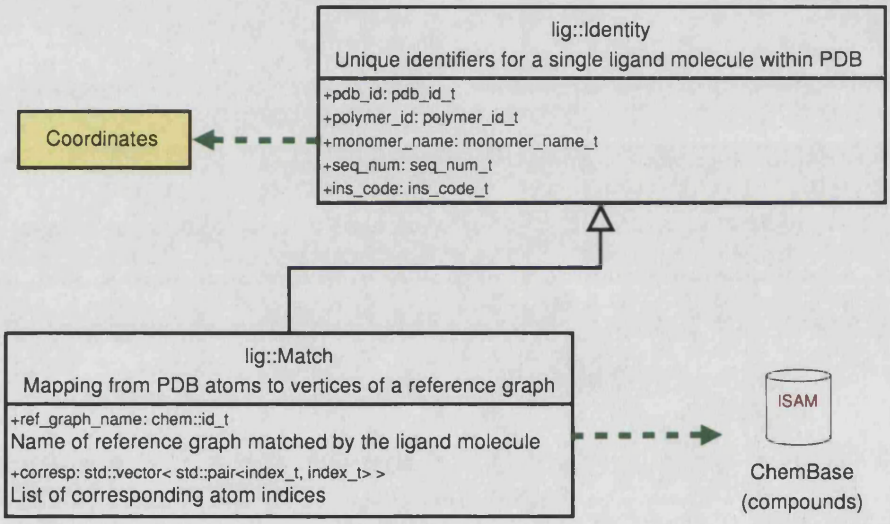

Figure 4.8: UML diagram of classes which represent ligand identity
The Match class inherits from the Identity class. Green dotted arrows indicate the primary data sources to which the objects' member variables refer. A MatchTable archive is therefore only meaningful when read in conjunction with the coordinate source and ChemBase archive used to construct it.

The `MatchTable` class stores a list of `Match` objects. The indices used to access this archive are the ligand descriptors mentioned above. As such, the table can serve as a queryable database of ligands present in the set of structures. Specifically, it can be used to rapidly return a list of all ligands of a given chemical type, or all ligand molecules bound to a specified PDB entry.

The class used to represent the actual coordinates of ligands and their environments is called `lig::Site`, and inherits from the `mmol::Molecule` class (§C.2.1). Its interface is as follows. Member functions allow the client to specify the ligand molecule of interest by providing a `Match` object; the `Site` class is able to store the identity of this ligand internally using the selection framework described previously. Once the ligand has been selected, other member functions may be called which identify all atoms and residues within a specified distance cutoff from the ligand; again, these are recorded as selections. By providing the appropriate `chem::Graph` object (*i.e.* the reference graph to which the ligand molecule was matched),

a transformation may be computed which superposes the ligand, or a fragment of it, onto the reference structure. This transformation is recorded inside the `Site` object, allowing the client at a later date to invert it, transforming the coordinates of the binding site back to the coordinate frame used in the original structure. Finally, a member function is defined which removes all parts of the original structure, save for the selected ligand and binding site region. Given a MatchTable archive and the original source of coordinate data which was used to build it, the `lig::Site` class provides a convenient framework which applications can use to manipulate the ligand(s) of interest.

4.3.3 Representation of ligand-domain contacts

For each atom of a ligand molecule, the residues which contact it are identified by the `build_contact_table` program. In order to store this information in a compact manner, the record for each ligand molecule contains the following data:

- A list of the domain identifiers which contact the ligand, stored as text (*e.g.* $\{1h8hD2, 1h8hD3\}$)
- For each atom of the ligand, a list of pairs of indices $\{(d_1,x_1),\ldots,(d_n,x_n)\}$ where each d_i is the index of a domain which contacts this atom, and the x_i is the sequential offset into that domain. For example, if the tenth residue of domain $1h8hD2$ contacts a given atom, its contact list would contain the index pair $(0,9)$.

Storing the data this way allows different types of questions to be asked about the ligand's contacts later on, specifically:

- Which domains contact the ligand?
- How many residues from each domain contact the ligand?
- Which parts of the ligand are contacted by a given domain?

Since no coordinate data need be queried in order to answer these questions, they can be processed very quickly.

Contact records are archived in an ISAM table in the same way used to store Match objects. As a consequence, once a list of the ligand molecules of interest has been generated, obtaining domain contact information for each one is a simple matter of querying the archive object.

4.3.4 Generation of the ligand dataset

Once the MatchTable archive has been constructed, generation of the dataset of all instances of a given ligand (or of ligands containing a given fragment) is a simple matter of querying the ISAM table. This is done by providing the name of either a ligand or a fragment to the `generate_ligand_dataset` program.

The `generate_ligand_dataset` program performs either one or both of the following roles:

1 Generate a list of the identities of either all ligands of a given type, or all ligands containing a given fragment, from the MatchTable archive.

2 For a list of ligands, apply the clustering protocol (§4.2), for a given level in the domain hierarchy and with a given dissimilarity threshold.

In order to perform the three-stage clustering described previously, the program is simply run three times, as shown in figure 4.9. The first time, the input is a ligand/fragment definition. The subsequent steps each consist of clustering the list of representatives obtained from the previous step.

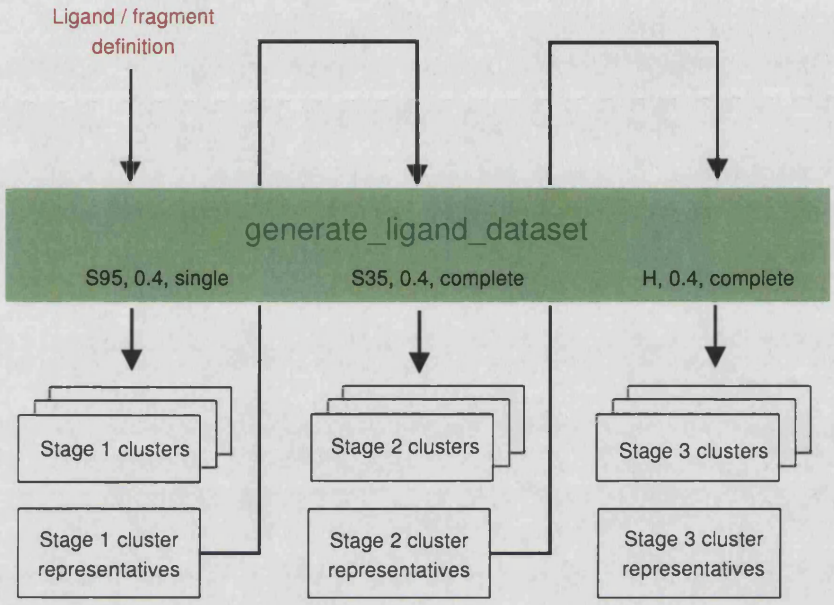

Figure 4.9: Generation of the ligand dataset
The `generate_ligand_dataset` program is used to generate, and then iteratively cluster, a list of validated instances of the required ligand or molecular fragment. At each stage, representatives from each cluster form the input to the subsequent stage. Parameters used for each clustering step are shown in the green box (see §4.2).

4.3.5 Maintainance of integrity

The data archives described above are intended primarily as read-only structures, and as such, they do not require the type of integrity checking mechanisms used in traditional databases (Silberschatz *et al.*, 1997). However, since different archives reference one another, a minimal check is needed to make sure that the correct version of an archive is being used.

Since GAMUT data archives are stored as normal files rather than being marshalled by a data management system of some kind, a timestamping mechanism is used in the pipeline. Whenever a binary file (such as a DomainTree object, or an ISAM archive) is generated, the time of creation is stored within it. When this file is then used in the generation of a second data file (such as when a MatchTable archive is used to build a ContactTable) the first file becomes a *dependency* of the second. In other words, it must be guaranteed that, at a later date, when the ContactTable and MatchTable archives are queried together, the correct instances of those archives are used. To do this, the timestamp of the dependency is stored within the dependent; here, the timestamp of the MatchTable archive is recorded within the ContactTable. By cross-referencing these numbers whenever the files are accessed, consistency is guaranteed.

The choice to construct much of the pipeline around binary file formats was taken for reasons of computational efficiency, as discussed in §2.3.4.1.4. However, this is obtained at the cost of transparency: the user cannot directly inspect the content of files generated at different steps of the pipeline. In addition, since these files are only readable by GAMUT applications, the data cannot directly be used by other programs.

Both of these concerns are addressed by providing utility programs which can be used to query and extract data from all of the binary file formats used in the pipeline. Command-line tools are available which allow either interactive querying or batch processing of each type of data archive. These can be used to generate human-readable reports of the data, column-separated files for import into spreadsheets or processing by other programs, and, where applicable, to export data in commonly-used file formats such as PDB or MOL2. The latter means that, although conceived and designed as a complete processing pipeline, individual modules from the schema shown in figure 4.6 may be used in isolation, with their output then being passed on for processing by other third-party tools.

A possible future development for the pipeline would be to replace some of the binary data files with a more portable format such as XML. The binary serialisation mechanism used in GAMUT is already abstracted to a significant degree from individual objects, so it could be extended fairly trivially to support XML serialisation.

4.3.6 Improving performance through parallelisation

The early stages of the pipeline described above are relatively time-consuming (ligand validation on ~20,000 PDB structures takes more than 24 hours on a single 2.4GHz workstation). Particularly during development and refinement of the method itself, the duration of these calculations were found to be prohibitive, so the programs `build_match_table` and `build_contact_table` were parallelised.

Both of these programs simply apply a single operation (in the first case graph matching, and in the second, geometric range querying) sequentially to a large number of ligand molecules. They are therefore ideal candidates for parallelisation. The strategy adopted here is based on a master-slave architecture. Given $N+1$ processes, we designate one to be the master, and the remaining N are the slaves. The master process reads the list of molecules to be processed, and then iterates through the list. At each step, it polls the group of slave processes to determine whether any are idle; if all slaves are busy, the master waits until one becomes free. The next molecule is then dispatched to a free slave, and the master progresses down the list.

Object-oriented programming techniques (§2.1.2) may be leveraged to simplify the process of parallelising an application. The first step is to encapsulate the 'driver' functionality (reading the list of inputs; iterating through it) and the 'worker' role (processing each entity in the list) each in a separate class. Once this is done, implementation of the serial version of the application is a simple matter of creating an instance of each of these classes, and then writing a couple of loops.

Writing the parallel version of the code requires only slightly more work: all that needs to be done is to augment the driver and worker classes by adding functions which allow them to communicate with one another. Specifically, the `Master` class, which inherits from `Driver`, needs a function to send the next entry

to a given slave, and a function to receive the results of that slave's processing. The `Slave` class requires corresponding functions which mediate its end of these communications (see figure 4.10). By isolating the data processing code from that which handles master-slave communication, the resulting program is considerably easier to understand.

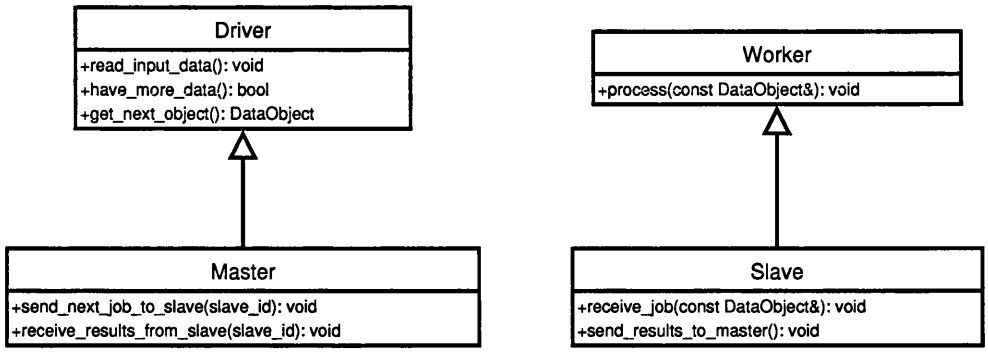

Figure 4.10: UML diagram of master/slave classes

Inter-process communication was performed using the Local Area Multicomputer (LAM) (Burns *et al.*, 1994) implementation of the Message Passing Interface (MPI) standard (Message Passing Interface Forum, 1998). Processing was carried out on a homogeneous Linux cluster providing up to 120 nodes. The speed increase upon parallelisation is roughly linear with respect to the number of processors used (results not shown). Utilising ~100 nodes, ligand validation can therefore be performed on all structures in the PDB in approximately 30 minutes.

4.4 Ligands in the PDB

The ligand validation procedure described in §4.1 was applied to all structures in the PQS database as of January 2005. This consisted of assemblies derived from 24,933 PDB entries. The dataset of 4857 compounds discussed in the previous section was used as the reference compound set. Molecules with fewer than 3 or more than 60 atoms were skipped. The remainder, a total of 110,988 molecules, were matched against the reference dictionary, allowing up to 2 mismatches per comparison. This is summarised in table 4.2.

4.4.1 Results of the validation procedure

4.4.1.1 Bound state of potential ligand molecules

Figure 4.11 shows the distribution of 'bound states' for all molecules inspected. The environment of each molecule was inspected to determine whether it was non-covalently or covalently bound to any other molecule. Where the ligand was more than 4Å away from any other molecule, it was classified as 'free'. Where it was within 4Å of a protein molecule, the ligand was classified as 'non-covalently bound'. Approximately a third of molecules inspected were covalently bonded to another residue; these cases were separated into those where the ligand is attached to a protein, and those where it is attached to another hetgroup molecule.

Source data	Number of compounds in MSDchem (January 2005)	5,955
	Number of compounds in reference compound set	4,857
	Source of coordinate data	PQS (January 2005)
	Number of structures processed	24,933
Pre-processing	Number of molecules inspected	164,727
	Number of molecules too small (< 3 atoms)	52,820
	Number of molecules too large (> 60 atoms)	919
Graph matching	Number of molecules checked	110,988
	Number of mismatched atoms tolerated	2
	Graph properties ignored	chirality, charge,aromaticity, bond order
	Graph properties retained	atom type, valence
	Bond tolerance	0.2Å
	Number of non-covalently bound ligands with validated identities	56,231 (from 12,629 entries)

Table 4.2: Summary of ligand validation procedure
This table summarises the key parameters used when applying the ligand identity validation procedure to generate the datasets used in the current study.

The 9% of molecules which were classified as 'free' almost exclusively consist of ions (mostly Ca^{2+}, Mg^{2+} and Na^{2+}), and other ingredients commonly found in crystallisation liquors, such as glycerol (compound name GOL) and acetate (ACT). Several are structures of intercalating agents crystallised with segments of nucleic acid chains (*e.g.* daunomycin in PDB entry 1O0K), or of prosthetic groups from low-resolution structures of membrane proteins in which the polypeptide chains were poorly resolved and therefore have missing coordinates (*e.g.* the light-harvesting complex in PDB entry 1VCR).

Approximately 19% of molecules surveyed were found to be covalently bonded to proteins. A large proportion of these molecules (around 11% of the total) are actually non-standard amino acids such as

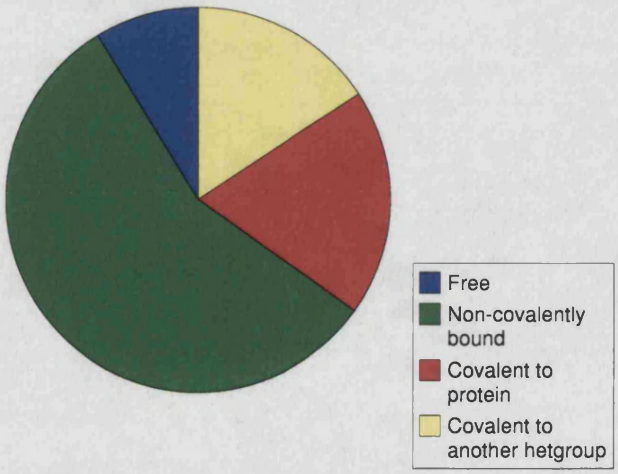

Figure 4.11: Distribution of the bound state
Distribution of bound states for all 110,988 molecules inspected during the validation procedure. 'Free' indicates that the molecule was more than 4Å away from any other molecule. 'Bound' indicates that the molecule was within 4Å of a protein. Where molecules were found to be covalently bonded to another molecule, a distinction is drawn between hetgroups bonded to protein, and hetgroups bonded to other hetgroups.

selenomethionine (MSE) and N-dimethyl-lysine (MLY), which were not recognised as protein constituents and therefore treated as potential ligands by the validation procedure. Unsurprisingly, the remainder consists overwhelmingly of post-translational modifications such as N-acetyl-glucosamine (NAG) and myristic acid (MYR). Attachment of these and other carbohydrates is one of the most common post-translational modifications applied to eukaryotic proteins, particularly those which are secreted or inserted into the membrane. Although there is no single function associated with these adornments, in many cases, they seem to lengthen the lifetime of secreted proteins by slowing their rate of clearance from the serum (Chitlaru *et al.*, 1998). In the case of membrane-bound proteins, these sugars are frequently involved in interactions with other proteins, including those which mediate cell-cell communication (Alberts *et al.*, 1994).

Also found in this group are 78 FAD molecules, which are known to be covalently attached in certain protein families (Dym and Eisenberg, 2001). In addition, 496 heme molecules were found to be covalently attached to proteins. These come from structures of c-type cytochromes which, for reasons which are not fully understood (Barker and Ferguson, 1999), appear to be unique among heme-utilising proteins in forming covalent bonds to the cofactor.

13% of the molecules checked were found to be covalently bonded to other hetero-group molecules. This set is quite diverse, containing substantial numbers of saccharide units such as NAG and mannose (MAN), and various small chemical groups such as methyl, phosphate, iodide and sialic acid. Several structures in which heme is bound to carbon monoxide (*e.g.* 1MZ0, 1VRE) are also found in this group.

The majority of the molecules studied, however (57%), and the set with which the remainder of this thesis will be concerned, are those which are non-covalently bound by protein.

4.4.1.2 Results of graph matching

Figure 4.12 shows the distribution of validation results for all molecules checked. The first thing to note is the large number of molecules (around 31%) discarded due to being too small (fewer than 3 non-hydrogen atoms). The size threshold was implemented specifically to exclude ions, and crystallisation solvents often found in crystal structures. Only a small proportion of molecules (0.5%) were excluded due to being too large (more than 60 atoms). These molecules, particularly cyclic compounds such as siroheme (SRM) and cyclodextrin (ACX) were found to significantly slow down the graph-matching procedure, and were therefore excluded from validation for purely pragmatic reasons.

In order to focus on 'true' ligands, rather than post-translational modifications and other covalently attached groups, in figure 4.13, the same data is re-plotted, this time omitting those molecules excluded from validation on the basis of their size, and only showing those molecules classified as non-covalently bound.

The majority of molecules in this set (84%) match the reference compound with the same name as the PDB residue name. A further 8% match to compounds which are stereochemical variants of the molecule named in the PDB entry. Only 8% of molecules either matched a different compound, or failed to match to any reference compound altogether. Taking those molecules which matched with 100% identity to the same isomer of the compound named in the PDB file, this gives a total set of 56,231 ligand molecules from 12,629

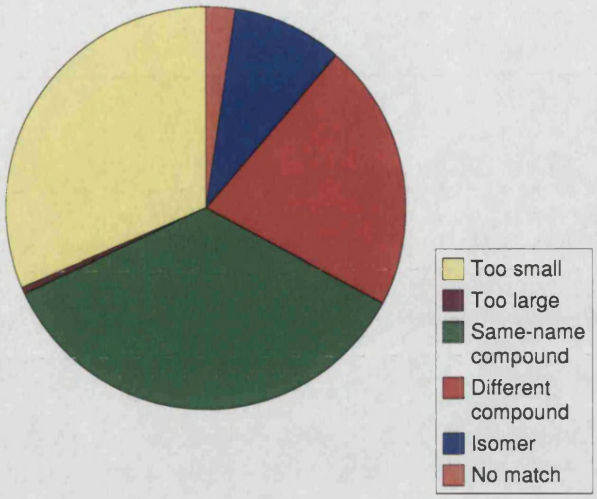

Figure 4.12: Distribution of matching results
Distribution of validation results for the 110,988 molecules surveyed. Meanings of the different classes are explained in the text.

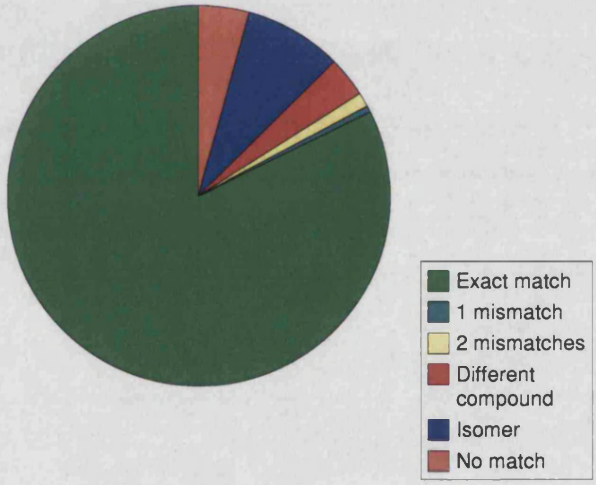

Figure 4.13: Bound ligand matching
This figure shows a subset of the data from figure 4.12. First, all molecules except those non-covalently bound to protein (see figure 4.11) were excluded. Of the remainder, molecules which were skipped during validation due to being either too large or too small, are omitted from the chart.

PDB entries for which chemical identity can be unambiguously assigned.

4.4.1.3 Examples of automatic identification of problems in ligand data

The following examples illustrate some of the inconsistencies discussed previously, which were automatically identified during the validation procedure.

PDB entry 1GY3, a structure of human CDK2 resolved to 2.7Å, contains two molecules whose residue name is ATP. They both match the reference graph for ADP, and indeed the PDB header states that the molecule was crystallised in the presence of Mg-ADP. The MSD page for 1gy3 identifies this ligand incorrectly as ATP.

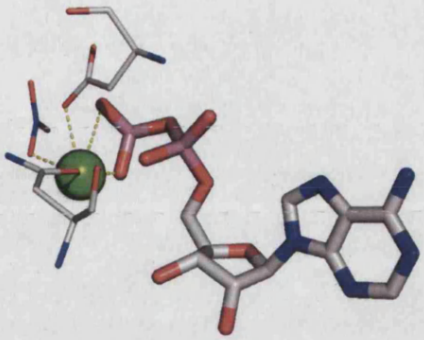

The ADP molecule from PDB entry 1GY3

PDB entry 1N48 is a structure of a bacterial DNA polymerase IV to 2.2Å. This protein is a member of a superfamily of polymerases known as the Y-family polymerases, which repair damaged DNA. The structure was solved in the presence of dideoxy-ATP (Ling *et al.*, 2001), but the ligand is named ATP in the PDB file. The validation procedure identified this molecule as being an instance of DAD (2',3'-didexoxy-ATP). The MSD page for 1N48 identifies this ligand incorrectly as ATP.

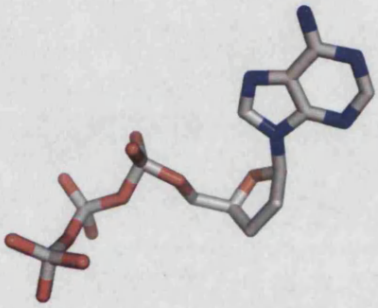

The ddATP molecule from PDB entry 1N48

In PDB entry 1K0U, a 3.0Å structure of rat S-adenosylhomocysteine hydrolase, the atom type of the NC3 atom, the carbon of the nicotinamide ring to which the carboxylamine group is attached, has been wrongly specified as nitrogen. This manifests itself as a single-vertex mismatch during validation.

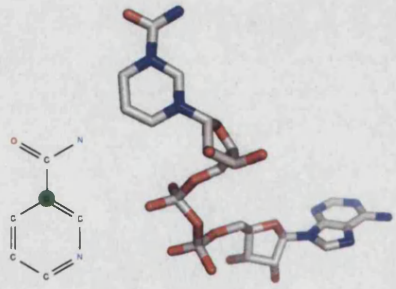

The NAD molecule from PDB entry 1K0U. The correct structure of a nicotinamide group is shown for comparison, with the NC3 carbon highlighted.

PDB entry 1IZL is a particularly low-resolution (3.7Å) structure of bacterial photosystem II. Only the porphyrin rings of the heme groups are resolved, resulting in these ligands failing to match any reference graph.

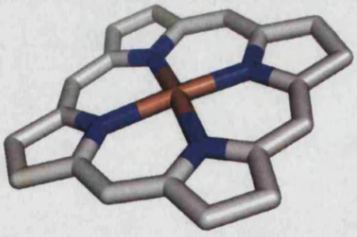

Coordinates of the partially resolved heme molecule from PDB entry 1IZL.

Of the four examples shown above, three come from structures of fairly poor quality, and could therefore be excluded by simply applying a threshold to the resolution of structures which are accepted for further analysis. However, the method shown here is more generic, and is capable of detecting problems, for example due to human error, which may still occur even where the crystallographic data itself is of a high standard.

4.4.1.4 The most common ligand types

The compounds which are most commonly found in complex with proteins are shown in figure 4.14. For each compound, the number of validated instances in the PDB are shown, along with the number of distinct PDB entries in which those instances were observed. The 20 most frequently observed molecules essentially consist of the most common biological cofactors (HEM, NAD(P), ADP, ATP, FAD, FMN) and widely used crystallisation buffer ingredients (PO4, DMS, EDO, FMT, TRS). Other molecules of biological interest are less frequently found, for example the guanosine nucleotides GDP (235 instances in 143 PDB entries), acetyl co-enzyme A (180/58) and GTP (122/46).

It should be remembered, however, that these counts simply reflect the number of times in which a given molecule has been co-crystallised with a protein. As such, they are influenced by the non-uniformity in the number of structures for a given protein family which have been deposited in the PDB. The prevalence of heme structures is an illustration of this: partly as a result of its historical status, myoglobin and the related protein hemoglobin have been heavily studied, resulting in a somewhat disproportionate number of their structures being present in the database.

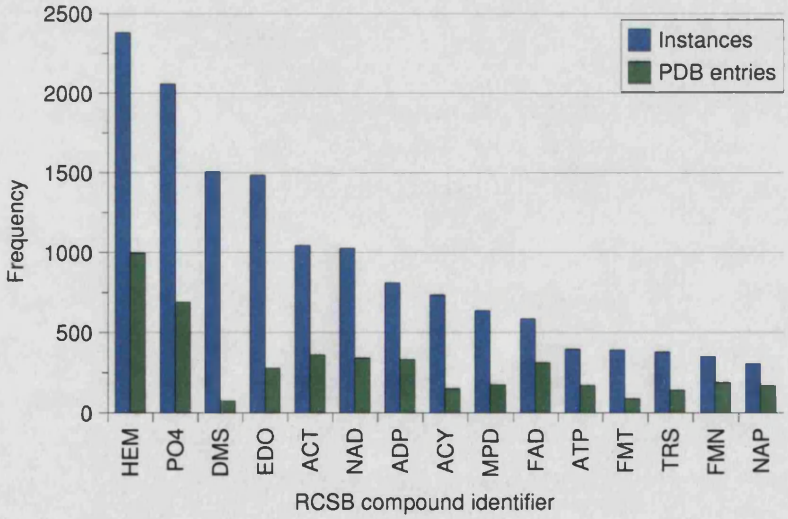

Figure 4.14: Most commonly-occurring hetgroups in the PDB
Blue bars indicate the number of instances of molecules which matched exactly to the reference graphs shown. Green bars represent the number of distinct PDB entries in which the matching molecules were found. The common names corresponding to the RCSB compound identifiers shown here are given in table 4.3. Note that the top two most commonly-occurring molecules, SO4 (sulphate ion, 11,867 instances) and GOL (glycerol, 3692 instances) have been omitted for clarity.

RCSB identifier	Common name	Likely biological ligand?
ACT	Acetate ion	⋆
ACY	Acetic acid	⋆
ADP	Adenosine diphosphate	✓
ANP	Phosphoaminophosphonic acid-adenylate ester	✓
ATP	Adenosine triphosphate	✓
COA	Coenzyme A	✓
DMS	Dimethyl sulfoxide	×
EDO	1,2-ethanediol	×
FAD	Flavin adenine dinucleotide	✓
FMN	Flavin mononucleotide	✓
FMT	Formic acid	×
GDP	Guanosine diphosphate	✓
GTP	Guanosine triphosphate	✓
GLC	Glucose	✓
HEC	Heme c	✓
HEM	Heme b	✓
MPD	2-methyl-2,4-pentanediol	×
NAD	Nicotinamide adenine dinucleotide	✓
NAP	Nicotinamide adenine dinucleotide phosphate	✓
PO4	Phosphate ion	⋆
TRS	2-amino-2-hydroxymethyl-propane-1,3-diol	×

Table 4.3: Common names corresponding to selected RCSB compound identifiers
Molecules most likely to be biological ligands were identified by manual inspection, and are indicated using the following symbols:
(×) most instances in crystal structures are probably experimental artefacts.
(⋆) some instances may be biologically relevant; others are probably due to crystallisation conditions.
(✓) most instances are likely to be the true biological ligand, or at least a close analogue of it.

4.4.2 Distribution of ligand types with respect to sequence and structure families

In order to gain a fairer picture of the distribution of different ligand types for which we have structural information, it is useful to enumerate the different protein folds, superfamilies and sequence families which interact with each type of compound. This is not intended to give a definitive picture of the relative occurrence of different molecules in metabolism, physiology or biological catalysis. Rather, it simply aims to provide a measure of the diversity, in evolutionary terms, of the structural data currently available for studies of ligand binding.

A ContactTable archive was built using CATH version 2.6.0; the data presented here were obtained simply by querying the MatchTable and ContactTable archives, and processing the results with Perl (Wall *et al.*, 2000) scripts in order to generate summary statistics.

4.4.2.1 Evolutionary diversity of proteins binding each ligand type

Figure 4.15 shows the distribution of the number of different protein folds which interact with each type of ligand. These counts represent the number of distinct CATH numbers, up to the topology level, among domains which contact the ligands. The majority of ligands (77%) bind either to just one fold (33% of all compounds), or two different folds[3] (40%). The number of compounds which are found in partnership with a large number of folds is very restricted: 107 compounds (2.2%) bind to more than 10 folds, 40 compounds

[3]To clarify, this is based simply on an enumeration of the number of different folds among all domains which contact the ligand in different structures; therefore these counts may represent ligands which are bound at a domain interface, or may be due to ligands which interact with one fold in one protein, and a different fold in another.

(0.8%) to more than 20 folds and only 25 compounds (0.5%) to more than 30.

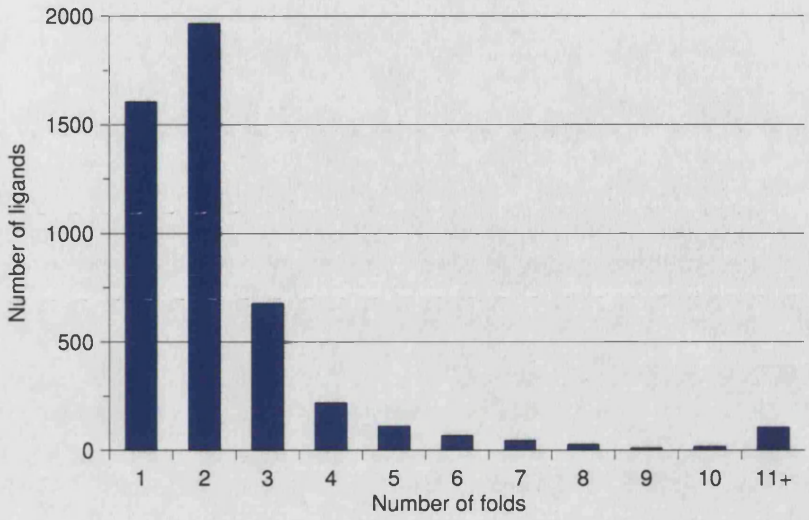

Figure 4.15: Distribution of numbers of distinct folds binding each ligand type
The chart shows the distribution of the number of distinct ligand types bound to each fold (*i.e.* to domains belonging to each CATH topology).

This is not a surprising result, since many of the compounds in the reference set are substrates specific to one or just a few enzymes, and hence would only be expected to bind to a limited number of folds. Conversely, the ubiquitous cofactors - which we expect to interact with a diverse set of proteins - make up only a small subset of the compound set. In order to quantify the degree of promiscuity of these common ligands, the number of protein families, superfamilies and folds with which each compound interacts was determined. This data is shown in figure 4.16. Compounds which were deemed by manual inspection unlikely to be biologically relevant ligands (see table 4.3) were excluded from the plot.

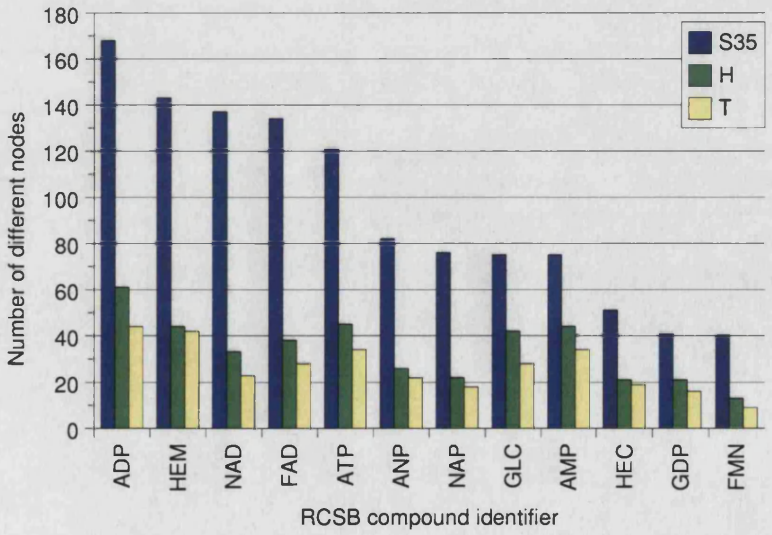

Figure 4.16: Ligands which bind to the most evolutionary diverse proteins
The twelve biological ligands which bind to the largest number of sequence families (CATH S35 families) are plotted. Also shown for each ligand is the number of distinct folds and homologous superfamilies to which it binds.

Comparing figures 4.14 and 4.16, it is unsurprising to see the compounds which ranked highest in terms of the raw counts of their occurrences in the PDB, also appear near the top of the list of compounds ordered by the number of protein families with which they interact. The adenosine nucleotides all rank much higher in terms of numbers of families which bind them, however, than in the list of occurrences (figure 4.14). The fact that the top-ranking compound in the non-redundant list (figure 4.16) is an adenosine nucleotide reflects the key role of ATP as the universal energy carrier in the cell. Similarly, the guanosine nucleotides, which also play a wide variety of cellular roles, are promoted once the redundancy present among PDB proteins is eliminated.

For both the adenosine and guanosine nucleotides, the diphosphate compound is more common than the triphosphate. This may not be an accurate reflection of the distribution of proteins for which the *cognate* ligand is, for example, ADP rather than ATP. Rather, it is likely that, during crystallisation of a protein which naturally recognises ATP, ADP has been supplied in the crystallisation liqor for experimental reasons.

Overall, the ratios of the numbers of families, superfamilies and folds which bind each compound are roughly constant over the common ligands shown here. The ratio between numbers of superfamilies and numbers of folds per ligand ranges between 1.05 (for HEM) and 1.44 (FMN). The ratio between numbers of families and numbers of superfamilies, on the other hand, is more variable; this is to be expected, since the number of families within each CATH superfamily varies considerably. The ligand with the minimum value of this ratio is AMP (1.7), while the three ligands with the highest value for this ratio are the redox cofactors NAD (4.15), NADP (3.45) and FAD (3.53).

The fact that these three cofactors bind proteins which exhibit the greatest sequence diversity per superfamily may be rationalised on the basis that the biological role of these ligands - namely, facilitating the oxidation/dehydrogenation of substrates - is fairly limited. The range of substrates which are modified by NAD(P) or FAD-dependent oxidoreductases, on the other hand, is extremely broad. We know that evolution of new substrate specificity while conserving the reaction often occurs through sequence divergence up to, but not beyond the point where fold also changes: see *e.g.* Hegyi and Gerstein (1999), Wilson *et al.* (2000), Todd *et al.* (2001). It is not surprising, therefore, that while relatively few folds have evolved to bind these cofactors, the diversity in terms of the number of sequence families *within* each of the fold groups is considerably larger.

4.4.2.2 Diversity of ligands binding each protein fold

Having assessed the evolutionary diversity of proteins binding each ligand, we now consider the inverse question: how many different types of ligand are bound by each fold? Figure 4.17 shows the protein folds which are most promiscuous in terms of the number of compounds with which they are partnered.

The first observation to make is that the numbers of small-molecule species found to interact with each fold type are surprisingly high. There are two reasons for this. Firstly, these counts include all compounds from the set of 56,231 molecules described in §4.4.1.2, and hence contain crystallisation artefacts as well as cognate ligands. As a result, a proportion of the counts shown here are due to a given fold being crystallised in the presence of different solvents, rather than due to it interacting with different ligands *in vivo*.

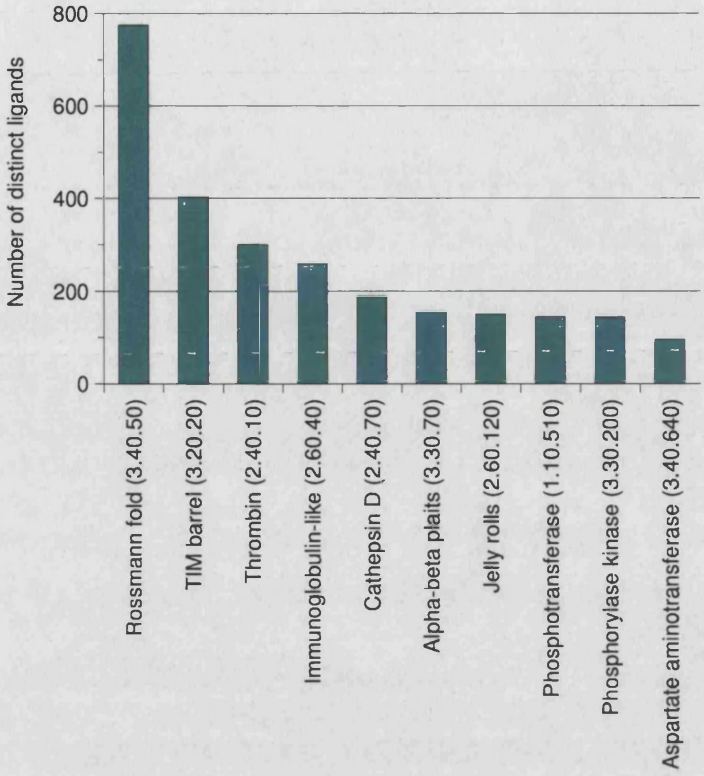

Figure 4.17: Most promiscuous folds
The protein folds which bind to the largest number of distinct ligand types are shown. For each, the CATH code up to the third level is given in parentheses.

The second reason is that the set of molecules which comprise the reference compound dictionary are not uniformly distributed in chemical space. That is to say, the compound set contains molecules which are very similar to one another (stereoisomers, and compounds which differ by minor substitutions of functional groups), as well as molecules which are very dissimilar. As a result, the fact that a given fold binds many different compounds does not necessarily imply a capability to interact with ligands which are chemically diverse. While these caveats diminish the meaning of the absolute values of the counts plotted here, it is still useful to discuss their relative magnitudes. It should be stressed, however, that what follows is a discussion of the relative occurrence of particular domain-ligand interactions *in the PDB* rather than in biology as a whole.

Considering the ten folds shown in figure 4.17, we see that five of them (the Rossmann fold, the TIM barrel, the immunoglobulin-like proteins, the αβ-plaits, and the jelly rolls) belong to the set of nine 'superfolds' which were identified more than a decade ago (Orengo *et al.*, 1994). Superfolds are defined as those which recur in proteins having neither sequence nor functional similarity[4].

[4]Since the publication of the original paper, the OB (oligonucleotide binding) fold has been added to this list, with eleven other CATH topologies currently proposed as potential superfolds (Orengo *et al.*, 1997).

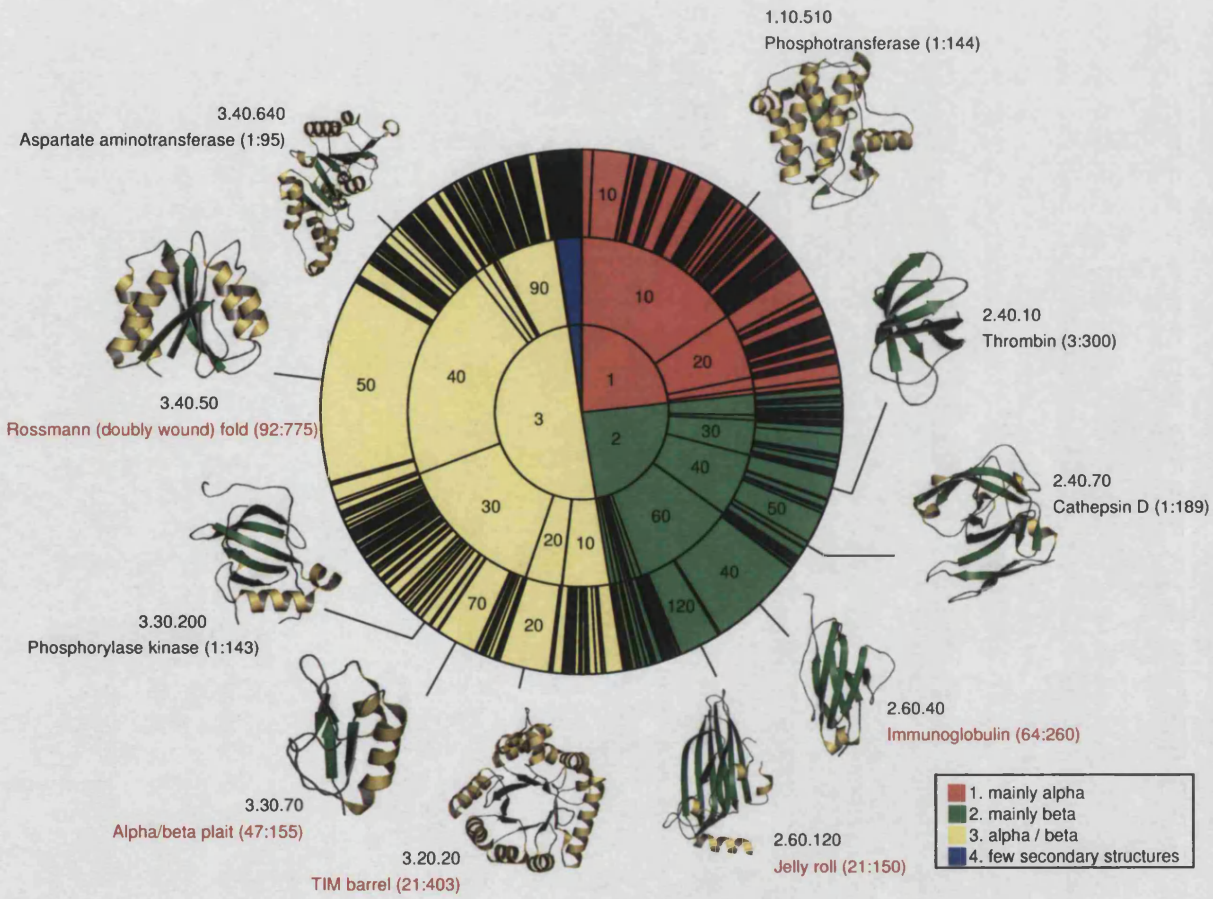

Figure 4.18: Most promiscuous folds compared with distribution of folds in protein space

The ten most promiscuous folds, in term of the number of compounds which they bind, are shown. The CATH wheel shows the relative populations of the first three levels (class, architecture, topology) of version 2.6.0 of the hierarchy: the size of the segment for each topology (in the outermost ring) is proportional to the number of homologous superfamilies which adopt that fold. Folds whose name is shown in red are those which have been identified as superfolds. Numbers in parentheses indicate, respectively the number of homologous superfamilies which adopt each fold, and the number of distinct ligands which are bound to domains with this fold. The colour of each segment corresponds to the CATH class, as shown in the key.

The evolutionary reasons for such widespread occurrence of certain folds in nature has been discussed extensively in the literature. The prevailing view is that, in most cases, proteins which share a common fold originated from a common ancestor; those structures which are for some reason particularly resilient to mutational changes without loss of stability therefore allow functional divergence to occur, whilst maintaining the same fold. An alternative hypothesis is that of convergent evolution - that is, the evolution of disparate sequences with no common ancestor to arrive at the same structure and/or function. If this were the case, then we may expect structural motifs which fold via fairly simply pathways, to occur more frequently. In either case, intrinsic structural stability would appear to be one likely explanation for the prevalence of the superfolds.

Figure 4.18 illustrates the relative occurrences in the CATH database of the ten folds which bind the largest numbers of compounds. The biological reasons for this promiscuity can be understood in some cases by considering the roles which proteins adopting each of these folds tend to play.

The **Rossmann fold** is the most highly populated of the α/β folds. It functions as a nucleotide binding domain, and is utilised in many oxidoreductases for recognition of the cofactor. Although it does not perform any catalysis, the fact that the NAD cofactor is bound quite deeply within it, with only the nicotinamide portion protruding to meet the catalytic partner domain (Bashton and Chothia, 2002), means that substrate molecules frequently contact the Rossmann domain as well as the catalytic unit. Since dehydrogenases act on a wide range of substrates, this accounts for the large number of molecules which are classified as interacting with Rossmann fold domains.

The **TIM barrel fold** is the most widely observed of all in crystal structures, the third most populous α/β fold, and it has been estimated that around 10% of all enzymes adopt it (Copley and Bork, 2000). Its usefulness as an enzymatic scaffold is illustrated by the fact that TIM barrels are associated with some 16 different EC numbers (Nagano *et al.*, 1999). Furthermore, several experiments have demonstrated that the catalytic function of enzymes with this fold can be successfully altered using directed evolution (Jurgens *et al.*, 2000, Altamirano *et al.*, 2000). It is therefore not surprising that it is found in complex with such a large number of ligand types.

The **thrombin fold** is named after the protein in which it was first discovered, a serine protease which initiates blood clotting in response to wound signals by cleaving the fibrinogen protein to release a rapidly aggregating peptide (Creighton, 1993). Several other common serine proteases, including the digestive enzymes trypsin, chymotrypsin and elastase share this fold. Each of these, although catalysing a similar endopeptidase reaction, has a different substrate specificity, with chymotrypsin cleaving peptide bonds flanked by bulky hydrophobic residues, trypsin cleaving bonds flanked with positively charged amino acids and elastase acting on peptide bonds between small, neutral residues (Hedstrom, 2002). Besides these preferences, however, these enzymes are not specific for particular peptide sequences; this is a necessary characteristic given their role in breaking down a wide range of foodstuffs, and indeed necessitates the protection of the enzyme from autodigestion, by producing it as an inactive precursor which is only set in action once it reaches the stomach. A number of proteins with thrombin folds are drug targets, explaining their high prevalence in the PDB.

The **immunoglobulin fold** was initially identified in proteins involved in the immune system, has since been observed in extracellular domains recognising a wide variety of ligands including small molecules (in the case of Fab proteins), peptides (MHC/HLA), DNA (the p53 DNA-binding domain) and other proteins (components of the extracellular matrix) (Bork *et al.*, 1994, and references therein). Among β folds, it contains the highest number of homologous superfamilies (64). Despite their broad-ranging substrate specificity, immunoglobulin-like domains do not appear to be directly involved in catalysis; no immunoglobulin fold domain is known to contain a naturally-present enzymatic active site. In the classical immunoglobulin G protein, ligand binding is mediated by loops which, due to high levels of recombination in the gene which encodes them (Tonegawa, 1983), exhibit a large amount of structural diversity. The majority of immunoglobulin-like domains, on the other hand, tend to interact with ligands via their β-sheets (Bork *et al.*, 1994).

The **cathepsin D** fold contains only one superfamily of aspartic proteases. These enzymes, involved in the catabolism of cartilage and connective tissue, have a similar substrate specificity to chymotrypsin (Barrett, 1977). As with the other proteases, cathepsin D folds are found in complex with a large number of different small peptides, which are classified as ligands in the MSD compound set. Like thrombin, several cathepsin D proteins are of particular pharmaceutical interest, meaning that they have been crystallised repeatedly with subtly different substrates.

α/β-plaits perform nucleotide binding functions in a wide variety of proteins ranging from the RNA-binding domains of various ribonucleoproteins, through viral DNA-binding proteins to ribosomal protein L3, which binds the 23S rRNA and may participate in the formation of the peptidyltransferase center of the ribosome (Orengo and Thornton, 1993). It is the third-most highly populated fold in CATH, following the Rossmann and TIM barrel folds. Inspection of the list of ligands which it binds shows that a large fraction are nucleotides, or nucleotide derivatives.

The **jelly roll** fold consists of two 'greek key' motifs linked by two connecting loops. It is found in a wide variety of proteins, including carbohydrate binding proteins, spherical virus coat proteins, influenza hemagluttinin and tumour necrotic factor. These are found in 21 distinct superfamilies. The ligands to which it is bound in the PDB are primarily carbohydrates.

The **phosphotransferase** and **aspartate aminotransferase** folds, like the cathepsin D proteins, are both *singlets*, *i.e.* they each consist of just one large superfamily. In the case of the phosphotransferase domain, it is partnered with a phosphorylase kinase domain. Aspartate aminotransferases catalyse the reversible transfer of the amino group from an amino acid to a 2-keto acid, using pyridoxal 5'-phosphate as a cofactor (Stryer, 1995). In contrast to many enzymes such as the proteases discussed previously, the aminotransferases react with both acidic substrates such as aspartate and glutamate, and neutral amino acids.

Overall, therefore, there appear to be three main reasons for ligand promiscuity in protein folds. The first is that certain folds are utilised by proteins with very diverse functions. This is the case for TIM barrels, and to a lesser extent, immunoglobulin folds and jelly rolls. In such cases, large evolutionary expansion of the superfamily has provided numerous opportunities for functional diversification. The reasons why this is

observed to such a large extent for some folds, and less so for others, are still not fully understood.

Another reason may be that the substrate specificity for a given protein is quite broad, resulting in many structures being present in the PDB, each crystallised with a slightly different partner. This is the case for many proteins which act on biopolymers, *e.g.* proteases and enzymes which catalyse modifications to DNA or RNA. The third reason is that protein families which are of particular biological interest are often deliberately crystallised many times with different substrates. This is particularly the case for drug targets. The over-representation of a particular fold in the PDB may be to one or a combination of these reasons: for example, the cathepsin D proteins are present in high numbers, probably due to both the second and third reasons given here.

4.4.2.3 Occurrence of multi-domain binding sites

In order to assess the frequency with which binding sites occur at domain interfaces, the number of domains contacting each ligand in the dataset was counted. Overall, 74% of binding sites were composed entirely from a single domain, with the remaining 26% consisting of residues from two or more domains. It is interesting to compare the proportion of multi-domain binding sites with the results of a previous study of a non-homologous set of 178 catalytic sites, which found that in all but 35 cases (20%), the entire complement of catalytic residues belongs to just a single domain (Bartlett *et al.*, 2002). The fact that the fraction of multi-domain binding sites is slightly larger than the fraction of multi-domain active sites is largely a product of the strict criteria which the authors used to define catalytic residues; this results in active sites consisting of a small number of closely-positioned residues.

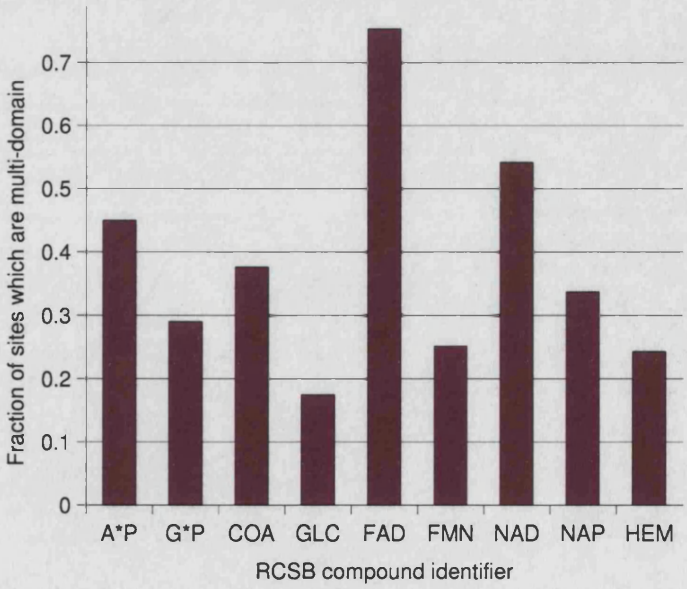

Figure 4.19: Fraction of binding sites for each ligand type composed of more than one domain
For each of the most common ligand types, the fraction of all binding sites which are comprised of more than one CATH domain is shown. Ligands ATP, ADP and AMP are collected together and plotted as A*T; guanosine nucleotides are similarly grouped as G*P.

Given both the differing sizes and diverse biological roles of different ligand types, however, this distribution would not be expected to be uniform across all compounds. Figure 4.19 shows the distribution of single- and multi-domain binding sites for several common ligands. The high frequency of multidomain binding sites for the redox cofactors NAD and FAD is not surprising given the tendency of proteins which bind them to have independent cofactor recognition and catalytic domains. Conversely, the common heme-binding proteins (hemoglobin, myoglobin, the cytochromes, and catalase) all bind the cofactor entirely within a single domain. The tendency of guanosine nucleotides to interact with only one domain is to be expected given their common role as signalling molecules that often bind to a single receptor domain, which in turn conveys the message to other effector domains within the protein. As the smallest molecule in this set, it is not surprising that glucose tends to interact with only one domain at a time. The reason for the striking difference between the fraction of FAD binding sites which contain more than one domain, and those for FMN, may simply be the difference in size between the two molecules.

4.4.3 Distribution of ligand types with respect to enzyme function

In order to obtain a general picture of the functional diversity of proteins which bind each type of compound, the fraction of each set which are annotated as enzymes was calculated. This was done by querying the MSD to obtain Enzyme Commission (EC) numbers for each protein chain which forms part of an enzyme. The MSD acquires this information by first searching each protein chain against the SWISS-PROT protein sequence database (Boeckmann *et al.*, 2003). The latter is a manually curated database which, for many proteins, contains extensive biological annotation including enzyme function. For every match to a SWISS-PROT sequence which is annotated with an EC number, this annotation can be transferred to the appropriate PDB chain(s), and hence to PDB entries. The SQL statement used to perform this query was as follows:

```
SELECT UNIQUE pdb.accession_code, swiss.chain_pdb_code, ec.ec_number
    FROM  entry pdb, swiss_prot_mapping swiss, ec_mapping ec
    WHERE swiss.entry_id = pdb.entry_id
    AND   ec.molecule_id = swiss.molecule_id;
```

The EC classification is a hierarchical system consisting of four levels; the meaning of each of these levels is shown in table 4.4. The level up to which two EC numbers are identical represents, to a first approximation, the degree of similarity between the two reactions concerned.

First digit (class)	Reaction type	Second digit	Third digit
1 (Oxidoreductases)	Oxidation / Reduction	Substrate acted upon	Type of Acceptor
2 (Transferases)	Transfer of a group between substrates	Description of the transferred group	More information about the group
3 (Hydrolases)	Bond cleavage by hydrolysis	Bond type being hydrolysed	Type of substrate
4 (Lyases)	Bond cleavage by elimination	Bond type being broken	Type of group eliminated
5 (Isomerases)	Transfer of groups within a molecule	Type of isomerism	Type of substrate
6 (Ligases)	Bond formation coupled to ATP hydrolysis	Bond type being formed	Type of compound formed

Table 4.4: Levels of the Enzyme Commission hierarchy
The meanings of the second and third digits of the EC classification vary according to the reaction class (the first digit). The fourth digit indicates a particular reaction.

Figure 4.20 shows the fraction of proteins binding each of the common ligands which were annotated with one or more EC number. The one unusual result is the low proportion of coenzyme A-binding proteins which were associated with an EC number. Manual inspection of several such proteins which were clearly enzymes - including some annotated as such in the PDB header records - showed that the MSD enzyme annotation protocol did not assign EC numbers to these proteins. As a result, the numbers shown here may underestimate the true number of enzymes which bind each ligand.

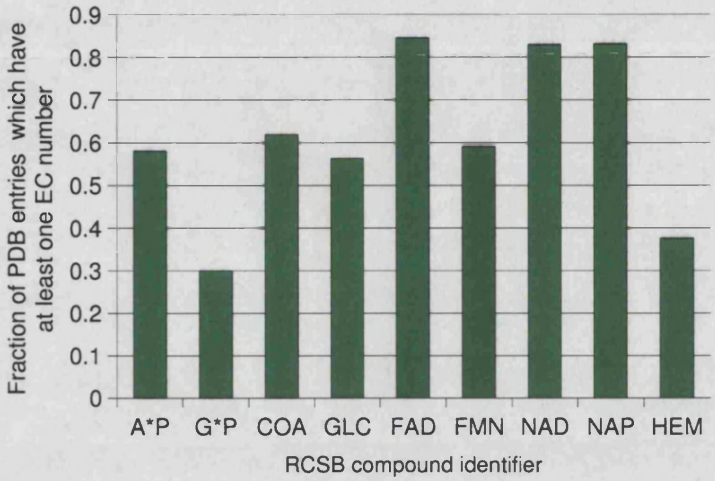

Figure 4.20: Fraction of proteins binding each ligand type which are annotated with enzyme functions
Enzyme function annotations were obtained from the MSD as described in the text. Ligands ATP, ADP and AMP are collected together and plotted as A*T; guanosine nucleotides are similarly grouped as G*P.

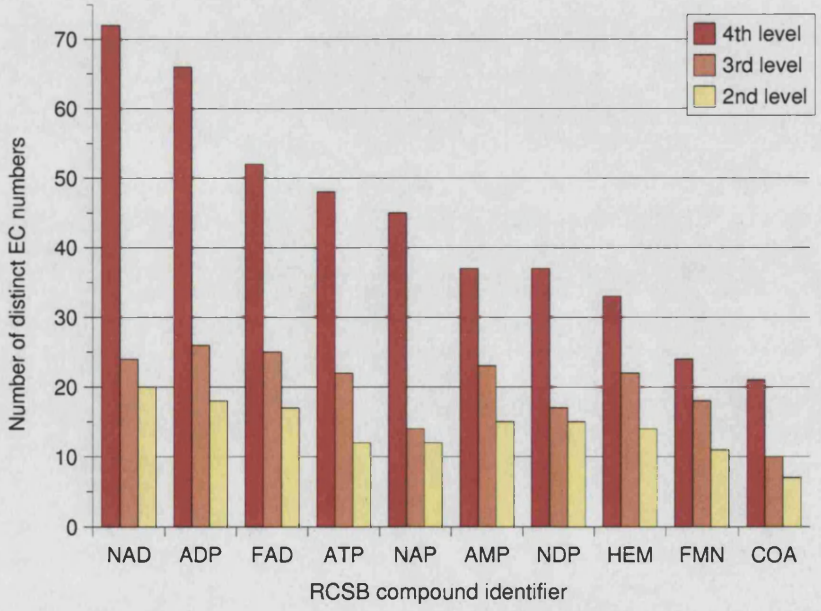

Figure 4.21: Ligands whose binding proteins have the widest range of enzyme functions
The ten ligands which bind to proteins with the largest range of EC numbers to the third level are plotted. Also shown for each ligand is the number of distinct EC numbers to the second and third levels, among the proteins to which it binds.

The range of functions catalysed by the enzymes discovered in the previous step was assessed by plotting the number of *distinct* EC numbers associated with each ligand, up to the second, third and fourth levels (see figure 4.21). Once again, the compounds whose proteins have the widest range of enzyme functions are the expected common biological ligands. It is interesting to note that while there is a considerable range in diversity at the fourth EC position among the ten ligands shown, the range of different numbers to the second and third levels is significantly less pronounced. This suggests that, for cofactors such as NAD, ATP and FAD, there are numerous enzymes which catalyse very similar reactions, whereas for coenzyme A, where the number of distinct EC numbers to the fourth level is only just over twice the number to the third level, the number of enzymes which have evolved to perform similar functions is much fewer. A more detailed analysis of the particular EC numbers associated with several key ligands is presented in the following section.

4.5 Datasets of ligands of particular biological interest

The ligands ATP, GTP, NAD and FAD were chosen for further analysis (see figure 1.2); for each, non-homologous datasets were generated using the clustering protocol described in §4.2. Details of the results of this clustering are tabulated in appendix D. Henceforth, the list of sites presented in tables D.1-D.4 will be referred to simply as 'the ligand dataset', and the numbers shown in the first column of those tables will be used to refer to the different third-level clusters for each ligand type. The domain composition of the binding sites in the largest clusters, and the functions of the associated proteins, are summarised in table 4.5.

There is large variance in the amount of functional diversity found among proteins within each cluster: the group with the widest range of functions are the ATP-binding proteins in the first cluster (P-loop containing NTP-hydrolyase domains), which are associated with four different primary EC numbers (IUPAC-IUB, 1983). The group of Rossmann-fold NAD-binding oxidoreductases, on the other hand, all catalyse similar types of reaction, but act on a wide range of substrates. Moving to smaller clusters, we find some which perform extremely specialised functions, such as the tRNA synthetases in ATP cluster 4, all of which catalyse the transfer of a particular amino acid onto the appropriate tRNA molecule. This group contains five members, each of which acts on a different amino acid type, and which, while sharing the same overall fold, exhibit only very low sequence similarity to one another.

4.5.1 Analysis of the clustering

4.5.2 Distribution of folds and superfamilies binding each ligand type

Figure 4.22 shows CATH wheels representing the distribution of different folds and superfamilies which interact with each of the four ligands considered here. For each site in the ligand dataset, the domain which contributes the largest fraction of the binding residues is determined. For example, site `1RDQ/A/ATP.600/B`, the representative for cluster 2 in the ATP dataset, consists of two domains - a phosphotransferase domain (CATH code 1.10.510.10) which contributes about a third of the binding residues, and a phosphorylase kinase domain (3.30.200.20) making up the remaining two thirds. In this case, the phosphorylase kinase domain is identified as the majority partner.

Ligand	Cluster	Size	Rep	Domains		Functions
ATP	1	22	1E2Q	3.40.50.300	P-loop containing nucleotide triphosphate hydrolases	Various
	2	9	1RDQ	3.30.200.20 1.10.510.10	Phosphorylase Kinase domain 1 Transferase (Phosphotransferase) domain 1	Kinases
	3	9	1MJH	3.40.50.620	Rossman fold ligase domain	Ligases; transferases
	4	5	1B8A	3.30.930.10	Bira Bifunctional Protein domain 2	tRNA synthetases
	5	3	1KJ8	3.30.470.20 3.30.1490.20	ATP grasp fold domain B -	Formyltransferase; synapsin I; biotin carboxylase
	6	3	1GZ4	3.40.50.720	NAD(P)-binding Rossmann-like	Malic enzyme; molybdopterin synthesis
GTP	1	6	1QRA	3.40.50.300	P-loop containing nucleotide triphosphate hydrolases	Signal proteins
NAD	1	54	1T2D	3.40.50.720*	Rossmann	Various oxidoreductases; UDP-glucose 4-epimerase
	2	4	1O04	3.40.605.10 3.40.309.10	Aldehyde Dehydrogenase domain 1 Aldehyde Dehydrogenase domain 2	Aldehyde dehydrogenase; Glyceraldehyde 3-phosphate dehydrogenase
	3	4	1NUU	3.40.50.620	Rossmann fold ligase domain	Adenylyltransferases
	4	4	1LW7	3.50.50.60	FAD/NAD(P)-binding domain	Glutathione reductase; ferredoxin reductase; NADH peroxidase; Dihydrolipamide reductase
	5	4	1GIQ	2.30.100.10	Toxin ADP-ribosyltransferase	ADP-ribosyltransferases
FAD	1	19	3GRS	3.50.50.60	FAD/NAD(P)-binding domain	Various oxidoreductases
	2	9	1GAW	2.40.30.10 3.40.50.80	Translation factors Nucleotide-binding domain	Ferredoxin-NADP+ reductase; cytochrome reductase; nitric oxide synthase
	3	5	1N62	3.30.465.10 3.30.43.10	Uridine Diphospho-n-acetylenolpyruvylglucosamine Reductase domains	Carbon monoxide dehydrogenase; nucleotide metabolism oxidoreductases
	4	5	1LQT	3.40.50.720	Rossmann	FPRA; dihyropyrimidine dehydrogenase; D-amino acid oxidase
	5	3	1E8G	3.30.465.20 3.30.43.10	Uridine Diphospho-n-acetylenolpyruvylglucosamine Reductase domains	Vanillyl-alcohol oxidase; cholesterol oxidase; D-lactate dehydrogenase
	6	3	1IQR	1.10.579.10 1.25.40.80	DNA Cyclobutane Dipyrimidine Photolyase domain 3 -	DNA photolyase

Table 4.5: Summary of the ligand datasets
For each cluster with three or more members, 'size' indicates the number of members, and 'rep' is the PDB entry ID of the cluster representative. The homologous superfamily level annotations of domains making up the binding sites in each cluster are shown along with their associated CATH numbers. Where the proteins in a cluster have a small range of functions, these are listed; in other cases, the range of functions is too large to list here. See appendix D for a more detailed version of this table.
($\star$) this domain binds the cofactor in partnership with other domains.

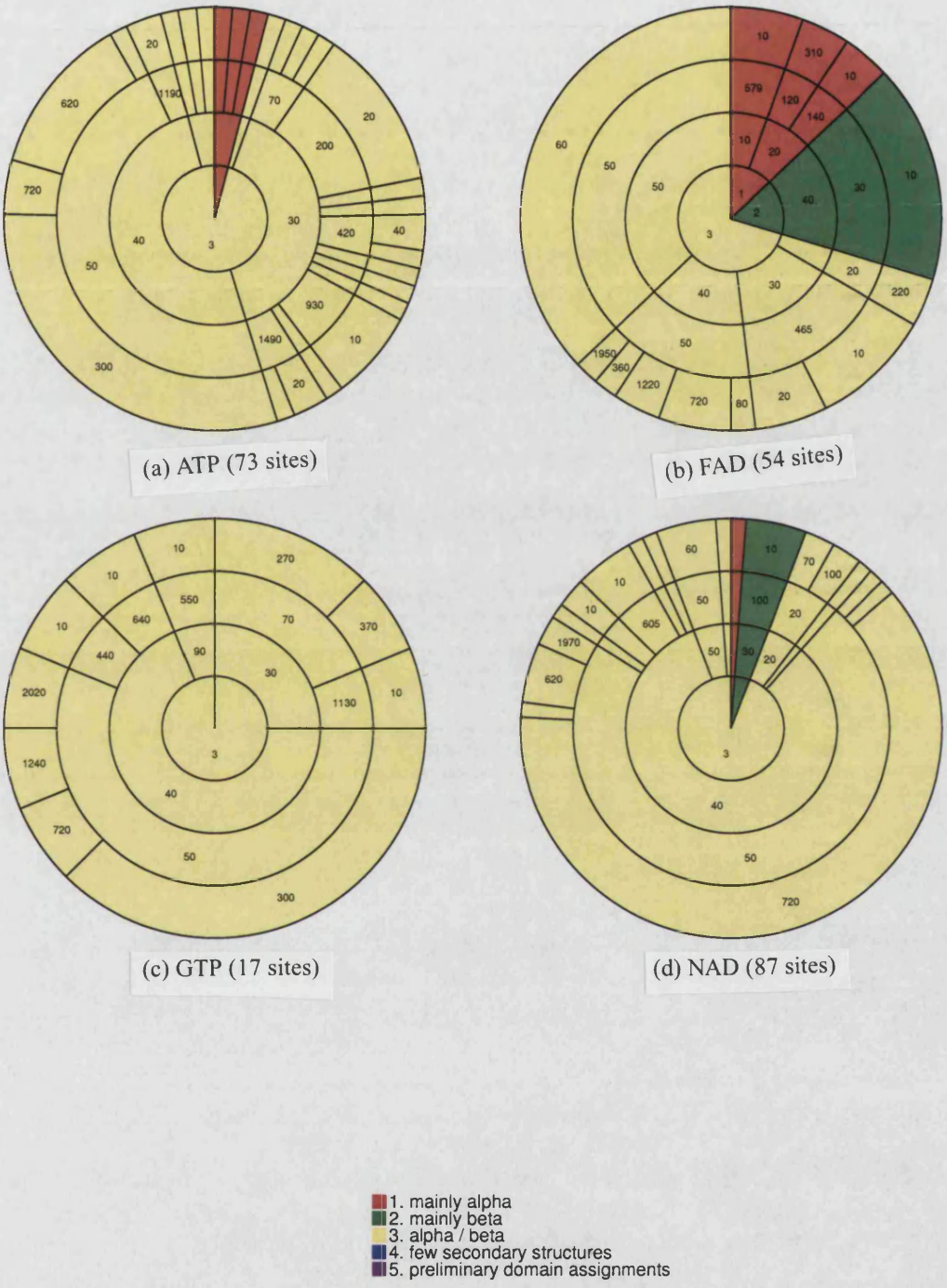

Figure 4.22: CATH wheels for the four ligands which were analysed in detail
For each representative binding site from the second stage of clustering (in which sites containing proteins with more than 35% sequence identity are clustered together), the CATH superfamily which contributes the majority of the binding site residues was identified. The angular size of each segment in the outermost ring is proportional to the number of sites in which that superfamily was identified as the largest constituent. Colours represent the different CATH classes, as shown in the key.

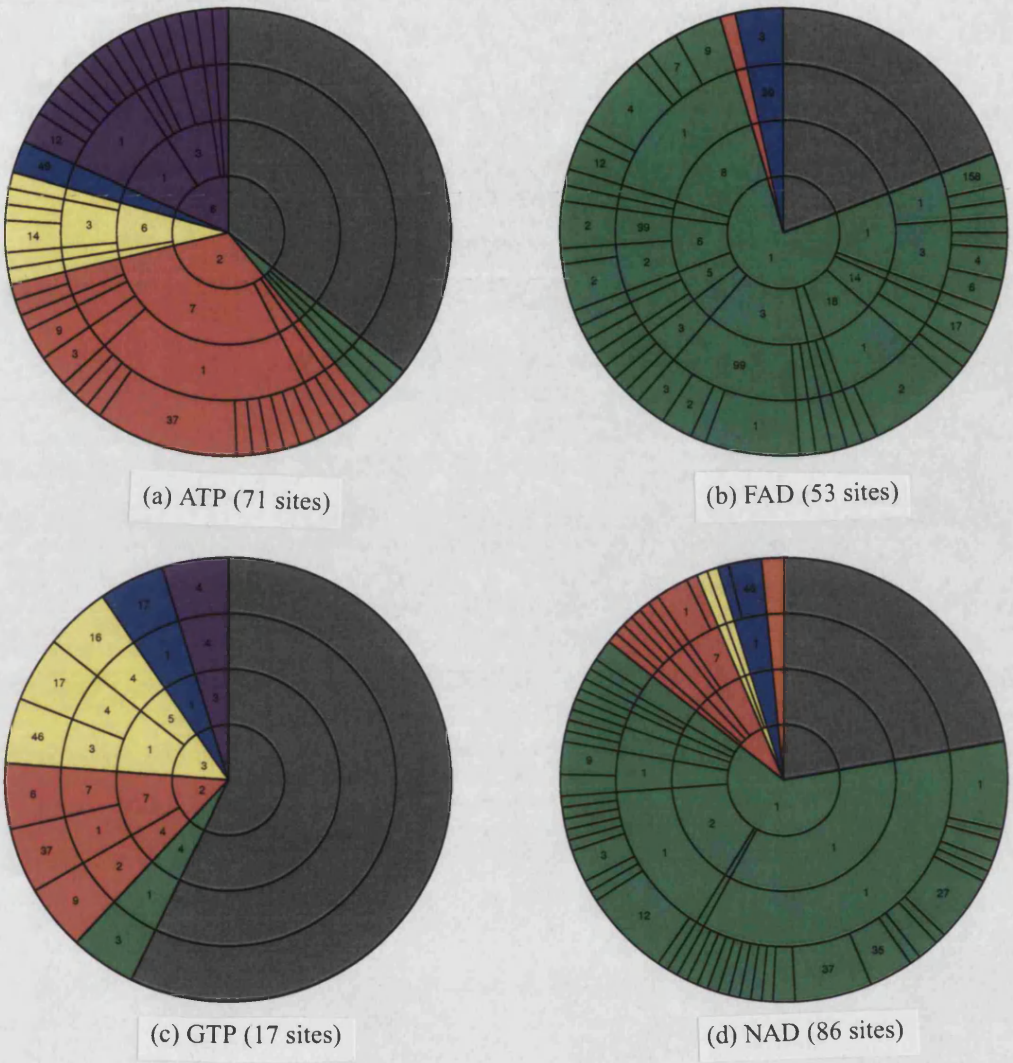

Figure 4.23: EC wheels for the four ligands which were analysed in detail
The angular size of each segment is proportional to the number of representative sites from the second stage of clustering (in which sites containing proteins with more than 35% sequence identity are clustered together) bound to proteins annotated with the corresponding EC number.

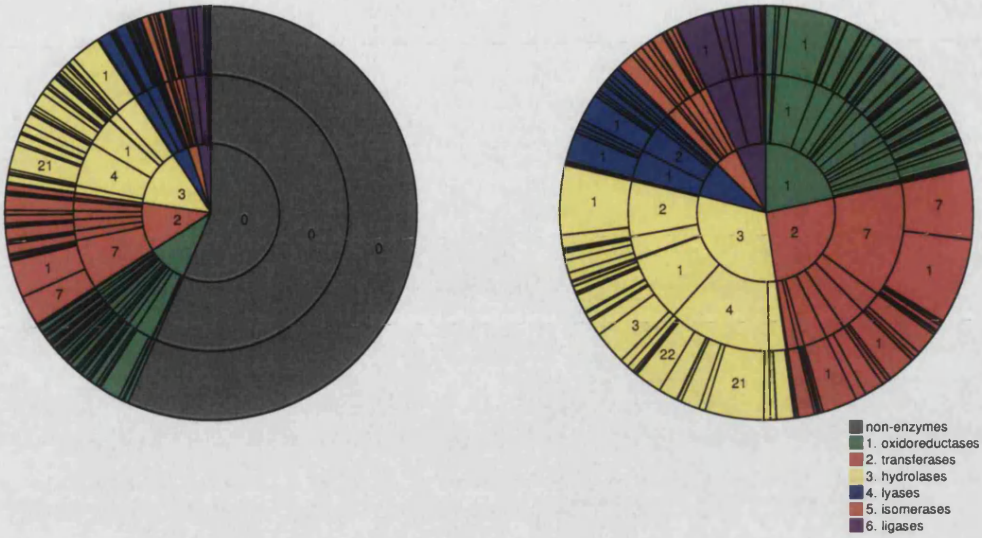

(a) All CATH S35 representatives

(b) CATH S35 representatives with EC numbers

Figure 4.24: EC wheels for the CATH S35 representatives

The CATH wheels represent the frequency of occurrence of each superfamily, counted in this way across all sites in each ligand dataset. Most of the binding sites are composed of α/β fold domains; exceptions to these patterns are quite rare: all GTP binding sites are composed of α/β domains, and for ATP, only two families adopt an α-helical fold. These are the GroEL proteins (cluster 10) and the ribonucleotide reductases (cluster 24). Both of these clusters are singlets.

Of the four nucleotide derivatives, FAD exhibits the widest diversity in the fold types which bind it. Although chiefly recognised by α/β domains, three FAD clusters belong to other classes. Sites in cluster 2, a diverse group originating from cytochromes and various oxidoreductases, bind the cofactor inside β-sheet domains belonging to the 'translation factor' superfamily (2.40.30.10). Two smaller clusters recognise FAD using α-helical folds: cluster 6, which contains three families of photolyase enzymes; and cluster 7, containing two short-chain dehydrogenases.

The degree of fold diversity in NAD binding sites is intermediate between those in the ATP and FAD datasets. The canonical NAD recognition motif is a β-sheet sandwiched between pairs of α-helices. The NAD molecule binds in a crevice formed at the 'switch point' of the β-sheet, where it is stabilised by interactions with the α-helical dipoles (Lesk, 1995). There are, however, other α/β folds which bind NAD, notably the α/β barrels (CATH architecture 3.20) found in the inosine-monophosphate dehydrogenases (cluster 7) and reductases acting on monosaccharides and the acids which are formed by their oxidation (cluster 8). There are two exceptions to the dominance of the α/β domains in the NAD dataset. Cluster 5 contains four families of ribosyltransferases, in which the NAD-binding domain is a β-sheet structure (2.30.100.10). Citrate synthase proteins (cluster 18), which fall into a single family, utilise an all-α-helical fold (1.10.580.10) for cofactor binding.

4.5.3 Distribution of enzyme functions among proteins binding each ligand type

Figure 4.23 shows EC wheels for each of the four ligand types. For each site in the dataset, annotation of enzyme function, where available, was obtained for its parent protein using the procedure described in §4.4.3. The angular size of each segment of the EC wheel indicates the number of sites which belong to enzymes catalysing the relevant reaction. In a few cases, the protein was assigned more than one EC number, for example site `1K87/C/FAD.2001` is from a bifunctional protein which can catalyse both pyrroline-carboxylate decarboxylation (EC number 1.5.1.12) and proline dehydrogenation (EC 1.5.99.8) reactions. These cases are extremely rare (2, 0, 1 and 1 examples for ATP, GTP, NAD and FAD respectively), and therefore were excluded from the analysis.

Figure 4.24 shows the distribution of enzyme functions among a non-homologous set of proteins. This set was generated by first taking the representative domains for each CATH S35 family. The EC number(s) associated with the parent protein of each domain were then plotted in the same way described above.

The most common enzyme functions for ATP-binding proteins reflect the chemistry most often performed upon it, namely hydrolysis of diphosphate esters. The most common EC numbers are 2.7.- (transferases transferring phosphate-containing groups), 6.1.- (ligases acting on C—O bonds), 3.6- (hydrolases acting on acid anhydrides) and 6.3- (ligases acting on C—N bonds).

Unsurprisingly, the wheels for FAD and NAD are dominated by oxidoreductase functions. The overall range of enzyme functions associated with GTP- and particularly ATP-binding proteins, on the other hand, is far broader, with ATP-binding proteins catalysing several transferase, hydrolase and ligase reactions, as well as a small number of oxidoreductase and lyase reactions.

4.6 Summary

In this chapter, automatic protocols for generating datasets of ligand binding sites have been described. These protocols include methods for determining the chemical identity of ligand molecules from their atomic coordinates, and a procedure for clustering binding sites based on relationships between the domains which constitute each of them.

The ligand identification/validation procedure has been applied to all structures in the PDB. The results show that several common biological ligands and cofactors are present in a large number of entries. The usefulness of the graph matching methodology for checking ligand identities is demonstrated by several cases in which ligands are mis-named in the PDB.

Analysis of the pairings of different protein folds and different ligand types shows that several of the folds which are most promiscuous in terms of the set of compounds with which they interact, are those which have been previously identified as occurring in many different protein superfamilies. Several promiscuous folds, however, correspond to only a small number of families; in these cases, arguments based on the specific functions of the proteins in these families can be invoked in order to explain their gregarious behaviour.

Due to biases affecting the selection of candidate proteins for crystallisation, as well as the compounds co-

crystallised with them, the data shown here should not be viewed as a direct reflection of the distribution of cognate ligands with respect to different protein folds. A more careful analysis in which ligand-protein interactions are checked for their biological relevance is currently under way (I. Nobeli, personal communication), and should clarify the extent to which the findings here can be extrapolated to biology as a whole. However, the fact that certain folds are capable of binding to such a large diversity of compounds, albeit sometimes under unphysiological conditions, does suggest that broadly similar patterns will be observed by more detailed analyses.

While the majority of ligand binding sites are composed of a single domain, the fraction of multi-domain binding sites among ligands and cofactors of interest, which tend to be among the larger compounds considered, is typically higher than average. This presents challenges for automated binding site clustering based on domain annotation. The method described here overcomes these methods using heuristics which appear to give reasonable clustering results.

Finally, datasets of binding sites for four ligands of particular interest were generated, and analysed both in terms of the domains which contribute to them, and in terms of the enzymatic functions of the proteins concerned. In the following two chapters, the structural properties of these binding sites will be investigated in detail, firstly from the point of view of ligand conformation, and then focussing on the diversity of their micro-environments.

Chapter 5

Conformational variability of bound ligands

The shape of a molecule depends on two factors. The first is, naturally, the chemical structure of the compound; that is, its complement of atoms and covalent bonds. As long as the molecule does not participate in any chemical reactions, this remains unchanged, while the second - the set of torsion angles around each of its rotable bonds - may vary dynamically through random thermal fluctuations, and as the molecule finds itself in different physical environments. This chapter is concerned with analysing the different conformations adopted by biological ligands. The variation in conformation is analysed first among ligands bound to evolutionarily unrelated binding sites, and secondly among ligands whose sites are composed of domains belonging to the same superfamily - that is, first between and then within the clusters defined as per §4.2. The aims of this study are to understand whether a given pair of interacting molecules (protein and ligand) always interact in the same way, and to what extent the different conformational states of the ligand are accessible when interacting with evolutionarily unrelated proteins.

5.1 Rationale for studying ligand conformation

Although small in comparison to proteins, many biological ligands are capable of considerable conformational variability. In the most abstract sense, the free energy landscape of a molecule with n rotable bonds may be considered to be an n-dimensional function, which may be replete with peaks (energy barriers), valleys (energy minima), and passes (saddle points). If we discretise this space by assuming that the i^{th} bond may exist in just one of a small number x_i of distinct, stable orientations, then the number of possible conformations of the molecule as a whole is given by the product $x_1 \times x_2 \times \ldots \times x_n$.

It is clear that the combinatorial effect of varying just a few rotable bonds leads to a large number of possibilities: if we assume that any one rotable bond can exist in three distinct rotational states, then a molecule with only ten such bonds can theoretically adopt $3^{10} = 59{,}049$ different conformations. Of course, many of these will be physically impossible due to steric clashes between atoms. Still others may be strongly disfavoured energetically, but a large number may have an energy not too distant from the global minimum, meaning that a considerable region of conformational space is potentially available for exploration by small organic molecules.

Upon binding to a protein, the conformational freedom of a ligand is typically restricted to a small number of states, which are often distinct from the optimum conformation of the solvated molecule, and in many cases may not even be close to a local energy minimum (Nicklaus *et al.*, 1995, Bostrom *et al.*, 1998). In some cases however, ligands retain considerable mobility even when complexed with proteins. Crystallographic and thermodynamic studies of natural and synthetic strepdavidin inhibitors showed that the ligand with the highest binding affinity also exhibited the greatest conformational variability in the binding site (Weber *et al.*, 1995). It must be remembered that while molecular recognition is thought to be driven in part by enthalpic change, and therefore characterised by the formation of specific interactions between the protein and the immobilised ligand, the favourable entropic effect of maintaining some ligand flexibility can in some cases compensate for weaker interactions between the two molecules.

Appreciation of the energetic constraints acting on bound ligands can shed light on how they perform their particular biological functions, be these as enzymatic cofactors, signalling molecules or labile substrates. In particular, strain induced in a ligand as a consequence of the shape which it is forced to adopt may promote its participation in chemical reactions. Alternatively, conformational change upon binding may expose a reactive atom or functional group which would otherwise be inacessible to other reactants. This is seen, for example, in the mechanism of DNA glycosylases, enzymes which catalyse the excision of damaged nucleotides from stretches of DNA. In order for catalysis to occur, the damaged base must be everted from the double helix to expose its C1′ atom to the enzymatic active site (Stivers and Jiang, 2003).

From a practical standpoint, the investigation of bound ligand conformations may prove valuable in the development of docking methods, where libraries of rotamers derived from bound ligand structures could be used to speed up conformational searches by *a priori* elimination of some of the large number of possible conformations mentioned previously. Furthermore, knowledge of the degree of conformational variation exhibited by bound ligands, both within and between protein families, should be useful in assessing the likely biological relevance of a proposed bound ligand pose. In particular, as high-throughput structure determination programmes begin to bear the promised fruit of complete coverage of the protein structure universe (Burley, 2000), we may be able to enumerate - at least for common ligands - the range of ligand conformations which occur in complex with proteins. This would be useful as a benchmark for *in silico* ligand binding prediction methods, for which the similarity between the predicted ligand pose with the set of conformations previously observed may be of use in judging its likelihood of being correct.

A slightly different application area where studies of small molecule conformation may be valuable is that of crystallographic refinement. Here, the comparative paucity of data on favoured ligand conformations, in comparison to those available for proteins themselves, can hamper the structure determination process, often leading to small molecule coordinates which are poorly refined. Although this is clearly something of a circular problem, increased understanding of the regions of conformational space which are most frequently explored by bound ligands, and particularly of the torsional deviations from theoretically stable states which may be tolerated when a ligand is in a protein environment (rather than an aqueous one), may lead to more robust assignments of ligand coordinates within complexes.

In summary, the primary motivations for the work presented in this chapter are as follows:

- To quantify the degree of conformational diversity of bound ligands, with a view to:
  1 Assessing the scale of the problem of predicting the cognate ligand for an uncharacterised structure: can searching be restricted to a small number of common conformations? Similar considerations apply during refinement of ligand coordinates during structure determination.
  2 Considering the advisibility of methods which attempt to predict ligand binding site specificity by comparison with databases of known sites: are ligands so flexible that fragment-based comparison methods are likely to meet with more success?
  3 Comparing ligand conformation variation within homologous superfamilies to that observed in ligands bound to unrelated proteins.
- To determine the extent to which ligand/cofactor conformation is correlated with protein function. In the cases where such correlation is observed, to investigate reasons why this should be so.
- To investigate whether ligands tend to bind with their bonds in the expected, low-energy orientations, or whether they are found in strained conformations.

5.2 Chemical theory pertinent to small molecule conformation

In §1.2, some contributions to the free energy of protein-ligand binding were discussed. The question of the internal strain energy of the ligand was previously omitted; since this is relevant to the current chapter, it is discussed briefly here.

5.2.1 Electron-pair repulsion

Let us consider the energy involved in rotating the carbon-carbon bond in an ethane molecule. The distance between the two carbon atoms in unchanged, but the distance between hydrogen atoms bonded to the two carbon atoms varies. It is simple to show that the minimum distance between a pair of hydrogen atoms is about 2.3Å, occurring when the molecule is in the conformation shown in figure 5.1a. The maximum distance is around 2.5Å (figure 5.1b). Since the distance of closest approach is only just less than twice the Van der Waals radius of hydrogen (1.2Å), the Van der Waals repulsion caused by the eclipsed conformation is small. However, measurements of the energy of this conformation show that it is in fact significantly higher than would be expected on the basis of steric hinderance alone.

This may be explained in part to repulsion between the electron pairs which constitute the C-H bonds. This type of repulsion is sometimes referred to as "eclipsing strain" or "torsional strain". The magnitude of this repulsion varies sinusoidally with respect to the torsion angle around the bond; the peaks of this energy function are known as the *rotational barriers* and its minima represent favoured conformations of the molecule. In the case of ethane the three minima are equally favourable, but this is not the case if the three substituents attached to each carbon atom are different.

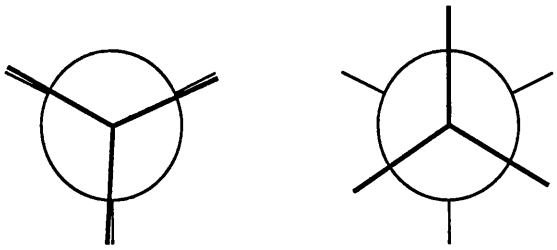

(a) Eclipsed (b) Staggered

Figure 5.1: Newman projections of eclipsed and staggered conformations of ethane

5.2.2 Electrostatic interaction

Where electronegative atoms are found in compounds, their negative charge-withdrawing effect induces dipoles within the molecule. These dipoles, in contrast to those discussed in §1.2.2.2 in relation to Van der Waals attraction, are permanent. Electrostatic interactions between these partial charges can cause some rotational states to be more stable than others. For example, consider 1,2-dibromoethane, which is an ethane molecule in which one hydrogen attached to each carbon atom has been replaced with a bromine atom. Each C-Br bond is polarised such that the bromine atom carries a partial negative charge. While the positively charged carbon atoms are covalently bonded, and thus cannot move away from one another, the negatively charged bromines can rotate to move as far apart as possible; the staggered conformation which places them on opposite sides of the C-C bond is known as the *anti* arrangement, and is shown in figure 5.2.

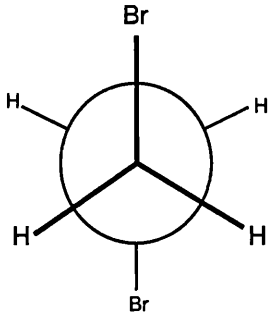

Figure 5.2: 1,2-dibromoethane in an *anti* staggered conformation
This is the most stable staggered conformation, since it provides maximal separation of the negatively charged bromine atoms. The other two staggered conformations are known as *gauche*.

5.2.3 Steric hinderance

The origin of Van der Waals attraction was discussed previously. As two atoms become closer, the Van der Waals attraction becomes balanced by a repulsive force due to the overlapping of their electronic orbits. This repulsive force is sometimes known as *Van der Waals repulsion*. The point at which the attractive and repulsive forces balance is the sum of the *Van der Waals radii* of the two atoms; the Van der Waals radius can therefore be seen as a measure of the size of an atom, including its electron cloud.

The sum of the attractive and repulsive Van der Waals forces is often approximated using a "Lennard-Jones potential" which takes the form

$$V(r) = 4\varepsilon\left[\left(\frac{\sigma}{r}\right)^{12} - \left(\frac{\sigma}{r}\right)^{6}\right]$$

where ε is the depth of the potential well and σ is the hard-sphere radius (see figure 5.3). The $\left(\frac{\sigma}{r}\right)^6$ term describes the attractive force and the $\left(\frac{\sigma}{r}\right)^{12}$ term describes the repulsive force. This is often referred to as a 6-12 potential.

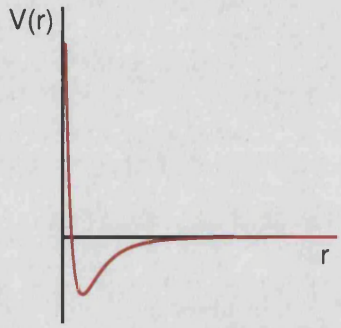

Figure 5.3: Lennard-Jones potential
The energy minimum occurs when the inter-atom separation r is equal to the sum of the two Van der Waals radii. As the two atoms move closer than this, the repulsive force increases very rapidly.

5.3 Previous work on ligand conformation

Ligand conformation has been analysed previously from a number of different perspectives. As is the case in many areas of structural bioinformatics, these can be roughly divided into those originating from first-principles consideration of the forces and energies acting on small molecules, and those take a 'knowledge-based' approach, focussing on comparisons of ligand conformations in complex with different proteins.

One of the earliest large-scale analyses of ligand conformation (Moodie and Thornton, 1993) compared the coordinates of protein-bound nucleotides to those in an unbound dataset obtained from the CSD. The latter consisted of crystal structures of deoxyribo- and ribonucleosides, nucleotides, dinucleotides and paired dinucleotides. The main finding was that few torsion angles were observed to undergo significant changes, and that these rotations tended to result in the nucleotides changing from folded to extended conformations upon binding to proteins. In addition, the authors found that the glycosidic bond within adenosine nucleotides had an overwhelming preference for adopting an *anti* orientation. At the time of the study, the available structural data for bound pyrimidine nucleotides was too scarce to allow the corresponding torsion angle in guanine nucleotides to be analysed.

The observations of pronounced ligand extension and the preference for an *anti* glycosidic bond were interpreted as being indicative of the need for ligands to expose as much of their surface area as possible, thereby facilitating more sensitive recognition. The authors suggest that the relatively small number of torsional changes which occur upon ligand binding are evidence that bound ligands exist predominantly

in low-energy conformations, since similar conformations in solution have been shown both theoretically and experimentally to be in low-energy states (Saenger, 1984).

This assumption does not hold for ligands in general however, according to a recent study which assessed the energetic effects of ligand reorganisation upon binding (Perola and Charifson, 2004). Working on a dataset of 150 diverse ligand-protein complexes, the authors used three different computational methods to compute both the global minimum conformation of the unbound ligand, and the global strain energy of the molecule when in complex with the protein (defined as the energy difference between the bound, bioactive conformation and the lowest energy conformation of the unbound ligand). They then compared the values obtained with the degree to which the ligand unfolds upon binding, and also with parameters describing the bound state, including number of hydrogen bonds formed, and the experimentally-determined binding affinity.

The energy calculations confirmed previous claims (Nicklaus *et al.*, 1995, Bostrom *et al.*, 1998) that ligands rarely bind in their lowest-energy conformation. Surprisingly, however, this study also found that in only about one third of cases were the bound conformations even within 0.5 kcal mol^{-1} of a *local* energy minimum. Moreover, no correlation was found between global strain energy of the bound ligands and either the number of polar interactions which they made with their proteins (contradicting the study of Nicklaus *et al.*), nor the binding affinity. These results suggest that even fairly energetically costly ligand rearrangements can be tolerated without penalising binding affinity. The authors also report that the ligands with the highest strain energies tended to be those which unfolded to the greatest degree upon binding. This finding, taken together with the lack of correlation between strain energy and number of hydrogen bonds, indicates that the primary stabilising factor offered to ligands by their binding sites is that of a generally hydrophobic environment which protects the uncovered nonpolar ligand regions from exposure to solvent.

A comparison of the binding sites for the redox cofactors NAD and NADP showed that, although they are structurally similar, these two molecules exhibit some noticeable differences in their interactions with proteins (Carugo and Argos, 1997). The authors report a total of 13 different conformations adopted by the two cofactors: eight of them by NADP and five by NAD. Interestingly, the two different compounds were never found in the same conformational cluster, indicating that even an apparently small chemical elaboration can significantly alter the constraints acting on the shape of a particular molecule. The relationship between the conformational clustering, and evolutionary similarities between the proteins is mentioned only in passing; the authors note that proteins with similar folds and/or functions tend to bind the cofactor in a similar conformation, but do not investigate this in detail.

Carugo and Argos then go on to look for conserved features of the NAD and NADP binding sites, reporting that, while several conserved interactions can be found among NAD-binding pockets, those which recognise NADP are more variable. The problem with this analysis is that it does not effectively deconvolute the effects of variability in ligand conformation from that of variation in the binding site. In other words, since their identification of conserved cofactor-protein interactions is based on a global superposition of the NAD(P) coordinates, the greater variability of NADP conformation compared with NAD may simply act to obscure any patterns in the binding sites. This type of problem was the driving force in developing a rigid-fragment-

centric protocol for binding site analysis, which will be discussed in the following chapter.

An interesting analysis of the sequence and structure of 32 families of FAD-binding proteins has been reported (Dym and Eisenberg, 2001). While the main stated aim of this study was the identification of sequence motifs diagnostic of the main fold groups within their dataset, the authors also comment on the conformation of the cofactors bound to each protein. They find that, while in some structural families (namely the p-cresol methylhydroxylase and pyruvate oxidase proteins), the cofactor conformation is essentially fixed, other groups (the glutathione reductase (GR) and ferredoxin reductase (FR) families) contain proteins which bind FAD in quite varied arrangements. Another interesting distinction of the FR family which they note is that it is the only one among the families studied in which the FAD is oriented with its isoalloxine ring, rather than the adenine ring, pointing towards the FAD-binding domain.

A structural basis for the variation of FR cofactor conformation is proposed in the paper: these proteins consist of two domains which are 'bridged' by the FAD molecule. Since, in different members of this family, the relative orientations of these two domains can vary, so the conformation of the cofactor must change in order to maintain its contacts. No explanation is given of the wide range in GR cofactor shapes, however; nor is the conformational variance of FAD *within* families compared to that observed *between* families.

Hansen and coworkers published a study of the relationship between protein sequence similarity and NAD cofactor conformation (Kho *et al.*, 2003). They obtained sequences of NAD(P)-utilising enzymes from SWISS-PROT, and then clustered them using a method which they term *protein keys*. These keys are strings of scores which represent the similarity of a given protein to every other sequence in the database, and hence describe the protein as a function of its sequence neighbourhood. Distances between these keys are used to generate sequence clusters, although since the authors fail to report the clustering thresholds used, it is difficult to estimate the sequence identity shared by proteins which fall into the same group. The authors then compare the sequence clusters obtained with a clustering based on the pairwise RMSDs between bound NAD(P) molecules retrieved from the PDB.

The main result reported in the paper is that each sequence family binds NAD(P) molecules in conformations which cluster together. This is not surprising, since the identification of protein relationships from sequence alone implies that more than 30% of their residues are identical, which in turn implies that function is conserved - and hence the cofactor should be expected to bind in the same way. Although relationships between higher-level protein similarities (*i.e.* superfamily or fold groupings) and cofactor conformation are not discussed at length, the overall finding is that members of the large structural families (Rossmann fold oxidoreductases and flavin-NAD(P)-coupled enzymes) both bind their cofactors in several different conformations, while the smaller families each map to just a single conformational cluster.

Intramolecular hydrogen bonding can be important in stabilising the conformation of small molecules. In an *ab initio* conformational analysis of the adenosine moiety for instance, it was found that hydrogen bonding between the adenine and ribose fragments was an important contributor to the stability of certain conformations (Lau *et al.*, 2003).

5.4 Methodology

In light of the existing corpus of literature on ligand conformation, the author felt that one area which has until now been insufficiently studied is the question of the extent to which *homologous* proteins may bind their ligands or cofactors in different conformations. As discussed previously, such a study would have value both in deepening understanding of the evolutionary constraints acting on molecular recognition, and in providing guidance on the permitted ranges of ligand conformation within any given family.

To gain an overall picture of the degree of ligand conformational variability between clusters for each ligand type, molecular superpositions were performed of the representatives of the third-level clustering. The reader will recall that each third-level cluster contains binding sites whose composition in terms of domains is similar up to the CATH H level (§4.2). For example, for ATP, this superposition consists of the 27 representative molecules (see table D.1).

A quantitative measure of overall conformational variation was obtained by calculating the radius of gyration (r_g) for each molecule. As discussed in §3.7.1, this parameter provides a crude measure of the extent to which a molecule is in an extended conformation, and is related to the measurement of its end-to-end distance.

It is interesting to compare similarities between the observed conformations of the bound ligands against relationships between the proteins which bind them. Firstly, we wished to compare the extent to which ligand conformations vary within and between families. Specifically, we wished to answer the following questions:

- What is the extent of conformation variation among ligands in the same cluster?
- Where variation is found within a cluster, it is manifested as a continuum, or are a number of distinct conformations preferred?
- How often do unrelated binding sites (*i.e.* those in different clusters) bind the ligand in the same conformation?

To approach these questions, we computed similarities between the shapes of all ligands in each dataset by performing least-squares superposition of all atoms in the molecule (see §3.6) to obtain RMSD values between each pair. These dissimilarities were then compared against the level-3 clustering assignment of the site to which each molecule is bound. In order to investigate the relationship between protein sequence similarity and ligand conformation, pairwise sequence identity values between ligand-binding domains were compared against the RMSD between their bound ligands.

Having investigated general trends in ligand shape, conformational differences were analysed in more detail by calculating torsion angles for several rotable bonds in each molecule. The objective of doing this was to establish which parts of each ligand type are the most flexible, and to identify molecules which are bound in particularly unusual conformations (as evidenced by torsion angles which lie outside preferred angular ranges). Where these outlying local conformations occur, they may simply be due to poor crystallographic refinement, or alternatively may reflect special structural or functional contraints acting on the bound ligand. The occurrences of both these contingencies are discussed later in the chapter.

5.5 Overall shape of bound ligands

5.5.1 Superpositions

Superpositions were performed using the method described in §3.6, which has been implemented in the GAMUT library. In order to show more clearly the conformational differences between individual molecules, the superpositions were performed on rigid fragments at their termini, rather than globally across the whole molecule, since the latter type of alignment tends to be very difficult to interpret visually. For ATP, the adenine ring was used; for GTP, the guanine ring; for NAD, the nicotinamide moiety; and for FAD, the isoalloxine group. Figures 5.4, 5.7, 5.8 and 5.11 show coordinate superpositions of all cluster representatives, for each ligand type studied. The initial observations which can be drawn from these plots are described for each ligand type in turn.

5.5.1.1 ATP

Visual inspection of figure 5.4 provokes three immediate reactions. The first is that the conformational diversity exhibited by ATP is considerable. Indeed, it is clear that the amount of variation in the shapes which this molecule can adopt - particularly in its triphosphate tail - are likely to preclude attempts to define a unique pharmacophore describing its recognition. The second is that, in agreement with previous studies, ATP is observed to adopt a generally fairly extended conformation. Thirdly, we note that the N-glycosidic bond is most often found in the *anti* orientation.

Although most bound ATP molecules are extended, this is not universally true: two representatives (1B8A and 3R1R) are seen to be bent to such a degree that the terminal phosphate atoms are almost in Van der Waals contact with the adenine ring. 1B8A is a structure of aspartyl-tRNA synthase. tRNA synthase enzymes, which catalyse the specific esterification of a given amino acid to the 3′ end of its corresponding tRNA, can be divided into two classes on the basis of sequence motifs (Eriani *et al.*, 1990). These classes each adopt different structural folds - class I enzymes adopt a Rossmann fold, while class II enzymes bind ATP using an antiparallel β-sheet motif. The conformations of ATP bound to these two classes (clusters 9 and 4 in the ATP dataset respectively) are shared, from the adenine moiety to the alpha phosphate (figure 5.5), with the beta phosphate bent back towards the adenine. This bending allows access to the alpha phosphate to which the tRNA molecule is esterified, as discussed in the paper describing PDB entry 1B8A (Schmitt *et al.*, 1998). It appears, then, that the subsequent bending of the gamma phosphate even closer to the adenine ring, which occurs only in class II enzymes, does not have a direct significance; Schmitt *et al.* report that, in structure 1B8A, this conformation is stabilised by a water molecule which forms bridging hydrogen bonds between the N7 atom and a magnesium ion coordinated by the triphosphate tail.

In the case of 3R1R, a structure of ribonucleotide reductase, the bent ATP conformation may be an experimental artefact. The authors report that ATP was not co-crystallised with the protein, but was soaked in afterwards, and that the soaking time may not have been sufficient for conformational changes to occur, which would accommodate the ligand in a more native conformation (Eriksson *et al.*, 1997).

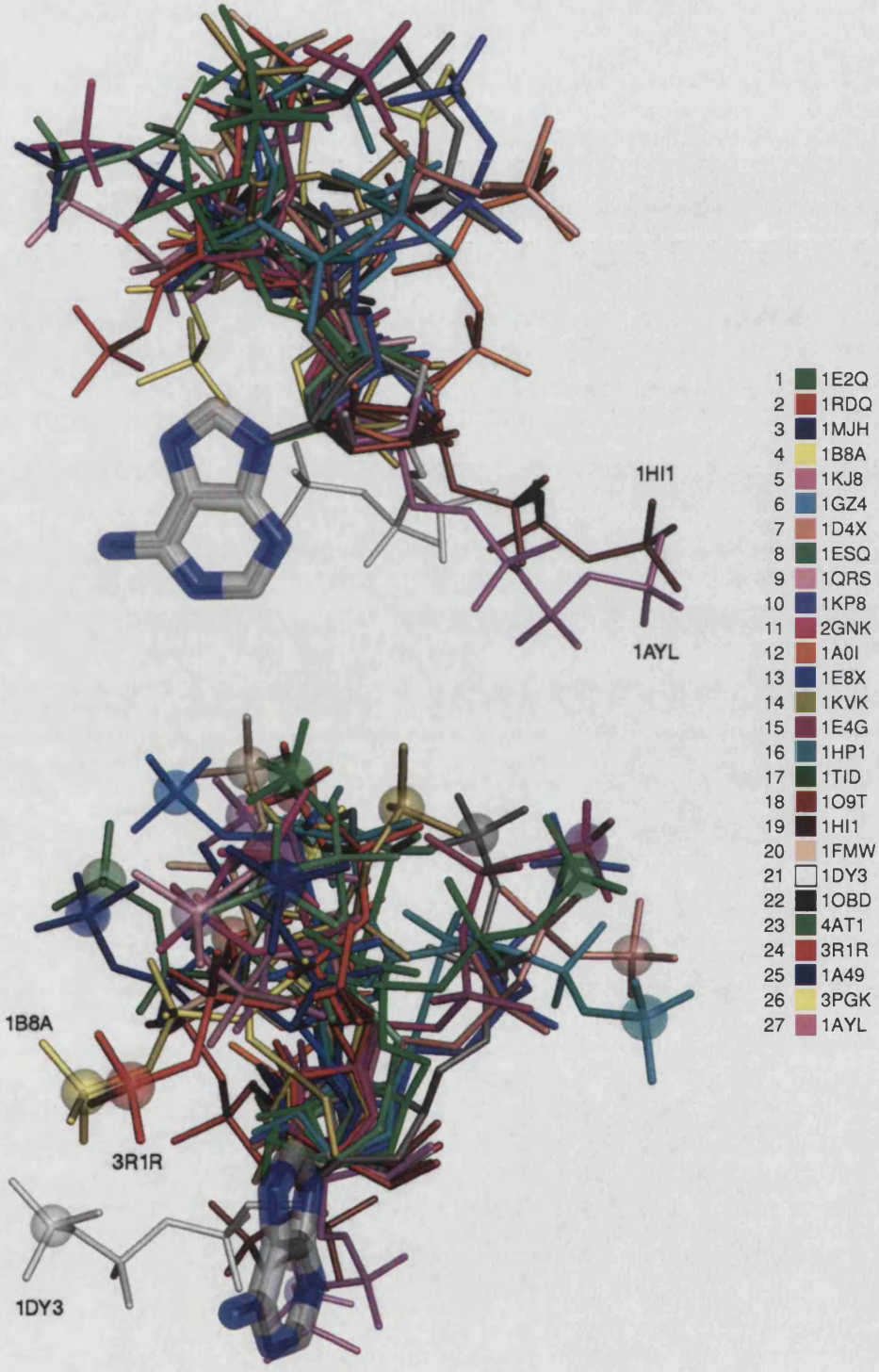

Figure 5.4: Superposition of ATP cluster representatives

The 27 ATP cluster representatives are shown, superposed on their adenine rings (highlighted). In the second image, the gamma phosphate atoms are shown with translucent spheres, to highlight the broad range of conformations adopted by the triphosphate tail. The key shows from which PDB entry each molecule was taken. Several particularly unusual conformations are indicated with labels on the plots themselves.

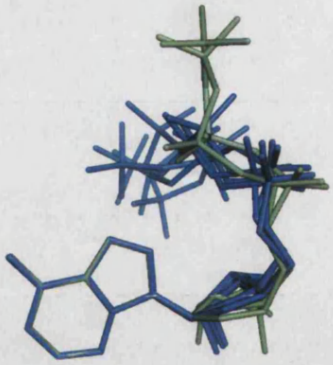

Figure 5.5: Conformation of ATP molecules bound to tRNA synthetase enzymes
ATP molecules from two class I (cluster 9, shown in green) and four class II tRNA synthetases (cluster 4, blue) are shown, superposed on their adenine rings. The conformation up to the alpha phosphate is conserved between the two structural classes.

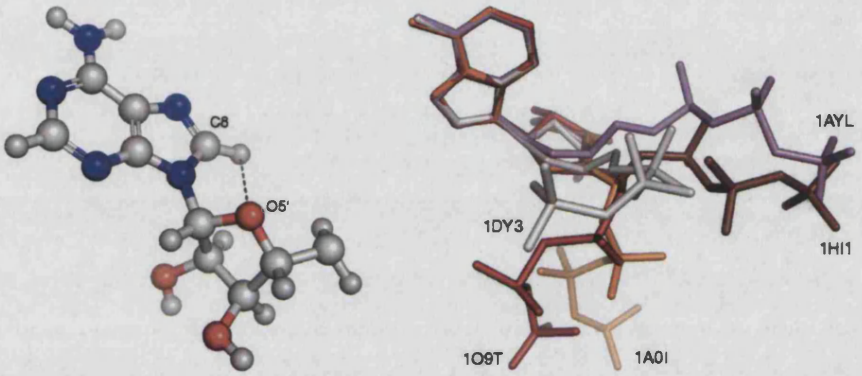

(a) Stabilisation of the *anti* conformation (b) *syn* conformations of ATP among the level-3 cluster representatives

Figure 5.6: The *syn* and *anti* conformations of ATP
(a) The *anti* orientation of the N-glycosidic bond may be stabilised by weak (C-H $\cdots$ O) hydrogen-bonding interactions between the ribose moiety and the base (Lau *et al.*, 2003). Coordinates taken from PDB entry 1QZ5; hydrogen atoms added using PyMOL (DeLano, 2002).
(b) Five examples of ATP in the *syn* conformation, found among the level-3 cluster representatives.

It has frequently been observed that the orientation of the N-glycosidic bond is one of the most conserved conformational descriptors of ATP, showing a significant preference for the *anti* orientation - see *e.g.* Saenger (1984), Moodie and Thornton (1993). This can be attributed to two factors: the steric hinderance of placing the bulky purine above the furanose ring, which would occur in the *syn* arrangement, and the stabilising effect of attractive interactions between the ribose O5′ and the base which are permitted by the *anti* orientation (see figure 5.6a). However, an *ab initio* quantum mechanical study of adenosine conformation suggested that the energy difference between the *anti* form and the most stable *syn* arrangement (where strain is relieved by switching the ribose ring pucker to the *endo* conformation) may be as little as 1.33 kcal mol^{-1} (Lau *et al.*, 2003). This suggests that a single extra hydrogen bond could be enough to stabilise the *syn* conformation. It should not be surprising, therefore, to find ATP molecules bound in this way to proteins, where the highly anisotropic environment could frequently be expected to offer the possibility to stabilise conformations distinct from those which predominate in aqueous environments. This is borne out by the current data: 5 of the 27 ATP cluster representatives have their N-glycosidic bond in the *syn* conformation (figure 5.6b).

Since these five proteins have quite diverse functions, it is not possible to posit any functional reason why they should bind ATP in this way; in all cases, upon visual inspection of the individual structures, interactions between the protein and the ligand can be identified which may contribute extra stability. These include hydrogen-bonding between the adenine ring and waters coordinating magnesium ions (1DY3), hydrophobic residues stacking against the face of the adenine ring (1AYL, 1A0I) and the fact that, for two proteins (1A0I and 1HI1), the catalytic mechanism involves the ATP becoming covalently attached to the protein via its ribose moiety.

It is interesting to note that, in all five of these cases (1A0I, 1O9T, 1HI1, 1DY3 and 1AYL), the level-3 clusters concerned (clusters 12, 18, 19, 21 and 27 respectively) are singlets. In other words, none of these five proteins has a relative which is distinct in sequence, but which belongs to the same superfamily. This may suggest that *syn* binding of ATP is an elaboration with fairly limited utility, and which has not therefore been propagated into other sequence families. This result may, on the other hand, simply reflect the current lack of structural data.

5.5.1.2 GTP

The conformations adopted by GTP bound to proteins are broadly similar to those of ATP (see figure 5.7). The *syn* conformation of the N-glycosidic bond seems to be more disfavoured when the base is guanine compared to adenine - only one GTP molecule (1JLR) has its N-glycosidic bond in the *syn* conformation. This is not surprising, given the presence of a bulky amine group attached to the C2 position of the guanine base, and the fact that the C8 atom in the guanine ring can make a weak hydrogen bond to ribose, similarly to the corresponding interaction in adenine.

5.5.1.3 NAD

Figure 5.8 shows the 19 representative NAD molecules, superposed on their nicotinamide rings. While most NAD molecules adopt a fairly extended shape, in agreement with previous studies, the degree of conformational diversity apparently permitted to the cofactor is striking. Two obvious exceptions to the tendency of NAD molecules to bind in extended forms are those from PDB entries 2BKJ and 1LW7.

2BKJ is a structure of flavin reductase from the luminous bacterium *Vibrio harvey*, with both NAD and FMN bound at one of its active sites. Flavin reductase enzymes catalyse the reduction of flavin using NAD(P)H as a cofactor. The substrate and cofactor are in close proximity in this structure, but the NAD molecule approaches FMN via its pyrophosphate moiety, with the adenine and nicotinamide rings stacked and pointing out of the binding cavity (figure 5.9a). This arrangement is not amenable to hydride transfer between the two bound molecules. In their paper describing the structure, the authors suggest that this arrangement is evidence for a mechanism whereby the NAD first binds in this folded conformation, then unfolding to its active conformation inside the binding site. Following reduction of the flavin, electrostatic repulsion between the protein and the positively charged nicotinamide ring may promote the return of the cofactor to its bent conformation and subsequent expulsion from the active site (Tanner *et al.*, 1999). The observed coordinates of NAD therefore could represent an intermediate between the solution structure and the fully bound, extended form.

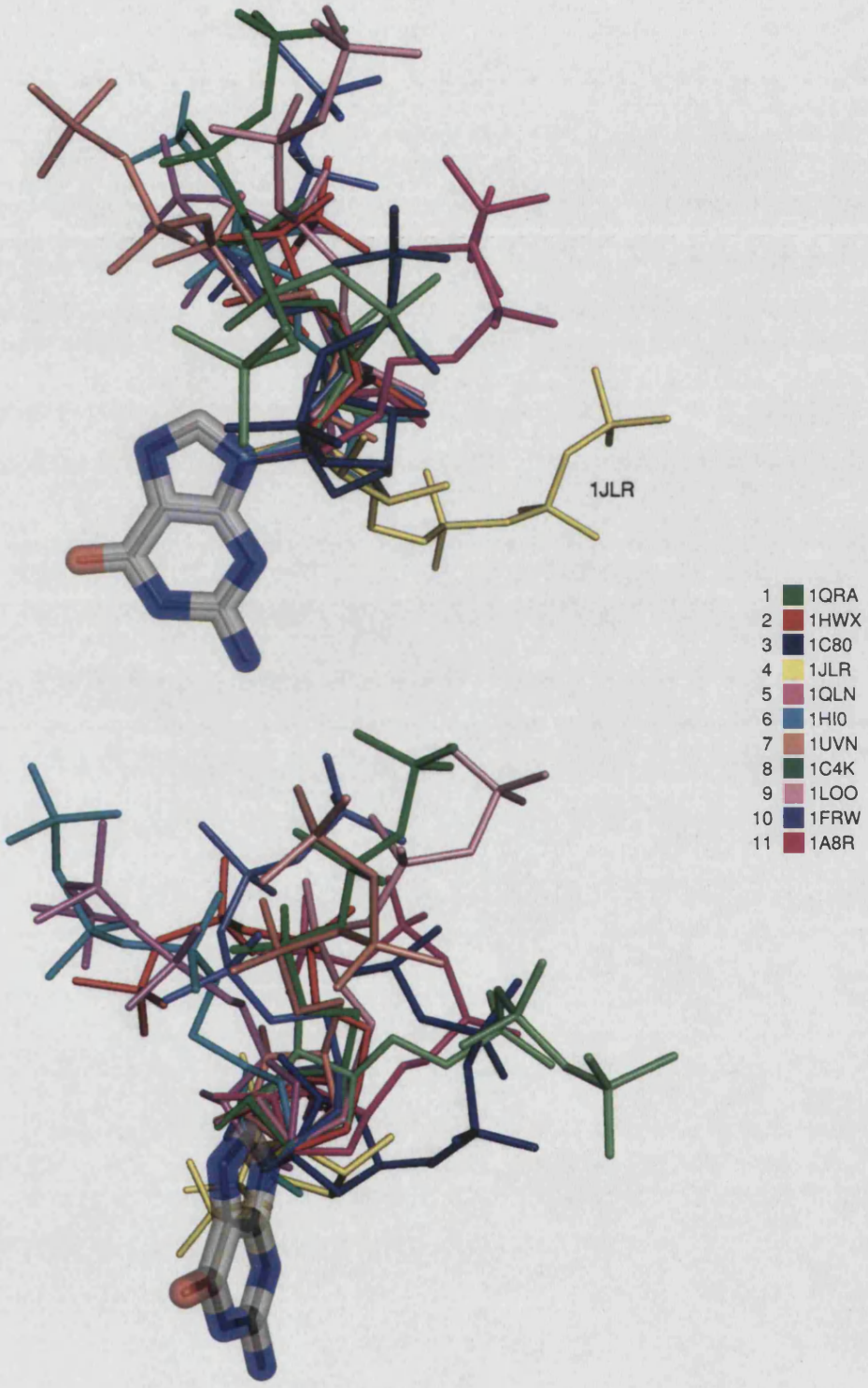

Figure 5.7: Superposition of GTP cluster representatives

The 11 GTP cluster representatives are shown, superposed on their guanine rings (highlighted). The key shows from which PDB entry each molecule was taken. One unusual example (1JLR), in which the N-glycosidic bond is unique in taking the *syn* orientation, is labelled.

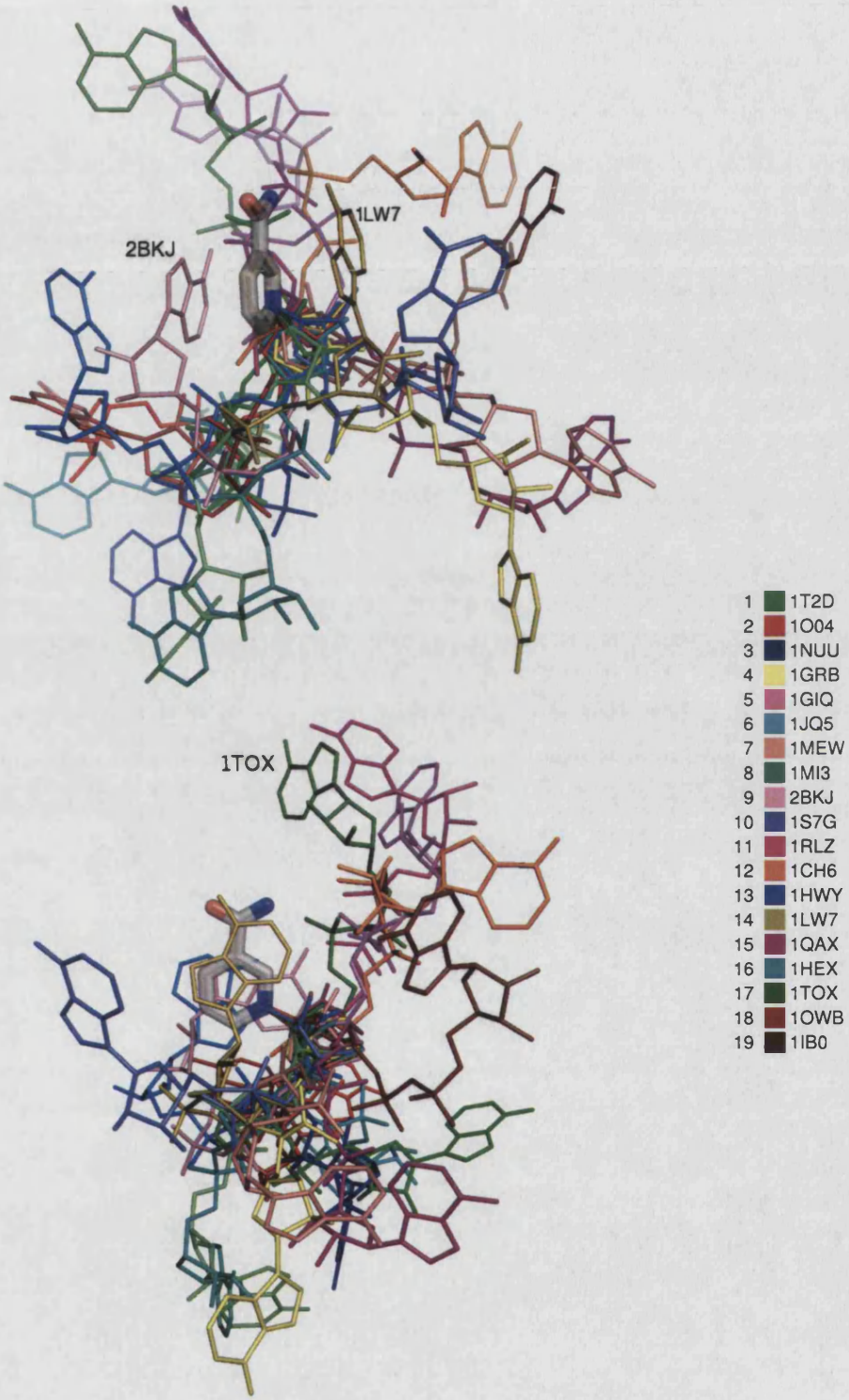

Figure 5.8: Superposition of NAD cluster representatives

The 19 NAD cluster representatives are shown, superposed on their nicotinamide rings (highlighted). Note that in some cases, the carboxyamide functionality is rotated 180° relative to the one shown here. The key shows from which PDB entry each molecule was taken. Two cases where the adenine and nicotinamide rings are in a stacked arrangement are labelled (2BKJ and 1LW7). The cofactor in diptheria toxin (1TOX), whose nicotinamide N-glycosidic bond adopts an unusual strained conformation, is also indicated.

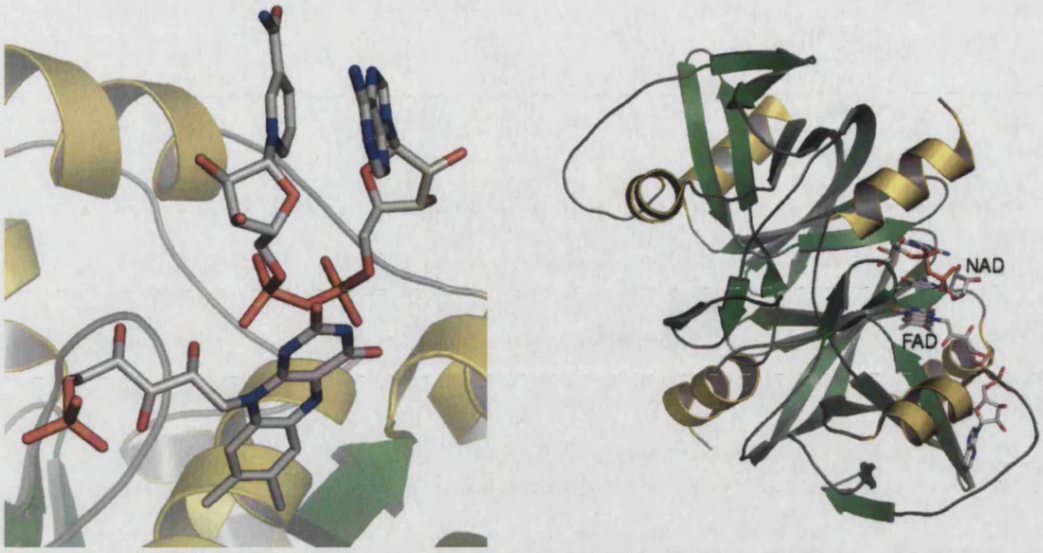

(a) Unproductive complex of folded NAD and FMN in PDB entry 2BKJ (2.1Å resolution)

(b) Productive complex of folded NAD and FAD in PDB entry 1RZ1 (2.1Å resolution)

Figure 5.9: Folded conformations of NAD in flavin reductase

Recent structural studies on another flavin reductase enzyme, however, cast doubt on this hypothesis. PDB entry 1RZ1[1] is a structure of flavin reductase PheA2 from *Bacillus thermoglucosidasius*, which displays no amino acid sequence similarity with the family of enzymes to which the *Vibrio harvey* belongs. It contains an NAD molecule, bound in a ring-stacked conformation, with the nicotinamide ring positioned close to an FAD molecule (see figure 5.9b). The authors report bleaching of the crystals upon addition of NAD, indicating that flavin reduction occurs, and therefore that the folded conformation of NAD persists during the reaction (van den Heuvel *et al.*, 2004).

1LW7 is a structure of the *H. influenzae* NadR protein. This is a bifunctional enzyme possessing both NMN adenylyltransferase and ribosylnicotinamide kinase activities (Singh *et al.*, 2002). The NAD molecule in the dataset, however, is not bound at an active site, and while it makes a number of specific contacts with the protein, its biological significance, if any, is unclear.

Another unusually-shaped NAD molecule is not as conspicuous as the ring-stacked examples - 1TOX, a structure of diptheria toxin (DT), binds NAD with the N-glycosidic bond of its nicotinamide nucleotide in an unusual conformation. This has been previously noted, and attributed to the particular catalytic mechanism of the toxin (Bell *et al.*, 1997). DT is an ADP-ribosyltransferase (ART) enzyme which catalyses the cleavage of the nicotinamide N-glycosidic bond followed by the transfer of the resulting ADP-ribose moiety to a post-translationally modified histidine residue of EF-2. By covalently linking the ADP-ribose to the elongation factor, protein synthesis is inhibited, resulting in cell death. The unusual strained conformation of the cofactor is thought to promote this reaction by exposing the reactive atom of NAD when bound within the active site.

Diptheria toxin is only one of a number of known ADP-ribosyltransferase enzymes. These include three other groups of prokaryotic toxins, each of which ADP-ribosylates a different type of target. One group, including cholera toxin, modifies heterotrimeric GTP-binding proteins (Fishman, 1990); another,

[1]These molecules are missing from the main datasets used here since 1RZ1 is not classified in CATH release 2.6.0.

including *C.botulinum* C3 exoenzyme, targets small GTP-binding proteins (Aktories *et al.*, 1988). A fourth group contains a number of toxins which ADP-ribosylate actin, with slightly different specificities - *C.botulinum* C2 toxin is restricted to modifying non-muscle actin, whereas *C.perfringens* iota toxin also causes depolymerisation of skeletal muscle actin (Tsuge *et al.*, 2003). In addition, two eukaryotic proteins with structural similarity to these bacterial toxins are known. These are the poly(ADP-ribsosyl)polymerase and ecto-ADP-ribosyltransferase families (Ruf *et al.*, 1996, Mueller-Dieckmann *et al.*, 2002). Each of these performs post-translational modifications on a wide range of targets.

In addition to that found in the DT structure, the NAD dataset contains four other molecules originating from ART enzymes. These are an iota toxin, two C3 exoenzyme-like toxins, and a rat ecto-ART. Inspection of the clustering revealed an error in the CATH database: whereas the NAD-binding domain from DT is classified as an α/β structure (CATH code 3.90.175.10), the domains which comprise the other four ART NAD-binding sites are classified as mostly β-sheet (2.30.100.10), and hence are placed in a separate cluster (cluster 5). These two domains share a common NAD-binding region consisting of a greek key motif, as shown in figure 5.10a and in SCOP, all five domains are classified as belonging to the same family. Figure 5.10b shows that all five ADP-ribosylating enzymes bind NAD in a similar conformation, with the torsion around the N-glycosidic bond being particularly well-conserved. Upon being notified of this problem, the CATH curators reclassified the NAD-binding domain of 1TOX: although it did not meet their criteria for being classified as homologous to the other ART domains, it has now been assigned to the same fold group, with a CATH number of 3.90.176.10.

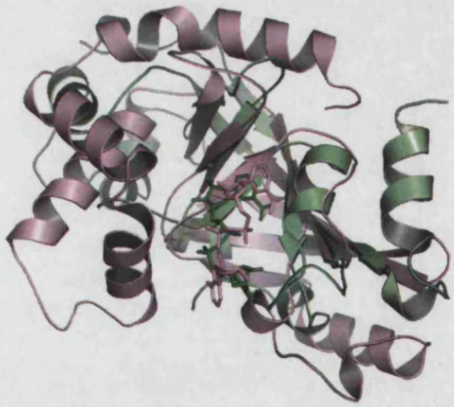

(a) Comparison of NAD-binding domains from diptheria toxin (1TOX, green) and *C.botulinum* iota toxin (1GIQ, pink). Superposition is based upon the coordinates of the protein backbones, and was performed using SSM (Krissinel and Henrick, 2004b).

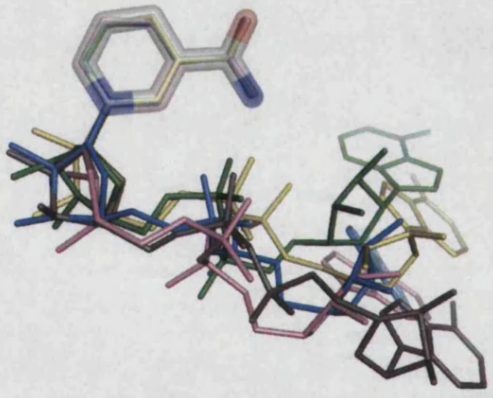

(b) Comparison of conformation of NAD in diptheria toxin (1TOX, green) and the four β-sheet ADP-ribosylating proteins from cluster 5 (1GIQ, pink; 1GZF, blue; 1OJZ, yellow; 1OG3, grey), superposed on the nicotinamide moiety. The shared orientation of the nicotinamide N-glycosidic bond is clearly visible.

Figure 5.10: NAD binding by ADP-ribosylating proteins

5.5.1.4 FAD

Superpositions of the 14 FAD cluster representatives, aligned upon their isoalloxine rings, are shown in figure 5.11. Visual inspection of the plots shows the conformations of FAD to be somewhat more homogeneous than those of NAD, with the main variation occurring around the ribitol-isoalloxine bond. The adenine nucleotide part of the molecule tends to be fairly extended, and FAD is the only molecule of the four studied here in

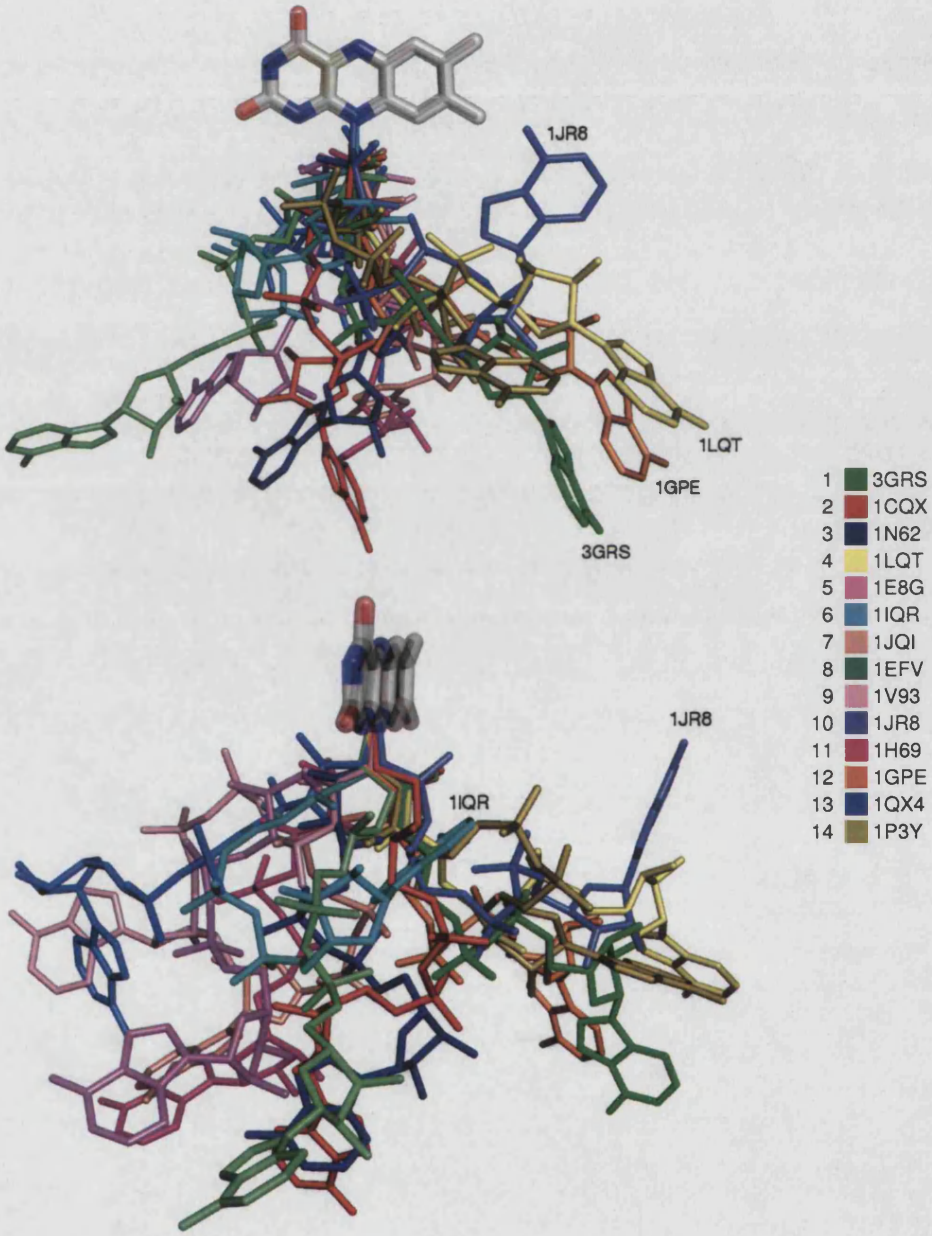

Figure 5.11: Superposition of FAD cluster representatives
The 14 FAD cluster representatives are shown, superposed on their isoalloxine rings (highlighted). The key shows from which PDB entry each molecule was taken.

which the adenosine N-glycosidic bond seems to adopt the *anti* conformation exclusively.

In contrast to NAD, no examples of FAD are seen where the molecule is bent enough to allow adenine-isoalloxine stacking interactions. The most bent conformation is that from PDB entry 1IQR (DNA photolyase from *Thermus thermophilus*), in which the centroids of the adenine and isoalloxine groups are separated by around 6.3Å, compared with 3.6Å and 4.0Å for the inter-ring distances in the NAD molecules from 2BKJ and 1LW7 respectively. There is no clear functional reason why the FAD in this enzyme should adopt such a compact conformation.

Three FAD molecules which have clearly similar conformations are 3GRS, 1LQT and 1GPE, which are the representatives from clusters 1, 4 and 12 respectively. Inspection of the clustering results shows that in all three cases, the FAD molecule is bound by a Rossmann fold domain (CATH code 3.50.50.60), but whereas in 3GRS (glutathione reductase), the FAD binding site is formed by two Rossmann fold domains, in both 1LQT (FprA, a mycobacterial oxidoreductase) and 1GPE (glucose oxidase), a single Rossmann domain binding the adenine is partnered with a second domain of a different type (see figure 5.12). The resulting change in the fraction of residue contributed by the Rossmann fold domain causes each site to be placed in a different cluster, although a human expert would classify them all as belonging to the glutathione reductase family (Dym and Eisenberg, 2001).

(a) Glutathione reductase (3GRS) (b) FprA (1LQT) (c) Glucose oxidase (1GPE)

Figure 5.12: FAD binding sites in the glutathione reductase family
In each case, the Rossmann fold domain which binds the adenine end of the FAD molecule is coloured red. Other colours indicate the following domains: green, Rossmann fold; yellow, enolase-like; blue, FAD/NAD(P)-binding; purple, glucose oxidase domain.

5.5.2 Radii of gyration

Having discussed several qualitative aspects of the bound conformations of the four ligands, we now proceed to analyse the degree of molecular compactness of each molecule, in order to quantify to what extent the general principal of ligand extension upon binding is realised in each case. Before looking at the radii of gyration calculated for each bound ligand in the dataset, it is instructive to explore the range of the possible values which this parameter could potentially take for each molecule. To estimate this, a set of artificially-generated conformations of each ligand were compiled, sampling the full extent of conformational space.

This was done by specifying a list of rotable bonds for each ligand, and a set of allowed rotamers for each bond. These rotable bonds were selected according to the criteria outlined in §2.3.4.3.1 and are shown diagrammatically in figures 3.13 and 3.14. For each bond, preferred angular ranges have been assigned by consideration of the hybridisation states of the pairs of bonded atoms, and by consulting previous literature on the subject. The atoms which define all rotable bonds used here, along with the preferred orientations, are shown in tables 5.1 - 5.3.

Angle	A	B	C	D	Preferred orientations
χ_{pur}	O4′	C1′	N9	C4	$+sc, 180° - 300°$
χ_{pyr}	O4′	C1′	N1	C2	$+sc, 180° - 300°$
γ	O5′	C5′	C4′	C3′	$\pm sc, ap$
β	PA	O5′	C5′	C4′	$\pm sc, ap$
α	O3	PA	O5′	C5′	$\pm sc, ap$
ξ_1	PB	O3A	PA	O5′	$\pm sc, ap$
ψ_1	O3B	PB	O3A	PA	$\pm sc, ap$
ξ_2	PG	O3B	PB	O3A	$\pm sc, ap$
ψ_2	O3G	PG	O3B	PB	$\pm sc, ap$

Table 5.1: Definition of torsion angles and associated minima for nucleotide derivatives
Torsion angles are ordered from the adenine end of the molecule to the triphosphate tail. χ_{pur} and χ_{pyr} refer to the definition of the torsion around the N-glycosydic bond for purines and pyrimidines respectively. See figure 3.13.

	Angle	A	B	C	D	Preferred orientations
Adenine nucleotide	χ_A	O4′_A	C1′_A	N9_A	C4_A	$+sc, 180° - 300°$
	γ_A	O5′_A	C5′_A	C4′_A	C3′_A	$\pm sc, ap$
	β_A	P_A	O5′_A	C5′_A	C4′_A	$\pm sc, ap$
	α_A	O3	P_A	O5′_A	C5′_A	$\pm sc, ap$
	ξ_A	P_N	O3	P_A	O5′_A	$\pm sc, ap$
Nicotinamide nucleotide	ξ_N	P_A	O3	P_N	O5′_N	$\pm sc, ap$
	α_N	O3	P_N	O5′_N	C5′_N	$\pm sc, ap$
	β_N	P_N	O5′_N	C5′_N	C4′_N	$\pm sc, ap$
	γ_N	O5′_N	C5′_N	C4′_N	C3′_N	$\pm sc, ap$
	χ_N	O4′_N	C1′_N	N9_N	C4_N	$+sc, 180° - 300°$
	θ_N	C2_N	C3_N	C7_N	NN7	sp, ap

Table 5.2: Definition of torsion angles and associated minima for NAD
Torsion angles are ordered from the adenine end of the molecule to the nucleotide moiety. See figure 3.14a.

	Angle	A	B	C	D	Preferred orientations
Adenine nucleotide	χ	O4′_A	C1′_A	N9_A	C4_A	$+sc, 180° - 300°$
	γ	O5′_A	C5′_A	C4′_A	C3′_A	$\pm sc, ap$
	β	P_A	O5′_A	C5′_A	C4′_A	$\pm sc, ap$
	α	O3	P_A	O5′_A	C5′_A	$\pm sc, ap$
	ξ_A	P	O3P	P_A	O5′_A	$\pm sc, ap$
Ribitol phosphate	ξ_R	P_A	O3P	P	O5′	$\pm sc, ap$
	θ_1	O3P	P	O5′	C5′	$\pm sc, ap$
	θ_2	P	O5′	C5′	C4′	$\pm sc, ap$
	θ_3	O5′	C5′	C4′	C4′	$\pm sc, ap$
	θ_4	C5′	C4′	C3′	C2′	$\pm sc, ap$
	θ_5	C4′	C3′	C2′	C1′	$\pm sc, ap$
	θ_6	C3′	C2′	C1′	N10	$\pm sc, ap$
	θ_7	C2′	C1′	N10	C10	sp, ap

Table 5.3: Definition of torsion angles and associated minima for FAD
Torsion angles are ordered from the adenine end of the molecule to the riboflavin moiety. See figure 3.14b.

A program was then written which generates all possible conformations of the molecule by systematically setting the rotable bonds to each combination of the allowed rotameric states. Each arrangement is then tested for steric clashes by checking whether any pair of non-bonded atoms approaches closer than the sum of their Van der Waals radii (values taken from Bondi (1964)). Atoms in the same ring system are excluded from this check. Since the restrictive definition of rotable bonds used here does not include bonds such as C−OH , it is possible that atoms which were found to clash in the conformations generated here would actually be free to rotate away from one another, were a more complete simulation of the molecule to be carried out. For this reason, clashes due to this type of atom (such as a hydroxyl hydrogen) were ignored. The set of arrangements which were found to be free of atomic clashes was taken to represent the extent of conformational space which may be explored by the molecule. No energy calculations were performed; therefore this set consists of those conformations which need satisfy only fairly liberal constraints.

The initial coordinates of each molecule used were the idealised coordinates retrieved from the MSD. These coordinates were originally generated using the CORINA program (Gasteiger *et al.*, 1990) (D. Dimitropoulis personal communication). Hydrogen atoms were included for the purposes of the steric hinderance check, but were excluded from the calculations of radius of gyration, to allow direct comparison of these values with those calculated from ligand coordinates taken from crystal structures. The allowed rotameric states for each bond were defined as the median values of each of the preferred angular ranges shown in tables 5.1 - 5.3.

The results of the conformation generation experiment are summarised in table 5.4. Figure 5.13 shows a number of the artificially-generated ligand conformations which exemplify the extrema and average values of r_g for each population.

Ligand	Number of rotable bonds*	Total number of possible conformations	Number of conformations free of steric clashes
ATP	8	4374	830
GTP	8	4374	826
NAD	11	52488	3054
FAD	13	1062882	4992

Table 5.4: Results of conformation generation experiment
(⋆) This is the number of bonds which were allowed to rotate in the current experiment, which is a subset of the total number of rotable bonds. A $C-NH_2$ bond, for instance, is not considered rotable for the purposes of this analysis. See §2.3.4.3.1 for more details. For each ligand, the total number of comformations resulting from all combinations of the rotamers defined previously is quoted. Following checks for steric clashes, a subset of these conformations is retained; these are taken to define the total conformational space of the molecule.

The generated conformations of ATP and GTP show that the *syn* orientation of the N-glycosidic bond is necessary to fold the molecules into their most compact forms. Most molecules in the datasets presented above, on the other hand, tend to adopt conformations intermediate between the median and extended forms.

For both FAD and NAD, in arrangements with an r_g close to the median value, the two rings tend to be separated from one another. The most compact NAD conformations are achieved by stacking the terminal ring systems in parallel; in the folded FAD structures, the adenine and isoalloxine rings are in close proximity, but do not lie in parallel. This suggests that the folded conformation of NAD in DNA photolyase (1IQR) is

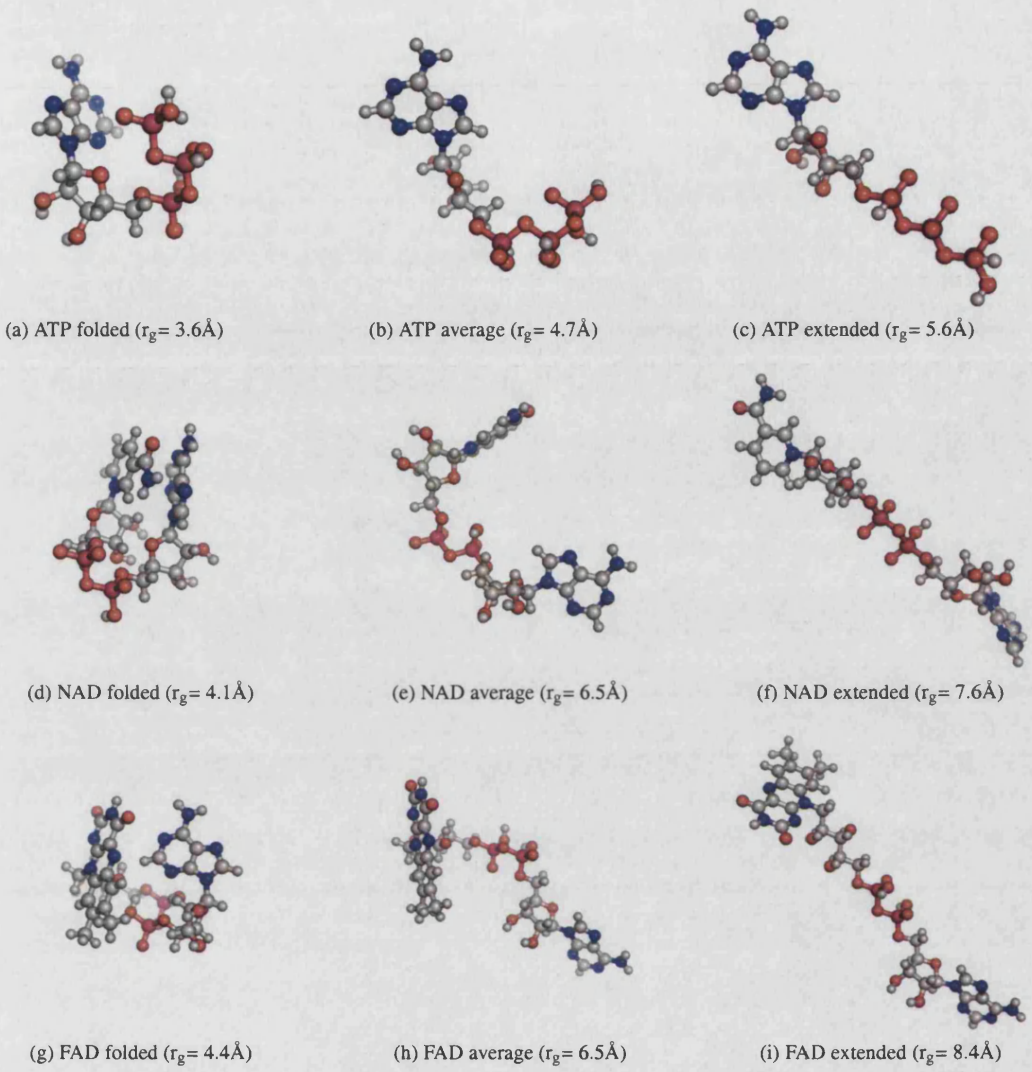

(a) ATP folded (r_g= 3.6Å) (b) ATP average (r_g= 4.7Å) (c) ATP extended (r_g= 5.6Å)

(d) NAD folded (r_g= 4.1Å) (e) NAD average (r_g= 6.5Å) (f) NAD extended (r_g= 7.6Å)

(g) FAD folded (r_g= 4.4Å) (h) FAD average (r_g= 6.5Å) (i) FAD extended (r_g= 8.4Å)

Figure 5.13: Generated ligand conformations
Artificially-generated ligand conformations which represent the minima, maxima and average values of r_g for each ligand type are shown. GTP is omitted since its conformations are essentially analogous to those shown for ATP.

in fact fairly close to the most compact possible arrangement of the cofactor. Circular dichroism experiments and molecular dynamics studies on NAD suggest that ring stacking occurs in this molecule when free in solvent (Thornton and Bayley, 1977); we may therefore take the folded conformation shown in figure 5.13d as being at least partially populated in an aqueous environment. Several authors have observed that, when in complex with proteins, the nicotinamide and adenine rings of NAD(P) tend to be approximately perpendicular and separated by around 15Å - see *e.g.* Stoddard *et al.* (1993). This corresponds to an intermediate conformation between the median and extended forms (figures 5.13e and 5.13f).

Having established the range of radii of gyration available to each ligand type, we can ask quantitatively how much of this range is explored by protein-bound ligand molecules. Table 5.5 shows statistics which describe the distributions of r_g for each ligand type, in both the 'real' (protein-bound) and artificially-generated datasets. Figure 5.14 shows histograms of these distributions. Structures of molecules from the dataset which illustrate the most compact and extended protein-bound forms of each ligand which were observed, as well as an example of a molecule with average extension, are included in each plot.

Ligand	Dataset*	n	Radius of gyration (r_g) /Å				Test of normality†		p (Wilcoxon test)▲
			Minimum	Maximum	μ	σ	W	p	
ATP	Artificial	830	3.58	5.60	4.63	0.40	0.99	1.13×10^{-6}	0.64
	Level 3	27	3.75	5.11	4.59	0.35	0.94	9.87×10^{-2}	
GTP	Artificial	826	3.60	5.73	4.71	0.42	0.99	1.06×10^{-5}	0.24
	Level 3	11	3.95	5.07	4.59	0.36	0.93	4.49×10^{-1}	
NAD	Artificial	3054	4.08	7.59	5.86	0.59	1.00	1.39×10^{-8}	0.17
	Level 3	19	4.21	6.53	5.63	0.66	0.92	1.28×10^{-1}	
FAD	Artificial	4992	4.38	8.44	6.43	0.69	0.99	6.38×10^{-14}	0.09
	Level 3	14	4.97	7.62	6.76	0.68	0.90	9.63×10^{-2}	

Table 5.5: Radii of gyration

(⋆) 'Artificial' refers to the set of generated ligand conformations; 'level 3' refers to the set of cluster representatives at the third level.

(†) The Shapiro-Wilks test, as implemented in the R (?) package e1071 (?), was used.

(▲) Wilcoxon 2-sample test, applied to determine whether the medians of the artifical and level-3 distributions differ significantly.

Comparison of the ranges of r_g values for the artificial and bound ligand conformations shows that, for all four ligand types, there are instances of the molecule which bind proteins in almost a maximally compact conformation. For ATP and GTP, the difference between the most tightly folded molecules in the generated and observed datasets seems to be that in the former, the N-glycosidic bond is in the *syn* conformation. While this does occur in the bound dataset, it tends to be accompanied by a fairly extended triphosphate tail (figure 5.6b); it is likely that the combination of the *syn* arrangement with a tightly bent triphosphate tail is energetically unfavourable, explaining its absence from the bound dataset.

At the other end of the distributions, there is a larger difference between the artificial and bound datasets, particularly for NAD and FAD. It appears that, while ligands often bind in extended conformations, these are not the *most* extended arrangements which they are capable of adopting. One explanation for this may be that this fully extended arrangement prevents coordination of metal ions by consecutive phosphate moieties, which is a commonly-observed motif in complexes of proteins with nucleotides and nucleotide derivatives.

Neither the r_g values for the artificially-generated conformations nor those for the bound ligand conformations are normally distributed, as shown by a Shapiro-Wilks test. This test measures the likelihood that the samples *are* drawn from normally-distributed populations (Royston, 1982); the p-values shown in table 5.5 show that, in most cases, this hypothesis is rejected with at least 90% confidence. This suggests that, rather than comparing the means and standard deviations of the distributions, more instructive statistics would be the measure of *skewness*.

Since the distributions are not normal, using a t-test to determine whether their means differ significantly is not appropriate. Instead, a Wilcoxon 2-sample test (two-tailed) was applied. The results indicate that, for all ligands except FAD, the medians of the two distributions are not significantly different - and therefore conflicts with previous assertions that these ligands bind in predominantly extended conformations. Rather, it seems that the bound conformations of ATP, GTP and NAD are drawn at random from the pool of possible conformations available to these molecules. When interpreting these findings, however, it must be remembered that the number of data points is quite small in all cases, and that increased amounts of data would allow for more substantial conclusions to be drawn.

An interesting observation which arises from comparison of the radii of gyration for ATP and GTP with those of NAD and FAD is that, for the latter pair of ligands, a slightly bimodal distribution is observed. Again, this should be treated with caution in light of the sparsity of data, but it appears that the mmost folded conformations of NAD and FAD are truly outliers, rather than being simply the lower extrema of smooth distributions.

5.5.3 General observations

In summary of the analysis of the overall shape of bound ligands, we find that, in conflict with previous studies, their degree of extension is not significantly different to the average degree of extension of all possible conformations. Indeed, rather than binding in exclusively extended arrangements, a small proportion of

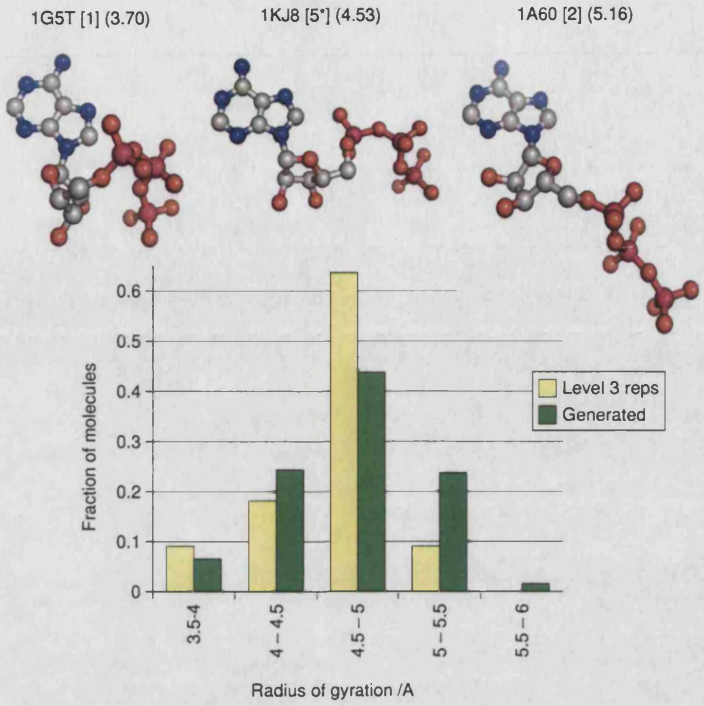

(a) ATP

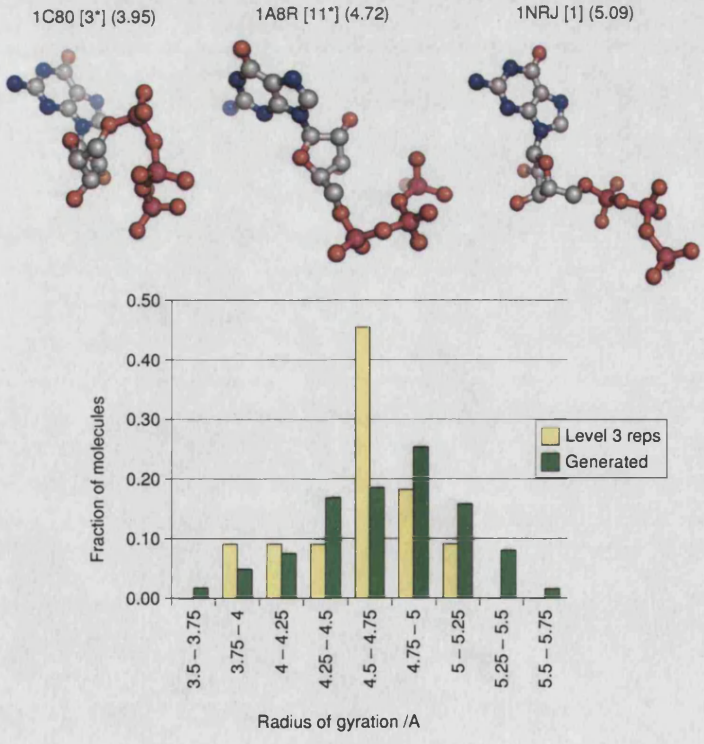

(b) GTP

Figure 5.14: Distribution of radii of gyration

The distribution of the radius of gyration among level-3 cluster representatives is compared against that obtained from the artificially generated conformations. Molecules from the dataset which represent the extrema and average of the distribution are shown. The level-3 cluster to which each molecule belongs is shown in square brackets; an asterisk indicates that the molecule is a cluster representative. The radius of gyration for each compound (in Å) is given in parentheses. Continued overleaf.

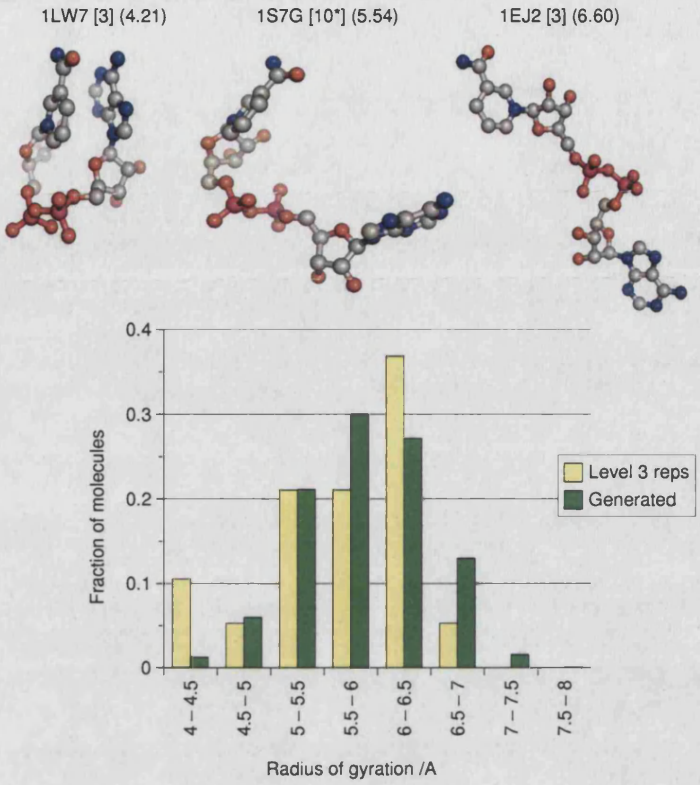

(c) NAD

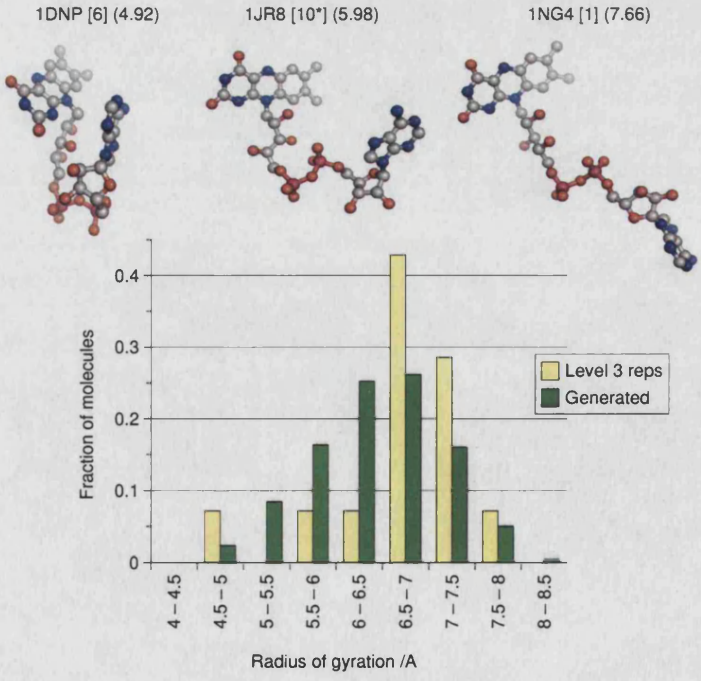

(d) FAD

Figure 5.14: Distribution of radii of gyration
Continued from previous page.

ligands appear to bind in very compact conformations; in some cases, these results may be due to biologically inactive complexes, but in others, genuine functional reasons can be posited to explain why this should be so.

Here, several cases in which ligands bind with part of the molecule in a strained or unfavourable arrangement have been identified. In some cases, this appears to promote catalysis, either by weakening a particular covalent bond, or by relieving steric hinderance around a reactive centre. In others, such as the *syn* conformations observed for the nucleoside moieties, the energetic impediment to adopting these orientations is not particularly high, and thus their occurrence may be explained as allowing for slightly more favourable protein-ligand interactions. Finally, the qualitative observation is made that the degree of variation between the conformations of a given ligand when bound by unrelated proteins is significant. The following section explores this finding in more detail.

5.6 Conformational differences between and within clusters

Having observed the large conformational variations between representative molecules of the level-3 clusters, the next phase of the analysis was to quantify that variation, and compare it against the extent to which molecules in *the same* cluster adopt different shapes.

5.6.1 Hierarchical clustering of ligand conformations

Similarities between the shapes of all level-2 representatives in each dataset were calculated by performing least-squares superposition of all atoms in the molecule (see §3.6). The RMSD values thus obtained were used to populate a distance matrix. This matrix was then analysed by applying complete-linkage clustering (§3.2). The relationships between the shapes of the ligands in the dataset, and the evolutionary relationships between the sites in which they are bound, were then compared by producing plots of the clustering dendrograms, labelling each leaf node with the index of the level-3 cluster to which the corresponding molecule belonged. In this way, clusters in which all members share a similar conformation are visible as leaf labels which are grouped together on the dendrogram; conversely, clusters which contain members with diverse conformations manifest themselves as labels which are scattered across the width of the tree. Note that the absolute ordering of nodes along the tree is not significant in and of itself: this can be changed arbitrarily by flipping a subtree around about its root node.

The clustering dendrograms are shown in figures 5.15 - 5.18. An initial comparison of these trees shows that of the four ligand types, ATP appears to exhibit the greatest degree of conformational variation within clusters. While, for GTP, NAD and FAD, most large clusters tend to have a large proportion of non-leaf nodes below the 1Å threshold, indicating that their members are similarly shaped, the two largest ATP clusters seem to be more distantly spread in conformational space, and hence appear more widely scattered along the leaves of the dendrogram (figure 5.15). Cluster 1 contains members which, although they all share a common Rossmann-fold ATP-binding domain, are diverse in terms of the protein function. Cluster 2, on the other hand, is composed almost exclusively of kinases (see table D.1). Qualitatively, the degree of conformational

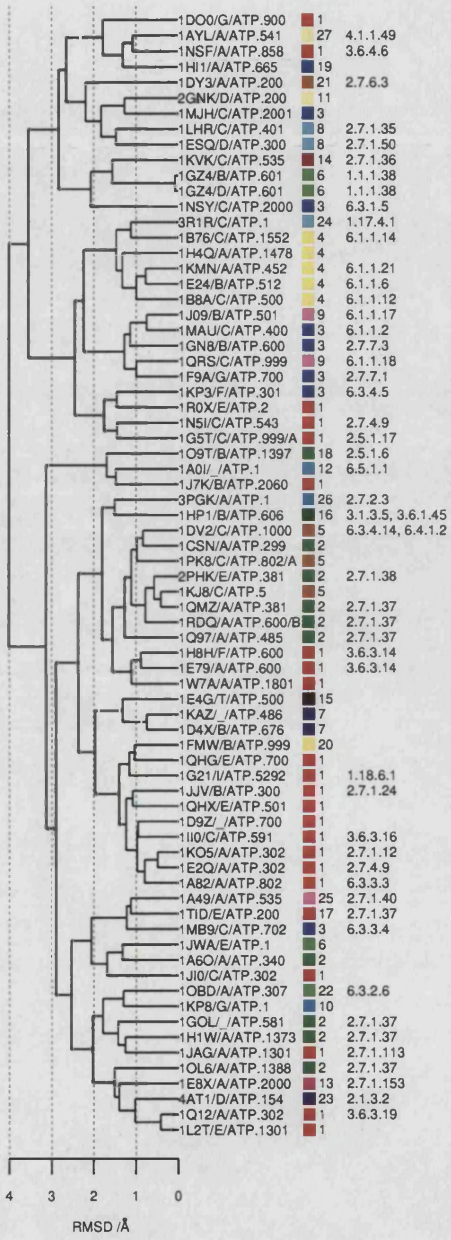

Figure 5.15: Comparison of ATP conformations with cluster assignments

The dendrogram represents the results of complete-linkage clustering, applied to the global RMSD values between all ligands in the ATP dataset. Coloured blocks and numbers indicate the level-3 cluster to which each molecule belongs. EC numbers associated with the protein binding each ligand molecule, where available, are shown alongside each leaf of the tree.

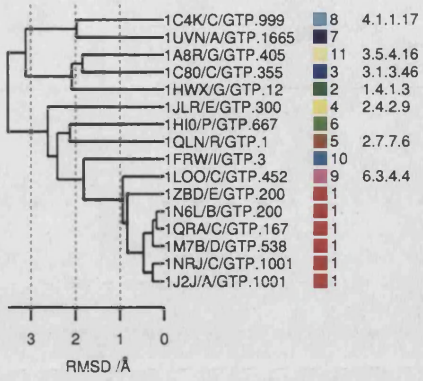

Figure 5.16: Comparison of GTP conformations with cluster assignments
The dendrogram represents the results of complete-linkage clustering, applied to the global RMSD values between all ligands in the GTP dataset. Coloured blocks and numbers indicate the level-3 cluster to which each molecule belongs. EC numbers associated with the protein binding each ligand molecule, where available, are shown alongside each leaf of the tree.

variance appears similar within each of these clusters, suggesting that similarity in protein function does not necessarily imply similarity in ligand binding mode.

In the case of NAD (figure 5.17), it is clear that cluster 1 (sites composed principally of Rossmann-fold domains from CATH superfamily 3.40.50.720) contains two distinct conformational subgroupings. Inspection of the χ_N angles for each molecule in cluster 1 shows that these groups correspond to the *syn* and *anti* orientations of the nicotinamide N-glycosidic bond (see figure 5.17). The other NAD clusters all consist of just a few members; most adopt similar conformations, with only occasional outliers (*e.g.* 1AD3 in cluster 2, 1LVL in cluster 4).

Looking at the FAD dendrogram, we see that there are several groups of clusters which seem to be close together in conformation space. For example, ligands in clusters 1, 4 and 12 adopt very similar conformations. These are all sites from glutathione reductase proteins, while clusters 3 and 5 are from members of the p-cresol methylhydroxylase family. The finding that FAD molecules binding to glutathione reductase proteins show quite conserved conformation is the reverse of that reported by Dym and Eisenberg. In contrast to the conserved FAD-binding mode of these proteins, sites from cluster 2 (flavin reductases) clearly show much more diversity. This is explored further below.

A final observation arising from the dendrograms is the lack of apparent correlation between ligand/cofactor conformation and the function of the protein, as represented by its EC number(s). For example, among the ATP molecules, sites from proteins with EC number 3.6.3.x (proton-pumping ATPases) sometimes occur very close together in conformation space (*e.g.* 1H8H and 1E79), but in other cases, bind ATP in very different forms (*e.g.* 1I10 and 1Q12). EC numbers 2.7.1.- appear across almost the full range of the tree, with little obvious grouping beyond that which we might expect due to members of the same superfamily showing conservation in both ligand conformation and protein function. Viewed in a biological context, this result is not surprising, however, since 2.7.1.- stand for phosphotransferases using an alcohol as the acceptor. There is no clear reason why fulfilment of this role should require a particular ATP conformation, so we may expect proteins which converge upon such a function to evolve distinct ATP-recognition mechanisms in the process.

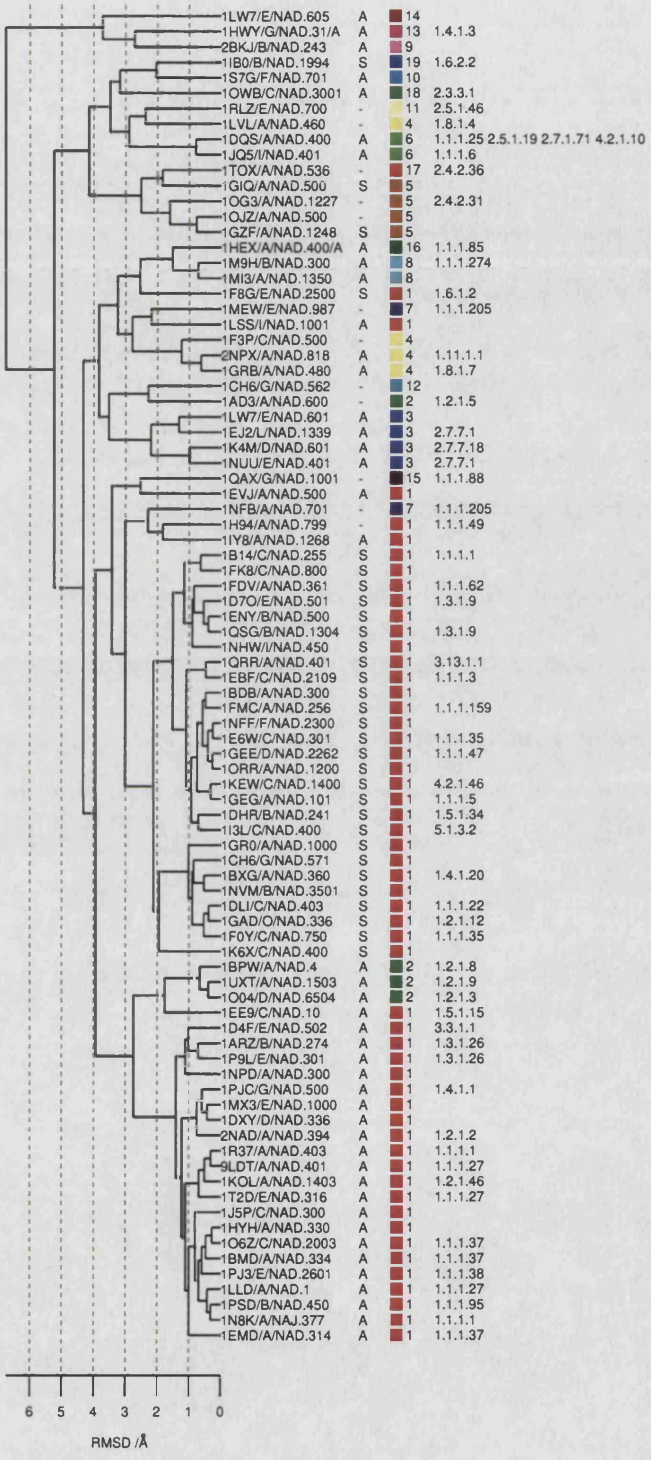

Figure 5.17: Comparison of NAD conformations with cluster assignments

The dendrogram represents the results of complete-linkage clustering, applied to the global RMSD values between all ligands in the NAD dataset. Coloured blocks and numbers indicate the level-3 cluster to which each molecule belongs. The orientation of the nicotinamide N-glycosidic bond is shown as S (*syn*), A (*anti*) or - (outside allowed ranges). EC numbers associated with the protein binding each ligand molecule, where available, are shown alongside each leaf of the tree.

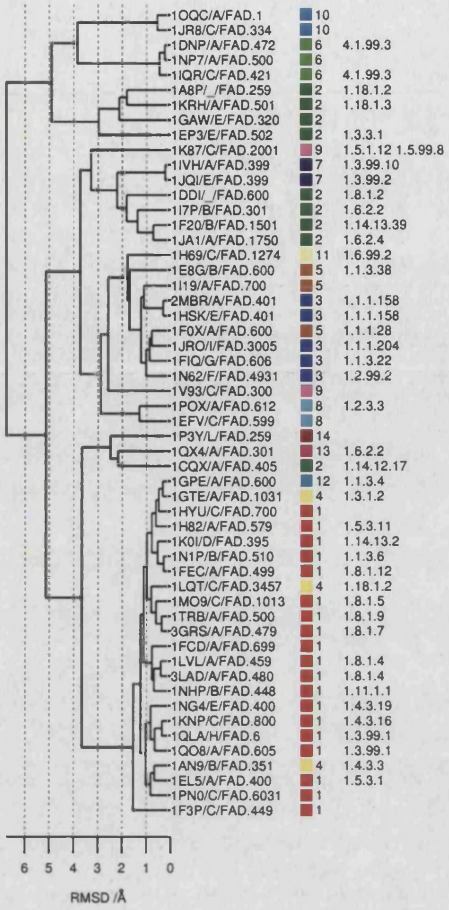

Figure 5.18: Comparison of FAD conformations with cluster assignments
The dendrogram represents the results of complete-linkage clustering, applied to the global RMSD values between all ligands in the FAD dataset. Coloured blocks and numbers indicate the level-3 cluster to which each molecule belongs. EC numbers associated with the protein binding each ligand molecule, where available, are shown alongside each leaf of the tree.

An exception is found in the tRNA synthetases. Cluster 9 contains two families of class I tRNA synthetases, which use a Rossmann fold to recognise the ATP molecule (Schmitt *et al.*, 1998); cluster 3 also contains a binding site from a class I tRNA synthetase (1MAU), as well as several other proteins of different functions which recognise ATP using a related domain. Cluster 4 contains five families of class II tRNA synthetases, whose ATP recognition site is built around an antiparallel β-sheet (Schmitt *et al.*, 1998). While the two classes of tRNA synthetase bind ATP in subtly distinct conformations, they still remain adjacent in the clustering dendrogram, indicating that although evolutionarily unrelated, these two groups have converged upon a similar ATP-recognition mode.

Among the NAD binding sites, the situation is slightly different. Stereospecificity in dehydrogenases has been extensively studied, and the tendency for enzymes which accept the same substrates to adopt the same cofactor stereospecificity previously noted (Glasfeld *et al.*, 1990). Although the amount of data shown in figure 5.17 is fairly small, we see that within cluster 1, where there are multiple families with the same EC number, they tend to cluster closely in conformational space with the N-glycosidic bond in the same orientation (*e.g.* 1D7O, 1QSG, 1F0Y; 1R37, 1N8K). An exception to this is the NAD binding site from 1B14. Like 1R37 and 1N8K, this is a structure of an alcohol dehydrogenase, but unlike these two, in entry

1B14, the substrate is not present, and the nicotinamide ring has rotated around to sit in the substrate-binding pocket.

For the FAD binding sites (figure 5.18), there is no clear pattern in the distribution of enzyme functions relative to cofactor conformation. Here, the main functional requirement - namely that the electron donor/acceptor group (flavin) be presented to the substrate - does not appear to impose any particular conformational constraints on the rest of the molecule. Although the shape of the cofactor may have an influence upon its redox potential, this is affected most by a bending of the flavin ring (Walsh and Miller, 2003), and less so by conformational rearrangements of the rest of the molecule. In any case, the redox potential is likely to be dominated by the composition of the binding site around the reactive part of the cofactor (Lostao *et al.*, 1997).

5.6.2 Multidimensional scaling of ligand conformational differences

Another way of comparing ligand conformation with the assignment of binding site clusters is by applying MDS to the RMSD matrices. As described in §3.3.1, this technique allows a set of data points to be projected into a high-dimensional Euclidean space, given only the matrix of distances between the points. By viewing only the the first two or three dimensions of this space, we can obtain an overview of relationships and patterns within the data. Since the separation of points in the MDS plot directly corresponds to the dissimilarity of the objects which they represent, this representation of the data may be easier to interpret than the clustering dendrograms.

Plots of the first two dimensions of the projection space are shown, for ATP, NAD and FAD, in figure 5.19. The results of the multidimensional scaling reinforce the findings obtained by inspecting the clustering dendrograms. The extent of variation within certain clusters is perhaps better highlighted in the MDS plots; see for example ATP cluster 3 and FAD cluster 2. In addition, they allow us to address the question of whether conformational variability is manifested continuously, or as distinct subgroups. The answer seems to be that this varies in different clusters: the variation in ATP cluster 1 shows a tendency to be divided into a number of groupings, while the conformations of ATP cluster 3 and FAD cluster 2 are fairly evenly distributed. Beyond these observations, there is little more to be gained by mere visual inspection of the plots.

Quantitative analysis

Once the data has been embedded in a space in this way - the result of the MDS will be referred to here as the 'projected space' - standard geometric concepts can be applied. For instance, we can easily calculate points which lie at the centroids of each cluster. This allows us to directly compare the spread of these points with the spread found within each cluster. This type of comparison is not possible in the original conformation space, since there is no robust way to define the 'average conformation' of an ensemble of molecules. We could of course compare the conformational variance of cluster representatives against the distributions within each cluster, but in this case, choice of an appropriate representative becomes problematic. Therefore the centroids of clusters in projection space are used here for 'between cluster' comparisons.

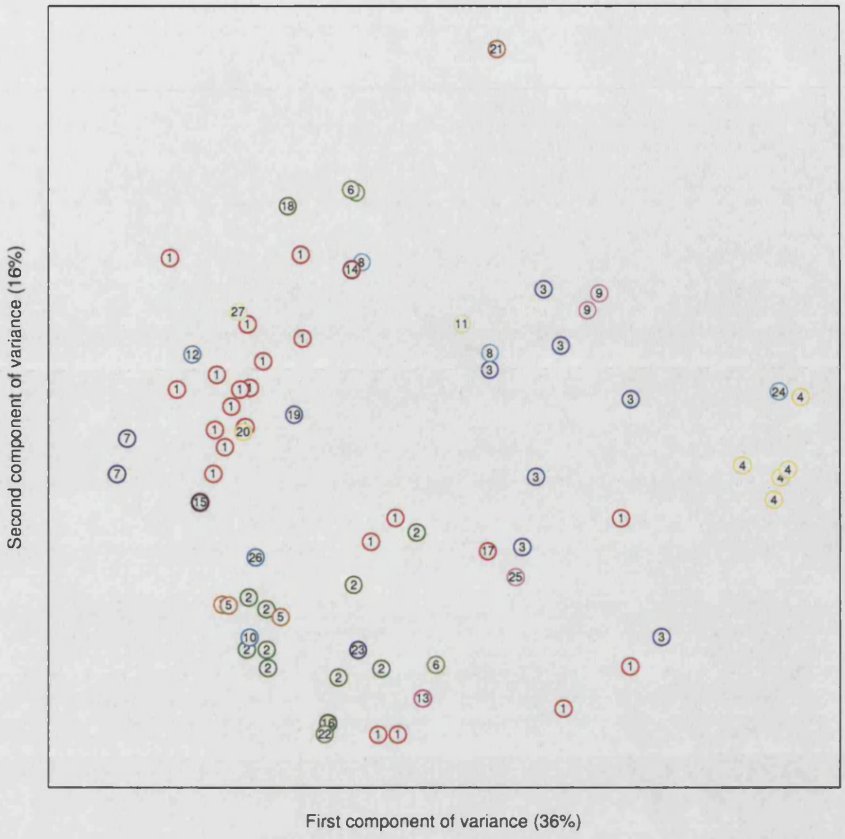

(a) ATP

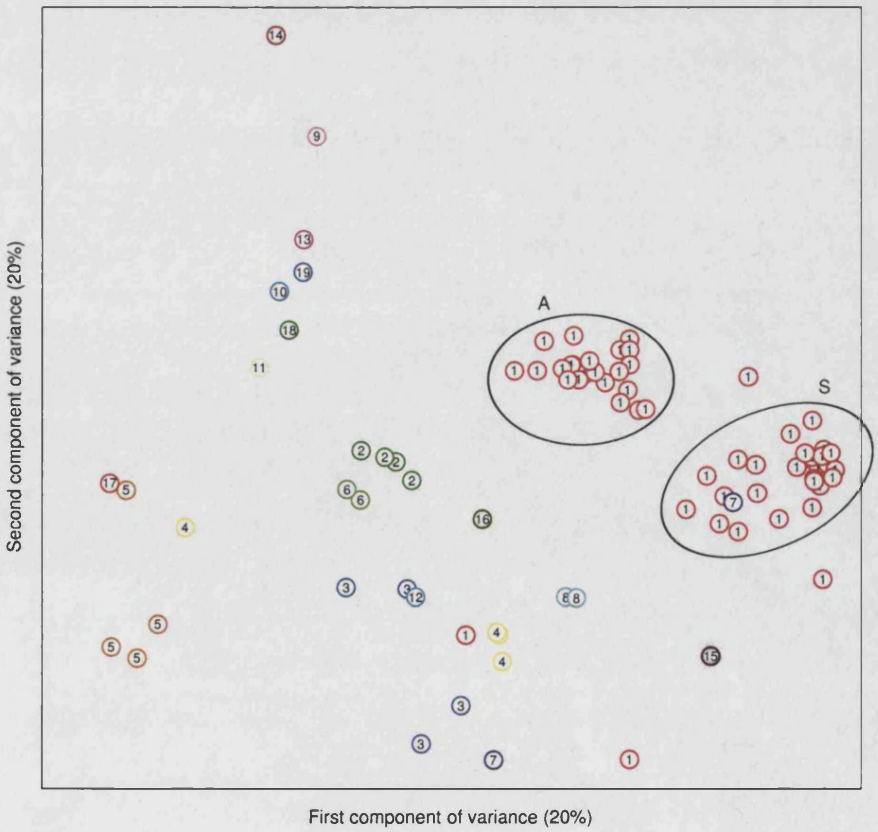

(b) NAD. The two distinct conformational subgroups visible in cluster 1 correspond to the *anti* (A) and *syn* (S) conformations of the N-glycosidic bond.

Figure 5.19: Multidimensional scaling of ligand conformational differences
Continued overleaf.

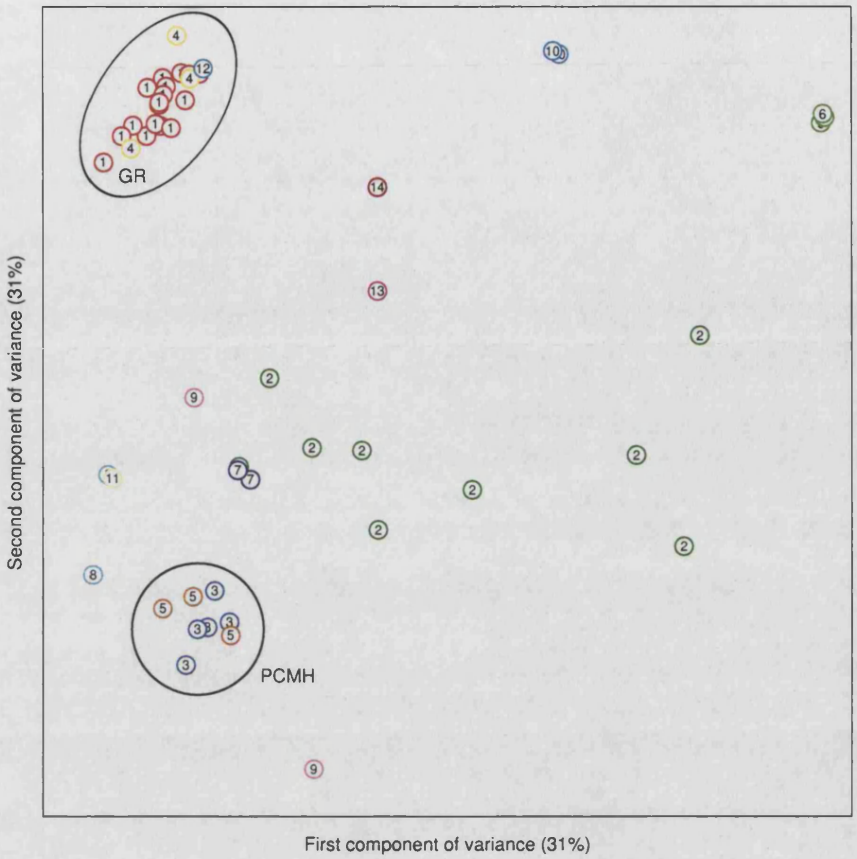

(c) FAD. Circles indicate conformational groupings which correspond to previously identified FAD-binding families: glutathione-reductase (GR) and p-cresol methylhydroxylase (PCMH). The flavin reductase family (clusters 2 and 13) exhibits the greatest range of FAD conformations.

Figure 5.19: Multidimensional scaling of ligand conformational differences
The two largest components of variance are shown; values shown on the axes indicate the proportion of total variance which is explained by each component. Numbers at each data point refer to the level-3 cluster to which the molecule belongs.

Before presenting the analysis of conformational variance within and between clusters, some 'thought experimentation' needs to be done. The total conformational space of a given molecule may be thought of as an n-dimensional space, where n is the number of rotable bonds possessed by the molecule; the axes of each dimension range from zero to 2π radians, representing the full rotation of each bond. Although it is continuous, this conformational space may, for some purposes, be treated as if it consists of an array of discrete voxels, by dividing each dimension of the space according to the number of low-energy rotamers of the corresponding bond. A subset of the total conformation space represents conformations in which the van der Waals spheres of non-bonded atoms intersect; these conformations are physically unfeasible, and therefore these region of conformational space are never explored.

Within the remaining region of space, each conformation is associated with a certain energy value; just as we can annotate a geographical map with contours indicating the height of the terrain, we can annotate each point in the multidimensional conformation map with an energy. In fact, since the favourability of any given conformation is influenced by the environment in which the molecule is situated, this annotation must be done separately for each physical context in which the ligand may exist. Simplistically, we may conceive of

two energy landscapes - one for the molecule in an aqueous context, and one when bound to protein. Now, by setting a hypothetical energy threshold, we obtain the set of ligand conformations which may exist stably when bound to protein (see figure 5.20).

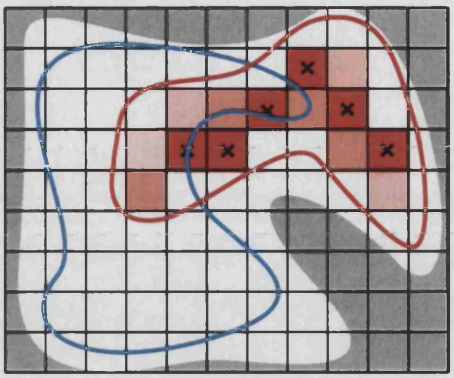

Figure 5.20: Hypothetical conformational energy landscape
The outer box represents all possible molecular conformations, with grid lines showing the discretisation according to bond rotamers. Grey shading shows the volume of conformation space which is inaccessible due to steric clashes. The blue region represents the conformational space explored by the molecule when in solvent; the red boundary encompasses conformations which are permitted when bound to protein. Red shading stands for the energy of each (discretised) conformation, with darker colours being more favourable. The set of allowed protein-bound conformations, according to some hypothetical energy cut-off, are marked with crosses.

Let us assume that the variance among the energies of these conformations is low - in other words that, to a first approximation, all of the allowed bound conformations are equally stable. Since non-homologous proteins have by definition evolved independently, we may assume that the 'choice' of which ligand conformation to bind is also independent for each, and hence that they are effectively sampling from the population of stable bound ligand conformations at random. This implies that the variance of ligand conformations among a randomly selected set of binding sites from evolutionarily unrelated proteins is an unbiased estimator of the variance of conformation among all stable, protein-bound arrangements of that particular ligand.

It is clear that the fact of being bound to a protein imposes certain constraints on ligand conformation; this is evidenced by the previously reported differences between solvent-exposed and protein-bound forms of certain molecules (Moodie and Thornton, 1993). One way of looking at conformational differences within and between clusters of related binding sites is to ask the question: does being bound to a protein *from a particular superfamily* impose any further constraints over and above the general requirements for being stable in a protein environment in general? In other words, are binding sites in domains belonging to the same superfamily sampling from the same pool of stable conformations as are unrelated sites, or do they 'pick' from a more restricted subset?

To test this, let us propose the following null and alternative hypotheses, noting that distance in projection space is equivalent to RMSD between conformations[2]:

[2]Note that, while in figure 5.19, only the first two components of variance are shown, for the distance calculations, all dimensions of projection space are used.

H_0: The average pairwise RMSD between ligands in the same cluster is the same as the average distance between cluster centroids in projection space.

H_1: The average pairwise RMSD between ligands in the same cluster is less than the average distance between cluster centroids in projection space.

Biological intuition tells us that H_1 is likely to be true: we expect that molecules bound to proteins belonging to the same superfamily should tend to adopt similar conformations. Therefore any clusters for which we fail to disprove the null hypothesis represent interesting cases, in which proteins within a single superfamily bind their ligands in very diverse ways.

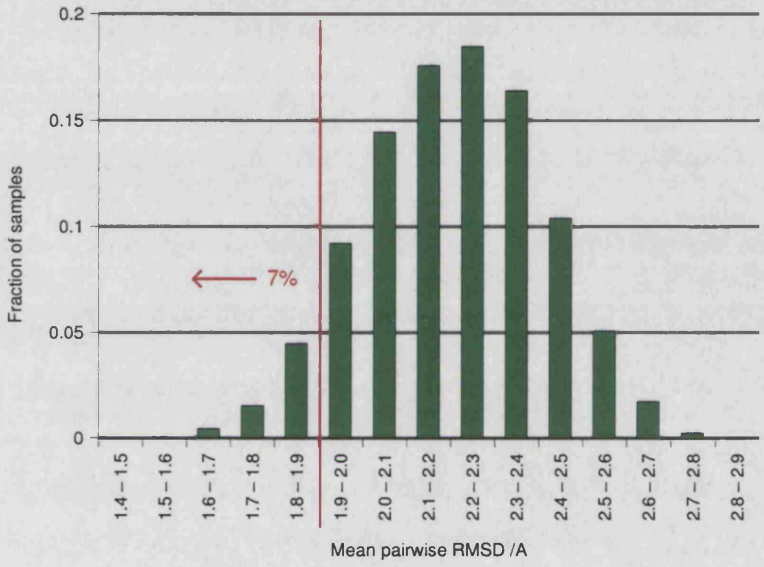

Figure 5.21: Significance testing of within-cluster mean pairwise RMSD
The distribution shown is that of the average ATP inter-centroid distance, from 10,000 samples of 7 centroids at a time. The red line indicates the value of the average within-cluster RMSD value for ATP cluster 3. This leads to a p-value for the significance test of 0.07.

We take the mean distance between all points (in projection space) belonging to a cluster as the statistic which measures the spread of that cluster. For a given cluster, let this quantity be denoted μ, and the number of members in the cluster by s. Were H_0 to be true, the observed value of μ would be the result of random sampling of s points from the pool of allowed protein-bound conformations. Since we assume that unrelated binding sites 'choose' their ligand conformations by random sampling from this pool, we can obtain the expected distribution of μ by repeatedly computing the mean pairwise distance between s randomly sampled centroids. The fraction of the resulting distribution which lies below μ is then the probability of observing this value by chance, if H_0 is true.

Ligand	No. of clusters	Between clusters: No. of centroid pairs*	Between clusters: Mean inter-centroid RMSD /Å	Cluster	No. of members	No. of pairs*	Pairwise RMSD within cluster /Å: Minimum	Maximum	Mean	p▲
ATP	27	351	2.21 ± 0.03	1	22	231	0.42	3.71	1.91 ± 0.04	$< 10^{-10}$
				2	9	36	0.47	2.26	1.58 ± 0.08	$< 10^{-10}$
				3	7	21	1.01	2.45	1.90 ± 0.08	6.69×10^{-2}
				4	5	10	0.77	1.39	1.12 ± 0.06	$< 10^{-10}$
				5	3	6	0.88	1.04	0.95 ± 0.03	3.00×10^{-4}
				6	3	6	0.07	2.86	1.93 ± 0.51	2.25×10^{-1}
GTP	11	55	2.51 ± 0.07	1	6	15	0.17	0.83	0.47 ± 0.06	0
NAD	19	171	3.58 ± 0.08	1	54	1431	0.24	4.13	1.83 ± 0.02	not calculated †
				2	4	6	0.39	2.45	1.47 ± 0.41	$< 10^{-10}$
				3	4	6	0.99	2.00	1.69 ± 0.18	$< 10^{-10}$
				4	4	6	0.63	3.88	2.38 ± 0.64	6.00×10^{-3}
				5	4	6	0.77	2.51	1.82 ± 0.27	$< 10^{-10}$
FAD	14	91	3.49 ± 0.13	1	19	171	0.29	1.54	0.87 ± 0.02	not calculated †
				2	9	36	0.72	4.83	2.78 ± 0.18	7.70×10^{-3}
				3	5	10	0.32	1.12	0.92 ± 0.07	$< 10^{-10}$
				4	3	3	0.61	1.23	0.97 ± 0.18	3.00×10^{-3}
				5	3	3	0.95	1.70	1.28 ± 0.22	6.60×10^{-3}
				6	3	3	0.24	0.47	0.35 ± 0.06	$< 10^{-10}$

Table 5.6: Comparison of conformational variance within and between clusters

This table shows statistics on the conformational variance within and between clusters for each ligand type. The variance was estimated using the mean pairwise distance between points in the projection space (for the within-cluster spread) and mean pairwise distance between cluster centroids (for between-cluster spread). (⋆) $\frac{n(n-1)}{2}$, where n is the number of clusters.

(†) insufficient number of cluster centroids available for sampling.

(▲) probability of observing a within-cluster conformational variance this large or greater, if the hypothesis that sites within a given cluster sample ligand conformation space at random is true. This was calculated according to the method described in the text.

For example, ATP cluster 3 has 7 members, and a mean pairwise within-cluster RMSD of 1.90Å. To estimate the probability of observing a conformational spread of this size or less at random, 7 points are selected at random from the 27 ATP cluster centroids, and the mean distance between the $\frac{7\times(7-1)}{2} = 21$ possible pairs is calculated. Repeating this procedure 10,000-fold results in the distribution shown in figure 5.21. 7% of this distribution lies below the value of 1.90Å, meaning that for this cluster, we fail to reject H_0 at the 5% significance level or greater.

Two clusters (NAD cluster 1 and FAD cluster 1) were excluded from this analysis because they contained more members than there were cluster centroids, thus rendering the sampling scheme described above impossible. Inspection of the MDS plots shows that these two clusters are clearly highly localised in projection space, indicating that H_0 would likely be strongly rejected for both, were sufficient data available.

Of the remaining clusters, the null hypothesis is rejected with $p < 0.01$ for all but two cases - ATP cluster 3 ($p = 0.07$) and ATP cluster 6 ($p = 0.23$) - see table 5.6. The latter contains only three members, of which two are highly similar, with one distant outlier; this result may not be particularly meaningful. There is no clear functional reason why cluster 3 should be so conformationally diverse: although its members catalyse a number of different functions, this is the case also for other clusters.

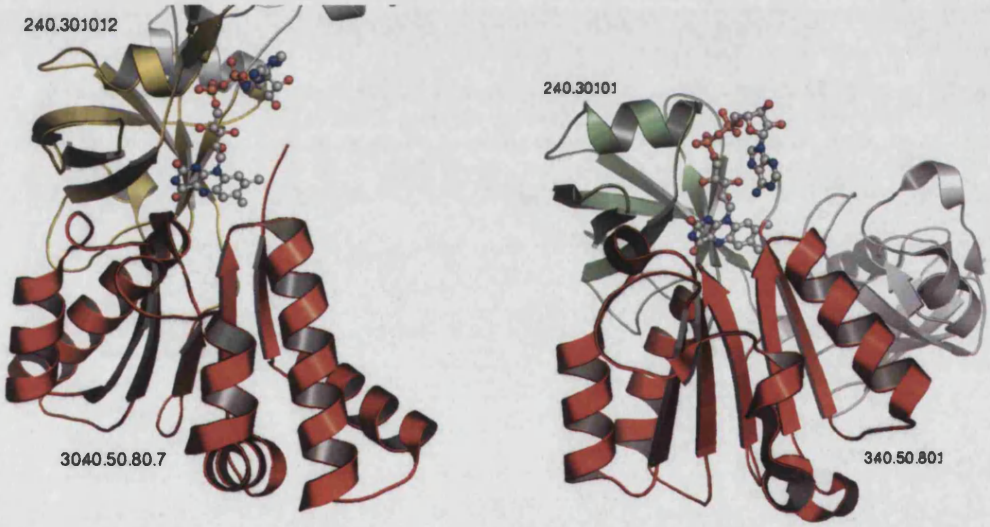

(a) Nitric oxide synthase (1F20, 1.9Å resolution)

(b) Benzoate 1,2-dioxygenase reductase (1KRH, 1.5Å resolution)

Figure 5.22: Variation in FAD conformation within the flavin reductase family
Small changes in the relative positions and structures of the two domains which interact with FAD cause concomitant changes in the cofactor conformation.

Although the spread within FAD cluster 2 was not found to be statistically significant, it is clearly the largest among all the FAD clusters. As pointed out by Dym and Eisenberg, this spread can be understood by inspecting the structure of the binding sites within the cluster. Each site in the flavin reductase family is composed principally of two domains - a nucleotide-binding domain with a Rossmann fold (CATH code 3.40.50.80) which binds the flavin end of the cofactor, and a β-sheet domain (CATH code 2.40.30.10) which interacts with the adenosine nucleotide part. The relative orientation of these two domains varies between different members of the FR family (see figure 5.22 for examples), resulting in differences in the conformation of the FAD which forms a bridge between them (figure 5.23).

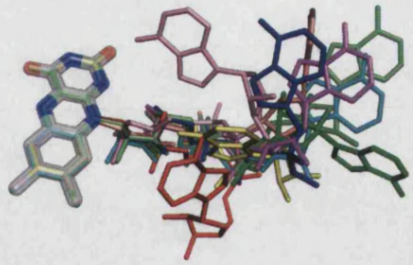

Figure 5.23: Variation in FAD conformation within the flavin reductase family
The figure shows the 9 FAD molecules from cluster 2 (flavin reductase proteins). The observed variation in cofactor conformation is due to differences in relative orientations of the two domains which contact the FAD molecule.

5.7 Relationship between protein sequence and ligand conformation

5.7.1 General trends

In 2001, a study was published which investigated the relationship between the protein sequence similarity of α-helical proteins and the molecular similarity of their ligands (Mitchell, 2001). This focussed on a dataset of 140 protein domain-ligand interactions. The main finding of the paper is that similar proteins do indeed tend to bind similar ligands, although the author expresses caution about the validity of extrapolating this result, derived as it was from PDB data, to biological systems in general.

Here, a related question is addressed - given a set of protein domains which bind the same ligand, do similar domains bind the ligand in similar conformations? To address this, the ligand datasets described previously were first filtered to remove all sites to which more than one domain makes a significant contribution. Any site in which no single domain contributes at least 80% of the residues contacting the ligand was excluded from this analysis. The number of binding sites remaining for each ligand is shown in table 5.7.

Ligand	Total number of sites	Number of single-domain sites
ATP	407	192
GTP	201	61
NAD	1045	671
FAD	684	327

Table 5.7: Number of predominantly single-domain binding sites for each ligand

For each ligand type, the sequence identity between each pair of single-domain binding sites was calculated by aligning the sequences of the domains which contribute the majority of residues to each site. These sequences were obtained from the CATH FTP server (ftp://ftp.biochem.ucl.ac.uk/pub/cathdata/v2.6.0), and aligned using the GAMUT implementation of the Needleman-Wunsch global alignment method (§3.5) with a BLOSUM45 matrix obtained from the NCBI FTP server (ftp://ftp.ncbi.nih.gov/blast/matrices). Scatter plots showing the RMSD between each pair of ligands, plotted against the sequence identity of the domains which bind them, are shown in figures 5.24 - 5.27.

As expected, the plots show that, when the sequence identity of a pair of binding domains is below 30%, the pairwise RMSD between their ligands may vary across the entire range observed for that particular ligand type. When sequence similarity is very high, most ligand pairs are close in terms of their conformation,

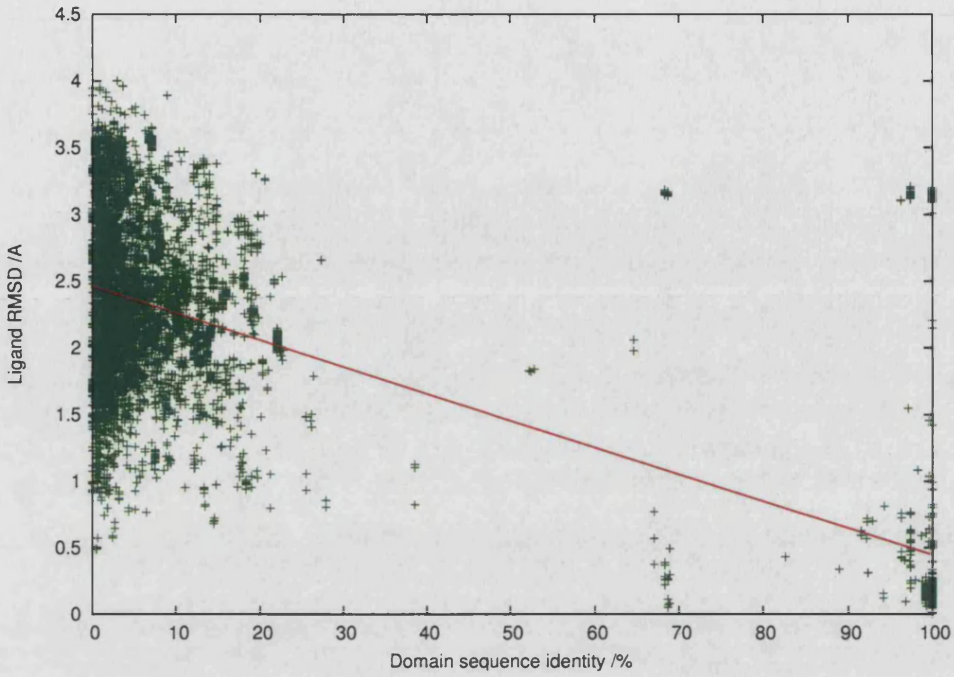

Figure 5.24: Sequence identity of ATP binding domains *versus* ligand conformational distance Result of linear regression (calculated using R) is shown as a red line ($r^2 = 0.29$).

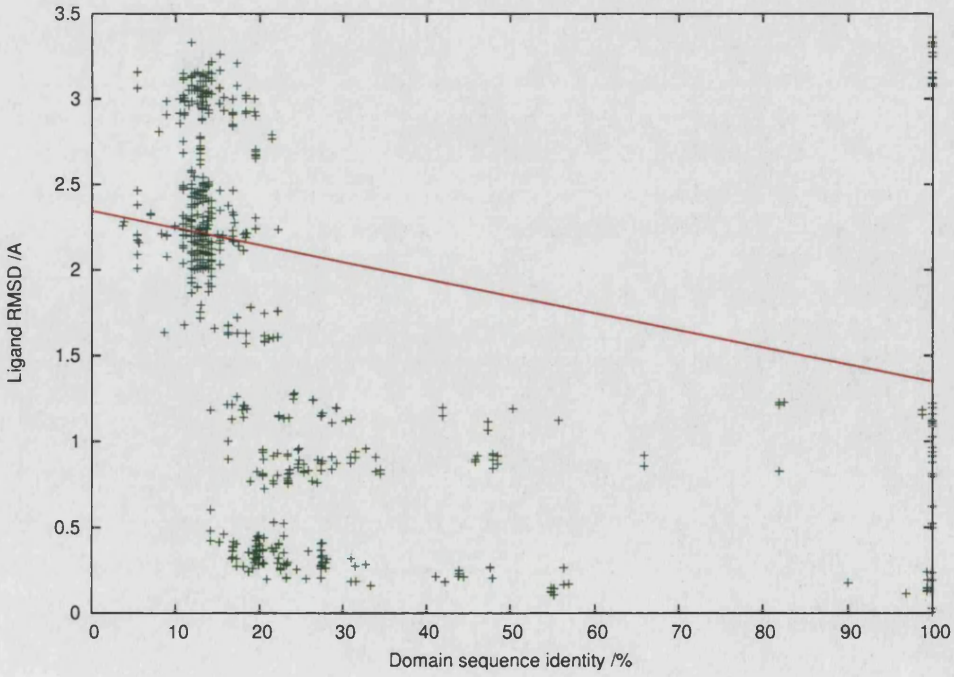

Figure 5.25: Sequence identity of GTP binding domains *versus* ligand conformational distance Result of linear regression (calculated using R) is shown as a red line ($r^2 = 0.14$).

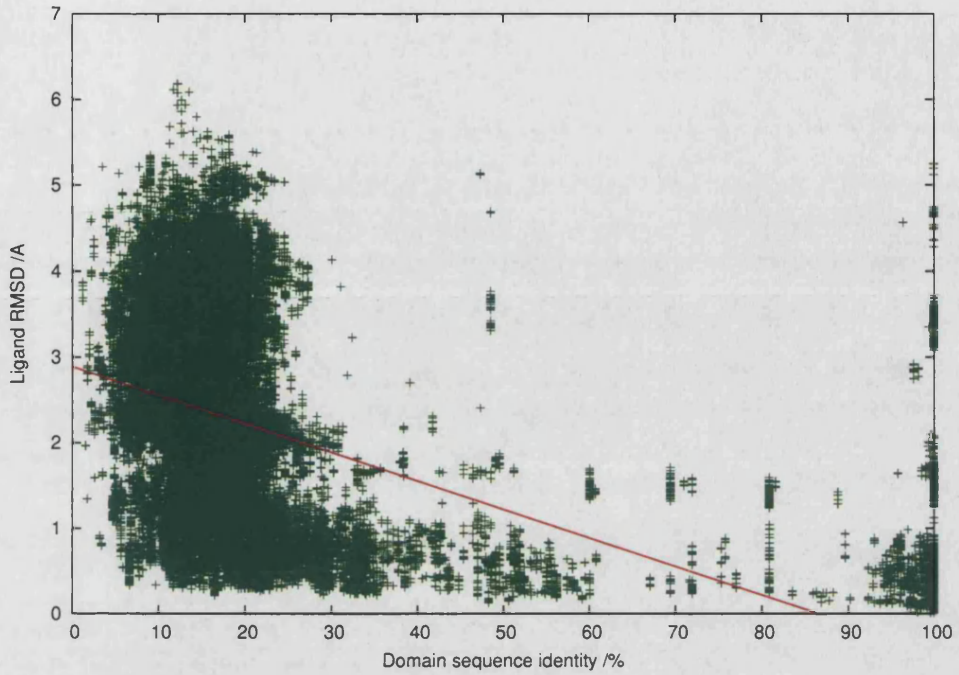

Figure 5.26: Sequence identity of NAD binding domains *versus* ligand conformational distance
Result of linear regression (calculated using R) is shown as a red line ($r^2 = 0.14$).

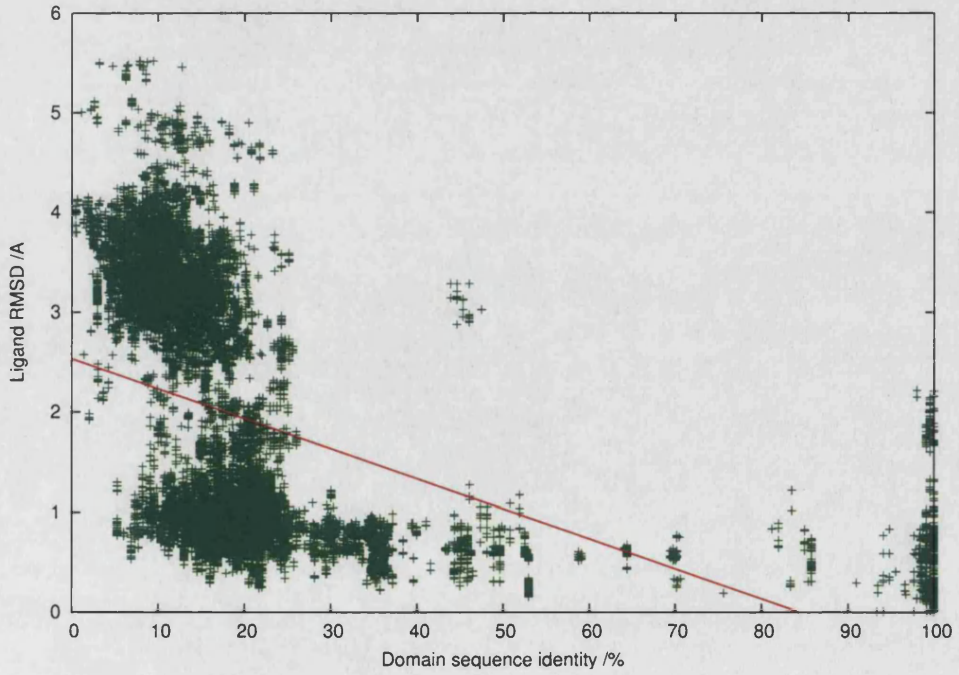

Figure 5.27: Sequence identity of FAD binding domains *versus* ligand conformational distance
Result of linear regression (calculated using R) is shown as a red line ($r^2 = 0.19$).

but for all ligands except FAD, there are several outlying pairs in which practically identical domains bind ligands in very disparate shapes. This may be due to conformational changes undergone at different stages of a reaction cycle. For example, in PDB entry 1PJ3, a 2.10Å structure of human malic enzyme, NAD molecules are bound to identical subunits of the protein in radically different arrangements.

The general trend, however, is for more similar domains to bind ligands in a more similar conformation. To quantify this, we can compute the standard linear regression coefficient. The nature of the data, however, means that the value obtained will necessarily be small. Firstly, there is a large variance in RMSD values corresponding to low sequence identities. Secondly, the inhomogeneous composition of the PDB means that there is a relative paucity of sequence pairs with identities in the range 50-80%, somewhat obscuring the general trend obeyed by these two variables. Table 5.8 shows the results of the linear regression, which in all cases indicates only weak correlation between the two variables; visual inspection of the plots suggests that an exponential or polynomial function may provide a better fit.

	Linear regression ($y = a + bx$)		
Ligand	a	b	r^2
ATP	2.43	-0.02	0.29
GTP	2.34	-0.01	0.14
NAD	2.88	-0.03	0.14
FAD	2.52	-0.03	0.19

Table 5.8: Linear regression between domain sequence identity and ligand conformation distance
Calculations were performed using R (Ihaka and Gentleman, 1996). r^2 is the linear regression correlation coefficient.

The data were then analysed by dividing the plots into discrete regions, and using a χ^2 test to determine whether the distributions observed are significantly different to what would be expected by chance. In doing so, we assume that the domain sequence identity and ligand RMSD variables are independent. The sequence identity values were divided into two ranges - low and high - using 45% as the cutoff value. This value is the same as that used in the analysis of Mitchell. It is generally held that pairs of proteins with this degree of sequence identity or greater are likely to be closely related in both evolutionary and structural terms (Orengo *et al.*, 1993). The RMSD values were divided using a cutoff of 1.5Å for ATP and GTP, and 2.0Å for NAD and FAD. These values were determined manually, and were chosen such that pairs of molecules with an RMSD below the threshold can be seen visibly to be in a very similar conformation; the larger value for NAD and FAD reflects the dependence of the RMSD value on the number of points used to calculate it.

The proportions of binding site pairs whose sequence similarity is high are 4%, 15%, 3% and 7% for ATP, GTP, NAD and FAD respectively. The corresponding proportions of pairs whose ligand RMSD is below the threshold are 8%, 30%, 35% and 56%. Making the assumption that these two variables are independent, we can construct a 2×2 contingency table as shown in table 5.9. Applying a χ^2 test to the values in these tables, with 1 degree of freedom, shows that in all cases, the hypothesis of independence is rejected with $p \ll 0.005$ (critical value = 7.879). The tendency for similar domains to bind the ligand in a similar conformation is expressed by the enrichment factor for the (high sequence similarity, low ligand RMSD) cell of the contingency table. This factor is the ratio between the number of observations in this cell compared to that which would be expected under the assumption of independence. Of the four ligand types, ATP has

	ATP	Sequence identity < 45% Observed	Expected	≥ 45% Observed	Expected	Total
RMSD	≥ 1.5Å	16,704	16,028.77	128	803.23	16,832 (0.92)
	< 1.5Å	757	1,432.23	747	71.77	1,504 (0.08)
$\chi^2 = 7259$ †		17,461 (0.96)		875 (0.04)		18,336

	GTP	Sequence identity < 45% Observed	Expected	≥ 45% Observed	Expected	Total
RMSD	≥ 1.5Å	1,212	1,089.65	72	194.35	1,284 (0.70)
	< 1.5Å	341	463.35	205	82.65	546 (0.30)
$\chi^2 = 304$ †		1,553 (0.85)		277 (0.15)		1,830

	NAD	Sequence identity < 45% Observed	Expected	≥ 45% Observed	Expected	Total
RMSD	≥ 2.0Å	146,262	141,907.31	478	4,832.69	146,740 (0.65)
	< 2.0Å	71,120	75,474.69	6,925	2,570.31	78,045 (0.35)
$\chi^2 = 11687$ †		217,382 (0.97)		7,403 (0.03)		224,785

	FAD	Sequence identity < 45% Observed	Expected	≥ 45% Observed	Expected	Total
RMSD	≥ 2.0Å	23,151	21,622.71	65	1,593.29	23,216 (0.44)
	< 2.0Å	26,492	28,020.29	3,593	2,064.71	30,085 (0.56)
$\chi^2 = 2789$ †		49,643 (0.93)		3,658 (0.07)		53,301

Table 5.9: χ^2 analysis of ligand conformation distance *versus* domain sequence identity
Numbers in parentheses show the fraction of total pairs for each ligand which fall into each row or column.
(†) The critical level for χ^2 at the 0.1% significance level, with one degree of freedom, is 10.83. Therefore the deviation from random is highly significant in all cases.

the highest enrichment factor (10.41), indicating that the relationship between sequence similarity and ligand conformations is strongest for this ligand.

The results of this analysis must be interpreted with caution, due to the degree of non-uniformity in the distribution of pairwise sequence similarities. Although the χ^2 analysis indicates a relationship between domain sequence similarity and bound ligand RMSD, the weak linear regression results, coupled with visual inspection of the scatter plots, show that this relation only really holds when sequence similarity is above around 30%.

5.7.2 Ligand conformation and sequence similarities in the 'twilight zone'

We know that, within homologous superfamilies, the overall structure of proteins tend to be conserved even though their primary sequences may diverge beyond the point at which their relatedness is detectable using standard sequence analysis methods. Pairs of sequences which lie below this similarity threshold,

commonly taken to be around 35% identity, are said to be 'in the twilight zone'. Here we ask whether pairs of domains towards the upper boundary of this sequence similarity interval tend to bind ligands in more similar conformations, or whether, once sequences have diverged so far, any relationship between evolutionary distance and ligand conformational similarity has been obscured to the point where it can no longer be observed.

In order to address this question, binding site clusters which satisfy the following three criteria were sought:

- Contain binding sites which are predominantly single-domain, such that sequence similarities between sites can be calculated in a straightforward manner;
- Contain several members (at least 10);
- Exhibit a reasonable degree of conformational diversity: must contain pairs of molecules which differ by at least 3Å

The only two clusters which satisfied all three of these requirements were ATP cluster 1 (P-loop hydrolase domains) and NAD cluster 1 (classical Rossmann-fold domain dehydrogenases). For each, pairwise sequence similarities and ligand conformational distances were calculated as above; scatter plots of the results are shown in figures 5.7.2 and 5.7.2 respectively. Visual inspection suggests that, for the ATP cluster, the two variables are uncorrelated below the 35% sequence identity threshold, while for NAD cluster 1, there is a weak correlation, with more similar domains tending to bind the cofactor in more similar conformations. This is confirmed by least squares linear regression analysis, which returns r^2 values for the two clusters of 0.004 and 0.15 respectively.

In order to better understand the relationship between pairwise domain sequence identity and NAD conformation among the Rossmann-fold domain dehydrogenases, a 'heat map' was constructed, in which a square matrix was plotted, with rows and columns corresponding to each site within the cluster. Each cell is coloured according to the sequence identity between the appropriate pair of domains, and the rows and columns are ordered according to a dendrogram obtained by clustering the cofactor conformations (figure 5.7.2).

The pattern which clearly emerges is that sequence identity, even within the 'twilight zone', is correlated with the stereospecificity of the cofactor conformation. This suggests that cofactor stereospecificity is non-random, but is in fact an evolutionarily conserved trait; this is in agreement with previous studies (Glasfeld *et al.*, 1990, and references therein). Moreover, it appears that altering dehydrogenase substrate specificity may require fewer mutational changes than those which are needed in order to permit the cofactor to bind with its nicotinamide ring positioned in the opposite direction. This is to be expected, since the latter may involve significant structural rearrangements, while facilitating recognition of a new substrate may simply be a matter of subtly changing the shape or electrostatic properties of the binding site.

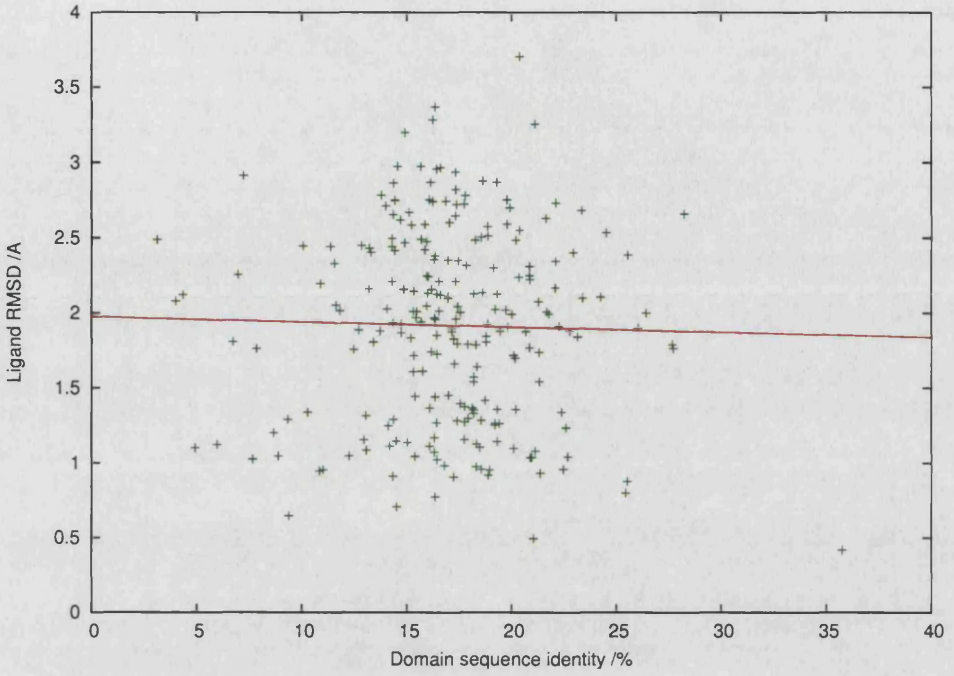

Figure 5.28: Sequence identity of P-loop hydrolase domains *versus* ATP RMSD values
Result of linear regression is shown as a red line ($r^2 = 0.004$).

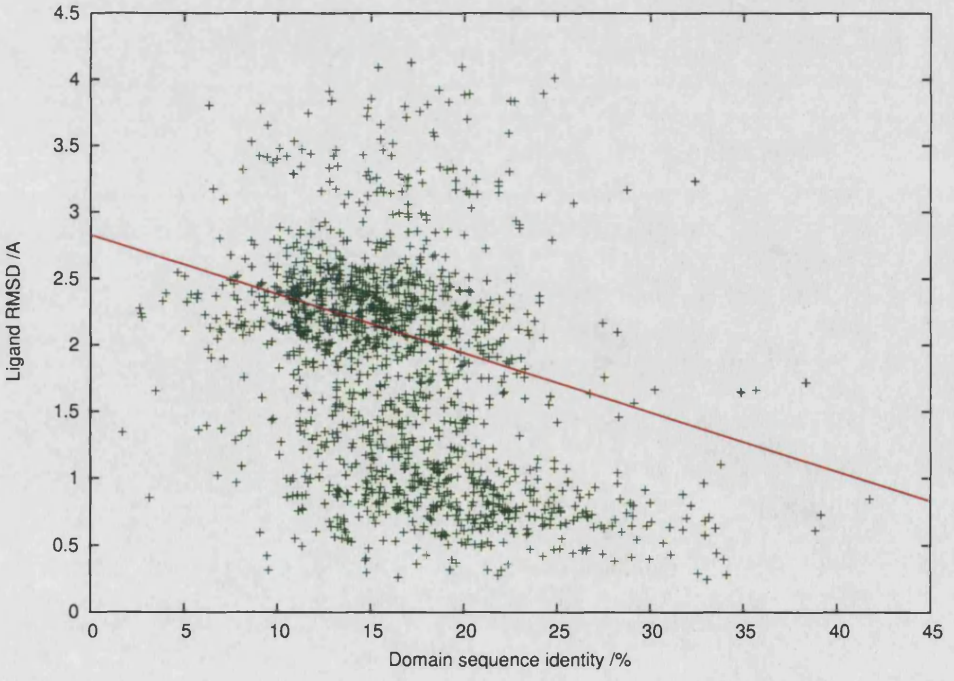

Figure 5.29: Sequence identity of Rossmann fold domains *versus* NAD RMSD values
Result of linear regression is shown as a red line ($r^2 = 0.15$).

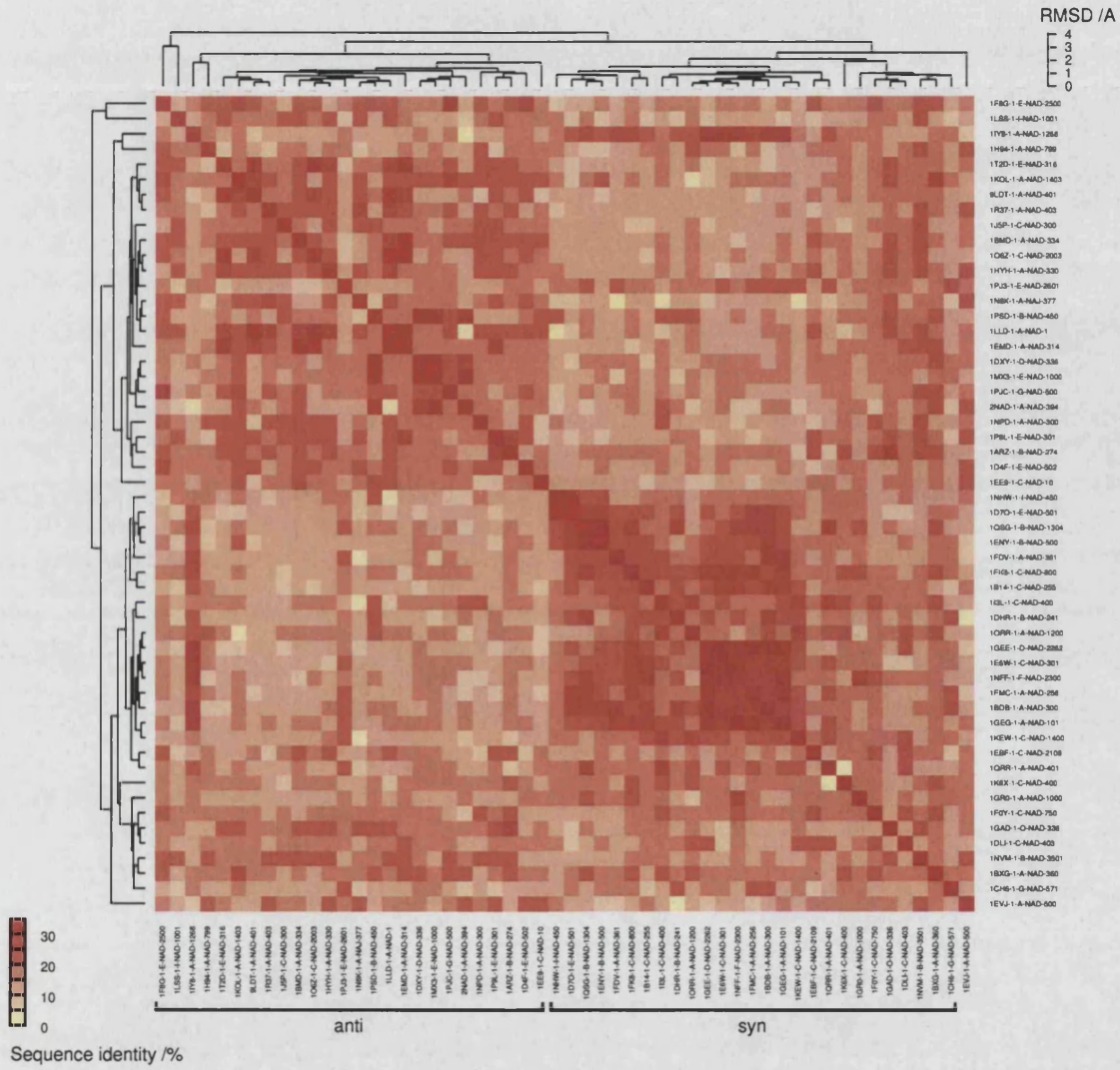

Figure 5.30: Sequence identity of Rossmann fold domains *versus* NAD conformational distance
Rossman fold domains within the same superfamily, but with sequence identities of less than 30%, and which bind NAD, were analysed. Cells of the matrix are coloured according to the sequence identity between the appropriate pair of domains, and the rows and columns are ordered according to a dendrogram obtained by clustering the NAD conformations. NAD molecules are distinguished according to the orientation of the nicotinamide N-glycosidic bond, as shown by the braces at the bottom of the plot.

5.8 Analysis of torsion angles

Another way of looking at ligand conformation is to measure the torsion angles of each rotable bond in the molecule. Comparison of the distribution of angles for each bond among a group of ligands can provide an overview of which parts of the molecule are the most variable.

As with all studies of ligand-protein interaction, the quality of the structural data used is of key importance when interpreting the results of this analysis. Torsion angles are particularly sensitive to experimental uncertainties - since the error in atomic coordinates in a structure resolved to 2.0Å is typically around 0.4Å, accurate calculation of bond torsions really requires data of at least this quality or better. In their discussion of the NAD(P) torsion angles, Carugo and Argos point out that, in many cases, these may be biased by restraints applied during crystallographic refinement (Carugo and Argos, 1997). Figure 5.31 shows the coordinates of NAD molecules taken from four structures of different resolutions, compared with the electron density observed in each crystallisation experiment. It is clear that, for data sets with resolutions of 2.5Å or worse, atomic positions cannot be unambiguously assigned from the electron density map alone.

An analysis of several hundred PDB structures (Morris *et al.*, 1992) found a clear dependency between the resolution of the structure and the standard deviations of the ϕ, ψ, χ_1 and χ_2 torsion angles. Even at the best resolutions of 1.3Å, standard deviations of the order 10-15° remained, and extrapolation of the best fit line to a hypothetical resolution of 0Å suggested that a residual deviation of between 2.9° and 9.3° would remain. From these results, it is clear that torsion angles should be regarded as a fairly approximate measure.

Figures 5.32 - 5.35 show the distribution of torsion angles for each rotable bond of ATP, GTP, NAD and FAD. These values were calculated using all level-3 cluster representatives as the input data. As such, they represent the conformations of all molecules bound to sites composed of non-homologous domains. For the reasons outlined above, the spokes of each torsion wheel are colour-coded according to the resolution of the structure from which the corresponding torsion angle was calculated.

The first observation which is prompted by inspection of these plots is that, among the four ligand types, ATP appears to exhibit the greatest spread in torsion angles, with a considerable number falling outside the theoretically favourable ranges. This is due in part to the structures in the ATP dataset being resolved to a lower resolution in general than those for the other three ligands. It is notable that the ATP bonds with the greatest variation, and which have the greatest proportion of examples in supposedly disfavoured regions, are those towards the phosphate tail of the molecule. This is the case even in structures of quite high resolution. This can be attributed to two factors. Firstly, since the adenine part of the molecule is that which tends to be bound by the protein, the phosphate moieties are often more exposed to solvent, and therefore can retain greater mobility when the ligand is bound. As a result, electron density for the γ and, to a lesser extent, β-phosphates is likely to be less well defined than for the adenine-ribose group. Secondly, the orientation of each phosphate is determined solely by the position of its four oxygen atoms. Since these are large, electronegative atoms which share a partial negative charge at physiological pH, they possess considerable electron density, which tends to blur out around the phosphate atom, thus presenting problems for accurate modelling of this part of the ligand coordinates.

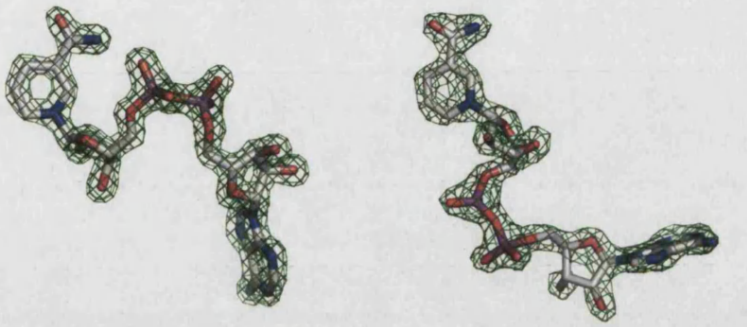

(a) 1HZJ. 1.5Å, R=0.179 (b) 1BTO. 2.0Å, R=0.174

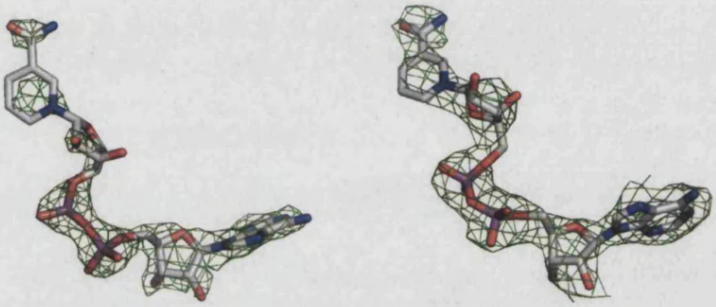

(c) 1E3L. 2.5Å, R=0.218 (d) 1AGN. 3.0Å, R=0.223

Figure 5.31: Coordinates of NAD molecules modelled into density maps at different resolutions
Each figure shows the coordinates of an NAD molecule, along with the electron density, contoured at 2σ (green chicken wire). The NAD molecules were arbitrarily chosen, from structures with a spread of different resolutions. They are from three structures of alcohol dehydrogenase (1BTO, 1E3L and 1AGN) and one of UDP-galactose 4-epimerase (1HZJ). Electron density maps were obtained from the Uppsala Electron Density Server (http://eds.bmc.uu.se). The density contours illustrate that, at a resolution of 2Å, robust assignment of coordinates is fairly straightforward, with the positions of most atoms clearly resolved. The 1.5Å map allows for completely unambiguous modelling, with even the holes in ring structures clearly visible. At resolutions of 2.5Å or poorer, coordinates can only be built by application of strict restraints, and therefore cannot be completely trusted. The maps in figures (c) and (d) show that the accuracy of torsion angles in particular may be limited.

It should be stressed that a wider range in the *local* orientations about a number of bonds does not necessarily lead to a similarly more diverse set of overall conformations. It is known that nearby torsion angles are correlated; therefore a change in one may be compensated for by another bond near to it in the molecule also being rotated. The combination of these two transformations may return the molecule to a global arrangement close to the original one.

Since ATP, NAD and FAD share a common adenosine nucleotide portion, we can directly compare the distributions of bonds 1-6 between these ligands. The general preferences of each bond are broadly similar for each ligand type. The χ and β angles (bonds 1 and 3 respectively) are particularly well-conserved, with all three ligands showing strong preferences for the *anti* orientation of the χ bond, and for the *ap* orientation of the β bond. These trends are to be expected given the steric hinderance caused by the other rotamers of each of these bonds.

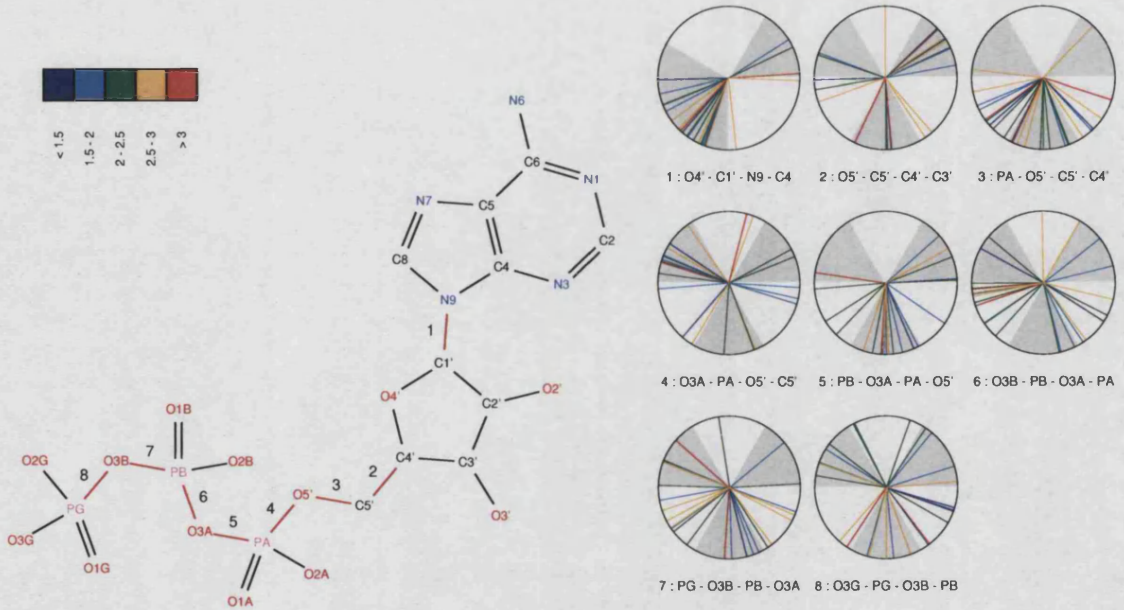

Figure 5.32: Variation in ATP torsion angles

For each of the rotable bonds, a wheel diagram showing the distribution of torsion angles among the 27 level-3 cluster representatives is plotted. The colours of the spokes represent the resolution of the structure from which the coordinates were taken, according to the scale bar shown (values in Å). Theoretically favourable angular ranges for each bond (see table 5.1) are shaded.

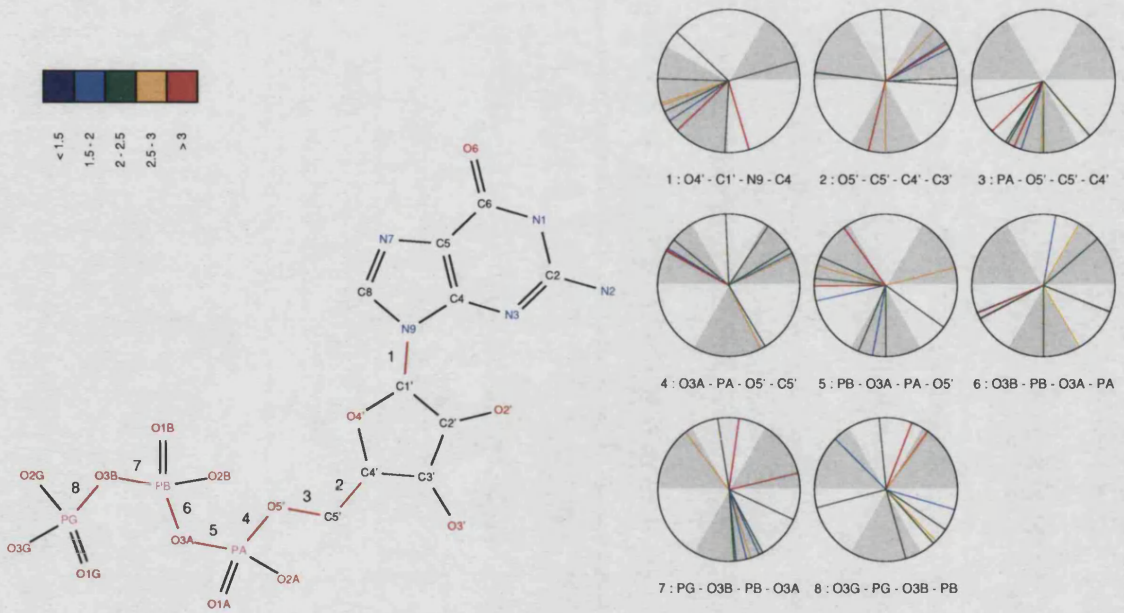

Figure 5.33: Variation in GTP torsion angles

For each of the rotable bonds, a wheel diagram showing the distribution of torsion angles among the 11 level-3 cluster representatives is plotted. The colours of the spokes represent the resolution of the structure from which the coordinates were taken, according to the scale bar shown (values in Å). Theoretically favourable angular ranges for each bond (see table 5.1) are shaded.

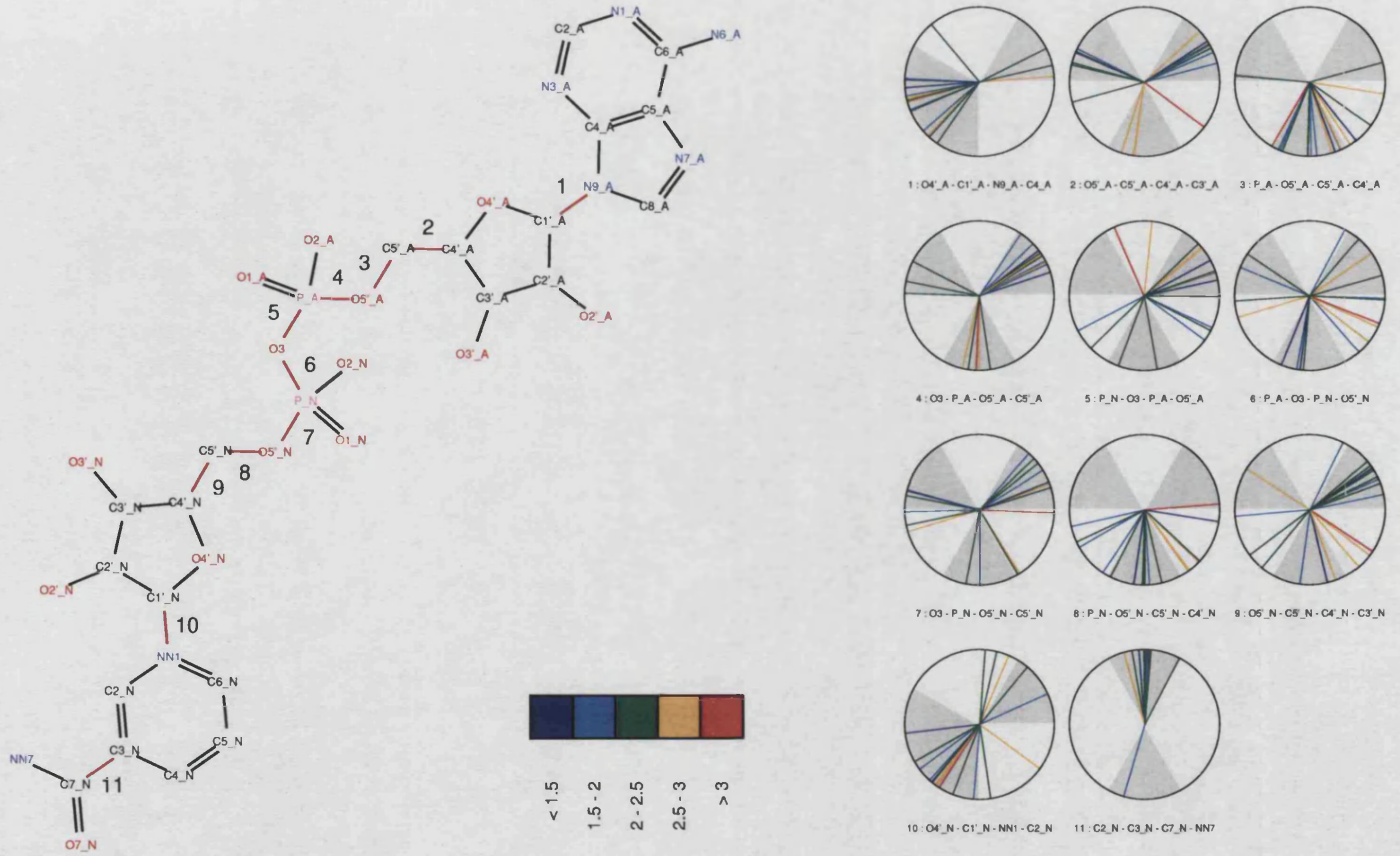

Figure 5.34: Variation in NAD torsion angles

For each of the rotable bonds, a wheel diagram showing the distribution of torsion angles among the 19 level-3 cluster representatives is plotted. The colours of the spokes represent the resolution of the structure from which the coordinates were taken, according to the scale bar shown (values in Å). Theoretically favourable angular ranges for each bond (see table 5.2) are shaded.

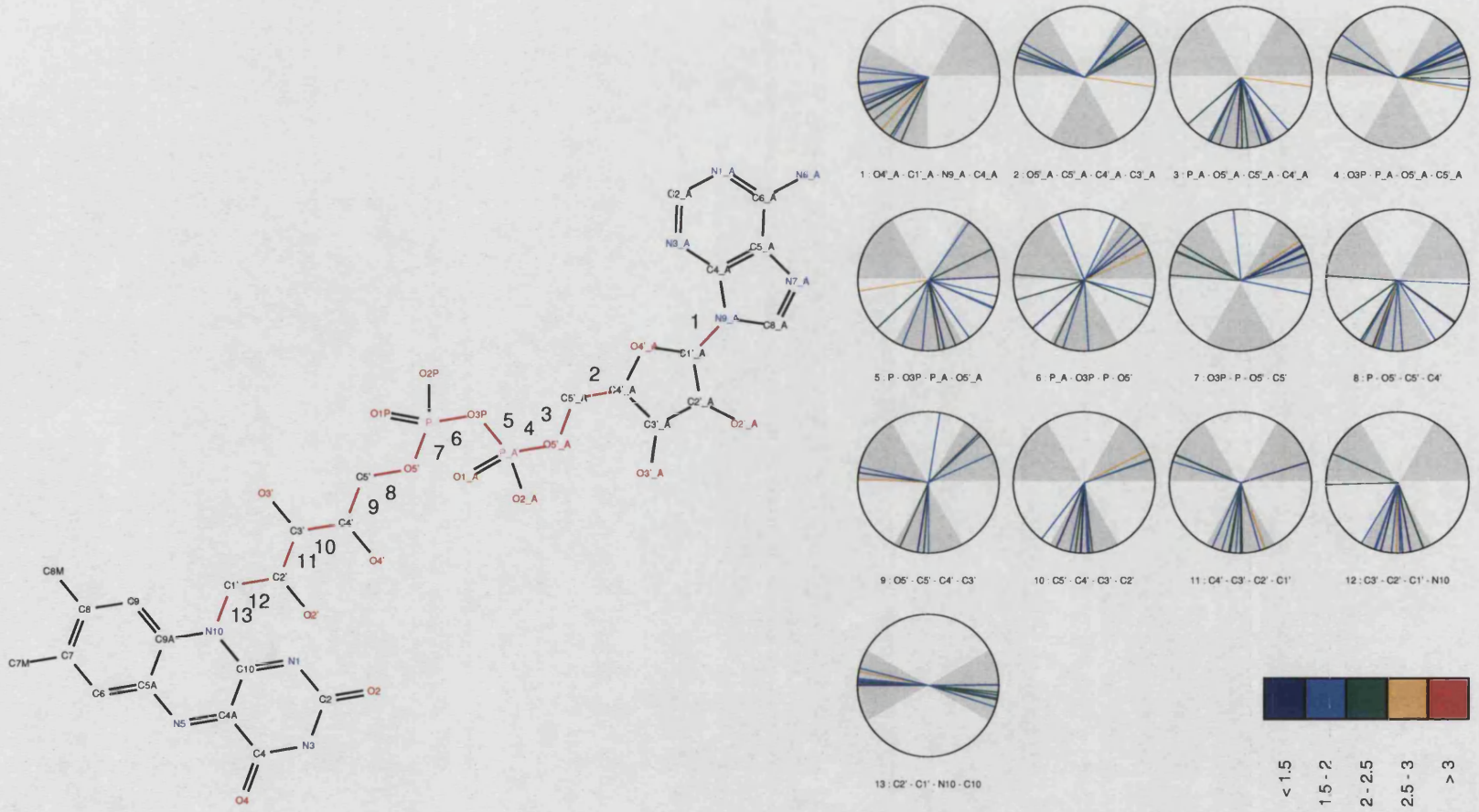

Figure 5.35: Variation in FAD torsion angles

For each of the rotable bonds, a wheel diagram showing the distribution of torsion angles among the 14 level-3 cluster representatives is plotted. The colours of the spokes represent the resolution of the structure from which the coordinates were taken, according to the scale bar shown (values in Å). Theoretically favourable angular ranges for each bond (see table 5.3) are shaded.

The preference at the γ bond (bond 2) appears to vary slightly between ATP and the two redox cofactors: while ATP shows a weak preference for *+sc* over *-sc*, both NAD and FAD show a roughly equal distribution between these two orientations. A *+sc* is expected to be favoured for this bond, as this promotes electrostatic interactions between the base and the O5′ atom of the ribose group (Saenger, 1984). Moving to the α bond (bond 4), ATP tends to bind with this bond in the *-sc* conformation, while NAD and FAD prefer *+sc*. A correlation between these two bonds is to be expected, since when γ is at *+sc*, an α orientation of *-sc* moves any groups distal to the α-phosphate away from the base and the sugar. When γ is at *-sc*, however, an α orientation of *+sc* is more sterically favourable.

5.9 Concluding remarks

In addition to the caveats mentioned throughout this chapter, it is worth pointing out some experimental artefacts which can complicate the analysis of ligand conformation. While these are not thought to invalidate the general trends discussed here, they need to be remembered when looking in more detail at individual cases.

When dealing with enzymatic cofactors, the conformation of the bound molecule may change during different stages of the reaction. This phenomenon has been observed several times in the case of the redox cofactors NAD and FAD. An example is found in the transhydrogenase enzyme, which couples stereospecific hydride transfer between NAD(H) and NADP(H) with proton translocation across the cell membrane in bacteria, or the mitochondrial membrane in eukaryotes. The proton gradient across the membrane induces conformational changes, which in turn shift the equilibrium towards formation of either NADH or NADPH. A recent crystal structure of transhydrogenase consists three copies of the heterotrimeric enzyme, two of which contains an interacting NAD/NADP pair. Analysis of differences between the two copies of the biological unit which contain these interacting pairs indicate that in one, the NAD cofactor is reduced, while in the other, it is oxidised (Sundaresan *et al.*, 2005). As shown in figure 5.36, the conformations of these two different redox forms of NAD are significantly different.

The need to take care to ensure that the oligomerisation state of a protein represented in a crystal structure is the same as the biological unit has been discussed previously (§1.3.1). The possibility that high-throughput studies of ligand binding may be misled by the presence of non-cognate ligands in the crystal has also been mentioned. The fickle nature of crystal structures does not end there, however. It has been known for some time that chemically similar inhibitors of a given protein may not all bind in the same way (Mattos *et al.*, 1994). In addition, several cases are known in which a ligand binds particularly 'loosely'; this is exemplified by the interaction of norcamphor with cytochrome P450, in which the ability of the ligand to rotate freely within the binding pocket can be seen by observing that hydroxylation occurs at several different positions in the molecule (Poulos, 1995).

A recent study of the effect of crystallisation conditions on the resulting structures of bovine trypsin complexed with inhibitors showed that small changes in pH can lead to radically different binding modes of *the same* inhibitor (Stubbs *et al.*, 2002). The fact that the inhibitor used was an unrefined lead with a relatively weak (μm) affinity for the target may have been a contributing factor in the change of binding

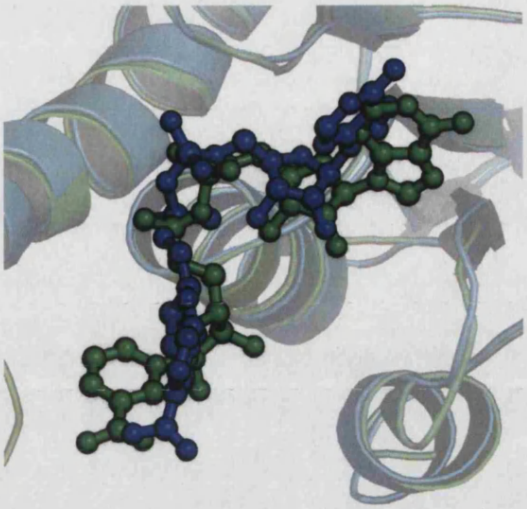

Figure 5.36: Conformational change of NAD in transhydrogenase
Two subunits of transhydrogenase (PDB entry 1XLT) are shown, superposed on the protein backbone. The NAD cofactor associated with each subunit is shown in ball-and-stick form, illustrating the different conformations which it can adopt. Chain B (green) is bound to an oxidised NAD cofactor while chain H (blue) contains a reduced NADH molecule (Sundaresan *et al.*, 2005). In both subunits, an NADP molecule (not shown) lies in close proximity to the nicotinamide functionality.

mode, but the paper nonetheless serves as a cautionary tale for those who may assume that the structure of a crystallised ligand-protein complex approximates the 'true' biological situation.

These findings show that even when we consider the interaction of a single ligand with a single protein, the recognition event is neither straightforward nor singular. On the contrary, the structure of the resulting complex which we see can vary depending on both the external conditions under which the system is observed, and as a result of changes internal to the system.

The main finding of this chapter is that the group of common biological ligands where were inspected adopt a wide range of conformations when bound by proteins. This has been shown by visual inspection of molecular superpositions, by analysis of matrices of the RMSD values calculated between the coordinates of different instances of each ligand, and by inspection of the distribution of torsion angles around their rotable bonds. Examination of a number of examples of ligands which bind in strained conformations here has shown that, in some cases, functional reasons for the binding mode can be proposed, while in others, it may be simply a result of particular features of the structure of the protein itself, and may not have any functional significance. In other cases, referring to the original literature shows that some outlying conformations may be experimental artefacts which do not resemble the true biological system.

In agreement with previous studies, the analysis presented here shows that the degree of extension of bound ligands is skewed towards more elongated conformations. The present study places this observation for the first time on a more quantitative footing by applying the concept of radius of gyration to ligand conformations. By exhaustively generating a set of all possible conformations for a given compound, the degree of extension of protein-bound ligands has been compared against the total extent of conformational space available to the molecule. In this way, it has been possible to show that, when bound to proteins, ligands explore a large extent of the available conformational space.

Among homologous proteins, the degree of conformational variation is not the same for all superfamilies. While most bind the ligand or cofactor in a reasonably conserved manner, several, notably the FAD-binding flavin reductase proteins, and proteins which contain a Rossmann-fold ATP-recognition domain, exhibit considerable variation in the binding mode. Statistical analysis shows that, for the latter family, the degree of ATP conformational variation is as great as that observed between homologous superfamilies.

Analysis of the relationship between the sequence similarity of protein domains binding a given ligand, and the similarities between the bound ligand conformations, shows that in general the correlation between these two variables is weak. Just as protein sequences with more than about 35% identity tend to fold into similar structures, domains above this threshold tend to bind ligands in fairly similar conformations. Below this sequence similarity cutoff, little correlation is evident. Next, the sequence similarity-ligand conformation relationship was explored among domains which are in the same superfamily but have less than 35% sequence identity. The two superfamilies examined showed quite different behaviour, with the ATP-binding P-loop hydrolase family showing no correlation, whereas the NAD-binding Rossmann-fold domains showed a clear relationship between primary sequence and cofactor stereospecificity.

Besides constraints of space and time, one reason why the current study was limited to the four molecules studied, was that a limitation of the automatic method for dataset generation used here is that it does not guarantee that the binding sites obtained are in complex with their cognate ligands. This is not too great a problem for the compounds studied here, where we can be reasonably confident that most of the interactions which they make are biologically relevant. Extending the study to more esoteric molecules, however, increases the risk that analogues, xenobiotic compounds and experimental artefacts will pollute the results. A resource which rectifies this problem by cataloguing the cognate ligands associated with each protein domain should soon be available (I. Nobeli, personal communication); application of the generic analytical methods presented here to a 'clean' dataset containing greater diversity of ligands would likely yield many interesting findings. In conclusion, the work presented in this chapter is intended as a 'pathfinding' report, which the author hopes will stimulate increased interest in the complex area of ligand conformational diversity, and which will encourage other researchers to explore its many ramifications across biology.

This work raises numerous questions which could be addressed in future studies. In particular, the relationship between protein evolution and ligand/cofactor conformation needs to be investigated in more detail. The findings shown here indicate that this relationship is complex, with no simple mapping between the similarity (in sequence or structure) of protein domains and the similarity of the shape of the bound ligand. This is most likely a product of the fact that the evolutionary pressure acting upon functional sites such as ligand binding pockets is not necessarily the same as that on the domain as a whole. By performing multiple sequence alignents and conservation analysis using previously published methods (Valdar and Thornton, 2001a), it would be possible to study the relationship between the evolutionary divergence of just the ligand-binding region, and the conformation of the ligand.

Another area which has been touched upon here, but which deserves further study, is the connection of cofactor conformation to enzymatic function. The results presented in this chapter suggest that this is weak at best, but this conclusion is drawn from a very small data set, and should therefore be more

thoroughly validated. It may be that more sensitive methods of ligand structure comparison than the superposition/RMSD approach taken here could uncover subtle relationships between conformation and function. The development of a method which attempts to predict the function of an enzyme based on the shape of its cofactor, using sophisticated spherical-harmonics based shape matching, is currently underway (T. Funkhouser, personal communication), and may go some way to addressing this point.

As stated previously, the main aim of the work in this thesis was to analyse the diversity of binding sites for a given ligand, as observed in structures retrieved from the PDB. In the light of the conformational variability so dramatically illustrated by the molecular superpositions shown here, it is clear that any attempts to compare binding sites simply by superposing the ligands as a whole will founder. As a result, it was decided to analyse the environments of rigid fragments of each ligand in turn, thus circumventing the problem of molecular flexibility. The following chapter describes a semi-automatic, generic method for identifying these rigid fragments, extracting and superposing their protein environments, and discusses several approaches for quantifying the structural and chemical diversity among these binding sites.

Chapter 6

Structural and chemical variability in ligand environments

The previous chapter established that the amount of conformational diversity shown by several common ligands when bound to different proteins is considerable. This has the effect of making patterns of interaction between ligands and proteins hard to detect, both visually and algorithmically. A natural response to this difficulty is to attempt to look for commonalities in those regions of ligand binding sites which surround rigid fragments of the ligand. In this way, ligand flexibility is eliminated, allowing comparatively simple approaches for binding site comparison to be designed.

A number of studies analysing interactions between rigid ligand fragments and proteins have been published. In several cases, structural motifs for fragment recognition have been identified which occur in unrelated proteins, suggesting that evolution may have converged upon a similar solution on a number of different occasions. Such cases of well-defined motifs, however, are the exception rather than the rule; despite extensive study, it appears that distilling the essential features of binding sites for a given ligand into a single structural 'template' - or even a manageable number of such templates - may prove intractable. Visual inspection of proteins interacting with several common ligand fragments suggests that, in terms of gross structural features such as sheets, helices and loops, and even in terms of local arrangements of amino acid residues, these sites exhibit almost limitless variability.

Trends can be identified, however, particularly when the binding sites are considered from the point of the view of the ligand - that is to say, when they are represented in terms of what the ligand 'sees' (*i.e.* a particular disposition of chemical properties), rather than what the crystallographer sees (that is, three-dimensional arrangements of amino acid residues). The first of part of this chapter describes a simple method for analysing groups of fragment environments in order to identify patterns of interaction. This is applied to a dataset of adenine binding sites, allowing a 'fuzzy template' - one which expresses the consensus pattern of interactions while also implicitly retaining information about binding site variation - to be defined.

The second part of the chapter is concerned with the development of a quantitative measure for binding site diversity. If elucidation of the *common* features of a group of binding sites may be considered analagous to finding the mean of a group of numbers, then measuring their diversity of the sites corresponds to calculating the variance. When comparing groups of biological sequences, tertiary structures, or very well-conserved

motifs such as catalytic sites, established methods exist for measuring the degree to which they are conserved (*i.e.* are lacking in diversity), both on the whole and locally. No such measure currently exists for binding sites. Such a quantity could be extremely useful, for example, in guiding computational searches for putative binding sites, in which a knowledge not only of which regions of known sites tend to show similarities, but also which exhibit significant levels of *variation*, would allow appropriate up- and down-weighting of the importance of those regions to the search. Here, the basis for such a method, defined by borrowing concepts from biological sequence analysis, is described, and examples of its application are shown.

6.1 Qualitative observations of binding site diversity

In order to demonstrate the degree of diversity found in the structure of ligand binding sites, consider the three ATP-binding proteins shown in figure 6.1. cAMP-dependent protein kinase (cAPK) is a member of a large superfamily of proteins which catalyse the transfer of the γ-phosphate from ATP onto serine, threonine or tyrosine residues on substrate proteins. This phosphorylation controls the activity, localization and overall function of many proteins, and plays a central role in many cellular processes, including signal transduction and regulation of the cell cycle. cAPK consists of two domains joined by a loop; the ATP-binding site is located between them, with the loop forming several specific polar interactions with the Watson-Crick edge of the adenine ring (figure 6.1a). The faces of the ring, on the other hand, are packed between a number of hydrophobic residues.

Lysyl-tRNA synthetase is one of a family of enzymes, each of which catalyses the 'charging' of a specific tRNA molecule with the appropriate amino acid. tRNA synthetases can be separated into two classes, which differ in both structure and mechanistic detail. Class I enzymes are normally monomeric, with the ATP molecule being bound by a classical Rossmann fold domain. Class II enzymes, of which lysyl-tRNA synthetase is an example, function as monomers, with the ATP being bound by a central antiparallel β-sheet motif. The amino acid transfer reaction proceeds in two steps. In the first step, the amino acid is activated by formation of an aminoacyl-adenylate, in which the carboxyl group of the amino acid is linked in to the alpha-phosphate of ATP, releasing pyrophosphate. When the correct tRNA is bound, the aminoacyl group of the aminoacyl-adenylate is transferred onto either the 2′ OH of the tRNA (in class I enzymes) or onto the 3′ OH (in most class II enzymes). Around the adenine moiety, the pattern of interactions in lysyl-tRNA synthetase is quite different to that seen in cAPK (see figure 6.1b). A phenylalanine ring lies across one face of adenine, and the only polar atom which is hydrogen bonded to the protein is N6, which donates two bonds.

Finally, we consider phosphoribosylgyclinamide formyltransferase. This enzyme catalyses the second step in the pathway of *de novo* purine biosynthesis, in which a formyl group is added to glycinamide ribonucleotide ('activated ribose'). This reaction also results in the terminal pyrophosphate bond of ATP being cleaved. As in cAPK, the ATP molecule is bound between two domains, with a connecting loop interacting with the Watson-Crick edge of adenine. However, in this case, an additional hydrogen bond is also formed at the *trans* position of N6, and N7 is unsatisfied (figure 6.1c). In this protein, N3 is exposed to solvent, with the position of an immobilised water molecule resolved nearby (not shown).

(a) cAMP-dependent protein kinase, catalytic subunit (1RDQ). The two domain which contact the ligand are coloured in pink and green.

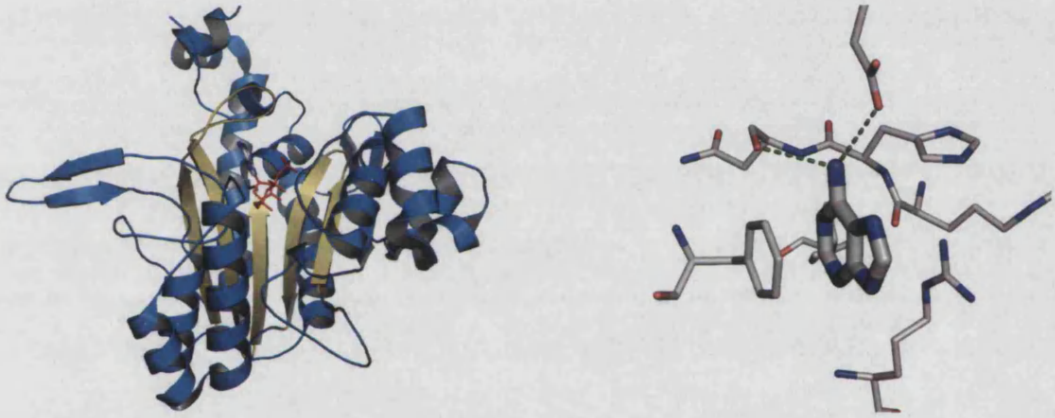

(b) Lysyl-tRNA synthetase (1E24). The central antiparallel β-sheet is shown in yellow; a loop at the top of it make up the adenine-binding pocket.

(c) Phosphoribosylgyclinamide formyltransferase (1KJ8). The two domains which contact the ligand are shown in blue and green. A loop connecting the two domains (yellow) makes four hydrogen-bonding interactions with adenine via consecutive residues.

Figure 6.1: Examples of diversity in adenine binding sites

The adenine-interacting regions of ATP-binding sites from three unrelated proteins are shown (PDB entry IDs are shown in parentheses). These images serve to demonstrate the great diversity in the structure of adenine-binding sites, both from a higher-level structural perspective (left), and in terms of the residues which contact the moiety (right). The three examples shown here have distinct patterns of hydrogen-bonding, as well as quite different non-polar contacts with the ligand.

These examples illustrate the point that the molecular recognition of adenine appears to be a complex problem, to which many different solutions can be constructed using the building blocks available in the structure of proteins. Although careful analysis of a small number of binding sites can elicit certain patterns, manual examination of a large number of structures quickly becomes cumbersome. Before describing the computational methods used here to study ligand binding sites, it is instructive to review the available literature on the recognition of adenylate, a moiety present in numerous key biological ligands.

6.2 Previous work on adenylate recognition

The ways in which proteins recognise and bind adenylate-containing ligands - especially interactions between protein and the adenine moiety - have been well studied. This is not surprising given the central biochemical roles of many adenlyate-containing ligands and cofactors - ATP, NAD(P), FAD, cyclic AMP and coenzyme A to name but a few. Early analyses focussed on identifying sequence motifs diagnostic of adenylate binding. One of the earliest was the 'P loop' or Walker A motif (Walker *et al.*, 1982), a consensus sequence of [G/A]X_4-GK[T/S] which forms an anion hole in which the phosphate groups of ATP sit. Other well-known ATP-binding signatures include the Walker B motif and the protein kinase and HSP70 signatures (Bairoch, 1991).

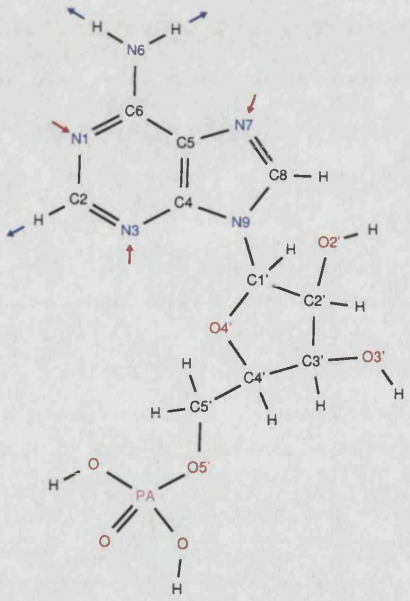

Figure 6.2: The adenylate moiety
Standard atom names used in reference to adenylate. Arrows indicate the potential hydrogen-bonding sites around adenine, including the weakly polarised C-H bond at position C2.

As more structural information has become available, this too has been scrutinised. In many cases, adenine appears to be the 'handle' via which the reactive parts of various molecules are attached to proteins. In an early study of adenylate recognition, Moodie *et al.* (1996) analysed a non-homologous dataset of 18 crystal structures of proteins bound to adenylate-containing nucleotides. The study encompassed calculation of interaction propensities for each amino acid with different parts of the adenylate fragment,

analysis of hydrogen bonding patterns and energy calculations. The authors found that hydrophobic and aromatic residues are particularly preferred in the adenine environment, in agreement with a previous study (Chakrabarti and Samanta, 1995). These residues tend to sandwich the adenine ring in a predominantly hydrophobic environment: interestingly, in addition to these non-polar residues, the basic side-chain of arginine is also noted to frequently lie across the face of the adenine ring.

From their analysis of the hydrogen bonding interactions between protein and adenylate, Moodie and coworkers conclude that there is no common motif for recognition of adenylate. Overall, fewer than one third of the theoretical total number of hydrogen bonds are formed to protein; some of the remainder of polar atoms in the ligands may interact with bulk solvent, but given the generally high degree to which adenylate tends to be buried in the protein (83.6% of adenine solvent accessible area is lost on average upon binding), the authors suggest that some hydrogen bonding sites may be completely occluded and hence remain unsatisfied. Of the four potential hydrogen bonding positions of adenine, the N6 donor make the most frequent interactions, while the N3 acceptor is reported to be involved in the least number of hydrogen bonds.

Moodie *et al.* conclude their paper by proposing the notion of a 'fuzzy template' for adenylate recognition, whereby different types of interactions may be described in broad geometric terms with respect to the ligand, but where precise templates of the form previously described for catalytic sites (Wallace *et al.*, 1996) may not be applicable. This type of approach to analysis of ligand recognition has proved enduringly popular: similar thinking can be seen to have motivated a number of studies including those based on the 'fuzzy functional forms' concept (Fetrow and Skolnick, 1998), investigations into recognition of heme (Taroni *et al.*, 2000) and sugars (Karmirantzou and Thornton, 1998), and the grid-based methods for the description of intermolecular interactions, X-SITE and IsoStar, which were described previously (§1.5.3.2).

One such analysis is that of Nobeli *et al.* (2001), which investigated the structural basis for the discrimination between the similarly shaped purine bases, adenine and guanine. They looked at a set of 97 adenine-protein complexes and 28 guanine-protein complexes to determine whether there were any salient differences between the two in terms of residue preference, burial or hydrogen bonding pattern. The paper as a whole serves to reinforce the fuzzy template concept since, while there are differences in the overall composition of binding sites for the two moieties, no clear patterns emerge which are characteristic of either one or the other. Experiments in which one base is substituted for the other within a structure *in silico* showed that the two key discriminating factors are (i) shape, with the added bulk of guanine's N2 amine group preventing it from fitting in some adenine binding sites and (ii) hydrogen bonds to the positions which differ between the two fragments (N6/O6, N1 and C2/N2).

Other studies have found particular structural motifs which are implicated in adenine/adenylate recognition. Kobayashi and Go (1997) described a geometrical method for comparing the environments of ligands wih the aim of finding common structural patterns. After applying their method to the set of all structures of adenine environments at that time, they reported that two unrelated protein families, cAMP-dependent protein kinase and D-Ala:D-Ala ligase (which has an ATP-grasp fold) bind adenine using a similar local arrangment of residues. Specifically, they describe a shared four-residue segment which makes two specific interactions

with the ligand: the carboxyl oxygen of the second residue accepts a hydrogen bond from the N6 amine group, while the backbone nitrogen of the fourth residue donates a hydrogen bond to the N1 atom (see figure 6.3).

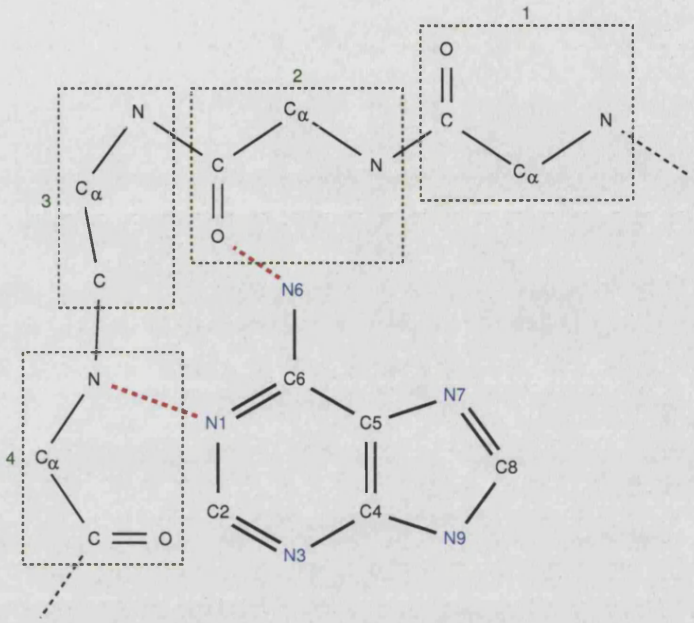

Figure 6.3: The adenine recognition motif described by Kobayashi and Go
This was described in Kobayashi and Go (1997). Red dashed lines represent hydrogen bond interactions between the adenine ring and the protein.

Denessiouk and Johnson (2000) generalised this finding somewhat by first noting that both groups of proteins identified by Kinoshita and Go shared a larger region of supersecondary structure around the adenine binding site, which they were then able to show was also present in the structure of ribonucleotide reductase R1 (RNR R1). Upon closer inspection of all three structures, the authors report an extended version of the original motif, in which the two hydrogen bonds to adenine are augmented with a hydrogen bond to the O2′ atom of the ribose, from the carboxy-terminal residue of the adenine-binding loop, and an invariant lysine residue which interacts with the α phosphate. Finally, they show that a total of 12 distinct ATP-binding folds exhibit the original adenine recognition motif, 8 of which also have the additional adenylate-interaction features which they newly define.

In a subsequent paper, the authors address the question of whether these ATP-recognition motifs are similarly found in sites which bind other adenylate-containing ligands (Denessiouk *et al.*, 2001). This issue is key to our understanding of molecular recognition: does the available data justify the application of a reductionist approach to the problem, whereby different parts of a ligand may be treated quasi-independently - or is the nature of protein-ligand recognition such that binding sites can only be appreciated when viewed in their entirety? The findings of this paper seem to suggest that, at least from a pattern-recognition perspective, the situation tends towards the former. In addition to the ATP-binding proteins previously reported, the authors find occurrences of similar adenine recognition motifs in numerous proteins which bind a range of ligands including coenzyme A, NAD, NADP and FAD. While this is striking, it must be pointed out that the

complement of protein-ligand complexes thus grouped together only accounts for less than a third of the total number of adenine environments in the PDB, meaning that many more ways of binding the moiety remain to be described.

More recently, the same authors noted that the donor-acceptor-donor (DAD) pattern along the Watson-Crick edge of the adenine group, which is recognised by the motif just described, is also present along two more edges of the base - the Hoogsteen (major groove) edge, and the sugar (shallow groove) edge (Denessiouk and Johnson, 2003). A thorough analysis of all protein-adenine complexes in the PDB shows that similar motifs exist to recognise these edges. Although the authors make no claim that these findings facilitate prediction of adenine binding sites, it should be pointed out that the notion of a structural motif has by this point become rather more abstract than the one originally identified by Kobayashi and Go, and could not be used to define a rigid structural template, for example, in the spirit of Wallace *et al.* (1996).

Cappello *et al.* (2002) take a slightly different approach, aiming not to discover particular motifs which bind adenine, but rather to describe the extent of diversity in the ways which evolution has produced to recognise it. By denoting each of the six potential hydrogen-bonding sites in adenine (five polar atoms plus the weak C-H donor of C2) as either satisfied or unsatisfied, they represent each protein-ligand complex using a six-digit binary string. Of the 64 possible combinations of interactions, the authors report that 33 are never observed. The most common situation is for no hydrogen bonds to be formed between adenine and the protein (around 40% of cases), with around 95% of structures belonging to one of 13 patterns. Of these, the most frequent combination is a pair of interactions with N6 and N1, as described by Denessiouk and Johnson. Capello *et al.* state in addition that in these cases, it is the *cis* hydrogen of N6 which is donated. Interestingly, C2 is found to be more often involved in hydrogen bonding than either N3 or N7, showing that even presumably weak donors can contribute significant interactions to the binding site.

A recent paper points out that, since previous studies have broadly agreed that many protein-ligand interactions are mediated via backbone atoms, defining the binding site in terms of atomic contacts, rather than the amino acid residues to which they belong, is a sensible starting point (Kuttner *et al.*, 2003). Given this premise, they describe a procedure for detecting spatial clusters containing atoms of similar types, in a coordinate frame defined by superposition of adenine. Applying this method to a non-redundant dataset of protein-adenine complexes, they define a number of clusters, most of which are in agreement with the distributions which would be expected given the chemical structure of the ligand. They then use these clusters as a search template to look for putative adenine binding sites in a test set of known adenine-binding proteins. The method suffers from a high false positive rate, but a number of post-search filters are described which reduce this considerably. However, the authors admit that their method is unlikely to be able to distinguish between proteins which bind adenine and those which do not.

The overall picture which emerges from these studies is that, in contrast to enzymatic active sites, well-conserved structural templates do not exist for ligand recognition. Rather, a given molecule may be recognised by interacting with one of a number of sites on its surface. Some of these interactions are more common than others, leading to regions of the binding sites which are more conserved. However, visual inspection tells us that, on the whole, the sites are extremely variable. The aim of this work is to quantify that

statement: *how* variable are ligand binding sites? Is this variability uniform among different families binding a given ligand?

6.3 Methodology

This section describes the methodological framework which is used to represent the fragment environments in a way which is amenable to the analyses which follow.

6.3.1 Definition of the binding site

When discussing protein-ligand interactions, the 'binding site' - that is, the parts of the protein which interact with the ligand molecule - may be defined in various different ways. Using one of the surfaces described in §3.8.1, the binding site may be defined as the region of the protein surface which is in proximity to, or accessible to the ligand. Note that this assumes that the coordinates of the ligand are known, an assumption which is made throughout this chapter. Alternatively, the binding site may be defined as the set of atoms or residues which lie within a given distance threshold of any part of the ligand. This definition of the binding site has the advantage that it is simple to compute, but brings the drawback that a distance cutoff large enough to include atoms interacting with the ligand via hydrogen bonds (around 3.5Å between atomic centres) also includes atoms in the second 'shell' around the ligand. In other words, atoms may be close to the ligand but occluded from being in direct contact with it, and hence should not be considered to form a functional part of the binding site.

Here, the binding site is defined as the set of atoms which expose a significant part of their Van der Waals surface to the ligand (or to the fragment of the ligand in which we are interested). In this way, atoms which cannot physically interact with the ligand are excluded. There is no requirement, however, that the atoms defined as comprising the binding site actually make attractive contacts with the ligand. The aim here was to obtain a purely knowledge-based description of the binding site, and therefore no detection of hydrogen bonding interactions or consideration of π-stacking geometries was applied. If we aim to map the distribution of *interactions* with respect to a ligand, as opposed to atom-type contacts, then the results will depend upon the particular model of interactions used. The present study aims to obtain a model-independent representation of the distribution of atomic contacts to a given ligand.

In detail, the algorithm used to define the binding site is as follows. Firstly, all atoms whose centres are within 3.5Å of the centre of any ligand atom are found using a kd-tree search (§3.4.2). Points are then distributed on the Van der Waals surface of each atom - from both the ligand and its neighbourhood - using the spherical design method described in §3.8.3.3. From each point on the ligand surface in turn, a ray-tracing method is then used to determine the set of environment surface points which are visible. This consists of a kd-tree search using a hemisphere of 2.5Å radius, projected from the ligand surface point, to obtain all potentially visible environment atom surface points. Each of these is then tested to determine whether the line of sight from ligand surface to environment atom surface is occluded by any other atom. If the line of sight is clear, the environment atom surface point is marked as visible.

Once this procedure is completed, each environment atom is inspected to determine the fraction of its surface points which were marked as visible from the ligand surface. Atoms exposing more than 10% of their Van der Waals surface to the ligand (equivalent to approximately 3.6Å^2 for a carbon atom) are considered to be making significant contacts with it. Using optimisations such as the kd-tree search and eliminating environment atom surface points once they have been marked as visible, means that this method is suitably efficient, at least on the relatively small number of atoms which need to be considered during ligand binding site analysis.

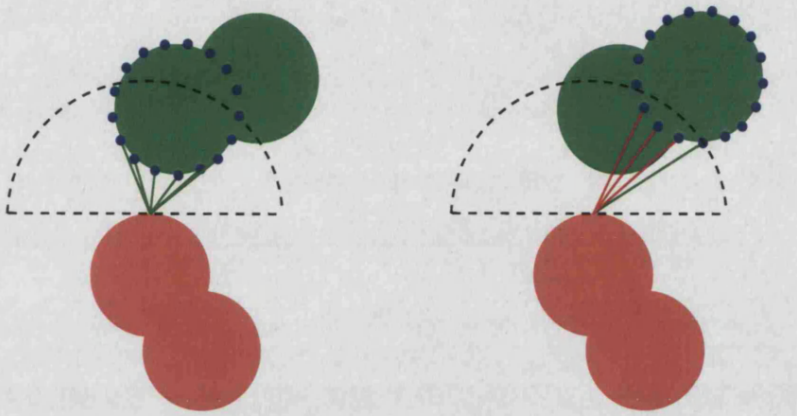

(a) A large portion of the surface of the nearer atom (green) is visible to the ligand surface point.

(b) Most of the rays to the further atom are occluded (shown in red).

Figure 6.4: Definition of the ligand binding site
Illustration of the ray-tracing method used to determining environment atom visibility.

6.3.2 Atom types

The atoms which make up each binding site are then classified into a set of predefined types. A number of atom type schemas have been previously described. One of the best-known is due to Engh and Huber (Engh and Huber, 1991), who extended a set of atom types originally used in the XPLOR refinement package to a total of 31 groupings. These types discriminate between atoms firstly on the basis of their chemical element, then according to the chemical context in which the atom is found, and finally depending on whether or not the atom is charged. For example, 18 types of carbon atoms are defined, with aliphatic carbons being separated from aromatic atoms, and both charged and uncharged states defined for carbon atoms liable to protonation (*e.g.* histidine $C^{\varepsilon 1}$).

In a study of covalent radii derived from protein crystal structures, Li and Nussinov defined 25 atom types, discriminating atoms firstly according to their chemical element and then by the number of hydrogen atoms to which they are bonded (Li and Nussinov, 1998). This results in a slightly different classification from that of Engh and Huber: for example, while in the older paper, histidine C^{δ} and C^{ε} are placed in separate classes, Li and Nussinov consider them chemically equivalent. Also, some atom types are missing from their classification altogether (*e.g.* arginine C^{ζ}, histidine C^{γ} and proline backbone nitrogen), since insufficient examples of them were found in their dataset.

Mitchell *et al.* (1999) generalise the concept of atom typing by describing a system (SATIS) for classifying any atom according to its element and those of its covalent partners. This does not require a previously defined set of atom types, and therefore can be applied automatically to any compound. However, for the purposes of this study, classification of atoms based on some accepted chemical notions are required, and therefore SATIS is not particularly useful here.

The atom classification schema used in the LPC software (Sobolev *et al.*, 1999) is attractive due to its simplicity. In this approach, atoms are defined according to whether they can donate or accept hydrogen bonds, and for non-polar atoms, whether they are part of aromatic systems and whether they are bonded to polar atoms.

The LPC schema forms the basis of the atom classification used in the present study, which is shown in table 6.1. It consists of six types, three polar and three primarily non-polar. Potential hydrogen bond acceptors and donors make up two types, with those atoms which can potentially both accept and donate hydrogen bonds (*e.g.* side-chain hydroxyl groups) belonging to a third class named 'hydrophilic'. The 'hydrophobic' atom type is composed of aliphatic side-chain carbon atoms, and aromatic side chain carbons belong to a fifth class. The final class, named 'neutral' contains carbon atoms which are covalently bonded to polar atoms, and which may therefore carry a small partial charge.

No atom typing system is perfect; indeed most suffer from two conspicuous drawbacks. The first is that, in specifying a rigid classification of atoms in this way, we are necessarily grouping atoms according to their *identity* rather than by the *role* which they play in a particular context. For example, although the atoms in the 'acceptor' class are all capable of accepting hydrogen bonds, this potential is no means realised in every instance of their occurrence. Depending on the local environment, a carboxyl oxygen atom making no hydrogen bonding interactions may not be particularly unfavourable.

The second drawback is that, even leaving aside the effects of different environments on the behaviour of certain chemical groups, it is clear that the properties (however they may be defined) of different functional groups - and therefore of individual atoms within them - form a continuum. A strict atom classification scheme is to some extent quite an unrealistic proposal. For instance, the aromatic atom type is clearly more similar to the hydrophilic class than, say, the acceptor type is to the hydrophobic class. Being able to enshrine these similarities in some type of quantitative measure would add greatly to the value of the atom classification model. In particular, it would allow us to compare two binding sites, and to determine in which regions of space they expose similar chemical properties to the ligand.

The difficulty of measuring similarities between a number of discrete classes also applies when considering proteins in terms of amino acids: of the twenty amino acids commonly found in proteins, some share more similar characteristics than others. One way of expressing these similarities is by dividing amino acids into a number of classes according to their phyisco-chemical properties. For instance, we may identify each amino acid type as being either 'aliphatic' (AGILPV), 'basic' (RHK), 'acidic' (DE), 'polar' (STCMNQ) or 'aromatic' (FWY)[1]. Taylor (1986) suggested a more complex classification in which he defined a number

[1] Amino acids belonging to each type are given parenthetically, using the standard one-letter code.

	Atom type	Included atoms
■	Acceptor	Backbone carboxyl oxygen Carboxylate oxygens of acidic sidechains (Asp $O^{\delta 1}$, $O^{\delta 2}$; Glu $O^{\varepsilon 1}$, $O^{\varepsilon 2}$) Carboxyl oxygen of asparagine and glutamine (Asn $O^{\delta 1}$; Gln $O^{\varepsilon 1}$)
■	Donor	Backbone nitrogen Nitrogens of basic sidechains (His $N^{\varepsilon 2\dagger}$; Lys N^{ζ}; Arg N^{ε}, $N^{\eta 1}$, $N^{\eta 2}$) Amine nitrogen of asparagine and glutamine (Asp $N^{\delta 2}$; Gln $N^{\varepsilon 2}$) Trytophan sidechain amine nitrogen (Trp $N^{\varepsilon 1}$)
■	Hydrophilic*	Sidechain hydroxyl groups (Ser O^{γ}; Thr $O^{\gamma 1}$; Tyr) His $N^{\delta 1\dagger}$
■	Hydrophobic	Backbone C^{α} atoms All C^{β} atoms except Cys, Ser, Thr All C^{γ} atoms except Asp, Asn, Phe, Tyr Aliphatic sidechain carbons (Ile $C^{\gamma 1}$, $C^{\gamma 2}$, $C^{\delta 1}$; Leu $C^{\delta 1}$, $C^{\delta 2}$; Lys C^{δ}; Thr $C^{\gamma 2}$; Val $C^{\gamma 1}$, $C^{\gamma 2}$)
■	Aromatic	Sidechain carbons of Phe ($C^{\delta 1}$, $C^{\delta 2}$, $C^{\varepsilon 1}$, $C^{\varepsilon 2}$, C^{γ}, C^{ζ}) Sidechain carbons of Trp except $C^{\delta 1}$ ($C^{\delta 2}$, $C^{\varepsilon 2}$, $C^{\varepsilon 3}$, $C^{\zeta 2}$, $C^{\zeta 3}$, $C^{\eta 1}$) Sidechain carbons of Tyr ($C^{\delta 1}$, $C^{\delta 2}$, $C^{\varepsilon 1}$, $C^{\varepsilon 2}$, C^{γ}, C^{ζ})
■	Neutral	Backbone carbonyl carbon atoms C^{β} atoms of Cys, Ser and Thr Sidechain carbons bonded to polar atoms (Arg C^{δ}, Arg C^{ζ}, Asn C^{γ}, Asp C^{γ}, Glu C^{δ}, Gln C^{δ}, His $C^{\varepsilon 1}$, His $C^{\delta 2}$, Lys C^{ε}, Met C^{ε}, Pro C^{δ}, Pro N, Trp $C^{\delta 1}$) Sulphur atoms (Met S^{δ}; Cys S^{γ})

Table 6.1: GAMUT atom classes

This table shows the six categories into which protein atoms are classified for the purposes of representing ligand binding sites in this study. Coloured boxes illustrate the colour-coding scheme used in diagrams throughout the chapter.
(†) note that the distinction between histidine $N^{\delta 1}$ and $N^{\varepsilon 2}$ atoms assumes a particular tautomeric state and therefore may be a source of some errors.
(⋆) atoms in this class can potentially both donate and accept hydrogen bonds.

of physical and chemical properties which were not mutually exclusive (*e.g.* small, charged, negative, polar, *etc.*), thereby constructing a Venn diagram in which each amino acid is classified according to the set of properties which it possesses. This has the advantage that the similarity of a pair of amino acids may be judged according to the number of properties which they share. A similar, if slightly simpler, classification was used by Zvelebil *et al.* (1987), in which amino acid properties are presented in the form of a truth table.

While these classifications are useful ways in which our understanding of the chemical properties of amino acids can be embodied, they are all somewhat *ad hoc*, and therefore not particularly suitable for statistical analysis of protein sequence and structure. By inspecting multiple alignments of protein sequences, the frequency with which each type of amino acid is observed to mutate to every other type can be calculated. This type of analysis, pioneered by Dayhoff *et al.* (1978) and later refined by Henikoff and Henikoff (1992), results in a 20×20 matrix of scores. Although they are actually mutation frequencies, the values in such matrices are often taken to represent amino acid similarity. This is rationalised on the basis that amino acids with more similar properties are more likely to be substituted for one another. Of course, mutation frequency also depends on other factors such as codon bias and secondary structural context - see *e.g.* Shi *et al.* (2001) - but to a first approximation, the inference of similarity from replaceability is generally considered to be

acceptable.

No such evolution-based model exists from which we can derive atom type similarities, but several studies have attempted to do so by analysing the frequency with which different atoms or functional groups are seen to play similar chemical roles. This phenomenon - specifically the observation of functional groups or molecules which have chemical and/or physical similarities producing broadly similar biological properties - is commonly referred to as *bioisosterism*. From a structural perspective, bioisosteres have been described as "molecules or functional groups that are structurally different but form similar intermolecular interactions". Watson *et al.* (2001) set out to quantify the degree of bioisosterism which exists between pairs of functional groups by comparing their spatial distributions with respect to various 'central group' fragments. In a similar study by Verdonk and coworkers, distributions obtained from the IsoStar database (Bruno *et al.*, 1997) are approximated by fitting three-dimensional Gaussian functions to peaks found in the density maps. For each pair of functional groups, a number of different similarity indices are then calculated, and averaged over all central fragments to give an indication of the frequency with which the contacting fragments form similar interactions. The authors show, by comparing their results against a curated database of bioisosteres, that their method is able to automatically identify functionally similar fragments. They point out, however, that the robust definition of threshold values on their scores, above which the degree of bioisosterism is significant, remains an unresolved problem.

In a similar study, Rantanen *et al.* (2001) obtain contact information obtained from the PDB, using ligand fragments as the central groups. While the study of Verdonk and coworkers analysed the distribution of chemical *fragments* around a reference group, in this paper, the contact distributions are calculated for a set of 25 atom types, adopted from Li and Nussinov (1998).These distributions are then approximated by a linear combination of Gaussian functions, using an expectation-minimisation algorithm to compute the fitting. In a subsequent paper (Rantanen *et al.*, 2002), each pair of Gaussian mixture models is compared to yield a dissimilarity matrix for the set of atom types. Their results suggest that many of the 25 atom types show distinct spatial distributions with respect to ligand fragments, with only a small number showing significant levels of similarity, therefore implying that they should be merged.

The results of Rantanen *et al.* were used to determine whether the GAMUT atom classification schema is a sensible one[2]. The dissimilarity matrix published in their paper was analysed using multidimensional scaling (§3.3.2); figure 6.5 shows a plot of the first two dimensions of the results, with each of the 25 atom types colour-coded according to which GAMUT class it belongs. The results shown here agree broadly with our intuition of the relationships between the atom types: there is a clear separation between polar atom types (acceptor, donor, hydrophilic) and non-polar types (hydrophobic, aromatic). Interestingly, atoms in the 'neutral' class, rather than being intermediate between the polar and non-polar atoms, occupy a quite distinct third section of the plot.

When the GAMUT atom classification was first devised, cysteine thiol (type 13) and methionine sulphide (type 14) sulphur atoms were classified in the hydrophilic and acceptor classes respectively. This was done

[2]Herein, the atom groupings of Rantanen *et al.* will be referred to as 'atom types', while the GAMUT classification will be referred to as 'atom classes', for clarity.

on the basis that they are both potential hydrogen-bonding partners, albeit weak ones. Inspection of the MDS plot, however, suggested that they should be moved into the neutral class.

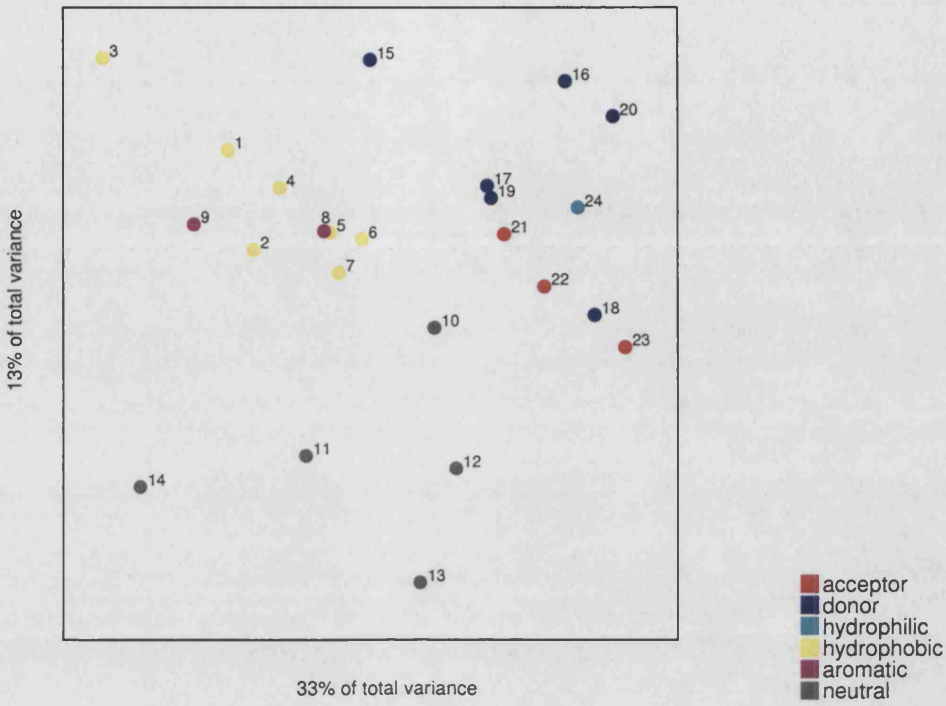

Figure 6.5: Dissimilarity between the atom types of Rantanen *et al.*
Multidimensional scaling plot of the distance matrix published in Rantanen *et al.* (2002). Numbers correspond to the 25 atom types used in the paper. Colours show to which GAMUT atom class each atom type belongs.

Among the hydrophobic atoms, type 3 (side-chain tertiary carbons of Ile, Leu, Thr and Val) is slightly separated from the main cluster. Of the hydrophobic atom types, atoms belonging to type 3 are the most distant - in terms of chemical connectivity - from any non-carbon atoms, so we may perhaps expect them to exhibit the most non-polar character. Conversely, atoms in types 6 (side-chain secondary methylene carbons adjacent to a charged group) and 7 (side-chain primary methyl carbons) are only one or two bonds away from charged or polar atoms, therefore their proximity in the plot to the acceptor and donor classes may be explained as being due to their slight polarisation.

Considering the polar atoms, there is a good separation between the acceptor and donor atom types, with the exception of type 18 (side-chain amide nitrogens of Asn and Gln). This may be a result of crystallographic errors in correctly identifying the atoms in the side-chains of these residues (discussed in §1.3.4). If the oxygen and nitrogen atoms were erroneously exchanged with sufficient frequency, it could lead to misleading dissimilarity values between these and the other atom types. In agreement with expectations, the hydroxyl oxygens (type 24), which can both accept and donate hydrogen bonds, are placed between the acceptor and donor groups.

With only six classes, the GAMUT schema is clearly of much lower granularity that that of Rantanen *et al.*, and therefore groups together some atom types which may have rather distinct characteristics. A schema with a small number of divisions is considerably more manageable however, and makes for easier comprehension

	acceptor	donor	hydrophilic	hydrophobic	aromatic	neutral
acceptor	0	0.59	0.49	0.90	0.94	0.82
donor	0.59	0	0.40	0.71	0.81	0.76
hydrophilic	0.49	0.40	0	0.91	1.00	0.86
hydrophobic	0.90	0.71	0.91	0	0.38	0.58
aromatic	0.94	0.81	1.00	0.38	0	0.64
neutral	0.82	0.76	0.86	0.58	0.64	0

Table 6.2: Dissimilarity between GAMUT atom classes
Distance matrix obtained by 'compressing' that published by Rantanen *et al.*, in order to group together those atom types which belong to each GAMUT atom class.

of the analyses later in this chapter. The atom classification used here may therefore be seen as a prototype for later, more sophisticated studies; here, for the purposes of exploring the analysis of binding site diversity, this schema is considered adequate.

We can now calculate a new distance matrix between the six GAMUT atom classes. In the projected space obtained by MDS analysis of the 25 × 25 distance matrix of Rantanen *et al.*, a point which represents each of the GAMUT atom classes can be calculated simply by computing the centroid of the atom types which constitute it. For example, the aromatic class is represented by a point located - in 25-dimensional space - mid-way between atom types 8 and 9. Thus we can obtain dissimilarity values between the GAMUT atom classes by calculating pairwise distances between the centroids. In this way the original 25 × 25 matrix is effectively compressed to a 6 × 6 matrix by grouping certain rows and columns. The resulting distance matrix, scaled so that the maximum distance is 1.0, is shown in table 6.2.

6.3.3 Generation of property maps

Once the set of atoms in contact with the ligand or fragment has been classified according to a specified schema, a density map is computed for each atom class. This is done by convoluting the coordinates of all atoms belonging to that class (*e.g.* hydrophobic, acceptor *etc.*) with a 3-dimensional Gaussian function, using a method similar to that used in, among others, the X-SITE program (Laskowski *et al.*, 1996).

The standard Gaussian function has the form

$$f(x) = ae^{-bx^2}$$

For generation of the property maps, the variable x represents the distance from the atomic centre; the parameter b is chosen such that the value of the function on the surface of the Van der Waals sphere of the atom is half that at its centre: in other words,

$$b = \frac{\ln 2}{r_{vdw}^2}$$

Although the function is defined over an infinite domain, it is evaluated only up to two Van der Waals radii away from the centre. The parameter a is chosen such that the sum of the function over all gridpoints within this range is 100 - this ensures that the total contribution of each atom to the density map is the same (figure 6.6).

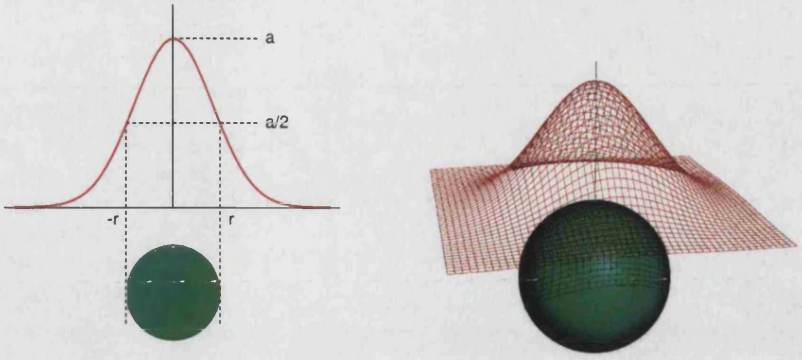

(a) The standard deviation of the normal curve is chosen such that the value of the function is half of its maximum value (p) at one Van der Waals radius (r) away from the centre of the atom. The magnitude of the function is set in order that the integral of the function sums to 100.0.

(b) A 2-dimensional analogue of the previous function. Extension to 3 dimensions is conceptually simple but cannot easily be represented on the page.

Figure 6.6: Convolution of atom coordinates with a Gaussian function

For reasons of computational efficiency, the values of this Gaussian function are not calculated exactly for every atom in every binding site. Rather, a 'mask function' is precomputed for each chemical element on a 3-dimensional grid large enough to accommodate a sphere of twice its Van der Waals radius (figure 6.7). When updating a property map with density due to a given atom, rather than evaluating the Gaussian function at each gridpoint in its vicinity, the precomputed mask is simply added to the map, positioning it so that its centre lies at the gridpoint closest to the atom centre. A small systematic error is thus introduced, due to the finite size of the grid spacing, but since the spacing used here (0.375Å) is significantly smaller than the atomic radii - and typically comparable to the experimental error in atom positions - this is not considered to be overly problematic. Other grid spacings were experimented with; the one used here was chosen as a compromise between granularity and computational cost.

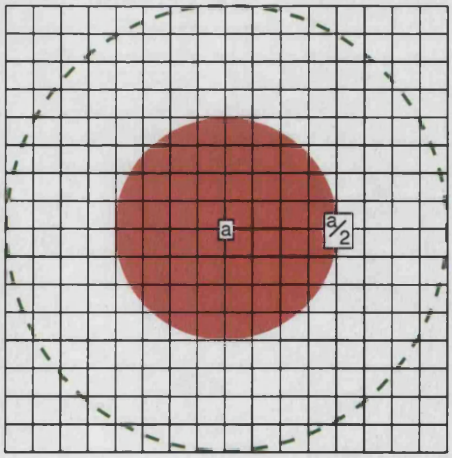

Figure 6.7: Precomputation of the 3-dimensional Gaussian function
The Van der Waals sphere of the atom is shown in pink. The Gaussian function is evaluated on all gridpoints lying within the green circle. As shown, the value of the function declines by one half at one Van der Waals radius from the centre of the atom.

The result of this procedure is a map for each atom type whose value, at all gridpoints inside the Van der

Waals sphere of an atom of that type, is $\frac{a}{2}$ or greater. Therefore, if a pair of atoms of the same class are covalently bonded, a contour at level $\frac{a}{2}$ envelops both atoms together (figure 6.8). Taking the set of maps for all k atom classes, we then obtain, at each gridpoint, a vectorial description of the composition of the binding site at that point: in regions of void space, the binding site is represented by the null vector, and in regions close to one or more atoms, the values in the vector represent the relative proximity of the point to nearby atoms of the k different classes.

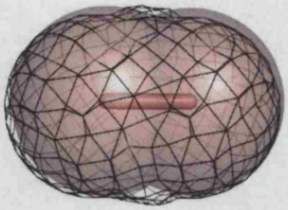

Figure 6.8: 'Smearing' effect of the Gaussian density convolution
Two covalently bonded atoms are shown as Van der Waals spheres. The mesh shows the contour of the resulting property map, calculated at half the peak value.

6.3.4 Generation of environment masks

The property maps are defined within a box enclosing the ligand molecule, but much of the volume inside the map is not of interest since it is too far away from the ligand. In addition, the volume occupied by the ligand itself must be excluded from analysis of the property maps, since this will necessarily be void. The method used to achieve this is to define an 'environment mask', which is simply a density map defined over the same region as the property maps, in which high values indicate those grid points which are considered as part of the environment of the ligand or fragment.

Construction of the environment mask consists of three stages (see figure 6.9). In the first, a map which marks the volume occupied by the ligand molecule itself is generated. Every point in the grid is tested to determine whether any ligand atoms lie in proximity to it, using a cutoff of 5.5Å. If so, the grid point is assigned a value by evaluating the Gaussian function with the distance to the nearest ligand atom.

Next, another map is created in which any point within 4Å of a ligand atom is set to 1.0. This map therefore contains non-zero values both within the volume occupied by the ligand, and in the space adjacent to it. In the third stage, the values in the first map are subtracted from those in the second. The result is a density map in which the only non-zero values are at grid points surrounding the fragment of interest, excluding the part of space at which the rest of the ligand is attached.

6.3.5 Mapping environment properties onto the fragment surface

For some analyses, it is desirable to map values from a density map onto a molecular surface. By so doing, the focus is changed from looking at the distribution of a certain property in space around a ligand, to the values of the property which the ligand 'sees', from each point on its surface. The specific advantages of mapping properties onto the surface are twofold:

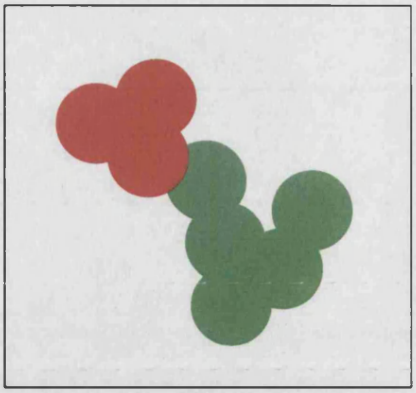

(a) Schematic representation of a ligand (green), with the fragment of interest marked in red

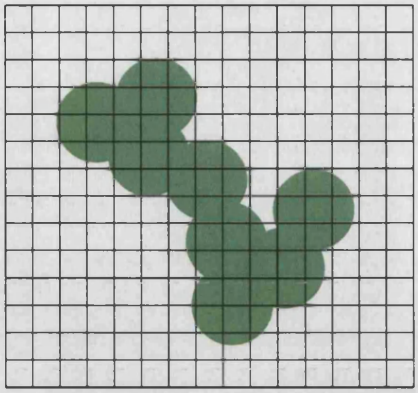

(b) Volume occupied by the ligand is marked out

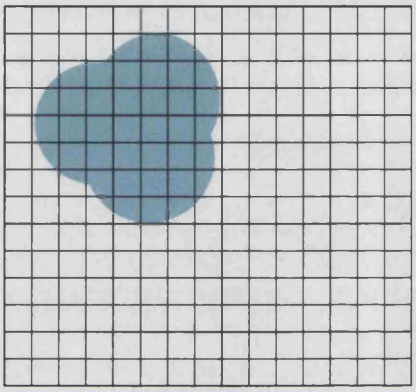

(c) Volume enclosing the fragment and its environment is defined using the approximate Gaussian convolution method

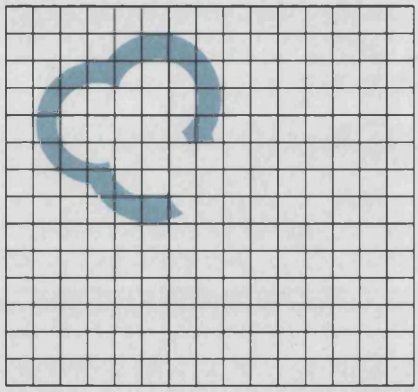

(d) Subtraction of the first map from the second leaves a mask defining the fragment environment

Figure 6.9: Creation of environment masks
Note that these figures are not to scale.

1 Visualising and interpreting three-dimensional scalar fields can be difficult, even with the aid of a graphics terminal and isocontouring tools. Conveying the same information comprehensibly on the printed page, however, is even more challenging. By mapping property values onto the surface, and showing these surfaces using a colour code to indicate different ranges of values, the essential features of the property map can be illustrated more simply.

2 Once the property has been mapped onto the surface, we can integrate it to obtain an average value. This enables the values of a certain property to be compared between different fragments, even if they are of differing shapes and sizes (for example adenine and nicotinamide).

The method used here to achieve this is simple, and is illustrated in figure 6.10. First, the molecular surface is calculated by computing a triangulated isosurface over the fragment (Lorensen and Cline, 1997). Then, normal vectors are calculated for each triangular facet on the surface. Normals from neighbouring facets are averaged in order to mitigate against the effects of local deformations in the surface. For every facet, the value of the density map at a point located a specified distance normal to it is obtained by first-order linear interpolation. Thus the values of the density map at points surrounding the fragment are projected onto its surface.

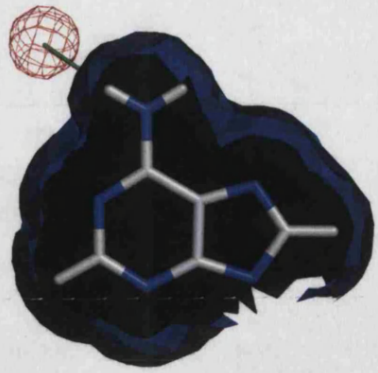

Figure 6.10: Mapping properties onto an atomic surface
The triangulated surface over an adenine moiety is shown. The surface normal of one facet is shown in green; in the example shown here, this facet would be assigned a high value, since the region of space which it is sampling falls inside a density isocontour.

6.4 Characterisation and comparison of fragment environments

Figure 6.11 shows the distribution of different atom types in contact with adenine. The dataset from which this image was generated contains a non-redundant subset of all adenine environments found in the PDB, regardless of the particular ligand in which the adenine moiety occurs. The dataset was generated using the method described in §4.2, counting only the residues in contact with the adenine part of each ligand when calculating their domain composition. This was done in order to allow the construction of a dataset of adenine binding sites, irrespective of the ligand type to which each adenine fragment belongs. This procedure resulted in 120 clusters; representatives of these clusters were used to generate the contact distributions shown here.

Certain patterns are evident from these images, notably two fairly distinct clusters of potential hydrogen bond acceptors proximal to the N6 hydrogen atoms, and a cluster of potential donors to the left of the picture, adjacent to N1. Less clear is a general preference for hydrophobic and aromatic contacts to occur above and below the plane of the ring rather than around its rim. Weaker preferences for donor and acceptor types which complement the other polar atoms of the fragment can also be discerned. Appreciating details of the patterns, however, such as comparing the shapes, spreads and intensities of localised enrichments for particular atom types, is almost impossible.

Identification of all but the most obvious patterns from this data by eye is difficult, partly because the sheer amount of information in each image is somewhat overwhelming, and also because the relative frequencies of occurrence of each type of atom in proteins as a whole are not equal. Picking out those interactions which are more than simply what would be expected by chance, therefore, is challenging. To overcome the first difficulty, the distributions of atomic positions were converted into density maps using the method described earlier. Isocontours of these maps can then be used to identify preferred interaction geometries; however, the choice of contouring level presents a new problem. To address this, the relative abundance of each atom type in a representative set of protein surfaces was computed, and these were used to convert raw density values into propensities, as described below.

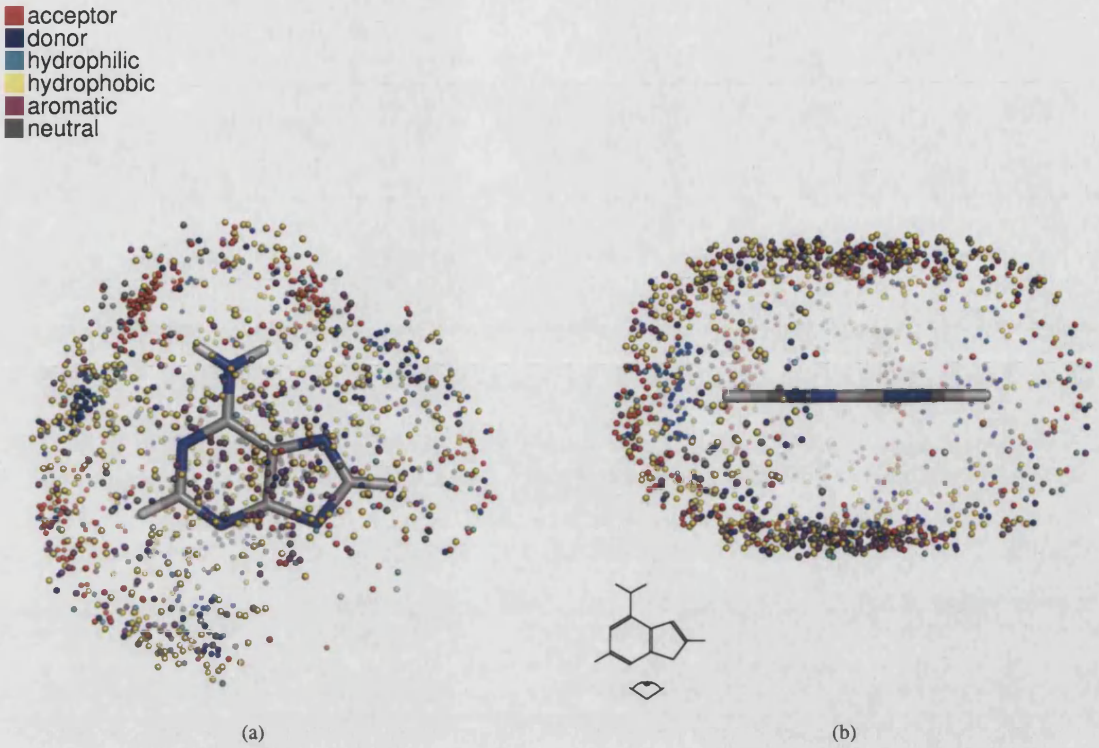

Figure 6.11: Spatial distribution of atom types contacting adenine
The plots show the distribution of atoms contacting adenine, taken from a non-redundant dataset of 120 protein-adenine complexes. Contacts were defined and classified as described in the text. Colours indicate the six atom types used (see key). The intensity of each atom fades in proportion to its distance from the viewer The intensity of each atom fades in proportion to its distance from the viewer. In part (b), the orientation of the adenine ring is indicated by the 'eye' logo shown below it.

6.4.1 Localised contact propensities

At each gridpoint, for each atom type, the values of the density maps over all binding sites are averaged. This average value is then converted into a propensity by taking into account the relative occurrence frequencies of the atom types. This calculation is performed as follows:

1 The relative occurrence of each atom type contacting the fragment in a non-redundant set of binding sites is calculated. These are designated $(f_1, f_2 \ldots f_k) : \Sigma_{i=1}^{k} f_i = 1.0$.

2 For each binding site, the k density values at each gridpoint in the environment region are summed. The average of these total density values is then computed over all gridpoints in the environment region. The values thus obtained for each binding site are then averaged to give the 'average total density per gridpoint', $\bar{\rho}$.

3 At each gridpoint in the i^{th} map, the density value $\rho_i(x)$ is converted to a propensity using the formula

$$\pi_i(x) = \frac{\rho_i(x)}{f_i \times \bar{\rho}}$$

One problem with this approach is that propensity values can only really be trusted when they are calculated over a fairly large number of binding sites. In the limiting case, where only one site is considered, every individual atom contacting the ligand would result in a high propensity value over its nearby gridpoints, since the density in that locale would be many times greater than expected by chance. The process of averaging

means, on the other hand, that high propensities are only obtained from large groups of sites where there is a genuine preference for a particular atom type in a particular region of space.

Figure 6.12 shows the distribution of polar atom types around adenine in the dataset of 120 complexes used previously, both as 'raw' scatter plots, and as propensity isocontours. As discussed previously, these plots do not show the distribution of hydrogen-bonding *interactions* relative to adenine, but rather the distribution of *potential* hydrogen-bond acceptors and donors. The location of an acceptor atom in a position where it could accept a hydrogen bond from the ligand does not necessarily imply that it does so, since the definition of atom contacts used here does not include any consideration of the geometry of the atoms to which the potential acceptor is bonded, which would be required to determine whether it really participates in an attractive interaction (see §1.2.2.1). Nevertheless, it is reasonable to assume that, where we see very high propensity values for acceptor or donor atoms in such positions, at least a significant proportion of them must be interacting with the ligand.

Inspection of the propensity contours in figure 6.12b shows that the most common interactions are with hydrogen bonds acceptors proximal to N6 and donors near N1. Moreover, the *cis* hydrogen of N6 appears to be donated more often than the *trans* hydrogen. This is consistent with the previous observation of motifs which interact with N6 and N1 via consecutive residues in the same chain. Closer examination of the distributions of acceptor atoms around N6 show that, while the deflection of *trans* acceptors perpendicular to the plane of the ring is approximately equal in both directions, the mean position of *cis* acceptors is shifted slightly towards the X-face[3] of the ring (see figure 6.12c). Enrichment for potential acceptors proximal to the hydrogen attached to C2 suggests that this bond is sufficiently polarised to participate in hydrogen-bonding interactions. The distribution of acceptor positions around this atom appears to be skewed towards the adenine Y-face (figure 6.12d). In agreement with previous studies, the density of donor atoms below N3 is fairly low. The contours visible behind the adenine ring are due to the nitrogen atoms in arginine side-chains which tend to stack against it (see figure 6.14c).

The distributions of figure 6.12 provide indications of the satisfaction of the hydrogen bonding potential of adenine by the proteins which bind it. We can also obtain information on the degree to which protein-bound adenine is still free to hydrogen-bond to bulk solvent, by examining the distribution of crystallographic water molecules around the adenine group. The resulting distribution, shown in figure 6.13, shows that the most solvent-accessible atom in adenine appears to be N7. The presence of density near N3 shows that the fact that this atom is rarely involved in interactions with protein (figure 6.12b) cannot entirely be explained using arguments based on steric hinderance by the rest of the ligand.

The preference for hydrophobic and aromatic contacts to the faces of the adenine ring is demonstrated in figure 6.14. Although not immediately apparent from the scatter plot, the propensity contours suggest that

---

3 While accepted nomenclature exists for referring to the two faces of nicotinamide, the author was unable to find any such convention for use with the adenine ring. Therefore, throughout this chapter, the two faces are designated 'X' and 'Y', as shown in the following picture:

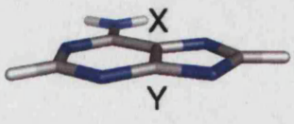

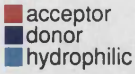

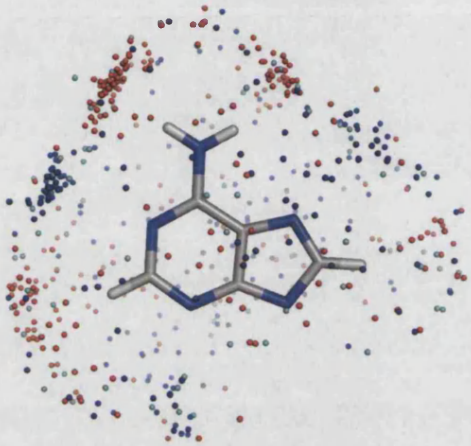

(a) Polar atom contacts

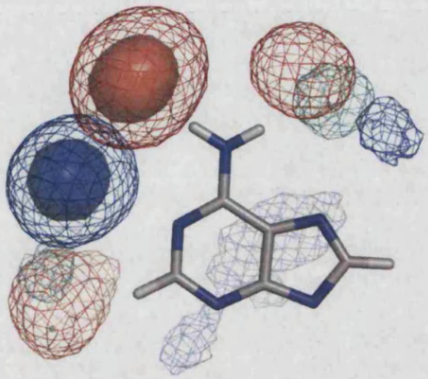

(b) Propensity contours for polar contacts

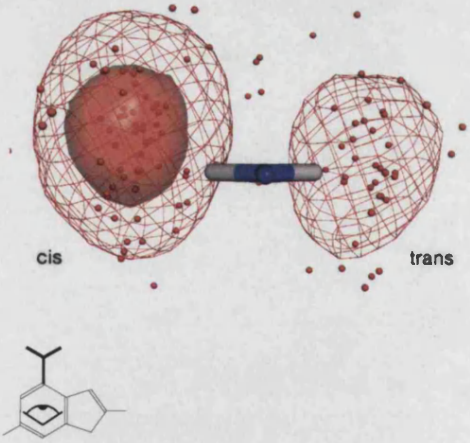

(c) Distribution of acceptors relative to N6. Only the amine group of adenine is shown, viewed along the C8-N6 bond

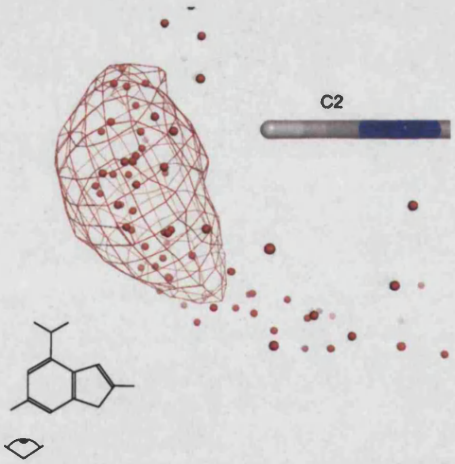

(d) Distribution of acceptors relative to C2, oriented so that C8-N6 points into the page

Figure 6.12: Spatial distribution of polar atoms contacting adenine

(a) the distribution of polar atoms contacting adenine, taken from the non-redundant dataset of 120 protein-adenine complexes. (b) contours indicating the regions of highest propensity for each polar atom type. Mesh contours were calculated at a level of $\pi = 15$; semi-solid contours show $\pi = 30$. (c) illustration of slight asymmetry in the location of potential hydrogen-bond acceptors *cis* to the N6 amine group. (d) illustration of asymmetry in the location of potential hydrogen-bond acceptors relative to the C2 atom.

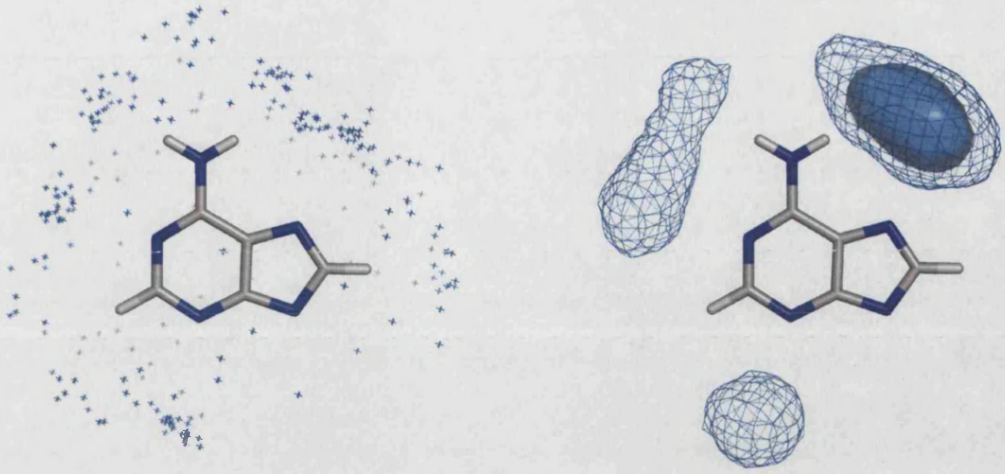

(a) Distribution of water oxygen atoms

(b) Density contours for water oxygen

Figure 6.13: Distribution of immobilised water molecules around adenine
(a) scatter plot of oxygen atoms from water molecules crystallographically visible around adenine in the 120 complexes analysed. (b) density contours showing most preferred regions: propensity values cannot be calculated for the water maps, so mesh contours are shown at $\sigma = 3$ and semi-solid contours at $\sigma = 5$ where σ is the standard deviation of values in the map.

this preference is not completely symmetrical with respect to the two faces of the ring. Aromatic contacts appear to be slightly more favoured on the X-face than the Y-face; conversely, there is a slightly greater density of hydrophobic/aliphatic contacts to the Y-face.

The distribution of arginine side-chains around arginine, which have been previously noted to frequently be found stacking in parallel against it, is shown in figure 6.14c. This demonstrates a striking asymmetry, with contacts to the Y-face being around four times more likely than those to the X-face (12 and 3 occurrences respectively). Figure 6.14d shows the distribution of aromatic side-chains around arginine. Phenylalanine and tyrosine are approximately equally likely to contact adenine (35 and 34 occurrences respectively), with tryptophan being less common (8 residues). Instances in which aromatic side-chains were oriented in parallel to, and stacked on the face of the adenine ring were identified by visual inspection. Counting the frequency of stacking interactions shows that contacts to the X-face are approximately twice as likely as those to the Y-face (14 versus 7 instances), with the majority of aromatic side-chains (56 residues) contacting adenine at an oblique angle.

Combining these propensity maps allows us to define the consensus binding site - or *pharmacophore* - for adenine, as shown in figure 6.15. This description, which is a realisation of the fuzzy template concept defined by Moodie and Thornton, is at the same time a feature-rich and easily comprehensible representation of the geometry of interactions made between proteins and this moiety.

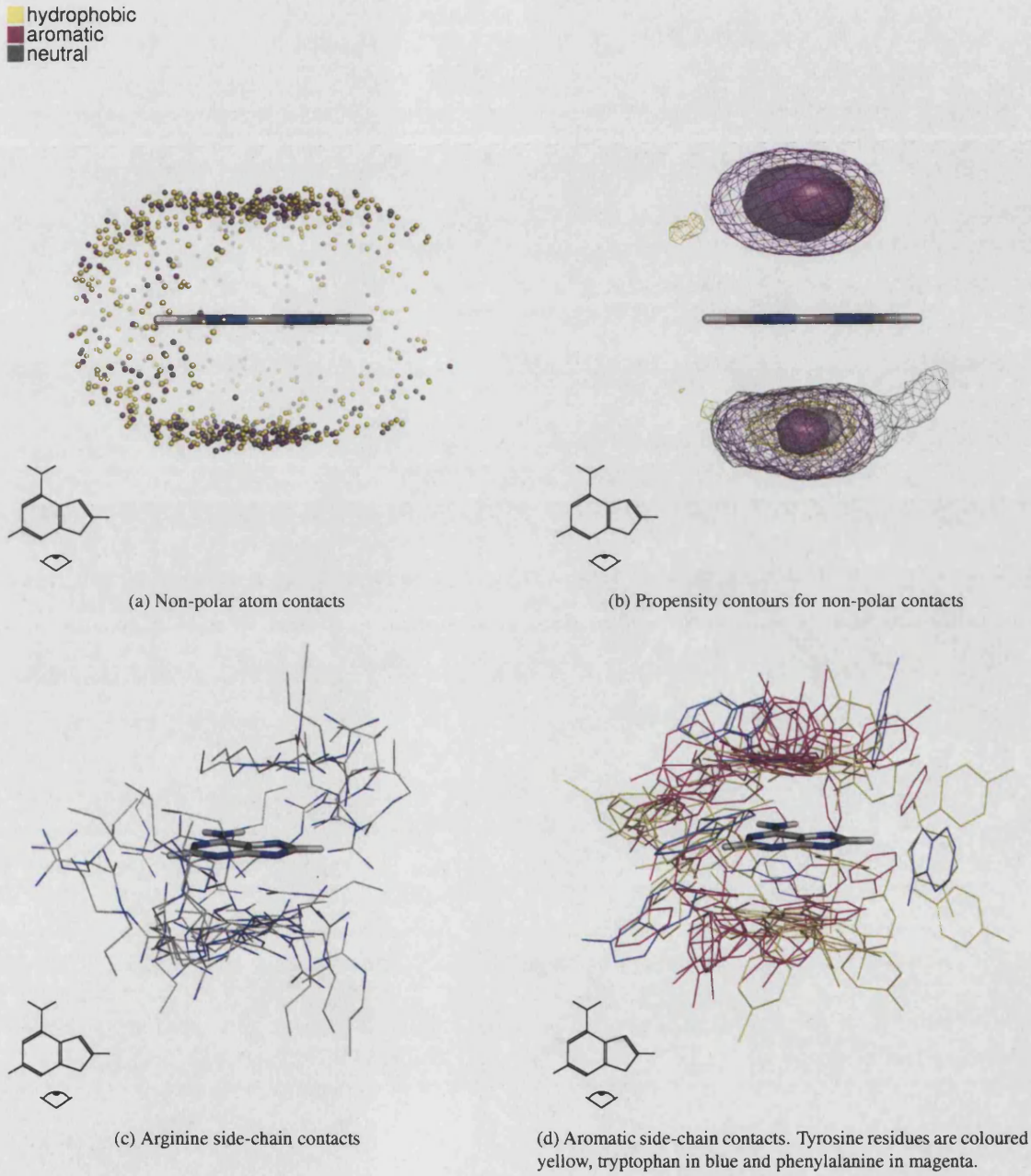

(a) Non-polar atom contacts

(b) Propensity contours for non-polar contacts

(c) Arginine side-chain contacts

(d) Aromatic side-chain contacts. Tyrosine residues are coloured yellow, tryptophan in blue and phenylalanine in magenta.

Figure 6.14: Spatial distribution of non-polar atoms contacting adenine

(a) the distribution of non-polar atoms contacting adenine, taken from a non-redundant dataset of 120 protein-adenine complexes. (b) contours indicating the regions of highest propensity for each polar atom type. Mesh contours were calculated at a level of $\pi = 15$; semi-solid contours show $\pi = 30$. (c) distribution of arginine side chain contacts, showing the tendency for arginine to stack against one side of the ring. (d) distribution of aromatic side chain contacts.

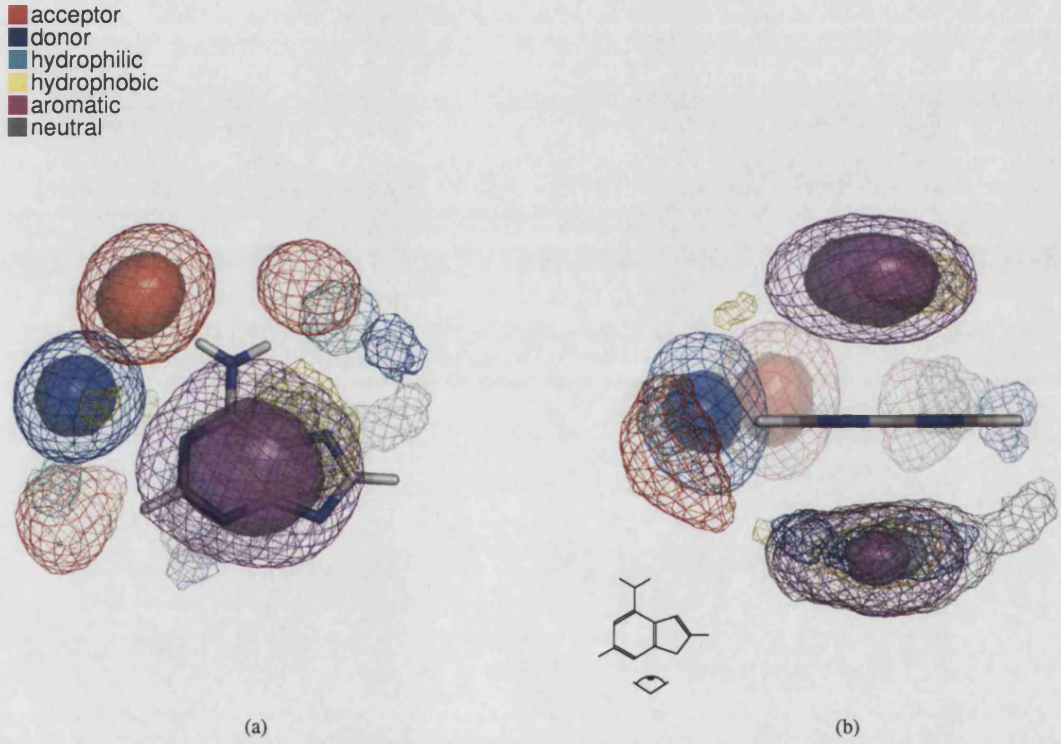

Figure 6.15: A composite picture of the adenine environments
Contours indicating the regions of highest propensity for each atom type, in a non-redundant dataset of 120 protein-adenine complexes. Mesh contours were calculated at a level of $\pi = 15$; semi-solid contours show $\pi = 30$.

6.5 Diversity of fragment environments

The concept of conservation has long been applied in the realm of sequence analysis (see Valdar (2002) and references therein), where analyses of multiple alignments of sequences belonging to a protein family is commonly used to delineate functionally important regions, or to identify sequence signatures diagnostic of the particular family being studied.

Several recent studies have combined conservation information from sequence and structure. A methodology known as 'evolutionary trace', was described by Lichtarge *et al.* (1996), and later refined by Pupko *et al.* (2002). These studies, while they also aim to produce a mapping of sequence position-specific conservation scores onto three-dimensional structure, may be distinguished from those mentioned above in that they derive their scores from a consideration of the phylogenetic relationships between the sequences. The paper of Ben-Tal and co-workers describes the application of their method to the SH2 domain, a component of an intracellular signalling cascade which is found in many proteins, and which recognises tyrosine-containing polypeptide fragments. They show that, in addition to the region of the domain surface which is involved in dimerisation, higher-than-average conservation scores are also found in the peptide-binding groove. The extent to which this is generally true for ligand-binding sites is still unclear. As mentioned previously, functional regions of proteins are often located in clefts which may be defined using purely geometric criteria. A problem which is encountered when applying cleft-detection methods is that the region of interest, if it is included in one of the resulting cavities at all, is typically restricted to a small fraction of its volume. Investigations are currently underway, therefore, to determine whether conservation scores can be used to 'zoom in' on the potential interaction sites within a cleft (F. Glaser, personal communication).

Valdar and Thornton describe a method of mapping residue conservation scores obtained from a multiple sequence alignment onto the three-dimensional structure of a representative protein from the family. They show that, considering residues on the surface of the protein, appropriately defined conservation scores are able to discriminate those regions which participate in subunit dimerisation (Valdar and Thornton, 2001a). In a later study (Valdar and Thornton, 2001b), the same authors report that conservation can also be used to distinguish between those subunit contacts in a crystal which are biologically important, and those which are merely due to crystal packing.

A slightly different approach involves mapping just the evolutionarily invariant *polar* residues onto a reference structure, then applying a spatial clustering procedure (Aloy *et al.*, 2001). The conserved clusters defined using this method were found to correctly identify the functional site of a protein (as defined by the SITE records in the PDB file) in around 80% of cases.

Local structural conservation has been studied in some detail for catalytic active sites. For many enzymes, a small number of residues can be identified as being responsible for the enzymatic function. By comparing the relative location of these residues in space, the extent to which their functional role places constraints on the local structure can be understood. A study of Ser-His-Asp catalytic triads among several convergently evolved groups of hydrolases, for example, found that the distances between the functional atoms of the Ser and Asp residues was within 1.4Å of the consensus distance over all examples analysed (Wallace *et al.*,

1996). A more recent study (Torrance *et al.*, 2005) showed that within most homologous enzyme families, the corresponding figure is below 1Å.

Similar studies of structural conservation of ligand-binding sites are more difficult. In enzymes, the same small number of residues are often clearly identifiable as being responsible for catalysing a particular reaction among proteins within - and sometimes between - homologous families. This permits residue equivalences to be unambiguously established between functional sites in different enzymes, thereby allowing them to be compared using standard geometrical measures such as RMSD. As has been previously stated, the situation is considerably less clear-cut for sites whose shared feature is not catalysis of a chemical reaction, but recognition of a particular chemical entity. Visual inspection of binding sites quickly reveals that there are far more ways to bind a given ligand than there appear to be for delivering efficient catalysis. The rest of this section is devoted to the development of a method for quantifying the extent to which this is so, and for visualising the regions of binding sites which tend to be the most variable.

6.5.1 Measures of diversity

6.5.1.1 Entropy

The concept of entropy was first introduced in 1865, and was defined as the amount of energy in a system which cannot be used to do work. During the course of studying thermodynamic transformations, Rudolf Clausius found that the introduction of this new quantity was required to explain why some transformations are reversible, and some are not: only those which do not result in an increase of entropy may be reversed. In 1877, Boltzmann looked at entropy from the standpoint of statistical mechanics, and redefined it in terms of the number of 'microstates' which a system may adopt, and which are consistent with its gross thermodynamic properties. Specifically, he defined entropy as

$$S = k\ln\Omega$$

where k is Boltzmann's constant and Ω is the number of microstates for the system (Atkins and de Paula, 2001). This leads to the idea of entropy as a measure of the amount of disorder within a system.

More recently, Shannon (1948) proposed a new definition of entropy for use in the analysis of information coding and transmission systems. The motivation for this new definition was to obtain a formula which, when applied to a source of information, would calculate the minimum channel capacity required to reliably transfer the data as a series of binary digits. The definition of *information entropy* of a discrete random event (as opposed to the thermodynamic entropy of a system discussed above) is

$$h(x) = -\sum_{i=1}^{k} p_i \log_2 p_i \tag{6.1}$$

where k is the number of possible outcomes for the event, and p_i is the probability of the i^{th} outcome. For instance, given a passage of text written in English, one could calculate the channel capacity necessary to transmit it by counting the occurrence within it of each letter of the alphabet. Assuming that the only punctuation in the text are spaces and full stops, we may then calculate its entropy as

$$H = -(p_a \log_2 p_a + p_b \log_2 p_b + \ldots + p_z \log_2 p_z + p_. \log_2 p_. + p_{space} \log_2 p_{space})$$

where p_a is the frequency of occurrence of the letter 'a' divided by the length of the passage.

Although originally defined for a particular purpose, Shannon's entropy measure tells us something about the nature of the signal - its *information content.* More specifically, it is a measure of the amount of information in a signal, over and above that which is strictly determined by - and hence predictable from - its inherent structure. Returning to the example of text, imagine an alphabet with only one letter, 'a'. The message 'aaaaa' written in this alphabet conveys no information, since we could have predicted its content perfectly prior to receiving it. *Any* message written in English, on the other hand, is more informative (in an information theoretic sense), since we cannot anticipate it from the relative frequencies of the different letters of the alphabet. It should be clear from the mathematical definition of information entropy given above that, for an alphabet with a given number of letters, the maximum entropy is reached when all are equally probable, and that, adding extra letters (with none-zero occurrence frequencies) to the alphabet will always increase its information content.

It is interesting to note that, although at first sight all that is shared by the information theoretic and thermodynamic formulations of entropy is a name, in fact the connection is much deeper. Given a uniformly distributed discrete random variable X with k possible values, let us ask what is the probability, after p observations of X, of seeing the distribution $(f_1, f_2 \ldots f_k)$, where f_i is the number of occurrences of outcome x_i. This probability follows a multinomial distribution

$$p = \frac{\Omega}{N}$$

where Ω is the number of combinations of outcomes fitting the observed distribution

$$\Omega = \frac{p!}{f_1! f_2! \ldots f_k!}$$

and N is the number of all possible outcomes, $N = k^p$. Applying the statistical mechanical formulation, the entropy of the system is given by the logarithm of the number of states, Ω. As the number of observations p tends towards infinity, $p!$ can be approximated by Stirling's approximation

$$\ln k! \cong k \ln k - k$$

Taking the logarithm of Ω, we thus obtain

$$\ln \Omega = -p \sum_{i=1}^{k} p_i \ln p_i$$

which is linearly related to the definition of H given in equation 6.1.

Entropy-based scores have been used previously to quantify the degree of conservation at each position of a multiple sequence alignment (Sander and Schneider, 1991, Gerstein and Altman, 1995). In the present study, a gridpoint in the space surrounding the ligand may be thought of as analagous to a column in the sequence

alignment, and each individual binding site to one of its rows. Although the binding site is characterised at each position by a k-dimensional vector of real numbers (one from each property map), we can easily convert each vector into a single symbol by applying a threshold value. If any of the k property maps have a value above half of the peak value ($\frac{a}{2}$ in figure 6.6a), then the gridpoint is labelled as possessing this property. If none of the maps is above the cutoff, the gridpoint is labelled as void. In this way, all points within the Van der Waals sphere of a given atom are assigned with the atom class to which it belongs. Therefore each gridpoint is assigned one of $k+1$ possible symbols: k different properties (*e.g.* acceptor, donor, aromatic *etc.*) and one symbol representing the absence of any atom type at that locus.

Once the set of n binding sites are represented in this way, it is simple to compute an entropy score for each gridpoint in the envelope region surrounding the fragment of interest. In order to ensure that the score is bounded by $[0,1]$, it is normalised as follows:

$$h(x) = \frac{-1}{\min(n, k+1)} \sum_{i=1}^{k+1} p_i \log_2 p_i \tag{6.2}$$

Figure 6.17 shows examples of entropy scores calculated for different combinations of symbols. Points at which no atom is present in any of the sites score zero entropy (a), as do points at which every site contains the same atom type (b). At the other end of the scale, points which exhibit the maximum possible diversity score 1.0. In this simple example, the number of sites is equal to $k+1$, so this case corresponds to each site having a different label at the gridpoint (h). Cases (c-g) illustrate the effect of increasing symbol diversity on the resulting entropy score. Note that the score is agnostic to the actual identity of the symbols, as shown by the fact that cases (d-f) all score the same. The entropy score therefore treats all properties (symbols) as orthogonal, whereas we know that some atom classes are more similar than others. Moreover, we may feel that column (f) is less diverse than (d) or (e), containing as it does only one atom type; the entropy score, however, treats the void symbol equally with all other symbol types.

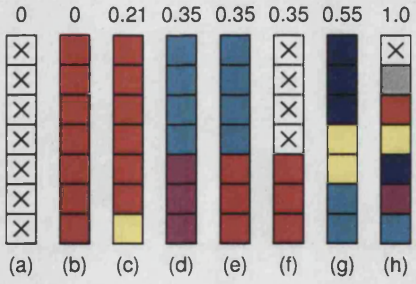

Figure 6.16: Example of entropy scoring
Each column represents a gridpoint in the fragment environment; each row represents a particular binding site. At each point in space, each site is classified either as containing an atom belonging to one of the six classes (colours - see table 6.1), or is marked as void (crosses). Values at the top of each column are normalised symbol entropy scores, calculated as described in the text.

6.5.1.2 Chemical diversity

By utilising the atom class dissimilarity matrix **D** calculated previously (table 6.2), we can formulate a diversity score which takes into account the degree to which, at any given point in space, different sites expose different chemical properties, rather than just different atom classes. At a point in space, x, let the i^{th}

site be represented by a k-dimensional 'property vector' $\mathbf{v}_i(x)$. If this point coincides with the centre of an atom, for example, this vector would take the form

$$v_i(x) = \begin{pmatrix} 0 & a & 0 & 0 & 0 & 0 \end{pmatrix}$$

where the index of the non-zero element corresponds to the atom class to which the atom belongs.

Using the matrix $\mathbf{M}$ which results from MDS analysis of the atom class dissimilarity matrix $\mathbf{D}$, we can compute the dissimilarity between two property vectors:

$$d(\mathbf{v}_i, \mathbf{v}_j) = \|\mathbf{M}\mathbf{v}_i - \mathbf{M}\mathbf{v}_j\|$$

If both the vectors $\mathbf{v}_i(x)$ and $\mathbf{v}_j(x)$ originate from gridpoints which coincide with centres of atoms from classes p and q, the value of this distance will simply be the $a\mathbf{D}_{pq}$ - in other words, the peak map value multiplied by the dissimilarity between these two atom classes.

In order to compute the chemical diversity at a particular gridpoint x, the following procedure is adopted.

1 The characteristic of each binding site at the gridpoint is represented by a single symbol, by applying a threshold in the same way as for the entropy calculations above.

2 For each of the m binding sites for which this symbol is not void, a property vector $\mathbf{v}(x)$ is composed. All values in this vector are set to zero except that which corresponds to the symbol representing the site, which is set to 1. For example, a gridpoint which was located near to an atom of the acceptor class would be represented by the property vector

$$\begin{pmatrix} 1 & 0 & 0 & 0 & 0 & 0 \end{pmatrix}$$

the acceptor class being arbitrarily the first among the six GAMUT atom classes.

3 Each property vector $v(x)$ is pre-multiplied with the matrix M, thus transforming it into the projection space:

$$\mathbf{w}(x) = \mathbf{M}\mathbf{v}(x)$$

4 The chemical diversity of the gridpoint is calculated as the average distance of the $\mathbf{w}$-vectors from their mean:

$$d(x) = \begin{cases} 0 & \text{if } m = 0 \\ \dfrac{2}{m}\sum_{i=1}^{m} \|\bar{\mathbf{w}}(x) - \mathbf{w}_i(x)\| & \text{otherwise} \end{cases} \tag{6.3}$$

The factor of 2 is applied in order that the score should be bounded by $[0, 1]$. To see why this is the case, consider a gridpoint at which half of the binding sites are labelled with the hydrophilic atom class, and half with the aromatic class. The dissimilarity value between these two classes is the largest in the distance matrix (1.0), so this column should score the maximum possible value. Since each $\mathbf{w}$ vector will be located at a distance of 0.5 from $\bar{\mathbf{w}}$, multiplying by 2 scales the score to be bounded by

$[0,1]$.

Figure 6.17 shows chemical diversity scores calculated for a number of hypothetical environment gridpoints. While it improves on the problems discussed in reference to the entropy score, the chemical diversity index has its own problems. Conspicuously, being based on calculation of a mean value, it is sensitive to outlying values, as shown by the value in column (c). Although this column is predominantly composed of acceptor classes, one hydrophobic symbol is sufficient to increase the diversity score from zero to 0.44. In addition, it is clear that, at gridpoints where most sites are devoid of atoms, the effect of a small number of atoms from dissimilar classes will be amplified.

However, cases (d-f) are more reasonably distinguished by the diversity score. At position (d), the binding sites have either hydrophilic or aromatic atoms, which are the most chemically dissimilar (table 6.2), resulting in a high diversity score. At (e), on the other hand, although the symbol diversity is the same, chemically the sites are more similar, as reflected by the score. Position (f) illustrates the difference in the response of the two scores to void values: here, the four void sites are ignored, and since all non-void sites have the same atom type, the chemical diversity is zero.

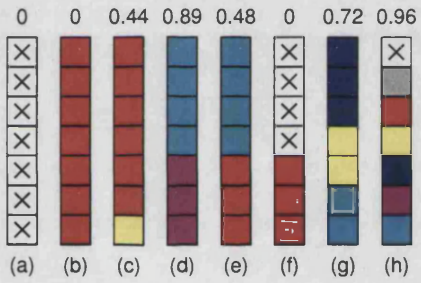

Figure 6.17: Example of chemical diversity scoring
Each column represents a gridpoint in the fragment environment; each row represents a particular binding site. At each point in space, each site is classified either as containing an atom belonging to one of the six classes (colours - see table 6.1), or is marked as void (crosses). Values at the top of each column are normalised chemical diversity scores, calculated as described in the text.

6.5.1.3 A combined diversity score

In order to play up the relative strengths of each score while compensating for their weaknesses, therefore, we define a new index which combines the two. In so doing, we follow a similar approach to that described by Valdar (2002). In this paper, the author was interested in comparing a range of scores for quantifying the degree of conservation of each column in a multiple sequence alignment. He identified three components of positional variability - namely symbol diversity, stereochemical diversity of the amino acids present, and the number of gaps. Choosing an appropriate measure for each of these quantities, bounded by $[0,1]$, the degree of conservation of a given column is then defined as

$$C(x) = (1-t(x))^{\alpha}(1-r(x))^{\beta}(1-g(x))^{\gamma}$$

where t, r and g represent the three quantities listed above, and where α, β and γ are parameters used to weight their relative importance.

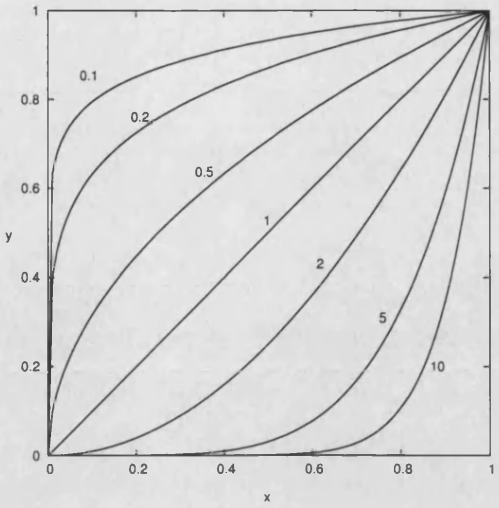

Figure 6.18: Effect of exponential parameters on components of the combined score
The graph shows plots of the function $y = x^{\alpha}$ for different values of the parameter α (shown adjacent to each curve).

In a multiple sequence alignment, a large number of gaps at a given position suggests that the residues at this point can be deleted without significantly impairing the protein function. As such, gappy columns should be considered to be less well conserved. The situation is quite different when considering binding sites: here, the absence of an atom at a particular point in space may well be a positively selected trait if, for example, it permits access to a functional group which is to participate in a reaction catalysed by the protein. It is not appropriate, therefore, to penalise gaps in the same way as they are in the sequence conservation score.

Following the approach of Valdar, the binding site diversity index used here is defined as follows

$$D(x) = (h(x))^{\alpha}(d(x))^{\beta} \tag{6.4}$$

where $h(x)$ and $d(x)$ are defined as per equations 6.2 and 6.3 respectively.

As shown in figure 6.18, values of the exponents greater than 1 serve to diminish the relative importance of changes in the value of their associated score which occur towards the lower end of the range; small changes in the score once it approaches 1 have a much greater impact on the output. Conversely, exponents less than 1 mean that changes in the score at the lower end of its range have a greater effect. In this chapter, parameters of $\alpha = 1.0$ and $\beta = 1.0$ have been used. It is recognised that this is a somewhat arbitrary choice; however, until the behaviour of the entropy and chemical diversity scores is better understood, there is no *a priori* reason for weighting either one more heavily than the other.

6.5.2 Diversity of unrelated adenine-binding sites

The entropy and diversity scores were calculated for the non-redundant dataset of 120 adenine binding sites used previously. Upon inspection of the density contours for each of these scores, it is immediately apparent that they are each sensitive to quite distinct aspects of binding site diversity.

Figure 6.19 shows isocontours for the entropy score, overlaid on the adenine-contacting atoms from all 120

sites. The first observation is that the entropy score is clearly dependent on the local 'crowding' of atoms: the higher entropy values are restricted to regions of space which are more frequently populated with contacts. This is to be expected given the way the the score is defined, since gridpoints where a high fraction of sites are classified 'void' obtain a low entropy score. The most noticeable high-entropy regions are those contacting the two faces of the adenine ring, with approximately equal degrees of disorder on both sides. In contrast, the areas around the rim of the ring tend to have quite low entropy scores, with only a few localised regions where the density values are above 0.3.

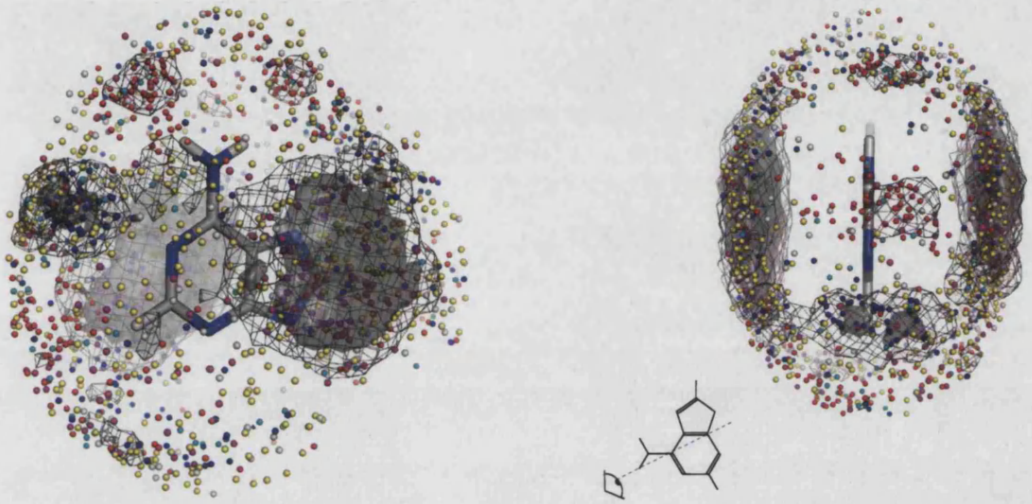

(a) (b)

Figure 6.19: Depiction of entropy scores for adenine environments
Mesh isocontours were calculated at a level of 0.3; semi-solid contours at 0.4. Adenine-contacting atoms from the binding sites are shown as spheres, colour-coded according to the atom class to which they are assigned (table 6.1).

Contact density is not the sole determining factor of the entropy score, however. This is evidenced by comparing the contours around the acceptor atoms *cis* to N6 and the donors proximal to N1. These two regions are similarly densely populated, but the latter has much higher atom type diversity. Inspection of the clusters of atoms at these points reveals that this is a good reflection of the type of contacts which occur: while around the N6 amine hydrogens, sites tend to be either void or occupied by acceptor atoms, next to N1, while there is a high concentration of donor contacts, we also see considerable numbers of other atom types.

Figure 6.20 shows contours describing the distribution of chemical diversity scores for the same dataset of adenine environments. It is immediately apparent that, in contrast to the entropy scores, the regions where this index is highest are those around the rim of adenine, with the two faces scoring relatively low values. Although it is difficult to see in figures 6.20a and 6.20b, interactive inspection of these distributions on a graphics workstation shows that there are clear 'holes' in the diversity contours at locations where contacts are made to the polar atoms of the adenine fragment. Most noticeable among these is a distinct region of low diversity at the *cis* position of N6, with a less well-pronounced reduction in scores around donors to N1 (figure 6.20c).

We can rationalise these findings by considering the nature of the interactions which are made to the face and the edges of adenine. Contacts to the faces can be characterised as being non-specific and diffuse: that is, the

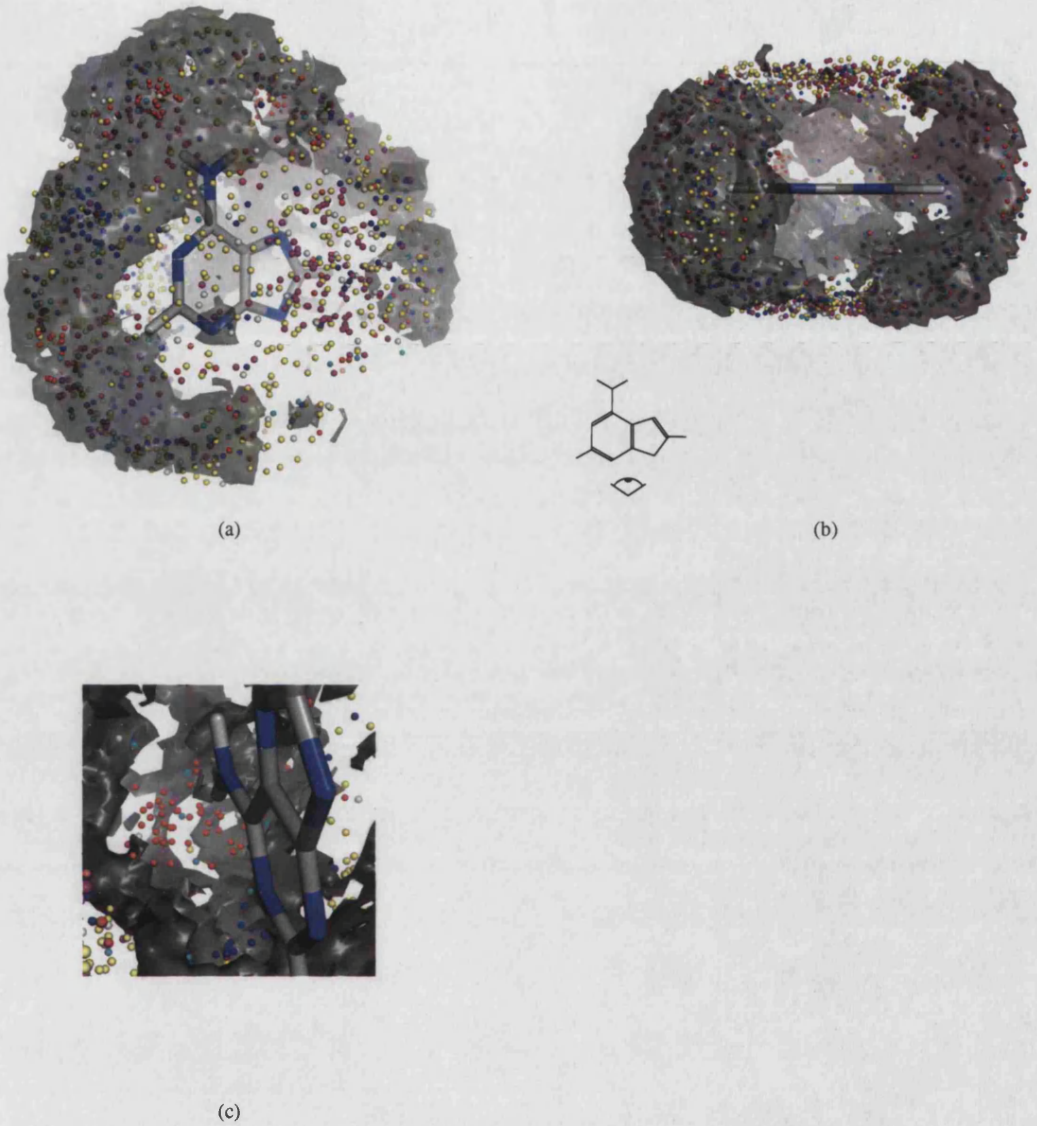

Figure 6.20: Depiction of chemical diversity scores for adenine environments
Isocontours were calculated at a level of 0.65. Adenine-contacting atoms from the binding sites are shown as spheres, colour-coded according to the atom class to which they are assigned.

geometrical requirements on the non-polar interactions which take place at these locations appear to be fairly loose. Therefore, even when comparing a group of sites, all of which contain an aliphatic side-chain packing against one of the adenine faces, the precise locations of the atoms in this side chain may vary considerably with respect to the ligand. Moreover, according to the MDS analysis presented previously, it appears that the two atom classes which predominantly contact the face regions (hydrophobic and aromatic) are fairly similar in their chemical characteristics. Taking these observations together, it is to be expected that, from the point of view of the entropy score, the face regions will evince a high degree of diversity, but when the atomic neighbourhood of the ligand is considered, albeit indirectly, in terms of its chemical characteristics, the perceived variance will be lower.

Conversely, around the rims, we see, as expected, several spatially compact clusters of polar contacts. As shown by Nobeli *et al.* (2001), these serve in part to distinguish between similarly-shaped nucleotide

bases during molecular recognition, and therefore should be both specific and accurate. The distribution of chemical diversity scores around the rim of the adenine ring suggests that, while there is a high degree of apparent variability in general, there are distinct regions where contacts to the ligand, if they are made, are of a particular type, with little tolerance for non-specific interactions.

Next we consider the effect of combining the entropy and diversity scores according to equation 6.4. A difficulty faced in doing so is that, while the relative simplicity of the two separate scores means that they can be understood in isolation, gaining an intuitive feel for what a particular value of the combined score *means* is more difficult. In addition, it is clear that the behaviour of the combined score will be quite sensitive to the choice of the two parameters α and β. Contour plots obtained from the combined score (with $\alpha = \beta = 1.0$) are shown in figure 6.21.

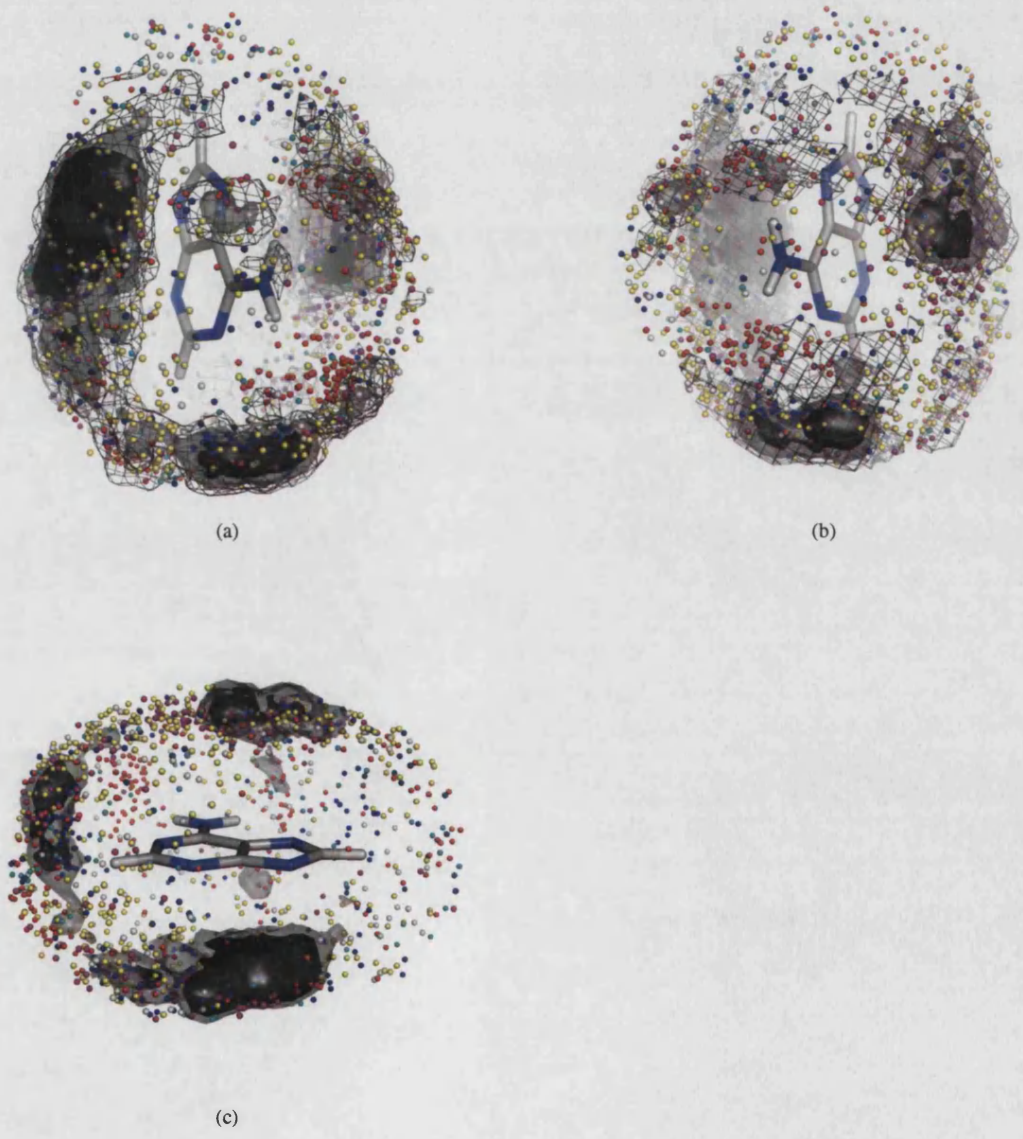

Figure 6.21: Depiction of combined diversity scores for adenine environments
Mesh isocontours were calculated at a level of 0.15, light semi-solid contours at 0.20 and dark semi-solid contours at 0.25. Adenine-contacting atoms from the binding sites are shown as spheres, colour-coded according to the atom class to which they are assigned.

Overall, the entropy score appears to dominate the combined results; interactive exploration of the density contours suggest that the variance in entropy scores is somewhat higher that in the diversity values. Nevertheless, the addition of the chemical diversity information has had some noticeable effects on the contour plots. Combined scores around the *cis* N6 acceptors are the lowest among the densely populated regions of the binding sites, reinforcing the intuitive impression that this interaction is among the most conserved. Conversely, while the areas around the C2 hydrogen atom have fairly low entropy scores, the presence in this region of several chemically diverse atom classes results in a relatively high combined diversity score.

Looking at the contours around adenine face contacts, we see that, although the two faces were fairly equal in terms of entropy scores, regions which abut the Y face have considerably higher combined diversity scores than those on the X face. This may be explained in part due to the previously noted high propensity for aromatic rings to stack against the X face, with a lower tendency in this region for aliphatic contacts. It appears that apolar contacts to the X face are slightly more homogeneous in nature, although inspection of the 'raw' coordinate superpositions of the binding sites shows that this is only a weak distinction.

In order to better understand the distribution of combined diversity scores around adenine, it is useful to map these values onto the fragment surface using the method described in §6.3.5. Plots of the surfaces, with each facet colour-coded according to the diversity score of its neighbourhood, are shown in figure 6.22. The most striking observation is the disparity in diversity scores between the two faces of the ring, with the Y face (figure 6.22a) being annotated with values peaking at around 0.4; values on the X face (figure 6.22b) are all below 0.3.

These plots recapitulate the result that the rim environment is less diverse than the regions which contact the ring faces. It is possible to see some slight differences between different regions around the rim, such as the higher scores around the *trans* N6 hydrogen than around the *cis* hydrogen, and the elevated values on the surface of the N1 atom (figure 6.22c). However, this type of visual analysis is hampered both by the difficulty of capturing the gradations of a score using only colour-coding, and by the fact that the more directional nature of polar interactions means that differences in diversity scores around the rim are projected onto relatively smaller surface areas than are those across the faces. In summary, it is extremely difficult to capture this type of three-dimensional information on the page, although the graphical techniques used here are considered to be sufficiently informative to convey at least the most important points.

6.5.3 Diversity of related adenine binding sites

Just as, in the previous chapter, the question "Do ligands bound to related proteins adopt more similar conformations than those bound to unrelated proteins?", here we ask whether the environments of adenine in related proteins are significantly more similar than those found in the non-redundant dataset.

The method used to do this is simple: the combined diversity scores mapped onto the fragment surface as in the previous section, are simply integrated across the adenine moiety to give an overall diversity score for any given collection of binding sites. Comparison of this value obtained from the non-redundant dataset described above, with those obtained by comparing binding sites in the same cluster, will be used to address

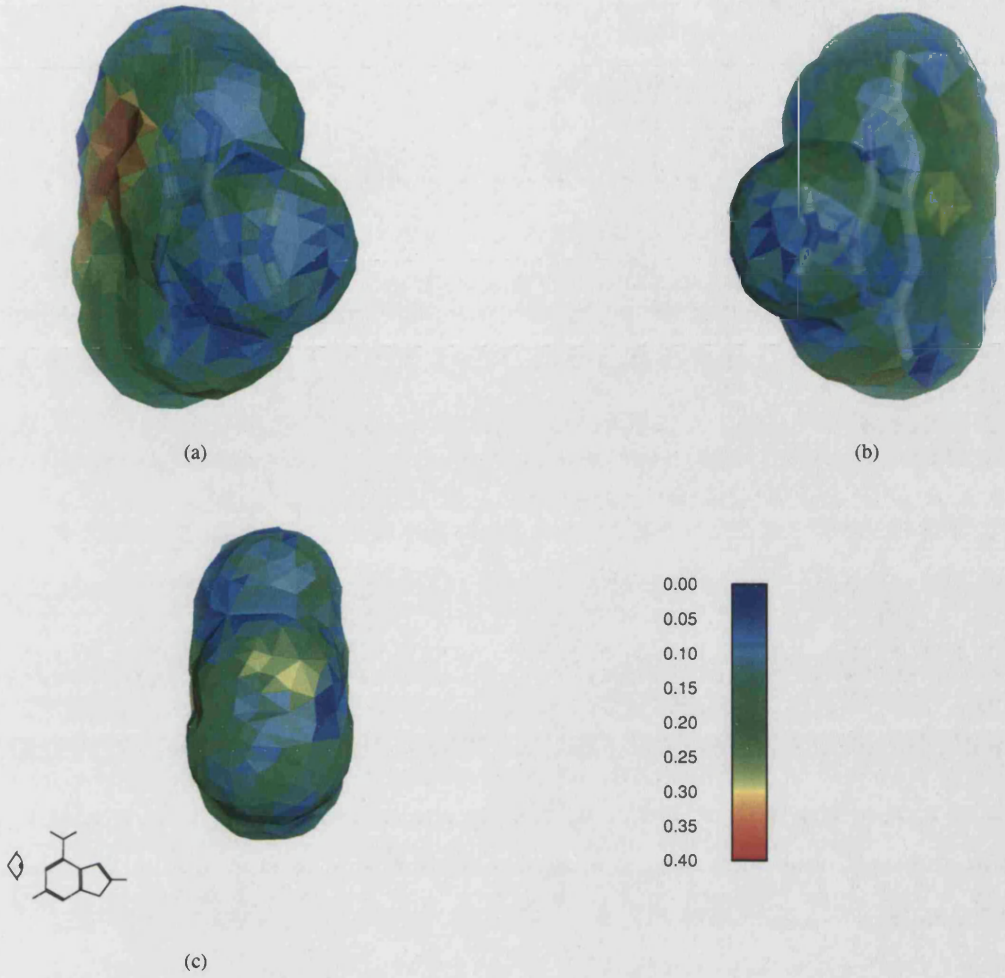

Figure 6.22: Combined diversity scores mapped onto adenine surface
In figures (a) and (b), the orientation of the ligand surface is shown by faintly overlaying a stick representation of adenine.

the question posed above. Before so doing, however, we must determine whether there is any dependence of this overall diversity score on the number of binding sites used to calculate it, since the number of sites in any one cluster is significantly fewer than the number of cluster representatives.

To do this, a random sampling procedure was devised. From the set of 120 binding sites in the non-redundant dataset, a subset of n sites was chosen at random, where n ranges from 2 to 120. The overall diversity measure was calculated for this subset of binding sites, and this was repeated 25 times. From these 25 values, the mean and variance of the overall diversity score was calculated for each n. In addition, the entropy and chemical diversity scores were integrated over the fragment surface independently, allowing any sample size dependence in the combined score to be deconvoluted into its two component parts. The results of this experiment are plotted in figure 6.23.

Both the entropy and diversity measures decline as decreasing numbers of binding sites are sampled. As this number drops below 7, the entropy score climbs once again, due to the effect of the $\min(n, k+1)$ term in the denominator of its correction factor (see equation 6.2). The monotonic decrease of the combined score as the sample size is reduced, is not a particularly desirable characteristic for a descriptive statistic: we would prefer

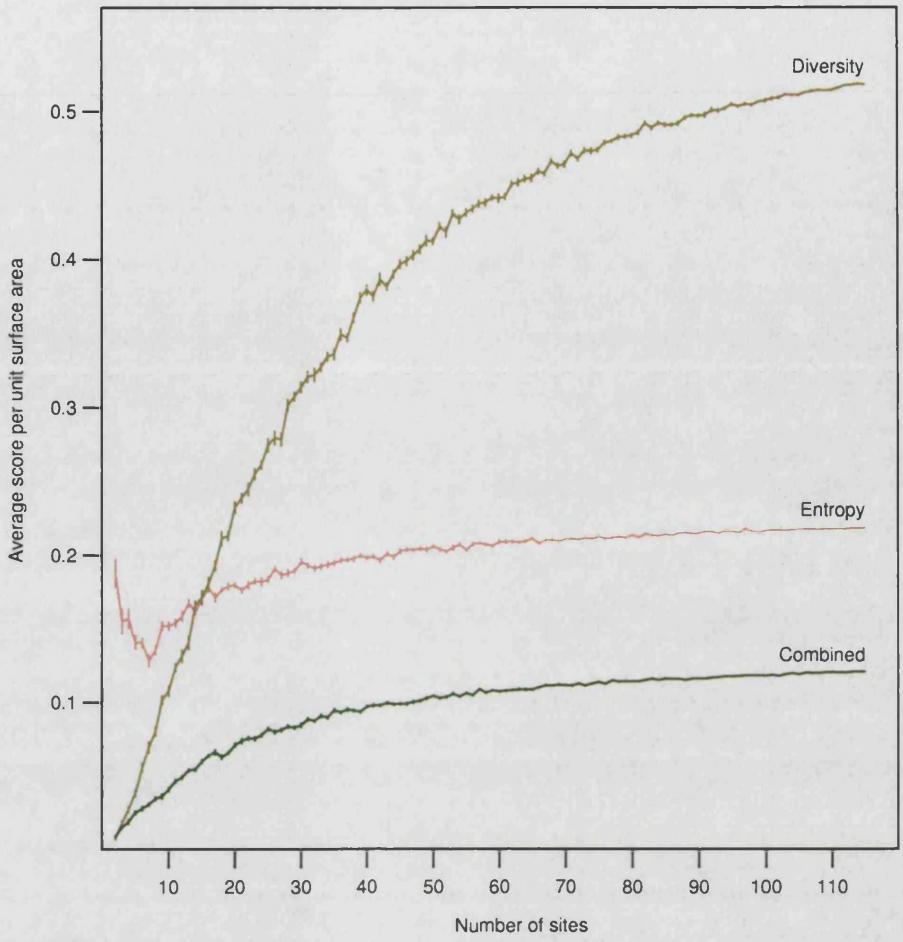

Figure 6.23: Sample size-dependence of the binding site diversity indices for adenine
The plot shows the dependence of the entropy, chemical diversity and combined score values, integrated over the adenine surface, on the number of binding sites used in the calculation.

it to remain fairly constant, as long as the number of binding sites used was above a reasonable minimum (say, around 10). However, for the purposes of this investigation, it is not particularly problematic - we must simply take it into account when comparing the scores obtained from the cluster representatives, with those computed within each cluster.

Table 6.3 summarises the clusters from the adenine dataset which have 10 or more members, and figure 6.24 shows the binding sites in each cluster, superposed on the adenine ring. Although the picture is complicated by the fact that some clusters have more members than others, it is apparent that the amount of structural variability in each not uniform. For instance, although the image of cluster 1, being the largest, appears at first sight to be very 'cluttered', closer inspection shows that the distribution of contacts to the ligand are far from random. Cluster 2, on the other hand, although smaller, contains adenine binding sites which are far more diverse. Moving to smaller clusters, we see that cluster 3 and 4 show moderate variability, 5 slightly more so, and that the kinases in cluster 6 have very well-conserved adenine recognition pockets. Similarly, the HSP90 domains in cluster 7 show little variability, while clusters 8 and 9 are slightly more disordered.

Cluster	Size	Ligands	Domains		Functions
1	94	NAD(P), FAD	3.40.50.720	NAD(P)-binding Rossmann-like	Dehydrogenases; reductases
2	48	ATP, ADP	3.40.50.300	P-loop containing NTP hydrolases	Kinases; transferases
3	30	FAD	3.50.50.60	FAD/NAD(P)-binding domain	Mostly ferredoxin reductase family
4	26	SAM	3.40.50.150	Rossmann	Methyltransferases
5	20	ATP, AMP	3.40.50.620	Rossmann	Class I tRNA synthetases; adenylyltransferases
6	12	ANP, ATP, ADP	3.30.200.20 1.10.510.10	Phosphorylase Kinase domain 1 Phosphotransferase domain	Kinases
7	11	ADP, ANP	3.30.565.10	HSP90	Heat shock proteins; DNA gyrase/topoisomerase; kinases
8	10	ADP	3.30.1490.20 3.30.470.20	Transferase ATP-grasp fold	Ligases; transferases
9	10	ATP, AMP	3.30.930.10	Bira Bifunctional Protein	Class II tRNA synthetases

Table 6.3: Summary of the adenine binding site clusters
For each cluster, 'Size' indicates the number of members, and 'Ligands' shows the adenine-containing molecules which predominate in this group. The homologous superfamily level annotations of domains making up the binding sites in each cluster are shown along with their associated CATH numbers. Where the proteins in a cluster have a small range of functions, these are listed.

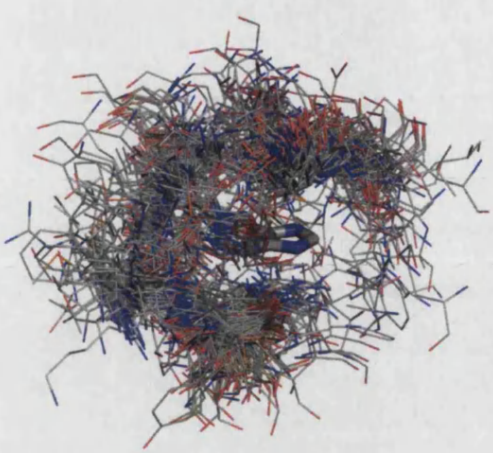

(a) Cluster 1 (94 members)

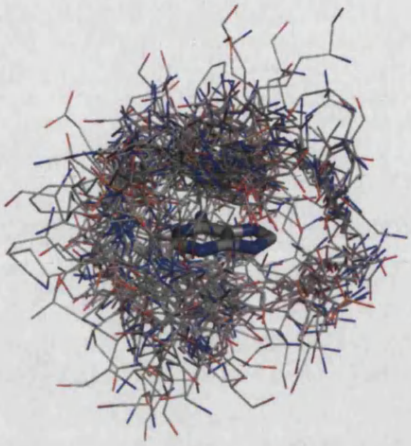

(b) Cluster 2 (48 members)

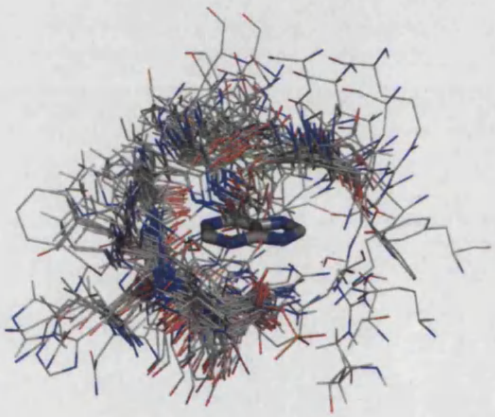

(c) Cluster 3 (30 members)

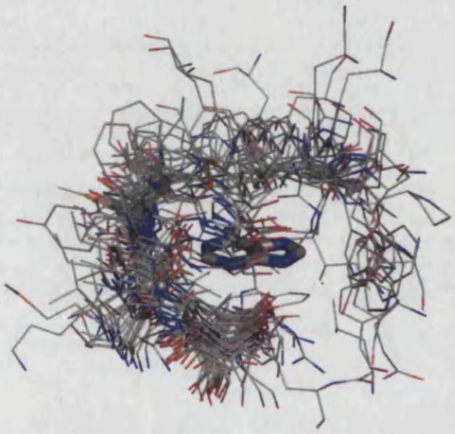

(d) Cluster 4 (26 members)

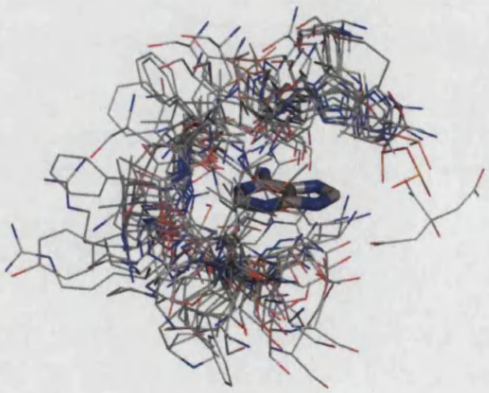

(e) Cluster 5 (20 members)

(f) Cluster 6 (12 members)

Figure 6.24: Diversity in adenine-binding site structure within superfamilies
The adenine-contacting residues from five sites randomly selected from the nine adenine-binding site clusters in table 6.4 are shown, demonstrating the different degrees of structural variability seen in adenine-binding sites from different superfamilies.

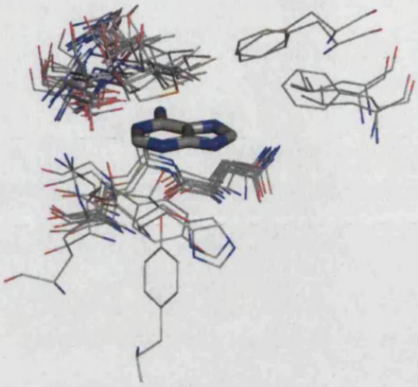

(g) Cluster 7 (11 members)

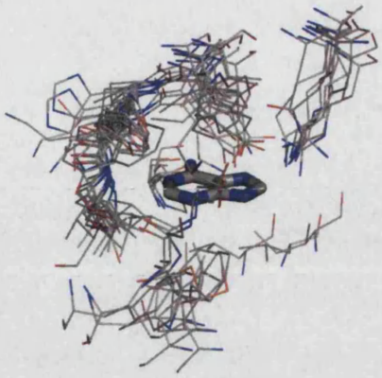

(h) Cluster 8 (11 members)

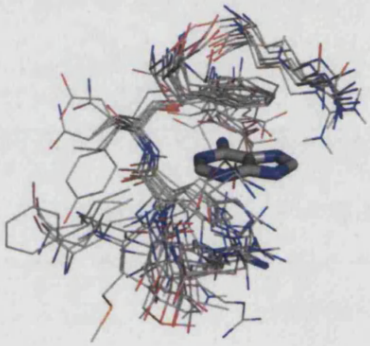

(i) Cluster 9 (10 members)

Figure 6.24: Diversity in adenine-binding site structure within superfamilies (continued)

Values of each of the three scores (entropy, chemical diversity and combined) calculated for each of these clusters are shown in table 6.4, alongside the mean and variance from the sampling experiment with the appropriate value of n. Figure 6.25 shows these scores plotted onto the graph illustrating the sample size dependency for each score type during random sampling. Making the assumption that the diversity values obtained in the sampling experiment follow a normal distribution, a Z-value is calculated for each score, for each cluster.

Looking first at the combined diversity scores, we see that they are in broad agreement with our intuitive notion of the degree of variation in each cluster. In all but two cases, the Z-score is negative, indicating that the binding sites in these clusters are significantly less variable than would be expected by sampling the same number of sites from the non-redundant dataset. The largest negative Z-score is for cluster 1, indicating that, although it is not immediately apparent by looking at the superposition plots, this cluster has the least diversity in the adenine binding pocket. Next are the scores for clusters 6 and 7, which were identified visually as bein particularly well conserved.

Cluster	No. of sites	Score used	Average score per unit area (Δ)	Random sampling Mean (μ)	Random sampling Standard error (SE)	Z†	
1	94	entropy	0.2062	0.2165	8.36×10^{-4}	-12.3	***
		diversity	0.3670	0.5019	1.23×10^{-4}	-1023.6	***
		combined	0.0907	0.1175	4.22×10^{-4}	-63.5	***
2	48	entropy	0.2244	0.2047	1.61×10^{-3}	12.2	***
		diversity	0.3655	0.4068	3.14×10^{-3}	-13.2	***
		combined	0.1086	0.1011	1.09×10^{-3}	6.88	***
3	30	entropy	0.1927	0.1960	2.35×10^{-3}	-1.4	
		diversity	0.1890	0.3140	3.92×10^{-3}	-31.9	***
		combined	0.0614	0.0846	1.85×10^{-3}	-12.6	***
4	26	entropy	0.2036	0.1910	1.98×10^{-3}	6.4	***
		diversity	0.1791	0.2797	4.92×10^{-3}	-20.4	***
		combined	0.0543	0.0800	1.50×10^{-3}	-17.1	***
5	20	entropy	0.1906	0.1801	1.87×10^{-3}	5.6	***
		diversity	0.2260	0.2326	4.09×10^{-3}	-1.6	
		combined	0.0810	0.0710	1.69×10^{-3}	5.92	***
6	12	entropy	0.1198	0.1590	3.70×10^{-3}	-10.6	***
		diversity	0.0118	0.1317	4.56×10^{-3}	-26.3	***
		combined	0.0040	0.0490	1.48×10^{-3}	-30.4	***
7	11	entropy	0.1005	0.1544	2.90×10^{-3}	-18.6	***
		diversity	0.0303	0.1238	3.14×10^{-3}	-29.8	***
		combined	0.0128	0.0464	1.26×10^{-3}	-26.7	***
8	11	entropy	0.1653	0.1544	2.90×10^{-3}	3.76	**
		diversity	0.0576	0.1238	3.14×10^{-3}	-21.1	***
		combined	0.0248	0.0464	1.26×10^{-3}	-13.3	***
9	10	entropy	0.1340	0.1523	3.08×10^{-3}	-5.9	***
		diversity	0.0406	0.1079	3.95×10^{-3}	-17.0	***
		combined	0.0156	0.0408	1.77×10^{-3}	-14.2	***

Table 6.4: Comparison of environment diversity within and between clusters of adenine binding sites

(†) $Z = \frac{\Delta - \mu}{SE}$

In two cases, however (2 and 5), the Z-score is positive, indicating that the binding sites are significantly *more* diverse than groups of sites randomly sampled from the non-redundant set. It is interesting to note that adenine cluster 5, consisting primarily of ATP/AMP molecules bound to class I tRNA synthetases and adenylyltransferases, corresponds roughly to cluster 3 from the ATP dataset. In the previous chapter, it was shown in §5.6.2 that this cluster showed significantly high levels of variation in the ATP conformation. Proteins belonging to these families, therefore, can be considered to be among the most variable in terms of their ATP binding sites, from both a ligand conformation perspective and when comparing the binding sites themselves.

Cluster 2, on the other hand, corresponds to ATP cluster 1. The conformational diversity shown by this group of ligands, although high, was not found to be statistically significant. Therefore we find that this group of proteins tends to bind the ligand in the same overall conformation, but stabilises it using a different

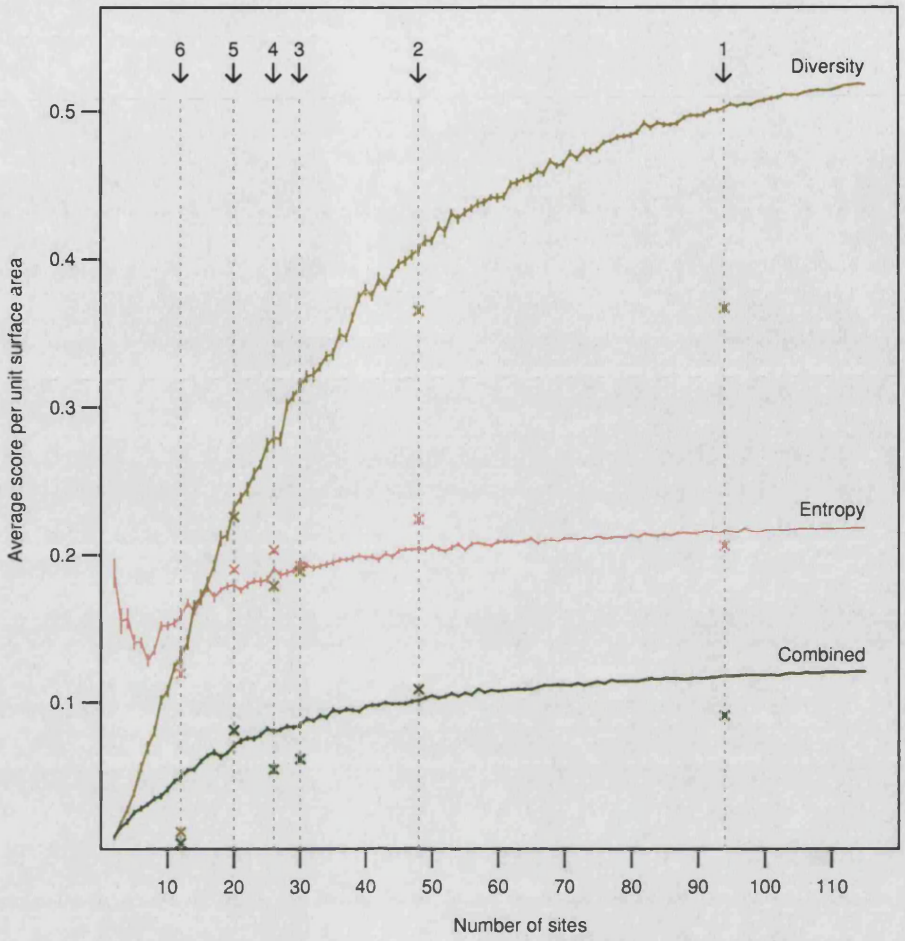

Figure 6.25: Diversity scores for adenine clusters compared to results of random sampling
Diversity scores for the six largest adenine clusters (see table 6.4) are shown in comparison to the values which were obtained in the random sampling experiment.

complement of interactions in different proteins.

Inspecting the entropy and chemical diversity scores for each cluster reveals an interesting observation: in all cases, the Z-scores for the chemical diversity index are negative. This appears to show that, even in clusters which are highly variable overall, a conserved pattern of chemical interactions is presented to the ligand. In other words, while the types of atoms contacting the ligand may change due to mutations in the binding site, and while in particular, the precise spatial location of non-directional (hydrophobic) contacts can vary, the chemical characteristics of the binding pocket are not so drastically altered. This is in keeping with our expectation of how binding sites may vary during evolution: the interactions which are necessary for molecular recognition must be conserved, while the remainder of the site - its structural scaffold - is free to undergo changes as long as these do not significantly alter the gross shape of the pocket.

6.5.4 Diversity of environments for different fragment types

Having asked how binding sites vary during evolution, we can now apply the diversity scoring method to a different problem: is the variation among *unrelated* binding sites for one fragment similar to that among sites specific for a different fragment? Given the widely varying biological roles played by ligands (§1.1.1), we

would expect their recognition pockets to be under quite different constraints. Where a fragment is usually used as a binding 'anchor', for example, its binding sites may be fairly similar, having evolved under one primary constraint - to recognise and bind the fragment tightly. On the other hand, those cofactor fragments which frequently play an active role in enzymatic catalysis would be expected to be found in quite diverse environments, according to which substrate was bound by any one protein.

To investigate this, the same procedure used to generate the adenine binding site dataset (see §4.2) was applied to create datasets of environments of guanine, nicotinamide and isoalloxine. This resulted in 35, 27 and 26 clusters respectively. Using the same protocol as described above for the adenine binding site clusters, the overall diversity scores obtained from the cluster representatives of each fragment was compared to that calculated from randomly selected groups of the same number of adenine sites. The resulting Z-scores therefore show whether the binding sites for each fragment are more or less variable overall than those for adenine. The results are shown in table 6.5.

Fragment	No. of sites	Average score per unit area (Δ)	Random sampling		$Z^{\dagger}$
			Mean (μ)	Standard error (SE)	
Guanine	35	0.0987	0.0947	1.55×10^{-3}	2.58 **
Nicotinamide	27	0.1052	0.0814	1.56×10^{-3}	15.3 ***
Isoalloxine	26	0.1314	0.0800	1.50×10^{-3}	24.3 ***

Table 6.5: Comparison of environment diversity scores of three different fragments
Combined diversity scores are compared against those calculated for adenine using the method described in the text.
(†) $Z = \frac{\Delta - \mu}{SE}$
(**) $p < 0.01$, two-tailed
(***) $p < 0.001$, two-tailed

The environments of all three fragments are found to be more diverse than those of adenine. Of the three, guanine shows only slightly more variability in its binding sites than adenine, while nicotinamide and isoalloxine are significantly more diverse. This is in agreement with the expectations outlined above - we may expect that a relatively small number of recognition strategies for binding adenine or guanine may have been selected during evolution, whereas the need to bind a variety of substrates in proximity to the redox group would necessitate greater binding site diversity around nicotinamide or isoalloxine.

These results suggest that knowledge-based binding site prediction methods may have more success with some ligand types than others. Moreover, their applicability in terms of function prediction may well be limited to fairly broad proclamations: while we might reasonably expect to be able to predict that a given protein binds, say, an NAD cofactor, and therefore is likely to be a redox enzyme, determination of its particular substrate specificity may be more difficult, and may well be better approached using docking methods.

6.6 Concluding remarks

This chapter has considered the structural and chemical variability exhibited by the regions of ligand binding sites which interact with rigid molecular fragments. By showing examples of the broad range of ways in

which proteins can apparently recognise a given moiety, the need for a score which quantifies binding site variability has been demonstrated.

A problem faced when designing this study was how to strike a balance between a purely knowledge-based approach to binding site representation, and one which is imbued with more chemical realism. Calculating the distribution of different functional groups or atom types around ligands is relatively simple to do, but suffers from the problem that some pairs of functionalities or atom types are more similar in their chemical properties than others. On the other hand, methods which attempt to analyse binding site similarities or differences by comparing various forcefields calculated over their volumes (see *e.g.* Kastenholz *et al.* (2000), Sheridan *et al.* (2002)), while potentially more realistic, are heavily dependent upon the reliability of the particular interaction mapping method used, which often cannot be easily assessed. The approach presented here, in which mixtures of atom-class densities are compared using empirically-determined atom-type similarity values, offers a simple and powerful means of taking into account chemical information when analysing structural data. While the set of atom classes used here may be criticised as being too coarse-grained, the modular analytical framework can allow different atom classification schema and dissimilarity to be 'plugged in' in a straightforward manner.

By representing each locus of a binding site in terms of a mixture of different atom types, and applying multidimensional scaling techniques to the atom type dissimilarity matrix, a simple method for comparing the chemical composition of a binding site at each point in space was described. Although its use was restricted here to a multi-way assessment of chemical diversity, it may also have applications in pairwise binding site comparison. Instead of the graph-matching approaches which are commonly employed to compute similarity between a pair of sites, we could represent each of them using the density mapping approach, and then compute a similarity index by applying the chemical diversity score discussed in this chapter. This would clearly be more computationally expensive, but may offer a more sensitive method of binding site comparison.

The main innovation of this chapter has been the prototyping of a novel diversity measure for application to ligand binding sites. Concepts previously applied in the analysis of protein sequence conservation - a one-dimensional problem - have been adapted in order that they could be leveraged on the three-dimensional information present in a collection of aligned ligand binding sites. The method which has been developed allows interactive exploration of the spatial distribution of binding site diversity, as well as calculation of an overall diversity metric which can be used to compare the variability of binding sites in different protein families and/or specific for different ligand fragments. Qualitative analysis of the score distributions obtained using this method suggest that it is capable of replicating our intuitive notions of what constitutes a variable - or conserved region of a binding site. Although more thorough validation would be necessary first, it is possible that this method could be used to help 'focus' binding site search methods, weighting the relative importance of different regions of the binding site according to the observed level of diversity.

Applying the diversity scoring method to a non-redundant set of adenine binding sites has shown that their variability can be roughly divided into two types, which are manifested in different regions of the ligand environment. The faces of the adenine rings are dominated by non-specific, non-polar contacts, which are

variable in terms of their precise spatial location and in terms of the atom types which are involved. The chemical characteristics of the binding sites in these regions, however, tends to be fairly homogeneous. Around the rim of the adenine fragment, however, we see a far greater diversity of chemical groups, with small islands of conserved interactions floating in a sea of variability. It appears, then, that these few specific interactions - with the N6 *cis* acceptor position being most prevalent - are capable of standing out sufficiently to ensure reliable recognition of the correct nucleotide.

As with the analysis of ligand conformational diversity, it appears that not all protein families are equal when we consider the conservation of their adenine binding sites. Comparison of the overall diversity scores for 9 clusters of adenine-binding sites showed that, while most are significantly well conserved, two families exhibited approximately the same level of diversity as we would expect by randomly sampling from unrelated sites. The biological reasons for this are not clear, and require further analysis.

The work presented in this chapter is by no means a definitive analysis of binding site variability, but it serves to illustrate an important point which should be heeded when designing any method for binding site comparison or prediction. The degree of variability varies greatly both between different regions of a binding site, and between the sites of different protein families. Therefore appropriate weighting should be applied when searching for geometric patterns in binding sites. Moreover, it should be appreciated that no single approach can be expected to work well when applied to all proteins: the fact that some families appear to be able to tolerate far greater diversity in their ligand-binding sites may mean that they will prove to be stumbling blocks for predictive methods.

Chapter 7

Discussion

This project set out to address two questions: comparing ligands bound to unrelated proteins (domains belonging to different superfamilies) with those bound to related proteins (non-identical domains from the same superfamily),

1 How much do the conformations of the ligand vary?

2 How much do the structure and properties of the binding sites vary?

In the course of providing answers to these problems, new software and methods were developed, and several novel insights into the phenomenon of molecular recognition were gained. This chapter draws together some of the main points from the body of the thesis, and suggests several areas in which further work could be done.

The GAMUT library

In addition to seeking answers to the biological questions stated above, the author took this doctoral research project as an opportunity to pursue an abiding interest in scientific programming techniques. The outcome of this part of the work was a software library called GAMUT, the details of which were covered in chapter 2. Besides providing the platform upon which all of the programs used for the analyses presented here were built, the design and implementation of GAMUT highlighted several important aspects of successful software development.

Perhaps the clearest of these is the need to strike a balance between expressivity and useability when designing software libraries. The former allows the library to fulfil a wide range of tasks, allowing it to serve as the main codebase for application development, thus reducing dependencies and simplifying the project. Expressivity is, however, often achieved at the expense of comprehensibility, since generic components tend to be less easily accessible to the programmer, requiring more time to understand how to access the required functionality. This can be particularly true in a language such as C++, where genericity is usually implemented using templates, which are burdensome both in terms of syntax and as a cause of 'code bloat' (both problems are covered extensively in the literature - see *e.g.* Alexandrescu (2001)). By using a range of techniques including template metaprogramming, much of the complexity inherent in the generic features of GAMUT has been hidden, such that, for example, clients may use the chemical graph class without needing to know that it inherits from a highly generic graph template class. Users with more complex needs, however, are free to employ the more powerful aspects of the library which come from harnessing these generic classes.

If the author were writing the library again from scratch, some design decisions would be taken differently. The implementation of GAMUT was seen not only as a means to an end (in terms of providing the tools necessary to perform certain analyses), but also as a educational vehicle for improving the author's programming skills. As such, some aspects of the library are overly complex, having been written in part to help understand the workings of a particular language feature. This is clearly not an ideal way to design software; nevertheless, the modular design of the library means that, while some parts should be re-written, such re-designs would not affect the overall structure of the system.

Diversity of structure and function of proteins binding a given ligand

The analysis presented in §4.4 provides a summary of the extent of macroscopic diversity - that is, diversity at the level of the whole protein - shown by proteins which contact ligands in the PDB. These must be viewed with caution since they include non-cognate interactions, and are adversely affected by biases present in the database, but nevertheless constitute a useful overview.

In terms of protein structure, most ligands tend to interact with only a small number of fairly similar proteins: over three quarters of ligands interact with only one or two folds (figure 4.15), and there are only 11 compounds which are bound by domains from more than 20 homologous superfamilies (figure 4.16). Considering function, only 9 ligands are bound by proteins with EC numbers distinct up to the second level (figure 4.21).

Conformational diversity of of bound ligands

In chapter 5, the considerable diversity in conformation of several common biological ligands was demonstrated, first pictorially, and then by application of a measure of compactness, the molecular radius of gyration. This showed that, while ligands often bind in an extended conformation, this is not always the case, and even when ligands do unfold upon binding, they are still free to explore a large region of conformational space.

Interestingly, the assumption that homologous proteins bind ligands in similar conformations was found not to hold universally. Indeed, the conformations of ligands bound to some families were found to be statistically as diverse as we would expect by sampling randomly from unrelated binding sites. This was demonstrated by application of a newly-developed technique for multi-way analysis of ligand conformation. The findings suggests that, firstly, the biological constraints on ligand conformation are not equal in all proteins, and secondly, that in many cases, ligands are likely to be only partially immobilised upon binding.

Structural and chemical diversity of ligand environments

Having established the high degree of ligand conformational variability, attention was turned in chapter 6 to assessing diversity in the ligand binding sites. Due to the findings of the previous chapter, this was done by concentrating on rigid fragments of ligands, primarily the adenine moiety. Here, binding sites were also shown to be highly diverse; conserved interactions were highlighted by using a propensity mapping approach to identify regions of space in which particular types of contacts to the ligand are statistically over-

represented. This method is a realisation of the 'fuzzy template' approach proposed previously (Moodie *et al.*, 1996), and may be a useful starting point for development of new binding site search techniques (discussed further below).

The remainder of chapter 6 describes a new method for quantifying binding site diversity. It should be stressed that this approach is currently only at a preliminary stage, but it appears that it is capable of providing a reasonable objective measure of the variance at each locus of a group of binding sites, which is in keeping with our own intuitive assessment.

Future work

Active development on GAMUT is likely to end with the completion of this thesis. However, were it to continue, the main threads would probably be the addition of a scripting layer, allowing the power of the library to be accessed from an interpreted library such as Python (Python Software Foundation, 1990), and the design of a web interface to the application programs, allowing users to perform analyses similar to those presented here on their own datasets.

Several aspects of the methodology used to generate the binding site datasets are worthy of further comment. The method used to validate ligand identities offered a simple and automatic means of guaranteeing that all instances of molecules identified as being of a particular type have a chemical structure which agrees with our notion of what that compound should be. It is somewhat stricter than the ligand validation applied in, for instance, the MSD, because ligands which are poorly resolved in the crystallography experiment are automatically excluded. From a biological perspective, however, it is less than ideal, since no checks are made on whether or not the ligand is cognate to the protein. In order to be more sure that findings from the type of high-throughput analysis described here are biologically relevant, this should be remedied in future work, particularly if more esoteric ligands are analysed.

The binding site clustering approach is similarly well-suited to large-scale analysis, but perhaps less reliable than it could be. The heuristic of clustering binding sites on the basis of their domain composition appears to be fairly effective, but may be misleading in that, for example, two binding sites which appear on homologous domains, but in different *locations* on the surface of those domains, would be clustered together. This means that conclusions drawn about the binding sites in this cluster may be the result of comparing sites which are, in truth, not directly comparable. This issue is not thought to be a particularly common problem, and therefore does not invalidate the general findings of this thesis, but could be rectified fairly simply in future work.

Finally, the overall architecture of the analytical pipeline described in chapter 4 could be improved by reducing its reliance on proprietary file formats.

The torsion angles of ligands in the four datasets in chapter 5 were treated only in passing; these deserve somewhat deeper analysis. In particular, the question of why so many torsion angles are observed to lie well outside preferred angular ranges - even in relatively high-resolution structures - needs to be addressed. It may be that, in some of these structures, although of generally high quality, the density into which the

ligands were fitted is less well-defined. Another explanation, stemming from anecdotal reports of structure determination practices, is that the refinement of ligand coordinates may in some cases not be as rigourously checked as that of the protein backbone. Thirdly, some of the strained angles will be the result of a particular conformation imposed on the ligand by the protein. An analysis which reveals the relative prevalence of each of these scenarios would be illuminating. In the first instance, this could be undertaken by a thorough analysis of temperature factors for all ligand coordinates in the datasets. An interesting experiment which could then be performed would be to obtain structure factors, where available, for each structure, and then systematically re-refine the coordinates of the ligand molecules using the same parameters for each, and then compare the results with the coordinates deposited in the PDB entry.

Another aspect of ligand conformational diversity which could be explored is the relationship between ligand conformation and binding site shape. Work is currently underway to develop methods for comparing the shape of binding pockets, with a view to predicting the ligand - or ligands - which may bind to a new protein (T. Funkhouser, personal communication). An interesting question which arises from this is, where we find domains which bind ligands in diverse conformations, does the shape of the binding pocket undergo concommittant deformations, or is it simply large enough to permit certain parts of the ligand to flex within an essentially rigid binding site?

In chapter 6, it was stated that the diversity scores could be used to focus geometric searches for potential binding sites. One way in which this proposal could be tested is as follows. For each fragment, templates could be constructed from the location of peak values in the propensity maps of each atom class. These templates could then be used to search for binding sites in a test set of structures (using appropriate cross-validation procedures), using an existing algorithm such as that recently described by Barker and Thornton (2003). This type of search would be expected to return a large number of false-positives; the utility of the diversity maps could then be tested by using them to calculate weights on each component of the template, and determining whether the extra information improved the specificity of the search.

Another avenue which could be explored using the diversity index is the relationship between sequence evolution and the increase in binding site diversity. Given a large, diverse protein family, one could sample groups of binding sites, of approximately equal size, gradually allowing more evolutionarily diverse sequences to join. By computing the binding site diversity for each group, one could begin to explore the effects of divergence on ligand binding sites.

Concluding remarks

In summary, the work presented in this thesis highlights the extremely high level of diversity among ligand binding sites. This goes some way to explaining the difficulties encountered by many researchers in developing ligand binding site prediction methods: the success of pattern-matching approaches is dictated by the signal-to-noise ratio of the data, which in this case is demonstrably low. Docking approaches offer an alternative which does not depend on analogy to previous examples, but instead is based on physico-chemical principles. Although these techniques allow us to build attractively realistic models of the forces involved in molecular recognition, the current level of accuracy in the free energy calculations based on these models is

too low to allow for robust predictions.

Ultimately, we must retain hope that reliable methods for predicting molecular interactions can and will be developed. All the information required for recognition is present in the atomic structures of the molecules involved; the correct partners are bound *in vivo*, so it should be possible for us to model the same processes *in silico*. Whether the most successful approach to this problem turns out to be knowledge-based, rooted in first principles, or a combination of the two remains to be seen. What we can say is that at present, there are some conspicuous gaps in our understanding of the process of molecular recognition, which will most likely be filled only after detailed inspection of many more experimentally studied interactions.

Appendix A

Graph theory

Graphs are mathematical abstractions useful for solving a wide range of problems. A thorough review of the whole field of graph theory is beyond the scope of this chapter; here, elementary graph theory is summarised, and some key algorithms are described in pseudocode.

The first modern application of graph theory is attributed to the Swiss mathematician Leonhard Euler, and was published in 1736. Euler wished to mathematically prove a widely held belief among residents of his town, Königsberg in East Prussia. The proposition was that it is impossible to cross each of the town's seven bridges (shown schematically in figure A.1a) exactly once during a single walk. Euler reformulated the problem by drawing a graph (figure A.1b) which represented the essential elements of the problem: the vertices correspond to the distinct land masses in the town, and its edges symbolise the bridges which join those land masses. Euler noted that, in the course of a walk around the town, the act of 'visiting' a new vertex corresponded to the use of two bridges (edges) - one used to arrive, and another to leave. It follows that, in order to avoid using the same bridge twice, the vertex must have an even number of incident edges. In order to carry out the type of walk described above, this condition must hold for *all but at most two* of the vertices in the graph - the remaining two being the vertices at which the path starts and ends. (Note that the starting and ending vertices may be the same, in which case the order of *every* vertex must be even.) It is clear that the Königsberg graph does not satisfy the constraint; whether this proof put an end to Sisyphean wandering on the part of Euler's fellow townsfolk is more difficult to say.

Graph theory has been applied in areas as diverse as chemistry, social sciences and computer networking. In this appendix, a basic review of graph theory is presented, in order to provide a foundation for the graph theoretic techniques applied to chemical structures in the rest of this thesis.

A.1 Definitions and terminology

Firstly, it is necessary to explain what is meant by the term 'graph', in a mathematical sense, and to define some terms commonly used in graph theory. More information and examples explaining the definitions given here may be found in Gibbons (1985).

A graph may be defined as a set of vertices, and a set of edges, where an edge is a connection between a pair of vertices within the graph. More precicely, a graph is a pair, $G = (V,E)$, where V is a finite set and E is a binary relation on V. The contents of the set $V = \{v_i\}_{i=1}^{N}$ are the graph vertices; we introduce

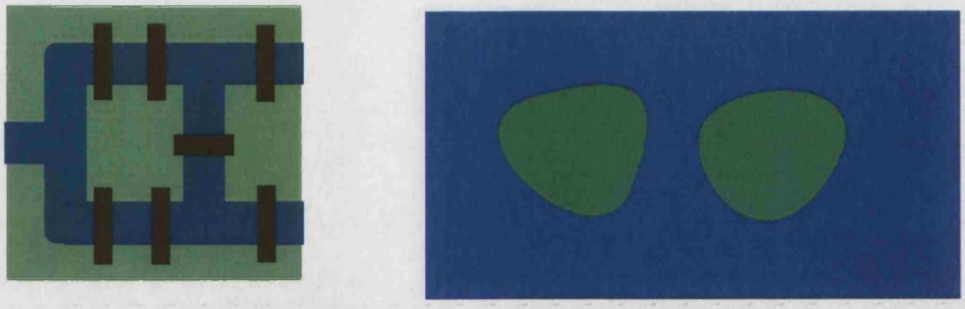

(a) Schematic representation of the arrangement of bridges in the city

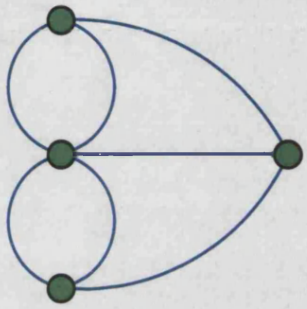

(b) Euler's graph formulation of the problem

Figure A.1: The Königsberg bridge problem

$v_i \in \mathcal{V}$ to represent the *properties* of the ith vertex, where $\mathcal{V}$ is the space of all possible vertex properties. The set $E = \{e_{ij}\}, 1 \leq i, j \leq N$ contains the edges of the graph, where i and j are the indices of the two vertices connected by an edge, and the properties of this edge are $e_{ij} \in \mathcal{E}$. $\mathcal{E}$ is the space of all possible edge properties; for example, if edges are labelled with real numbers, then $\mathcal{E} = \mathbb{R}^1$. Alternatively, vertices and edges may be labelled with *tuples* of properties; this is the case for many of the graphs considered in this thesis. Note that in the literature, the term *label* is often used in place of vertex/edge property. The edge e_{ij} is said to be *incident* on vertices i and j. The total number of edges incident on a vertex is referred to as the *order*, or *degree* of that vertex. For every edge e_{ij}, vertices i and j are said to be adjacent.

A fundamental property of a graph is whether it is *directed* or *undirected*. In directed graphs, the index pair (i, j) associated with each edge is ordered; in other words, each edge connects a source vertex to a target vertex. An edge in an undirected graph does not distinguish between the pair of vertices which it joins. The two edges e_{ij} and e_{ji}, therefore, are distinct in a directed graph, but refer to the same edge in an undirected graph. In a directed graph, the edge e_{ij} is said to be an *out-edge* of vertex i and an *in-edge* of vertex j. Graphs which contain both directed and undirected edges are said to be *mixed*; a *null graph*, on the other hand, is one which contains only isolated vertices, *i.e.* $E = \emptyset$. Here, we shall consider only undirected graphs, since our aim is to describe the use of graphs to represent chemical structures, whose edges (bonds) have no intrinsic directionality.

Graphs in which at most one edge is permitted to connect any pair of vertices are *simple* graphs (see figure A.2a). If parallel edges are permitted; that is, multiple edges between the same pair of vertices (figure A.2b, the graph is known as a *multigraph*. While in most graphs, vertices are not permitted to be connected directly to themselves, if this restriction is removed, *pseudographs* can be constructed (figure A.2c).

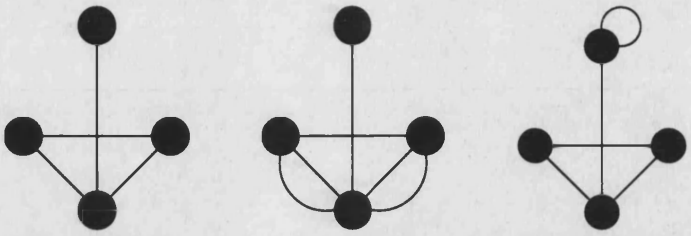

(a) A simple graph (b) A multigraph (c) A pseudograph

Figure A.2: Types of graphs, organised in terms of connectivity

Graphs in which every vertex is directly or indirectly connected to every other; that is, in which one can construct a walk along one or more edges from any vertex to any other, are said to be *connected*. Once again, as we focus on chemical graphs, the following discussions consider only simple connected graphs.

A *path* on a graph is defined as a set of vertices $\{v_1, v_2, \cdots, v_n\}$ which are sequentially connected; in other words, the edge set $\{e_{12}, e_{23}, \cdots, e_{n-1n}\}$ is a subset of the edges in the graph. A path in which the first vertex is also the last, is called a *cycle*, or, with particular reference to chemical graphs, a *ring* Downs (2003).

If the vertex and edge sets of a graph H are subsets of the vertex and edge sets respectively of another graph G, then H is a *subgraph* of G. Given a subset V' of the vertices G, an *induced subgraph* can be constructed by selecting a set E' from the edge set of G such that both endpoints of each edge in E' are in V'. The pair $I = (V', E')$ then constitutes the subgraph of G induced by the vertex set V'. This is illustrated in figure A.3

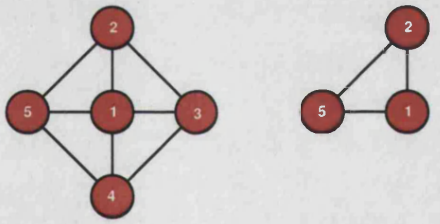

(a) A graph (b) Subgraph induced by the vertex set $\{1,2,5\}$

Figure A.3: An example of an induced subgraph

An *ismorphism* between two graphs is a one-to-one mapping between their two sets of vertices. If just some parts of a pair of graphs can be mapped onto one another, we may define a *subgraph isomorphism*. Strictly, a subgraph isomorphism between a pair of graphs G, H is an isomorphism between subgraphs G', H' of G and H. If, however, one of these subgraphs is in fact equal to its parent graph (*i.e.* $G' = G$), then a special case exists in which one graph, G, can be entirely mapped to a subgraph of H. For clarity, this type of subgraph isomorphism shall be referred to as an Exact Subgraph Isomorphism. This is shown schematically in figure A.4b. The term Common Subgraph Isomorphism will be used to describe the case where both G' and H' are subsets of the parent graphs G and H, as shown in figure A.4c. Note that common subgraph isomorphisms can be distinguished according to whether or not they are *connected* in each graph. An isomorphism is connected within one of the two graphs if each vertex within the subgraph is connected to every other by a path. A connected subgraph is also known as a *clique*. Finally, figure A.4a depicts an isomorphism in which all vertices from both graphs are mapped; this will be referred to as a *full graph ismorphism*.

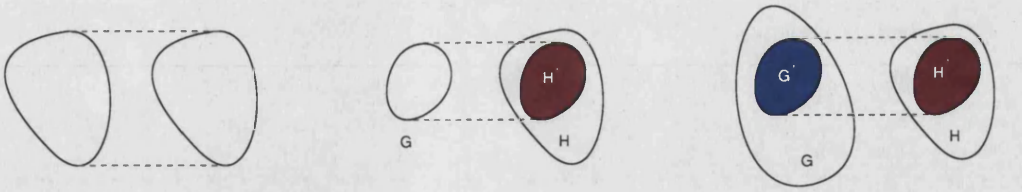

(a) A full graph isomorphism (b) An exact subgraph isomorphism (c) A common subgraph isomorphism

Figure A.4: Types of graph isomorphism

A.2 Representation of graphs

We may conceive of a number of ways of representing the structure of graphs. Consider the graph in figure A.5.

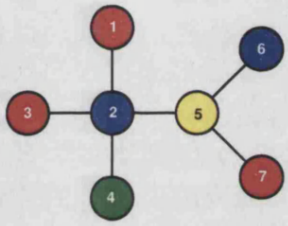

Figure A.5: An example graph
The vertex properties v_i are the colours of the circles. Edges do not have any properties in this graph.

The simplest representation is the *edge list*, which is simply the set E. In the case presented here, edges are unlabelled, so each member in the set E is simply an unordered pair of indices indicating the pair of vertices which are connected by the edge. The edge list for the graph in figure A.5 is as follows:

$$(1,2)\ (2,3)\ (2,4)\ (2,5)\ (5,6)\ (5,7)$$

An alternative is the *adjacency list*, in which a list of adjacent vertices is stored for each vertex in the graph. For instance, vertex 2 has adjacent vertices 1, 3, 4 and 5; the complete adjacency list is:

$$\begin{array}{ll} 1: & 2 \\ 2: & 1,3,4,5 \\ 3: & 2 \\ 4: & 2 \\ 5: & 2,6,7 \\ 6: & 5 \\ 7: & 5 \end{array}$$

The *adjacency matrix* is a third representation. Since edges are unlabelled, the adjacency matrix in this case is a *boolean matrix*; that is, a matrix in which each cell M_{ij} simply indicates the presence or absence of an edge connecting the *ith* and *jth* vertices. The values stored in the $|V| \times |V|$ boolean matrix M are given by

$$M_{ij} = \begin{cases} \begin{cases} 1 & : \quad e_{ij} \in E \\ 0 & : \quad \text{otherwise} \end{cases} & : \quad i \neq j \\ 0 & : \quad otherwise \end{cases}$$

For labelled graphs, each cell in the adjacency matrix would contain either the properties of an edge, if it is present, or else a defined null value indicating that the edge is absent. The adjacency matrix for the graph in figure A.5 is shown here:

$$\begin{pmatrix} 0 & 1 & 0 & 0 & 0 & 0 & 0 \\ 1 & 0 & 1 & 1 & 0 & 0 & 0 \\ 0 & 1 & 0 & 0 & 0 & 0 & 0 \\ 0 & 1 & 0 & 0 & 0 & 0 & 0 \\ 0 & 1 & 0 & 0 & 0 & 1 & 1 \\ 0 & 0 & 0 & 0 & 1 & 0 & 0 \\ 0 & 0 & 0 & 0 & 1 & 0 & 0 \end{pmatrix}$$

Other possibilities for the edge representation exist, for example the *winged edge* and *half edge* representations. These are not used in GAMUT and are therefore not discussed further; for more information on these and other topics related to graph theory, the reader is advised to consult de Berg *et al.* (1997).

When choosing the appropriate graph representation for a given problem domain, the usual two considerations apply, namely how much space (memory) the representation requires, and how rapidly the data can be accessed.

A.2.1 Storage requirements

For the construction of a database of graphs which is queried infrequently for instance, the storage requirements of a given representation are paramount. The most important determinant of the storage space required is the *sparsity* of the graph(s) themselves. Graphs in which each vertex is connected to many other vertices are said to be *dense* graphs. Mathematically, the density of a graph is given by the relationship of the numbers of vertices and edges in it; dense graphs have $|E| \approx |V|^2$, whereas sparse graphs have $|E| = \alpha|V|, \alpha \ll |V|$. It follows from the observation that, since the vertices of chemical graphs are naturally of low order, all but the smallest molecular graphs are sparse.

It can be seen that the amounts of storage required for the edge list, adjacency list and adjacency matrix representations of a sparse graph are $O(E)$, $O(E+V)$ and $O(V^2)$ respectively. While the edge list is clearly the most efficient way of storing a sparse graph in terms of storage requirements, it is often the case that other representations are often more efficient from an algorithmic standpoint.

A.2.2 Speed requirements

Graph algorithms may involve accessing the data held in a graph in a variety of ways, including:

1 Iteration through all vertices in the graph in no particular order

2 Iteration through all edges in the graph in no particular order

3 Iteration through all vertices connected to a particular source vertex

4 Iteration through all edges incident on a particular source vertex

5 Asking whether a particular pair of vertices are connected by an edge

For a graph with V vertices and E edges, we can derive orders of complexity for these operations, using each of the representations described above. These orders are shown in table A.1.

Clearly, no one representation is optimal for all possible operations; rather, the choice of representation used by a given algorithm is often a heuristic one, based largely on the types of graphs which are expected to be processed.

Representation	All vertices iteration	All edges iteration	Adjacent vertices iteration	Incident edges iteration	Edge existence test
Edge list	$O(V)$	$O(E)$	$O(E)$	$O(E)$	$O(E)$
Adjacency list	$O(V)$	$O(E)$	$O(\frac{E}{V})$	$O(\frac{E}{V})$	$O(\frac{E}{V})$
Edge matrix	$O(V)$	$O(\frac{1}{2}V^2)$	$O(V)$	$O(V)$	*constant*

Table A.1: Average orders of complexity for common graph operations

A.3 Common graph operations

Two fundamental types of graph iteration are the Depth-first search (DFS) and Breadth-first search (BFS) . They are described briefly here; the following, more in-depth discussion of several graph algorithms will refer to these traversal methods. Both DFS and BFS are methods for visiting all vertices in a graph G which are reachable from a given source vertex v_s; in a connected graph, this means that all vertices are visited eventually.

In BFS, the search proceeds by first visiting all neighbours of - that is, vertices adjacent to - the current vertex. Next, the vertices adjacent to those neighbours are visited, and so on. In this way, the search propagates outwards from the initial vertex, until all vertices have been visited. A formal description of the BFS is presented in algorithm A.1.

In DFS, by contrast, the search moves forward, deeper into the graph, as soon as it reaches a new vertex. That is, it will pick the next adjacent unvisited vertex until reaching a vertex that has no unvisited adjacent vertices. The algorithm will then backtrack to the previous vertex and continue along any as-yet unexplored edges from that vertex. DFS is formalised in algorithm A.2.

A.4 Graph algorithms

There are many types of graph algorithms, reflecting the widespread applicability of graph theory to different problem domains. Among them are methods for detecting cycles in graphs (e.g. Figueras (1996)), determining minimum path lengths between pairs of vertices, and generating 2-dimensional depictions of graphs. The family of graph theoretic algorithms most used in the current study are those for matching pairs of graphs; two such algorithms are discussed in detail in §3.1.

Recursive breadth-first search on an undirected graph $G = (V,E)$, starting at vertex v_s
The VISIT() *function may be a user-defined event which should occur as each new vertex is discovered*

Function BREADTHFIRSTSEARCH(G, v_s) :
Initialise the set of unvisited vertices
$R \leftarrow V - v_s$
Visit the initial vertex
VISIT(v_s)
BFS_RECURSIVE(v_s, R, E)

Function BFS_RECURSIVE(v_c, R, E) :
Get the set of unvisited vertices adjacent to the current vertex v_c
$N \leftarrow \{v_i \in R \mid \exists\, e_{ci} \in E\}$
Visit neighbours of the current vertex
for each $v \in N$:
VISIT(v)
Recursively call the function to visit neighbours-of-neighbours
for each $v \in N$:
$R \leftarrow R - v$
BFS_RECURSIVE(v, R, E)

Algorithm A.1: Breadth-first search in an undirected graph

Recursive depth-first search on an undirected graph $G = (V,E)$, starting at vertex v_s
The VISIT() *function may be a user-defined event which should occur as each new vertex is discovered*

Function DEPTHFIRSTSEARCH(G, v_s) :
Initialise the set of unvisited vertices
$R \leftarrow V - v_s$
Visit the initial vertex
VISIT(v_s)
DFS_RECURSIVE(v_s, R, E)

Function DFS_RECURSIVE(v_c, R, E) :
Get the set of unvisited vertices adjacent to the current vertex v_c
$N \leftarrow \{v_i \in R \mid \exists\, e_{ci} \in E\}$
Visit neighbours of the current vertex; proceed forward from each new vertex immediately
for each $v \in N$:
VISIT(v)
$R \leftarrow R - v$
DFS_RECURSIVE(v, R, E)

Algorithm A.2: Depth-first search in an undirected graph

A.4.1 Ring perception

Firstly, let us elaborate on the definition of a graph cycle presented previously. If no pair of vertices in a cycle is joined by an edge which is not part of the cycle, it is a *simple* cycle; other cycles are *complex*. Since all chemical graphs are simple graphs, all cycles found in them are by definition simple.

Given a graph with v vertices and e edges, consisting of n connected components [1], the number of rings which make up a *fundamental basis set* is given by the Cauchy formula:

$$\mu = e - v + n$$

[1] Here, n is always equal to 1, since we are only considering graphs which represent individual molecules, and hence contain only one connected component

A fundamental basis set is a set of rings from which all others, in a non-trivial ring system, can be produced by combining subsets of them.

A.4.1.1 Ring sets

For complex ring systems, a range of cycles can be perceived. Figure A.6 shows the seven possible cycles in a complex ring system consisting of three fused simple cycles. A common problem is how to select a set of rings which is in some way optimal for the given graph. For instance, if we require that a ring set should satisfy the criterion that it contains each vertex in the ring system at least once, then we may enumerate the following possible combinations:

$$\{a,b,c\};\{a,e\};\{b,d\};\{c,f\}$$

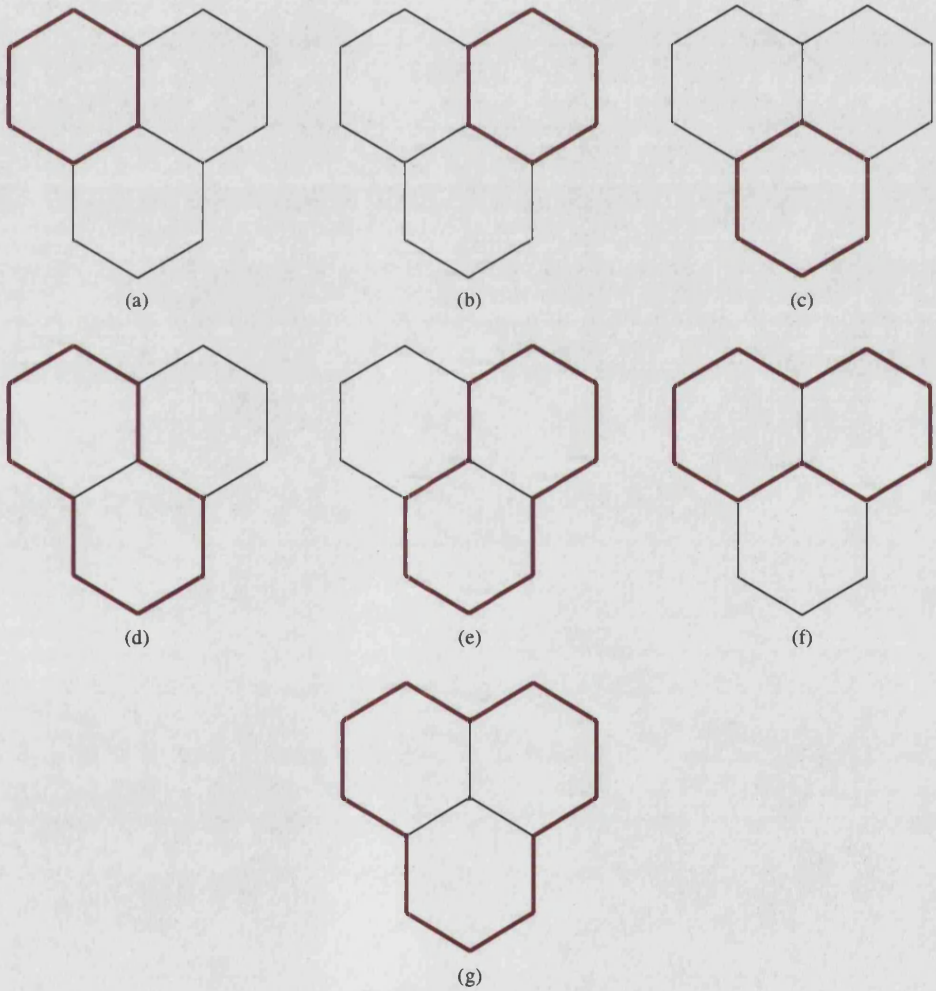

Figure A.6: Cycles in a complex ring set

For most applications in cheminformatics, the most useful type of ring set is the smallest set of smallest rings, otherwise known as the minimal cycle basis. Definition of the SSSR is a preliminary step in the identification of rigid molecular fragments, which can be created by removing all acyclic single bonds from a molecule. For certain applications however, other types of ring sets may be more applicable. For example, a ring set known as the Essential Set of Essential Rings (ESER) has been used in analysis of changes in catalytic sites

during enzymatic reactions. Further details on different types of ring sets are available in Gibbons (1985).

A.4.1.2 SSSR perception algorithms

Several algorithms for perceiving the SSSR have been published (Qian *et al.* (1990), Fan *et al.* (1993), Balducci and Pearlman (1994), Figueras (1996)).

Figureas' method is summarised in pseudocode as algorithm A.3. The essence of the algorithm is as follows:

1 Remove all vertices whose degree is less than 2.
2 Determine the smallest degree of the remaining vertices. If it is greater than 2, temporarily remove edges from the lowest-degree vertex to reduce its degree to 2.
3 Select a vertex of degree 2, and perform a breadth-first search to find the smallest ring which contains this vertex.
4 Remove a degree-2 vertex from the ring just found, thus breaking it.
5 Repeat from step 3 until all nodes of degree 2 have been eliminated.

In order to illustrate the breadth-first search method, consider the graph shown in figure A.7. The algorithm begins by assigning intial values to the paths leading from the source vertex (1) to its neighbouring vertices, 2 and 5.

$$path[2] = [1,2]$$

$$path[5] = [1,5]$$

The search progresses by moving from vertex 2 on to vertex 3. First, a check is made to determine whether $path[3]$ is empty. It is, so a closed path has not been found; the value of $path[3]$ is then updated:

$$path[3] = path[2] + 3 = [1,2,3]$$

This procedure progresses until a non-empty path is encountered. Referring to step figure A.7b, we see that extending the path from vertex 4 to vertex 3 will meet a non-empty path. At this stage, the intersection of the two paths is computed; here:

$$intersection = path[4] \times path[3] = [1,5,4] \times [1,2,3] = [1]$$

The fact that the intersection contains just a single vertex indicates that the closed path is a valid ring. Contrast this with the situation when the path leading around the four-membered ring is extended from vertex 6 to vertex 4:

$$intersection = path[6] \times path[4] = [1,5,7,6] \times [1,5,4] = [1,5]$$

This indicates that the target vertex, 4, can be reached by more than one path from the source. The ring $\{1,5,7,6,4,3,2\}$ is not therefore a member of the SSSR.

Function FIGUERAS($G(V,E)$) :

$W \leftarrow V$
$Rings \leftarrow \emptyset$
$M \leftarrow$ adjacency matrix of G

while $W \neq \emptyset$ **do**
Remove degree-zero vertices from W
Remove degree-one vertices from W

$deg_{min} \leftarrow$ smallest degree in W
if $deg_{min} < 2$ **then**
return
if $deg_{min} > 2$ **then**
Temporarily remove edges from lowest ring-connectivity vertex in W to reduce its degree to 2
else
Find smallest ring for each vertex with degree 2
for each $v \in W : degree(v) = 2$ **:**
$r \leftarrow$ GETRING(G, v, M)
Add r to *Rings* unless it is a permutation of an existing ring

Perform a breadth-first search to find the smallest ring containing v
Function GETRING($G(V,E), v, M$) :
Initialise an empty FIFO queue Q
Create new ring r

Initialise paths array; each array is a bit-mask of length $|V|$
$paths \leftarrow array[|V|]$

Push all vertices adjacent to v onto the queue
for each $w \in G : M_{vw} = 1$ **:**
ENQUEUE($\{w, v\}, Q$)

while Q is not empty **do**
$\{x, y\} \leftarrow$ DEQUEUE(Q)
$p_x \leftarrow paths[x]$

Loop over all vertices adjacent to x, except y, which has already been visited
for each $z \in G : M_{xz} = 1, z \neq y$ **:**
$p_z \leftarrow paths[z]$
if $p_z.count = 0$ **then**
Vertex z is encountered for the first time; record the path which has been travelled to reach it
$p_z \leftarrow p_x$
$p_z[z] = true$
ENQUEUE($\{z, x\}, Q$)
else
Compute the intersection of paths p_x *and* p_z
$p_{inter} \leftarrow p_x \cap p_z$
if $p_{inter}.count = 1$ **then**
Construct a new ring, whose vertices are given by the bits set in the union of paths p_x *and* p_z

$p_{inter} \leftarrow p_x \cup p_z$
for $i \leftarrow 1 to |V|$ **:**
if $p_{inter}[i]$ **then**
$r \leftarrow r + V_i$
return r
return r

Algorithm A.3: Ring perception by breadth-first search

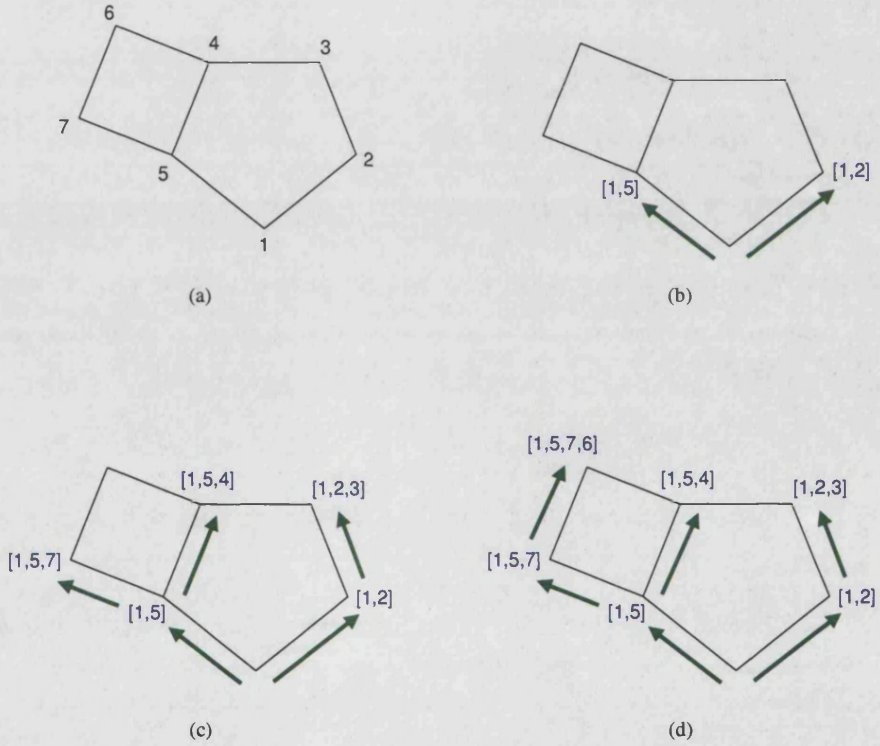

Figure A.7: Ring perception by breadth-first search

Appendix B

Coding principles and techniques

This appendix describes, first, the conventions which were adhered to while writing the library. An appreciation of these principles, particularly those which relate to names, should aid the reader when he/she reads the GAMUT code. The rest of the appendix details several programming techniques which were used in various points of the library.

B.1 General principles

- Pointers are avoided in the public interfaces of classes; references are preferred.
- Objects are passed by `const` reference rather than by value wherever possible.
- C-style casts are not used; the new C++ casting operators are used instead.
- `static_cast<>` is only used where there is a strong advantage to doing so, either from a performance or simplicity standpoint.
- The `const` keyword is used wherever possible.
- const-ness is respected within classes; `const_cast<>` is avoided.
- Macros are used in the following reasons only:
  - Header inclusion guards
  - Control of conditional compilation, *e.g.* debugging code
  - For recursive metaprogramming (*e.g.* typelists)
  - To throw GAMUT exceptions, which report the file and line number where they originated
  - In certain special cases where their use improves readability of the code *e.g.* for initialisation of static class members used by the I/O system

The source code for the library was organised using the following guidelines:

- Header files have the suffix .h
- Source code files have the suffix .cpp
- Template function definitions are in files with suffix .hxx
- Inline function definitions are in files with suffix .inl. Inlining of member functions is controlled by a macro which is set during library configuration. The macros look like this:

```
#ifdef GAMUT_INLINING
#define GAMUT_INLINE inline
#else
#define GAMUT_INLINE
#endif
```

The body of potentially inlined member functions in the .inl file is written as follows:

```
GAMUT_INLINE void MyClass::myfunc() { /* ... */ }
```

If inlining is enabled, this file is included in the appropriate header, making the implementation of the function visible to all callers of it. If inlining is disabled, the file is appended to the .cpp file, meaning that the functions are compiled into the library itself.

- All header files are protected with macros which prevent multiple inclusion.
- The hierarchy of namespaces is reflected in the directory structure of the library code. For example, a class which is in the `gamut::mmol` namespace would be found in the gamut/mmol/ subdirectory of the source tree.

Names for classes and functions were chosen according to the following rules:

- Class names are capitalised, and multiple words concatenated, *e.g.* `ScalarField`.
- Functions are named in lower case, with multiple words joined by underscores, *e.g.* `read_data`.
- Private and protected class members are named with a trailing underscore (*e.g.* `data_`).
- Private and protected class functions are named with a trailing underscore (*e.g.* `void init_();`).
- Typedef names are given the `_t` (for *type*) suffix (*e.g.* `matrix_t`).
- Macros and static class constants are named all in upper case.
- Everything in the GAMUT library belongs to the `gamut` namespace. Subcomponents of the library lie in nested namespaces (*e.g.* the chemistry components are all defined in namespace `gamut::chem`).

B.2 Memory management

GAMUT is designed in such a way that clients should rarely need to use the `new` and `delete` keywords to create and dispose of library objects. This is achieved primarily by having complex objects (*e.g.* the macromolecular structure and graph classes) manage the lifetime of their constituent components internally (here, *e.g.* atoms and vertices respectively), allowing clients access to those objects by passing references to them. Where the copy constructor and assigment operator (`operator=`) of a class are public, they should perform deep copying. For example, copying the root node of a tree will also cause the subtree of that node to be copied recursively. For some classes, copying is explicitly prevented by making these operators private. This is typically for those objects whose existence is managed by other objects; for example, macromolecule selection objects are managed by a selection manager, which provides functions for creating, copying and disposing of them.

B.3 Deferred evaluation

A problem which recurs in the design of complex classes is how best to maintain the integrity of internal class data, with minimal computational cost. As an example, consider a hypothetical class `C` which stores a list `L` of some kind of object. In addition, `C` is required to maintain several indices, through which the client may perform look-ups into `L`. For example, `L` may be a list of graph objects, and the indices may be derived properties of those graphs, such as the number of cycles in each.

These indices are derived from the objects stored in `L`. Now assume that, whenever objects are added to, or removed from `L`, the indices become invalidated, and must be rebuilt. The problem is that this rebuilding process may be relatively computationally expensive, and, until a look-up is requested, is not strictly necessary. The technique of *deferred evaluation*[1] is used to address this problem, by postponing rebuilding of the indices until access to them is needed. This is typically achieved by storing a flag which indicates whether, at any time, a given internal data field is up to date. Operations on `L` in this example would clear the up-to-date flag; look-up operations would first check this flag to see whether to rebuild the indices, before accessing them. Deferred evaluation is utilised in many of the GAMUT classes.

The implementation of deferred evaluation typically relies upon *mutable* data members, *i.e.* those which are permitted to be modified by even those class member functions which are qualified with the `const` keyword. The reason for using the `mutable` keyword is related to the definition of *const-ness* as applied to an object. To return to the example above, rebuilding of the indices certainly violates the *physical const-ness* of `C`; that is, the bits and bytes which constitute the `C` object are altered by the re-indexing operation. However, this operation should not violate the object's *logical* const-ness. That is, it should not change the contents of the object *as seen by an outside observer.* Since the index stored by `C` is not really a part of the data which defines the object, but rather a peripheral data member which only exists to facilitate proper operation of its parent object, it may be altered even by functions which are defined to be non-mutating, or `const`.

The example code presented in listing B.1 illustrates the use of this technique.

B.4 The composite dispatch technique

At various stages while writing the library, the following problem was encountered: *I have a class, C, which, under certain circumstances, should use A as its base class, and under others, should used B.* For example, let us say that we are writing a container class `C`, templated on the value stored within it (let this type be named `T`). If that data type is numeric, a certain set of interface functions should be exposed; if it is non-numeric, another set should be. The obvious way to do this is somehow to define the numerical-values interface in one class (`A`), and the non-numerical interface in another (`B`). Now, it is trivial to write a mechanism which determines whether or not `T` is numeric by using the *type traits* pattern. But how should we change the base class of `C` depending upon the result?

The author has invented a technique for doing this, and has named it 'composite dispatch'. The use of

[1] The name is chosen in analogy to the technique of *lazy evaluation* which is employed in functional programming paradigms to delay evaluation of a functional argument until its value is required.

```
template<class T>
class C {

    std::vector<T>                          data;
    mutable std::map<unsigned, unsigned>    indices;
    mutable bool                            up_to_date;

    void rebuild_index() const {

        indices.clear();

        // Compute an index for each data value.  Here we assume that
        // class T defines a compute_index() function which returns
        // an integer value.
        for(unsigned i=0; i<data.size(); ++i)
            indices[data[i].compute_index()] = i;

        up_to_date = true;
    }

    public:

        C() : up_to_date(true) { }


        void add_data(const T& x) {

            // Add the data object to the list
            data.push_back(x);

            // Mark the index as invalidated
            up_to_date = false;
        }


        // Look up a value in the container according to its index
        const T& get_value(unsigned index) const {

            // If the index is currently out of date, rebuild it
            if(not up_to_date) rebuild_index();

            // Find the required index in the map
            std::map<unsigned, unsigned>::const_iterator i =
                indices.find(index);

            // Throw an exception if the index was not found
            if(i == indices.end()) throw std::range_exception;

            // Return the appropriate data value
            assert(i->second < data.size());
            return data[i->second];
        }
};
```

Listing B.1: The deferred evaluation technique

different base classes to contribute parts of the functionality of a derived class is known as the Composite design pattern (Gamma *et al.*, 1995), and the compile-time selection of different parts of code via the template mechanism is commonly referred to as 'compile-time dispatch'.

The code in listing B.2 illustrates how the technique works.

```
// Selector classes - these are typically just empty structs
struct A_Tag { };
struct B_Tag { };

// Two potential base classes; one of these will be inherited from
// by the class C, defined below
class A { /* ... */ };
class B { /* ... */ };

// Definition of the class which selects the appropriate base for C
template<class Tag> struct Selector { };

// Specialisations of the selector map tags onto base classes
template<> struct Selector<A_Tag> { typedef A base_t; };
template<> struct Selector<B_Tag> { typedef B base_t; };

// The class which we actually instantiate
template<class Tag>
class C : public Selector<Tag>::base_t
{ /* ... */ };

// Two example instantiations using different base class selectors
C<A_Tag> c_inheriting_from_A;
C<B_Tag> c_inheriting_from_B;
```

Listing B.2: The composite dispatch technique

This idiom allows the programmer to define a class whose base class is determined by passing a template 'selector' parameter.

B.5 Customisation of the behaviour and form of objects

In several places through the GAMUT library, the problem of how to permit *customisation* of objects was encountered. Specifically, how best to allow a client to modify the way an object behaves, within the bounds of the definition of the role of that class, using simple and intutive programming techniques? This object customisation came in two flavours, which are discussed separately below: customisation of *behaviour* and customisation of *form*.

B.5.1 Behavioural customisation

Consider the design of a class which implements a particular algorithm. The client instantiates an object of this class, provides the input data, and then instructs it to execute the algorithm. Finally, the client can request the result of the algorithm from this object.

Most algorithms, however, allow some degree of parameterisation. In some cases, this may be simple - for example, a clustering algorithm may require the client to supply some kind of threshold value; clearly this can be easily implemented with a single member function of the algorithm object. However, suppose the algorithm permits some more complex adjustment of its behaviour. For example, a simulated annealing algorithm may allow the client to alter the mathematical function which controls the way the system 'cools'.

It is not so immediately obvious how this should be implemented: whereas before we simply needed to pass a value, now it seems that we require a function into which we can pass *a piece of code*. In fact this is not so far-fetched, and there are several ways to achieve it. GAMUT utilises two, which shall be described here.

B.5.1.1 Behavioural functors

The first approach is to use a *functor* (or "function object"). This is an object which defines the application operator, `operator()`, as a member function, and hence may be thought of as a free function which has been 'wrapped' inside an object. By passing a functor to our algorithm object, we are effectively passing it a piece of code, and can therefore alter its behaviour at runtime. Function objects used in this context are referred to as *behavioural functors* in order to distinguish them from the many other uses of functors in C++.

Let us look more closely at the anatomy of a simple functor. The code snippet in listing B.3 shows how we might write a base class for functors which express a cooling function for a simulated annealing algorithm.

```
struct CoolingFunctor {

    // Cloning function - returns a copy of the cooling functor,
    // dynamically created on the heap.
    virtual CoolingFunctor* clone() const = 0;

    // The cooling function.  Given previous temperature and time
    // elapsed, it returns the new, cooler temperature.
    virtual float operator()(float temp, float time) const = 0;
};
```

Listing B.3: An example functor

This abstract base class mandates that any cooling functor provide at least two functions: one which dynamically creates a copy of itself, returned in the form of a base class pointer, and one which computes the new, cooled temperature which results after a given time lapse. A sketch of part of the annealing algorithm object may now look as shown in listing B.4.

Note that the use of function objects to customise the behaviour of an object is potentially very powerful. While the functor demonstrated above is very simple, a functor may in fact be quite complex, containing its own data, and exposing any number of member functions. The only requirement is that functors used in this way should be derived from an abstract base class which defines a cloning function, and in which all member functions required by the algorithm object are also virtual.

B.5.1.2 Behavioural policies

Another design methodology which has some similarities with the functor technique is that of *policies*. As with behavioural functors, policies Alexandrescu (2001) are *small classes which are used to specify a behavioural or structural part of a larger class*. The key difference between functors and policies as they are used in GAMUT is that while functors are used for run-time customisation, policies must be specified at compile-time, as template parameters of a template class or template member function.

Suppose that we wished to rewrite the algorithm class outlined above, using policies rather than functors to specify the cooling function. This would be the result of a design decision that execution speed was more

```
struct AnnealingAlgorithm {

    CoolingFunctor*     cooling;
    float               time_per_step;
    float               temp;

    // Algorithm is initialised with some default cooling function
    AnnealingAlgorithm()
    :   cooling(new DefaultCoolingFunctor), time_per_step(1.0)
    { }

    // Destructor disposes of the cooling functor
    ~AnnealingAlgorithm()
    { delete cooling; }

    // This function allows the client to specify a new cooling function
    void set_cooling_function(const CoolingFunctor& cf) {

        delete cooling;
        cooling = cf.clone();
    }

    // This function is called by the algorithm at each step of the annealing
    // It applies the cooling function expressed by the functor
    void cool_down()
    { temp = (*cooling)(temp, time_per_step); }
};
```

Listing B.4: A sketch of code for a simulated annealing algorithm

important than runtime flexibility, since changing the cooling function would require actual modification of client code, rather than being possible through, for example, command-line switches. The following code shows one possible cooling policy:

```
struct ExponentialCoolingPolicy {


    static float new_temp(float temp, float time)
    { return temp / (2^time); }
};
```

Now the annealing algorithm should be rewritten in order to take a cooling policy in the form of a template parameter, as shown in listing B.5.

```
template<class CoolingPolicy>
struct AnnealingAlgorithm {

    float               time_per_step;
    float               temp;

    AnnealingAlgorithm()
    :   time_per_step(1.0)
    { }

    // This function is called by the algorithm at each step of
    // the annealing.
    // It applies the cooling function expressed by the policy class
    void cool_down()
    { temp = CoolingPolicy::new_temp(temp, time_per_step); }
};
```

Listing B.5: Design of a simulated annealing algorithm using policy classes

It should be apparent that behavioural functors and policies can be used to achieve the same aims, but that

the design of the object which is to be parameterised, is significantly different in each case. So, in what circumstances is each of these approaches desirable? Since functors are passed using references or pointers to an abstract base class which defines the functor interface, their interfaces must consist of virtual functions, thereby incurring the usual penalties of runtime polymorphism. Policy classes, on the other hand, can be written using normal member functions, and can therefore provide greater efficiency of execution. On the other hand, the runtime flexibility afforded by the use of functors can in certain circumstances make them more useful than policy classes.

B.5.2 Customisation of form: tuples and property maps

While, in the previous section, we were concerned with how to alter the *behaviour* of a class, another similar (and yet orthogonal, in OOP terms) problem is how to alter the *contents* of a class. That is, how to design a generic class to which we can easily add data members. As an example, consider the design of a graph vertex class. For some applications, there may be no information stored at each vertex; for others, each vertex may be given a label in the form of the string. For still other applications, the client may wish to associate a colour, or a more complex data structure with each vertex. A similar situation exists in the design of a generic tree node class.

The problem, therefore, is how to enable the client to customise the type of information which is stored at each node in a tree, or at each vertex and each edge in a graph. The 'classical' OOP solution to this problem would be to define an unlabelled graph or tree node as the base class, then to inherit from it, adding labels as member variables of the derived class, as shown in listing B.6. This approach has several drawbacks, notably that, for every type of node class derived from the generic base, code for various functions such as serialising the data, or printing it to the screen, has to be specially written. A far better approach would be to parameterise the base class on the type of data stored in it.

```
// Generic base node
class Node {

    // Contains code for iterating through child nodes, managing lifetime of
    // children, etc.
};

// Derived node type - we wish to label each node with a number
class LabelledNode : public Node {

    // Label is a member variable of the derived class
    int label;

    // Now we must write code for serialising the label, etc.
};
```

Listing B.6: Naieve design for a generic tree node class

C++ provides the capability for parameterising a class through the use of templates, which are orthogonal to inheritance. The STL defines several container templates, which may be instantiated by the client to allow any type of object to be stored inside them. One limitation of templates, however, is that one must specify the number of template parameters which a class should take; in other words, a naive parameterisation of the

base class allows us only to change the types of a *fixed number* of labels. For example, specifying the type of a generic graph vertex class as

```
template<class Label1, class Label2> class Vertex
```

states that each vertex is labelled with exactly two variables. We cannot specify an instantiation of the vertex template which has one, three or four labels.

Let us define the vertex template as taking just one parameter, then. Now, if we wish to instantiate a vertex type with three labels, we simply define a 'label object', and specify that as the template parameter:

```
template<class Label> class Vertex;
struct MyLabels { int i; float f; std::string s; };
typedef Vertex<MyLabels> MyVertex;
```

The problem with this approach is that we now need to write a set of member functions for `MyLabels`, which take care of I/O operations and the like. This means that some of the genericity of the `Vertex` template is lost, and the use of templates has gained us little over simply inheriting from an unlabelled base and adding the label data to the derived class.

The solution used in GAMUT is to use *property maps*. The first step of their implementation is to define a *tuple* class, that is, a fixed-size, heterogeneous collection of elements. Each node, vertex or edge contains a tuple, whose number and type of elements is determined at compile time by providing a *type list*. Typelists (Czarnecki and Eisenecker, 2000, Alexandrescu, 2002) are lists of types which a recursively defined: a typelist is a type, followed by a typelist, as shown below. The end of a typelist is marked by the presence of a 'null typelist' in the second position.

```
template<class Head, class Tail>
struct TypeList {
    typedef Head head;
    typedef Tail tail;
};
```

Just as we may recursively build up a list of types, a tuple is constructed by recursively building a list of *variables*, the type of each one being obtained from a typelist. This 'construction' occurs at compile-time; the run-time overhead of constructing a tuple is identical to that which would be incurred for construction of a normal structure containing the same variable types. The advantage of using tuples over structures is that generic code for serialising the tuple data, for printing the list of tuple elements to the screen and so forth, may be written just once, in the tuple template. This code is then valid for all combinations of types for the elements contained in the tuple; as such, the tuple class represents a truly generic software component. Moreover, an empty tuple may be optimised by the compiler to take up no storage space, and little or no runtime overhead. Using tuples to store the label data, we may define the generic node class as shown below.

```
// The LabelTypes parameter should be a typelist, containing the types
// of label(s) which are stored at each node in the tree.  The typelist may
// be empty, in which case the nodes are unlabelled
template<class LabelTypes> class Node {

    // A tuple of labels is aggregated into the vertex
    Tuple<LabelTypes> labels;
};
```

Accessing specific elements of a tuple by their index in the complete list of elements can be fairly easily implemented, but this is not very convenient for accessing the labels of a vertex, node or edge. For example, when defining a graph in which vertices each have a name (stored as a string), and a colour (stored as an integer), the vertex type would be defined using code something like the following:

```
typedef Vertex<TYPELIST(std::string, int)> vertex_type;
```

Now, when we wish to access the colour of a vertex, we must remember that it is in the second position within the list of labels. Given a vertex which has many different labels, this could be burdensome; a system in which we could refer to a specific label using its name, rather than its index, would be preferable, and closer in spirit to the usual situation in OOP, whereby member variables are accessed through *getter* and *setter* methods whose names are similar to that of the variable being referred to.

The provision of a more intuitive look-up system is the final step in the property map implementation. A property map is an extension of the tuple concept, whereby each element in the tuple is associated with a name, or key. The key is itself a C++ type, and a property map is defined by passing two typelists: the first specifies a list of key types, and the second specified the list of elements stored in the tuple. Elements may then be referred to using either their indices, or their keys, as shown in listing B.7. Now, we may simply inherit from the `PropertyMap` class when designing the vertex or node classes. In this way, the vertex and node classes become customisable in just the way described above.

```
// First, define types used as property keys - these are simply empty structures
struct name_key     { };
struct colour_key   { };

// Definition of a property map type
// Here, TYPELIST is a macro which recursively constructs a list of types
typedef PropertyMap<
    TYPELIST(name_key, colour_key),          // List of key types
    TYPELIST(std::string, int)               // List of element types
> property_map_type;

// Create an instance of the property map type
property_map_type P(''joebloggs'', 5);

// Access elements of the property map using tuple indices
std::string name = P.elem<0>();              // Returns ''joebloggs''
P.elem<1>() = 10;                            // Sets colour to 10

// Access elements of the property map using property keys
std::string name2 = P.property<name_key>();  // Returns ''joebloggs''
int colour2 = P.property<colour_key>();      // Returns 10
```

Listing B.7: Property maps

Appendix C

Implementation of the GAMUT library

This appendix is concerned with the technical details of the implementation of the GAMUT library. It aims to show how the design of the library delivers both efficiency of execution and ease of use to the programmer.

C.1 Implementation of the generic components layer

In this and the next section, the implementation of each component of GAMUT is discussed in more detail. Here, we focus upon the generic component layer upon which more complex classes are built. Where possible, the inter-relationships between different classes in the library are illustrated using Unified Modelling Language (UML) diagrams (Object Management Group, 1995). The description presented here is, at times, necessarily quite technical in nature; as such, a working knowledge of the C++ language will be necessary to fully understand certain salient points. For a summary of the general coding principles adhered to when writing the library, the reader is referred to appendix B.1; the appendices which follow it discuss some more specialised programming issues which relate to the design and implementation of certain parts of the library.

Short sections of GAMUT code are included here where necessary in order to illustrate a particular concept. In order to fully understand all details of the library, however, interested readers are advised to inspect the library home page.

C.1.1 Arrays

As described in §2.3.4.1.1, the two main types of array class defined in GAMUT are fixed-size, one-dimensional arrays, and a three-dimensional array class with associated indexing and addressing features. The fixed-size array class is a template class, which is simply a wrapper around a standard C array. Its function is to endow arrays with the object-oriented features (such as iterators, proper copy semantics, *etc.*) expected of data types in C++, which are missing from the C array type. Since the only data member of the class is the aggregated C array, and since almost all member functions are inline, the array class nonetheless offers performance comparable to the C array type.

The implementation of the three-dimensional array class is broken into two pieces: a *dimension* class, and the *array* class itself, which holds the data values. The dimension class is responsible for index-address conversions, and for determining whether a given index or address is within bounds. The array class proper is responsible for managing and providing access to the data values (the latter being possible using iterators,

views or random access). The array class inherits from the dimension class, thus exposing the indexing functions of the latter to the client.

The array class is naturally templated on the type of value being stored within it. Where this type is numerical, a composite dispatch technique[1] is used to add arithmetical operators to the array interface, as described in the design section.

C.1.2 Graphs

The graph components within GAMUT were originally written to facilitate the representation and comparison of chemical structures. In their original incarnation, they were heavily based on the graph components in the CCP4 Coordinate Library (Krissinel, 2002). Since then, the graph objects have been substantially redesigned, with much inspiration taken from the Boost Graph Library (The Boost Committee, 1998).

The fundamental components of the GAMUT graph framework are the `Graph`, `Vertex` and `Edge` class templates. Of these, the only class of which users create objects directly is `Graph`; `Vertex` and `Edge` objects are created and 'owned' by the `Graph` class, with users gaining access to vertices and edges via references returned from `Graph` methods.

GAMUT graphs are parameterised on seven characteristics, namely:

1 Vertex type
2 Edge type
3 Properties attached to the graph itself
4 Edge representation
5 Vertex container type
6 Edge container type
7 Containment policy

These are explained below.

C.1.2.1 Vertex and edge types

The vertex and edge classes used in GAMUT graphs are parameterised on the type of data stored in each. This data is stored and accessed using a technique called 'property maps'; more details on this are available in appendix B.5.2. A graph type is defined by first defining the types of its vertices and edges, and then instantiating the `Graph` template with these parameters. All three of the class templates `Vertex`, `Edge` and `Graph` may be assigned labels using the property map framework. The whole process is illustrated in listing C.1.

[1] See appendix B.4 for a description of the composite dispatch technique.

```
using namespace gamut::graph;

// Define the set of colours from which each vertex may be annotated
enum colour { BLACK=0, WHITE, RED, YELLOW, BLUE, GREEN };

// Definition of the vertex type
typedef TYPELIST_2(vertex_label_key, vertex_colour_key) vertex_keys_t;
typedef TYPELIST_2(unsigned int, colour)                vertex_props_t;
typedef Vertex<vertex_keys_t, vertex_props_t>           vertex_t;

// Definition of the edge type
typedef TYPELIST_1(edge_weight_key)                     edge_keys_t;
typedef TYPELIST_1(float)                               edge_props_t;
typedef Edge<edge_keys_t, edge_props_t>                 edge_t;

// Definition of the graph properties
typedef TYPELIST_1(graph_label_key)                     graph_keys_t;
typedef TYPELIST_1(std::string)                         graph_props_t;

// Finally, we define the graph type itself
// Note that here, only three graph characteristics (vertex type, edge type
// and graph properties) are defined.
typedef Graph<vertex_t, edge_t, graph_keys_t, graph_props_t>    graph_t;
```

Listing C.1: Syntax for definition of a GAMUT graph type
This code shows the syntax used to define a graph type whose vertices each have a label, which is an unsigned integer, and a colour. The edges of the graph are each associated with a weight, which is a floating point number. In addition, the graph itself has a label.

C.1.2.2 Graph properties

The `Graph` class itself also inherits from `PropertyMap`, so that properties can be specified for the graph as well as for its component vertices and edges. The typelists for the graph property keys and property types are provided as template parameters, as shown in listing C.1.

C.1.2.3 Edge representation

While vertices are always stored by `Graph` objects in a simple list structure, GAMUT provides three different edge representations for graphs:

- Edge list
- Adjacency list
- Adjacency matrix

For a description of the differences between these representations, andthe computational/algorithmic implications of choosing a particular representation, see appendix A.

Selecting the type of edge representation is simple: it is done by passing a template parameter which identifies the required representation, as shown in the code below.

```
using namespace gamut::graph;
typedef Graph<
    vertex_t,
    edge_t,
    TYPELIST_1(graph_label_key),
    TYPELIST_1(std::string),
    AdjacencyListSelector                    // A special 'tag' class
> adjacency_list_graph_t;
```

Internally, each different type of edge representation is defined as a separate class. When the `Graph` template is instantiated using a particular edge representation selector tag, the appropriate edge representation class is used as a base class for the graph. This is achieved using the *composite dispatch* technique described in appendix B.4.

Interconversion between different representations of the same type of graph is automatically handled by the library:

```
// Declare an edge list graph object
edge_list_graph_t g1;

// Populate g1 with some data - this code is omitted for brevity

// Create an adjacency list representation of g1
adjacency_list_graph_t g2 = g1;
```

This allows the client to very easily 'reformat' the graph data into the edge representation most suitable for a particular algorithm or application.

C.1.2.4 Vertex and edge container types, and the containment policy

As stated earlier, the `Graph` class manages the lifetime of its consituent vertices and edges. Internally, these are both stored in STL containers, which may be instantiations of `std::vector`, `std::list` or `std::set`. For details of the differences between these containers, the user is referred to the STL documentation (Inc., 1994).

The type of container used to store vertices may be important depending on the application. For example, while `std::vector` guarantees constant-time random access to its elements, finding a particular element within the vector is a linear time operation. Conversely, finding an element in a `std::set` is guaranteed to be possible in, at worst, logarithmic time, but obtaining an element by its index is not directly possible. In order to provide maximum genericity, GAMUT allows clients to specify which STL container is used for both vertex and edge storage.

The mechanism used to achieve this flexibility is to define a *container wrapper* template. This is a class which contains an instance of one of the STL containers described above, and which exposes an interface which is invariant over the set of possible containers. To illustrate briefly what this means, consider random access to elements stored in a container. The `std::vector` container facilitates this directly, via its `operator[]`; however, `std::list`, although a sequential container, does not provide random access to its contents. However, we may implement a random access function for `std::list`, simply by incrementing an

iterator from the beginning of the list, by the required number of steps. Clearly this is a linear-time operation, compared with the constant-time amortization of `std::vector::operator[]`.

The `ContainerWrapper` template class exposes a number of member functions, including `operator[]`, each of which may either be a forwarding function to the aggregated STL container, if a suitable function exists, or may be implemented within `ContainerWrapper` using member functions of the STL container. In this way, we may create containers which, although internally implemented using different STL components, expose a common interface, and which therefore may be used interchangably inside other classes such as `Graph`.

The inheritance hierarchy of the `Graph` class is illustrated in figure C.1.

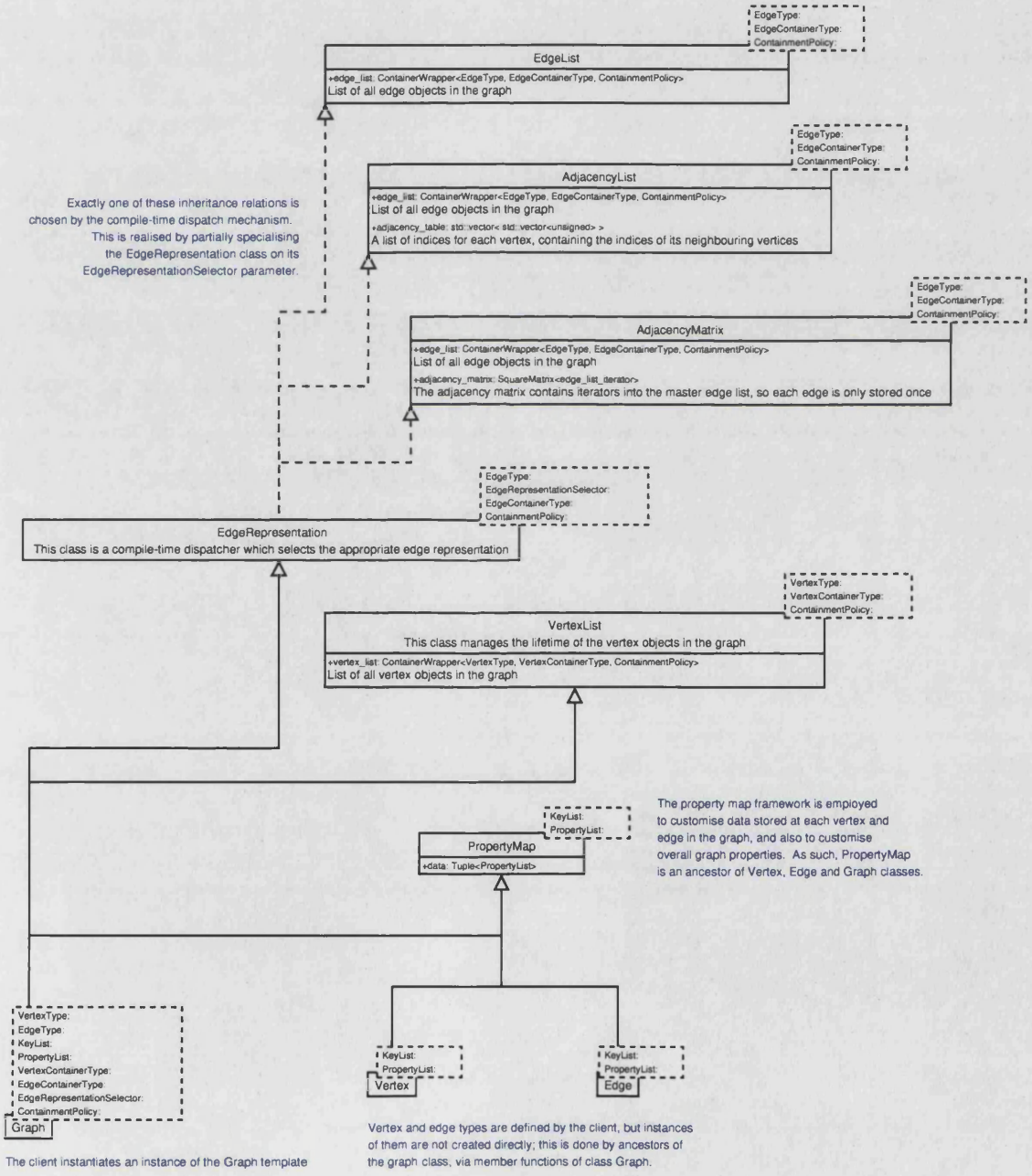

Figure C.1: UML diagram of the inheritance hierarchy of the `Graph` class

C.1.2.5 The graph interface

As mentioned in §2.3.4.1.2, one requirement of the graph framework was that is should expose an intutive interface which should be, as far as possible, invariant over different combinations of the graph parameters. In other words, the client should be able to manipulate a coloured, edge-list graph in much the same was as he/she would interact with an uncoloured, adjacency-matrix graph. To achieve this, a set of interface functions which should be available for any vertex and edge representations was mandated during the design phase; this is summarised in tables C.1 and C.2. A use of the graph interface, to populate a graph with data, is illustrated in listing C.2.

C.1.2.6 Graph algorithms

In the GAMUT graph framework, each type of graph algorithm is implemented as a template class, parameterised on the type of graph which it processes. In order to run an algorithm on a given graph, the client creates an instance of the algorithm object, passes it a reference to the graph, and then calls the `run` member function of the algorithm. The results of the algorithm may then be accessed through other member functions of the algorithm object.

Graph algorithms are divided into *unary* algorithms, which operate on one graph at a time (such as a ring perception algorithm), and *binary* algorithms, which operate upon a pair of graphs (such as a maximum common subgraph detection algorithm). Every unary algorithm class inherits from the `UnaryAlgorithm` class, which holds a pointer to the subject graph, and has responsibility for logging functions. A similar `BinaryAlgorithm` base class is also defined. Figure C.2 shows part of the inheritance hierarchy of the graph algorithm classes. It should be noted that this hierarchy was consciously designed in such a way as to facilitate the easy addition of more than one algorithm of the same type. For example, should the client wish to implement a new subgraph isomorphism algorithm, he/she should do so by inheriting from the `MCSAlgorithm` class. In this way, two benefits are realised: firstly, much of the 'housekeeping code' necessary for the algorithm is inherited from the base class, and secondly, the new algorithm object can be substituted for any other subgraph isomorphism object in client code, since they share the same interface.

Function	Return type	Description
`n_vertices() const`	`size_t`	Number of vertices in the graph
`vertex(size_t n)`	`vertex_type&`	Get reference to the nth vertex
`vertex(size_t n)`	`const vertex_type&`	Get const reference to the nth vertex
`n_visible_vertices() const`	`size_t`	Number of vertices in the graph which are not hidden. Each vertex can be temporarily hidden, which means that it is ignored by any algorithms which operate on the graph.
`visible_vertex(size_t n)`	`vertex_type&`	Get reference to the nth visible vertex
`visible_vertex(size_t n)`	`const vertex_type&`	Get const reference to the nth visible vertex
`vertex_begin()`	`vertex_iterator`	Get iterator to the first vertex in the graph
`vertex_end()`	`vertex_iterator`	Get iterator past the last vertex in the graph
`vertex_begin() const`	`const_vertex_iterator`	Get iterator to the first vertex in the graph
`vertex_end() const`	`const_vertex_iterator`	Get iterator past the last vertex in the graph
`visible_vertex_begin()`	`visible_vertex_iterator`	Get iterator to the first visible vertex in the graph
`visible_vertex_end()`	`visible_vertex_iterator`	Get iterator past the last visible vertex in the graph
`visible_vertex_begin() const`	`const_visible_vertex_iterator`	Get iterator to the first visible vertex in the graph
`visible_vertex_end() const`	`const_visible_vertex_iterator`	Get iterator past the last visible vertex in the graph
`erase_vertex(vertex_iterator)`	`vertex_iterator`	Erase a vertex from the graph
`add_vertex(const vertex_properties_t&)`	`vertex_iterator`	Add a vertex to the graph, and give it the specified properties

Table C.1: Vertex-related functions in the graph interface

Function	Return type	Description
`n_edges() const`	`size_t`	Number of edges in the graph
`edge_exists(size_t i, size_t j) const`	`bool`	Returns true if the specified pair of vertices are adjacent
`edge_properties(size_t i, size_t j)`	`edge_properties_t&`	Returns a reference to the properties of the specified edge
`edge_properties(size_t i, size_t j) const`	`const edge_properties_t&`	Returns a reference to the properties of the specified edge
`out_edge_begin(size_t i)`	`out_edge_iterator`	Get iterator to first out-edge of ith vertex. When dereferenced, this iterator returns a reference to the properties of the out-edge.
`out_edge_end(size_t i)`	`out_edge_iterator`	Get iterator past last out-edge of ith vertex
`out_edge_begin(size_t i) const`	`const_out_edge_iterator`	Get iterator to first out-edge of ith vertex
`out_edge_end(size_t i) const`	`const_out_edge_iterator`	Get iterator past last out-edge of ith vertex
`adjacent_begin(size_t i) const`	`adjacent_iterator`	Get adjacency iterator to first neighbour of ith vertex. When dereferenced, this type of iterator returns the index of the neighbouring vertex.
`adjacent_end(size_t i) const`	`adjacent_iterator`	Get adjacency iterator past last neighbour of ith vertex.
`add_edge(size_t i, size_t j, const edge_properties_t&)`	Varies according to edge representation	Add an edge between ith and jth vertices, with specified properties

Table C.2: Edge-related functions in the graph interface

```
// The graph type graph_t is defined as per the previous listing
graph_t G;

// This code shows how to generate the following graph:
/*
```

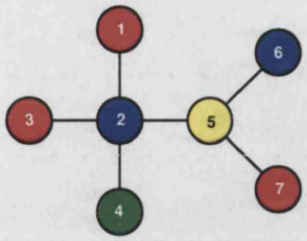


```
*/

// Add vertices
G.add_vertex(vertex_t::properties_t(1, RED));
G.add_vertex(vertex_t::properties_t(2, BLUE));
G.add_vertex(vertex_t::properties_t(3, RED));
G.add_vertex(vertex_t::properties_t(4, GREEN));
G.add_vertex(vertex_t::properties_t(5, YELLOW));
G.add_vertex(vertex_t::properties_t(6, BLUE));
G.add_vertex(vertex_t::properties_t(7, RED));

// Add edges - each edge is defined using a pair of vertex
// indices and the edge properties (here, a floating-point
// weight value). The vertex indices are zero-based and
// correspond to the order in which vertices were added to
// the graph
G.add_edge(0, 1, edge_t::properties_t(0.6));
G.add_edge(1, 2, edge_t::properties_t(0.6));
G.add_edge(1, 3, edge_t::properties_t(0.6));
G.add_edge(1, 4, edge_t::properties_t(0.6));
G.add_edge(4, 5, edge_t::properties_t(0.6));
G.add_edge(4, 6, edge_t::properties_t(0.6));
```

Listing C.2: Population of a graph object with data

The graph algorithms currently implemented in GAMUT are listed in table C.3.

Class	Algorithm	Reference
Clique detection	Bron-Kerbosch	Bron and Kerbosch (1973)
Subgraph isomorphism detection	Clique detection	Bron and Kerbosch (1973)
Subgraph isomorphism detection	CSI	Krissinel and Henrick (2004a)
Ring perception	Ring perception by breadth-first search	Figueras (1996)
Layout	Force-directed	N/A
Shortest path	Floyd-Warschall all pairs shortest path	Floyd (1962)
Traversal	Depth-first search	Gibbons (1985)
Traversal	Breadth-first search	Gibbons (1985)

Table C.3: Graph algorithms currently implemented in GAMUT

As with many algorithms in GAMUT, the graph algorithms each allow their behaviour to be customised to a degree. For example, the `RingPerceptionAlgorithm` class allows the client to specify the size of the smallest ring which should be considered. The subgraph isomorphism algorithms require that the client specify what criteria must be met by a pair of vertices, in order that they can be considered equivalent by the matching algorithm. For one application, simply sharing the same colour may be sufficient to consider two vertices compatible; for another, the user may wish to define a more complex function on the properties of the two

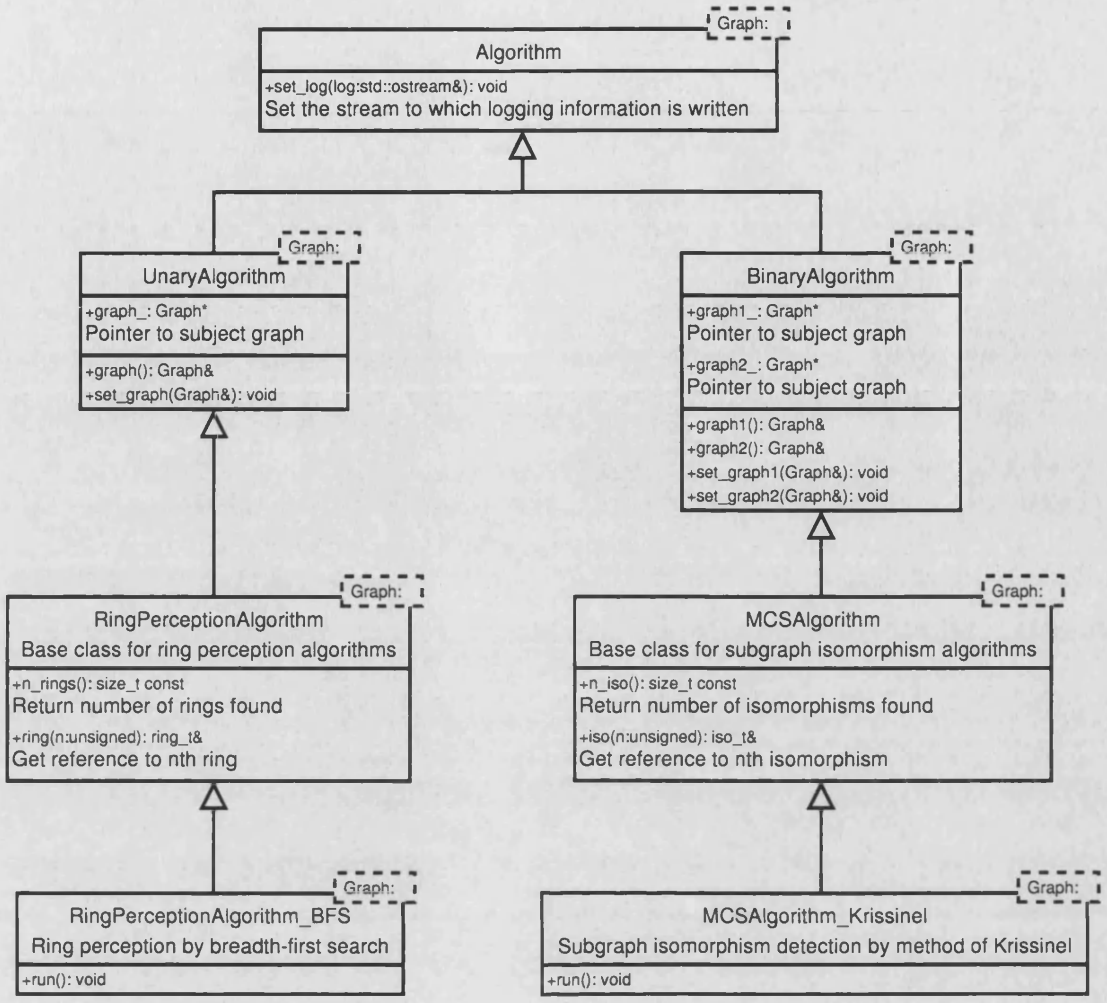

Figure C.2: UML diagram of the inheritance hierarchy of two graph algorithm classes

vertices.

These two examples of behavioural parameterisation fall into distinct classes: the first is easily achieved by a member function which modifies a scalar value in the algorithm object, while the second essentially requires that the client be able to effectively pass a bundle of code into the algorithm. As in several places through the library, the latter type of parameterisation is implemented using *behavioural functors*[2]. The vertex matching criteria discussed above may be encapsulated in a functor of the following form:

```
template<class VertexType>
struct VerticesMatch {

    bool operator()(const VertexType& u, const VertexType& v) const;
};
```

This functor takes as its arguments a pair of vertex references, and returns a boolean value indicating whether they are compatible, and hence, may form part of a graph isomorphism. The `MCSAlgorithm` class allows the client to register a vertex-matching functor of this type, and a corresponding functor for the edge-matching criteria, before running the algorithm.

[2]See appendix B.5 for a discussion of behavioural customisation using function objects.

C.1.2.6.1 Layout algorithms

For the case of graph layout methods, the algorithm in question calculates the 2D coordinates of each vertex in the layout, but does not 'know' how to draw the vertices and edges onto a graphics device. Again, functors are used; this time, the functors are vertex and edge 'depiction generators', each of which returns a graphics object for a given vertex or edge. In this way, the client is free to write a functor which represents each vertex as a circle, a triangle, or any other depiction of arbitrary complexity. The usefulness of this approach is exemplified in the implementation of the chemical structure diagram generation class (described in detail in §C.2.2.3). In order to produce diagrams with a standardised apperance, each atom in the structure should be represented in the appropriate way (*i.e.* the atomic symbol, with a superscript indicating its formal charge). Implementing this is simple: a functor was written which generates the appropriate glyphs, and simply 'plugged in' to the layout framework.

The graph layout algorithm base class inherits directly from `graphics::Collection`, a container class for graphics objects (see §C.1.6). This means that the, after the initial layout phase, the client can easily perform various manipulations on the layout (*e.g.* rotations, scaling *etc.*) in order to tailor it to the requirements of the application. An example is presented in listing C.3.

```
// Let graph_t be a typedef for the graph type we are using
graph_t G;

// Populate graph with data - code omitted here

// Declare a layout object.  This is an instance of the random
// layout class, which simply assigns random 2D coordinates to
// each vertex.
graph::LayoutRandom<graph_t> layout(G);

// Run the algorithm
layout.layout();

// Scale the collection of graphics objects to fit inside a
// given bounding box, while maintaining the aspect ratio of
// the original layout
layout.fit_maintain_aspect(100, 100, 500, 500);

// Open a PostScript file, and draw the graph layout into it
graphics::PostScript out(''graph.ps'');
layout.draw(out);
```

Listing C.3: Graph layout example

C.1.3 Linear algebra

The fundamental components of GAMUT's linear algebra framework are classes for representing vectors and matrices. Each of these may be divided into to two broad types: those whose size is fixed at compile-time, and those which may be dynamically re-sized. Objects which can be dynamically re-sized incur an extra overhead compared to those whose size is statically determined, both in terms of extra data members which must be maintained (to store the current size of the object and the amount of memory which has been allocated to it), and a runtime speed penalty. As such, fixed-size linear algebra components are preferred for applications such as 3D geometry, in which the size of the vectors and matrices will always be the same.

On the other hand, applications such as those which manipulate distance matrices for clustering or pricipal component analysis require the ability to change the size of the linear algebra objects at runtime.

The implementation consequences of choosing whether a linear algebra component is statically or dynamically sized are as follows:

- **Storage**: statically sized components may store their data by aggregating a statically C array; dynamic components should aggregate an STL container instead. The container used in the dynamic component implies extra overhead in terms of both required storage and runtime performance.
- **Runtime checks**: vector and matrix algebra operations can be carried out on statically sized objects without any runtime checks to ensure that the operands are compatible in dimension.
- **Construction**: vectors and matrices which have a fixed size may have their elements initialised directly by the constructor; since the length of the list elements required for a dynamic component is not known *a priori*, it cannot be passed to the constructor. This means that statically sized components may be constructed more efficiently.

The templates which are defined in the linear algebra module are listed in listing C.4. Elementary linear algebra operations, for example matrix multiplication, are implemented as member functions of these classes. More complex operations, such as matrix diagonalisation and singular value decomposition, are implemented as classes in the same way as the graph algorithms described above.

```
// Statically sized classes
template<typename T, size_t N>  class Vector;
template<typename T, size_t N>  class SquareMatrix;

// Classes whose size may be specified at runtime
template<typename T>            class DynamicVector;
template<typename T>            class DynamicMatrix;
template<typename T>            class DynamicSquareMatrix;
```

Listing C.4: Classes defined in the linear algebra component

C.1.4 Geometric range querying

Geometric range querying (§3.4) is a common operation in structural bioinformatics applications. The geometric range query framework implemented in GAMUT allows any type of data to be stored in the query map, as long as each data object is associated with a k-dimensional coordinate. This allows it to be used, for instance, to index the positions of atoms in space such that the set of atoms which fall inside a given geometric region may be rapidly determined.

GAMUT defines an abstract base class named `Region` providing functions which answer these questions. `Region` is templated on the dimensionality of the space, and on the type used to represent coordinates in this space. A set of shapes including (hyper)spheres, (hyper)cubes and (hyper)annuli, which inherit from `Region` are defined. Of course, the client is free to define other regions in a similar manner; in this way, the geometric query framework is fully extensible. An outline of the classes which comprise the geometric region framework is presented in listing C.5.

```
// Abstract base class for regions in D-dimensional space
// C is the type of coordinate used
template<typename C, size_t D> class Region {

    virtual bool contains_point(const Vector<C,D>&) const = 0;
    virtual bool intersects_box(const Vector<C,D>&, const Vector<C,D>&) const = 0;

    // Functions which return the geometric centre of the region, and
    // the distance of its furthest extremity from this point
    virtual Vector<C,D> centre() const = 0;
    virtual C           extent() const = 0;
};

// Concrete classes which inherit from the abstract region
template<typename C, size_t D> class Sphere  : public Region<C,D> { /* ... */ };
template<typename C, size_t D> class Cube    : public Region<C,D> { /* ... */ };
template<typename C, size_t D> class Annulus : public Region<C,D> { /* ... */ };
```

Listing C.5: An outline of the framework for describing geometric regions

C.1.5 Trees

A tree is mathematically equivalent to a Directed Acyclic Graph (DAG) ; as such, it would be possible to implement a tree data structure directly using the graph template described above. However, certain features of the graph template render it unsuitable for the types of uses to which trees are put within GAMUT As such, a separate tree component was written from scratch.

Within GAMUT, types trees are distinguished on two primary criteria:

- **Arity of children**: binary trees, where each node has exactly two children, are distinguished from *N-ary* trees, where each node may have any number of children (including zero). The former type is used to represent data structures such as clustering hierarchies and kd-trees, while the second forms the basis for molecular structure and domain classification hierarchies.
- **Heterogeneity**: in some trees, all nodes are of the same type, while other trees may be heterogeneous in their composition. For example, in a clustering tree, every node in the tree represents a single clustering division, and therefore each node stores the same type of data. Taking the example of a tree representing a molecular structure, some nodes represent residues, others atoms *etc.*. This distinction is important from an implementational standpoint, as is clear when one considers the operation of copying a tree. Where the nodes are *monomorphic*, this is straightforward, but for a *polymorphic* tree, it is necessary to store the children of each node using base-class pointers, with the concrete type of each newly-created node being determined by inspecting the type of the source node.

In GAMUT, there is no such class as `Tree`; rather, a tree is created simply by declaring a node object, which represents the root. Node objects 'own' their child nodes, such that when the destructor of a node is called, it destroys all its children automatically. This leads to the recursive destruction of the entire subtree of that node. It should be clear, therefore, that a node class should:

- contain its child nodes, either
  - in the form of pointers to dynamically-allocated objects, which are explicitly deleted by the parent's destructor

  - directly, by aggregation: in this case, child nodes will be automatically disposed of when the parent is destroyed

- contain a pointer to the parent node, which is null if the node is a root

C.1.5.1 Classes

Due to the quite different characteristics exhibited by each of the types of tree described above, they are modelled using four different class templates, all defined in namespace `gamut::tree`:

- `BinaryNode`
- `PolymorphicBinaryNode`
- `NaryNode`
- `PolymorphicNaryNode`

However, since all node types share the characteristic that they contain a pointer to their parent, each of these classes inherits from a common base, `Node`. The binary node classes each contain a pair of pointers to their left and right children. The N-ary nodes aggregate a container of child nodes, in the form of a `ContainerWrapper` object, as described in §C.1.2.4.

C.1.5.2 Traversals

Whereas, for the graph classes, traversals such as breadth-first and depth-first searches are implemented as standalone classes, it was more convenient in the tree framework to implement these as different types of *iterators*. There are five 'flavours' of iterators defined, as shown in table C.4.

Type	Result of incrementing	Result of decrementing	Stopping condition
vertical	Move to first child	Move to parent	Current node has no children
horizontal	Move to next node at current depth	Move to previous node at current depth	Current node is last at current depth
depth-first	Move to next node in depth-first-search	Move to previous node in depth-first-search	Current node is last in the tree
breath-first	Move to next node in breadth-first-search	Move to previous node in breadth-first-search	Current node is last in the tree
children	Move to next child of current node	Move to previous child of current node	Already at last child of current node

Table C.4: Types of tree iterators
The five flavours of tree iterator are described. Each one defines the increment and decrement operators ++ and --; the effect of calling each of these is described. As with all types of iterators, there must be a means of determining when the iteration should be stopped; this is described as the 'stopping condition'.

The interface for performing tree iterations is common across all types of tree; for example, in order to iterate through all children of a particular node, one would write code with the following form:

```
SomeNodeType n;
for(SomeNodeType::child_iterator i = n.child_begin();
    i != n.child_end(); ++i)
    const SomeNodeType& child = *i;
```

The syntax for performing other types of iteration is similar to this.

C.1.5.3 Layout algorithms

Two simple tree layout algorithms are implemented in GAMUT; the diagrams in figure C.3 illustrate the difference between them. The architecture of the tree layout classes is very similar to the graph layout algorithms described previously. As for graphs, the tree `Layout` classes

- inherit from `graphics::Collection`
- can have their output customised using the *behavioural functor* technique: here, the client provides a 'node depiction generator' functor, which creates a graphics object for each node.

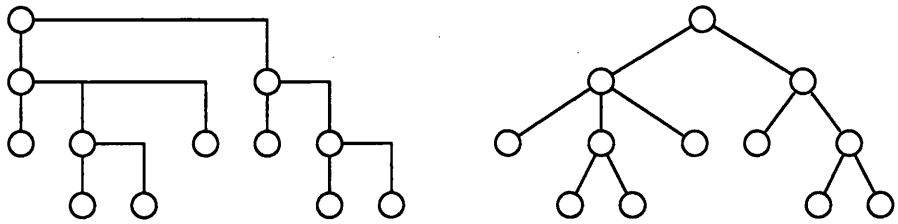

Figure C.3: Tree layout algorithms

C.1.6 Graphics

In order to display certain types of data, such as the structure of graphs, a simple 2D graphics framework has been implemented in GAMUT. This consists of the following components:

- **Graphical primitives**: A set of classes which represent geometric primitives such as circles, lines, polygons and text. These classes inherit from a common base class, `graphics::Object`, which defines an interface allowing operations such as scaling, translation, rotation and drawing to be carried out polymorphically via `Object` pointers or references.
- **Graphics containers**: Classes which contain heterogeneous collections of graphics objects, stored as `Object*` pointers. The container classes themselves also inherit from `Object`, such that the client may easily manipulate whole groups of graphics objects at a time.
- **Colours**: Classes which represent colours as either Red, Green, Blue (RGB) or Hue, Saturation, Value (HSV) triplets, and functions to convert between the two formats.
- **Graphics devices**: An abstract graphics device is defined, providing an interface which allows the user to draw any of the primitives described above. A single concrete graphics device is implemented at present; this class generates PostScript (Adobe Systems Incorporated, 1990) format images.

The graphics framework is required to visualise the graph and tree layouts generated by the algorithms described above.

C.1.7 Persistence

A pair of stream classes, `io::Ostream` and `io::Istream`, are defined in GAMUT, and are used for binary serialisation of library objects; these classes are instantiations of the standard library templates `std::ostream`

and `std::istream`. The interface to the stream objects consists of a pair of functions named `gwrite` and `gread`, for "generic write" and "generic read":

```
template<typename T> Ostream& Ostream::gwrite(const T& x);
template<typename T> Istream& Istream::gread(T& x);
```

These functions are described as generic in the sense that they are capable of writing or reading any type of object, as long as it is either

- A GAMUT object
- A POD (plain old data) type, such as `char`, `int`, `float`, *etc.*

The way these functions work is as follows. If the object `x` passed to the `gwrite` function is a POD type, a specialised version of gwrite is called (a specialised version of the function exists for every POD type). This function writes `x` to the stream using the standard library function `std::ostream::write`. By convention, GAMUT objects are stored in little-endian format. When performing binary I/O on floating point values, is is required that the machine represents floating point numbers internally using the IEEE 754 standard (Institute of Electrical and Electronic Engineers, 1987); on all platforms inspected to date, this has been found to be the case.

If the object is not a POD type, it cannot match the signature of any of the specialised forms of `gwrite`, so the generic (nonspecialised) version of the function is called. This version attempts to call `x.write(*this)`. All GAMUT objects define a pair of functions which implement its serialisation; these functions have the signatures

```
void write(io::Ostream&) const;
void read(io::Istream&);
```

The call to the nonspecialised `gwrite` function can only compile if the compiler can find an appropriate `write` function defined in the `T` class - in other words, if `x` is a GAMUT object.

To summarise, the GAMUT `Ostream` class facilitates the writing of any type of object (POD or GAMUT) to the stream using the same function call (`gwrite`), with the appropriate implementation of this function being chosen by the rules of C++ template instantiation, and endianness being automatically accounted for. Symmetrically, any type of POD or GAMUT object may be read from an `Istream` using the `gread` function. The result of this is that the implementation of the serialisation functions within each GAMUT class becomes very simple, as shown in listing C.6.

C.1.7.1 Indexed file storage

In addition to simple serialisation, GAMUT provides the capability to create indexed files. Indexed files are useful when a large number of objects of the same type need to be stored, and accessed efficiently. By indexing the archive file, only those items of data to which the client requests access, need be read into memory.

The indexed file mechanism implemented in GAMUT is based on the ISAM principle. The idea is that two disk files are created. The first, known as the data file, simply contains data objects serialised one after

```
// An example GAMUT object
class AGamutObject {

    // Member variables
    int                 i;      // A POD type
    std::string         s;      // An STL type
    AnotherGamutObject  o;      // A GAMUT type

    public:

        void write(io::Ostream& out) const {

            out.gwrite(i);      // Calls out.write(&i, sizeof(int))
            out.gwrite(s);      // Calls a GAMUT function which writes strings
            out.gwrite(o);      // Calls o.write(out)
        }

        void read(io::Istream& in) {
            in.gread(i);        // Calls in.read(&i, sizeof(int))
            in.gread(s);        // Calls a GAMUT function which reads strings
            in.gread(o);        // Calls o.read(in)
        }
};
```

Listing C.6: Implementation of serialisation functions for a GAMUT object

another. The second file is the index file, and contains, for each data object, one or more keys, associated with the offset into the data file at which the record of the appropriate data object begins. The ISAM file organisation is illustrated in figure C.4.

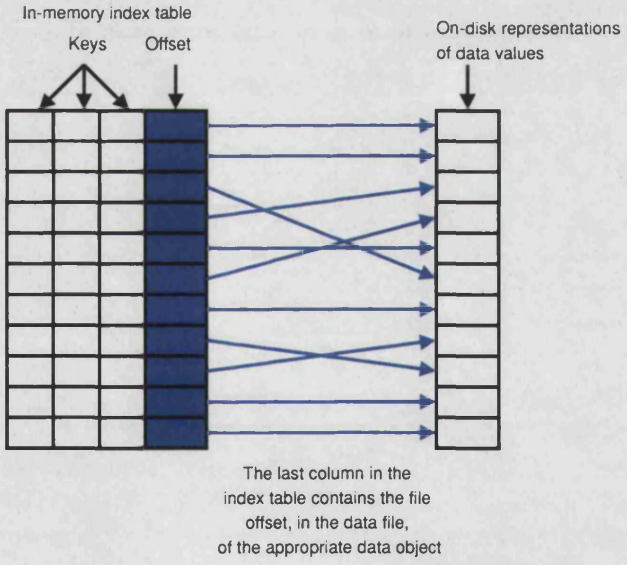

Figure C.4: Organisation of an ISAM archive
The diagram shows the relationship between the two components of the ISAM archive - the index file and the data file.

When an ISAM archive is opened, the index file is read in its entirety, and an in-memory map from the keys to a set of 'data object proxies' is built. Each proxy contains two members: the offset of its respective data object in the data file, and a pointer, which is initialised to null. When the client requests access to a particular data object, by looking up its key(s) in the index, the ISAM archive object inspects the appropriate proxy. If its pointer is null, the data file is accessed, and the data object loaded into memory, with the read operation starting at the file offset stored in the proxy. A pointer to the newly loaded data object is stored in the proxy,

and a reference to the same object returned to the client.

If, when a proxy is inspected, its pointer is found to be non-null, this means that the data object has already been loaded into memory, and a reference to it can be returned immediately, without further disk access. This scheme, which is known as *pointer swizzling*, therefore minimises the amount of access which needs to be made to the data file, which is typically large in size.

The description of ISAM behaviour thus far has assumed that the archive is a read-only object. GAMUT does indeed allow an ISAM archive to be opened read-only, but it may also be opened with write access enabled. In this case, the library must keep track of changes which have been made to the archive. The archive may be changed by adding, deleting, or modifying data objects held in it. Changes are only made to the in-memory representation of the archive data; the client must explicitly call a `commit` function in order to commit these changes to disk. At this point, the index and data files are reorganised to bring them into syncrony with the in-memory data. All of the steps described above are illustrated in figure C.5.

The implementation of the ISAM archive class in GAMUT consists of three parts. The first of these is the definition of a class which handles the mapping from a tuple of keys, to the file offset. GAMUT contains a template class, `TupleMap`, which maps a tuple onto a single data value. Internally, `TupleMap` contains N separate maps, where N is the number of elements in the key tuple. This allows queries to be performed either on a single key element, or on a combination of several key elements.

The second component of the ISAM archive is the proxy class. As described above, the proxy contains the file offset of the data object which it represents, as well as a pointer to that object. In addition, each proxy contains a pointer to a file stream which is connected to the data file. This allows the definition of a member function in the proxy, `Proxy::operator*()` which automatically loads the data object, if required, and returns a reference to it. As such, the proxy represents an autonomous pointer swizzler, transparently returning its data object when required, leaving the client unaware whether or not disk access has taken place. In addition, the `Proxy` class contains a record of the *status* of its data object, which records whether the object is new, modified, or still synchronised with the on-disk representation.

The third part of the ISAM implementation is the class which clients actually utilise, named `isam::Table`. The table class contains a `TupleMap` from tuple keys to `Proxy` objects, and provides the member functions necessary to allow the client to access data in the archive. The `Table` class is responsible for orchestrating all disk access to the ISAM files, in particular maintaining the integrity between the index and data files, and reorganising data objects such that no gaps are created in the data file by removal or modification of data values.

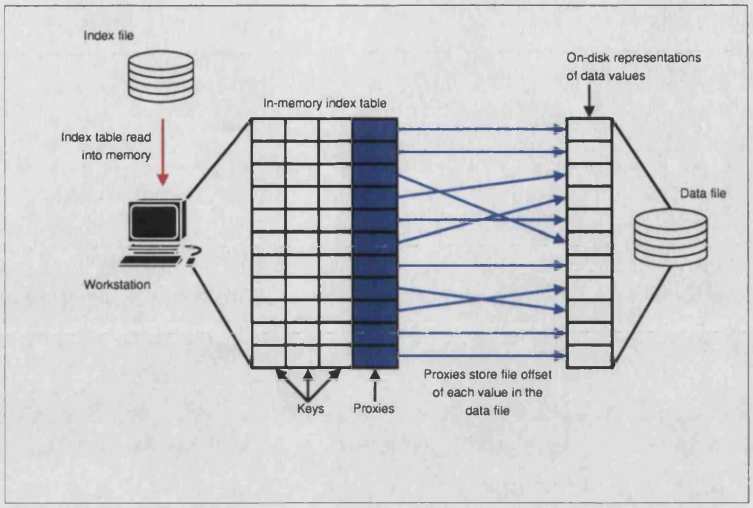

(a)

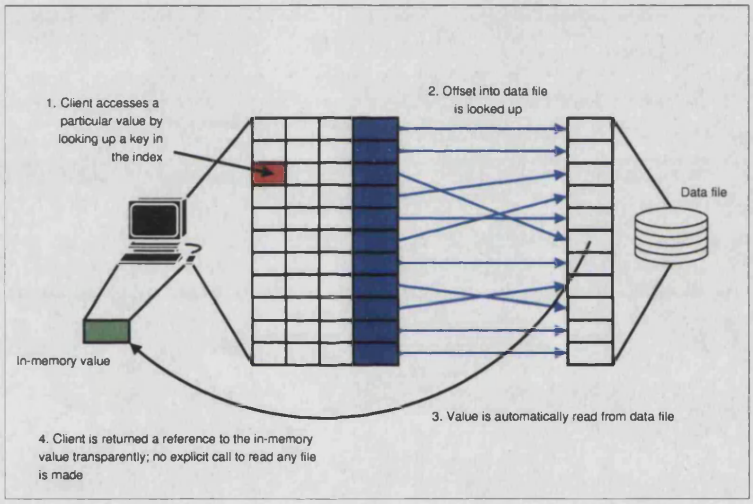

(b)

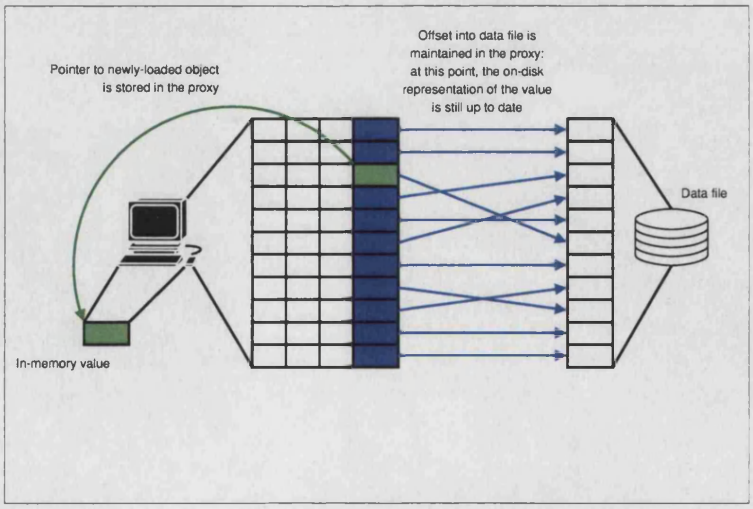

(c)

Figure C.5: Pointer swizzling

(a) Index is loaded into memory; (b,c) swizzling occurs when data values are requested by the client. Continued overleaf.

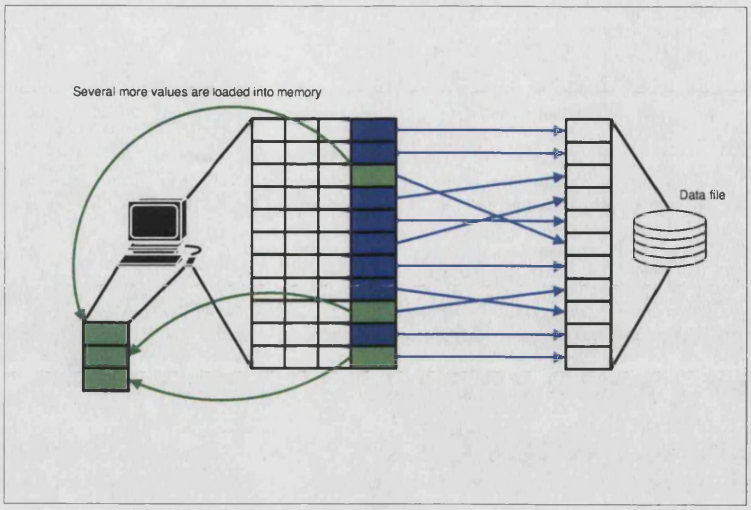

(d)

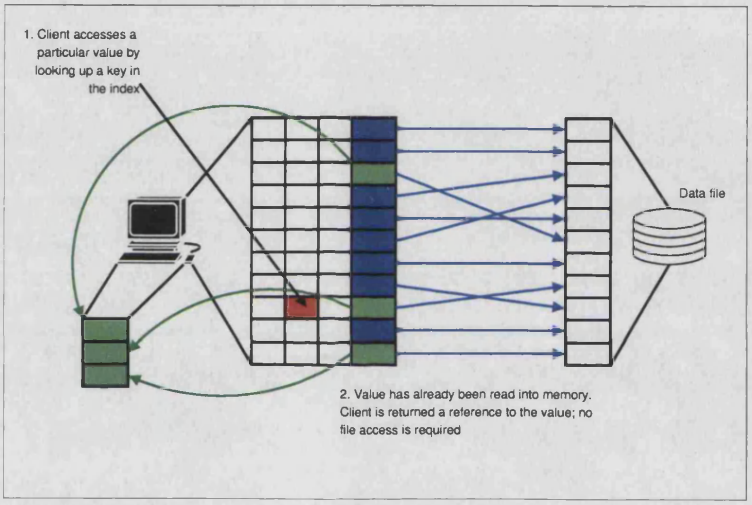

(e)

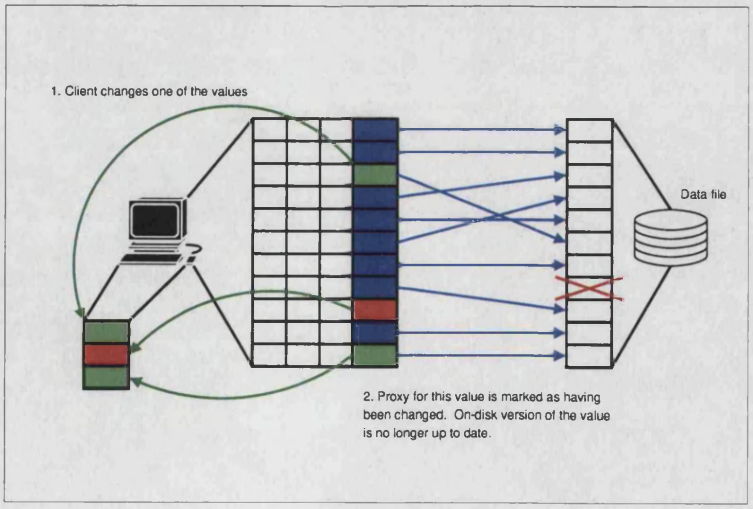

(f)

Figure C.5: Pointer swizzling (continued)
(d) swizzling occurs when data values are requested by the client; (e) cached values can be returned immediately without file access; (f) altered values are marked. Continued overleaf.

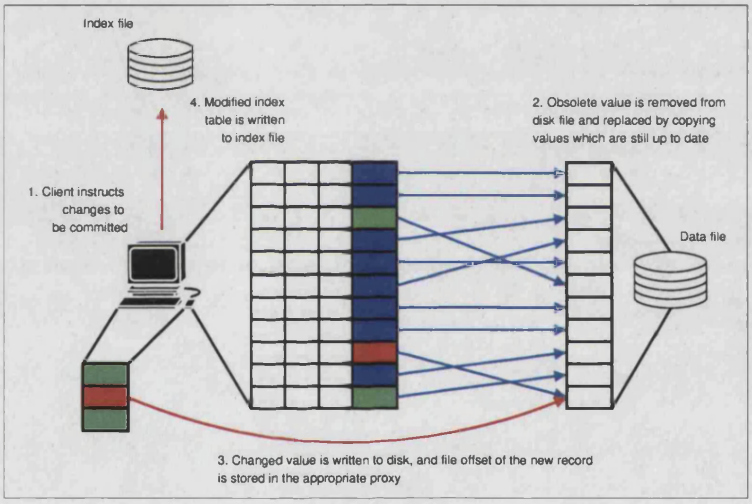

(g)

Figure C.5: Pointer swizzling (continued)
(g) changes are committed to disk.

C.2 Implementation of the bioinformatics layer

C.2.1 Macromolecular structure

Classes for representing macromolecular coordinate data are defined in namespace `gamut::mmol`.

C.2.1.1 Nodes of the molecular tree

Each of the levels in the molecular tree is populated with objects of a different type, namely, `Model`, `Polymer`, `Monomer` and `Atom` objects. Each of these classes inherits from an instance of the `PolymorphicNaryNode` template described in §C.1.5, allowing them to be part of a polymorphic tree.

C.2.1.2 `Molecule` as a manager class

Internally, `Molecule` is required to perform multiple housekeeping roles. Its primary purpose is to act as the root of the molecular tree: as such, it 'owns' each `Model` of the molecule, and therefore indirectly, also owns all of the `Polymer`, `Monomer` and `Atom` objects. In addition to being the ultimate owner of all nodes in the molecular tree, a `Molecule` object is also the owner of all selections made upon it, as well as all bonds between its atoms.

Each of these 'object manager' roles is separated in the implementation of `Molecule`, through the use of inheritance. Management of each type of objects (node, selection and bond) is undertaken by one of the base classes of `Molecule`, as illustrated in figure C.6.

C.2.1.2.1 The coordinate manager

The coordinate manager is responsible for the lifetime of the objects which constitute the molecular hierarchy. Each `CoordinateManager` object stores by aggregation the root node of this hierarchy, through which all nodes in the tree may be accessed. For example, in order to iterate through all nodes in the second level down from the tree, the client would recursively iterate through the children of the root, and the children of those nodes in turn.

For many applications, the ancestry of each node may not be important; if, for example, the client simply wishes to iterate through each monomer in the molecule, doing so by traversing the tree would be quite inefficient (see figure C.7). For this reason, the `CoordinateManager` class also stores a list of pointers to the objects at each lebel of the molecular tree (atoms, residues, chains and models). Clients may iterate through these lists using member functions of the manager. It is evidently important that the coordinate manager should ensure that these lists are consistent at all times with the nodes present in the tree; this is done using the deferred evaluation technique described above.

Another responsibility of the coordinate manager class is to maintain a *geometric query map* (see §3.4) of atomic positions. This allows the client to rapidly perform queries which return the set of atoms lying in any given region of space; the interface through which these queries are actually performed is defined in the selection manager class described below. Once again, deferred evaluation is used to keep the query map up

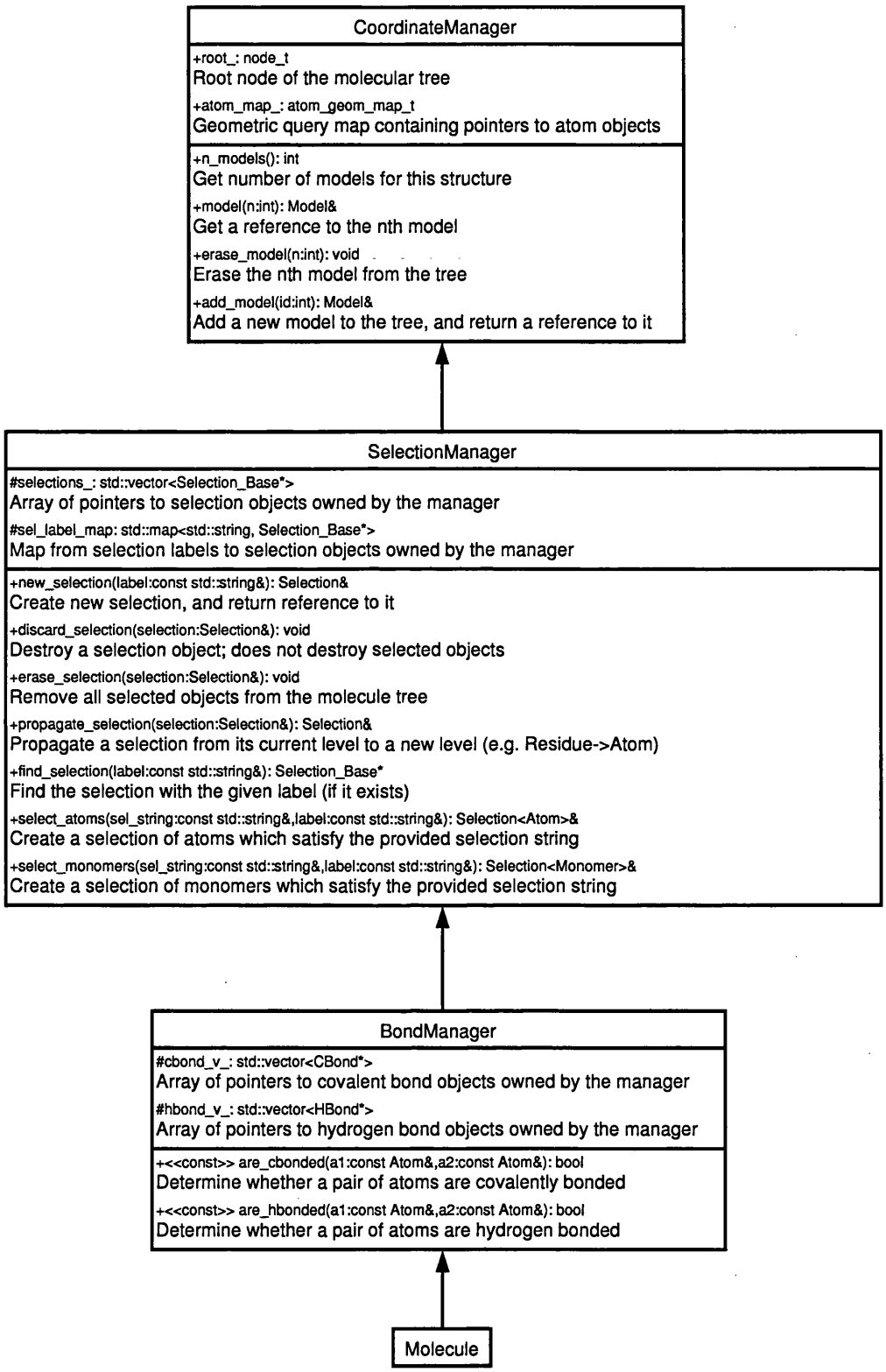

Figure C.6: Separation of the 'object manager' roles of the `Molecule` class

Almost all of the functionality of `Molecule` is inherited from its base classes, each of which takes responsibility for managing a different type of information. The lists of class attributes and methods shown here is incomplete, and is intended to serve as an illustration of the function of each base class.

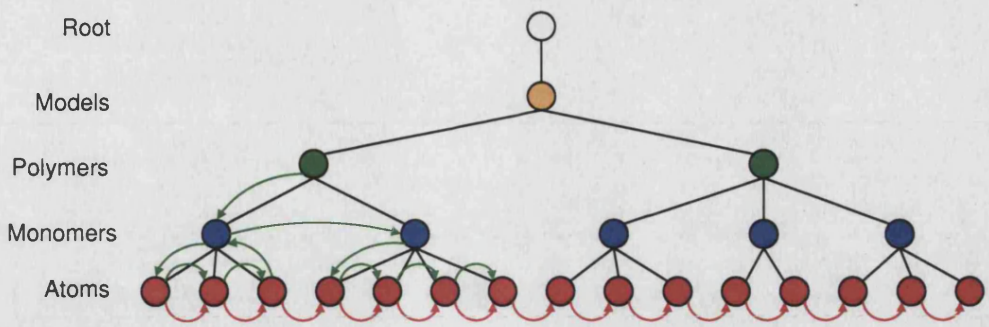

Figure C.7: Different types of iteration through nodes of the molecular tree
The green arrows indicate the process of iterating through all atoms of a given polymer, by recursively traversing the tree using member functions of its nodes. The red arrows indicate the process of iterating through all atoms in a molecule, using the lists stored by the `CoordinateManager` class. Clearly the latter represents a more efficient means for traversal of all nodes at a particular level.

to date. Finally, the coordinate manager provides the ability for the client to perform certain operations to all objects in the tree *en masse*, such as rotations and translations.

C.2.1.2.2 The selection manager

GAMUT allows the client to construct selections at any level of the molecular tree, and provides a mechanism conferring persistence upon the selections. The classes which constitute the selection framework are illustrated in figure C.8. Each selection is represented by a `Selection<T>` object, where `T` is a template parameter determining the type of objects in the selection; the selection object contains a list of pointers to the objects which constitute it. Clients are granted access to the selected objects via member functions of the selection class.

The mechanism used to keep the list of selected objects up to date is a deferred evaluation[3] approach based on bit-masks. Each selection object is associated with a bit-mask, in which all bits except one are set to zero. Similarly, every node in the molecular tree has a bit-mask of the same length. Any number of bits in the masks associated with node objects may be set; each bit which is set indicates membership of that node in a given selection; see figure C.9. In order to rebuild the list of selected objects therefore, a `Selection` object needs simply to query its associated `CoordinateManager` object (to which a pointer is held), iterating through all nodes in the appropriate level of the tree and checking the bit mask of each. Whenever a node is encountered in whose bit-mask the bit corresponding to the selection object is set, a pointer to the node is added to the list of selected objects. This procedure is carried out whenever a `Selection` member function is called which requires access to the list of selected objects, and when that list is found to have been marked out-of-date.

Creation and disposal of `Selection` objects is orchestrated by the `SelectionManager` class. When the client requests creation of a new selection, the first task of the selection manager is to generate a bit-mask which is orthogonal to all masks currently in use. This is done by maintaining a count of the number of masks generated to date: if, for example, 3 selections have already been made, the newly-generated mask would be `<000100...>`. When a client no longer requires a given selection, the `SelectionManager::discard_selection`

[3] see appendix B.3 for a brief discussion of the deferred evaluation technique.

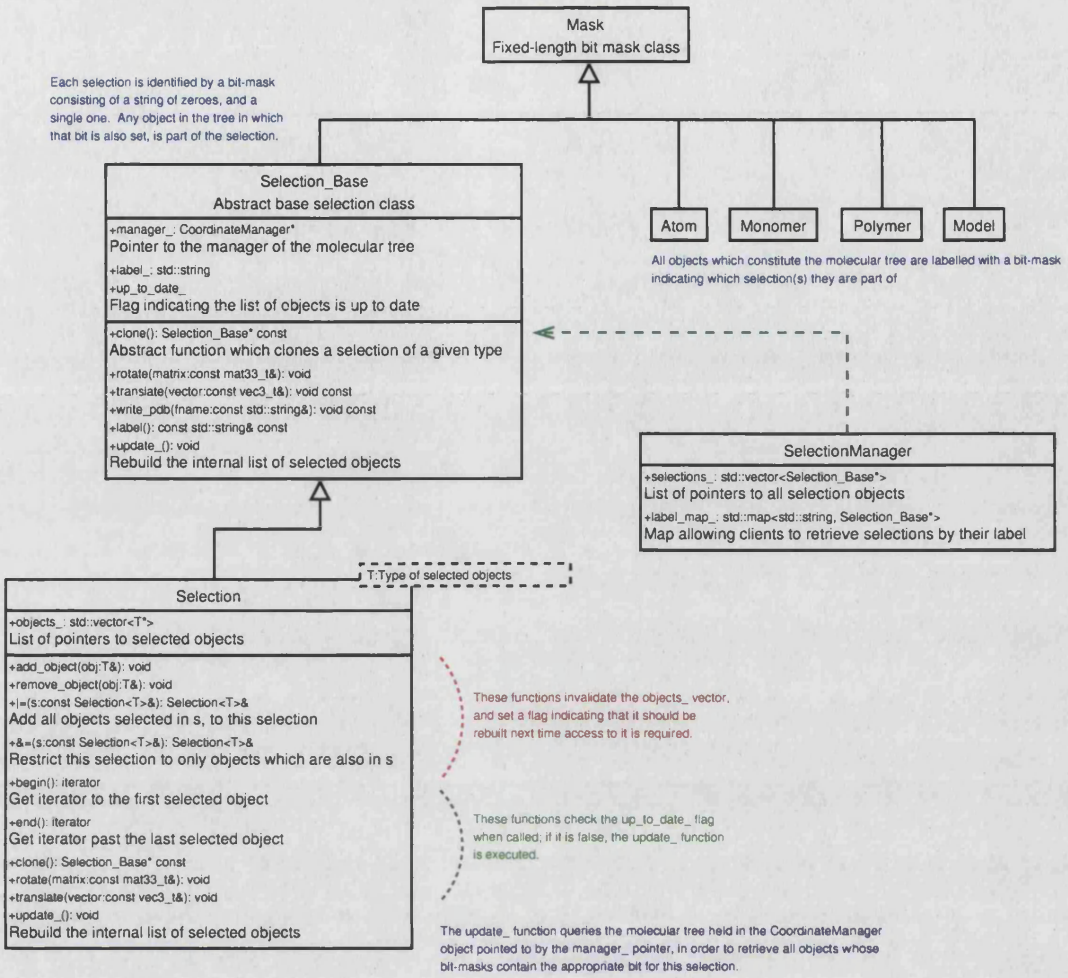

Figure C.8: Classes which constitute the selection framework

The member data and functions listed here do not fully describe the classes, but serve to illustrate the relationship between the selection objects and the selection manager. The `SelectionManager` functions which are used to create selections are described elsewhere.

function may be called. This has three effects: firstly, the selection mask is subtracted bitwise from the mask of every selected object. Secondly, the mask is added to a pool of 'recycled' masks maintained by the selection manager object. These masks may now be re-used for new selections, thus allowing any number of selections to be created on a given molecule, as long as no more that `N` are in use at any time, where `N` is the length of the bit-masks (128 in the current implementation). Finally, the `Selection` object itself is destroyed.

In order to create selections based on object identities, such as atom name, or residue sequence number, a system of selection *predicates* is used. Each of the molecular node classes (`Atom`, `Monomer`, `Polymer` and `Model`) define a nested type called `predicate`, which is in fact a unary functor returning either true or false. For example, the atom predicate class has the following form:

```
struct predicate
{ bool operator()(const Atom&) const; };
```

Each node class also defines static member functions which generate predicate objects representing certain criteria. For example, the `Atom::metal` function creates a predicate object which returns true when presented with a metal atom, and false otherwise. Similar functions exist to create predicates which return true if the atom has a certain name, if the residue sequence number lies within a given range, and so forth. Now, let us

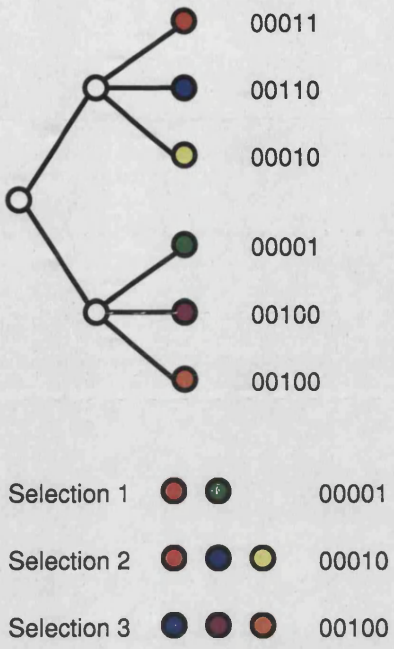

Figure C.9: Selection bitmasks
A section of the molecular tree is shown, with the bit masks associated with each leaf node. The objects which constitute each selection are illustrated below the tree.

say we wish to select all residues in chain 'A' of the first model of a molecule, whose sequence number is within the range 10 to 20. The `SelectionManager` class defines a function with the following signature:

```
Selection<Monomer>& select_monomers(
    const Model::predicate&,
    const Polymer::predicate&,
    const Monomer::predicate&,
    const std::string& label
);
```

In order to create the selection described above, we simply need to provide three predicate objects which define the selection criteria at the model, polymer and monomer levels, as follows:

```
Selection<Monomer>& my_selection = my_molecule.select_monomers(
    Model::id_equals(1),                  // Model predicate
    Polymer::id_equals('A'),              // Polymer predicate
    Monomer::seq_num_in_range(10, 20),    // Monomer predicate
    ''some_informative_name''             // Label
);
```

Similar functions exist for selections at each level of the tree, with the number of predicate arguments required corresponding to the depth of that level from the root node.

The selection object is populated by performing a depth-first search of the molecular tree. When each new node is discovered by the search, it is checked against the appropriate predicate to determine whether it matches; if not, the search down that branch of the tree is terminated. When an object at the last level (here, the monomer level) is encountered, which matches its predicate, a pointer to it is added to the selection list, the mask of the object is bitwise-OR'ed with that of the selection object, and the search moves back up the tree.

Rather than using predicate objects, the client may make the same selection by providing a selection string, complying with a predefined format. Without going into the details of this format, the selection string corresponding to the example given here is `/1/A/.10-20`; internally, this is parsed by the selection manager and converted into a series of predicate objects which are passed to the function above. The power of the predicate-based approach, however is its flexibility: any number and combination of predicates may be supplied to the selection function, as long as they can be expressed in the form of unary boolean functors. The standard logical operations AND, OR and NOT are defined on the predicate classes, such that the client can write predicate expressions such as

```
Selection<Monomer>& my_selection = my_molecule.select_monomers(
    Model::any(),
    not Polymer::id_equals('A'),
    Monomer::name_equals{''GLY''} and Monomer::seq_num_in_range(1,50)
);
```

As discussed previously, in addition to selections based on object identity, geometrically-defined selections were also required. These were divided into two types: selection of all objects lying in an arbitrary geometric region, and those which are defined by proximity to objects in an existing selection.

When specifying a region-based selection, it is necessary to clarify exactly what qualifies a particular entity as being 'inside' a given region. For example, considering an amino acid residue, do we simply require any atom of the residue to fall inside the region, or do we want the stricter criterion that the centre (geometric, or centre of mass) of the residue be within the query region? In GAMUT, these 'insideness criteria' are specified using *policies*[4].

The available insideness criteria policies are:

- `GeometricCentre_InsidenessCriterion` - object is inside the region if its geometric centre is inside the region.
- `MassCentre_InsidenessCriterion` - object is inside the region if its centre of mass is inside the region.
- `GeometricCentreOfChildren_InsidenessCriterion` - object is inside the region if the geometric centre of any of its child nodes is inside the region.

The following statements illustrate the creation of selections in which, in the first case, any atom of a monomer inside a given sphere qualifies the monomer as 'selected', then the geometric centre and centre of mass of each monomer must be inside the sphere. The first statement shows how to create selections in which any atom of a monomer inside a given sphere qualifies the monomer as 'selected':

```
select_region<GeometricCentreOfChildren_InsidenessCriterion>
    (sphere_t(vec3_t(0,0,0), 5));
```

If, on the other hand, the geometric centre or centre of mass of each monomer must be inside the sphere in order to qualify it as selected, the following statements should be used:

[4]See appendix B.5 for a discussion of the use of policy classes for behavioural parameterisation.

```
select_region<GeometricCentre_InsidenessCriterion>
    (sphere_t(vec3_t(0,0,0), 5));
select_region<MassCentre_InsidenessCriterion>
    (sphere_t(vec3_t(0,0,0), 5));
```

When defining a new selection by proximity to an existing selection, another criterion must be specified, namely from which part(s) of the existing selection distances should be measured. That is, do we wish to select objects near to the geometric centre of the existing selection, or close to any object in that selection? This choice is expressed using a 'relative selection origin' policy. The available relative selection origin policies are:

- `GeometricCentreOfSelection_OriginCriterion` - distances are measured from the geometric centre of the existing selection.
- `GeometricCentreOfEachElement_OriginCriterion` - the distance of a given point from the selection is taken as the distance from that point to the nearest member of the existing selection.
- `GeometricCentreOfEachChildOfEachElement_OriginCriterion` - the distance of a given point from the selection is taken as the distance from that point to the nearest child of any member of the selection.

In order to illustrate the use of the selection policies, consider the code snippet in listing C.7, which shows the selection of a ligand based upon its identity, followed by geometric selection of all residues which have at least one atom in proximity to any atom of the ligand.

```
// Selection of the ligand molecule.
Selection<Monomer> ligand =
    M.select_monomers(``/1/A/ATP.1'', ``ligand'');

// Selection of all residues which contact the ligand
Selection<Monomer> environment =
    M.select_relative<
        GeometricCentreOfChildren_InsidenessCriterion,
        GeometricCentreOfEachChildOfEachElement_OriginCriterion
    >
```

Listing C.7: Example of using selection functions to pick out a ligand binding site

C.2.1.2.3 The bond manager

By default, bonds between atoms in a molecular structure are not explicitly stored in a `Molecule` object. However, facilities are provided for representing both covalent and hydrogen bonds. Both types of bond inherit from a common `Bond` base class, which contains pointers to the two bonded atoms. All bond objects are managed by the `BondManager` class, which, like the `SelectionManager` maintains a list of all bonds.

By referring to a table of standard covalent radii for each element, the bond manager class is able to infer covalent bonds between atoms within and between residues. This allows the atomic coordinates of a monomer (protein residue, or ligand) to be converted into a graph which represents the connectivity of the molecule.

C.2.1.3 File I/O

In order to read coordinate data into `Molecule` objects, a parser for PDB format files was implemented. In addition to extracting coordinate data, the parser may also obtain sequence data and additional annotations such as EC number from the PDB file, although the latter is often recorded in a non-standard fashion, and therefore cannot be reliably retrieved. The inconsistencies present in PDB files are well-known, and the GAMUT parser attempts to check for some of these as it reads the file. For example, the parser can be instructed to throw an exception if it encounters two atoms with identical name and alternative location fields, belonging to the same residue. A variety of other checks may be optionally enabled or disabled by the client depending upon the level of strictness required. PDB format files may be also written by GAMUT objects, in order to export data for use in other programs.

C.2.2 Chemical structure

Namespace `gamut::chem` contains the classes which deal with chemical connectivity data.

C.2.2.1 The chemical graph class

Implementation of the chemical graph class was fairly straightforward given the generic graph template described above. As mentioned earlier, `chem::Graph` is not in fact simply an instantiation of the generic `Graph` template; rather, it is derived from such an instantiation. The reason for doing this is to add extra member functions to the graph object, which perform functions such as computing the valence of each atom of the compound, from the connectivity information stored within the graph.

One point worthy of discussion is the representation of atom properties. The atomic properties of atomic number, chirality, valence, number of hydrogens and charge may all be represented as integer values; since the upper bound on each value is small, it is possible to store them concisely as a single 32-bit integer using a bit-masking system, as illustrated in figure C.10. The advantage of doing this is realised when chemical structures are compared using graph isomorphism algorithms. If, for a given application, the chirality of an atom is not considered relevant for the graph-matching procedure, it can trivially be hidden by masking out the appropriate bits from the composite atom property value.

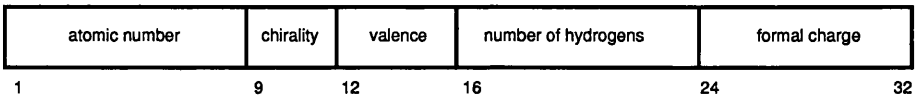

Figure C.10: Concise storage of atom properties using a bit-masking approach
The 32 bits of the integer value are partitioned into 'chunks', each of which represents one of the properties of the atom.

C.2.2.2 The chemical compound archive class

As described above, an archive was required in which collections of chemical structures (in the form of graph objects) could be persistently stored, and from which those structures could be easily retrieved. The implementation of this archive class, called `ChemBase`, was based upon the generic ISAM table class described previously, and was therefore trivial.

`ChemBase` archives can be built using several different application programs, which are discussed further in chapter 4. In essence, these allow the user either to provide a collection of compounds in the form of MOL2 files, or to query the MSD database of chemical entities found in the PDB. In either case, the result is a binary file containing the relevant chemical compounds, stored in the form of GAMUT chemical graphs, and therefore ready for use in a variety of analyses.

C.2.2.3 Structure diagram generation

The layout algorithm chosen for implementation in GAMUT was adapted from that found in the Chemistry Development Kit (Dortu *et al.*, 2000) and is outlined in pseudocode as algorithm C.1.

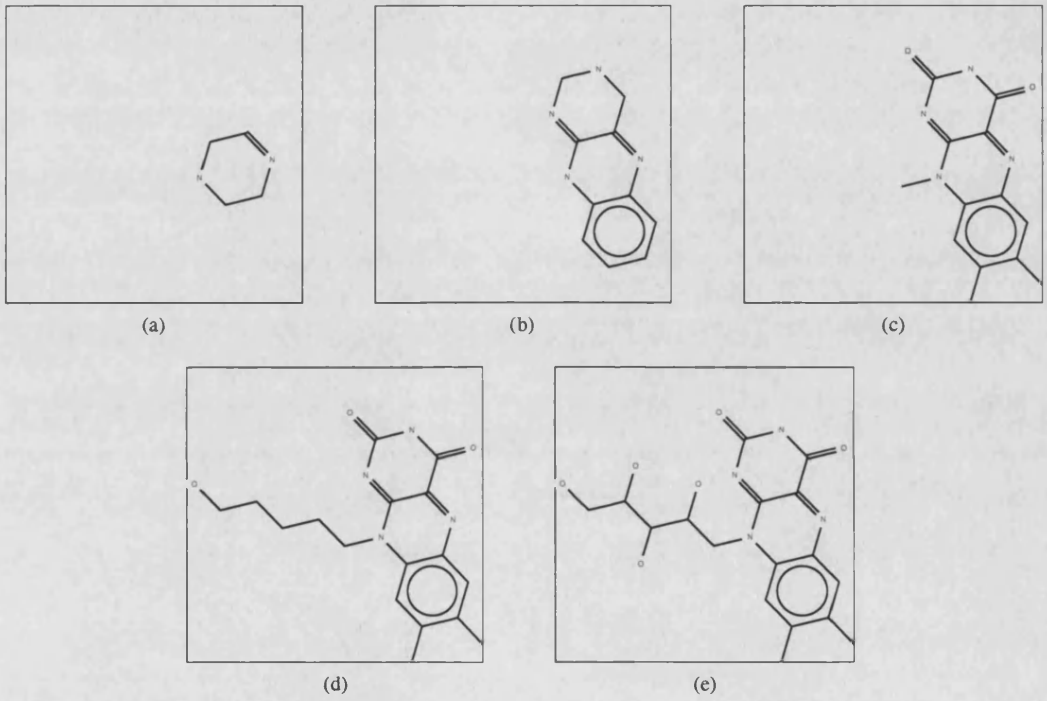

Figure C.11: Example of the chemical structure layout algorithm
This figure shows the progress of the layout algorithm when applied to riboflavin. (a) placement of the most connected ring; (b) placement of other rings in the same ring system; (c) distribution of substituents around this ring system; (d) placement of the longest unplaced aliphatic chain; (e) substituents to this chain are added.

The progress of structure diagram generation is illustrated for riboflavin in figure C.11. The cycle perception algorithm detects three rings, which together make up a connected ring system. Of these, the middle ring is the most connected, since it is joined to two other rings, while each of the others only neighbours one ring. The six vertices which make up the middle ring are placed on a regular hexagon. The placement of the remaining two rings is determined by the position of the bonds which they share with the first ring. Once all three rings are placed, their immediate substituents are distributed around their periphery. Now the algorithm checks to see whether unplaced vertices remain; this is found to be true, so the longest aliphatic chain is placed next. Its orientation is determined by pointing it away from the ring system to which it is bonded, and its bonds are angled each at 120° from the previous bond. Finally, the substituents of this aliphatic chain are positioned to complete the diagram.

The initial layout generated in this way may then be *refined* in order to improve its appearance. The approach

used here is to 'flip' single acyclic bonds with the aim of reducing clashes between atoms in the diagram. This is done by computing a penalty function based on the proximity of all pairs of non-covalently-bonded atoms in the structure. Each single acyclic is inspected to determine whether flipping it would decrease the value of this function; if so, the change is accepted, otherwise it is ignored. By applying this to each flippable bond, and then repeating the whole cycle a number of times, the appearance of the layout may be improved.

Several other examples of diagrams generated by the layout algorithm are shown in table C.5.

The power of having this algorithm implemented internally within the library, rather than simply writing a MOL2 file for the compound, and depicting it using an external program, is that it allows the details of the diagram to be programmatically modified. For example, in order to illustrate the parts of two compounds which are matched in a subgraph isomorphism, the programmer can easily 'instruct' the layout object to highlight the matched atoms in a different colour.

C.3 Ligand binding sites

Implementation of the ligand binding site components described in §2.3.4.4 consists of three core classes, defined in namespace `gamut::lig`:

- `Identity`: this class contains all information needed to unambiguously identify a single ligand molecule within the PDB archive, namely:
  - PDB entry
  - chain identifier
  - residue name
  - sequence number
  - insertion code

  In addition, where the molecule was observed to exist in more than one location within the crystal, the `Identity` class also records the alternative location indicator for the conformation seen to have the highest occupancy.
- `Match`: this class inherits from `Identity`; in addition to the fields listed above, it also contains:
  - name of the reference compound to which the ligand was matched
  - correspondances between the atoms of the ligand molecule, and the vertices of the reference graph. These are stored as pairs of indices, where the first refers to the index of the reference vertex, and the second to the index of the ligand atom.
  - whether the ligand is covalently or non-covalently bound to protein within the PDB entry
- `MatchTable`: this is an ISAM archive which stores `Match` objects. Its indices allow clients to look up ligand matches by PDB entry, residue name, reference compound name, bound state, or any combination of the above.

In addition to these classes, the ligand binding site component contains numerous utilities for performing functions including

Function LAYOUT($G(V,E)$) :

Find all ring systems in the graph
This is done using the Figueras ring perception algorithm, which is not described here
RingSystems ← FINDRINGSYSTEMSBYBREADTHFIRSTSEARCH(G)

Create a starting point by laying out either the largest ring system, if there is one, or the longest aliphatic chain
if *RingSystems* $\neq \emptyset$ **then**
If rings were found, place the largest connected ring set
PLACERINGSYSTEM(*RingSystems*[0])
PLACERINGSUBSTITUENTS(*RingSystems*[0])

else
Find the longest chain, using Floyd's all-pairs shortest path algorithm
Chain ← FINDLONGESTCHAIN()
Place the chain with its first bond oriented along the x-axis
PLACELINEARCHAIN(*Chain*, (1,0))

Place the remaining vertices relative to those which have already been placed
while *UnplacedVertices* $\neq \emptyset$ **do**
If a placed atom with unplaced aliphatic neighbours exists, distribute its neighbours and place the aliphatic chain
LAYOUTALIPHATICPARTS()
If an unplaced ring system is left, place it
PLACENEXTRINGSYSTEM()

Function PLACERINGSYSTEM(RS,V) :
Find the most connected ring $M \in RS$*, and place it with the first bond of the system oriented along V*
Iteratively place all other rings in RS relative to M

Function PLACERINGSUBSTITUENTS(R) :
for each $v \in R$:
Distribute unplaced neighbouring vertices of v evenly around v, on the outer side of R

Function PLACENEXTRINGSYSTEM() :
Find a placed vertex v, with an unplaced neighbour n which is in a ring system RS; if such a vertex is not found, return
Compute a bond vector V which will orient RS away from the other neighbours of v
PLACERINGSYSTEM(RS,V)

Function PLACELINEARCHAIN(C,V) :
Place an aliphatic chain using alternating bond angles of +/- 120 degrees, with the first bond oriented along the given vector

Function LAYOUTALIPHATICPARTS() :
Find a vertex v with an unplaced neighbour n which is not in a ring; if such a vertex is not found, return
Compute a bond vector V which points away from the remaining neighbours of v
Find the longest unplaced chain C, which originates from n
PLACELINEARCHAIN(C,V)

Algorithm C.1: Chemical structure diagram generation algorithm
Adapted from the Java implentation found in the Chemistry Development Kit (Dortu *et al.*, 2000). The outline presented here is far from complete, and is intended only to convey the basic structure of the algorithm.

- Deriving a chemical graph from the atomic coordinates of a ligand molecule
- Computing a least-squares rigid superposition of one molecule onto another, given a list of atom-atom correspondances
- Computing torsion angles from atomic coordinates of a molecule
- Determining the handedness of the chiral stereocentres of a molecule from its coordinates

The details of how these operations are carried out are discussed further in chapter 4.

C.4 Density maps

As stated above, the density map class is simply an instantiation of the generic scalar field template, with the added capability of reading and writing CCP4 format map files. Since GAMUT maps are always defined as orthonormal grids, the library will generate an error when reading a CCP4 map unless it has been saved in mode 2, will all cell skew angles equal to 90°.

Name	PDB HET code	Diagram
Cyclic AMP	CMP	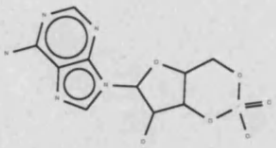
Estradiol	EST	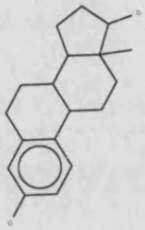
Indinavir	MK1	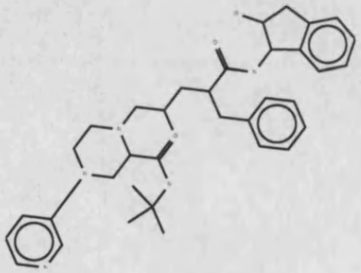
Riboflavin	RBF	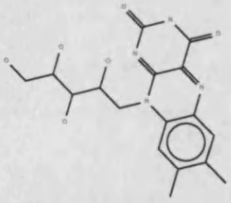
N-acetyl serotonin	ASE	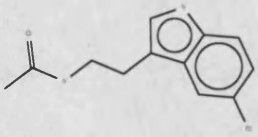

Table C.5: Examples of diagrams generated by chemical graph layout algorithm

Appendix D

Ligand datasets

This appendix contains tabulated summaries of the datasets for the four ligands (ATP, GTP, NAD and FAD) whose analysis forms the main body of the thesis. The information contained in each column is as follows:

- **Cluster**: the number of each third-level cluster (see §4.2), which is used to refer to it in the rest of the thesis. Clusters are ordered by size.
- **Ligand**: the identity of each ligand, as found in the PQS database. This has the following form: `PDB ID /chain ID / residue ID.`
- **Protein**: the name of the protein, as recorded in the PDB file header.
- **Family size**: the number of non-identical sites which belong to each second-level cluster; in other words, the number of first-level representatives which belong to this cluster.
- **Resolution**: the resolution of the structure in which each molecule was found. Where the structure was solved by X-ray crystallography, this is the crystallographic resolution in angstroms; NMR structures are denoted 'NMR'.
- **EC**: the EC number(s) associated with the protein to which each ligand is bound (see §4.4.3).
- **Domain**: this column contains the CATH numbers for each superfamily which contacts the ligand. The names of each of these superfamilies can be obtained by consulting the table in appendix E.
- **Fraction**: the fractional contribution of each superfamily to the binding site (see §4.2.3).

Table D.1: Summary of the ATP dataset

Cluster	Ligand	Protein	Family size	Resolution	EC	Domain	Fraction
1	1E2Q/A/ATP.302/	Thymidylate kinase	1	1.7	2.7.4.9	3.40.50.300	1.00
	1G5T/C/ATP.999/A	Cobalamin adenosyltransferase	1	1.8	2.5.1.17	3.40.50.300	0.86
	1A82/A/ATP.802/	Dethiobiotin synthetase	1	1.8	6.3.3.3	3.40.50.300	1.00
	1N5I/C/ATP.543/	Thymidylate kinase	1	1.9	2.7.4.9	3.40.50.300	1.00
	1L2T/E/ATP.1301/	Hypothetical ABC transporter ATP-binding protein MJ0796	2	1.9		3.40.50.300	1.00
	1NSF/A/ATP.858/	N-ethylmaleimide sensitive factor	1	1.9	3.6.4.6	1.10.8.60 3.40.50.300	0.14 0.86
	1R0X/E/ATP.2/	Cystic fibrosis transmembrane conductance regulator	1	2.2		3.40.50.300	1.00
	1W7A/A/ATP.1801/	DNA mismatch repair protein (MutS)	1	2.3		3.40.50.300	1.00
	1KO5/A/ATP.302/	Gluconate kinase	1	2.3	2.7.1.12	3.40.50.300	1.00
	1II0/C/ATP.591/	Arsenical pump-driving ATPase	1	2.4	3.6.3.16	3.40.50.300	1.00
	1E79/A/ATP.600/	ATP synthase, α chain heart isoform	1	2.4	3.6.3.14	1.10.1140.10 3.40.50.300	0.07 0.80
	1QHX/E/ATP.501/	Chloramphenicol phosphotransferase	1	2.5		3.40.50.300	1.00
	1Q12/A/ATP.302/	Maltose/maltodextrin transport ATP-binding protein (MalK)	1	2.6	3.6.3.19	3.40.50.300	1.00
	1JAG/A/ATP.1301/	Deoxyguanosine kinase	1	2.8	2.7.1.113	3.40.50.300	1.00
	1H8H/F/ATP.600/	Bovine mitochondrial F1-ATPase	1	2.9	3.6.3.14	1.10.1140.10 3.40.50.300	0.22 0.78
	1DO0/G/ATP.900/	Heat shock locus U	2	3.0		1.10.8.60 3.40.50.300	0.25 0.75
	1G21/I/ATP.5292/	Nitrogenase molybdenum-iron protein, α chain	1	3.0	1.18.6.1	3.40.50.300	1.00
	1J7K/B/ATP.2060/	Holliday junction DNA helicase (RuvB)	1	1.8		1.10.8.60	0.22

Table D.1 : Summary of the ATP dataset (continued from previous page)

Cluster	Ligand	Protein	Family size	Resolution	EC	Domain	Fraction
						3.40.50.300	0.78
	1JI0/C/ATP.302/	ABC transporter	1	2.0		3.40.50.300	1.00
	1JJV/B/ATP.300/	Dephospho-CoA kinase	1	2.0	2.7.1.24	3.40.50.300	1.00
	1QHG/E/ATP.700/	ATP-dependent helicase (PcrA)	1	2.5		3.40.50.300	1.00
	1D9Z//ATP.700/	Excinuclease UvrABC component (UvrB)	1	3.1		3.40.50.300	1.00
	1RDQ/A/ATP.600/B	cAMP-dependent protein kinase, α-catalytic subunit	2	1.3	2.7.1.37	1.10.510.10 3.30.200.20	0.31 0.62
	1CSN/A/ATP.299/	Casein kinase-1	1	2.0		1.10.510.10 3.30.200.20	0.35 0.65
	1H1W/A/ATP.1373/	3-phosphoinositide dependent protein kinase-1	1	2.0	2.7.1.37	1.10.510.10 3.30.200.20	0.24 0.76
	1QMZ/A/ATP.381/	Cell division protein kinase 2	1	2.2	2.7.1.37	1.10.510.10 3.30.200.20	0.30 0.60
2	2PHK/E/ATP.381/	Phosphorylase kinase	1	2.6	2.7.1.38	1.10.510.10 3.30.200.20	0.36 0.50
	1A6O/A/ATP.340/	Protein kinase CK2, α-subunit	1	2.1		1.10.510.10 3.30.200.20	0.44 0.56
	1Q97/A/ATP.485/	SR protein kinase	1	2.3	2.7.1.37	1.10.510.10 3.30.200.20	0.37 0.63
	1OL6/A/ATP.1388/	Serine/threonine kinase 6	1	3.0	2.7.1.37	1.10.510.10 3.30.200.20	0.21 0.79

Table D.1 : Summary of the ATP dataset (continued from previous page)

Cluster	Ligand	Protein	Family size	Resolution	EC	Domain	Fraction
	1GOL//ATP.581/	Transferase	1	NMR	2.7.1.37	1.10.510.10 3.30.200.20	0.55 0.45
3	1MJH/C/ATP.2001/	ATP-binding domain of protein MJ0577	1	1.7		3.40.50.620	1.00
	1GN8/B/ATP.600/	Phosphopantetheine adenylyltransferase	1	1.8	2.7.7.3	3.40.50.620	1.00
	1KP3/F/ATP.301/	Argininosuccinate synthetase	1	2.0	6.3.4.5	3.40.50.620	0.89
	1F9A/G/ATP.700/	Hypothetical protein MJ0541	1	2.0	2.7.7.1	3.40.50.620	1.00
	1NSY/C/ATP.2000/	NAD synthetase	1	2.0	6.3.1.5	3.40.50.620	1.00
	1MB9/C/ATP.702/	β-lactam synthetase	1	2.1	6.3.3.4	3.40.50.620	1.00
	1MAU/C/ATP.400/	Tryptophan-tRNA ligase	1	2.1	6.1.1.2	1.10.240.10 3.40.50.620	0.27 0.73
4	1B8A/C/ATP.500/	Aspartyl-tRNA synthetase	2	1.9	6.1.1.12	3.30.930.10	1.00
	1E24/B/ATP.512/	Lysyl-tRNA synthetase	1	2.4	6.1.1.6	3.30.930.10	0.82
	1KMN/A/ATP.452/	Histidyl-tRNA synthetase	1	2.8	6.1.1.21	3.30.930.10	0.94
	1H4Q/A/ATP.1478/	Prolyl-tRNA synthetase	1	3.0		3.30.930.10	1.00
	1B76/C/ATP.1552/	Glycyl-tRNA synthetase	1	3.4	6.1.1.14	3.30.930.10	1.00
5	1KJ8/C/ATP.5/	Phosphoribosylglycinamide formyltransferase 2	1	1.6		3.30.470.20 3.30.1490.20	0.44 0.50

Table D.1 : Summary of the ATP dataset (continued from previous page)

Cluster	Ligand	Protein	Family size	Resolution	EC	Domain	Fraction
	1PK8/C/ATP.802/A	Rat synapsin 1	2	2.1		3.30.470.20	0.43
						3.30.1490.20	0.43
	1DV2/C/ATP.1000/	Biotin carboxylase	1	2.5	6.3.4.14	3.30.470.20	0.47
					6.4.1.2	3.30.1490.20	0.53
6	1GZ4/D/ATP.601/	NAD-dependent malic enzyme	1	2.2	1.1.1.38	3.40.50.720	0.88
	1GZ4/B/ATP.601/	NAD-dependent malic enzyme	1	2.2	1.1.1.38	3.40.50.720	0.81
	1JWA/E/ATP.1/	Molybdopterin biosynthesis protein (MoeB)	1	2.9		3.40.50.720	0.95
7	1D4X/B/ATP.676/	Actin	6	1.8		3.30.420.40	0.76
						3.90.640.10	0.24
	1KAZ//ATP.486/	Hydrolase	1	NMR		3.30.420.40	0.70
						3.90.640.10	0.30
8	1ESQ/D/ATP.300/	Hydroxyethylthiazole kinase	1	2.5	2.7.1.50	3.40.1190.20	1.00
	1LHR/C/ATP.401/	Pyridoxal kinase	1	2.6	2.7.1.35	3.40.1190.20	1.00
9	1QRS/C/ATP.999/	Glutaminyl-tRNA synthetase	1	2.6	6.1.1.18	1.10.1160.10	0.25
						3.40.50.620	0.75

Table D.1 : Summary of the ATP dataset (continued from previous page)

Cluster	Ligand	Protein	Family size	Resolution	EC	Domain	Fraction
	1J09/B/ATP.501/	Glutamyl-tRNA synthetase	1	1.8	6.1.1.17	1.10.1160.10 3.40.50.620	0.33 0.53
10	1KP8/G/ATP.1/	GroEL protein	1	2.0		1.10.560.10	0.80
11	2GNK/D/ATP.200/	Nitrogen regulatory protein	1	2.0		3.30.70.120	1.00
12	1A0I//ATP.1/	Ligase	1	NMR	6.5.1.1	3.30.470.30 3.30.1490.70	0.29 0.50
13	1E8X/A/ATP.2000/	Phosphatidylinositol 3-kinase, catalytic subunit	1	2.2	2.7.1.153	1.10.1070.11 3.30.1010.10	0.32 0.68
14	1KVK/C/ATP.535/	Mevalonate kinase	1	2.4	2.7.1.36	3.30.230.10	1.00
15	1E4G/T/ATP.500/	Cell division protein (FtsA)	1	2.6		3.30.420.40 3.30.420.90	0.28 0.44

Table D.1 : Summary of the ATP dataset (continued from previous page)

Cluster	Ligand	Protein	Family size	Resolution	EC	Domain	Fraction
16	1HP1/B/ATP.606/	5′-nucleotidase	1	1.7	3.1.3.5 3.6.1.45	3.90.780.10	1.00
17	1TID/E/ATP.200/	Anti-sigma F factor	2	2.5	2.7.1.37	3.30.565.10	0.89
18	1O9T/B/ATP.1397/	S-adenosylmethionine synthetase	1	2.9	2.5.1.6	3.30.300.10	0.89
19	1HI1/A/ATP.665/	P2 protein	1	3.0		3.30.70.270 3.90.900.10	0.33 0.50
20	1FMW/B/ATP.999/	Myosin II heavy chain	1	2.1		3.30.538.10	1.00
21	1DY3/A/ATP.200/	7,8-dihydro-6-hydroxymethylpterin-pyrophosphokinase	1	2.0	2.7.6.3	3.30.70.560	0.95
22	1OBD/A/ATP.307/	Phosphoribosylamidoimidazole-succinocarboxamide synthase	1	1.4	6.3.2.6	3.30.200.20	0.71

Table D.1 : Summary of the ATP dataset (continued from previous page)

Cluster	Ligand	Protein	Family size	Resolution	EC	Domain	Fraction
						3.30.470.20	0.29
23	4AT1/D/ATP.154/	Aspartate carbamoyltransferase (aspartate transcarbamylase)	1	2.6	2.1.3.2	3.30.70.140	1.00
24	3R1R/C/ATP.1/	Ribonucleotide reductase R1	1	3.0	1.17.4.1	1.10.40.20	0.91
25	1A49/A/ATP.535/	Pyruvate kinase	1	2.1	2.7.1.40	3.20.20.60	0.81
26	3PGK/A/ATP.1/	Phosphoglycerate kinase	2	2.5	2.7.2.3	3.40.50.1270	1.00
27	1AYL/A/ATP.541/	Phosphoenolpyruvate carboxykinase	2	1.8	4.1.1.49	2.170.8.10 3.90.228.20	0.20 0.80

Table D.2: Summary of the GTP dataset

Cluster	Ligand	Protein	Family size	Resolution	EC	Domain	Fraction
1	1QRA/C/GTP.167/	Transforming protein p21/h-ras-1	3	1.6		3.40.50.300	1.00
	1J2J/A/GTP.1001/	ADP-ribosylation factor 1	3	1.6		3.40.50.300	1.00
	1NRJ/C/GTP.1001/	Signal recognition particle receptor, α subunit homolog	1	1.7		3.40.50.300	1.00
	1M7B/D/GTP.538/	Rnd3/rhoe small GTP-binding protein	2	2.0		3.40.50.300	1.00
	1ZBD/E/GTP.200/	Rab-3a	1	2.6		3.40.50.300	1.00
	1N6L/B/GTP.200/	Ras-related protein rab-5a	1	1.6		3.40.50.300	1.00
2	1HWX/G/GTP.12/	Glutamate dehydrogenase	1	2.5	1.4.1.3	3.40.50.720	1.00
3	1C80/C/GTP.355/	Fructose-2,6-bisphosphatase	1	2.2	3.1.3.46	3.40.50.1240	1.00
4	1JLR/E/GTP.300/	Uracil phosphoribosyltransferase	1	2.5	2.4.2.9	3.40.50.2020	1.00
5	1QLN/R/GTP.1/	Bacteriophage T7 RNA polymerase	1	2.4	2.7.7.6	3.30.70.370	1.00
6	1HI0/P/GTP.667/	P2 protein	1	3.0		3.30.70.270 3.90.900.10	0.64 0.36

Table D.2 : Summary of the GTP dataset (continued from previous page)

Cluster	Ligand	Protein	Family size	Resolution	EC	Domain	Fraction
7	1UVN/A/GTP.1665/	RNA-dependent RNA polymerase	1	3.0		1.10.1360.10 3.30.70.270	0.36 0.55
8	1C4K/C/GTP.999/	Ornithine decarboxylase	1	2.7	4.1.1.17	3.40.640.10	1.00
9	1LOO/C/GTP.452/	Adenylosuccinate synthetase	1	2.2	6.3.4.4	3.40.440.10 3.90.170.10	0.56 0.44
10	1FRW/I/GTP.3/	Molybdopterin-guanine dinucleotide biosynthesis protein	1	1.8		3.90.550.10	1.00
11	1A8R/G/GTP.405/	GTP cyclohydrolase 1	1	2.1	3.5.4.16	3.30.1130.10	0.90

Table D.3: Summary of the NAD dataset

Cluster	Ligand	Protein	Family size	Resolution	EC	Domain	Fraction
	1T2D/E/NAD.316/	L-lactate dehydrogenase	4	1.1	1.1.1.27	3.40.50.720	0.82
						3.90.110.10	0.18
	1N8K/A/NAJ.377/	Alcohol dehydrogenase, chain E	6	1.1	1.1.1.1	3.40.50.720	0.61
						3.90.180.10	0.39
	1I3L/C/NAD.400/	UDP-glucose 4-epimerase	2	1.5	5.1.3.2	3.40.50.720	1.00
	1K6X/C/NAD.400/	NMRA	1	1.5		3.40.50.720	0.86
	1ORR/A/NAD.1200/	CDP-tyvelose-2-epimerase	1	1.5		3.40.50.720	0.89
	1GEE/D/NAD.2262/	Glucose 1-dehydrogenase	1	1.6	1.1.1.47	3.40.50.720	1.00
	1IY8/A/NAD.1268/	Levodione reductase	1	1.6		3.40.50.720	1.00
	1KOL/A/NAD.1403/	Formaldehyde dehydrogenase	1	1.6	1.2.1.46	3.40.50.720	0.71
						3.90.180.10	0.29
	1GEG/A/NAD.101/	Acetoin reductase	1	1.7	1.1.1.5	3.40.50.720	1.00
	1E6W/C/NAD.301/	Short chain 3-hydroxyacyl-CoA dehydrogenase	2	1.7	1.1.1.35	3.40.50.720	1.00
	1NVM/B/NAD.3501/	4-hydroxy-2-oxovalerate aldolase	1	1.7		3.30.360.10	0.27
						3.40.50.720	0.73
	1QSG/B/NAD.1304/	Enoyl-[acyl-carrier-protein] reductase	2	1.8	1.3.1.9	3.40.50.720	1.00
	1GAD/O/NAD.336/	D-glyceraldehyde-3-phosphate dehydrogenase	9	1.8	1.2.1.12	3.30.360.10	0.11
						3.40.50.720	0.89
	1NFF/F/NAD.2300/	Putative oxidoreductase RV2002	2	1.8		3.40.50.720	1.00
	1FMC/A/NAD.256/	7 α-hydroxysteroid dehydrogenase	1	1.8	1.1.1.159	3.40.50.720	1.00
	1F0Y/C/NAD.750/	L-3-hydroxyacyl-CoA dehydrogenase	2	1.8	1.1.1.35	3.40.50.720	0.87
	1KEW/C/NAD.1400/	dTDP-D-glucose 4,6-dehydratase	3	1.8	4.2.1.46	3.40.50.720	0.97

Table D.3 : Summary of the NAD dataset (continued from previous page)

Cluster	Ligand	Protein	Family size	Resolution	EC	Domain	Fraction
	1BMD/A/NAD.334/	Malate dehydrogenase	3	1.9	1.1.1.37	3.40.50.720	0.86
						3.90.110.10	0.14
	1EMD/A/NAD.314/	Malate dehydrogenase	1	1.9	1.1.1.37	3.40.50.720	0.88
						3.90.110.10	0.12
	1J5P/C/NAD.300/	Aspartate dehydrogenase	1	1.9		3.30.360.10	0.17
						3.40.50.720	0.83
	1DXY/D/NAD.336/	D-2-hydroxyisocaproate dehydrogenase	3	1.9		3.40.50.720	0.96
	1D7O/E/NAD.501/	Enoyl-[acyl-carrier protein] reductase precursor	1	1.9	1.3.1.9	3.40.50.720	1.00
	1GR0/A/NAD.1000/	Myo-inositol-1-phosphate synthase	1	1.9		3.30.360.10	0.13
						3.40.50.720	0.87
	1FK8/C/NAD.800/	3-α-hydroxysteroid dehydrogenase/carbonyl reductase	1	1.9		3.40.50.720	1.00
	1O6Z/C/NAD.2003/	Malate dehydrogenase	1	1.9	1.1.1.37	3.40.50.720	0.64
						3.90.110.10	0.23
	1MX3/E/NAD.1000/	C-terminal binding protein 1	1	1.9		3.40.50.720	0.93
	2NAD/A/NAD.394/	NAD-dependent formate dehydrogenase	1	2.0	1.2.1.2	3.40.50.720	0.93
	1PJC/G/NAD.500/	L-alanine dehydrogenase	1	2.0	1.4.1.1	3.40.50.720	1.00
	1BDB/A/NAD.300/	Cis-biphenyl-2,3-dihydrodiol-2,3-dehydrogenase	1	2.0		3.40.50.720	1.00
	9LDT/A/NAD.401/	Lactate dehydrogenase	2	2.0	1.1.1.27	3.40.50.720	0.84
						3.90.110.10	0.16
	1LLD/A/NAD.1/	L-lactate dehydrogenase	3	2.0	1.1.1.27	3.40.50.720	0.76
						3.90.110.10	0.24
	1F8G/E/NAD.2500/	Nicotinamide nucleotide transhydrogenase	1	2.0	1.6.1.2	3.40.50.720	0.81
	1PJ3/E/NAD.2601/	NAD-dependent malic enzyme, mitochondrial	2	2.1	1.1.1.38	3.40.50.720	0.81

Table D.3 : Summary of the NAD dataset (continued from previous page)

Cluster	Ligand	Protein	Family size	Resolution	EC	Domain	Fraction
	1ENY/B/NAD.500/	Enoyl-acyl carrier protein reductase	1	2.2		3.40.50.720	1.00
	1HYH/A/NAD.330/	L-2-hydroxyisocaproate dehydrogenase	1	2.2		3.40.50.720	0.85
						3.90.110.10	0.15
	1EBF/C/NAD.2109/	Homoserine dehydrogenase	1	2.3	1.1.1.3	3.40.50.720	1.00
	1BXG/A/NAD.360/	Phenylalanine dehydrogenase	1	2.3	1.4.1.20	3.40.50.720	1.00
	1DHR/B/NAD.241/	Dihydropteridine reductase	1	2.3	1.5.1.34	3.40.50.720	1.00
	1LSS/I/NAD.1001/	Trk system potassium uptake protein TrkA homolog	1	2.3		3.40.50.720	1.00
	1R37/A/NAD.403/	NAD-dependent alcohol dehydrogenase	1	2.3	1.1.1.1	3.40.50.720	0.66
						3.90.180.10	0.34
	1P9L/E/NAD.301/	Dihydrodipicolinate reductase	1	2.3	1.3.1.26	3.30.360.10	0.05
						3.40.50.720	0.90
	1NPD/A/NAD.300/	Hypothetical shikimate 5-dehydrogenase-like protein YdiB	1	2.3		3.40.50.720	0.91
	1DLI/C/NAD.403/	UDP-glucose dehydrogenase	1	2.3	1.1.1.22	3.40.50.720	0.85
	1NHW/I/NAD.450/	Enoyl-acyl carrier reductase	1	2.4		3.40.50.720	0.92
	1B14/C/NAD.255/	Alcohol dehydrogenase	1	2.4	1.1.1.1	3.40.50.720	1.00
	1H94/A/NAD.799/	Glucose 6-phosphate 1-dehydrogenase	1	2.5	1.1.1.49	3.30.360.10	0.06
						3.40.50.720	0.94
	1ARZ/B/NAD.274/	Dihydrodipicolinate reductase	1	2.6	1.3.1.26	3.30.360.10	0.05
						3.40.50.720	0.95
	1EVJ/A/NAD.500/	Glucose-fructose oxidoreductase	1	2.7		3.30.360.10	0.19
						3.40.50.720	0.81
	1PSD/B/NAD.450/	D-3-phosphoglycerate dehydrogenase	1	2.8	1.1.1.95	3.40.50.720	0.92
	1D4F/E/NAD.502/	(phosphoglycerate dehydrogenase) S-adenosylhomocysteine hydrolase	1	2.8	3.3.1.1	3.40.50.720	0.60

Table D.3 : Summary of the NAD dataset (continued from previous page)

Cluster	Ligand	Protein	Family size	Resolution	EC	Domain	Fraction
						3.40.50.1480	0.20
	1CH6/G/NAD.571/	Glutamate dehydrogenase	1	2.9		3.40.50.720	0.71
	1EE9/C/NAD.10/	5,10-methylenetetrahydrofolate dehydrogenase	1	3.0	1.5.1.15	3.40.50.720	0.95
	1FDV/A/NAD.361/	17-β-hydroxysteroid dehydrogenase	1	3.1	1.1.1.62	3.40.50.720	1.00
	1QRR/A/NAD.401/	Sulfolipid biosynthesis protein	1	1.6	3.13.1.1	3.40.50.720	0.88
2	1O04/D/NAD.6504/	Aldehyde dehydrogenase, mitochondrial precursor	4	1.4	1.2.1.3	3.40.309.10	0.14
						3.40.605.10	0.86
	1UXT/A/NAD.1503/	Glyceraldehyde-3-phosphate dehydrogenase	1	2.2	1.2.1.9	3.40.309.10	0.18
						3.40.605.10	0.68
	1AD3/A/NAD.600/	Aldehyde dehydrogenase (class 3)	1	2.6	1.2.1.5	3.40.309.10	0.32
						3.40.605.10	0.68
	1BPW/A/NAD.4/	Aldehyde dehydrogenase	1	2.8	1.2.1.8	3.40.309.10	0.15
						3.40.605.10	0.81
3	1NUU/E/NAD.401/	FKSG76 (NMN adenylyltransferase)	2	1.9	2.7.7.1	3.40.50.620	1.00
	1EJ2/L/NAD.1339/	Nicotinamide mononucleotide adenylyltransferase	1	1.9	2.7.7.1	3.40.50.620	1.00
	1K4M/D/NAD.601/	NAMN adenylyltransferase	1	1.9	2.7.7.18	3.40.50.620	1.00
	1LW7/E/NAD.601/	Transcriptional regulator NADR	1	2.9		3.40.50.620	1.00

Table D.3 : Summary of the NAD dataset (continued from previous page)

Cluster	Ligand	Protein	Family size	Resolution	EC	Domain	Fraction
4	1GRB/A/NAD.480/	Glutathione reductase	2	1.9	1.8.1.7	3.50.50.60	0.88
	1F3P/C/NAD.500/	Ferredoxin reductase	1	2.4		3.50.50.60	0.83
	2NPX/A/NAD.818/	NADH peroxidase	1	2.4	1.11.1.1	3.50.50.60	0.85
	1LVL/A/NAD.460/	Dihydrolipoamide dehydrogenase	1	2.5	1.8.1.4	3.50.50.60	1.00
5	1GIQ/A/NAD.500/	Iota toxin component IA	2	1.8		2.30.100.10	1.00
	1GZF/A/NAD.1248/	Mono-ADP-ribosyltransferase c3	1	1.9		2.30.100.10	1.00
	1OJZ/A/NAD.500/	ADP-ribosyltransferase	1	2.0		2.30.100.10	1.00
	1OG3/A/NAD.1227/	T-cell ecto-ADP-ribosyltransferase 2	1	2.6	2.4.2.31	2.30.100.10	1.00
6	1JQ5/I/NAD.401/	Glycerol dehydrogenase	1	1.7	1.1.1.6	1.20.1090.10	0.23
						3.40.50.1970	0.77
	1DQS/A/NAD.400/	3-dehydroquinate synthase	1	1.8	1.1.1.25	1.20.1090.10	0.26
					2.5.1.19	3.40.50.1970	0.74
					2.7.1.71		
					4.2.1.10		
7	1MEW/E/NAD.987/	Inosine-5′-monophosphate dehydrogenase	1	2.1	1.1.1.205	3.20.20.70	1.00
	1NFB/A/NAD.701/	Inosine-5′-monophosphate dehydrogenase 2	1	2.9	1.1.1.205	3.20.20.70	1.00

Table D.3 : Summary of the NAD dataset (continued from previous page)

Cluster	Ligand	Protein	Family size	Resolution	EC	Domain	Fraction
8	1MI3/A/NAD.1350/	Xylose reductase	1	1.8		3.20.20.100	1.00
	1M9H/B/NAD.300/	2,5-diketo-D-gluconic acid reductase A	1	2.0	1.1.1.274	3.20.20.100	1.00
9	2BKJ/B/NAD.243/	Flavin reductase	1	2.1		3.40.109.10	1.00
10	1S7G/F/NAD.701/	NAD-dependent deacetylase 2	1	2.3		3.40.50.1220	0.85
11	1RLZ/E/NAD.700/	Deoxyhypusine synthase	1	2.1	2.5.1.46	3.40.910.10	0.97
12	1CH6/G/NAD.562/	Glutamate dehydrogenase	1	2.9		3.40.192.10	1.00
13	1HWY/G/NAD.31/A	Glutamate dehydrogenase	1	3.2	1.4.1.3	3.40.50.720 3.40.192.10	0.40 0.44
14	1LW7/E/NAD.605/	Transcriptional regulator NADR	1	2.9		3.40.50.300 3.40.50.620	0.75 0.25

Table D.3 : Summary of the NAD dataset (continued from previous page)

Cluster	Ligand	Protein	Family size	Resolution	EC	Domain	Fraction
15	1QAX/G/NAD.1001/	3-hydroxy-3-methylglutaryl-CoA reductase	1	2.8	1.1.1.88	3.30.70.420 3.90.770.10	0.56 0.24
16	1HEX/A/NAD.400/A	3-isopropylmalate dehydrogenase	1	2.5	1.1.1.85	3.40.718.10	1.00
17	1TOX/A/NAD.536/	Diphtheria toxin	1	2.3	2.4.2.36	3.90.175.10	0.94
18	1OWB/C/NAD.3001/	Citrate synthase	1	2.2	2.3.3.1	1.10.580.10	1.00
19	1IB0/B/NAD.1994/	NADH-cytochrome b5 reductase	1	2.3	1.6.2.2	3.40.50.80	0.89

Table D.4: Summary of the FAD dataset

Cluster	Ligand	Protein	Family size	Resolution	EC	Domain	Fraction
	3GRS/A/FAD.479/	Glutathione reductase	3	1.5	1.8.1.7	3.50.50.60	0.95
	1MO9/C/FAD.1013/	ORF3	1	1.6	1.8.1.5	3.50.50.60	0.84
	1PN0/C/FAD.6031/	Phenol 2-monooxygenase	1	1.7		3.50.50.60	0.86
	1FEC/A/FAD.499/	Trypanothione reductase	2	1.7	1.8.1.12	3.50.50.60	0.95
	1K0I/D/FAD.395/	P-hydroxybenzoate hydroxylase	1	1.8	1.14.13.2	3.50.50.60	0.92
	1H82/A/FAD.579/	Polyamine oxidase	1	1.9	1.5.3.11	3.50.50.60	0.79
	1NHP/B/FAD.448/	NADH peroxidase	1	2.0	1.11.1.1	3.50.50.60	0.75
	1TRB/A/FAD.500/	Thioredoxin reductase	2	2.0	1.8.1.9	3.50.50.60	0.97
	1HYU/C/FAD.700/	Alkyl hydroperoxide reductase subunit F	1	2.0		3.50.50.60	0.91
1	1QO8/A/FAD.605/	Flavocytochrome c3 fumarate reductase	3	2.1	1.3.99.1	3.50.50.60	0.87
	3LAD/A/FAD.480/	Dihydrolipoamide dehydrogenase	5	2.2	1.8.1.4	3.50.50.60	0.89
	1QLA/H/FAD.6/	Fumarate reductase flavoprotein subunit	3	2.2	1.3.99.1	3.50.50.60	0.87
	1NG4/E/FAD.400/	Glycine oxidase	1	2.3	1.4.3.19	3.50.50.60	0.81
	1F3P/C/FAD.449/	Ferredoxin reductase	1	2.4		3.50.50.60	0.87
	1LVL/A/FAD.459/	Dihydrolipoamide dehydrogenase	1	2.5	1.8.1.4	3.50.50.60	0.95
	1FCD/A/FAD.699/	Flavocytochrome c sulfide dehydrogenase (FCSD)	1	2.5		3.50.50.60	0.94
	1KNP/C/FAD.800/	L-aspartate oxidase	1	2.6	1.4.3.16	3.50.50.60	0.95
	1N1P/B/FAD.510/	Cholesterol oxidase	2	0.9	1.1.3.6	3.50.50.60	0.89
	1EL5/A/FAD.400/	Sarcosine oxidase	1	1.8	1.5.3.1	3.50.50.60	0.69
	1CQX/A/FAD.405/	Flavohemoprotein	2	1.8	1.14.12.17	2.40.30.10	0.70

Table D.4 : Summary of the FAD dataset (continued from previous page)

Cluster	Ligand	Protein	Family size	Resolution	EC	Domain	Fraction
						3.40.50.80	0.17
	1EP3/E/FAD.502/	Dihydroorotate dehydrogenase B (pyrd subunit)	1	2.1	1.3.3.1	2.10.240.10 2.40.30.10 3.40.50.80	0.20 0.65 0.10
	1GAW/E/FAD.320/	Ferredoxin-NADP$^+$ reductase	6	2.2		2.40.30.10 3.40.50.80	0.76 0.24
	1KRH/A/FAD.501/	Benzoate 1,2-dioxygenase reductase	1	1.5	1.18.1.3	2.40.30.10 3.40.50.80	0.62 0.24
	1JA1/A/FAD.1750/	NADPH-cytochrome P450 reductase	1	1.8	1.6.2.4	1.20.990.10 2.40.30.10	0.06 0.78
	1F20/B/FAD.1501/	Nitric-oxide synthase	1	1.9	1.14.13.39	2.40.30.10 3.40.50.80	0.70 0.25
	1I7P/B/FAD.301/	NADH-cytochrome b5 reductase	3	2.0	1.6.2.2	2.40.30.10 3.40.50.80	0.85 0.15
	1DDI//FAD.600/	Oxidoreductase	1	NMR	1.8.1.2	1.20.990.10 2.40.30.10 3.40.50.80	0.23 0.59 0.18
	1A8P//FAD.259/	Oxidoreductase	1	NMR	1.18.1.2	2.40.30.10 3.40.50.80	0.64 0.36
	1N62/F/FAD.4931/	Carbon monoxide dehydrogenase, small chain	1	1.1	1.2.99.2	3.30.43.10 3.30.465.10	0.30 0.48

Table D.4 : Summary of the FAD dataset (continued from previous page)

Cluster	Ligand	Protein	Family size	Resolution	EC	Domain	Fraction
	1HSK/E/FAD.401/	UDP-N-acetylenolpyruvoylglucosamine reductase	1	2.3	1.1.1.158	3.30.43.10	0.29
						3.30.465.10	0.57
	1FIQ/G/FAD.606/	Xanthine oxidase	1	2.5	1.1.3.22	3.30.43.10	0.29
						3.30.465.10	0.58
	1JRO/I/FAD.3005/	Xanthine dehydrogenase, chain A	1	2.7	1.1.1.204	3.30.43.10	0.31
						3.30.465.10	0.47
	2MBR/A/FAD.401/	Uridine diphospho-N-acetylenolpyruvylglucosamine reductase	1	1.8	1.1.1.158	3.30.43.10	0.37
						3.30.465.10	0.47
4	1LQT/C/FAD.3457/	FPRA	2	1.1	1.18.1.2	3.40.50.720	0.61
						3.50.50.60	0.26
	1GTE/A/FAD.1031/	Dihydropyrimidine dehydrogenase	1	1.6	1.3.1.2	3.40.50.720	0.79
						3.50.50.60	0.12
	1AN9/B/FAD.351/	D-amino acid oxidase	1	2.5	1.4.3.3	3.40.50.720	0.84
5	1E8G/B/FAD.600/	Vanillyl-alcohol oxidase	1	2.1	1.1.3.38	3.30.43.10	0.28
						3.30.465.20	0.50
	1I19/A/FAD.700/	Cholesterol oxidase	1	1.7		3.30.43.10	0.34
						3.30.465.20	0.59
	1F0X/A/FAD.600/	D-lactate dehydrogenase	1	1.9	1.1.1.28	3.30.43.10	0.44
						3.30.465.20	0.53

Table D.4 : Summary of the FAD dataset (continued from previous page)

Cluster	Ligand	Protein	Family size	Resolution	EC	Domain	Fraction
6	1IQR/C/FAD.421/	Photolyase	2	2.1	4.1.99.3	1.10.579.10	0.57
						1.25.40.80	0.43
	1NP7/A/FAD.500/	DNA photolyase	1	1.9		1.10.579.10	0.54
						1.25.40.80	0.46
	1DNP/A/FAD.472/	DNA photolyase	1	2.3	4.1.99.3	1.10.579.10	0.54
						1.25.40.80	0.46
7	1JQI/E/FAD.399/	Short chain acyl-CoA dehydrogenase	4	2.2	1.3.99.2	1.20.140.10	0.61
						2.40.110.10	0.39
	1IVH/A/FAD.399/	Isovaleryl-CoA dehydrogenase	1	2.6	1.3.99.10	1.20.140.10	0.62
						2.40.110.10	0.38
8	1EFV/C/FAD.599/	Electron transfer flavoprotein	2	2.1		3.40.50.1220	0.84
	1POX/A/FAD.612/	Pyruvate oxidase	1	2.1	1.2.3.3	3.40.50.1220	0.77
						3.40.50.970	0.23
9	1V93/C/FAD.300/	5,10-methylenetetrahydrofolate reductase	2	1.9		3.20.20.220	1.00
	1K87/C/FAD.2001/	Proline dehydrogenase	1	2.0	1.5.1.12	3.20.20.220	1.00

Table D.4 : Summary of the FAD dataset (continued from previous page)

Cluster	Ligand	Protein	Family size	Resolution	EC	Domain	Fraction
					1.5.99.8		
10	1JR8/C/FAD.334/	Erv2 protein, mitochondrial	1	1.5		1.20.120.310	1.00
	1OQC/A/FAD.1/	Augmenter of liver regeneration	1	1.8		1.20.120.310	1.00
11	1H69/C/FAD.1274/	NAD(P)H dehydrogenase 1	4	1.9	1.6.99.2	3.40.50.360	1.00
12	1GPE/A/FAD.600/	Glucose oxidase	2	1.8	1.1.3.4	3.50.50.60 4.10.450.10	0.44 0.34
13	1QX4/A/FAD.301/	NADH-cytochrome b5 reductase	1	1.8	1.6.2.2	2.40.30.10 3.40.50.80	0.31 0.69
14	1P3Y/L/FAD.259/	MRSD protein	1	2.5		3.40.50.1950	0.92

Appendix E

CATH superfamily names

The following table gives both the CATH code and the descriptive name for all superfamilies which are discussed or referenced elsewhere in the text.

Table E.1: Mapping from CATH codes to superfamily names

CATH code	Description
1.10.8.60	Helicase, Ruva Protein; domain 3
1.10.40.20	Ribonucleotide Reductase Protein R1; domain 1
1.10.240.10	Tyrosyl-Transfer RNA Synthetase
1.10.246.10	Serum Albumin; chain A, domain 1
1.10.420.10	Peroxidase; domain 2
1.10.468.10	Photosynthetic Reaction Center; subunit C, domain 2
1.10.489.10	Chloroperoxidase
1.10.490.10	Globins
1.10.510.10	Transferase(Phosphotransferase) domain 1
1.10.520.10	Peroxidase; domain 1
1.10.560.10	GROEL; domain 1
1.10.579.10	DNA Cyclobutane Dipyrimidine Photolyase; subunit A, domain 3
1.10.580.10	Citrate Synthase; domain 1
1.10.630.10	Cytochrome p450
1.10.640.10	Myeloperoxidase; subunit C
1.10.710.10	Cytochrome C554; chain A
1.10.760.10	Cytochrome c
1.10.780.10	Hydroxylamine Oxidoreductase; chain A, domain 1
1.10.1070.11	Phosphatidylinositol 3-kinase Catalytic Subunit; chain A, domain 5
1.10.1130.10	Flavocytochrome C3; chain A
1.10.1140.10	Bovine Mitochondrial F1-atpase; Atp Synthase Beta Chain; chain D, domain 3
1.10.1160.10	Glutamyl-trna Synthetase; domain 2
1.10.1360.10	RNA dependent RNA polymerase; C-terminal domain
1.20.120.10	Four Helix Bundle (Hemerythrin (Met); subunit A)
1.20.120.310	Four Helix Bundle (Hemerythrin (Met); subunit A)
1.20.140.10	Butyryl-CoA Dehydrogenase; subunit A, domain 3
1.20.210.10	Cytochrome C Oxidase; chain A
1.20.810.10	Cytochrome Bc1 Complex; chain C

Table E.1: Mapping from CATH codes to superfamily names (continued from previous page)

CATH code	Superfamily name
1.20.850.10	Hydroxylamine Oxidoreductase; chain A, domain 2
1.20.910.10	Heme Oxygenase; chain A
1.20.950.10	Fumarate reductase cytochrome b subunit;
1.20.990.10	NADPH-cytochrome p450 Reductase; chain A, domain 3
1.20.1090.10	Dehydroquinate synthase-like - alpha domain
1.20.1260.10	Ferritin
1.20.1270.40	Substrate Binding Domain Of Dnak; chain A; domain 2
1.25.40.80	Serine Threonine Protein Phosphatase 5, Tetratricopeptide repeat
2.10.240.10	Dihydroorotate dehydrogenase b (pyrk subunit); domain 3
2.30.100.10	Toxin ADP-ribosyltransferase; chain A; domain 1
2.40.30.10	Translation factors
2.40.110.10	Butyryl-CoA Dehydrogenase; subunit A, domain 2
2.40.128.20	Lipocalin
2.40.180.10	Catalase HpII; chain A, domain 1
2.60.40.830	Immunoglobulin-like
2.60.40.1210	Immunoglobulin-like
2.60.120.10	Jelly Rolls
2.110.10.10	Hemopexin
2.170.8.10	Phosphoenolpyruvate Carboxykinase; domain 2
3.10.120.10	Flavocytochrome B2; subunit A, domain 1
3.20.20.60	Phosphoenolpyruvate-binding domains
3.20.20.70	Aldolase class I
3.20.20.100	NADP-dependent oxidoreductase
3.20.20.220	TIM Barrel
3.30.43.10	Uridine Diphospho-n-acetylenolpyruvylglucosamine Reductase; domain 2
3.30.70.120	Alpha-Beta Plaits
3.30.70.140	Alpha-Beta Plaits
3.30.70.270	Alpha-Beta Plaits
3.30.70.370	Alpha-Beta Plaits
3.30.70.420	Alpha-Beta Plaits
3.30.70.560	Alpha-Beta Plaits
3.30.200.20	Phosphorylase Kinase; domain 1
3.30.230.10	Ribosomal Protein S5; domain 2
3.30.300.10	GMP Synthetase; chain A, domain 3
3.30.360.10	Dihydrodipicolinate Reductase; domain 2
3.30.420.40	Nucleotidyltransferase; domain 5
3.30.420.90	Nucleotidyltransferase; domain 5
3.30.450.20	Beta-Lactamase
3.30.465.10	Uridine Diphospho-n-acetylenolpyruvylglucosamine Reductase; domain 3
3.30.465.20	Uridine Diphospho-n-acetylenolpyruvylglucosamine Reductase; domain 3
3.30.470.20	ATP-grasp fold; B domain
3.30.470.30	D-amino Acid Aminotransferase; chain A, domain 1

Table E.1: Mapping from CATH codes to superfamily names (continued from previous page)

CATH code	Superfamily name
3.30.538.10	Myosin fragment; domain 2
3.30.565.10	Heat Shock Protein 90
3.30.930.10	Bira Bifunctional Protein; domain 2
3.30.1010.10	Phosphatidylinositol 3-kinase Catalytic Subunit; chain A, domain 4
3.30.1130.10	GTP Cyclohydrolase I; domain 2
3.30.1490.20	Dna Ligase; domain 1
3.30.1490.70	Dna Ligase; domain 1
3.30.1500.10	Heme-binding Protein A; chain A;
3.40.50.80	Nucleotide-binding domain of ferredoxin-NADP reductase (FNR) module
3.40.50.300	P-loop containing nucleotide triphosphate hydrolases
3.40.50.360	Rossmann fold
3.40.50.620	Rossmann fold
3.40.50.720	NAD(P)-binding Rossmann-like domain
3.40.50.970	Rossmann fold
3.40.50.1220	TPP-binding domain
3.40.50.1240	Phosphoglycerate mutase-like
3.40.50.1270	Rossmann fold
3.40.50.1480	Rossmann fold
3.40.50.1950	Rossmann fold
3.40.50.1970	Rossmann fold
3.40.50.2020	Rossmann fold
3.40.109.10	NADH Oxidase
3.40.192.10	Leucine Dehydrogenase; chain A, domain 1
3.40.309.10	Aldehyde Dehydrogenase; chain A, domain 2
3.40.440.10	Adenylosuccinate Synthetase; subunit A, domain 1
3.40.605.10	Aldehyde Dehydrogenase; chain A, domain 1
3.40.640.10	Type I PLP-dependent aspartate aminotransferase-like (Major domain)
3.40.718.10	Isopropylmalate Dehydrogenase
3.40.910.10	Deoxyhypusine Synthase
3.40.1190.20	UDP-N-acetylmuramoyl-L-alanine:D-glutamate ligase
3.50.50.60	FAD/NAD(P)-binding domain
3.90.10.10	Cytochrome C3
3.90.110.10	L-2-Hydroxyisocaproate Dehydrogenase; subunit A, domain 2
3.90.170.10	Adenylosuccinate Synthetase; subunit A, domain 3
3.90.175.10	Diphtheria Toxin; domain 1
3.90.180.10	Medium-chain alcohol dehydrogenases; catalytic domain
3.90.228.20	Phosphoenolpyruvate Carboxykinase; domain 3
3.90.340.10	Nitric Oxide Synthase; chain A, domain 1
3.90.550.10	Spore Coat Polysaccharide Biosynthesis Protein SpsA; chain A
3.90.640.10	Actin; chain A, domain 4
3.90.770.10	3-hydroxy-3-methylglutaryl-coenzyme A Reductase; chain A, domain 2
3.90.780.10	5'-nucleotidase; domain 2

Table E.1: Mapping from CATH codes to superfamily names (continued from previous page)

CATH code	Superfamily name
3.90.900.10	RNA dependent RNA polymerase; fingers domain
3.90.910.10	Cytochrome C nitrite reductase; domain 2
4.10.450.10	Glucose Oxidase; domain 2

Abbreviations and nomenclature

API	Application Programming Interface
ART	ADP-ribosyltransferase
ASCII	American Standard Code for Information Interchange
ATP	Adenosine triphosphate
BBSRC	Biotechnology and Biological Sciences Research Council
BFS	Breadth-first search
BLOSUM	Block Substitution Matrix
cAMP	Cyclic AMP
CSD	Cambridge Structural Database
CSI	Common Subgraph Isomorphism
DAG	Directed Acyclic Graph
DFS	Depth-first search
DHFR	Dihydrofolate reductase
EBI	European Bioinformatics Institute
EC	Enzyme Commission
EMBL	European Molecular Biology Laboratory
ESER	Essential Set of Essential Rings
ESI	Exact Subgraph Isomorphism
FAD	Flavin adenine dinucleotide
FMN	Flavin mononucleotide
FTP	File Transfer Protocol
GAMUT	Gareth's Macromolecular Utility Toolkit
HMM	Hidden Markov Model
HSV	Hue, Saturation, Value
HTML	Hypertext Markup Language

ISAM	Indexed Sequential Access Management
LAM	Local Area Multicomputer
MAD	Multiple wavelength Anomalous Dispersion
MCS	Maximum Common Subgraph
MDS	Multidimensional Scaling
MPI	Message Passing Interface
MR	Molecular Replacement
MSD	Macromolecular Structure Database
NAD	Nicotinamide adenine dinucleotide
NADP	Nicotinamide adenine dinucleotide phosphate
NCBI	National Center for Biotechnology Information
NMR	Nuclear Magnetic Resonance
OOP	Object-Oriented Programming
PCA	Principal Components Analysis
PDB	Protein Data Bank
PQS	Protein Quaternary Structure
RCSB	Research Collaboratory in Structural Bioinformatics
RGB	Red, Green, Blue
RMSD	Root Mean Squared Deviation
SAXS	Small-angle X-ray Scattering
SCOP	Structural Classification of Proteins
STL	C++ Standard Template Library
SVD	singular value decomposition
UCL	University College London
UML	Unified Modelling Language
VMM	Vertex Mapping Matrix
XML	Extensible Markup Language

References

Abrahams, D., 2003. Boost.Python. http://www.boost.org/libs/python.

Adobe Systems Incorporated, 1990. PostScript Language Reference Manual, 2nd Edition. Addison-Wesley, Reading, MA.

Aktories, K., Rosener, S., Blaschke, U., Chhatwal, G. S., 1988. Botulinum ADP-ribosyltransferase C3. Purification of the enzyme and characterization of the ADP-ribosylation reaction in platelet membranes. Eur. J. Biochem. 172, 445–450.

Alberts, B., Bray, D., Lewis, J., Raff, M., Roberts, K., Watson, J. D., 1994. Molecular Biology of the Cell, 3rd Edition. Garland, New York and London.

Alexandrescu, A., Feb. 2001. Modern C++ Design. Addison-Wesley, Reading, MA.

Alexandrescu, A., Feb. 2002. Generic Programming: Typelists and Applications. C/C++ Users Journal 2.

Algorithmic Solutions Software, G., 2001. LEDA. http://www.algorithmic-solutions.com/.

Allen, F. H., 2002. The Cambridge Structural Database: a quarter of a million crystal structures and rising. Acta Cryst. B58 (3), 380–8.

Aloy, P., Querol, E., Aviles, F. X., Sternberg, M. J., 2001. Automated structure-based prediction of functional sites in proteins: applications to assessing the validity of inheriting protein function from homology in genome annotation and to protein docking. J. Mol. Biol. 311 (2), 395–408.

Altamirano, M. M., Blackburn, J. M., Aguayo, C., Fersht, A. R., 2000. Directed evolution of new catalytic activity using the alpha/beta-barrel scaffold. Nature 403 (6770), 617–22.

Anderson, E., Bai, Z., Bischof, C., Blackford, S., Demmel, J., Dongarra, J., Du Croz, J., Greenbaum, A., Hammarling, S., McKenny, A., Sorenson, D., 1999. LAPACK Users' Guide, 3rd Edition. Society for Industrial and Applied Mathematics, Philadelphia, PA.

Andreeva, A., Howorth, D., Brenner, S. E., Hubbard, T. J., Chothia, C., Murzin, A. G., 2004. SCOP database in 2004: refinements integrate structure and sequence family data. Nucleic Acids Res. 32 (Database issue), D226–9.

Ashburner, M., Ball, C. A., Blake, J. A., Botstein, D., Butler, H., Cherry, J. M., Davis, A. P., Dolinski, K., Dwight, S. S., Eppig, J. T., Harris, M. A., Hill, D. P., Issel-Tarver, L., Kasarskis, A., Lewis, S., Matese, J. C., Richardson, J. E., Ringwald, M., Rubin, G. M., Sherlock, G., 2000. Gene ontology: tool for the unification of biology. The Gene Ontology Consortium. Nature Genetics 25 (1), 25–9.

Atkins, P., de Paula, J., 2001. Physical Chemistry, 7th Edition. OUP, Oxford, UK.

Autumn, K., Sitti, M., Liang, Y. A., Peattie, A. M., Hansen, W. R., Sponberg, S., Kenny, T., Fearing, R., Israelachvili, J., Full, R., 2002. Evidence for van der Waals adhesion in gecko setae. Proc. Natl. Acad. Sci. USA 99 (19), 12252–6.

Bairoch, A., 1991. PROSITE: a dictionary of sites and patterns in proteins. Nucleic Acids Res 19, 2241–5.

Baker, E. N., Hubbard, R. E., 1984. Hydrogen bonding in globular proteins. Prog. Biophys. Mol. Biol. 44, 97–197.

Balducci, R., Pearlman, R. S., 1994. Efficient exact solution of the ring perception problem. J. Chem. Inf. Comp. Sci. 34 (4), 822–831.

Barker, J., Thornton, J., 2003. An algorithm for constraint-based structural template matching: application to 3D templates with statistical analysis. Bioinformatics In press.

Barker, P. D., Ferguson, S. J., 1999. Still a puzzle: why is haem covalently attached in c-type cytochromes? Structure 7, R281–R290.

Baron, M., Norman, D. G., Campbell, L. D., 1991. Protein Modules. Trends Biochem. Sci. 16, 13–17.

Barrett, A. J., 1977. Proteinases in mammalian cells and tissues. Elsevier, New York, Ch. Cathepsin D and other carboxyl proteinases, pp. 209–248.

Bartlett, G. J., Porter, C. T., Borkakoti, N., Thornton, J. M., 2002. Analysis of catalytic residues in enzyme active sites. J. Mol. Biol. 324 (1), 105–21.

Bashton, M., Chothia, C., 2002. The geometry of domain combination in proteins. J. Mol. Biol. 315 (4), 927–39.

Bell, C. E., Yeates, T. O., Eisenberg, D., 1997. Unusual conformation of nicotinamide adenine dinucleotide (NAD) bound to diphtheria toxin: a comparison with NAD bound to the oxidoreductase enzymes. Protein Sci. 6 (10), 2084–96.

Bellman, R. E., 1984. Eye of the Hurricane: An Autobiography. World Scientific, Singapore.

Berman, H. M., Westbrook, J., Feng, Z., Gilliland, G., Bhat, T. N., Weissig, H., Shindyalov, I. N., Bourne, P. E., 2000. The Protein Data Bank. Nucleic Acids Res. 28 (1), 235–42.

Betts, M. J., Sternberg, M. J., 1999. An analysis of conformational changes on protein-protein association: implications for predictive docking. Protein Eng. 12 (4), 271–83.

Bhattacharya, M., Babwah, A. V., Ferguson, S. S., 2004. Small GTP-binding protein-coupled receptors. Biochem. Soc. Trans. 32 (6), 1040–4.

Binkowski, T. A., Naghibzadeh, S., Liang, J., 2003. CASTp: Computed Atlas of Surface Topography of proteins. Nucleic Acids Res. 31 (13), 3352–5.

Boeckmann, B., Bairoch, A., Apweiler, R., Blatter, M. C., Estreicher, A., Gasteiger, E., Martin, M. J., Michoud, K., O'Donovan, C., Phan, I., Pilbout, S., Schneider, M., 2003. The SWISS-PROT protein knowledgebase and its supplement TrEMBL in 2003. Nucleic Acids Res. 31 (1), 365–70.

Bondi, J., 1964. Van der Waals Volumes and Radii. J. Phys. Chem. 68, 441–451.

Bork, P., Holm, L., Sander, C., 1994. The Immunoglobulin Fold: Structural Classification, Sequence Patterns and Common Core. J. Mol. Biol. 242, 309–320.

Bostrom, J., Norrby, P. O., Liljefors, T., 1998. Conformational energy penalties of protein-bound ligands. J. Comp. Aided Mol. Des. 12 (4), 383–96.

Brady, Jr, G. P., Stouten, P. F., 2000. Fast prediction and visualization of protein binding pockets with PASS. J. Comp. Aided Mol. Des. 14 (4), 383–401.

Brenner, S. E., Chothia, C., Hubbard, T. J., 1997. Population statistics of protein structures: lessons from structural classifications. Curr. Op. Struct. Biol. 7 (3), 369–76.

Bron, C., Kerbosch, J., 1973. Algorithm 457: Finding all cliques of an undirected graph. Communications of the A.C.M. 16, 575–577.

Brooks, B. R., Bruccoleri, R. E., Olafson, B. D., States, D. J., Swaminathan, S., Karplus, M., 1983. CHARMM: A Program for Macromolecular Energy, Minimization, and Dynamics Calculations. J. Comp. Chem. 4, 187–217.

Bruno, I. J., Cole, J. C., Lommerse, J. P., Rowland, R. S., Taylor, R., Verdonk, M. L., 1997. IsoStar: a library of information about nonbonded interactions. J. Comp. Aided Mol. Des. 11 (6), 525–37.

Burley, S. K., 2000. An Overview of Structural Genomics. Nature Struct. Biol. 7, 928.

Burns, G., Daoud, R., Vaigl, J., 1994. LAM: An Open Cluster Environment for MPI. In: Proceedings of Supercomputing Symposium. pp. 379–386.

Cahn, R. S., Ingold, C., Prelog, V., 1966. Specification of molecular chirality. Angew. Chem. Intl. Ed. 5, 385–415.

Cappello, V., Tramontano, A., Koch, U., 2002. Classification of proteins based on the properties of the ligand-binding site: the case of adenine-binding proteins. Proteins 47 (2), 106–15.

Carugo, O., Argos, P., 1997. NADP-dependent enzymes. I: Conserved stereochemistry of cofactor binding. Proteins 28 (1), 10–28.

Chakrabarti, P., Samanta, U., 1995. CH/pi interaction in the packing of the adenine ring in protein structures. J. Mol. Biol. 251 (1), 9–14.

Chang, W., Shindyalov, I. N., Bourne, P. E., 1994. Design and Application of PDBlib, a C++ Macromolecular Class Library. CABIOS 10 (6), 575–586.

Chen, L., DeVries, A. L., Cheng, C. H., 1997. Convergent evolution of antifreeze glycoproteins in Antarctic notothenioid fish and Arctic cod. Proc. Natl. Acad. Sci. USA 94 (8), 3817–22.

Chitlaru, T., Kronman, C., Zeevi, M., Kam, M., Harel, A., Ordentlich, A., Velan, B., Shafferman, A., 1998. Modulation of circulatory residence of recombinant acetylcholinesterase through biochemical or genetic manipulation of sialylation levels. Biochem J. 336 (3), 647–58.

Chothia, C., 1984. Principles that determine the structure of proteins. Ann. Rev. Biochem. 53, 537–72.

Chothia, C., 1992. Proteins. One thousand families for the molecular biologist. Nature 357 (6379), 543–4.

Collaborative Computational Project Number 4, 1994. The CCP suite: Programs for protein crystallography. Acta Cryst. D50, 760–763.

Copley, R. R., Bork, P., 2000. Homology among (betaalpha)(8) barrels: implications for the evolution of metabolic pathways. J. Mol. Biol. 303 (4), 627–41.

Cowtan, K., 2000. The Clipper Project. http://http://www.ysbl.york.ac.uk/~cowtan/clipper/clipper.html.

CRAN, 1996. The Comprehensive R Archive Network. http://lib.stat.cmu.edu/R/CRAN.

Creighton, T. E., 1993. Proteins: Structure and Molecular Properties, 2nd Edition. W.H. Freeman, New York.

Czarnecki, K., Eisenecker, U., 2000. Generative Programming: Methods, Tools, and Applications. Addison-Wesley, Reading, MA.

Dalby, A., Nourse, J. G., Hounshell, W. D., Gushurst, A. K. I., Grier, D. L., Leland, B. A., Laufer, J., 1992. Description of several chemical structure file formats used by computer programs developed at Molecular Design Limited. J. Chem. Inf. Comp. Sci. 32 (3), 244–255.

Dayhoff, M., Schwartz, R., Orcutt, B., 1978. Atlas of Protein Sequence and Structure. Vol. 5. National Biomedical Research Foundation, Washington, D.C., Ch. A model of evolutionary change in proteins, pp. 345–352.

de Berg, M., van Kreveld, M., Overmars, M., Schwarzkopf, O., 1997. Computational Geometry (Algorithms and Applications). Springer-Verlag, Berlin Heidelberg.

DeLano, W. L., 2002. The PyMOL molecular graphics program. http://www.pymol.org.

Denessiouk, K., Johnson, M., 2000. When fold is not important: a common structural framework for adenine and AMP binding in 12 unrelated protein families. Proteins 38 (3), 310–26.

Denessiouk, K., Johnson, M., 2003. "Acceptor-donor-acceptor" motifs recognize the Watson-Crick, Hoogsteen and Sugar "donor-acceptor-donor" edges of adenine and adenosine-containing ligands. J. Mol. Biol. 333 (5), 1025–43.

Denessiouk, K., Rantanen, V., Johnson, M., 2001. Adenine recognition: a motif present in ATP-, CoA-, NAD-, NADP-, and FAD-dependent proteins. Proteins 44 (3), 282–91.

Dortu, F., Gezelter, D., Guha, R., Han, Y., Hartmann, K., Horlacher, O., Howard, M., Josten, G., Krassavine, A., Kuhn, S., Luttmann, E., Mazuir, N., Michels, S., Murray-Rust, P., Pudney, C., Rienstra-Kiracofe, J., Robinson, D., Sandhu, B., Senecal, J.-S., Sild, S., Smith, B., Steinbeck, C., Tomkinson, S., Wegner, J., Werner, S., Willighagen, E., Zhang, Y., 2000. The Chemistry Development Kit. http://cdk.sourceforge.net.

Downs, G. M., 2003. Handbook of Cheminformatics: From Data to Knowledge. Vol. 1. Wiley-VCH, Weinheim, Ch. Ring Perception, pp. 161–177.

Dym, O., Eisenberg, D., 2001. Sequence-structure analysis of FAD-containing proteins. Protein Sci. 10 (9), 1712–28.

Edgar, R. C., 2004. MUSCLE: multiple sequence alignment with high accuracy and high throughput. Nucleic Acids Res. 32 (5), 1792–7.

Eisen, M. B., Wiley, D. C., Karplus, M., Hubbard, R. E., 1994. HOOK: a program for finding novel molecular architectures that satisfy the chemical and steric requirements of a macromolecule binding site. Proteins 19 (3), 199–221.

Engh, R. A., Huber, R., 1991. Accurate bond and angle parameters for X-ray protein structure refinement. Acta Cryst. A47, 392–400.

Eriani, G., Delarue, M., Poch, O., Gangloff, J., Moras, D., 1990. Partition of tRNA synthetases into two classes based on mutually exclusive sets of sequence motifs. Nature 347 (6289), 203–6.

Eriksson, M., Uhlin, U., Ramaswamy, S., Ekberg, M., Regnstrom, K., Sjoberg, B. M., Eklund, H., 1997. Binding of allosteric effectors to ribonucleotide reductase protein R1: reduction of active-site cysteines promotes substrate binding. Structure 5 (8), 1077–92.

Fan, B. T., Panaye, A., Doucet, J. P., Barbu, A., 1993. Ring perception. A new algorithm for directly finding the smallest set of smallest rings from a connection table. J. Chem. Inf. Comp. Sci. 33 (5), 657–662.

Felsenstein, J., 1985. Confidence limits on phylogenies - an approach using the bootstrap. Evolution 39 (4), 783–791.

Fersht, A. R., 1999. Structure and Mechanism in Protein Science. W.H. Freeman, New York.

Fetrow, J., Skolnick, J., 1998. Method for prediction of protein function from sequence using the sequence-to-structure-to-function paradigm with application to glutaredoxins/thioredoxins and T1 ribonucleases. J. Mol. Biol. 281 (5), 949–68.

Figueras, J., 1996. Ring Perception Using Breadth-First Search. J. Chem. Inf. Comp. Sci. 36 (5), 986–991.

Fishman, P. H., 1990. ADP-ribosylating Toxins and G Proteins. American Society of Microbiology, Washington, DC, Ch. Mechanism of action of cholera toxin, pp. 127–140.

Flower, D. R., 1996. The lipocalin protein family: structure and function. Biochem. J. 318 (1), 1–14.

Floyd, R. W., 1962. Algorithm 97: Shortest path. Communications of the A.C.M. 5 (6), 345.

Gamma, E., Helm, R., Johnson, R., Vlissides, J., 1995. Design patterns: elements of reusable software. Addison-Wesley, Reading, MA.

Gardiner, E. J., Willett, P., Artymiuk, P. J., 2000. Graph-theoretic techniques for macromolecular docking. J. Chem. Inf. Comp. Sci. 40 (2), 273–9.

Garey, M., Johnson, D., 1979. Computers and Intractability; A Guide to the Theory of NP-Completeness. Freeman, New York.

Garman, E., 1999. Cool data: quantity AND quality. Acta Cryst. D55 (10), 1641–53.

Gasteiger, J., Rudolph, C., Sadowski, J., 1990. Automatic Generation of 3D-Atomic Coordinates for Organic Molecules. Tetrahedron Comput. Methodol. 3, 537–547.

Gerstein, M., Altman, R., 1995. Average core structures and variability measures for protein families: application to the immunoglobulins. J. Mol. Biol. 251 (1), 161–75.

Gibbons, A., 1985. Algorithmic Graph Theory. Cambridge University Press, Cambridge, UK.

Glasfeld, A., Leanz, G. F., Benner, S. A., 1990. The stereospecificities of seven dehydrogenases from Acholeplasma laidlawii. The simplest historical model that explains dehydrogenase stereospecificity. J. Biol. Chem. 265 (20), 11692–9.

Goodford, P., 1985. A computational procedure for determining energetically favorable binding sites on biologically important macromolecules. J. Med. Chem. 28 (7), 849–57.

Halperin, I., Ma, B., Wolfson, H., Nussinov, R., 2002. Principles of docking: An overview of search algorithms and a guide to scoring functions. Proteins 47 (4), 409–43.

Hammes, G. G., 2002. Multiple conformational changes in enzyme catalysis. Biochemistry 41 (26), 8221–8.

Hardin, N. H., Sloane, N. J. A., 1996. McLaren's Improved Snub Cube and Other New Spherical Designs in Three Dimensions. Discrete and Computational Geometry 15, 429–441.

Harrison, A., Pearl, F., Sillitoe, I., Slidel, T., Mott, R., Thornton, J., Orengo, C., 2003. Recognizing the fold of a protein structure. Bioinformatics 19 (14), 1748–59.

Hedstrom, L., 2002. Serine protease mechanism and specificity. Chem. Rev. 102 (12), 4501–24.

Hefti, M. H., Vervoort, J., van Berkel, W. J., 2003. Deflavination and reconstitution of flavoproteins. Eur. J. Biochem. 270 (21), 4227–42.

Hegyi, H., Gerstein, M., 1999. The relationship between protein structure and function: a comprehensive survey with application to the yeast genome. J. Mol. Biol. 288 (1), 147–64.

Hendlich, M., Rippmann, F., Barnickel, G., 1997. LIGSITE: automatic and efficient detection of potential small molecule-binding sites in proteins. J. Mol. Graph. Model. 15 (6), 359–63.

Henikoff, S., Henikoff, J., 1992. Amino acid substitution matrices from protein blocks. Proc. Natl. Acad. Sci. U S A 89 (22), 10915–9.

Henrick, K., Thornton, J., 1998. PQS: a protein quaternary structure file server. Trends Biochem. Sci. 23 (9), 358–61.

Higgins, C. L., Muralidhara, B. K., Wittung-Stafshede, P., 2005. How do cofactors modulate protein folding? Protein Pept. Lett. 12 (2), 165–70.

Higgins, D. G., Sharp, P. M., 1989. Fast and sensitive multiple sequence alignments on a microcomputer. Comp. Appl. Biosci. 5 (2), 151–3.

Hinsen, K., 2000. The molecular modeling toolkit: A new approach to molecular simulations. J. Comp. Chem. 21 (2), 79–85.

Ho, C. M., Marshall, G. R., 1990. Cavity search: an algorithm for the isolation and display of cavity-like binding regions. J. Comp. Aided Mol. Des. 4 (4), 337–54.

Holm, L., Sander, C., 1995. Dali: a network tool for protein structure comparison. Trends Biochem. Sci. 20 (11), 478–80.

IBM, 1954. Preliminary Report, Specifications for the IBM Mathematical FORmula TRANslation System, FORTRAN. Tech. rep., IBM Corporation, New York.

Ihaka, R., Gentleman, R., 1996. R: A language for data analysis and graphics. Journal of Computational and Graphical Statistics 5 (3), 299–314.

Ihlenfeldt, W. D., Takahashi, Y., Abe, H., Sasaki, S., 1994. Computation and Management of Chemical Properties in CACTVS: An extensible Networked Approach toward Modularity and Flexibility. J. Chem. Inf. Comp. Sci. 34, 109–116.

Inc., S. M., 1994. Standard Template Library. http://www.sgi.com/tech/stl/.

Inc., S. M., 1995. Java programming language. http://java.sun.com.

Institute of Electrical and Electronic Engineers, 1987. IEEE standard 754. Tech. rep., Institute of Electrical and Electronic Engineers.

ISO/IEC Information Technology Task Force, 1998. Programming Language C++. Tech. Rep. 14882:1998, International Organization for Standardization.

IUPAC Commission, 1974. Rules for the nomenclature of organic chemistry, Section E: Stereochemistry, Recommendations. Pure Appl. Chem. 45, 11–30.

IUPAC-IUB, 1983. Nomenclature Committee of IUB (NC-IUB) and IUB-IUPAC Joint Commission on Biochemical Nomenclature (JCBN): Newsletter 1983. Biochem J 209 (1), I–IV.

Jackson, R. M., Gabb, H. A., Sternberg, M. J., 1998. Rapid refinement of protein interfaces incorporating solvation: application to the docking problem. J. Mol. Biol. 276 (1), 265–85.

Jardine, N., Sibson, R., 1971. Mathematical Taxonomy. Wiley, London.

Jeffrey, G. A., Saenger, W., 1991. Hydrogen Bonding in Biological Structures. Springer-Verlag, Berlin.

Jones, S., Stewart, M., Michie, A., Swindells, M. B., Orengo, C., Thornton, J. M., 1998. Domain assignment for protein structures using a consensus approach: characterization and analysis. Protein Sci. 7 (2), 233–42.

Jurgens, C., Strom, A., Wegener, D., Hettwer, S., Wilmans, M., Sterner, R., 2000. Directed evolution of a (beta alpha)8-barrel enzyme to catalyze related reactions in two different metabolic pathways. Proc. Natl. Acad. Sci. USA 97 (18), 9925–30.

Karmirantzou, M., Thornton, J., 1998. Rational Molecular Design in Drug Research. Alfred Benzon Symposium 42, Munksgaard, Copenhagen, Denmark, Ch. Computational approaches to protein ligand interactions: protein-heme complexes, pp. 264–279.

Kastenholz, M., Pastor, M., Cruciani, G., Haaksma, E., Fox, T., 2000. GRID/CPCA: a new computational tool to design selective ligands. J. Med. Chem. 43 (16), 3033–44.

Kearsley, S. K., 1989. On the orthogonal transformation used for structural comparisons. Acta Cryst. A45, 208–210.

Kho, R., Baker, B. L., Newman, J. V., Jack, R. M., Sem, D. S., Villar, H. O., Hansen, M. R., 2003. A path from primary protein sequence to ligand recognition. Proteins 50 (4), 589–99.

Kinoshita, K., Furui, J., Nakamura, H., 2002. Identification of protein functions from a molecular surface database, eF-site. J. Struct. Funct. Genomics. 2 (1), 9–22.

Kleywegt, G. J., Jones, T. A., 1994. Detection, delineation, measurement and display of cavities in macromolecular structures. Acta Cryst. D50 (2), 178–85.

Klyne, W., Prelog, V., 1960. Experientia 16, 521–523.

Kobayashi, N., Go, N., 1997. A method to search for similar protein local structures at ligand binding sites and its application to adenine recognition. Eur. Biophys. J. 26 (2), 135–44.

Kohlbacher, O., Lenhof, H., 2000. BALL - Rapid Software Prototyping in Computational Molecular Biology. Bioinformatics 16 (9), 815–824.

Koshland, D. E., 1958. Application of a theory of enzyme specificity to protein synthesis. Proc. Natl. Acad. Sci. USA 44, 98–123.

Krebs, E. G., 1989. Role of the cyclic AMP-dependent protein kinase in signal transduction. JAMA 262, 1815–1818.

Krissinel, E. B., 2002. CCP4 Coordinate Library Project, http://www.ebi.ac.uk/keb/cldoc/.

Krissinel, E. B., Henrick, K., 2004a. Common subgraph isomorphism detection by backtracking search. Softw. Pract. Exper. 34 (6), 591–607.

Krissinel, E. B., Henrick, K., 2004b. Secondary Structure Matching (SSM), a new tool for fast protein structure alignment in 3D. Acta Cryst. D60 (12), 2256–68.

Kruskal, J. B., Wish, M., 1977. Multidimensional scaling. Sage Publications, Beverly Hills, CA.

Kuttner, Y., Sobolev, V., Raskind, A., Edelman, M., 2003. A consensus-binding structure for adenine at the atomic level permits searching for the ligand site in a wide spectrum of adenine-containing complexes. Proteins 52 (3), 400–11.

Labute, P., 2005. On the perception of molecules from 3D Atomic Coordinates. J. Chem. Inf. Model. 45 (2), 215–21.

Lamdan, Y., Wolfson, H., 1988. Geometric hashing: A general and efficient model-based recognition scheme. In: Proceedings of the International Conference of Computer Vision.

Lamport, L., 1985. LaTeX: A Document Preparation System. Addison Wesley.

Lanyon, S. M., 1985. Detecting internal inconsistencies in distance data. Systematic Zoology 34 (4), 397–403.

Laskowski, R. A., 1995. SURFNET: a program for visualizing molecular surfaces, cavities, and intermolecular interactions. J. Mol. Graph. 13 (5), 323–30, 307–8.

Laskowski, R. A., MacArthur, M. W., Moss, D. S., Thornton, J. M., 1993. PROCHECK: A program to check the stereochemical quality of protein structures. J. Appl. Cryst. 26, 283–291.

Laskowski, R. A., Thornton, J. M., Humblet, C., Singh, J., 1996. X-SITE: use of empirically derived atomic packing preferences to identify favourable interaction regions in the binding sites of proteins. J. Mol. Biol. 259 (1), 175–201.

Laskowski, R. A., Watson, J. D., Thornton, J. M., 2003. From protein structure to biochemical function? J. Struct. Funct. Genomics 4 (2-3), 167–77.

Lau, S. K., Chass, G. A., Lovas, S., Penke, B., Csizmadia, I. G., 2003. An exploratory ab initio conformational analysis of selected fragments of nicotinamide adenine dinucleotide (NAD+). Part II: adenosine. J. Mol. Struct. (THEOCHEM) 666, 431–437.

Laurie, A. T., Jackson, R. M., 2005. Q-SiteFinder: an energy-based method for the prediction of protein-ligand binding sites. Bioinformatics 21 (9), 1908–16.

Lennon, B. W., Williams, C. H. J., Ludwig, M. L., 1999. Crystal structure of reduced thioredoxin reductase from Escherichia coli: Structural flexibility in the isoalloxine ring of the flavin adenine dinucleotide cofactor. Protein Sci. 8, 2366–2379.

Lesk, A. M., 1995. NAD-binding domains of dehydrogenases. Curr. Op. Struct. Biol. 5 (6), 775–83.

Levitt, D. G., 2001. A new software routine that automates the fitting of protein X-ray crystallographic electron-density maps. Acta Cryst. D57 (7), 1013–9.

Levitt, D. G., Banaszak, L. J., 1992. POCKET: a computer graphics method for identifying and displaying protein cavities and their surrounding amino acids. J. Mol. Graph. 10 (4), 229–34.

Levitt, M., Chothia, C., 1976. Structural patterns in globular proteins. Nature 261 (5561), 552–8.

Li, A., Nussinov, R., 1998. A set of van der Waals and coulombic radii of protein atoms for molecular and solvent-accessible surface calculation, packing evaluation, and docking. Proteins 32 (1), 111–27.

Lichtarge, O., Bourne, H. R., Cohen, F. E., 1996. An evolutionary trace method defines binding surfaces common to protein families. J. Mol. Biol. 257 (2), 342–58.

Ling, H., Boudsocq, F., Woodgate, R., Yang, W., 2001. Crystal structure of a Y-family DNA polymerase in action: a mechanism for error-prone and lesion-bypass replication. Cell 107 (1), 91–102.

Lipman, D. J., Altschul, S. F., Kececioglu, J. D., 1989. A tool for multiple sequence alignment. Proc. Natl. Acad. Sci. USA 86 (12), 4412–5.

Lorensen, W. E., Cline, H. E., 1997. Marching Cubes: A High Resolution 3D, Surface Construction Algorithm. Proceedings of SIGGRAPH '87 21 (4), 163–169.

Lostao, A., Gomez-Moreno, C., Mayhew, S. G., Sancho, J., 1997. Differential stabilization of the three FMN redox forms by tyrosine 94 and tryptophan 57 in flavodoxin from Anabaena and its influence on the redox potentials. Biochemistry 36 (47), 14334–44.

Madej, T., Gibrat, J. F., Bryant, S. H., 1995. Threading a database of protein cores. Proteins 23 (3), 356–69.

Mattos, C., Rasmussen, B., Ding, X., Pestko, G. A., Ringe, D., 1994. Analagous inhibitors of elastase do not always bind analagously. Nature Struct. Biol. 1, 55–58.

Message Passing Interface Forum, 1998. MPI: A Message-Passing Interface Standard (version 1.2). http://www.mpi-forum.org.

Meyer, B., 1997. Object-Oriented Software Construction. Prentice Hall PTR, New Jersey.

Milligan, G. W., Cooper, M. C., 1985. An examination of procedures for determining the number of clusters in a data set. Psychometrika 50, 159–179.

Miranker, A., Karplus, M., 1991. Functionality maps of binding sites: a multiple copy simultaneous search method. Proteins 11 (1), 29–34.

Mitchell, J., Alex, A., Snarey, M., 1999. SATIS; Atom Typing from Chemical Connectivity. J. Chem. Inf. Comp. Sci. 39, 751–757.

Mitchell, J. B., 2001. The relationship between the sequence identities of alpha helical proteins in the PDB and the molecular similarities of their ligands. J. Chem. Inf. Comp. Sci. 41 (6), 1617–22.

Mitchell, P., 1961. Coupling of Phosphorylation to Electron and Hydrogen Transfer by a Chemiosmotic Type of Mechanism. Nature 191, 144–148.

Mojena, R., 1977. Hierarchical grouping methods and stopping rules: an evaluation. Computer Journal 20, 359–363.

Moodie, S. L., Mitchell, J. B., Thornton, J. M., 1996. Protein recognition of adenylate: an example of a fuzzy recognition template. J. Mol. Biol. 263 (3), 486–500.

Moodie, S. L., Thornton, J. M., 1993. A study into the effects of protein binding on nucleotide conformation. Nucleic Acids Res. 21 (6), 1369–80.

Morris, A. L., MacArthur, M. W., Hutchison, E. G., Thorton, J. M., 1992. Assessing the Accuracy of Protein Structural Coordinates. Proteins 12, 345–364.

Moult, J., Melamud, E., 2000. From fold to function. Curr. Op. Struct. Biol. 10 (3), 384–9.

Mueller-Dieckmann, C., Ritter, H., Haag, F., Koch-Nolte, F., Schulz, G. E., 2002. Structure of the ecto-ADP-ribosyl transferase ART2.2 from rat. J. Mol. Biol. 322 (4), 687–96.

Murzin, A. G., Brenner, S. E., Hubbard, T., Chothia, C., 1995. SCOP: a structural classification of proteins database for the investigation of sequences and structures. J. Mol. Biol. 247 (4), 536–40.

Nagano, N., Hutchison, E. G., Thornton, J. M., 1999. Barrel structures in proteins: automatic identification and classification including a sequence analysis of TIM barrels. Protein Sci. 8, 2072–2084.

Najmanovich, R., Kuttner, J., Sobolev, V., Edelman, M., 2000. Side-chain flexibility in proteins upon ligand binding. Proteins 39 (3), 261–8.

Needleman, S. B., Wunsch, C. D., 1970. A general method applicable to the search for similarities in the amino acid sequence of two proteins. J. Mol. Biol. 48 (3), 443–53.

Nicklaus, M. C., Wang, S., Driscoll, J. S., Milne, G. W., 1995. Conformational changes of small molecules binding to proteins. Bioorg. Med. Chem. 3 (4), 411–28.

Nobeli, I., Laskowski, R., Valdar, W., Thornton, J., 2001. On the molecular discrimination between adenine and guanine by proteins. Nucleic Acids Res 29 (21), 4294–309.

Notredame, C., Higgins, D. G., Heringa, J., 2000. T-Coffee: A novel method for fast and accurate multiple sequence alignment. J. Mol. Biol. 302 (1), 205–17.

Object Management Group, 1995. Unified Modelling Language. http://www.uml.org.

Orengo, C. A., 1999. CORA–topological fingerprints for protein structural families. Protein Sci. 8 (4), 699–715.

Orengo, C. A., Flores, T. P., Taylor, W. R., Thornton, J. M., 1993. Identification and classification of protein fold families. Protein Eng. 6 (5), 485–500.

Orengo, C. A., Jones, D. T., Thornton, J. M., 1994. Protein superfamilies and domain superfolds. Nature 372 (6507), 631–4.

Orengo, C. A., Michie, A. D., Jones, S., Jones, D. T., Swindells, M. B., Thornton, J. M., 1997. CATH–a hierarchic classification of protein domain structures. Structure 5 (8), 1093–108.

Orengo, C. A., Pearl, F. M. G., Thornton, J. M., 2003. Structural Bioinformatics. Wiley-Liss, Hobocken, NJ, Ch. The CATH Domain Structure Database, pp. 249–272.

Orengo, C. A., Taylor, W. R., 1996. SSAP: sequential structure alignment program for protein structure comparison. Methods Enzymol. 266, 617–35.

Orengo, C. A., Thornton, J. M., 1993. Alpha plus beta folds revisited: some favoured motifs. Structure 1 (2), 105–20.

Patthy, L., 1991. Modular exchange principles in proteins. Curr. Op. Struct. Biol. 1, 351–361.

Pearl, F., Todd, A., Sillitoe, I., Dibley, M., Redfern, O., Lewis, T., Bennett, C., Marsden, R., Grant, A., Lee, D., Akpor, A., Maibaum, M., Harrison, A., Dallman, T., Reeves, G., Diboun, I., Addou, S., Lise, S., Johnston, C., Sillero, A., Thornton, J., Orengo, C., 2005. The CATH Domain Structure Database and related resources Gene3D and DHS provide comprehensive domain family information for genome analysis. Nucleic Acids Res. 33 (Database issue), D247–51.

Pearson, K., 1901. On lines and planes of closest fit to systems of points in space. Phil. Mag. 2, 559–72.

Perola, E., Charifson, P. S., 2004. Conformational analysis of drug-like molecules bound to proteins: an extensive study of ligand reorganization upon binding. J. Med. Chem. 47 (10), 2499–510.

Perrakis, A., Sixma, T. K., Wilson, K. S., Lamzin, V. S., 1997. wARP: improvement and extension of crystallographic phases by weighted averaging of multiple-refined dummy atomic models. Acta Cryst. D53 (Pt 4), 448–55.

Pickering, S., Bulpitt, A., Efford, N., Gold, N., Westhead, D., 2001. AI-based algorithms for protein surface comparisons. Comput. Chem. 26 (1), 79–84.

Pitt, W. R., Williams, M. A., Steven, M., Sweeney, B., Bleasby, A. J., Moss, D. S., 2001. The Bioinformatics Template Library - generic components for biocomputing. Bioinformatics 17 (8), 729–737.

Poulos, T. L., 1995. Cytochrome P450. Curr. Op. Struct. Biol. 5, 767–774.

Pupko, T., Bell, R., Mayrose, I., Glaser, F., Ben-Tal, N., 2002. Rate4Site: an algorithmic tool for the identification of functional regions in proteins by surface mapping of evolutionary determinants within their homologues. Bioinformatics 18 (Suppl 1), S71–7.

Python Software Foundation, 1990. Python programming language. http://www.python.org.

Qian, C., Fisanick, W., Hartzler, D. E., Chapman, S. W., 1990. Enhanced algorithm for finding the smallest set of smallest rings. J. Chem. Inf. Comp. Sci. 30 (2), 105–110.

Ramachandran, G. N., Sasisekharan, V., 1968. Conformation of polypeptides and proteins. Adv. Protein. Chem. 23, 283–438.

Rantanen, V., Denessiouk, K., Gyllenberg, M., Koski, T., Johnson, M., 2001. A fragment library based on Gaussian mixtures predicting favorable molecular interactions. J. Mol. Biol. 313 (1), 197–214.

Rantanen, V. V., Gyllenberg, M., Koski, T., Johnson, M. S., 2002. A dissimilarity matrix between protein atom classes based on Gaussian mixtures. Bioinformatics 18 (9), 1257–63.

Ratkiewicz, A., Truong, T. N., 2003. Application of chemical graph theory for automated mechanism generation. J. Chem. Inf. Comp. Sci. 43 (1), 36–44.

Raymond, J. W., Willet, P., 2002. Effectiveness of graph-based and fingerprint-based similarity measures for virtual screening of 2D, chemical structure databases. J. Comp. Aided Mol. Des. 16 (1), 59–71.

Reddy, B. V. B., Bourne, P. E., 2003. Structural Bioinformatics. Wiley-Liss, Hobocken, NJ, Ch. Protein Structure Evolution and the SCOP Database, pp. 239–248.

Rhodes, G., 2000. Crystallography Made Crystal Clear, 2nd Edition. Elsevier, New York.

Ringe, D., Mattos, C., 1999. Analysis of the binding surfaces of proteins. Med. Res. Rev. 19 (4), 321–31.

Romesburg, H. C., 1984. Cluster Analysis for Researchers. Lifetime Learning Publications, Belmont, CA.

Rossmann, M. G., 1990. The molecular replacement method. Acta Cryst. A46 (2), 73–82.

Royston, P., 1982. Algorithm AS 181: The W Test for Normality. Applied Statistics 31, 176–180.

Ruf, A., Mennissier de Murcia, J., de Murcia, G., Schulz, G. E., 1996. Structure of the catalytic fragment of poly(AD-ribose) polymerase from chicken. Proc. Natl. Acad. Sci. USA 93 (15), 7481–5.

Russell, R. B., Sasieni, P. D., Sternberg, M. J., 1998. Supersites within superfolds. Binding site similarity in the absence of homology. J. Mol. Biol. 282 (4), 903–18.

Saenger, W., 1984. Principles of Nucleic Acid Structure. Springer-Verlaf, New York.

Sander, C., Schneider, R., 1991. Database of homology-derived protein structures and the structural meaning of sequence alignment. Proteins 9 (1), 56–68.

Schaffer, A. A., Wolf, Y. I., Ponting, C. P., Koonin, E. V., Aravind, L., Altschul, S. F., 1999. IMPALA: matching a protein sequence against a collection of PSI-BLAST-constructed position-specific score matrices. Bioinformatics 15 (12), 1000–11.

Schmitt, E., Moulinier, L., Fujiwara, S., Imanaka, T., Thierry, J. C., Moras, D., 1998. Crystal structure of aspartyl-tRNA synthetase from Pyrococcus kodakaraensis KOD: archaeon specificity and catalytic mechanism of adenylate formation. EMBO J. 17 (17), 5227–37.

Schmitt, S., Kuhn, D., Klebe, G., 2002. A new method to detect related function among proteins independent of sequence and fold homology. J. Mol. Biol. 323 (2), 387–406.

Shannon, C., 1948. A mathematical theory of communication. Bell System Tech. J. 27, 379–423.

Sheridan, R., Holloway, M., McGaughey, G., Mosley, R., Singh, S., 2002. A simple method for visualizing the differences between related receptor sites. J. Mol. Graph. Model. 21 (1), 71–9.

Shi, J., Blundell, T., Mizuguchi, K., 2001. FUGUE: sequence-structure homology recognition using environment-specific substitution tables and structure-dependent gap penalties. J. Mol. Biol. 310 (1), 243–57.

Shindyalov, I. N., Bourne, P. E., 1998. Protein structure alignment by incremental combinatorial extension (CE) of the optimal path. Protein Eng. 11 (9), 739–47.

Shrake, A., Rupley, J. A., 1973. Environment and exposure to solvent of protein atoms. Lysozyme and insulin. J. Mol. Biol. 79 (2), 351–71.

Silberschatz, A., Korth, H. F., Sudarshan, S., 1997. Database System Concepts, 3rd Edition. McGraw-Hill, Maidenhead, Berkshire.

Silberstein, M., Dennis, S., Brown, L., Kortvelyesi, T., Clodfelter, K., Vajda, S., 2003. Identification of substrate binding sites in enzymes by computational solvent mapping. J. Mol. Biol. 332 (5), 1095–113.

Singh, S. K., Kurnasov, O. V., Chen, B., Robinson, H., Grishin, N. V., Osterman, A. L., Zhang, H., 2002. Crystal structure of Haemophilus influenzae NadR, protein. A bifunctional enzyme endowed with NMN, adenyltransferase and ribosylnicotinimide kinase activities. J. Biol. Chem. 277 (36), 33291–9.

Skolnick, J., Fetrow, J. S., 2000. From genes to protein structure and function: novel applications of computational approaches in the genomic era. Trends Biotech. 18 (1), 34–9.

Smith, T. F., Waterman, M. S., 1981. Identification of common molecular subsequences. J. Mol. Biol. 147 (1), 195–7.

Sobolev, V., Sorokine, A., Prilusky, J., Abola, E., Edelman, M., 1999. Automated analysis of interatomic contacts in proteins. Bioinformatics 15 (4), 327–32.

Sokal, R. R., Rohlf, F. J., 2003. Biometry, 3rd Edition. WH Freeman, New York.

Sonnhammer, E. L., Kahn, D., 1994. Modular arrangement of proteins as inferred from analysis of homology. Protein Sci. 3 (3), 482–92.

Stivers, J. T., Jiang, Y. L., 2003. A mechanistic perspective on the chemistry of DNA, repair glycosylases. Chem Rev. 103 (7), 2729–59.

Stock, D., Leslie, A. G., Walker, J. E., 1999. Molecular architecture of the rotary motor in ATP, synthase. Science 286 (5445), 1700–5.

Stoddard, B. L., Dean, A., Koshland, Jr, D. E., 1993. Structure of isocitrate dehydrogenase with isocitrate, nicotinamide adenine dinucleotide phosphate, and calcium at 2.5-A resolution: a pseudo-Michaelis ternary complex. Biochemistry 32 (36), 9310–6.

Stroustrup, B., 1995. The C++ Programming Language, 1st Edition. Addison-Wesley, Reading, MA.

Stryer, L., 1995. Biochemistry, 4th Edition. W.H. Freeman, New York.

Stubbs, M. T., Reyda, S., Dullweber, F., Moller, M., Klebe, G., Dorsch, D., Mederski, W. W., Wurziger, H., 2002. pH-dependent binding modes observed in trypsin crystals: lessons for structure-based drug design. Chembiochem 3 (2-3), 246–9.

Sundaresan, V., Chartron, J., Yamaguchi, M., Stout, C., 2005. Conformational diversity in NAD(H) and interacting transhydrogenase nicotinamide nucleotide binding domains. J. Mol. Biol. 346 (2), 617–29.

Tanner, J. J., Tu, S. C., Barbour, L. J., Barnes, C. L., Krause, K. L., 1999. Unusual folded conformation of nicotinamide adenine dinucleotide bound to flavin reductase P. Protein Sci. 8 (9), 1725–32.

Taroni, C., Jones, S., Thornton, J. M., 2000. Analysis and prediction of carbohydrate binding sites. Protein Eng. 13 (2), 89–98.

Taylor, W., 1986. The classification of amino acid conservation. J. Theor. Biol. 119 (2), 205–18.

Terwilliger, T. C., 2000. Maximum-likelihood density modification. Acta Cryst. D56 (8), 965–72.

The Boost Committee, 1998. C++Boost. http://www.boost.org/.

The OpenBabel Team, 2001. OpenBabel. http://sourceforge.net/projects/openbabel/.

Thornton, J. M., Bayley, P. M., 1977. Conformational energy calculations for dinucleotide molecules: a study of the nucleotide coenzyme nicotinamide adenine dinucleotide (NAD+). Biopolymers 16 (9), 1971–86.

Todd, A. E., Orengo, C. A., Thornton, J. M., 2001. Evolution of function in protein superfamilies, from a structural perspective. J. Mol. Biol. 307 (4), 1113–43.

Tonegawa, S., 1983. Somatic generation of antibody diversity. Nature 302 (5909), 575–81.

Torrance, J. W., Bartlett, G. J., Porter, C. T., Thornton, J. M., 2005. Using a library of structural templates to recognise catalytic sites and explore their evolution in homologous families. J. Mol. Biol. 347 (3), 565–81.

Tsuge, H., Nagahama, M., Nishimura, H., Hisatsune, J., Sakaguchi, Y., Itogawa, Y., Katunuma, N., Sakurai, J., 2003. Crystal structure and site-directed mutagenesis of enzymatic components from Clostridium perfringens iota-toxin. J. Mol. Biol. 325 (3), 471–83.

Ullman, J. R., 1976. An algorithm for subgraph isomorphism. Journal of the Association for Computing Machinery 23, 31–42.

Valdar, W., 2002. Scoring residue conservation. Proteins 48 (2), 227–41.

Valdar, W., Thornton, J., 2001a. Protein-protein interfaces: analysis of amino acid conservation in homodimers. Proteins 42 (1), 108–24.

Valdar, W. S., Thornton, J. M., 2001b. Protein-protein interfaces: analysis of amino acid conservation in homodimers. Proteins 42 (1), 108–24.

van den Heuvel, R. H., Westphal, A. H., Heck, A. J., Walsh, M. A., Rovida, S., van Berkel, W. J., Mattevi, A., 2004. Structural studies on flavin reductase PheA2 reveal binding of NAD in an unusual folded conformation and support novel mechanism of action. J. Biol. Chem. 279 (13), 12860–7.

van Heesch, D., 1997. Doxygen. http://http://www.stack.nl/~dimitri/doxygen/.

Vaughan, G. V., 2000. GNU Autoconf, Automake and Libtool. Macmillan, Indianapolis, PA.

Velankar, S., McNeil, P., Mittard-Runte, V., Suarez, A., Barrell, D., Apweiler, R., Henrick, K., 2005. E-MSD: an integrated data resource for bioinformatics. Nucleic Acids Res. 33 (Database issue), D262–5.

Verdonk, M. L., Cole, J. C., Taylor, R., 1999. SuperStar: a knowledge-based approach for identifying interaction sites in proteins. J. Mol. Biol. 289 (4), 1093–108.

Verdonk, M. L., Cole, J. C., Watson, P., Gillet, V., Willett, P., 2001. SuperStar: improved knowledge-based interaction fields for protein binding sites. J. Mol. Biol. 307 (3), 841–59.

Walker, J., Saraste, M., Runswick, M., Gay, N., 1982. Distantly related sequences in the alpha- and beta-subunits of ATP synthase, myosin, kinases and other ATP-requiring enzymes and a common nucleotide binding fold. EMBO J 1 (8), 945–51.

Wall, L., Christiansen, T., Orwant, J., 2000. Programming Perl, 3rd Edition. O'Reilly, Sebastopol, CA.

Wallace, A. C., Laskowski, R. A., Thornton, J. M., Feb. 1995. LIGPLOT: a program to generate schematic diagrams of protein-ligand interactions. Protein Eng. 8 (2), 127–34.

Wallace, A. C., Laskowski, R. A., Thornton, J. M., 1996. Derivation of 3D coordinate templates for searching structural databases: application to Ser-His-Asp catalytic triads in the serine proteinases and lipases. Protein Sci. 5 (6), 1001–13.

Walsh, J. D., Miller, A.-F., 2003. Flavin reduction potential tuning by substitution and bending. J. Mol. Struct. (THEOCHEM) 623, 185–195.

Walsh, M. A., Evans, G., Sanishvili, R., Dementieva, I., Joachimiak, A., 1999. MAD data collection - current trends. Acta Cryst. D55 (10), 1726–32.

Watson, P., Willett, P., Gillet, V., Verdonk, M., 2001. Calculating the knowledge-based similarity of functional groups using crystallographic data. J. Comput. Aided. Mol. Des. 15 (9), 835–57.

Weber, P. C., Pantoliano, M. W., Salemme, F. R., 1995. Crystallographic and thermodynamic comparison of structurally diverse molecules binding to streptavidin. Acta Cryst. D51 (4), 590–596.

Weber, S., 2005. Light-driven enzymatic catalysis of DNA repair: a review of recent biophysical studies on photolyase. Biochim. Biophys. Acta. 1707 (1), 1–23.

Weiner, S. J., Kollman, P. A., Case, D. A., Singh, U. C., Ghio, C., Alagona, G., Profeta, S., Weiner, P., 1984. A new force field for molecular mechanical simulation of nucleic acids and proteins. J. Am. Chem. Soc. 106, 765–784.

Westbrook, J., Feng, Z., Jain, S., Bhat, T. N., Thanki, N., Ravichandran, V., Gilliland, G. L., Bluhm, W., Weissig, H., Greer, D. S., Bourne, P. E., Berman, H. M., 2002. The Protein Data Bank: unifying the archive. Nucleic Acids Res. 30 (1), 245–8.

Wilson, C. A., Kreychman, J., Gerstein, M., 2000. Assessing annotation transfer for genomics: quantifying the relations between protein sequence, structure and function through traditional and probabilistic scores. J. Mol. Biol. 297 (1), 233–49.

Yap, K. L., Ames, J. B., Swindells, M. B., Ikura, M., 1999. Diversity of conformational states and changes within the EF-hand protein superfamily. Proteins 37 (3), 499–507.

Young, G., Householder, A., 1938. Discussion of a set of points in terms of their mutual distances. Psychometrika 3, 19–22.

Zvelebil, M., Barton, G., Taylor, W., Sternberg, M., 1987. Prediction of protein secondary structure and active sites using the alignment of homologous sequences. J. Mol. Biol. 195 (4), 957–61.